frontiers | Research Topics

Drug resistance, global epidemiology and virulence of acinetobacter

Edited by
Raffaele Zarrilli, Paolo Visca, Remy A. Bonnin and Emmanuelle Dé

Published in
Frontiers in Microbiology
Frontiers in Cellular and Infection Microbiology

ISSN 1664-8714
ISBN 978-2-83251-838-0
DOI 10.3389/978-2-83251-838-0

About Frontiers

Frontiers is more than just an open access publisher of scholarly articles: it is a pioneering approach to the world of academia, radically improving the way scholarly research is managed. The grand vision of Frontiers is a world where all people have an equal opportunity to seek, share and generate knowledge. Frontiers provides immediate and permanent online open access to all its publications, but this alone is not enough to realize our grand goals.

Frontiers journal series

The Frontiers journal series is a multi-tier and interdisciplinary set of open-access, online journals, promising a paradigm shift from the current review, selection and dissemination processes in academic publishing. All Frontiers journals are driven by researchers for researchers; therefore, they constitute a service to the scholarly community. At the same time, the *Frontiers journal series* operates on a revolutionary invention, the tiered publishing system, initially addressing specific communities of scholars, and gradually climbing up to broader public understanding, thus serving the interests of the lay society, too.

Dedication to quality

Each Frontiers article is a landmark of the highest quality, thanks to genuinely collaborative interactions between authors and review editors, who include some of the world's best academicians. Research must be certified by peers before entering a stream of knowledge that may eventually reach the public - and shape society; therefore, Frontiers only applies the most rigorous and unbiased reviews. Frontiers revolutionizes research publishing by freely delivering the most outstanding research, evaluated with no bias from both the academic and social point of view. By applying the most advanced information technologies, Frontiers is catapulting scholarly publishing into a new generation.

What are Frontiers Research Topics?

Frontiers Research Topics are very popular trademarks of the *Frontiers journals series*: they are collections of at least ten articles, all centered on a particular subject. With their unique mix of varied contributions from Original Research to Review Articles, Frontiers Research Topics unify the most influential researchers, the latest key findings and historical advances in a hot research area.

Find out more on how to host your own Frontiers Research Topic or contribute to one as an author by contacting the Frontiers editorial office: frontiersin.org/about/contact

Drug resistance, global epidemiology and virulence of acinetobacter

Topic editors

Raffaele Zarrilli — University of Naples Federico II, Italy
Paolo Visca — Roma Tre University, Italy
Remy A. Bonnin — Université Paris-Saclay, France
Emmanuelle Dé — Rouen Normandy University, France

Citation

Zarrilli, R., Visca, P., Bonnin, R. A., Dé, E., eds. (2023). *Drug resistance, global epidemiology and virulence of acinetobacter*. Lausanne: Frontiers Media SA. doi: 10.3389/978-2-83251-838-0

Table of contents

frontiers | Frontiers in Microbiology

TYPE Editorial
PUBLISHED 21 February 2023
DOI 10.3389/fmicb.2023.1151462

OPEN ACCESS

EDITED AND REVIEWED BY
Rustam Aminov,
University of Aberdeen, United Kingdom

*CORRESPONDENCE
Raffaele Zarrilli
✉ rafzarri@unina.it

SPECIALTY SECTION
This article was submitted to Antimicrobials, Resistance and Chemotherapy, a section of the journal Frontiers in Microbiology

RECEIVED 26 January 2023
ACCEPTED 30 January 2023
PUBLISHED 21 February 2023

CITATION
Zarrilli R, Visca P, Bonnin RA and Dé E (2023) Editorial: Drug resistance, global epidemiology and virulence of *Acinetobacter*. *Front. Microbiol.* 14:1151462. doi: 10.3389/fmicb.2023.1151462

Editorial: Drug resistance, global epidemiology and virulence of *Acinetobacter*

Raffaele Zarrilli[1]*, Paolo Visca[2], Remy A. Bonnin[3] and Emmanuelle Dé[4]

[1]Department of Public Health, University of Naples Federico II, Naples, Italy, [2]Department of Sciences, Roma Tre University, Rome, Italy, [3]Team "Resist" Unité Mixte de Recherche (UMR) 1184 "Immunology of Viral, Auto-Immune, Hematological and Bacterial Diseases (IMVA-HB)," Institut National de la Santé et de la Recherche Médicale (INSERM), Université Paris-Saclay, CEA, LabEx LERMIT, Faculty of Medicine, Le Kremlin-Bicêtre, France, [4]University of Rouen Normandie, National Institute of Applied Sciences (INSA) Rouen Normandie, Centre National de la Recherche Science (CNRS), Lab. Polymers, Biopolymers, Surfaces (PBS), Unité Mixte de Recherche 6270, Rouen, France

KEYWORDS

***Acinetobacter*, antimicrobial resistance, genomic epidemiology, virulence, environmental fitness**

Editorial on the Research Topic
Drug resistance, global epidemiology and virulence of *Acinetobacter*

Bacteria belonging to the genus *Acinetobacter* are Gram-negative coccobacilli that are a frequent cause of health-care associated infections. *Acinetobacter baumannii* and the emergent species of *A. baumannii* (Ab) group like *A. pittii*, *A. nosocomialis*, *A. seifertii* and *A. lactucae* are the most clinically relevant species (Wong et al., 2017). Global epidemiology of *A. baumannii* showed a clonal population structure dominated by two major global clonal lineages (GC1 and GC2) and few additional epidemic clones (Gaiarsa et al., 2019). The most successful *A. baumannii* clones show resistance to a broad range of antimicrobials and disinfectants and share virulence features such as biofilm formation on abiotic surfaces, resistance to desiccation and adherence to epithelial cells, which contribute to their survival in the hospital environment and spread among patients (Giannouli et al., 2013).

This Research Topic collected original updates on the drug resistance, global epidemiology and virulence of *Acinetobacter*.

Three studies of This Topic investigated the genomics of antimicrobial resistance in *A. baumannii*. Vijayakumar et al. analyzed the mobile genetic elements associated with carbapenem resistance in *A. baumannii* clinical isolates from multiple hospitals in India between 2018 and 2019. They observed an increased prevalence of bla_{OXA-23} followed by dual carbapenemases, bla_{OXA-23}, and bla_{NDM} and identified variations of AbaR4 and AbGRI resistance islands (RI). The majority of the isolates belonged to the dominant international clonal lineage 2, followed by less prevalent clones assigned to PasteurST25 and PasteurST10. Hamed et al. analyzed the genomic structure of RI in multidrug resistant and extensive drug resistant *A. baumannii* clinical isolates from Egypt. The majority of the isolates belonged to high-risk global clones (GC1, GC2, and GC9) and disclosed at least nine configurations of genomic RI, three of which (AbaR4, AbaR4b, and AbGRI1-like-2) carried bla_{OXA-23} carbapenemase within Tn*2006*. An additional RI (RI-PER-7), carrying the resistance genes *armA* and bla_{PER-7}, was also identified on a plasmid into the strain M03. Yadav and Singh analyzed CRISPR-Cas type I-F1 and type I-F2 systems and its association with phage invasion in 4,977 genomes of *A. baumannii*. Of the 689 CRISPR-Cas positive genomes, 67.48% isolates harbored type I-F1, 28.59% had type I-F2, and 3.7% had co-existence of both type I-F1 and type I-F2 systems. A significantly reduced number of integrated phages in

isolates with co-existence of type I-F1 + F2 compared with other counterparts was observed ($p = 0.0041$). In addition, the isolates carrying type I-F1 + F2 did not exhibit reduced resistance and virulence genes compared to CRISPR-Cas (–) and CRISPR-Cas (+) type I-F1 and type I-F2. This suggested that that the co-existence of CRISPR-Cas type I-F1 and F2 systems in *A. baumannii* imparts the hyperactivity against phages without affecting the presence of resistance genes.

The genetic elements responsible for horizontal gene transfer of antimicrobial resistance in *Acinetobacter* were also analyzed. Mindlin et al. showed that the population of natural *Acinetobacter* strains contains a significant number of conjugative mega-plasmids and revealed the presence of the genes for resistance to heavy metals in the plasmids from environmental strains, while the accumulation of antibiotic resistance genes carried by transposons and integrons in plasmids from clinical strains. Conjugative mega-plasmids may play a key role in the dissemination of multi-drug resistance among *Acinetobacter* species. The acquisition of blaOXA genes encoding different carbapenem-hydrolyzing class-D β-lactamases represents a main determinant of carbapenem resistance in *A. baumannii*. Giacone et al. investigated the contribution of pXerC/D-mediated recombination to the generation of structural diversity between resistance plasmids carrying pXerC/D-bounded blaOXA-58- and TnaphA6-containing resistance modules. They showed the existence of different pairs of recombinationally-active pXerC/D sites in these plasmids, some mediating reversible intramolecular inversions and others reversible plasmid fusions/resolutions.

Other studies investigated the role of efflux pumps (EPs) in antimicrobial resistance and tolerance to disinfectants in *A. baumannii*. The TetA(G) efflux pump of *A. baumannii* confers resistance to a variety of tetracyclines. Sumyk et al. studied the binding of tetracycline to TetR repressor of *A. baumannii* AYE (AbTetR). They showed that Arg104 and Arg135 residues, which are embedded at the entrance of the AbTetR binding pocket, play important roles in the recognition of tetracyclines, and act as a barrier to prevent the release of tetracycline from its binding pocket upon AbTetR activation. This might provide further insight for the development of new tetracycline antibiotics to overcome the efflux resistance mechanism deployed by *A. baumannii*. López-Siles et al. analyzed the promoter region markers associated with altered expression of three operons coding for Resistance-Nodulation-Division (RND) antibiotic efflux pumps (EPs) in *A. baumannii*. They *in silico* identified the genetic alterations leading to the constitutive upregulation of specific promoter regions of RND operons and then fused DNA of upstream sequences of RND operons to a luciferase reporter system. In sum, they developed a computational-experimental pipeline containing all components required for identifying the upstream regulatory resistome in *A. baumannii*. The management of infections caused by *A. baumannii* is hindered by its intrinsic tolerance to a wide variety of biocides. Migliaccio et al. investigated the role of different *A. baumannii* EPs in tolerance to chlorhexidine (CHX) and benzalkonium (BZK) and identified non-toxic compounds able to restore susceptibility to CHX and BZK in *A. baumannii*. They demonstrated that tolerance to CHX and BZK in *A. baumannii* ATCC 19606 was mediated by the activation of AdeB, AceI, and AmvA EPs, AdeB playing a major role. Importantly, inhibition of EP genes expression by either piperine or resveratrol at non-toxic concentrations restored CHX and BZK susceptibility in *A. baumannii*.

Several of the published manuscripts analyzed the molecular mechanisms of virulence in *A. baumannii*. To highlight critical molecular determinants of *A. baumannii* biofilm formation, Robin et al. used proteomic approaches on ATCC17978 and SDF strains. They identified the MacAB-TolC EP system as a contributor to biofilm formation on solid surfaces. Indeed, this EP is involved in the envelope stress response (maintenance of membrane rigidity, tolerance to high osmolarity conditions) but also in the maintenance of iron and sulfur homeostasis. This system could help *A. baumannii* to face deleterious conditions occurring in mature biofilms. Understanding regulation of genes involved in virulence and biofilm formation is essential to develop new strategies of infection control. It was previously shown that members of LysR-type transcriptional regulator (LTTR) family regulated numerous genes involved in these essential bacterial functions. To understand the genetic mechanisms regulating the interconvertion between virulent opaque (Vir-O) and avirulent translucent (AV-T) colony variants in *A. baumannii*, Tierney et al. examined the function of the LysR-type transcriptional regulator (LTTR), *ABUW_1132*. This global regulator, able to stimulate the expression of 74 genes by ≥2-fold, regulated positively the switch from Vir-O to AV-T and also impacted quorum sensing molecule secretion and surface-associated motility. Its deletion in AV-T variant promoted capsule formation and increased virulence. This suggests that AV-T variant, which has advantages in natural environments due to an increased ability to form biofilm, may also exist in virulent state, in case of *ABUW_1132* downregulation. LeuO, another LTTR, was characterized by Islam et al. *via* the construction of a *leuO* deletion mutant. Phenotypic characterization of this mutant showed that LeuO act as a repressor of biofilm synthesis by regulating genes within the *csuA/BABCDE* chaperon-usher pili system or the *A1S_0112-A1S_0119* acinetin operon, known as critical for biofilm formation. Several mutations in *leuO* gene from clinical strains were associated with a hyper-biofilm phenotype. Also, *leuO* gene disruption increased pathogenicity of *A. baumannii* in mouse infection model, while decreased motility and epithelial cell adhesion.

The molecular mechanisms responsible for environmental persistence were also investigated. Tajuelo et al. analyzed the role of the peptidoglycan recycling pathway enzymes AmpD and AnmK, which contribute to intrinsic fosfomycin resistance in *A. baumannii*, and also to virulence. They demonstrated that bacterial growth, fitness, biofilm formation and twitching motility were reduced in mutant strains *A. baumannii* ATCC 17978 Δ*ampD*::Kan and Δ*anmK*::Kan compared to the wild type strain. Also, Zhou et al. investigated the role of *gigA*/*gigB* genes of *A. baumannii* ATCC 17978, in bacterial growth, stress resistance, evading macrophage defense, and killing of *Galleria mellonella* larvae. The deletion of *gigA/gigB* conferred growth and replication defects within murine macrophages and an inability to kill *G. mellonella* larvae, while were dispensable for other stress-resistance survival phenotypes, including aminoglycoside resistance.

In conclusion, the spread of multi-drug resistant *A. baumannii* is a global public health threat. Understanding the mechanisms of antimicrobial resistance, virulence and adaptation to stressful conditions is important to prevent and control infections by this challenging pathogen.

Author contributions

All authors listed have made a substantial, direct, and intellectual contribution to the work and approved it for publication.

Acknowledgments

We are grateful to all reviewers who put their efforts to analyze the manuscripts. ED thanks the Normandie Region (SéSAD research network, France) and European Union for their support. Europe gets involved in Normandie with European Regional Development Fund.

Conflict of interest

The authors declare that the research was conducted in the absence of any commercial or financial relationships that could be construed as a potential conflict of interest.

Publisher's note

All claims expressed in this article are solely those of the authors and do not necessarily represent those of their affiliated organizations, or those of the publisher, the editors and the reviewers. Any product that may be evaluated in this article, or claim that may be made by its manufacturer, is not guaranteed or endorsed by the publisher.

References

Gaiarsa, S., Batisti Biffignandi, G., Esposito, E. P., Castelli, M., Jolley, K. A., Brisse, S., et al. (2019). Comparative analysis of the two Acinetobacter baumannii multilocus sequence typing (MLST) schemes. *Front. Microbiol.* 10, 930. doi: 10.3389/fmicb.2019.00930

Giannouli, M., Antunes, L., Marchetti, V., Triassi, M., Visca, P., and Zarrilli, R. (2013). Virulence-related traits of epidemic Acinetobacter baumannii strains belonging to the international clonal lineages I-III and to the emerging genotypes ST25 and ST78. *BMC Infect. Dis.* 13, 1–11. doi: 10.1186/1471-2334-13-282

Wong, D., Nielsen, T. B., Bonomo, R. A., Pantapalangkoor, P., Luna, B., and Spellberg, B. (2017). Clinical and pathophysiological overview of Acinetobacter infections: a century of challenges. *Clin. Microbiol. Rev.* 30, 409–447. doi: 10.1128/CMR.00058-16

frontiers in Microbiology

ORIGINAL RESEARCH
published: 19 July 2021
doi: 10.3389/fmicb.2021.711158

Binding of Tetracyclines to *Acinetobacter baumannii* TetR Involves Two Arginines as Specificity Determinants

Manuela Sumyk†, Stephanie Himpich†, Wuen Ee Foong, Andrea Herrmann, Klaas M. Pos and Heng-Keat Tam†‡*

Institute of Biochemistry, Goethe-University Frankfurt, Frankfurt, Germany

OPEN ACCESS

Edited by:
Paolo Visca, Roma Tre University, Italy

Reviewed by:
Winfried Hinrichs, University of Greifswald, Germany
Fabio Polticelli, Roma Tre University, Italy

***Correspondence:**
Heng-Keat Tam
tamhk60@hotmail.com

†These authors have contributed equally to this work and share first authorship

‡Present address:
Heng-Keat Tam, Hengyang Medical College, University of South China, Hengyang, China

Specialty section:
This article was submitted to Antimicrobials, Resistance and Chemotherapy, a section of the journal Frontiers in Microbiology

Received: *18 May 2021*
Accepted: *23 June 2021*
Published: *19 July 2021*

Citation:
Sumyk M, Himpich S, Foong WE, Herrmann A, Pos KM and Tam H-K (2021) Binding of Tetracyclines to Acinetobacter baumannii TetR Involves Two Arginines as Specificity Determinants. Front. Microbiol. 12:711158. doi: 10.3389/fmicb.2021.711158

Acinetobacter baumannii is an important nosocomial pathogen that requires thoughtful consideration in the antibiotic prescription strategy due to its multidrug resistant phenotype. Tetracycline antibiotics have recently been re-administered as part of the combination antimicrobial regimens to treat infections caused by *A. baumannii*. We show that the TetA(G) efflux pump of *A. baumannii* AYE confers resistance to a variety of tetracyclines including the clinically important antibiotics doxycycline and minocycline, but not to tigecycline. Expression of *tetA(G)* gene is regulated by the TetR repressor of *A. baumannii* AYE (AbTetR). Thermal shift binding experiments revealed that AbTetR preferentially binds tetracyclines which carry a O-5H moiety in ring B, whereas tetracyclines with a 7-dimethylamino moiety in ring D are less well-recognized by AbTetR. Confoundingly, tigecycline binds to AbTetR even though it is not transported by TetA(G) efflux pump. Structural analysis of the minocycline-bound AbTetR-Gln116Ala variant suggested that the non-conserved Arg135 interacts with the ring D of minocycline by cation-π interaction, while the invariant Arg104 engages in H-bonding with the O-11H of minocycline. Interestingly, the Arg135Ala variant exhibited a binding preference for tetracyclines with an unmodified ring D. In contrast, the Arg104Ala variant preferred to bind tetracyclines which carry a O-6H moiety in ring C except for tigecycline. We propose that Arg104 and Arg135, which are embedded at the entrance of the AbTetR binding pocket, play important roles in the recognition of tetracyclines, and act as a barrier to prevent the release of tetracycline from its binding pocket upon AbTetR activation. The binding data and crystal structures obtained in this study might provide further insight for the development of new tetracycline antibiotics to evade the specific efflux resistance mechanism deployed by *A. baumannii*.

Keywords: transcription repressor, antibiotic resistance, *Acinetobacter baumannii*, TetR family, tetracycline transporter, tetracycline, tigecycline

INTRODUCTION

Acinetobacter baumannii is an opportunistic human pathogen, that has been recently classified by the World Health Organization as the most prevalent clinical bacterium, in need for novel antibiotics due to its multidrug resistance (MDR) phenotype (World Health Organisation [WHO], 2017). The intrinsic antibiotic resistance and the propensity to acquire MDR determinants cause a tremendous problem in public health, leading to high morbidity and mortality associated with nosocomial infections (Touchon et al., 2014; Morris et al., 2019). A prominent MDR mechanism employed by *A. baumannii* is the deployment of multidrug efflux pumps that actively remove a variety of antibiotics from the cells across bacterial membranes (Rumbo et al., 2013; Yoon et al., 2015). The gene expression of multidrug efflux pumps is often modulated by various types of transcriptional regulators including LysR-type transcriptional regulators, TetR-type regulators, and two-component transcriptional regulatory systems (Marchand et al., 2004; Coyne et al., 2010; Rosenfeld et al., 2012; Liu et al., 2018).

Tetracyclines are bacteriostatic antibiotics that function through reversible binding to the A site of the 30S ribosomal subunit, thereby inhibiting bacterial protein synthesis (Chopra and Roberts, 2001). Due to their broad spectrum of activity and relatively low cost, tetracyclines are used extensively in human and animal infections. In many countries, tetracyclines are incorporated into livestock feed at subtherapeutic doses as growth promoters for metaphylaxis purposes (Chattopadhyay, 2014; Granados-Chinchilla and Rodríguez, 2017). The misuse of tetracyclines in the poultry sector has led to an increase in acquired tetracycline resistance and these resistance mechanisms are attributed to efflux pumps, inactivating enzymes, ribosomal protection, and/or target modification (Nguyen et al., 2014). Tetracycline resistance genes in bacteria are typically located in mobile plasmids, transposons, conjugative transposons, and integrons, enabling these genes to move between species and into a wide range of genera by conjugation (Chopra and Roberts, 2001). In the late twentieth century, tigecycline has been specifically developed to overcome the emerging efflux-mediated tetracycline resistance (e.g., TetA) in Gram-negative bacteria, and exhibits an increase in antimicrobial potency against clinically important pathogens (Petersen et al., 1999). The enhanced antimicrobial activity of tigecycline compared to other tetracyclines is attributed to its increased binding affinity for the ribosome (Olson et al., 2006). Notably, the bulky 9-*tert*-butylglycylamido moiety at position C9 of tigecycline has enabled this antibiotic to escape the TetA-mediated extrusion of tigecycline, most likely due to the steric hindrance effect to TetA caused by this bulky substituent (Hirata et al., 2004).

In Gram-negative bacteria, it became evident that tetracyclines are transported out of the cells in a synergy between the single component efflux pumps (e.g., TetA) and the Resistance Nodulation cell Division (RND)-type tripartite efflux pumps, both energized by the proton motive force (McMurry et al., 1980; Foong et al., 2020). In *A. baumannii*, tetracyclines are initially transported from the cytoplasm to the periplasm by TetA, from where subsequently, RND-type efflux pumps (e.g., AdeABC, AdeFGH, and AdeIJK) remove the antibiotics from the periplasm across the outer membrane (Foong et al., 2020). The expression of *tetA* is tightly regulated by TetR, a member of TetR-family transcriptional regulators (TFR) and *tetA* expression is induced by sub-inhibitory tetracycline concentrations (Takahashi et al., 1986). TFRs harbor a highly variable C-terminal sensory ligand-binding domain (LBD) and a conserved N-terminal DNA-binding domain (DBD) (Ramos et al., 2005; Cuthbertson and Nodwell, 2013). The DBD is composed of three α-helices forming a helix-turn-helix (HTH) motif, and interacts with the DNA major groove (Hinrichs et al., 1994; Orth et al., 2000). The LBD is responsible for ligand binding and oligomerization (Hinrichs et al., 1994; Kisker et al., 1995). In the absence of the ligand, the dimeric TFR repressor binds to a specific operator sequence, preventing the transcription of its target genes. Upon ligand binding, conformational changes of the TFR repressor trigger a pendulum movement of the DBD, thereby leading to the release of repressor from the operator DNA. The dissociation of the TFR repressor from the operator DNA subsequently activates the expression of TFR target genes (Kisker et al., 1995; Orth et al., 2000).

A recent study has indicated that TetA(G) of *A. baumannii* AYE confers resistance to the clinically important tetracycline antibiotics doxycycline and minocycline. Genome sequence analysis of *A. baumannii* AYE revealed the presence of a divergently transcribed TFR gene (ABAYE3639, hereafter referred to as *A. baumannii AbtetR*) located downstream of the *tetA* gene (Fournier et al., 2006). Here, we show that expression of the *A. baumannii tetA(G)* gene in *E. coli* Δ*mdfA*Δ*emrE* confers resistance to various tetracyclines except tigecycline. The *tetR* gene encodes a transcriptional regulator that controls the *tetA(G)* expression. In this study, we found that AbTetR binds to an intercistronic region between *tetA* and *tetA(G)* genes. In addition, thermal shift binding experiments revealed that AbTetR prefers to bind tetracyclines, which carry a O-5H moiety in ring B. In contrast, tetracyclines (e.g., minocycline and tigecycline) with a 7-dimethylamino moiety are less well recognized by AbTetR. Structural analysis of a minocycline bound AbTetR-Gln116Ala variant showed that Arg104 and Arg135, which are embedded at the entrance of the binding pocket, are important for tetracycline recognition and act as a barrier to prevent the release of tetracycline from the AbTetR binding pocket.

MATERIALS AND METHODS

Cloning of *A. baumannii tetA(G)* and *tetR* and Site-Directed Mutagenesis

A. baumannii tetR and *tetA(G)* genes were cloned into pET24a and pTTQ18, respectively (Foong et al., 2020), via the Gibson assembly method (Gibson et al., 2009). Briefly, *tetR* and *tetA(G)* were amplified from chromosomal DNA of *A. baumannii* AYE. Amplified genes and vectors were mixed with the Gibson assembly mixture containing T5 exonuclease (Epicenter), Phusion polymerase (Thermo Fisher Scientific) and Taq DNA ligase (NEB). AbTetR substitution variants were generated by the ExSite protocol (Stratagene) with 5′-phosphorylated primers.

Plasmids were verified by sequencing (Eurofins Scientific). All primers used in this study are listed in **Supplementary Table 1**.

Drug Susceptibility Assay

Drug susceptibility assays were conducted as previously described (Foong et al., 2019). Briefly, overnight cell cultures of *E. coli* BW25113 Δ*emrE*Δ*mdfA* harboring empty vector (pTTQ18) or pTTQ18abtetG were adjusted to an OD_{600} of 10^0–10^{-5} and 4 μl of the diluted cultures were spotted on a LB agar plate supplemented with 100 μg ml^{-1} ampicillin, 0.2 mM isopropyl-β-D-1-thiogalactopyranoside (IPTG) and a variety of tetracycline antibiotics (**Supplementary Figure 1**) at the indicated concentrations (**Figure 1**). Plates were incubated at 37°C overnight.

Overproduction and Purification of AbTetR

E. coli C43 (DE3) Δ*acrAB* harboring pET24abtetR_{His} was grown overnight in LB liquid medium supplemented with 50 μg ml^{-1} kanamycin (LB_{Kan}). Two ml of overnight culture was inoculated into fresh LB_{Kan} liquid medium (1 l in a 5 l baffled Erlenmeyer flask), grown at 37°C at 100 rpm until OD_{600} of 0.6–0.7 before induction with 0.3 mM IPTG (final concentration). Subsequently, the culture was incubated at 20°C for 16 h, at 100 rpm. All protein purification steps were conducted at 4°C. Cells were harvested by centrifugation and suspended in ice-cold Buffer A (50 mM Tris, pH8.0, 500 mM NaCl, 20 mM Imidazole, 10% Glycerol) before passage through the chamber of a Pressure Cell Homogeniser (Stansted, United Kingdom) at 15,000 psi. Insoluble debris was removed by centrifugation at 120,000 × *g* for 45 min. The supernatant was loaded onto a HisTrap HP Ni^{2+} affinity column (GE Healthcare) pre-equilibrated with Buffer A. After two wash steps with 50 column volumes of the same buffer supplemented with 30 and 50 mM imidazole, respectively, bound proteins were eluted in the same buffer supplemented with 230 mM imidazole. The eluted proteins were concentrated to 1–2 ml with Amicon Ultra-15 Centrifugal Filter unit (30 kDa MWCO) (Merck). Subsequently, concentrated proteins were subjected to size-exclusion chromatography (Superdex 75 HiLoad 16/60 column, coupled to an Äkta Prime system, GE Healthcare) using Buffer B (20 mM HEPES, pH8.0, 195 mM NaCl, 5 mM KCl, 5 mM DTT, 5% Glycerol) as running buffer at 0.4 ml min^{-1}.

Thermal Shift Assay

Thermo stability of AbTetR was determined using a Rotor Gene-Q cycler (Qiagen, Hilden, Germany) with Sypro Orange dye as an unfolding reporter (Niesen et al., 2007). Briefly, 2 μl of AbTetR (20 μM) was mixed with 22 μl Buffer B. For ligand-induced melting temperature shifts, chlortetracycline, demeclocycline, doxycycline, meclocycline, methacycline, minocycline, oxytetracycline, tetracycline, or tigecycline was added (300 μM final concentration) to the protein solution and incubated at room temperature for 10 min. Samples were subjected to centrifugation at 13,000 × *g* for 5 min at room temperature, to remove any traces of precipitate. Subsequently, samples were mixed with 1.1 μl of 250× Sypro

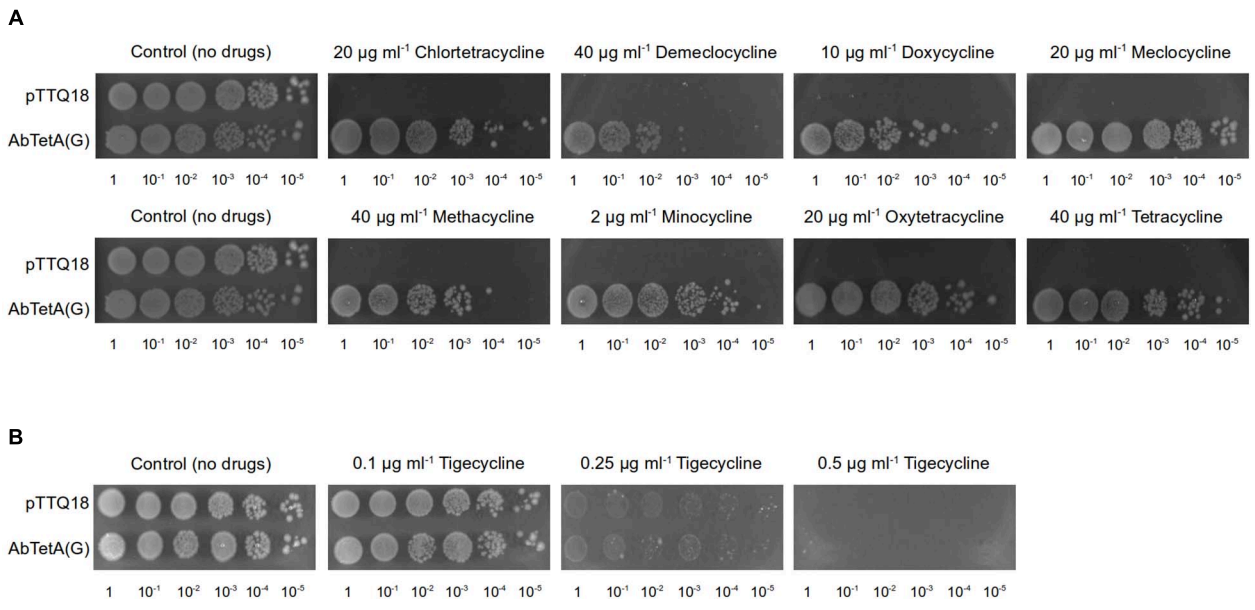

FIGURE 1 | TetA(G) from *A. baumannii* confers resistance to *E. coli* BW25113 Δ*emrE*Δ*mdfA* toward diverse tetracyclines. Drug susceptibility assays were conducted by spotting diluted cell cultures (OD_{600} = 10^0–10^{-5}, as indicated below the respective images) on LB agar plate supplemented with 0.2 mM IPTG and 100 μg ml^{-1} ampicillin containing **(A)** tetracyclines (20 μg ml^{-1} chlortetracycline, 40 μg ml^{-1} demeclocycline, 10 μg ml^{-1} doxycycline, 20 μg ml^{-1} meclocycline, 40 μg ml^{-1} methacycline, 2 μg ml^{-1} minocycline, 20 μg ml^{-1} oxytetracycline, or 40 μg ml^{-1} tetracycline). Both of the control plates are identical and both represent the same biological repeat in the same experiment (a representative). **(B)** tigecycline (0.1–0.5 μg ml^{-1}). As a negative control, cells harboring pTTQ18 (empty vector) were spotted on the same agar plate. Experiments were conducted three times (biological repeats) and the results shown are representative.

Orange (Invitrogen). Thermal denaturation was induced by increasing the temperature from 25 to 75°C at a rate of 1°C min^{-1}. The fluorescence of the dye was monitored (excitation and emission wavelength of 470 and 555 nm, respectively) during the heating process. The unfolding temperature (T_m) was determined by fitting the fluorescence curve to a Boltzmann sigmoid function (GraphPad Prism). The melting curves are shown in **Supplementary Figure 2**.

Electrophoretic Mobility Shift Assay

Electrophoretic mobility shift assay (EMSA) was performed with SYBR Green as a DNA binding probe. Primers used for amplification of the intercistronic region with different DNA sequence length used in the EMSA are listed in **Supplementary Table 1**. Approximately 100 ng of amplified DNA fragments were incubated with 5 μM AbTetR in binding buffer containing 10 mM Tris, pH7.5, 1 mM EDTA, 100 mM KCl, 5 mM dithiothreitol, 5% glycerol, 0.01 mg ml^{-1} BSA, and 70 ng poly [d(I-C)] as a non-specific competitor. The samples were incubated at 25°C for 30 min and subjected to electrophoresis on a 10% non-denaturing polyacrylamide gel in 1× TBE buffer in an ice-bath at 120 V for 2 h. Subsequently, the gel was stained with 1× SYBR Green in 1× TBE buffer at room temperature for 1 h before de-staining with water. The protein-DNA complexes and free DNAs were detected on an ImageQuant LAS 4000 [Excitation with Epi-RGB (Cy2) and emission filter of Y515Di (Cy2)] (GE Healthcare BioSciences AB, Uppsala, Sweden).

Crystallization of AbTetR

Crystals of AbTetR were obtained by sitting drop vapor diffusion within 1 week by incubation of equal volumes of protein solution (15 mg ml^{-1}) and precipitant solution containing 0.1 M Tris, pH8.5, 0.2 M magnesium chloride hexahydrate, 0.2 M sodium sulfate, and 25% PEG2000 MME. Crystals were cryo-protected by soaking in mother liquor supplemented with increasing PEG2000 MME concentration to 35% before flash-cooling in liquid nitrogen. Crystals of minocycline bound AbTetR-Gln116A were obtained by co-crystallization. Briefly, 8 mg ml^{-1} of AbTetR-Gln116Ala (Gln116Ala) variant was incubated with 1 mM minocycline, dissolved in Buffer B (20 mM HEPES, pH8.0, 195 mM NaCl, 5 mM KCl, 5 mM DTT, 5% Glycerol) at room temperature for 10 min. Subsequently, sample was centrifuged at 13,000 × *g* for 5 min at room temperature to remove any precipitates. Crystals of minocycline-Gln116Ala binary complex were obtained by sitting drop vapor diffusion within 3 days by incubation of equal volumes of the minocycline-Gln116Ala complex solution and precipitant solution containing 0.1M sodium cacodylate, pH5.5, 11% PEG Smear Broad (Molecular Dimension), 3% Tacsimate, pH7.0 (Hampton Research), and 10% ethylene glycol. Crystals were flash-cooled in liquid nitrogen directly from the drop without any cryo-protectant.

X-Ray Diffraction Data Collection, Processing, and Refinement

Datasets were collected on beam line Proxima 2A at the Soleil Synchrotron, Saint-Aubin, France using a Eiger detector (Dectris), and subsequently indexed and integrated with XDS (Kabsch, 2010). A molecular replacement solution for wildtype AbTetR was obtained using MrBUMP (Keegan and Winn, 2008) using a modified structure by Sculptor (Bunkóczi and Read, 2011) of TetR(D) variant (1A6I) (Orth et al., 1998) as a search model. Structural models were built in COOT (Emsley et al., 2010), refined with REFMAC5 (Murshudov et al., 2011) and validated with MolProbity (Chen et al., 2010). 100% of the residues are in favored regions of the Ramachandran plot for both structures reported in this manuscript. Polder electron density maps were calculated using phenix.polder (Liebschner et al., 2017).

Tetracycline Bound AbTetR Models

The electron density of minocycline in the Gln116Ala structure was used as a template for ligand (chlortetracycline, demeclocycline, doxycycline, meclocycline, methacycline, oxytetracycline, tetracycline, and tigecycline) fitting with Coot (Emsley et al., 2010). Structural models were refined with REFMAC5 (Murshudov et al., 2011). These structural models were used to interpret the thermal shift binding experiments as shown in **Figure 7**.

RESULTS

The *A. baumannii tetR* gene is part of a divergently transcribed regulon, comprises the putative tetracycline transporter gene *tetA(G)*, and the putative transcriptional regulator *tetR* (*abtetR*). AbTetR is presumably involved in the regulation of *tetA(G)* expression. To identify all possible ligands of AbTetR, we first analyzed the substrate transport profile of *A. baumannii* TetA(G) in *Escherichia coli*, followed by subsequent biophysical characterization of AbTetR binding to the identified ligands and operator DNA.

TetA(G) From *A. baumannii* AYE Confers Resistance to Various Tetracyclines

A previous study reported that *E. coli* expressing *A. baumannii tetA(G)* confers resistance to tetracycline, minocycline, and doxycycline (Foong et al., 2020). In addition to the aforementioned tetracyclines, overexpression of *tetA(G)* in *E. coli* exerted a protective effect against the bacteriostatic effect of other tetracyclines such as chlortetracycline, demeclocycline, meclocycline, methacycline, and oxytetracycline (**Figure 1A** and **Supplementary Figure 1**). Consistent with previous result (Foong et al., 2020), cells expressing *A. baumannii tetA(G)* were susceptible to tigecycline (**Figure 1B** and **Supplementary Figure 1**), indicating tigecycline is not recognized by the AbTetA(G) efflux pump.

Mapping of the DNA Binding Site of AbTetR

TFRs bind mostly to palindromic inverted repeat (IR) sequences at the promoter region to modulate the expression of their target genes (Orth et al., 1998; Rodikova et al., 2007). In the

genome of *A. baumannii* AYE, *tetA(G)* and *tetR* genes are arranged in a divergently orientated direction, and the 103-bp intercistronic sequence between *tetA(G)* and *tetR* contains two IR sequences of 13-bp (designated as IR1) and 14-bp (designated as IR2) in length (**Figure 2A**). IR1 is located 21-bp upstream of the *tetR* gene and IR2 is located 15-bp upstream of the *tetA(G)* gene (**Figure 2A**). To determine whether AbTetR binds to this intercistronic sequence, DNA fragments of different lengths containing IR1 and/or IR2 were amplified and these DNA fragments were subjected to EMSA in the presence of purified AbTetR (**Figure 2B**). All amplified DNA sequences containing the intercistronic region showed an electrophoretic mobility shift of the DNA fragment in the presence of AbTetR, implying that AbTetR binds to the amplified DNA fragments (**Figure 2C**). In constrast, a lack of AbTetR binding to DNA was observed when AbTetR was incubated with an amplified 96-bp non-binding DNA sequence between the downstream genes ABAYE3642 and ABAYE3644 (**Figure 2C**). These results indicated that AbTetR binds to the intercistronic region between *tetA* and *tetR* of *A. baumannii* AYE.

AbTetR Shows Low Affinity Binding for Minocycline and Tigecycline, but High Affinity for Meclocycline

Since AbTetR binds to the intercistronic sequence between *tetA(G)* and *tetR* and potentially modulates the expression of *tetA(G)* (**Figure 2C**), we tentatively assumed that the substrates of the TetA(G) efflux pump are also substrates of AbTetR. To test this notion, AbTetR was purified and subjected to thermal shift assay (TSA) in the absence or presence of tetracyclines. The T_m value of the wildtype AbTetR is 45.6°C (**Table 1**), indicating that AbTetR is less stable in solution compared to TetR(D) (T_m = 51.8°C) and other globular proteins (Vedadi et al., 2006; Palm et al., 2020). Interestingly, the T_m value of AbTetR increased to 63.0°C in the presence of tetracycline, with a ΔT_m [ΔT_m = T_m(liganded) – T_m(unliganded)] of 17.4°C (**Table 1**),

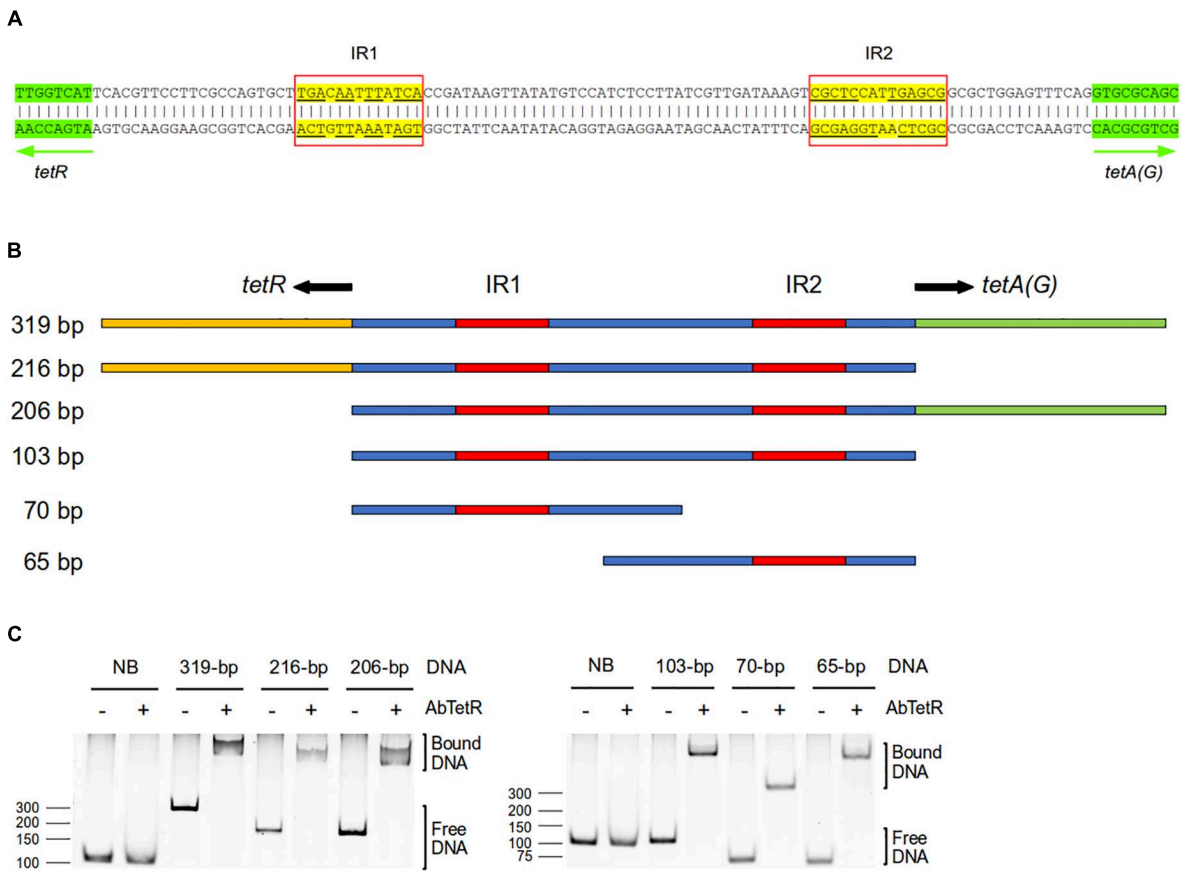

FIGURE 2 | Intercistronic region of *tetR* and *tetA(G)*. **(A)** The *A. baumannii* AYE intercistronic region of *tetR-tetA(G)* was analyzed for operator sequences using the EMBOSS palindromes prediction tool (Rice et al., 2000). The intergenic sequence located between *tetR* and *tetA(G)* genes contains two inverted repeat (IR) sequences, IR1 and IR2, highlighted in yellow. The divergently orientated genes *tetR* and *tetA(G)* are indicated by arrows and highlighted in green. **(B)** Schematic representation of the amplified dsDNA of the intercistronic region between *tetR* and *tetA(G)* genes of *A. baumannii* AYE. PCR products of different length consisting IR1 and/or IR2 (319–65 bp) were amplified from genomic DNA of *A. baumannii* AYE. The starts of the open reading frames of the *tetR* and *tetA(G)* genes are indicated in yellow and green, respectively. The intergenic region is indicated in blue and the IRs are highlighted in red. **(C)** Binding of dsDNA containing IR1 and/or IR2 to TetR in the electrophoretic mobility shift assay.

TABLE 1 | Melting temperatures of AbTetR variants in the absence or presence of various tetracycline antibiotics.

Mutant	Apo	Chl	ΔT_m	$\Delta\Delta T_m$	Dem	ΔT_m	$\Delta\Delta T_m$	Dox	ΔT_m	$\Delta\Delta T_m$	Mec	ΔT_m	$\Delta\Delta T_m$	Met	ΔT_m	$\Delta\Delta T_m$	Min	ΔT_m	$\Delta\Delta T_m$	Oxy	ΔT_m	$\Delta\Delta T_m$	Tet	ΔT_m	$\Delta\Delta T_m$	Tig*	ΔT_m	$\Delta\Delta T_m$
Wildtype	45.6 ± 0.2	62.3± 0.3	16.7	–	62.6 ± 0.1	17.0	–	66.4± 0.2	20.8	–	67.7± 0.3	22.1	–	66.0± 0.3	20.4	–	57.1± 0.3	11.5	–	65.5± 0.3	19.9	–	63.0± 0.3	17.4	–	56.6± 0.3	11.0	–
H64A	n.d.	45.5± 0.4	n.d.	n.d.	46.4± 0.3	n.d.	n.d.	47.7± 0.2	n.d.	n.d.	51.1± 0.5	n.d.	n.d.	47.4± 0.2	n.d.	n.d.	n.d.	n.d.	n.d.	45.6± 0.2	n.d.	n.d.	44.8 ± 0.5	n.d.	n.d.	39.7± 0.9	n.d.	n.d.
N82A	41.5± 0.3	43.5± 0.3	2.0	−14.7	45.7± 0.3	4.2	−12.8	42.8± 0.2	1.3	−19.5	47.1± 0.2	5.6	−16.5	44.1± 0.2	2.6	−17.8	42.4± 0.2	0.9	−10.6	42.4± 0.2	0.9	−19.0	42.3± 0.2	0.8	−16.6	n.d.	n.d.	n.d.
F86A	n.d.	45.1± 0.3	n.d.	n.d.	45.9± 0.1	n.d.	n.d.	49.1± 0.3	n.d.	n.d.	54.2± 0.1	n.d.	n.d.	48.3± 0.2	n.d.	n.d.	n.d.	n.d.	n.d.	46.6± 0.1	n.d.	n.d.	45.6± 0.4	n.d.	n.d.	36.9± 0.7	n.d.	n.d.
H100A	45.9± 0.2	57.3± 0.2	11.4	−5.3	58.7± 0.1	12.8	−4.2	60.9± 0.2	15.0	−5.8	64.8± 0.1	18.9	−3.2	60.8± 0.1	14.9	−5.5	49.1± 0.5	3.2	−8.3	57.0± 0.1	11.1	−8.8	55.4± 0.3	9.5	−7.9	47.7± 0.2	1.8	−9.2
T103A	46.8± 0.1	57.8± 0.2	11.0	−5.7	60.6± 0.3	13.8	−3.2	62.9± 0.2	16.1	−4.7	64.9± 0.2	18.1	−4.0	62.6± 0.3	15.8	−4.6	53.3± 0.2	6.5	−5.0	61.1± 0.3	14.3	−5.6	59.7± 0.3	12.9	−4.5	53.0± 0.2	6.2	−4.8
R104A	40.9± 0.2	**60.6± 0.4**	**19.7**	**3.0**	**60.1± 0.5**	**19.2**	**2.2**	60.9± 0.3	20.0	−0.8	63.1± 0.3	22.2	0.1	61.2± 0.3	20.3	−0.1	52.0± 0.7	11.1	−0.4	**63.4± 0.3**	**22.5**	**2.6**	**60.4± 0.3**	**19.5**	**2.1**	**53.2± 0.4**	**12.3**	**1.3**
Q116A	n.d.	54.4± 0.2	n.d.	n.d.	54.9± 0.1	n.d.	n.d.	59.4± 0.2	n.d.	n.d.	60.2± 0.1	n.d.	n.d.	59.0± 0.1	n.d.	n.d.	49.8± 0.4	n.d.	n.d.	57.1± 0.2	n.d.	n.d.	54.9± 0.3	n.d.	n.d.	44.1± 0.3	n.d.	n.d.
R135A	41.7± 0.2	62.2± 0.2	20.5	3.8	62.7± 0.1	21.0	4.0	**70.1± 0.2**	**28.4**	**7.6**	68.8± 0.1	27.1	5.0	**70.0± 0.2**	**28.3**	**7.9**	57.2± 0.1	15.5	4.0	**67.9± 0.2**	**26.2**	**6.3**	**65.8± 0.2**	**24.1**	**6.7**	56.9± 0.1	15.2	4.2
S138A	42.9± 0.1	59.7± 0.3	16.8	0.1	60.8± 0.1	17.9	0.9	63.4± 0.3	20.5	−0.3	65.7± 0.2	22.8	0.7	62.9± 0.2	20.0	−0.4	53.2± 0.1	10.3	−1.2	62.3± 0.3	19.4	−0.5	60.1± 0.3	17.2	−0.2	53.5± 0.4	10.6	−0.4
E147A	44.8 ± 0.1	56.6 ± 0.2	11.8	−4.9	58.3± 0.1	13.5	−3.5	59.2± 0.1	14.4	−6.4	64.4± 0.1	19.6	−2.5	59.5± 0.1	14.7	−5.7	48.3± 0.2	3.5	−8.0	55.9± 0.2	11.1	−8.8	53.7± 0.2	8.9	−8.5	49.0± 0.4	4.2	−6.8
R104A_ R135A*	n.d.	56.1± 0.2	n.d.	n.d.	54.4± 0.2	n.d.	n.d.	55.5± 0.2	n.d.	n.d.	57.7± 0.4	n.d.	n.d.	57.0± 0.2	n.d.	n.d.	n.d.	n.d.	n.d.	55.5± 0.2	n.d.	n.d.	54.1± 0.1	n.d.	n.d.	53.9± 0.2	n.d.	n.d.

*The indicated melting temperature (Tm) were derived using thermal shift assays. Apo, Unliganded; Chl, chlortetracycline; Dem, demeclocycline; Dox, doxycycline; Mec, meclocycline; Met, methacycline; Min, minocycline; Oxy, oxytetracycline; Tet, tetracycline; Tig, tigecycline. Experiments were repeated five times (technical repeats) except for * = three technical repeats. Mean Tm values and standard errors are shown. n.d. = not detected. ΔTm = Tm(liganded) – Tm(unliganded). $\Delta\Delta Tm = \Delta Tm(Variant) - \Delta Tm(Wildtype)$. The numbers represent in °C as unit. Values in boldface represent T_m values of the substrate preferences of the respective AbTetR variants.*

indicating that tetracycline binds to AbTetR, thereby stabilizing the protein. The pronounced thermostabilization of tetracycline-AbTetR complex is comparable to the ΔT_m of tetracycline bound TetR(D), with a ΔT_m of 19.4°C (Palm et al., 2020). In addition to tetracycline, several other tetracyclines stabilized the wildtype AbTetR as well, and caused an apparent increase in T_m (**Table 1**). As expected, we observed a significant increase in T_m of AbTetR in the presence of tigecycline, even though it is not a TetA(G) substrate (**Table 1** and **Figure 1B**). The increase in T_m of liganded proteins can be correlated to the binding affinity of the ligand (Brandts and Lin, 1990; Matulis et al., 2005). We standardly used tetracycline concentrations of 300 μM in the TSA experiments and therefore, concluded that minocycline and tigecycline are the weakest binders with a ΔT_m of only 11.5 and 11.0°C, respectively (**Table 1**). In contrast, the largest increase in ΔT_m of the liganded AbTetR was obtained in the presence of meclocycline, with an increase of 22.1°C, indicating that meclocycline is the tightest binder. The remaining tetracyclines (chlortetracycline, demeclocycline, doxycycline, methacycline, and oxytetracycline) shifted the ΔT_m of the liganded AbTetR in the range of 16.7–20.8°C (**Table 1** and **Supplementary Figure 1**). The relative binding affinity of these tetracyclines to AbTetR is minocycline = tigecycline < chlortetracycline = demeclocycline = tetracycline < doxycycline = methacycline = oxytetracycline < meclocycline.

Structure of the Unliganded AbTetR and the Minocycline Bound AbTetR-Gln116Ala

The unliganded AbTetR fused to a C-terminal hexahistidine-tag was crystallized in space group $P2_1$ with two molecules per asymmetric unit, arranging in a twofold rotational symmetry, suggesting a dimer in nature (**Figure 3A** and **Supplementary Table 2**). As expected, each of the unliganded AbTetR protomers (Monomer A: AbTetR-A and Monomer B: AbTetR-B) exhibits a typical TFR topology, containing 10 α-helices (Cuthbertson and Nodwell, 2013; **Figure 3A**), which is well superimposed with other homologous TetR repressors (r.m.s.d. of C_α = 1.6–2.4 Å) (**Supplementary Figure 3**). Both AbTetR protomers are structurally invariant (1.1 Å r.m.s.d. of C_α over 176 residues) except for helices α1-α4 and α9, as a result of the involvement of helices α1-4 in crystal packing, whereas helix α9 is highly mobile (**Figure 3B**). The AbTetR protomer is organized in two core domains, with one core domain being a LDB and the second one being a DBD (**Figure 3A**). The DBD is composed of helices α1-α3 that form the HTH motif whereas helix α4 connects the DBD and LBD. In contrast, helices α4-α8 form the LBD, whereas helices α8/α8' and α10/α10' of the AbTetR-A and AbTetR-B protomers are involved in the formation of a four-helix bundle, thereby contributing to the stabilization of AbTetR dimer.

Extensive crystallization experiments to obtain the crystal structure of the wildtype AbTetR in complex with tetracycline antibiotics were unsuccessful. To obtain AbTetR in complex with tetracyclines, a less active AbTetR variant was used for co-crystallization experiments. Interestingly, the AbTetR-Gln116Ala (Gln116Ala) variant fused to a C-terminal hexahistidine-tag was crystallized in space group $P2_12_12_1$ with four molecules per asymmetric unit (**Figure 3C** and **Supplementary Table 2**). All the Gln116Ala protomers are invariant (0.45–0.56 Å r.m.s.d. of C_α over 168 residues) except for helices α7 and α9, indicating a marginal difference in the asymmetric protomers of the Gln116Ala-AB and Gln116A-CD dimers (discussed later). Similar to the wildtype AbTetR structure, helix α9 of the Gln116Ala variant is likely to be highly mobile even upon minocycline binding, except for the Gln116Ala-B protomer due to the crystal packing (**Figure 3D**). Minocycline was assigned to the non-proteinaceous electron density in each of the four monomers, and its presence was confirmed by polder electron density map analysis (Liebschner et al., 2017; **Figure 3C** and **Supplementary Figure 4**).

Residues (His64, Asn82, Phe86, His100, Thr103, Arg104, Gln116, and Glu147) involved in the tetracycline binding are highly conserved among TetR regulators (Hinrichs et al., 1994; Orth et al., 1998; **Figures 4**, **5** and **Supplementary Figure 5**). Similar to the liganded TetR(D) (Hinrichs et al., 1994), the minocycline binding site of AbTetR is defined by helices α4-α6 and α8 (**Figure 3C**). The entrance of the AbTetR binding pocket consists of helices α7 and α8 from one protomer, and helix α9' and loop α8'/α9' from the other protomer (its symmetry-related protomer). Ring A of minocycline engages in hydrogen bond (H-bond) interactions with His64 and Asn82 (**Figure 4** and **Supplementary Figure 5**). Additionally, the O-12aH moiety of minocycline interacts with the phenyl side chain of Phe86 via OH···π interaction. In contrast, Leu134 contributes to the van der Waals interaction with the 4-dimethylamino moiety of ring A. A common feature of TetR members is the coordination of the tetracycline-Mg^{2+} complex in the binding pocket via a H-bond network (Takahashi et al., 1986; Hinrichs et al., 1994). In the minocycline bound Gln116Ala structure, Mg^{2+} is coordinated in an octahedral fashion by the keto-enolate group O-11/O-12 of minocycline, His100, and three water molecules (**Figure 4**). These water molecules form a H-bond network with Thr103, Ser138, and Glu147' (residue from the symmetry-related protomer). Of note, the involvement of Ser138 in this H-bond network is novel in the minocycline-bound AbTetR structure and this interaction is absent in other TetR regulators (Hinrichs et al., 1994; Kisker et al., 1995; **Figures 4**, **5** and **Supplementary Figure 5**). Ring D of minocycline is surrounded by hydrophobic residues (Pro105, Phe110, Ala113, Val131, Ile134, Val163', and Phe176'), where it is sandwiched between Pro105 and Arg135 by hydrophobic and cation-π stacking interactions, respectively (**Figure 4**). Notably, Arg135 is not conserved among the TetR-type repressors and this residue is replaced by either serine or methionine in the other TetR repressors (**Figure 5** and **Supplementary Figure 5**). Interestingly, the cation-π stacking interaction between Arg135 and ring D of the tetracycline antibiotics is substituted by a hydrophobic interaction in TetR(B) (Phe177') and TetR(D) (Met177') structures (Hinrichs et al., 1994; **Supplementary Figure 5**). Additionally, the O-10H moiety of minocycline forms a H-bond with Nε of Arg104 in the Gln116Ala structure, but notably this interaction is absent in the

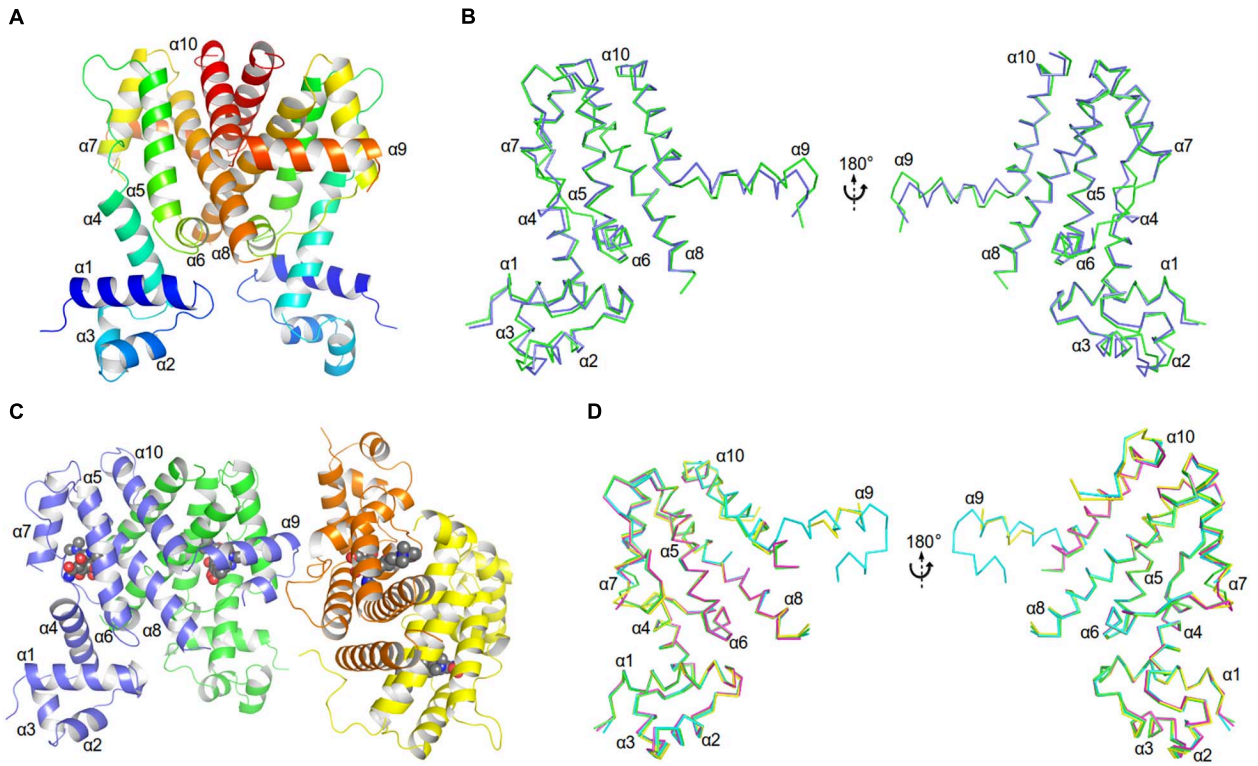

FIGURE 3 | Crystal structures of AbTetR and the minocycline bound AbTetR-Gln116Ala variant. **(A)** Crystal structure of TetR of *A. baumannii* AYE (rainbow color, N terminus: blue, C terminus: red). **(B)** Superimposition of AbTetR-A (green) and AbTetR-B (blue). **(C)** Binary structure of two dimeric Gln116Ala variants in complex with minocycline. Minocycline molecules are depicted as spheres (carbon: black; oxygen: red; nitrogen: blue). **(D)** Superimposition of the four monomers of minocycline-bound Gln116Ala (Gln116Ala-A: green, Gln116Ala-B: cyan, Gln116Ala-C: magenta, Gln116Ala-D: yellow).

other TetR repressors in complex with minocycline (**Figure 4** and **Supplementary Figure 5**).

Conformational Changes of AbTetR and the Minocycline Bound State

As discussed above, both protomers of the unliganded AbTetR are virtually indistinguishable except for helices α1-4 and α9 (**Figure 3B**). Helix α4 of the AbTetR-A protomer is elongated by one helical turn (residues 61–65) in comparison to helix α4 of the AbTetR-B protomer (**Figure 3B**). Surprisingly, helix α4 of the AbTetR-B protomer adopts a similar conformation akin to the helix α4 of the minocycline bound Gln116Ala structure (**Figure 6A**). Due to one additional helical turn in helix α4 of the AbTetR-A protomer, Arg63 on helix α4 flips 180° from the solvent exposed position to occupy the position where His64 is located in the liganded state or in the unliganded AbTetR-B protomer, thereby forming H-bonds with Asn82 and Ser138 (**Supplementary Figure 6**). In addition to the aforementioned H-bond network, Arg63 also engages in a cation-π stacking interaction with Phe86 (**Supplementary Figure 6**). These unique features enable His64 to adopt a more solvent exposed conformation compared to His64 in the minocycline-bound state. However, we cannot rule out the possibility that this conformation is an artifact due to the interaction between AbTetR-A protomer and its neighboring symmetry protomer.

Binding of minocycline to AbTetR appears to induce subtle conformational changes in helix α6, which is comprised of the conserved residues His100–Thr103, forming a type II β-turn (**Figure 6A**). Notably, the type II β-turn is a typical feature of the induced state in the liganded TetR regulators (Hinrichs et al., 1994; Kisker et al., 1995; Werten et al., 2014). The formation of the β-turn in TetR(D) is mainly attributed to the H-bond network between the Thr103 side chain, the CO moiety of His100, and the tetracycline/Mg^{2+} complex (Orth et al., 1998; Werten et al., 2016). Of note, it has been reported that Thr103 is the key residue in the TetR induction event (Scholz et al., 2000; Werten et al., 2016). Additionally, the β-turn formation in TetR(D) is further stabilized by the salt bridge interaction between Arg104 and Asp178' (Glu180' in AbTetR) and the H-bond interaction between Gly102 (conserved in AbTetR) and His151' (Ser151' in AbTetR) (Orth et al., 1998). Surprisingly, the β-turn of the minocycline bound Gln116Ala structure is stabilized by a complex H-bond network comprised of Arg49, Asp53, Arg98, Ile99, Ala101, Thr103, Arg104, Asp154', the minocycline/Mg^{2+} complex and water molecules (**Figure 6B**). A closer inspection of the AbTetR binding pocket indicated that the β-turn induces a rotation of helix α7 by ∼7.1–8.2°, which is associated with a rotation of helix α4 by 9.9–11.4°, thereby facilitating a pendulum

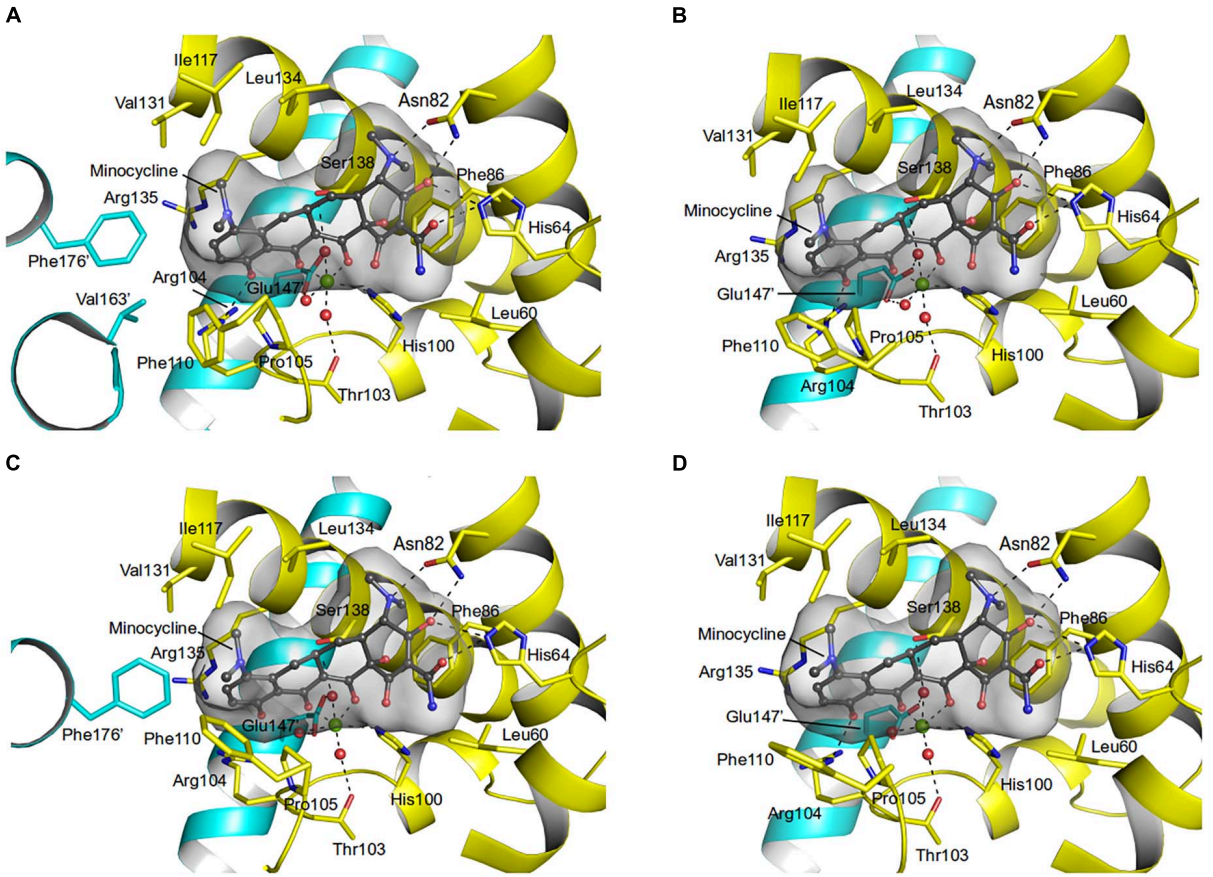

FIGURE 4 | Minocycline binding sites of the AbTetR-Gln116Ala variant. Minocycline bound to **(A)** Monomer A; **(B)** Monomer B; **(C)** Monomer C; and **(D)** Monomer D. Residues from the symmetry-related protomer are colored in cyan. Water molecules and the Mg^{2+} are depicted as red and green spheres, respectively.

movement of the DBD (**Figure 6A**). Interestingly, the β-turn formation in the liganded Gln116Ala structure also induces a conformational change of loop α6/α7, which is highly mobile in the unliganded state. Conformational changes of loop α6/α7 include, (i) the formation of one additional helical turn in helix α7 of the Gln116Ala-A protomer; (ii) a poorly defined loop in Gln116Ala-B protomer; and (iii) the formation of a 3_{10} helix in Gln116Ala-C protomer. Rigid body superimposition of the unliganded AbTetR dimer and the minocycline bound Gln116Ala dimer (Gln116Ala-AB, Gln116Ala-CD, and vice versa) revealed a more compact protein folding in the liganded state (**Supplementary Figure 7**). Binding of minocycline to one liganded protomer, such as the Gln116Ala-A protomer of the Gln116Ala-AB dimer or vice versa (similar to the Gln116Ala-CD dimer or vice versa), leads to a rotation of helices α7'/α8' in the Gln116Ala-B protomer, resulting in the movement of these helices toward the binding pocket of the Gln116Ala-B protomer (**Supplementary Figure 7**). The aforementioned motion is followed by a rotation of helices α9'10' in the Gln116Ala-B protomer toward the binding pocket of the Gln116Ala-A protomer. Taken together, the unique motions of helices α7–α10 in the Gln116Ala-A and Gln116Ala-B protomers trigger a rotation of helices α5/α5' in the Gln116Ala-AB dimer, inducing pendulum-like movements of helices α4/α4' and the DBDs in the AbTetR dimer, thereby displacing the AbTetR regulator from the operator DNA (**Figure 6A** and **Supplementary Figure 7**).

Molecular Determinants for Tetracyclines Binding to AbTetR

To elucidate the role of residues embedded in the minocycline binding site, we characterized single alanine AbTetR substitution variants by TSA analysis in the presence of tetracycline antibiotics (**Table 1**). The unliganded Arg104Ala and Arg135Ala variants exhibited a slightly lower thermal stability than the wildtype AbTetR (T_m of Arg104Ala = 40.9°C; T_m of Arg135Ala = 41.7°C) (**Table 1**). Interestingly, TSA experiments clearly indicated that the $\Delta\Delta T_m$ [$\Delta\Delta T_m = \Delta T_m$(variant) – ΔT_m(wildtype)] of the Arg104Ala variant under the treatment of chlortetracycline, demeclocycline, oxytetracycline, tetracycline, and tigecycline (between +2.1 and +3.0°C) was higher than the same protein under the treatment of doxycycline, meclocycline, methacycline, and minocycline (between −0.8 and +0.1°C) (**Table 1**). These results indicate that the Arg104Ala variant exhibits a preference for tetracyclines with a 6-OH substituent except for tigecycline (**Table 1** and **Supplementary Figure 1**). To our surprise, the

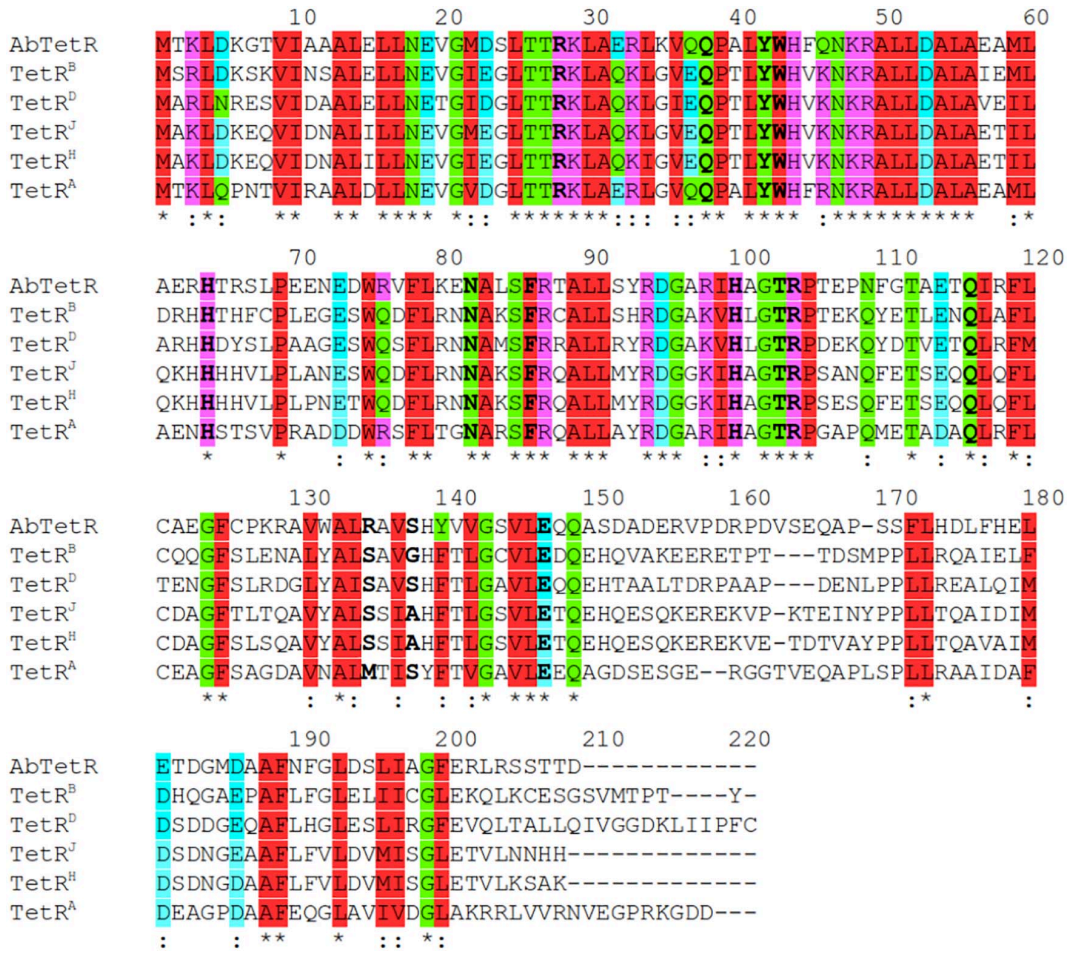

FIGURE 5 | Protein sequence alignment of TetR members. AbTetR: TetR class G of *A. baumannii* AYE (Genbank accession number: CAM88408); TetR^{B}: TetR class B of transposon Tn*10* (Genbank accession number: ELD20529); TetR^{D}: TetR class D of *Escherichia coli* (Genbank accession number: P0ACT4); TetR^{J}: TetR class J from *Proteus mirabilis* (Genbank accession number: AAD12754); TetR^{H}: TetR class H from *Pasteurella multocida* (Genbank accession number: CAA75662); TetR^{A}: TetR class A from *Pseudomonas* sp. (PDB: 5MRU). Substituted residues are indicated in bold.

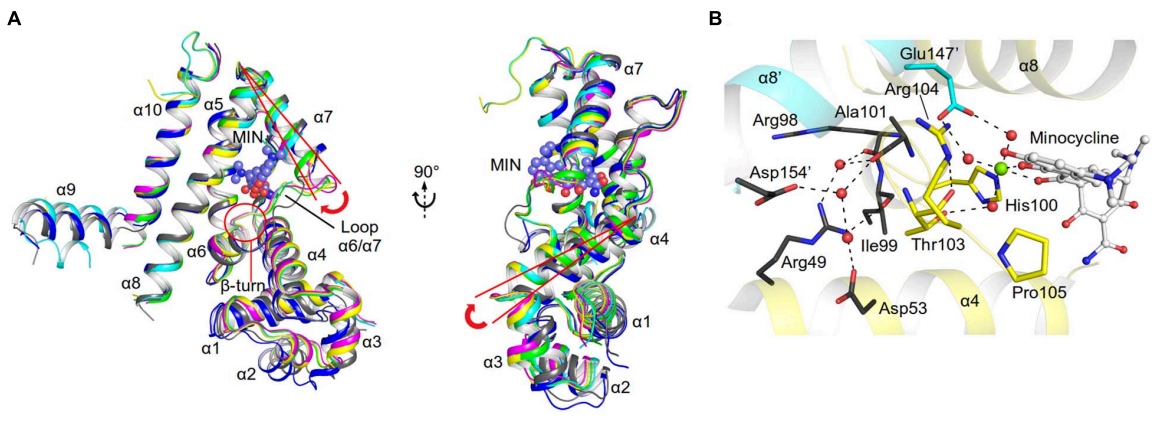

FIGURE 6 | Minocycline (MIN) binding induced conformational changes of AbTetR. **(A)** Conformational changes of the DNA binding domain of the unliganded AbTetR and the liganded Gln116Ala structures. Structural superimposition was performed based on the main chain atoms of helices α8 and α10 (Yu et al., 2010). (AbTetR-A: black, AbTetR-B: blue, Gln116Ala-A: green, Gln116Ala-B: cyan, Gln116Ala-C: magenta, Gln116Ala-D: yellow). **(B)** Water-mediated stabilization of the β-turn upon minocycline binding. Water molecules and the Mg^{2+} are depicted as red and green spheres, respectively.

thermal stability of the Arg135Ala variant increased by 2.4–4.0°C in the presence of doxycycline, methacycline, oxytetracycline, and tetracycline compared to the wildtype AbTetR incubated with the same tetracyclines (**Table 1**). The thermal stability of the liganded form of the Arg104Ala_Arg135Ala variant was reduced by 2.7–10.9°C in comparison to the wildtype AbTetR upon treatment with tetracyclines, in all cases except for minocycline (**Table 1**). These results indicate that all tetracyclines bind to the Arg104Ala_Arg135Ala variant except for minocycline. In contrast, the single arginine substitution variants were able to bind minocycline (**Table 1**).

It has been reported that the TetR(D) substitution variants (His100Ala, Thr103Ala, and Glu147Ala) are more stable than the wildtype protein and binding of tetracycline to these variants increases the thermostability of these proteins by 3.0–8.2°C (Palm et al., 2020). However, the binding affinity of these TetR(D) substitution variants for tetracycline is lower than the binding affinity of the wildtype protein (Palm et al., 2020). Surprisingly, the unliganded AbTetR His100Ala, Thr103Ala, and Glu147Ala variants exhibited comparable T_m values to the unliganded wildtype AbTetR. As expected, our binding data suggest a slight decrease in the binding affinities of His100Ala, Thr103Ala, and Glu147Ala variants for all tetracyclines except for meclocycline (**Table 1**). These data are in line with previous reports that His100, Thr103, and Glu147 play a role in tetracycline binding (Palm et al., 2020). Interestingly, the thermostability of the unliganded Ser138Ala variant (T_m of 42.9°C) was slightly lower compared to the unliganded wildtype AbTetR (T_m of 45.6°C) (**Table 1**). However, addition of tetracyclines to the Ser138Ala variant further stabilized this variant, leading to T_m values similar to the liganded wildtype AbTetR. These results indicate that Ser138 is not important for the coordination of the tetracycline-Mg^{2+} complex. In the minocycline bound Gln116Ala structure, Asn82 is involved in extensive H-bonding with the 4-dimethylamino and 3-enolate moieties of minocycline (**Figure 4** and **Supplementary Figures 1**, **5**). Surprisingly, the unliganded Asn82Ala variant exhibited a lower T_m value (41.5°C) compared to the wildtype AbTetR (**Table 1**). Previous study indicated that tetracycline binding thermostabilizes the TetR(D)-Asn82Ala variant, leading to a marginal increase in T_m value (ΔT_m = 2.2°C) (Palm et al., 2020). As expected, tetracyclines except for demeclocycline, and meclocycline, did not show a pronounced stabilization effect for the AbTetR-Asn82Ala variant, with T_m values of 42.3–44.1°C (**Table 1**). Interestingly, incubation of Asn82Ala variant with demeclocycline and meclocycline increased the ΔT_m value by 4.2 and 5.6°C, respectively. His64Ala, Phe86Ala, and Gln116Ala variants were unstable in solution at temperature $\geq$ 25°C when compared to other AbTetR variants (**Table 1**), but addition of tetracyclines stabilized these variants to a certain extent. Interestingly, no clear protein unfolding event was observed for the His64Ala and Phe86Ala variants when these variants were incubated with minocycline. These results indicate that minocycline is not able to bind to the His64Ala and Phe86Ala variants. Moreover, tetracyclines stabilized the Phe86Ala variant less well compared to all the other liganded AbTetR variants (T_m = 36.9–54.2°C), except for the Asn82Ala variant. Taken together, these results indicate that His64, Asn82, and Phe86 are the most important residues for tetracycline binding. In contrast, Arg104 and Arg135 play a role in tetracycline selectivity.

DISCUSSION

The binding affinity of tetracyclines to AbTetR is mainly determined by the chemical properties of the tetracycline antibiotics (**Table 1**, **Figure 7**, and **Supplementary Figure 1**). The 7-dimethylamino moiety in ring D is only present in the weakest binders (minocycline and tigecycline) (**Table 1** and **Supplementary Figure 1**). In addition, both minocycline and tigecycline do not have a functional group at position 6 in ring C, whereas the other tetracyclines carry either a methyl, methylene or hydroxyl moiety at this position (**Figure 7** and **Supplementary Figure 1**). Interestingly, addition of the bulky 9-*tert*-butyl-glycylamido moiety in ring D of tigecycline does not affect its binding affinity for AbTetR, as shown by similar T_m values of the minocycline and tigecycline bound AbTetR complexes (**Table 1** and **Supplementary Figure 1**). Binding of tigecycline to TetR is not unprecedented. In fact, it has been shown experimentally that *tetB* expression is induced by the binding of tigecycline to TetR in *E. coli* (Hirata et al., 2004).

It has been shown that Arg104 plays an important role in the binding of tetracyclines to TetR (Müller et al., 1995). However, our data suggest that Arg104 plays an important role in tetracycline selectivity (**Table 1**). Interestingly, the Arg104Ala variant exhibits a clear preference for tigecycline and tetracycline antibiotics containing a O-6H moiety in ring C (**Table 1** and **Supplementary Figure 1**). We speculate that substitution of Arg104 to alanine might augment the size of the AbTetR binding pocket associated with alleviating the steric hindrance between the 9-*tert*-butyl-glycylamido moiety of tigecycline and the guanidinium moiety of Arg104, thereby increasing the binding affinity for tigecycline (**Figure 7C** and **Supplementary Figure 1**). In contrast, the binding affinity for tigecycline is not affected by the substitution of Arg135 to alanine (**Table 1**). Our results show that the non-conserved Arg135 is involved in the cation-π stacking interaction with the ring D of minocycline (**Figures 4**, **5** and **Supplementary Figure 5**). To our surprise, the Arg135Ala variant shows an increased binding affinity for tetracyclines devoid of a functional moiety at position 7 (**Table 1** and **Supplementary Figure 1**). We therefore speculate that the removal of the Arg135 guanidinium group might create a different local environment in the binding pocket associated with the alteration of binding geometry for tetracyclines compared to the wildtype AbTetR.

One common feature of the tight binding of tetracyclines (doxycycline, oxytetracycline, methacycline, and meclocycline) to AbTetR is the presence of the O-5H moiety in ring B. Indeed, Gln116 putatively interacts with O-5H by H-bonding, as shown by our docking model, thereby increasing the stability of the protein-ligand complexes (**Figures 7A,B**). The major difference between meclocycline and the other tight binders is the 7-chloro moiety (**Supplementary Figure 1**). However, the 7-chloro moiety alone cannot be ascribed to an increase in

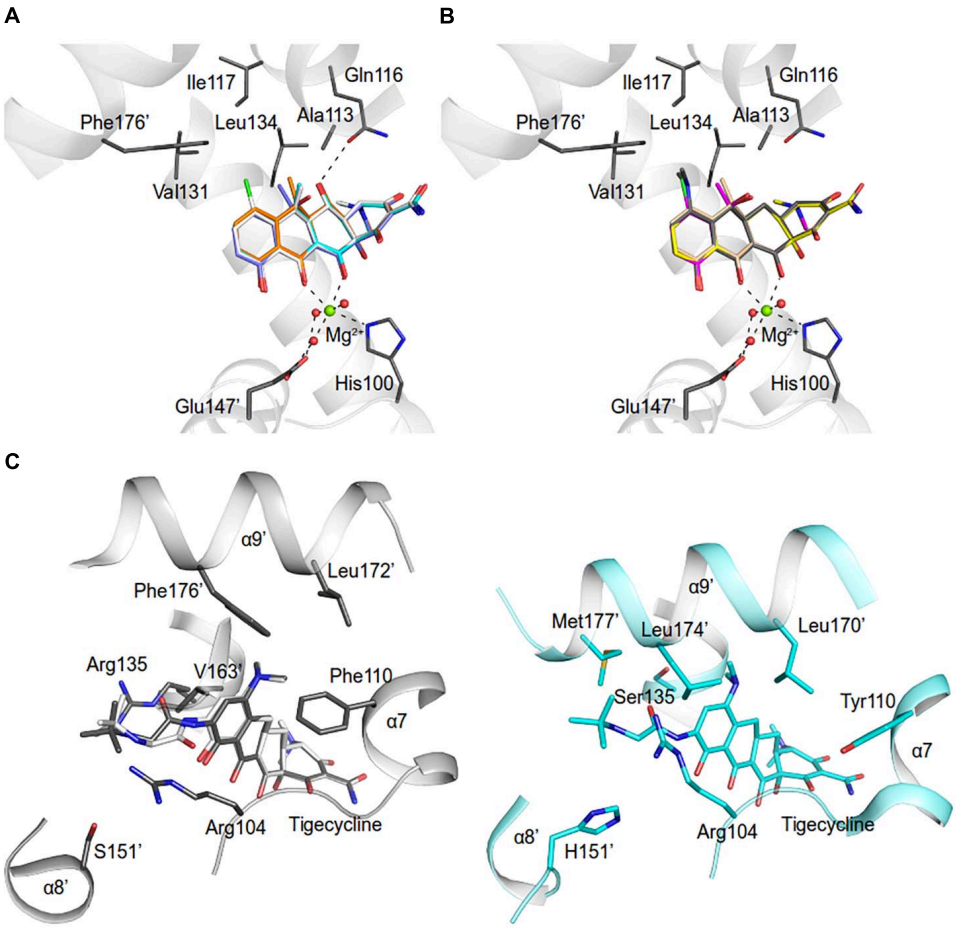

FIGURE 7 | Model of tetracycline antibiotics in the AbTetR binding pocket. Tetracycline antibiotics and Q116 were modeled to the AbTetR structure. Only residues (except for H100 and E147') that are involved in the interaction with C5, C6, and C7 of tetracyclines are shown as black sticks. Water molecules are depicted as red spheres. Tetracyclines are shown as sticks **(A)** Carbon colored as orange: doxycycline; white: meclocycline; cyan: methacycline; slate: oxytetracycline. **(B)** Carbon colored as magenta: chlortetracycline; yellow: demeclocycline; gray: minocycline; and wheat: tetracycline. **(C)** Tigecycline binding site of TetR(D) (PDB: 4ABZ) (right) and AbTetR (left). Two tigecycline binding modes were modeled to the AbTetR structure. For clarity, only residues that are involved in the interaction with ring D of tigecycline are depicted.

binding affinity for meclocycline, since both chlortetracycline and demeclocycline only show a moderate increase in T_m (**Table 1** and **Supplementary Figure 1**). Therefore, the O-5H moiety in ring B of meclocycline and doxycycline (absent in chlortetracycline and demeclocycline) plays a crucial role in the binding of these tetracyclines to AbTetR (**Supplementary Figure 1**). We speculate that the H-bond interaction between the O-5H moiety and Gln116 might further improve the positioning of the meclocycline 7-chloro moiety in the hydrophobic environment, which is comprised of Phe110, Ala113, Ile117, Val131, and Phe176', thereby contributing to the overall stability of meclocycline in the AbTetR binding pocket (**Figures 7A,B**).

His64, Asn82 and Phe86 of AbTetR are key residues in the binding of tetracycline antibiotics (**Table 1**), which corroborates the data from binding studies of TetR(D) (Müller et al., 1995; Scholz et al., 2000; Palm et al., 2020). According to previous studies (Werten et al., 2016; Palm et al., 2020), Asn82 is the most important residue for tetracycline binding that contributes most of the binding energy for the formation of the tetracycline-Mg^{2+} complex in TetR(D) (Palm et al., 2020). Confoundingly, only one tetracycline molecule is identified to bind to one of the two binding pockets in the dimeric TetR(D)-Asn82Ala structure, while the other binding pocket is occupied by an irrelevant molecule (Werten et al., 2016). In contrast, our data suggest that four different tetracyclines (chlortetracycline, methacycline, demeclocycline, and meclocycline) are able to bind to the Asn82Ala variant, as indicated by a slight increase in ΔT_m value of the protein-ligand complexes (**Table 1**). Finally, the decrease in thermal stability of the liganded Gln116Ala variant is most likely attributed to the lack of H-bonding between Gln116 and ring A of tetracyclines (Hinrichs et al., 1994; **Figures 7A,B** and **Supplementary Figures 1**, **5**).

In the unliganded state, loop α6/7, loop α8/9 and helix α9 of AbTetR are highly mobile in order to facilitate the binding of minocycline. As expected, binding of the minocycline-Mg^{2+} complex to AbTetR facilitates the formation of a type II β-turn

associated with a rotation of helix α7 toward the minocycline binding pocket, thereby inducing a rigid body motion of helices α8-α10 from its symmetry-related protomer (**Supplementary Figure 7**). Conformational changes of helices α8 and α8' in the AbTetR dimer lead to the coordination of Mg^{2+} by Glu147' in a water-mediated manner, resulting in a rigid body movement of helices α9-α10, α8'/α9', and loops α8/α9, thereby closing the binding pocket as well as preventing the release of minocycline (**Supplementary Figure 7**). Surprisingly, binding of minocycline to the Gln116Ala-B and Gln116Ala-D protomers does not induce a complete closure of the binding pocket by helix α9' from their respective symmetry-related protomer (**Figures 4B,D**). The partial closure of the binding pocket by helix α9' is unusual as helix α9' of the TetR(D) is required to prevent the release of tetracycline from its binding pocket upon TetR(D) induction (Orth et al., 1998). A closer inspection of the AbTetR binding pocket indicated that a complete closure of helices α9/α9' is not necessary in the AbTetR dimer when minocycline is bound. We speculate that Arg104 and Arg135 embedded at the entrance of AbTetR binding pocket might play an important role as a barrier, together with Pro105, Phe110, and Val131, forming hydrophobic and cation-π traps to prevent the release of minocycline from its binding pocket (**Figures 4B,D** and **Supplementary Figure 5**). Additionally, we also speculate that helix α9 plays a role in the retention of minocycline in the binding pocket. Taken together, we propose that the release of AbTetR from its cognate DNA is attributed to cooperativity between two protomers in the AbTetR dimer upon AbTetR induction by tetracycline/Mg^{2+} binding. This cooperativity is mediated by a conformational change of the LDB (helices α7-α10 and α7'-α10') associated with a pendulum-like motion of helices α4/α4' and both DBDs, resulting in the release of AbTetR from its cognate DNA (**Figure 6A** and **Supplementary Figure 7**).

Tetracyclines are not commonly prescribed to treat the infections caused by *A. baumannii*, however, doxycycline and minocycline have been recently administered in combination with other antibiotics to improve clinical effectiveness in eradicating *A. baumannii* infections (Falagas et al., 2015). It has recently been shown that AbTetA(G) confers resistance to clinically important doxycycline and minocycline (Foong et al., 2020). In fact, our results show that AbTetA(G) exhibits resistance to almost all of the tetracycline antibiotics except for tigecycline (**Figure 1**). AbTetR, a transcriptional regulator involved in *tetA(G)* expression, can bind various types of tetracycline antibiotics with different binding affinities (**Table 1**). Interestingly, we show that tigecycline can bind to AbTetR, even though TetA(G) is not able to recognize and transport tigecycline. This result is in line with previous data that *tetB* expression is induced by tigecycline through tigecycline binding to TetR (Hirata et al., 2004). Therefore, we speculate that tigecycline binds to AbTetR, which would render the release of DNA from the repressors, inducing the expression of *tetA(G)*.

The *tetR* and *tetA(G)* genes are embedded within the Tn*7*-like AbaR1 resistance island (Fournier et al., 2006; Rose, 2010). Interestingly, the Tn*7*-like AbaR1 resistance island shows a high similarity to the mobilizable *Salmonella* genomic island 1 of *Proteus mirabilis*, which harbors an antibiotic resistance gene cluster (Siebor and Neuwirth, 2013). It was recently shown that the genomic island 1 is acquired from *Salmonella* spp. (Boyd et al., 2001; Siebor and Neuwirth, 2013), indicating that *A. baumannii* might have acquired the Tn*7*-like AbaR1 resistance island from these species. Alarmingly, it has been demonstrated that the TetA efflux pump confers resistance against tigecycline in *A. baumannii* (Foong et al., 2020). A potential event of horizontal gene transfer between tetracycline susceptible strains and resistant strains, together with a natural selection of tetracycline efflux pumps on tigecycline and an unbridled expression of these genes might pose a serious threat in hospitals. Therefore, the administration of tetracyclines in hospitals has to be carried out with high precaution.

DATA AVAILABILITY STATEMENT

Atomic coordinates and structure factors for the reported crystal structures have been deposited with the Protein Data Bank under accession number 6RX9 (unliganded AbTetR) and 6RXB (AbTetR-Gln116Ala in complex with minocycline).

AUTHOR CONTRIBUTIONS

H-KT conceptualized the work and performed structural analysis. MS, SH, WF, and H-KT conducted all experiments with assistance from AH. H-KT, WF, and KP wrote the manuscript. All authors contributed to the article and approved the submitted version.

FUNDING

This work was supported by a grant from the Deutsche Forschungsgemeinschaft through DFG Research Unit FOR 2251 "Adaptation and persistence of the emerging pathogen *Acinetobacter baumannii* subproject 06" to KP.

ACKNOWLEDGMENTS

We acknowledge the SOLEIL Synchrotron in Saint Aubin, France, for provision of synchrotron radiation facilities. We would like to thank Gavin Fox and William Shepard for assistance in using beamline Proxima 2A (Proposal Numbers: 20160833 and 20170761). We are grateful to Hartmut Michel (Max-Planck Institute of Biophysics, Frankfurt am Main, Germany) for the use of the X-ray diffractometer at INSTRUCT Core Centre G.

SUPPLEMENTARY MATERIAL

The Supplementary Material for this article can be found online at: https://www.frontiersin.org/articles/10.3389/fmicb.2021.711158/full#supplementary-material

REFERENCES

Boyd, D. A., Peters, G. A., Cloeckaert, A., Boumedine, K. S., Chaslus-Dancla, E., Imberechts, H., et al. (2001). Complete nucleotide sequence of a 43-kilobase genomic island associated with the multidrug resistance region of *Salmonella enterica* serovar Typhimurium DT104 and its identification in phage type DT120 and serovar Agona. *J. Bacteriol.* 183, 5725–5732. doi: 10.1128/JB.183.19.5725-5732.2001

Brandts, J. F., and Lin, L. N. (1990). Study of strong to ultratight protein interactions using differential scanning calorimetry. *Biochemistry* 29, 6927–6940. doi: 10.1021/bi00481a024

Bunkóczi, G., and Read, R. J. (2011). Improvement of molecular-replacement models with *Sculptor*. *Acta Crystallogr. D Biol. Crystallogr.* 67, 303–312. doi: 10.1107/S0907444910051218

Chattopadhyay, M. K. (2014). Use of antibiotics as feed additives: a burning question. *Front. Microbiol.* 5:334. doi: 10.3389/fmicb.2014.00334

Chen, V. B., Arendall, W. B. III, Headd, J. J., Keedy, D. A., Immormino, R. M., Kapral, G. J., et al. (2010). MolProbity: all-atom structure validation for macromolecular crystallography. *Acta Crystallogr. D Biol. Crystallogr.* 66, 12–21. doi: 10.1107/S0907444909042073

Chopra, I., and Roberts, M. (2001). Tetracycline antibiotics: mode of action, applications, molecular biology, and epidemiology of bacterial resistance. *Microbiol. Mol. Biol. Rev.* 65, 232–260. doi: 10.1128/MMBR.65.2.232-260.2001

Coyne, S., Rosenfeld, N., Lambert, T., Courvalin, P., and Périchon, B. (2010). Overexpression of resistance-nodulation-cell division pump AdeFGH confers multidrug resistance in *Acinetobacter baumannii*. *Antimicrob. Agents Chemother.* 54, 4389–4393. doi: 10.1128/AAC.00155-10

Cuthbertson, L., and Nodwell, J. R. (2013). The TetR family of regulators. *Microbiol. Mol. Biol. Rev.* 77, 440–475. doi: 10.1128/MMBR.00018-13

Emsley, P., Lohkamp, B., Scott, W. G., and Cowtan, K. (2010). Features and development of Coot. *Acta Crystallogr. D Biol. Crystallogr.* 66, 486–501. doi: 10.1107/S0907444910007493

Falagas, M. E., Vardakas, K. Z., Kapaskelis, A., Triarides, N. A., and Roussos, N. S. (2015). Tetracyclines for multidrug-resistant *Acinetobacter baumannii* infections. *Int. J. Antimicrob. Agents* 45, 455–460. doi: 10.1016/j.ijantimicag.2014.12.031

Foong, W. E., Tam, H. K., Crames, J. J., Averhoff, B., and Pos, K. M. (2019). The chloramphenicol/H^+ antiporter CraA of *Acinetobacter baumannii* AYE reveals a broad substrate specificity. *J. Antimicrob. Chemother.* 74, 1192–1201. doi: 10.1093/jac/dkz024

Foong, W. E., Wilhelm, J., Tam, H. K., and Pos, K. M. (2020). Tigecycline efflux in *Acinetobacter baumannii* is mediated by TetA in synergy with RND-type efflux transporters. *J. Antimicrob. Chemother.* 75, 1135–1139. doi: 10.1093/jac/dkaa015

Fournier, P. E., Vallenet, D., Barbe, V., Audic, S., Ogata, H., Poirel, L., et al. (2006). Comparative genomics of multidrug resistance in *Acinetobacter baumannii*. *PLoS Genet.* 2:e7. doi: 10.1371/journal.pgen.0020007

Gibson, D. G., Young, L., Chuang, R. Y., Venter, J. C., Hutchison, C. A. III, and Smith, H. O. (2009). Enzymatic assembly of DNA molecules up to several hundred kilobases. *Nat. Methods* 6, 343–345. doi: 10.1038/nmeth.1318

Granados-Chinchilla, F., and Rodríguez, C. (2017). Tetracyclines in food and feeding stuffs: from regulation to analytical methods, bacterial resistance, and environmental and health implications. *J. Anal. Methods Chem.* 2017:1315497. doi: 10.1155/2017/1315497

Hinrichs, W., Kisker, C., Duvel, M., Müller, A., Tovar, K., Hillen, W., et al. (1994). Structure of the Tet repressor–tetracycline complex and regulation of antibiotic resistance. *Science* 264, 418–420. doi: 10.1126/science.8153629

Hirata, T., Saito, A., Nishino, K., Tamura, N., and Yamaguchi, A. (2004). Effects of efflux transporter genes on susceptibility of *Escherichia coli* to tigecycline (GAR-936). *Antimicrob. Agents Chemother.* 48, 2179–2184. doi: 10.1128/AAC.48.6.2179-2184.2004

Kabsch, W. (2010). XDS. *Acta Crystallogr. D Biol. Crystallogr.* 66, 125–132. doi: 10.1107/S0907444909047337

Keegan, R. M., and Winn, M. D. (2008). MrBUMP: an automated pipeline for molecular replacement. *Acta Crystallogr. D Biol. Crystallogr.* 64, 119–124. doi: 10.1107/S0907444907037195

Kisker, C., Hinrichs, W., Tovar, K., Hillen, W., and Saenger, W. (1995). The complex formed between Tet repressor and tetracycline-Mg^{2+} reveals mechanism of antibiotic resistance. *J. Mol. Biol.* 247, 260–280. doi: 10.1006/jmbi.1994.0138

Liebschner, D., Afonine, P. V., Moriarty, N. W., Poon, B. K., Sobolev, O. V., Terwilliger, T. C., et al. (2017). Polder maps: Improving OMIT maps by excluding bulk-solvent. *Acta Crystallogr. D Biol. Crystallogr.* 73, 148–157. doi: 10.1107/S2059798316018210

Liu, Q., Hassan, K. A., Ashwood, H. E., Gamage, H. K. A. H., Li, L., Mabbutt, B. C., et al. (2018). Regulation of the aceI multidrug efflux pump gene in *Acinetobacter baumannii*. *J. Antimicrob. Chemother.* 73, 1492–1500. doi: 10.1093/jac/dky034

Marchand, I., Damier-Piolle, L., Courvalin, P., and Lambert, T. (2004). Expression of the RND-type efflux pump AdeABC in *Acinetobacter baumannii* is regulated by the AdeRS two-component system. *Antimicrob. Agents Chemother* 48, 3298–3304. doi: 10.1128/AAC.48.9.3298-3304.2004

Matulis, D., Kranz, J. K., Salemme, F. R., and Todd, M. J. (2005). Thermodynamic stability of carbonic anhydrase: measurements of binding affinity and stoichiometry using ThermoFluor. *Biochemistry* 44, 5258–5266. doi: 10.1021/bi048135v

McMurry, L., Petrucci, R. E., and Levy, S. B. (1980). Active efflux of tetracycline encoded by four genetically different tetracycline resistance determinants in *Escherichia coli*. *Proc. Natl. Acad. Sci. U.S.A.* 77, 3974–3977. doi: 10.1073/pnas.77.7.3974

Morris, F. C., Dexter, C., Kostoulias, X., Uddin, M. I., and Peleg, A. Y. (2019). The mechanisms of disease caused by *Acinetobacter baumannii*. *Front. Microbiol.* 10:1601. doi: 10.3389/fmicb.2019.01601

Müller, G., Hecht, B., Helbl, V., Hinrichs, W., Saenger, W., and Hillen, W. (1995). Characterization of non-inducible Tet repressor mutants suggests conformational changes necessary for induction. *Nat. Struct. Biol.* 2, 693–703. doi: 10.1038/nsb0895-693

Murshudov, G. N., Skubák, P., Lebedev, A. A., Pannu, N. S., Steiner, R. A., Nicholls, R. A., et al. (2011). REFMAC5 for the refinement of macromolecular crystal structures. *Acta Crystallogr. D Biol. Crystallogr.* 67, 355–367. doi: 10.1107/S0907444911001314

Nguyen, F., Starosta, A. L., Arenz, S., Sohmen, D., Dönhöfer, A., and Wilson, D. N. (2014). Tetracycline antibiotics and resistance mechanism. *Biol. Chem.* 395, 559–575. doi: 10.1515/hsz-2013-0292

Niesen, F. H., Berglund, H., and Vedadi, M. (2007). The use of differential scanning fluorimetry to detect ligand interactions that promotes protein stability. *Nat. Protoc.* 2, 2212–2221. doi: 10.1038/nprot.2007.321

Olson, M. W., Ruzin, A., Feyfant, E., Rush, T. S., O'Connell, J., and Bradford, P. A. (2006). Functional, biophysical,and structural bases for antibacterial activity of tigecycline. *Antimicrob. Agents Chemother.* 50, 2156–2166. doi: 10.1128/AAC.01499-05

Orth, P., Cordes, F., Schnappinger, D., Hillen, W., Saenger, W., and Hinrichs, W. (1998). Conformational changes of the Tet repressor induced by tetracycline trapping. *J. Mol. Biol.* 279, 439–447. doi: 10.1006/jmbi.1998.1775

Orth, P., Schnappinger, D., Hillen, W., Saenger, W., and Hinrichs, W. (2000). Structural basis of gene regulation by the tetracycline inducible Tet repressor-operator system. *Nat. Struct. Biol.* 7, 215–219. doi: 10.1038/73324

Palm, G. J., Buchholz, I., Werten, S., Girbardt, B., Berndt, L., Delcea, M., et al. (2020). Thermodynamics, cooperativity and stability of the tetracycline repressor (TetR) upon tetracycline binding. *Biochim. Biophys. Acta Proteins Proteom* 1868:140404. doi: 10.1016/j.bbapap.2020.140404

Petersen, P. J., Jacobus, N. V., Weiss, W. J., Sum, P. E., and Testa, R. T. (1999). In vitro and in vivo antibacterial activities of a novel glycylcycline, the 9-t-butylglycylamido derivative of minocycline (GAR-396). *Antimicrob. Agents Chemother.* 43, 738–744. doi: 10.1128/AAC.43.4.738

Ramos, J. L., Martínez-Bueno, M., Molina-Henares, A. J., Terán, W., Watanabe, K., Zhang, Z., et al. (2005). The TetR family of transcriptional repressors. *Microbiol. Mol. Biol. Rev.* 69, 326–356. doi: 10.1128/MMBR.69.2.326-356.2005

Rice, P., Longden, I., and Bleasby, A. (2000). EMBOSS: the European molecular biology open Software Suite. *Trends Genet.* 16, 276–277. doi: 10.1016/s0168-9525(00)02024-2

Rodikova, E. A., Kovalevskiy, O. V., Mayorov, S. G., Budarina, Z. I., Marchenkov, V. V., Melnik, B. S., et al. (2007). Two HlyIIR dimers bind to a long perfect inverted repeat in the operator of the hemolysin II gene from *Bacillus cereus*. *FEBS Lett.* 581, 1190–1196. doi: 10.1016/j.febslet.2007.02.035

Rose, A. (2010). TnAbaR1: a novel Tn7-related transposon in *Acinetobacter baumannii* that contributes to the accumulation and dissemination of large

repertoires of resistance genes. *Biosci. Horizons* 3, 40–48. doi: 10.1093/biohorizons/hzq006

Rosenfeld, N., Bouchier, C., Courvalin, P., and Périchon, B. (2012). Expression of the resistance-nodulation-cell division pump AdeIJK in *Acinetobacter baumannii* is regulated by AdeN, a TetR-type regulator. *Antimicrob. Agents Chemother.* 56, 2504–2510. doi: 10.1128/AAC.06422-11

Rumbo, C., Gato, E., López, M., Ruiz de Alegría, C., Fernández-Cuenca, F., Martínez-Martínez, L., et al. (2013). Contribution of efflux pumps, porins, and β-lactamases to multidrug resistance in clinical isolates of *Acinetobacter baumannii*. *Antimicrob. Agents Chemother.* 57, 5247–5257. doi: 10.1128/AAC.00730-13

Scholz, O., Schubert, P., Kintrup, M., and Hillen, W. (2000). Tet repressor induction without Mg^{2+}. *Biochemistry* 39, 10914–10920. doi: 10.1021/bi001018p

Siebor, E., and Neuwirth, C. (2013). Emergence of *Salmonella* genomic island 1 (SGI1) among *Proteus mirabilis* clinical isolates in Dijon. France. *J. Antimicrob. Chemother.* 68, 1750–1756. doi: 10.1093/jac/dkt100

Takahashi, M., Altschmied, L., and Hillen, W. (1986). Kinetic and equilibrium characterization of the Tet repressor-tetracycline complex by fluorescence measurements: evidence for divalent metal ion requirement and energy transfer. *J. Mol. Biol.* 187, 341–348. doi: 10.1016/0022-2836(86)90437-7

Touchon, M., Cury, J., Yoon, E. J., Krizova, L., Cerqueira, G. C., Murphy, C., et al. (2014). The genomic diversification of the whole *Acinetobacter* genus: origins, mechanisms, and consequences. *Genome Biol. Evol.* 6, 2866–2882. doi: 10.1093/gbe/evu225

Vedadi, M., Niesen, F. H., Allali-Hassani, A., Fedorov, O. Y., Finerty, P. J., Wasney, G. A., et al. (2006). Chemical screening methods to identify ligands that promote protein stability, protein crystallization, and structure determination. *Proc. Natl. Acad. Sci. U.S.A.* 103, 15835–15840. doi: 10.1073/pnas.0605224103

Werten, S., Dalm, D., Palm, G. J., Grimm, C. C., and Hinrichs, W. (2014). Tetracycline repressor allostery does not depend on divalent metal recognition. *Biochemistry* 50, 7990–7998. doi: 10.1021/bi5012805

Werten, S., Schneider, J., Palm, G. J., and Hinrichs, W. (2016). Modular organisation of inducer recognition and allostery in the tetracycline repressor. *FEBS J.* 283, 2102–2114. doi: 10.1111/febs.13723

World Health Organisation (WHO) (2017). *Global Priority List of Antibiotic-Resistant Bacteria to Guide Research, Discovery, and Development of New Antibiotics*. Geneva: WHO, 1–7.

Yoon, E. J., Chabane, Y. N., Goussard, S., Snesrud, E., Courvalin, P., Dé, E., et al. (2015). Contribution of resistance-nodulation-cell division efflux systems to antibiotic resistance and biofilm formation in *Acinetobacter baumannii*. *mBio* 6, e309–e315. doi: 10.1128/mBio.00309-15

Yu, Z., Reichheld, S. E., Savchenko, A., Parkinson, J., and Davidson, A. R. (2010). A comprehensive analysis of structural and sequence conservation in the TetR family transcriptional regulators. *J. Mol. Biol.* 400, 847–864. doi: 10.1016/j.jmb.2010.05.062

Conflict of Interest: The authors declare that the research was conducted in the absence of any commercial or financial relationships that could be construed as a potential conflict of interest.

frontiers in Microbiology

ORIGINAL RESEARCH
published: 04 August 2021
doi: 10.3389/fmicb.2021.723949

The *gigA/gigB* Genes Regulate the Growth, Stress Response, and Virulence of *Acinetobacter baumannii* ATCC 17978 Strain

Hua Zhou[1,2], Michael J. Gebhardt[2†], Daniel M. Czyz[2,3], Yake Yao[1] and Howard A. Shuman[2]*

[1] Department of Respiratory and Critical Care Medicine, The First Affiliated Hospital, Zhejiang University School of Medicine, Hangzhou, China, [2] Department of Microbiology, University of Chicago, Chicago, IL, United States, [3] Department of Microbiology and Cell Science, University of Florida, Gainesville, FL, United States

OPEN ACCESS

Edited by:
Remy A. Bonnin, Université Paris-Saclay, France

Reviewed by:
William T. Doerrler, Louisiana State University, United States
Paul Stokes Hoffman, University of Virginia, United States

***Correspondence:**
Hua Zhou
zhouhua1@zju.edu.cn

†Present address:
Michael J. Gebhardt, Division of Infectious Diseases, Boston Children's Hospital, Harvard Medical School, Boston, MA, United States

Specialty section:
This article was submitted to Antimicrobials, Resistance and Chemotherapy, a section of the journal Frontiers in Microbiology

Received: *11 June 2021*
Accepted: *16 July 2021*
Published: *04 August 2021*

Citation:
Zhou H, Gebhardt MJ, Czyz DM, Yao Y and Shuman HA (2021) The gigA/gigB Genes Regulate the Growth, Stress Response, and Virulence of Acinetobacter baumannii ATCC 17978 Strain. Front. Microbiol. 12:723949. doi: 10.3389/fmicb.2021.723949

Acinetobacter baumannii is an important pathogen of nosocomial infection. Recently, a group of genes, named "*gig*" (for Growth in *Galleria*), have been identified in a contemporary multi-drug resistant clinical isolate of *A. baumannii*—strain AB5075. Among these so-called *gig* genes, *gigA* and *gigB* were found to promote antibiotic resistance, stress survival, and virulence of AB5075 by interacting with the nitrogen phosphotransferase system (PTS^{Ntr}). This study aimed to investigate the roles of *gigA/gigB*, which appear to comprise a stress-signaling pathway (encoding for an atypical two-component system response regulator and a predicted anti-anti-sigma factor, respectively), and the involvement of *ptsP* (encoding the Enzyme I component of the PTS^{Ntr}) in the growth, stress resistance, and virulence of the widely studied *A. baumannii* strain ATCC 17978. Genetic analyses of strains harboring mutations of *gigA* and *gigB* were performed to investigate the roles of these genes in bacterial growth, stress resistance, evading macrophage defense, and killing of *Galleria mellonella* larva. In contrast with findings from strain AB5075 where *gigA* and *gigB* contribute to aminoglycoside resistance, the data presented herein indicate that the loss of *gigA/gigB* does not impact antibiotic resistance of strain ATCC 17978. Interestingly, however, we found that deletion of *gigA/gigB* in the ATCC 17978 background imparts a general growth in laboratory medium and also conferred growth and replication defects within murine macrophages and an inability to kill *G. mellonella* larvae. Importantly, studies as well as the loss of *ptsP* restored the phenotypes of the *gigA/gigB* mutant to that of the wild-type. The data presented herein indicate that in *A. baumannii* ATCC 17978, the *gigA/gigB* genes play a key role in both growth and virulence traits, but are dispensable for other stress-resistance survival phenotypes, including aminoglycoside resistance. Our findings thus highlight several similarities and also important differences between the *gigA/gigB* stress-signaling pathway in two commonly studied isolates of this troublesome pathogen.

Keywords: *Acinetobacter baumannii*, nitrogen phosphotransferase system, *Galleria mellonella*, *gigA*, *gigB*, *ptsP*

INTRODUCTION

Acinetobacter baumannii is a Gram-negative bacterium responsible for approximately 20% of intensive care unit infections worldwide and is the top-ranking pathogen on the World Health Organization's list of priority antibiotic-resistant pathogens (Lee et al., 2017; WHO, 2017; Karalewitz and Miller, 2018). Many circulating *A. baumannii* strains exhibit a multidrug-resistant phenotype due to a combination of intrinsic and acquired traits (Peleg et al., 2012; Gottig et al., 2014). Identification of virulence determinants and understanding of the mechanisms underlying the pathogenesis of *A. baumannii* are important for combating *A. baumannii* infection.

Recently, Gebhardt et al. (2015) have identified a group of genes, named "*gig*" (for Growth in *Galleria*), that are required for growth of the highly virulent and highly antibiotic resistant *A. baumannii* strain AB5075 in *Galleria mellonella* larvae. Among these genes, *gigA* and *gigB* were found to promote antibiotic resistance, stress survival, and virulence of AB5075 by interacting with the nitrogen phosphotransferase system (PTS^{Ntr}) (Gebhardt and Shuman, 2017). *gigA* encodes a protein phosphatase 2C-type phosphatase, and *gigB* encodes a putative anti-anti-sigma factor. GigA was shown to dephosphorylate GigB, which in turn regulates the phosphate level on NPr, a key component of the PTS^{Ntr}. Disruption of the GigA/GigB signaling pathway led to the altered expression of numerous stress response genes. Thus, the intersection of GigA/GigB with the PTS^{Ntr} promotes stress survival (Gebhardt and Shuman, 2017).

The *ptsP* gene encodes the enzyme I component of the PTS^{Ntr}. Mutations in *ptsP* increases tobramycin resistance (Schurek et al., 2008; Scribner et al., 2020; Abisado et al., 2021). In AB5075, deletion of *ptsP* in either a Δ*gigA* or Δ*gigB* background suppresses the *gig* mutant phenotypes to near-wild-type levels, including restoration of aminoglycoside resistance, stress survival, and growth in *Galleria* larvae (Gebhardt and Shuman, 2017). Our previous work has revealed that in *A. baumannii* AB5075 mutants lacking both *gigA* and *gigB* (i.e., a Δ*gigAB* double mutant), only concurrent complementation of both *gigA* and *gigB* can restore kanamycin resistance to wild-type levels, suggesting that *gigA* and *gigB* are inseparable in the pathogenesis of *A. baumannii* (Gebhardt and Shuman, 2017). However, the role played by *ptsP* in the survival and virulence of an *A. baumannii* Δ*gigAB* mutant strain remains unknown.

ATCC 17978 is among the best-studied strains of *A. baumannii* and is an ideal model for genetic manipulation compared with clinical isolates due to its sensitivity to most antibiotics and high genome homology to current *A. baumannii* isolates (Sahl et al., 2011; Jacobs et al., 2014a). In this study, we investigated the roles of *gigA*/*gigB* and the involvement of *ptsP* in the growth, stress response, and virulence of ATCC 17978. Our results may provide new information about the roles of *gigA*/*gigB* and the PTS^{Ntr} system in the pathogenesis of *A. baumannii* infection.

MATERIALS AND METHODS

Bacterial Strains and Culture

A. baumannii ATCC 17978 was purchased from The American Type Culture Collection (Manassas, VA, United States). *Escherichia coli* DH5α was obtained from Invitrogen (Carlsbad, CA, United States). The tetracycline-resistant and sucrose-sensitive plasmid pMJG42, apramycin-resistant pMJG120, and gentamicin-resistant pMJG125 plasmids were kept in our laboratory at the University of Chicago (Chicago, IL, United States). The bacteria were cultured in lysogeny broth (LB) medium at 37°C. When required, the antibiotics added for selection were tetracycline (10 μg/mL), apramycin (50 μg/mL), and gentamicin (10 μ g/mL).

Generation of Gene Deletion and Complementation Plasmids

Gene deletion and complementation plasmids were generated as previously described (Jacobs et al., 2014b; Gebhardt et al., 2015; Gebhardt and Shuman, 2017). Briefly, gene deletions were performed using allelic exchange plasmid pMJG42. The resulting plasmids (pMJG42-Δ*gigAB,* pMJG42-Δ*ptsP*) were transformed into ATCC 17978 via electroporation to obtain ATCC 17978 Δ*gigAB* and ATCC 17978 Δ*ptsP* mutants. After tetracycline selection and sucrose counterselection, the clones were subjected to colony PCR. Gene deletions were confirmed by sequencing. For complementation of the deleted *gigA*/*gigB*, the entire open reading frames of *gigA*/*gigB* were amplified by PCR, cloned into pMJG120 or pMJG125 to obtain pMJG120-*gigAB* or pMJG125-*gigAB*, and transformed into ATCC 17978 Δ*gigAB* via electroporation to obtain ATCC 17978 Δ*gigAB* pMJG120-*gigAB* or ATCC 17978 Δ*gigAB* pMJG125-*gigAB*.

ATCC 17978 Δ*gigAB* was transformed with pMJG42-*gigA*/*gigB* to generate ATCC 17978' with *in situ* complementation of *gigA* and *gigB*. ATCC 17978 Δ*ptsP* was transformed with *pMJG42-gigAB* to generate ATCC 17978 Δ*ptsP*Δ*gigAB*. All bacterial strains, plasmids, and primers in this study were summarized in **Supplementary Tables 1–3**.

Whole-Genome Sequencing

Eight strains of ATCC 17978 Δ*gigAB* were randomly selected from different batches for whole-genome sequencing. Genomic DNA was prepared using the QIAamp DNA Mini Kit (Qiagen, Germany) and then subjected to whole genome sequencing (WGS) using the Illumina Hiseq2500 platform (Illumina, CA, United States) following the 2 × 100 bp protocol. The average sequencing throughput was 1 Gb. Raw fastq reads were trimmed by Trimmomatic for quality control (Bolger et al., 2014) and subsequently mapped against the reference genome of ATCC 17978-mff (Accession No. CP012004) with Bowtie2 (Langmead and Salzberg, 2012). Variant calling was performed using the bcftools call function with the default parameters (Danecek et al., 2021). We had submitted all of these data to NCBI BioProject database under the BioProject ID PRJNA738724.[1]

[1]http://www.ncbi.nlm.nih.gov/bioproject/738724

Calculation of Gene Deletion Efficiency

After antibiotics selection and sucrose counterselection, 24 clones were randomly selected for colony PCR. Gene deletions were confirmed by sequencing. The gene deletion efficiency was calculated as (the number of the clones with successful deletion mutation)/24 × 100% The experiment was repeated three times, and data were expressed as the mean ± standard deviation (SD).

Efficiency of Plating Analysis

Overnight cultures of the indicated strains were back-diluted into fresh LB and grown for 2 h. After outgrowth, aliquots of the cultures were serially diluted. Then, a 10-μL aliquot was spotted onto LB agar plates with or without stressors as follows: HCl (medium adjusted to pH 5.5), $ZnCl_2$ (final concentration = 1.25 mmol/L). Colony forming units (CFU) were counted at 12 h after incubation at 37 or 50°C. Efficiency of plating (EOP) was calculated as (CFU recovered on stress medium)/(CFU recovered on plain medium at 37°C).

Bacterial Growth Curves

ATCC 17978, ATCC 17978 Δ*gigAB*, ATCC 17978 Δ*ptsP*, and ATCC 17978 Δ*ptsP* Δ*gigAB* were cultured in LB medium without antibiotics. ATCC 17978 Δ*gigAB* pMJG120 and ATCC 17978 Δ*gigAB* pMJG120-*gigAB* were cultured in LB medium containing 50 mg/L apramycin. ATCC 17978 Δ*gigAB* pMJG125 and ATCC 17978 Δ*gigAB* pMJG125-*gigAB* was cultured in LB medium containing 10 mg/L gentamicin, in the presence or absence of 1% (w/v) arabinose.

Each strain was grown overnight on the appropriate LB agar plate, and a single colony was picked and expanded in 2 mL LB broth overnight. A 1 μL aliquot was diluted at 1:1,000, and the dilution was added into triplicate wells of a 96-well plate at 200 μL/well. LB medium without bacteria was used as a blank. The OD_{600} was determined every 15 min using a Biotek plate reader (Winooski, VT, United States). Growth curves were generated using GraphPad Prism 5 (San Diego, CA, United States). Each experiment was performed in triplicate and repeated three times. The mean was calculated for each experiment, and data were presented as the mean of three experiments.

Antibiotic Sensitivity Testing

Antibiotic sensitivity testing was performed as previously described (Gebhardt et al., 2015). The antibiotics used in this study are summarized in **Table 1**. Data were expressed as minimum inhibitory concentration (MIC).

Isolation of Mouse Bone Marrow-Derived Macrophages (BMDMs)

Bone marrow-derived macrophages (BMDMs) were obtained from 8 to 12 week old female C57BL/6J (Jackson Laboratories) mice as previously described (Toda et al., 2021). Briefly, bone marrow cells were collected from the femur and tibia of mice and maintained in RPMI 1640 medium (Gibco, Thermo Fisher Scientific, Waltham, MA, United States) supplemented with 10 ng/mL mouse macrophage colony-stimulating factor (mMCSF; Gibco), 10% fetal bovine serum (Gibco), and 1% Pen/Strep (Gibco) at 37°C in a humidified atmosphere of 5% CO_2 for 7 days.

Bacterial Killing Assay

Mouse BMDMs were plated in a 96-well plate at a density of 50,000 cells/well and cultured overnight. Cells were infected with wild-type ATCC 17978, ATCC 17978 Δ*gigAB*, or ATCC 17978 Δ*gigAB* pMJG120-*gigAB* at 5×10^5 CFU/mL. The plate was centrifuged at 2,170 rpm for 30 min at room temperature, followed by incubation at 37°C for 30 min. After replacing the medium with RPMI 1640 containing 100 mg/L gentamicin to kill extracellular bacteria, the infected cells were incubated for an additional 1 h (t = 0 h). Then, the infected cells were cultured in RPMI 1640 supplemented with 25 mg/L gentamicin (wild type and Δ*gigAB* strains) or 1.5 mg/L polymyxin (Δ*gigAB* pMJG120-*gigAB* strain). Cell lysates were collected at 0, 2, and 6 h post infection using phosphate buffered saline (PBS) containing 1% Triton-X100, serially diluted, and plated on LB agar plates. CFU were enumerated after 18 h of growth at 37°C. Each experiment was performed in triplicate and repeated three times. The mean CFU of surviving bacteria was calculated for each experiment, and data were presented as the mean of three experiments.

G. mellonella Killing Assay

Infection of *Galleria mellonella* larvae (Knutson's LiveBait, Brooklyn, MI) was performed as described previously (Jacobs et al., 2014a; Gebhardt and Shuman, 2017). Briefly, the bacteria were grown overnight in an orbital shaker (37°C, 200 rpm), and overnight cultures were resuspended in PBS to a final OD_{600} of 1.0. *G. mellonella* larvae were randomly divided into three groups (n = 10/group). A total of 10 μL cultures (5×10^6 CFU/mL) were inoculated into the last left proleg of each larva. After injection, larvae were incubated at 37°C. The number of dead larvae was recorded hourly. Each experiment was performed in triplicate and repeated three times. The mean larval survival was calculated for each experiment, and data were presented as the mean of three experiments.

Statistical Analysis

Data were expressed as the mean ± SD. Statistical analysis was performed using GraphPad Prism 5. Differences among groups were compared using one-way ANOVA followed by Dunnett's *post-hoc* test. Killing curves were plotted using the Kaplan-Meier method. A P-value of < 0.05 was considered statistically significant.

RESULTS

gigA/gigB Are Important for the Growth but Not Required for the Survival of ATCC 17978

In our preliminary study, we noticed that the *gigA/gigB* deletion efficiency in wild-type 17978 was only 4.2%, suggesting that loss of *gigA/gigB* inhibits the growth of 17978 (**Table 2**). To further explore how the genetic background affects the efficiency

TABLE 1 | Antibiotic susceptibilities of deletion strains (MIC, mg/L).

	ATCC 17978	ATCC 17978Δ *ptsP*	ATCC 17978Δ *ptsP*Δ *gigAB*	ATCC 17978 Δ *gigAB*
Ampicillin	>128	128	>128	>128
Apramycin	8	4	4	2
Chloramphenicol	64	64	32	32
Gentamicin	0.5	0.5	0.5	< 0.25
Hygromycin	128	128	128	128
Kanamycin	2	2	1	1
Streptomycin	16	16	16	16
Tetracycline	0.5	1	0.5	0.5
Polymyxin B	0.5	1	0.5	0.5

MIC, minimum inhibitory concentration.

of *gigA/gigB* deletion, we assessed Δ*gigAB* mutation efficiency in various 17978 genetic backgrounds. All gene deletions and complementation were confirmed by sequencing. The results of these analyses are shown in **Table 2**, and indicate that strains harboring either a *ptsP* deletion or *in trans*-complementation of *gigA/gigB* greatly increased the frequency of isolating the *gigA/gigB* double deletion mutation, suggesting that *ptsP* deletion and *gigA/gigB* complementation can compensate for the apparent growth defect caused by loss of *gigA/gigB*.

In the arabinose-inducible pMJG125 vector-based complementation of *gigA/gigB* background, we observed that the Δ*gigAB* colonies were smaller than wild-type colonies in the absence of arabinose; this phenotype was eliminated by the supplementation with 1% arabinose (**Table 2** and **Supplementary Figure 1**). This finding further confirms that *gigA/gigB* are important for the growth of 17978 and that complementation of *gigA/gigB* with arabinose supplementation promotes the growth of Δ*gigAB* mutant to the wild-type level.

To determine if the loss of *gigA/gigB* required the generation of suppressing mutations, we performed whole genome sequencing on eight 17978 Δg*igAB* clones isolated from different batches of gene knockout experiments. We found that, other than the *gigA/gigB* deletion, the genome of each of the sequenced Δg*igAB* clones was 100% identical to the genome of ATCC 17978-mff reference strain, suggesting that deletion of the *gigA/gigB* genes does not require suppressing/compensatory mutations and that ATCC 17978 can survive without *gigA/gigB*. Thus, *gigA/gigB* are important for the growth but not required for the survival of ATCC 17978 under our routine laboratory culturing conditions.

Loss of *ptsP* and/or *gigAB* Does Not Affect Antibiotic Resistance of ATCC 17978

To explore the roles of *ptsP* and *gigA/gigB* in the antibiotic resistance of ATCC 17978, we performed antibiotic susceptibility tests in the wild type and gene deletion strains. As shown in **Table 1**, although the MIC of apramycin, chloramphenicol, and kanamycin were decreased in at least two deletion mutation strains compared with those in wild-type ATCC 17978, the results did not reach statistical significance. These data suggest that, in contrast to our previous findings in the *A. baumannii* AB5075 strain background, *ptsP* and *gigA/gigB* are not required for antibiotic resistance of ATCC 17978.

Loss of *ptsP* Restores the Growth of 17978 Δ*gigAB* to the Wild-Type Level

To explore the involvement of *ptsP* in *gigA/gigB*-mediated growth of ATCC 17978, we performed growth curve analyses. As shown in **Figure 1A**, 17978 Δ*gigAB* exhibited remarkably suppressed growth compared with the wild-type, whereas 17978 Δ*ptsP* exhibited a comparable growth rate to the wild-type, suggesting that *gigA/gigB* contribute to 17978 growth. Interestingly, 17978 Δ*ptsP*Δ*gigAB* showed comparable growth to the wild-type strain, indicating that loss of *ptsP* alleviates the growth defect associated with the loss of *gigA/gigB*. In addition, pMJG125-based complementation of *gigA/gigB* also restored the growth of 17978 Δ*gigAB* to the wild-type level in the presence of arabinose (**Figure 1B**).

gigA/*gigB* Mediate *in vitro* High-Temperature Resistance of ATCC 17978

We next sought to explore any additional roles of *gigA*/*gigB* and *ptsP* in stress resistance of ATCC 17978. Although the wild-type 17978 grown at 50°C showed a moderately reduced colony size phenotype when compared with those grown at 37°C, no significant loss of CFU was observed (EOP = 1; **Figure 2A**, left panel). However, loss of both *gigA* and *gigB* resulted in a dramatic reduction in CFU at 50°C (EOP = 10^{-5}; **Figure 2A**, right panel), suggesting that *gigA* and *gigB* contribute to high-temperature resistance of 17978. In the absence of arabinose, complementation of both *gigA* and g*igB* partially restored the growth of Δ*gigAB* mutant at 50°C (EOP = 10^{-3}; **Figure 2B**, left panel). Importantly, arabinose supplementation further restored the growth of Δ*gigAB* mutant with *gigA/gigB* complementation to the wild-type level at 50 °C (EOP = 1; **Figure 2B**, right panel), despite the small sizes of the colonies. This finding suggests that *gigA/gigB* contribute to high-temperature resistance of 17978 on solid media. As observed in the growth curves described above, 17978 Δ*ptsP* Δ*gigAB* and 17978 Δ*ptsP* exhibited comparable growth at 50°C (EOP = 1; **Figure 2C**), suggesting that loss of *ptsP* restores the growth of Δ*gigAB* mutant under high-temperature

TABLE 2 | The efficiency of *gigA/gigB* deletion in ATCC 17978 of different gene background.

Gene background	Extrachromosomal *gigA/gigB* expression	*gigA/gigB* deletion efficiency (%)
ATCC17978	–	4.2
ATCCATCC17978Δ*ptsP*	–	52.1
ATCC17978 pMJG120	–	4.2
ATCC17978 pMJG120-*gigAB*	+	47.8
ATCC17978Δ*ptsP* pMJG120	–	68.8
ATCC17978Δ*ptsP* pMJG120-*gigAB*	+	42.9
ATCC17978'	–	8.4
ATCC17978 pMJG125-*gigAB* (with 1% arabinose)	+	54.2
ATCC17978 pMJG125-*gigAB* (without 1% arabinose)	+/–	Large colonies: wild-type Small colonies: Δ*gigAB*

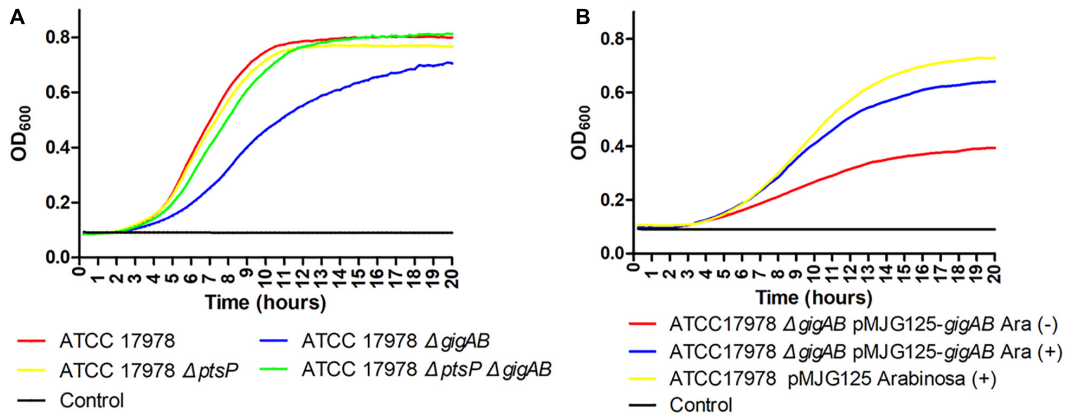

FIGURE 1 | Growth curves of different ATCC 17978 stains. **(A)** The indicated strains were grown for 20 h at 37°C in LB. **(B)** The strains indicated were grown for 96 h at 37°C in LB with or without 1% arabinose. Growth was measured by determining the OD_{600} every 15 min. Each experiment was performed in triplicate and repeated three times, and the most representative curves were presented.

stress. Taken together, these results suggest that *gigA/gigB* mediate high-temperature resistance of 17978 on LB agar plates, whereas *ptsP* negatively regulates this response.

When we examined the ability of the Δ*gigAB* strain to survive acid stress (pH = 5.5), we did not observe significant differences in the growth between the wild-type and Δ*gigAB* mutant strains (EOP = 1; **Figure 3A**), suggesting that the 17978 strain is not sensitive to pH stress as measured herein, and that the loss of *gigA* and *gigB* does not confer an acid stress sensitivity on the 17978 strain.

When cultured on LB containing Zn^{2+}, both wild-type and Δ*gigAB* mutant demonstrated significantly suppressed growth compared with those cultured on LB without Zn^{2+} (EOP = 10^{-4}, **Figure 3B**). No major difference was observed in the growth between the wild-type and Δ*gigAB* mutant. This finding suggests that factors other than *gigA* and *gigB* mediate zinc resistance of ATCC 17978.

gigA/gigB Protect ATCC 17978 From BMDM Killing

Evading macrophage phagocytosis is critical for the survival of pathogens *in vivo* (Rosales and Uribe-Querol, 2017). To investigate the roles of *gigA/gigB* in macrophage killing evasion of ATCC 17978, we infected murine BMDMs with the wild-type, Δ*gigAB* mutant, and *gigAB* complementation strains and monitored their survival and replication. When BMDMs were infected with wild-type 17978, we observed a 10-fold reduction of intracellular live bacteria at 2 h after infection (**Figure 4**). On the other hand, when BMDMs were infected with Δ*gigAB* mutant, we observed a 300-fold reduction of live bacteria in BMDMs at 2 h after infection (**Figure 4**), suggesting a decreased replication ability of the Δ*gigAB* mutant. Importantly, the Δ*gigAB* pMJG120-*gigAB* complementation strain exhibited a similar trend of survival and replication and comparable CFU at different time points to the wild-type 17978 (**Figure 4**). These results suggest that *gigA* and *gigB* promote macrophage killing evasion of ATCC 17978.

gigA/gigB Are Required for Killing *G. mellonella*

To examine the roles of *gigA/gigB* in the virulence of ATCC 17978, we performed a *G. mellonella* killing assay. As shown in **Figure 5**, inoculation of *G. mellonella* larvae with wild-type 17978 resulted in a rapid killing of the larvae starting 8 h after inoculation. No killing was observed in the larvae that received Δ*gigAB* mutant within 48 h after inoculation. Complementation of both *gigA* and *gigB* restored the virulence of bacteria to nearly

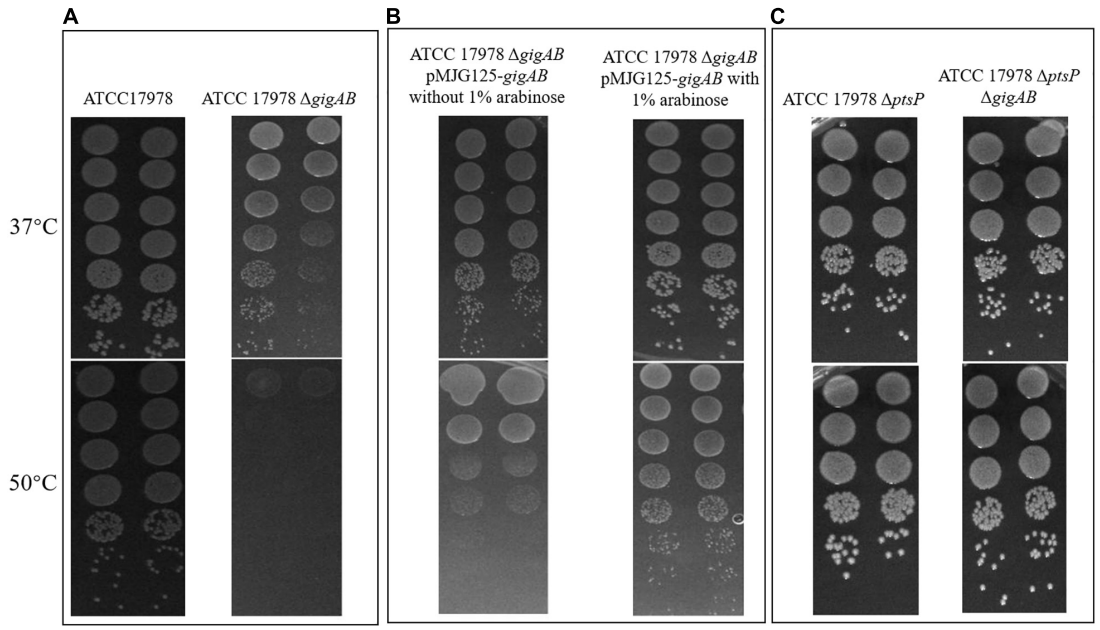

FIGURE 2 | The roles of *gigA/gigB* in ATCC 17978 in response to high temperature. **(A)** Images of wild-type ATCC 17978 and ATCC 17978 Δ*gigAB* mutant grown on LB at 37 or 50°C. **(B)** Images of ATCC 17978 Δ*gigAB* pMJG125-*gigAB* grown on LB without or with 1% arabinose at 37 or 50°C. **(C)** Images of ATCC 17978 Δ*ptsP* and ATCC 17978 Δ*ptsP*Δ*gigAB* grown on LB at 37 or 50°C.

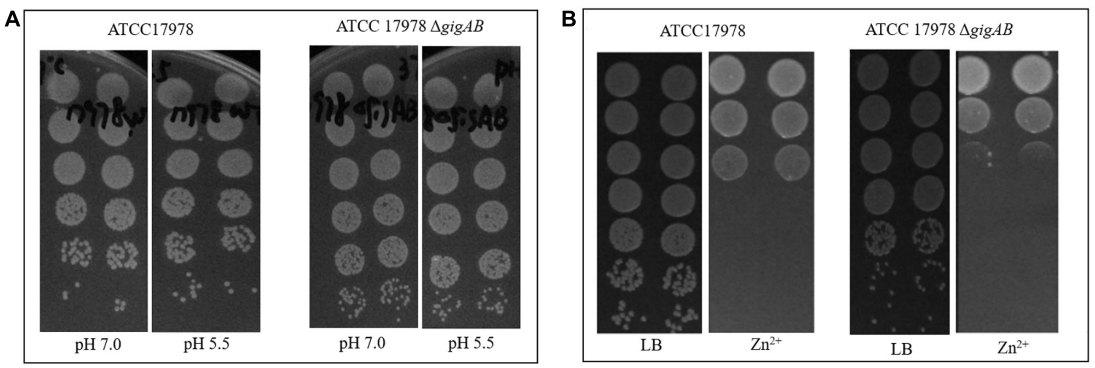

FIGURE 3 | The roles of *gigA/gigB* in ATCC 17978 in response to acid or zinc. **(A)** Images of wild-type ATCC 17978 and ATCC 17978 Δ*gigAB* mutant grown on LB at pH 7.0 or pH 5.5. **(B)** Images of wild-type ATCC 17978 and ATCC 17978 Δ*gigAB* mutant grown on LB with or without 1.25 mmol/L Zn^{2+}.

wild-type level. Thus, *gigA/gigB* are required for the virulence of ATCC 17978. Much like for the growth and temperature studies described above, both the 17978 Δ*pstP* and 17978 Δ*ptsP* Δ*gigAB* strains killed larvae with similar kinetics as the wild-type 17978 strain, suggesting that the loss of *ptsP* restores the virulence defect caused by the Δ*gigAB* deletion.

DISCUSSION

In this work, we sought to investigate the roles of *gigA*/*gigB* in the survival, stress resistance, macrophage killing evasion, and virulence of *A. baumannii* ATCC 17978 as well as the involvement of *ptsP* in *gigA*/*gigB* signaling. We found that *gigA*/*gigB* are important for growth of *A. baumannii* ATCC 17978, but are not explicitly required for survival of 17978. Indeed, the Δ*gigAB* mutant strain exhibited growth defects at both 37°C and 50°C compared with the wild-type strain, which was effectively restored by pMJG125-based *gigA*/*gigB* complementation in the presence of arabinose or loss of *ptsP*. Furthermore, *gigA*/*gigB* protected 17978 from murine BMDM killing and were required for the virulence of 17978 in *G. mellonella*.

Bacterial genetics remains an important and powerful tool for revealing the function(s) of specific genes. Efficient construction of gene knockouts or other types of mutations in bacteria often requires modifications of genetic background (Xu and Zhang, 2016). Our preliminary data have shown that

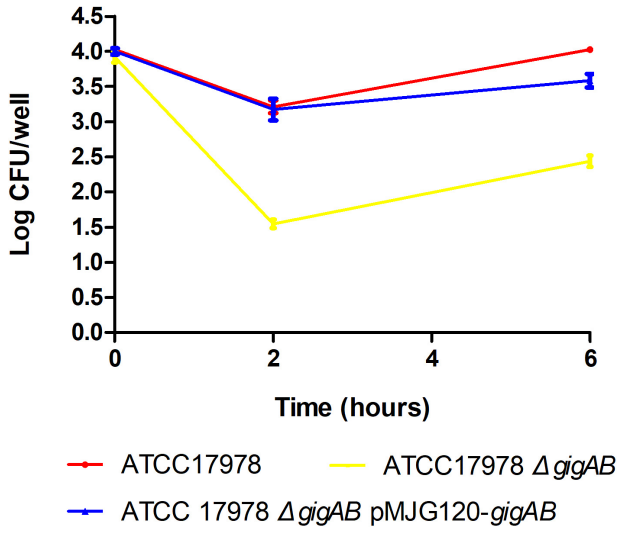

FIGURE 4 | Bone marrow-derived macrophage killing of wild-type and mutant ATCC 17978. Murine bone marrow derived macrophage (BMDMs) were cultured for 24 h, then challenged with wild-type ATCC 17978, ATCC 17978 Δ*gigAB*, or ATCC 17978 Δ*gigAB* pMJG120-*gigAB* at 5 × 10^4 colony forming unit count (CFU)/mL in the presence of 1 mM IPTG. BMDMs were lysed at 0, 2, or 6 h after challenge and surviving bacteria were quantified via standard plate count method.

the *gigA/gigB* deletion efficiency in wild-type 17978 was only 4.2%, suggesting that *gigA/gigB* are critical for the survival of ATCC 17978. We further found that *gigA/gigB* complementation or *ptsP* deletion significantly improved *gigA/gigB* deletion efficiency, suggesting that *gigA/B* complementation or *ptsP* deletion compensates for the lack of *gigA/B* in 17978. This is consistent with our previous study showing that loss of *ptsP* in the *A. baumannii*Δ*gigA* or Δ*gigB* mutant restores the growth of *A. baumannii* in *G. mellonella* larvae (Gebhardt and Shuman, 2017).

When studying genes essential for bacterial growth and/or survival, it is not uncommon to inadvertently isolate clones which harbor compensatory or suppressing mutations that alleviate the phenotype of the particular genes being studied (MacLean and Vogwill, 2014). To exclude the possibility that the Δ*gigAB* strain acquired such compensatory mutations, we performed whole genome sequencing in multiple independently derived Δ*gigAB* clones and found that, with the exception of the *gigA/gigB* deletion, the genome of Δ*gigAB* clones displayed 100% identity to the genome of the wild-type strain, suggesting that *gigA/gigB* deletion does not require subsequent compensatory mutations, further confirming that 17978 can survive without *gigA/gigB*.

When we knocked out *gigA/gigB* in the genetic background of pMJG125-*gigAB* conditional strain, we observed that in the absence of arabinose, the colonies of Δ*gigAB* mutants were smaller than those of the wild-type (**Table 2** and **Supplementary Figure 1**). In addition, Δ*gigAB* mutant still showed growth defect even after the complementation of *gigA/gigB* in the absence of arabinose (**Figure 1**). Of note, arabinose supplementation effectively reversed these effects. We attribute these observations to leaky basal expression from the arabinose-promoter on the multi-copy pMJG125 plasmid.

In addition to the growth in LB medium, we also investigated the roles of *gigA/gigB* in ATCC 17978 in response to several environmental stresses, including antibiotics, high temperature, Zn^{2+}, and acid. Neither the wild-type nor the Δ*gigAB* mutant showed significant growth defect to acid stress (**Figure 3A**). Additionally, we did not observe significant differences for MIC values for various antibiotics (**Table 1**) and colony formation in the presence of Zn^{2+} (**Figure 3B**) between the wild-type and the mutant strain lacking both *gigA* and *gigB*. These results suggest that factors other than *gigA/gigB* regulate the responses of ATCC 17978 to antibiotics and Zn^{2+} stresses, in contrast to what was previously observed in the more virulent AB5075 strain (Gebhardt et al., 2015; Gebhardt and Shuman, 2017; Blaschke et al., 2018). For example, it has previously been reported that the chromosomally-encoded efflux pump CraA, AdeAB efflux system, and incubation temperature regulate antibiotic resistance of ATCC 17978 (Adams et al., 2018; De Silva et al., 2018; Kroger et al., 2018). Additionally, transcriptional analyses have shown that zinc resistance efflux pumps are responsible for zinc

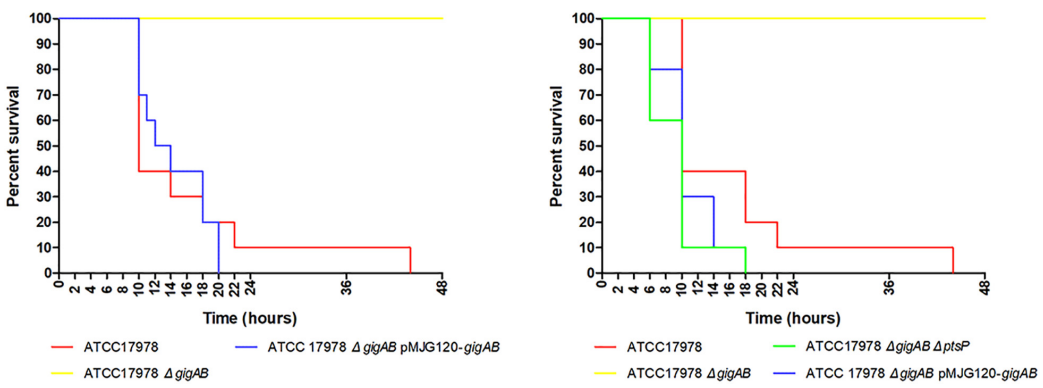

FIGURE 5 | Killing of *G. mellonella* larvae. *G. mellonella* larvae were inoculated with 5 × 10^6 CFU/mL of wild-type ATCC 17978, ATCC 17978 Δ*gigAB*, or ATCC 17978 Δ*gigAB* pMJG120-*gigAB* (*n* = 10 larvae/group). After injection, larvae were incubated at 37°C. The number of dead larvae was recorded hourly.

stress response in ATCC 17978, including two cation diffusion facilitator transporters, one heavy metal efflux transporter, and one P-type ATPase (Hassan et al., 2017). That there are differential consequences of *gigA/gigB* deletion in the AB5075 background (i.e., aminoglycoside and zinc sensitivity) and the ATCC 17978 background (i.e., growth defect under routine culture conditions) suggests that some of the inputs and/or outputs of the GigA/GigB signaling pathway have diverged since the two strains separated; yet, other facets of the pathway, such as growth at elevated temperature and virulence, have remained intact. Further research will be required to understand the molecular mechanisms that underlie the different stress responses that are regulated by GigA/GigB amongst these two isolates.

Of note, our results showed that complementation of the Δ*gigAB* deletion strain with a plasmid-borne copy of *gigA/gigB* restored growth on agar plates at high temperature and that a subsequent deletion of *ptsP* in the Δ*gigAB* background also alleviated the high temperature growth defect caused by the loss of both *gigA* and *gigB* (**Figure 2**), consistent with previous observations in the AB5075 strain (Gebhardt and Shuman, 2017).

We finally examined the roles of *gigA/gigB* in evading macrophage phagocytosis and killing *G. mellonella* larvae. Our data indicate that *gigA/gigB* are required for 17978 in killing *G. mellonella*: no larvae died within 48 h after inoculation with Δ*gigAB* mutant. Additionally, we found that *gigA/gigB* contribute to the macrophage killing evasion of ATCC 17978, as evidenced by the decreased intracellular live bacteria and the suppressed bacterial replication in murine BMDMs infected with Δ*gigAB* mutant compared with those infected with the wild-type strain (**Figure 5**). As it has been reported that RNA chaperone Hfq and superoxide dismutase of ATCC 17978 also play important roles in evading macrophage phagocytosis (Heindorf et al., 2014; Kuo et al., 2017), it will be interesting to examine if the loss of *gigA* and/or *gigB* leads to altered expression of these virulence factors.

CONCLUSION

In this study, we demonstrate that *gigA/gigB* are important for the growth of *A. baumannii* strain ATCC 17978, although they are not explicitly required. The Δ*gigAB* mutant exhibits growth defects at both 37 and 50°C, which can be restored either through *gigA/gigB* complementation or by loss of *ptsP*. In contrast to findings in the *A. baumannii* AB5075 background (Gebhardt and Shuman, 2017), *gigA/gigB* do not appear to alter the response of strain 17978 to antibiotics or Zn^{2+} stress. Finally, like strain AB5075, the *gigA/gigB* genes are required for the virulence traits of strain ATCC 17978 in both resisting killing by macrophage and the *G. mellonella* infection model.

DATA AVAILABILITY STATEMENT

The datasets presented in this study can be found in online repositories. The names of the repository/repositories and accession number(s) can be found below: http://www.ncbi.nlm.nih.gov/bioproject/, PRJNA738724.

ETHICS STATEMENT

The animal study was reviewed and approved by the Ethics Committee of the University of Chicago Medical Center.

AUTHOR CONTRIBUTIONS

HZ performed the all stepss of experiment, analyzed the experimental data, and drafted the manuscript. MG helped construct *A. baumannii* ATCC17978 mutants. DC helped perform the BMDM isolation and bacterial killing experiments. YY analyzed whole genome sequences and helped to analyze data. MG and DC revised the manuscript. HS designed the study and revised the manuscript. All authors read and approved the final manuscript.

FUNDING

This work was supported by a research grant from the National Natural Science Foundation of China (81971897) and a research grant from the Natural Science Foundation of Zhejiang Province LQ20H0006). The funders had no role in the study design, data collection and interpretation, or the decision to submit the work for publication.

SUPPLEMENTARY MATERIAL

The Supplementary Material for this article can be found online at: https://www.frontiersin.org/articles/10.3389/fmicb.2021.723949/full#supplementary-material

REFERENCES

Abisado, R. G., Kimbrough, J. H., Mckee, B. M., Craddock, V. D., Smalley, N. E., Dandekar, A. A., et al. (2021). Tobramycin adaptation enhances policing of social cheaters in *Pseudomonas aeruginosa*. *Appl. Environ. Microbiol.* 87:e0002921.

Adams, F. G., Stroeher, U. H., Hassan, K. A., Marri, S., and Brown, M. H. (2018). Resistance to pentamidine is mediated by AdeAB, regulated by AdeRS, and influenced by growth conditions in *Acinetobacter baumannii* ATCC 17978. *PLoS One* 13:e0197412. doi: 10.1371/journal.pone.0197412

Blaschke, U., Suwono, B., Zafari, S., Ebersberger, I., Skiebe, E., Jeffries, C. M., et al. (2018). Recombinant production of A1S_0222 from *Acinetobacter baumannii* ATCC 17978 and confirmation of its DNA-(adenine N6)-methyltransferase activity. *Protein Expr. Purif.* 151, 78–85. doi: 10.1016/j.pep.2018.06.009

Bolger, A. M., Lohse, M., and Usadel, B. (2014). Trimmomatic: a flexible trimmer for Illumina sequence data. *Bioinformatics* 30, 2114–2120. doi: 10.1093/bioinformatics/btu170

Danecek, P., Bonfield, J. K., Liddle, J., Marshall, J., Ohan, V., Pollard, M. O., et al. (2021). Twelve years of SAMtools and BCFtools. *Gigascience* 10:giab008.

De Silva, P. M., Chong, P., Fernando, D. M., Westmacott, G., and Kumar, A. (2018). Effect of incubation temperature on antibiotic resistance and virulence factors

of *Acinetobacter baumannii* ATCC 17978. *Antimicrob. Agents Chemother.* 62:e01514-17.

Gebhardt, M. J., Gallagher, L. A., Jacobson, R. K., Usacheva, E. A., Peterson, L. R., Zurawski, D. V., et al. (2015). Joint transcriptional control of virulence and resistance to antibiotic and environmental stress in *Acinetobacter baumannii*. *mBio* 6, e01660-15.

Gebhardt, M. J., and Shuman, H. A. (2017). GigA and GigB are master regulators of antibiotic resistance, stress responses, and virulence in *Acinetobacter baumannii*. *J. Bacteriol.* 199:e00066-17.

Gottig, S., Gruber, T. M., Higgins, P. G., Wachsmuth, M., Seifert, H., and Kempf, V. A. (2014). Detection of pan drug-resistant *Acinetobacter baumannii* in Germany. *J. Antimicrob. Chemother.* 69, 2578–2579.

Hassan, K. A., Pederick, V. G., Elbourne, L. D., Paulsen, I. T., Paton, J. C., Mcdevitt, C. A., et al. (2017). Zinc stress induces copper depletion in *Acinetobacter baumannii*. *BMC Microbiol.* 17:59. doi: 10.1186/s12866-017-0965-y

Heindorf, M., Kadari, M., Heider, C., Skiebe, E., and Wilharm, G. (2014). Impact of *Acinetobacter baumannii* superoxide dismutase on motility, virulence, oxidative stress resistance and susceptibility to antibiotics. *PLoS One* 9:e101033. doi: 10.1371/journal.pone.0101033

Jacobs, A. C., Thompson, M. G., Black, C. C., Kessler, J. L., Clark, L. P., Mcqueary, C. N., et al. (2014a). AB5075, a highly virulent isolate of *Acinetobacter baumannii*, as a model strain for the evaluation of pathogenesis and antimicrobial treatments. *mBio* 5:e01076-14.

Jacobs, A. C., Thompson, M. G., Gebhardt, M., Corey, B. W., Yildirim, S., Shuman, H. A., et al. (2014b). Genetic manipulation of *Acinetobacter baumannii*. *Curr. Protoc. Microbiol.* 35, 6G.2.1-11.

Karalewitz, A. P., and Miller, S. I. (2018). Multidrug-resistant *Acinetobacter baumannii* chloramphenicol resistance requires an inner membrane permease. *Antimicrob. Agents Chemother.* 62:e00513-18.

Kroger, C., Mackenzie, K. D., Alshabib, E. Y., Kirzinger, M. W. B., Suchan, D. M., Chao, T. C., et al. (2018). The primary transcriptome, small RNAs and regulation of antimicrobial resistance in *Acinetobacter baumannii* ATCC 17978. *Nucleic Acids Res.* 46, 9684–9698. doi: 10.1093/nar/gky603

Kuo, H. Y., Chao, H. H., Liao, P. C., Hsu, L., Chang, K. C., Tung, C. H., et al. (2017). Functional characterization of *Acinetobacter baumannii* Lacking the RNA Chaperone Hfq. *Front. Microbiol.* 8:2068. doi: 10.3389/fmicb.2017.02068

Langmead, B., and Salzberg, S. L. (2012). Fast gapped-read alignment with Bowtie 2. *Nat. Methods* 9, 357–359. doi: 10.1038/nmeth.1923

Lee, C. R., Lee, J. H., Park, M., Park, K. S., Bae, I. K., Kim, Y. B., et al. (2017). Biology of *Acinetobacter baumannii*: pathogenesis, antibiotic resistance mechanisms, and prospective treatment options. *Front. Cell Infect. Microbiol.* 7:55. doi: 10.3389/fcimb.2017.00055

MacLean, R. C., and Vogwill, T. (2014). Limits to compensatory adaptation and the persistence of antibiotic resistance in pathogenic bacteria. *Evol. Med. Public Health* 2015, 4–12. doi: 10.1093/emph/eou032

Peleg, A. Y., De Breij, A., Adams, M. D., Cerqueira, G. M., Mocali, S., Galardini, M., et al. (2012). The success of acinetobacter species; genetic, metabolic and virulence attributes. *PLoS One* 7:e46984. doi: 10.1371/journal.pone.0046984

Rosales, C., and Uribe-Querol, E. (2017). Phagocytosis: a fundamental process in immunity. *Biomed. Res. Int.* 2017:9042851.

Sahl, J. W., Johnson, J. K., Harris, A. D., Phillippy, A. M., Hsiao, W. W., Thom, K. A., et al. (2011). Genomic comparison of multi-drug resistant invasive and colonizing *Acinetobacter baumannii* isolated from diverse human body sites reveals genomic plasticity. *BMC Genomics* 12:291. doi: 10.1186/1471-2164-12-291

Schurek, K. N., Marr, A. K., Taylor, P. K., Wiegand, I., Semenec, L., Khaira, B. K., et al. (2008). Novel genetic determinants of low-level aminoglycoside resistance in *Pseudomonas aeruginosa*. *Antimicrob. Agents Chemother.* 52, 4213–4219. doi: 10.1128/aac.00507-08

Scribner, M. R., Santos-Lopez, A., Marshall, C. W., Deitrick, C., and Cooper, V. S. (2020). Parallel evolution of tobramycin resistance across species and environments. *mBio* 11:e00932-20.

Toda, G., Yamauchi, T., Kadowaki, T., and Ueki, K. (2021). Preparation and culture of bone marrow-derived macrophages from mice for functional analysis. *STAR Protoc* 2:100246. doi: 10.1016/j.xpro.2020.100246

WHO (2017). *Global Priority List of Antibiotic-Resistant Bacteria to Guide Research, Discovery and Development of New Antibiotics*. Geneva: World Health Organization.

Xu, J. Z., and Zhang, W. G. (2016). Strategies used for genetically modifying bacterial genome: site-directed mutagenesis, gene inactivation, and gene over-expression. *J. Zhejiang Univ. Sci. B* 17, 83–99. doi: 10.1631/jzus.b1500187

Conflict of Interest: The authors declare that the research was conducted in the absence of any commercial or financial relationships that could be construed as a potential conflict of interest.

Publisher's Note: All claims expressed in this article are solely those of the authors and do not necessarily represent those of their affiliated organizations, or those of the publisher, the editors and the reviewers. Any product that may be evaluated in this article, or claim that may be made by its manufacturer, is not guaranteed or endorsed by the publisher.

frontiers in Microbiology

ORIGINAL RESEARCH
published: 21 September 2021
doi: 10.3389/fmicb.2021.728644

Ubiquitous Conjugative Mega-Plasmids of *Acinetobacter* Species and Their Role in Horizontal Transfer of Multi-Drug Resistance

*Sofia Mindlin[1], Olga Maslova[1], Alexey Beletsky[2], Varvara Nurmukanova[1], Zhiyong Zong[3], Andrey Mardanov[2] and Mayya Petrova[1]**

[1] Institute of Molecular Genetics of National Research Center "Kurchatov Institute", Moscow, Russia, [2] Institute of Bioengineering, Research Center of Biotechnology of the Russian Academy of Sciences, Moscow, Russia, [3] Center of Infectious Diseases, West China Hospital, Sichuan University, Chengdu, China

Conjugative mega-plasmids play a special role in adaptation since they carry a huge number of accessory genes, often allowing the host to develop in new niches. In addition, due to conjugation they are able to effectively spread themselves and participate in the transfer of small mobilizable plasmids. In this work, we present a detailed characterization of a recently discovered family of multiple-drug resistance mega-plasmids of *Acinetobacter* species, termed group III-4a. We describe the structure of the plasmid backbone region, identify the *rep* gene and the origin of plasmid replication, and show that plasmids from this group are able not only to move between different *Acinetobacter* species but also to efficiently mobilize small plasmids containing different *mob* genes. Furthermore, we show that the population of natural *Acinetobacter* strains contains a significant number of mega-plasmids and reveal a clear correlation between the living conditions of *Acinetobacter* strains and the structure of their mega-plasmids. In particular, comparison of the plasmids from environmental and clinical strains shows that the genes for resistance to heavy metals were eliminated in the latter, with the simultaneous accumulation of antibiotic resistance genes by incorporation of transposons and integrons carrying these genes. The results demonstrate that this group of mega-plasmids plays a key role in the dissemination of multi-drug resistance among *Acinetobacter* species.

Keywords: *tra*-operon, replication initiation protein, iterons, plasmid backbone, accessory region, phylogenetic analysis, mobilization

OPEN ACCESS

Edited by:
Raffaele Zarrilli,
University of Naples Federico II, Italy

Reviewed by:
Steve Petrovski,
La Trobe University, Australia
Raul Raya,
CONICET Centro de Referencia para Lactobacilos (CERELA), Argentina

****Correspondence:***
Mayya Petrova
petrova@img.ras.ru

Specialty section:
This article was submitted to Antimicrobials, Resistance and Chemotherapy, a section of the journal Frontiers in Microbiology

Received: *21 June 2021*
Accepted: *25 August 2021*
Published: *21 September 2021*

Citation:
Mindlin S, Maslova O, Beletsky A, Nurmukanova V, Zong Z, Mardanov A and Petrova M (2021) Ubiquitous Conjugative Mega-Plasmids of Acinetobacter Species and Their Role in Horizontal Transfer of Multi-Drug Resistance. Front. Microbiol. 12:728644. doi: 10.3389/fmicb.2021.728644

INTRODUCTION

The genus *Acinetobacter* includes species of different life-styles, from free-living saprophytes to human and animal pathogens (Touchon et al., 2014). *Acinetobacter* species occur in diverse natural and artificial environments such as forest and agricultural soils, animal and human skin and gut, fresh- and seawater, or even sewage and activated sludge (Peleg et al., 2012; Touchon et al., 2014). Due to the importance of *Acinetobacter* strains in the clinic, the number of publications devoted to the study of this genus has increased significantly in recent years. The most studied *Acinetobacter* species is the human pathogen *A. baumannii* (Peleg et al., 2012; Salgado-Camargo et al., 2020), which has attracted exceptional attention because of its pathogenicity and multi-drug resistance (Göttig et al., 2014). However, despite their high prevalence in most environments, the distribution

and ecological roles of various *Acinetobacter* species, apart from pathogenic and nosocomial species with clinical importance, have remained poorly explored. While non-baumannii acinetobacters live in a wide range of environments including habitats contaminated with heavy metals (Turton et al., 2010; Mindlin et al., 2016), the mechanisms of horizontal gene transfer and, in particular, the role of various groups of plasmids in this process in *Acinetobacter* have not been studied in much detail.

Conjugation is the main process by which genes (including antibiotic−resistance genes) are horizontally transferred from one bacterium to another and is therefore a major contributor to bacterial genome plasticity, evolution and adaptation (Brovedan et al., 2020; von Wintersdorff et al., 2016). Conjugative plasmids play a key role in the physical transfer of DNA from cell to cell. Any conjugative plasmid contains the backbone or core region, a set of genes and elements that ensure its replication, maintenance in the cell and transfer to other cells, and a varying number of accessory genes, which may encode for drug resistance or have other adaptive functions (Thomas, 2000). The number of sequenced *Acinetobacter* plasmids in genomic databases has exceeded 3,000 and continues to grow rapidly. It should be noted that the genus *Acinetobacter* is characterized by the presence of numerous plasmids in the same strain (Feng et al., 2016; Brovedan et al., 2019; Mindlin et al., 2020), and most of them contain the relaxase gene (*mobA*), which suggests their potential ability to be mobilized (Francia et al., 2004; Garcillán-Barcia et al., 2009). Large conjugative plasmids are usually found in the study of clinical antibiotic-resistant strains of *Acinetobacter*, but only some of them are studied in detail. Despite the fact that the ability to carry out conjugative transfer has been confirmed experimentally for several plasmids (Silva et al., 2018; Wibberg et al., 2018), it remained largely unexplored whether they are able to mobilize other non-conjugative plasmids containing the relaxase gene.

To date, three groups of conjugative plasmids are known in *Acinetobacter*, for which their ability to move from one strain to another has been experimentally proven. Each group was formed on the basis of a high level of homology of the backbone regions. A group of plasmids closely related to pACICU2 (64,366 bp) (NC_010606.1) was identified first (Hamidian and Hall, 2014). These plasmids were assigned to the LN_1 lineage in the classification of *A. baumannii* plasmids (Salgado-Camargo et al., 2020). It was shown that pACICU2 contains a complete conjugative apparatus and its relaxase gene belongs to the MOB_F family. Some plasmids from this group contain the bla_{oxa23} gene and are widespread mainly in *A. baumannii* strains (Bertini et al., 2010; Nigro et al., 2015). Conjugative plasmids from the second group [prototype pLS488 (NZ_MF078634)] were found in *Acinetobacter* strains belonging to different species, but are less common than representatives of the first group. In most cases they contain antibiotic resistance genes (Silva et al., 2018). All of them contain a complete set of genes involved in the conjugation process and a gene encoding a replication initiator protein. Its relaxase gene belongs to the MOB_P family. In the work of Mindlin et al. (2020), this group of plasmids was designated III-1a. In contrast, neither the relaxase gene nor the gene encoding the replication initiator protein could be identified in the third group of conjugative mega-plasmids, represented by the prototype plasmid pA297-3 (Hamidian et al., 2016; Nigro and Hall, 2017). At the same time, it was shown that this plasmid is able to actively move between different strains (Hamidian et al., 2016; Nigro and Hall, 2017). The authors believe that the relaxase gene should be present in the plasmid, but the corresponding protein belongs to a new, not yet described relaxase family (Hamidian et al., 2016). It should be noted that other groups of plasmids (for example, related to pAVAci1 or pABTJ1) containing conjugative transport genes are revealed in *Acinetobacter* strains, but the functional activity of these genes remains unknown to date.

At the end of 2020, another group of *Acinetobcater* conjugative plasmids was discovered simultaneously by two teams of researchers (Ghaly et al., 2020; Mindlin et al., 2020). In Mindlin et al. (2020), this group was designated III-4a. It includes mega-plasmids with the size of about 300 kb, which also do not contain known replicase and relaxase genes. It was found that plasmids of this group are widely distributed in predominantly clinical strains of various *Acinetobacter* species. Analysis of the genomes of plasmids from this group suggested that they play an important role in adaptation, since different geographical regions are characterized by their own sets of adaptive genes, while sharing a conserved core genome (Ghaly et al., 2020).

In this work, we performed a detailed characterization of group III-4a plasmids, including: (1) description of the structure of the backbone region; (2) identification of the *rep* gene and the origin of plasmid replication; (3) demonstration that plasmids from group III-4a are conjugative and can efficiently mobilize small plasmids containing different *mobA* genes; (4) data on the wide distribution of plasmids of the III-4a group among environmental strains of *Acinetobacter*.

MATERIALS AND METHODS

Media and Growth Conditions

Bacteria were grown in lysogeny broth (LB) medium or solidified agar LB medium (LA) (Sambrook and Russell, 2001) at 30°C. When required, LB agar was supplemented with antimicrobial agents at the following final concentrations (μg/ml): $HgCl_2$ (Hg) 4–5; $K_2Cr_2O_7$ (Cr) 70–140; streptomycin (Sm) 100–200; chloramphenicol (Cm) 20; gentamycin (Gm) 5; rifampicin (Rif) 25; nalidixic acid (Nal) 20; ceftazidime (Cef) 200; tetracycline (Tc) 10.

Bacterial Strains and Plasmids

Both mercury resistant (Hg-r) and mercury-sensitive (Hg-s) *Acinetobacter* strains from the IMG collection were used in this study (**Supplementary Table 1**). The host strain of pALWED1.1 (*A. lwoffii* ED23-35) was isolated from permafrost sample aged forty thousand years. Part of the *Acinetobacter* sp. strains was isolated from mercury mines in different regions of the former Soviet Union. Additional strains from the collections were isolated from soils and water samples from different geographical regions (**Supplementary Table 1**; Petrova et al., 2002; Kholodii et al., 2004; Mindlin et al., 2005). The strain *A. wuhouensis* WCHAW010062 containing pOXA23_010062 was

kindly provided by A. Nemec. The strains *A. baylyi* BD413rif and *A. lwoffii* BSW27-2nal were used as recipients in matings. Small mobilizable plasmids used in this work are presented in **Table 1**.

Standard DNA Manipulations

Standard protocols were used for agarose gel electrophoresis, and colony hybridization (Sambrook and Russell, 2001). GeneJET Genomic DNA Purification kit (Thermo Fisher Scientific) was used for total genomic DNA isolation. PCR was performed with a Mastercycler (Eppendorf) using Taq DNA polymerase with supplied buffer (Thermo Fisher Scientific) and a dNTP mixture (Thermo Fisher Scientific). The primers trbC-F: ggtctacctgtttatgcatcc and trbC-R: aattcgccgttgtgctgtcc were used to amplify the fragment of *trbC* gene (20950–22249 position in the sequence KX426227) and rep-F: tgtctgaactctctttaccg and rep-R: gtatgcacatcagctgcagc—to amplify the fragment of the putative *rep* gene (228166–229724 position).

Screening of Plasmids Related to pALWED1.1 Among Modern *Acinetobacter* Strains

We screened 57 environmental strains of *Acinetobacter* isolated in our laboratory from samples of soil and water (**Supplementary Table 1**). At the first stage of screening, the colonies of all strains were hybridized with a probe (1,300 bp) containing the *trbC* gene encoding the coupling protein (CP) from pALWED1.1 (20950–22249 position in the sequence KX426227). At the second stage of screening, genomic DNA was isolated from all hybridization positive strains and PCR was performed with primers for the putative *rep* gene and the gene *trbC* from pALWED1.1.

Analysis of the Frequency of Conjugation Transfer of pALWED1.1-Related Plasmids

The ability to transfer resistance markers during conjugation was tested for 6 from 13 strains containing plasmids related to pALWED1.1. These strains were as resistant to mercury as the original strain ED23-35 and one of them was resistant to streptomycin and tetracycline. In addition to them, we tested the conjugative transfer of the plasmid pOXA23_010062 (CP033130.1), also belonging to group III-4a, from the strain *A. wuhouensis* WCHAW010062. All the analyzed strains were crossed with rifampicin-resistant mutants of the *A. baylyi* BD413 strain that does not contain its own plasmids. Matings were performed overnight on the surface of LA plates. Cultures of the donor and recipient in the late logarithmic growth phase were mixed in a ratio of 1: 1; the mixture was plated on the LA surface and incubated at 30° for 18–20 h. The mixed growth was then scrapped off the plate, resuspended, and suitable dilutions were spread on appropriate selective plates. Parent strains were plated in parallel with the matings and then processed similarly to the matings as controls. Isolated colonies from matings and of parental strains were used to identify recombinants and parental forms.

TABLE 1 | Mobilizable plasmids analyzed.

Plasmid	Natural host	MOB family, Group*	Resistance to
pALWED 3.5	*A. lwoffii* ED9-5a	MOB_Q, II-1b	Chromium (Cr)
pALWVS1.4	*A. lwoffii* VS15	MOB_Q, I-1c	Chloramphenicol (Cm)
p7_010062	*A. wuhouensis* WCHAW010062	MOB_Q, I-1a	Tetracycline (Tc)
RSF1010	Different gamma-proteobacteria	MOB_Q, -	Streptomycin (Sm)

**Group number according to plasmid classification in Mindlin et al. (2020).*

Mobilization Assays

The small mobilizable plasmids (**Table 1**) were transformed into *A. baylyi* BD413rif. The conjugative plasmid pALWED1.1 was then transferred to these strains by conjugation with the strain *A. lwoffii* ED23-35. The standard procedure of mating a donor strain harboring two plasmids (conjugative and non-conjugative) with a recipient strain (nalidixic acid-resistant mutant of the strain BSW27-2) was used (Brasch and Meyer, 1986). Matings were performed overnight on the surface of LA plates as described above. Transconjugants were selected on LA plates supplemented with appropriate antimicrobial agents. The mobilization frequency was calculated according to Brasch and Meyer (1986).

Identification of the Backbone Region of pALWED1.1

The genes involved in conjugation [*mob* genes and mating pair formation (MPF) genes] were identified by amino acid similarity with genes of previously described plasmids. The plasmid R64 (AB027308.1, NC_005014) from *Salmonela enterica* and plasmid pA297-3 (KU744946.1) isolated from *A. baumannii* A297 (Hamidian et al., 2016) were used as references for the MPF I group of the T4SS system and CPT4 from the MOB_F family.

Previously, neither we nor other researchers (Ghaly et al., 2020) were able to detect the *rep* gene of mega-plasmids. In this paper, we conducted a more careful search. To this end, the backbone regions presented in all mega-plasmids, including an extended region containing the genes involved in conjugation, were determined and hypothetical proteins presented in all plasmids were identified. The identified hypothetical proteins were analyzed using the BLAST Protein on NCBI site (Altschul et al., 1997), which allowed us to find the gene encoding the putative replication initiation protein. The putative iterons of mega-plasmids were revealed manually by the analysis of the region next to the putative *rep* gene.

Search for Plasmids Related to pALWED1.1 in GenBank

Plasmids related to pALWED1.1 from modern *Acinetobacter* strains were identified using the BLASTp program. The sequence of pALWED1.1 was used as query to search for related plasmids in NCBI database containing complete plasmid genomes on April 1, 2021. All plasmids that had the query cover >50% and the identity of the common region >98.5% were considered as

related to pALWED1.1. Since all the detected plasmids contained genes encoding the CP TrbC and the putative replication initiator protein Rep, the sequences of these two genes were used as queries to search for related sequences in the NCBI database containing whole-genome shotgun contigs.

Bioinformatic Analysis

Phylogenetic trees were built in the following way. First, we constructed multiple alignment of the plasmid complete genomes using Mauve v2.4.0. A Mauve genome alignment results in a set of alignment blocks, each of which is a conserved region across multiple sequences. Alignment blocks present in all plasmid genomes were concatenated and used as an input for tree construction in Phyml v3.3 with default parameters. The concatenated alignment was 352,008 bases in length. Blast comparison between pALWED1.1 and pAHTJR1 plasmid genomes was visualized using Easyfig (Sullivan et al., 2011), alignments with minimum length of 1,000 bp and e value >1e-3 were used.

RESULTS

The Molecular Structure of Plasmid pALWED1.1 as a Typical Representative of Group III-4a

Plasmid pALWED1.1 (original designation pKLH208) was isolated from the ancient permafrost strain ED23-35 of *A. lwoffii* resistant to mercury salts (Petrova et al., 2002). It was shown that it is a large plasmid that is able to transfer mercury resistance by conjugation (Kholodii et al., 2004). Initially, only the plasmid region containing the genes of the *mer*-operon encoding mercury resistance was sequenced and studied (Kholodii et al., 2004). Later, thanks to the complete sequencing of pALWED1.1 (287,631 bp) it became possible to study the structure of extended plasmid regions containing determinants of resistance to heavy metal salts (Mindlin et al., 2016). Finally, due to the appearance of a large number of complete genomes of *Àcinetobacter* plasmids, it became clear that pALWED1.1 is a typical representative of an extensive group of plasmids, designated III-4a (Ghaly et al., 2020; Mindlin et al., 2020). However, the structure of the backbone region of the plasmids of this group remained unexplored. Therefore, one of the goals of this work was to describe the structure of the backbone region of plasmids belonging to the group III-4a on the example of pALWED1.1.

Backbone Region of pALWED1.1

Identification of Genes Involved in Conjugation

The transfer of plasmids by conjugation is carried out by several groups of proteins encoded by plasmid genes. The relaxosome complex is responsible for DNA cleavage at the origin of transfer (*oriT*) and formation of relaxosome (Smillie et al., 2010). The MPF complex is involved in the building of pilus and pore necessary for translocation of single-stranded DNA. The MPF complex and relaxosome are linked via the ATPase CP, one of the key proteins of conjugation apparatus (Smillie et al., 2010; Llosa and Alkorta, 2017).

We identified the putative transfer region of pALWED1.1 and found that it contains a set of MPF genes belonging to the MPF I group of these genes found in other conjugative plasmids (**Table 2**). In particular, we identified genes *traU* and *traO* as well as other genes necessary for functioning of the T4SS system (**Figure 1**). All the genes of the MPF module as well as the gene *trbC* encoding the coupling protein T4CP are located in a single plasmid region. Besides the T4SS genes, the genes *parABM* encoding the system of plasmid partitioning are also present in the same region (**Figure 1**).

We found homology between the Tra proteins of the pALWED1.1 plasmid and the T4SS system proteins from the R64 plasmid belonging to the MOB_F family, suggesting that the *tra* genes of this group of mega-plasmids can be placed into the MOB_F family. However, the gene *mobA* encoding relaxase, the protein necessary for nicking DNA and forming the relaxasome, was not found, and none of the pALWED1.1 plasmid genes showed significant similarities with any of the known relaxase genes. It can therefore be proposed that the relaxase gene of pALWED1.1 belongs to a new not yet described family. Indeed, in some other conjugative plasmids a gene encoding relaxase also has not been identified. Such plasmids in Acinetobacters are the mega-plasmid pA297-3 described by Hamidian et al. (2016) and pNDM-BJ01 and related plasmids described by Hu et al. (2017). Similar observations were made for relaxases of other bacterial plasmids (Smillie et al., 2010; Guzman-Herrador and Llosa, 2019).

Identification of the Replication Module of pALWED1.1

In the initial analysis of the pALWED1.1 genome (Mindlin et al., 2016), we were unable to find the gene(s) encoding the protein related to the described plasmid replication initiation proteins.

TABLE 2 | Identification of the pALWED1.1 genes involved into the formation of MPF complex.

Gene	Coordinates	Identity (%) of aa sequences found in R64 AB027308.1 (%)	Identity (%) of aa sequences found in pA297-3 (KU744946.1) (%)
traY	273149–276157	24	50
trbA	284947–286476	–	44
parA	296–1132	–	51
stbA	3072–4178	–	34
traJ	4484–5779	31	49
traI	5807–6616	22	37
traH	6654–7100	–	39
traM	9613–10389	–	38
traN	10394–11350	40	43
traO	11372–12895	33	38
traU	17222–20404	29.7	47
trbC	20527–23319	33	40.8

"–" not found.

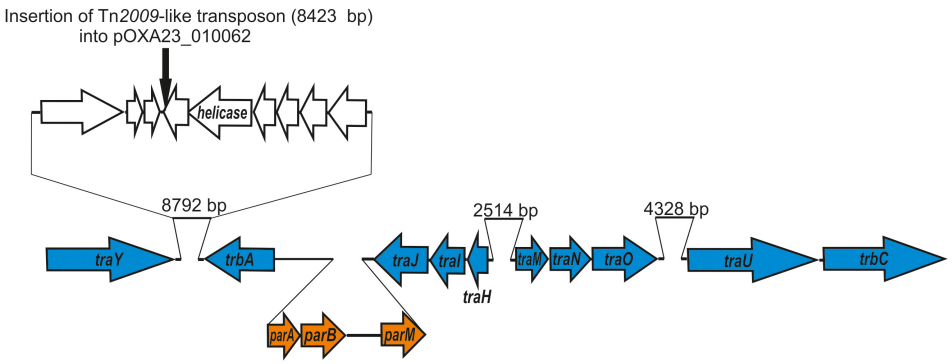

FIGURE 1 | Genetic structure of pALWED1.1 region involved in conjugation. The location and polarity of genes are shown with arrows. Genes of MPF complex are marked in blue; genes encoding partitioning process—in orange. In the top the site of insertion of Tn*2009* (black arrow) into the plasmid pOXA23_010062 is shown.

But with a more careful search we found a candidate protein with low similarity to proteins from pfam01051, presumably including plasmid replication proteins, localized in the plasmid region 228158–229948 (**Figure 2A**). We hypothesize that this particular gene might encode the replication gene. In support of this conclusion, all mega-plasmids from this group contain a gene that is almost identical to the putative *rep* gene of pALWED1.1 in the same region.

Since many plasmid replicons contain directly oriented AT rich sequences near their *rep* genes, iterons, we analyzed the structure of the intergenic region separating the putative *rep* gene of pALWED1.1 from the neighboring genes. It was revealed that a significant part (about 1,200 bp) of this region is rich in adenine and thymine residues (65%). Moreover, at the distance of 830 bp from the start codon of the putative *rep* gene we found 10 tandem repeats, 83–84 bp each (**Figure 2A**). From the 10 copies revealed, three copies are identical, two differ by 1–2 bp, and the rest by 4–14 bp (**Figure 2B**). We found such repeats in all mega-plasmids of the III-4a group, and in all cases their number and relative location remain unchanged. Therefore, we assumed that these repeats are plasmid iterons.

It should be noted that most of previously described iterons are 17–22 bp long, and they are located at a close distance (5–200 bp) from the starting codon of the *rep* gene. The number of their copies is usually 4–5 (Bertini et al., 2010), sometimes more (Konieczny et al., 2014). However, significantly longer iterons were found in some plasmids (Page et al., 2001; Gilmour et al., 2004; Konieczny et al., 2014). In particular, a replicon containing twelve 80–81 bp iterons located at a distance of about 500 bp from the *rep* (*repHI2*) gene was discovered in the large conjugative plasmid R478 isolated from *Serratia marcesens* (Gilmour et al., 2004), and cloning experiments suggested their functional activity (Page et al., 2001).

Despite the lack of significant sequence similarity between the plasmids R478 and pALWED1.1, these replicons share many similar features: (i) both contain long iterons (81 and 83 bp, respectively); (ii) the number of iterons in both plasmids significantly exceeds the usual number of short iterons (12 and 10 vs. 3–5); (iii) in both plasmids they are located at a considerable distance from the replicase gene (500 and 830 bp, respectively); (iv) in both plasmids, iterons are located in the region adjacent to the initiation codon of the replicase gene (**Figure 2**). This suggests that we did probably succeed in identifying the replicon of mega-plasmids of the III-4a group.

Backbone Region of Megaplasmids

The region occupied by the genes of the conjugative complex is highly homologous in all mega-plasmids (**Supplementary Table 2**). In addition, a significant portion of the region located between the replication initiation control locus and the conjugative complex genes in pALWED1.1 (228.2–287.6 kb) is also present in all related plasmids. **Figure 3** shows, using the example of plasmid pAHTJR1, which genes from this region are present in most related plasmids, and which can be replaced. Thus, the main region of this group of mega-plasmids has a total length of 85.2 kb: 1–25 kb (25.8 kb, conjugative genes) and 228.2–287.6 kb (59.4 kb), in the coordinates pALWED1.1 (**Figure 3**). It is also noteworthy that the non-homologous regions of pALWED1.1 are occupied by heavy metal resistance genes, while those of pAHTJR1 are occupied by antibiotic resistance genes.

Accessory Regions of Group III-4a Plasmids Carrying Resistance Genes

To obtain more detailed information on the molecular structure and properties of this group of mega-plasmids, we carried out comparative genomic analysis of the 28 plasmids in the size range of 200–300 kb with backbones closely related to those of pALWED1.1 found in the GenBank databases as of April 1, 2021 (**Table 3**). The main attention was given to the identification of antibiotic and heavy metal resistance determinants and mobile elements that contribute to their spread, and to the study of the conjugative and mobilization properties of these plasmids.

Bioinformatic analysis conducted by Ghaly et al. (2020) showed that different variants of the group III-4a plasmids from strains living within the same geographical region usually have a similar structure of accessory regions, whereas in their core genomes they are often evolutionarily distant members of group III-4a. In addition, the authors provided a brief characterization of the accessory regions of group III-4a plasmids, including

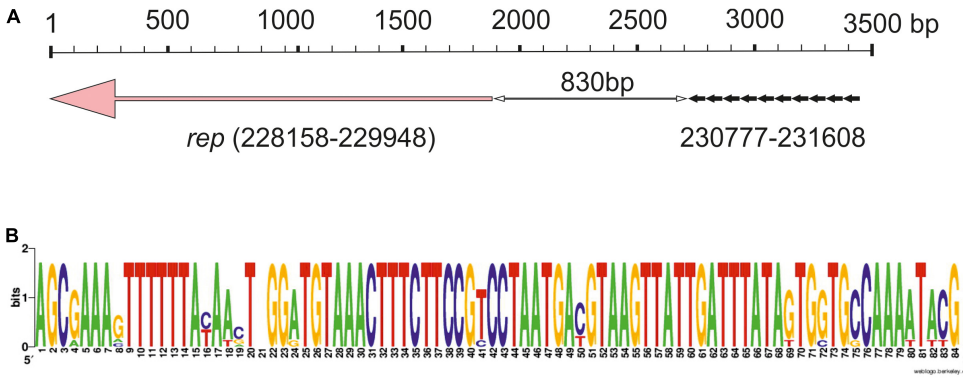

FIGURE 2 | Iteron-controlled putative replicon of pALWED1.1. **(A)** The relative location of the replication initiator gene and the iterons. Pink arrow indicate the *rep* gene, little black arrows indicate surrounding repeat sequences (iterons). **(B)** Consensus sequence of the iterons of pALWED1.1.

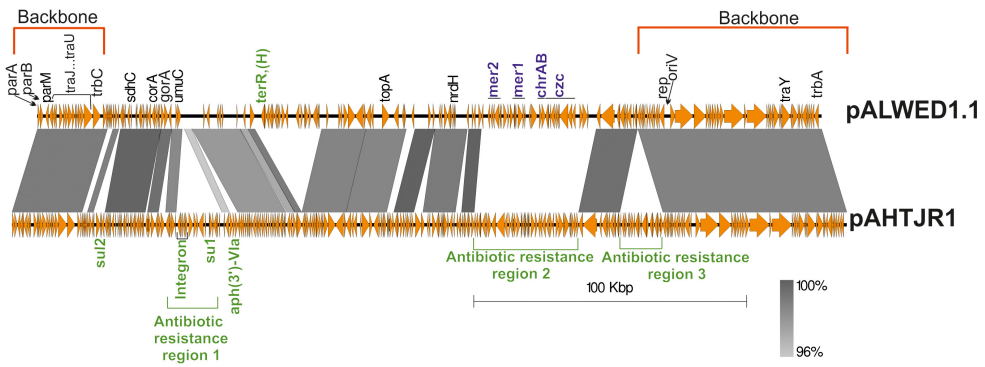

FIGURE 3 | Comparative linear map of plasmids pALWED1.1 and pAHTJR1. The location and polarity of genes and ORFs are shown with arrows. The extent of homologous regions is indicated in the dark gray shading. The backbones regions of plasmids are delimited by square red brackets and antibiotic resistance regions in pAHTJR1—by green. Antibiotic resistance genes are colored in green and genes of resistance to salts of heavy metals—in blue. Antibiotic resistance region 1 contains integron with the cassette genes *arr-3*- (rifamycine resistance) and *aacA4* (aminoglycoside resistance) and the gene *aph(3′′)-V1a* (aminoglycoside resistance). Antibiotic resistance region 2 contains the genes *oxa58* (carbapenem resistance), the *msrE* and *mphE* (macrolide resistance) and the *floR* (phenicol resistance). Antibiotic resistance region 3 contains the aminoglycosides resistance genes *aph(3′′)-1b* and *aph(6) -1d* and tetracycline resistance genes *tet*(Y) and *tetR*. Other genes: *sdhC*, succinate dehydrogenase, cytochrome b556 subunit; *corA*, magnesium and cobalt transport protein CorA; *gorA*, glutathione-disulfide reductase; *umuC*, DNA polymerase V subunit UmuC; *topA*, topoisomerase IA; *nrdH*, putative NrdH-redoxin family protein.

the total number and distribution of antibiotic resistance genes and associated mobile genetic elements (integrons and MITEs, miniature inverted-repeat transposable elements), as well as heavy metal resistance genes (Ghaly et al., 2020). In this paper, we focus on some features of the genetic structure of the accessory regions of plasmids of this group not described previously.

It was revealed that while having similar backbone regions, the plasmids differ significantly in the structure of accessory regions. Thus, some plasmids (7 out of 28) retain the mercury resistance operon(s) in their genome (**Supplementary Table 3**) that are part of remnants of transposons that are unable to transpose (Kholodii et al., 2004). At the same time, all plasmids contain genes for resistance to various antibiotics, the set of which differs in various plasmids. It was shown that most clinical plasmids contain a kanamycin resistance transposon (Tn*aph6*), two plasmids (pOXA23_010062 and pAS74-1) contain the transposon Tn*2009* with the bla_{OXA-23} gene, 14 from 20 plasmids don't carrying mercury resistance determinants contain classI integrons with various set of antibiotic resistance genes (**Supplementary Table 3** and **Figure 4**). It should be noted that most of the integrons are flanked by 439 bp MITEs likely facilitating mobilization of the integron by transposition (Gillings et al., 2009; Domingues et al., 2011, 2013).

The most complex mosaic structure was revealed in the plasmid pXBB1-9 (Zong, 2014), containing a complex Tn*402*-like class 1 integron (Ia) with the *arr3* and *aacA4* cassettes. In addition, it contains a 5.7 kb fragment with IS*CR1* and the metallo-beta-lactamase (bla_{PER1}) gene. The same genetic element (type Ia) is found in the plasmids pAHTJR1 and pOXA58_010055 (**Supplementary Table 3**). The mechanism of the acquisition of the IS*CR1*-bla_{PER-1} region is not completely clear (Zong, 2014).

The rest of the integrons present in plasmids of group III-4a have a standard structure, except that they contain MITE elements on the flanks. The integrons differ between themselves in the number and set of gene cassettes (**Supplementary Table 3** and **Figure 4**). Sometimes one of the MITE copies

TABLE 3 | List of pALWED1.1-related mega-plasmids.

Strain	Plasmid	Size, bp	Source	Country/Region	Accession number
A. lwoffii ED23-35	pALWED1.1	287,631	Permafrost	Russia: Kolyma	KX426227.1
A. haemolyticus TJR01	pAHTJR1	306,131	Human	China: Tianjin	CP038010.1
A. pittii 2014N21-145	p2014N21-145-1	323,995	Human	Taiwan	CP033569.1
A. pittii C54	pC54_001	256,887	Human	Australia: Sydney	CP042365.1
A. johnsoni Acsw19	pAcsw19-2	351,885	Sewage	China: Luzhou	CP043309.1
Acinetobacter sp. WCHA55	pOXA58_010055	372,328	Sewage	China: Sichuan, Chengdu	CP032285.1
A. baumannii 34AB	p34AB	277,864	Pig (caecum at slaughter)	China: Jiangsu	MK134375.1
A. pittii 2014S07-126	p2014S07-126-1	284,051	Human	Taiwan	CP033531.1
A. wuhouensis WCHAW010062	pOXA23_010062	311,749	Sewage	China: Sichuan, Chengdu	CP033130.1
A. defluvii WCHA30	pOXA58_010030	355,075	Hospital sewage	China: Chengdu, Sichuan	CP029396.2
A. johnsoni XBB1	pXBB1-9	398,857	Hospital sewage	China: Chengdu, Sichuan	CP010351.1
A. baumannii E47	pE47_001	327,867	Hospital, room 7	Australia: Sydney	CP042557.1
A. ursingii RIVM0051	pRIVM0051_IMP-4	259,278	Human	Netherlands: Bilthoven	MH220286
A. ursingii RIVM0002	pRIVM0002_IMP-4	317,191	Human	Netherlands: Bilthoven	MH220285
A. ursingii RIVM0061	pRIVM0061_IMP-4	313,407	Human	Netherlands: Bilthoven	MH220287
A. baumannii ABF9692	pABF9692	264,805	Duck	China: Guangdong province	CP048828.1
A. pittii AP43	pAP43-OXA58-NDM1	268,263	Human	China: Hangzhou	CP043053.1
A. seifertii AS4	pAS4-1	276,086	Human	Taiwan	CP061688.1
A. seifertii AS23	pAS23-1	290,682	Human	Taiwan	CP061673.1
A. seifertii AS70	pAS70-1	281,459	Human	Taiwan	CP061572.1
A. seifertii AS74	pAS74-1	336,046	Human	Taiwan	CP061557.1
A. nosocomialis	pWM08B	255,232	Human	Australia	MT742183
A. lwoffii	pR4WN_12CE1	270,906	Prawn	East Australian Fisheries	MT742180
Acinetobacter sp. TTH0-4	pR4WN_IBD1	284,751	Prawn	East Australian Fisheries	MT742182
A. johnsoni	pR4WN_E10B	259,080	Prawn	East Australian Fisheries	MT742181
A. pittii JXA13	pHNJXA13-1	206,931	Dog	China; Nanchang	CP054138
A. baumannii ABF9692	pAB9692	264,805	Trachea of duck	China	CP048828.1
Acinetobacter sp. CS-2	unnamed2	283,930	Hospital wastewater	China	CP67021.1

is absent (for instance, see integron type II in the plasmid pC54_001 from A. *pittii* C54, **Figure 4**). In most cases, plasmids contain a single integron. The exceptions are plasmids found in *A. ursingii* strains which contain two or three different integrons. For example, three integrons of plasmid pRIVM0061_IMP-4 from strain RIVM0061 of *A. ursingii* contain cassette genes *arr-3-aacA4*, *IMP-4-aacA4-catB3*, and bla_{PSE}, correspondingly (**Supplementary Table 3**). In this case, the first of the integrons (type I) is located at a considerable distance from the other two (types II and V), located next to each other. Noteworthy, both MITE copies in second and third integrons are absent. It should be also noted that two from three integrons contain distinct genes for beta lactam resistance (bla_{IMP-4}; bla_{PSE}), encoding functionally different proteins.

It is interesting to note that the type VIII intregron, which was only found in plasmids pR4WN_12CE1, pR4WN_IBD1 and pR4WN_E10B from prawns, contain four cassette genes and three of them unrelated to antibiotic resistance and possibly involved in the cell metabolism. These were *msrA* and *msrB*, encoding peptide methionine sulfoxide reductase, the gene encoding an organic cation transport protein that mediates the transport of organic cations across the cell membrane, and *aadA* responsible to streptomycin/spectinomycin resistance encoding aminoglycoside 3′′-adenyl-transferase. Interestingly, while the *msrA* and *msrB* genes are commonly found in plasmids or in chromosomes (Koepsell et al., 2003), we could not find the gene encoding the organic cations transport protein in *Acinetobacter* strains, apart from this integron found in strains inhabiting prawns. It can be assumed that the transport protein contributes to the survival of the corresponding *Acinetobacter* strains in prawns.

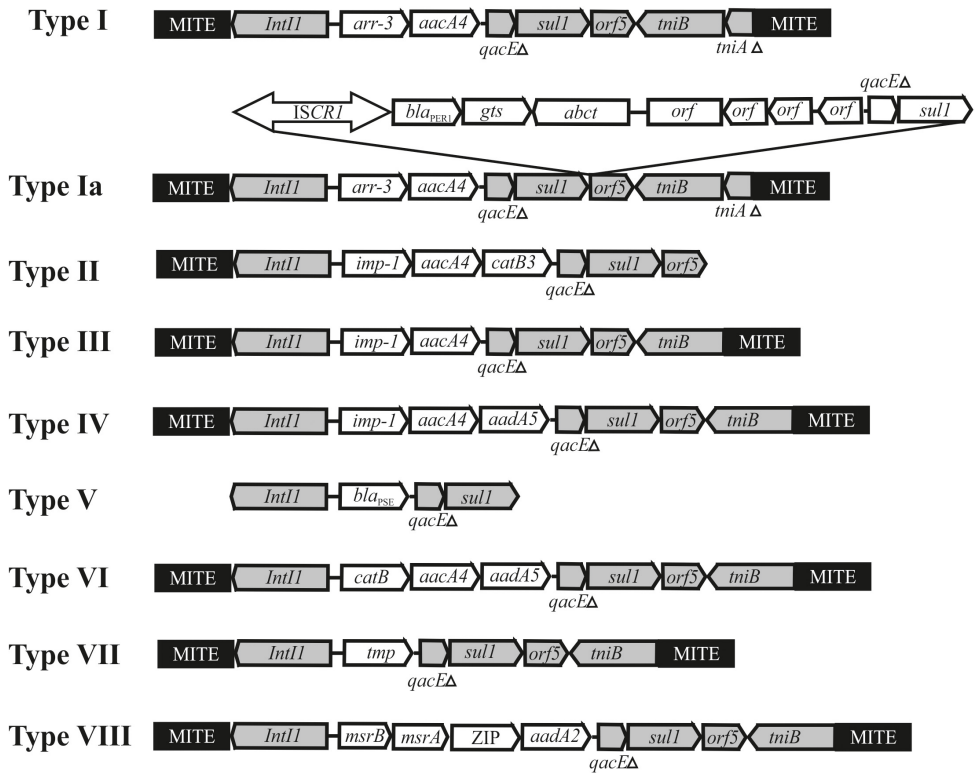

FIGURE 4 | Genetic structure of integrons found in Acinetobacter mega-plasmids belonging to the group III-4a. The location and polarity of genes are shown with arrows. The conserved regions of integrons: 5′-conserved segment—intI1-integrase and 3′-conserved segment—*qacE*Δ, *sul1*, *orf5*, *tniB*, *tniA*Δ. Cassette genes: *arr3*—rifamycin-resistance; *aacA4*, *aadA2* and *aadA5*—aminoglycoside resistance; *catB*, *catB3*—phenicols resistance; bla_{PSE}—beta-lactam resistance; *imp-1*—metallo-β-lactamase, *msrA* and *msrB*—peptide methionine sulfoxide reductase, ZIP-cation transport. MITE–a miniature inverted-repeat transposable elements facilitating mobilization of integron by transposition. Other elements: IS*CR1*-bla_{PER-1} contains gene bla_{PER-1} encoding beta-lactamase.

While nine plasmids related to plasmid pALWED1.1 did not contain integrons, they were also characterized by multiple resistance to antibiotics, due to the presence of transposons and various determinants of resistance. At the same time, most plasmids of this group lacked the determinants of resistance to mercury or other heavy metals, and some contained incomplete sets of the metal resistance genes.

Due to the diversity of the mega-plasmid habitat, we tried to determine the presence / absence of a relationship between the habitat conditions of plasmids and the structure of their genome. For this purpose, two groups of mega-plasmids were selected and compared: (1) plasmids originating from clinical strains of *Acinetobacter* isolated from humans (13 strains) and (2) plasmids originating from environmental strains from sewages and permafrost (7 strains). Although this division into groups is quite conditional, clear differences between strains of the two groups were revealed. Most of the strains of the first group (10 out of 13) contained integrons and only three of them were characterized by resistance to mercury. In contrast, the majority of plasmids of the second group (5 from 7) did not contain integrons and the most of them were resistant to mercury (5 from 7). It should be noted that all modern plasmids were characterized by multiple resistance to antibiotics unlike a permafrost plasmid. Nevertheless, plasmids from wastewater on average contained 1–2 less resistance genes than those isolated from humans. Thus, it can be assumed that the process of adaptation of environmental *Acinetobacter* strains to the existence in the clinic was accompanied by the loss of resistance to mercury and the acquisition of integrons and of multiple resistance to antibiotics. This was achieved by inserting various mobile elements (transposons, integrons) into the plasmid genome. Interestingly, some plasmids contain two and even three integrons.

Distribution of Group III-4a Plasmids Among Modern Strains

We analyzed the distribution of plasmids from the group III-4a among modern strains of *Acinetobacter*. It was previously shown that these plasmids are widely found in the sequenced genomes of clinical strains of *Acinetobacter* (Ghaly et al., 2020; Mindlin et al., 2020). It should be noted that the number of complete genomes of plasmids of group III-4a is growing rapidly: in addition to 21 mega-plasmids present in the fall of 2020 (Ghaly et al., 2020), 7 more sequences were added until April 1, 2021, thus bringing their total number to 28 (**Table 3**). In addition, we found the *trbC* and putative *rep* genes, belonging to the backbone region of

the mega-plasmids of this group, in unassembled genomes of 59 *Acinetobacter* strains deposited in the GenBank (**Supplementary Table 4**). Since most *Acinetobacter* strains in the database are of clinical origin, we also screened our collection of *Acinetobacter* environmental strains for the group III-4a plasmids (section "Materials and Methods"). Of the 56 tested strains 14 contained simultaneously the *trbC* and putative *rep* genes highly similar to pALWED1.1 (**Supplementary Table 1**). Thus, plasmids from group III-4a are widely distributed among both clinical and environmental strains of *Acinetobacter*.

Functional Activity of Plasmids From Group III-4a

We previously showed that the plasmid pAWED1.1 not only moves itself with a frequency of 8×10^{-3} from the original strain of *A. lwoffii* ED23-35 to the cells of *A. baylyi* BD413rif, but also mobilizes the small plasmid pALWED1.8 (MOB_{HEN} family, group I-2b) contained in the same strain, with a similar frequency of 3×10^{-3} (Kurakov et al., 2016). In this work, we investigated the ability of pAWED1.1 to mobilize *Acinetobacter* plasmids belonging to different groups of the MOB_Q family (**Table 1**), according to the classification of mobilizable plasmids developed by us (Mindlin et al., 2020), and also checked the conjugation activity of other plasmids from group III-4a.

It was found that pALWED1.1 was able to mobilize all the small *Acinetobacter* plasmids studied, although mobilization events were less efficient than conjugative transfer, which is consistent with the observations of Brasch and Meyer (1986). The frequency of mobilization was different (**Table 4**). The transfer of the pALWVS1.4 plasmid occurred with a frequency, which was 20 times lower than that of pALWED1.1 itself, while the frequency of transfer of the p7_010062 plasmid was 100 times lower. We also tested the possibility of mobilizing a wide-host range plasmid RSF1010, whose derivatives are widely distributed in clinical strains of various gamma-proteobacteria. Plasmid pALWED1.1 did not mobilize RSF1010. Hence, the pALWED1.1 conjugation system is able to mobilize only *Acinetobacter* plasmids that belong to different groups of the MOB_Q and MOB_{HEN} families.

The backbone regions of all mega-plasmids belonging to group III-4a includes genes of the conjugative complex (**Supplementary Table 2**). Unfortunately, the ability of these plasmids to conjugate has not been previously investigated. Since, in addition to pALWED1.1, we had at our disposal another related mega-plasmid with a known nucleotide sequence, pOXA23_010062, we also determined its conjugation transfer frequency. The conjugation transfer of the pOXA23_010062 occurred at a frequency of 2.0×10^{-7}, which is four orders of magnitude less than that of pALWED1.1. The reason for this was established by a detailed comparison of the structure of the genomes of the two plasmids. It turned out that the pOXA23_010062 genome, in contrast to pALWED1.1, contained an insertion of the Tn*2009*-like transposon carrying the bla_{OXA23} gene (**Figure 1**). It is essential that the insertion occurred into a gene located next to the *traY* gene, i.e., in the region where the main genes of the conjugative complex are located. At the same time, the available data on the widespread distribution of closely related mega-plasmids leave no doubt that most of them are highly conjugative.

To confirm this assumption, we tested the ability of seven strains in which we found genes *trbC* and *rep* similar to pALWED1.1 (see above) to transmit their resistance markers due to conjugation. It turned out that all strains are able to transmit markers of resistance to mercury or antibiotics to the *A. baylyi* BD413 (**Table 5**). In most strains, the transfer frequency was similar to pALWED1.1, and in two, NC13-1 and LS12-1, it was drastically reduced. Perhaps this is related with the presence of changes in the structure of their *tra* operons, similar to what we found in pOXA23_010062. All the data obtained indicate that the majority of plasmids from group III-4a are active disseminators of genetic information between cells of different strains of *Acinetobacter* both in the clinical and environmental settings.

TABLE 4 | Mobilization of different small plasmids by pALWED1.1.

Mating		Transconjugants frequency (per recipient)*		Ratio
Donor	**Recipient**	**pALWED1.1 (A)**	**Small plasmids (B)**	**A/B**
BD413rif (p7_010062 + pALWED1.1)	BSW27-2nal	2.6×10^{-4}	2.3×10^{-6}	116
BD413rif (pALWVS1.4 + pALWED1.1)	BSW27-2nal	6.8×10^{-4}	2.9×10^{-5}	23
BD413rif (pALWED 3.5 + pALWED1.1)	BSW27-2nal	3.0×10^{-3}	4.0×10^{-5}	75
BD413rif (RSF1010 + pALWED1.1)	BSW27-2nal	6.0×10^{-4}	$<1\times10^{-8}$	–

**Average of three experiments.*

TABLE 5 | Frequency of conjugative transfer of environmental plasmids from the group III-4a.

Mating		Transconjugants frequency (per recipient)*
Donor	**Recipient**	
ED45-25	BD413rif	4.5×10^{-3}
KHP18	BD413rif	2.5×10^{-3}
NC13-1	BD413rif	1.5×10^{-6}
LS12-1	BD413rif	2.3×10^{-7}
Z13-16	BD413rif	2.2×10^{-1}
W14	BD413rif	5.5×10^{-2}
ANS7-7 (Tc-R)	BD413rif	2.7×10^{-3}
ANS7-7 (Str-R)	BD413rif	6.2×10^{-2}
WCHAW010062	BD413rif	2.0×10^{-7}

**Average of three experiments. To rule out that the transconjugants were not spontaneous rifampicin mutants of donor cells the morphological characters of isolated colonies from matings and donor cells were compared because these in parental strains are differed significantly.*

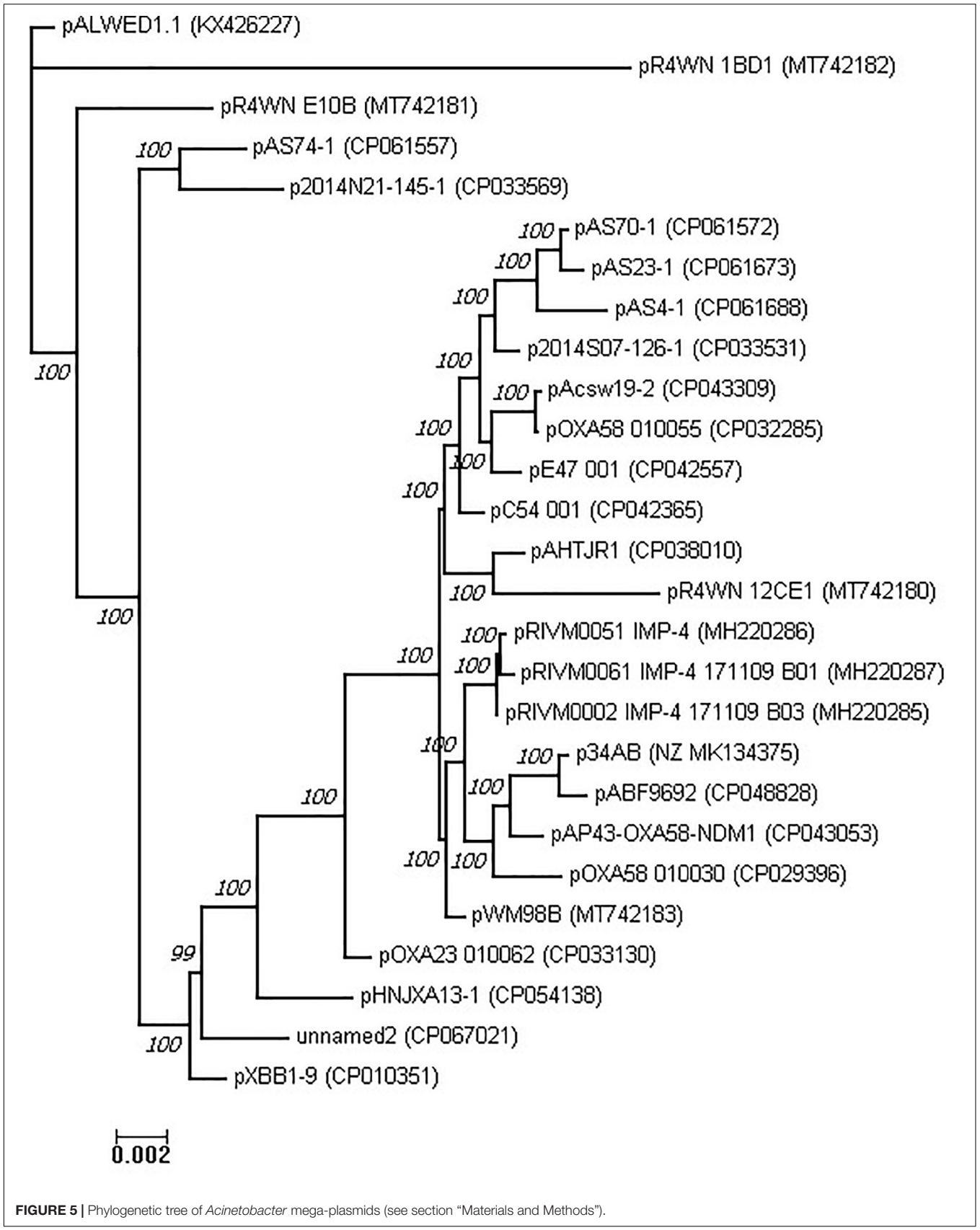

FIGURE 5 | Phylogenetic tree of *Acinetobacter* mega-plasmids (see section "Materials and Methods").

Phylogeny and Evolution of the Plasmids Belonging to the Group III-4a

Previously, Ghaly et al. (2020) used a total of eight genes belonging to the plasmid core genome for phylogenetic analysis of the group III-4a plasmids. In our analysis, we constructed multiple alignment of the complete genomes of 28 plasmids of this group. The concatenated alignment was 352,008 bases in length. This alignment was used to construct a phylogenetic tree of the group III-4a plasmids (**Figure 5**). In general, the topology of the tree obtained by us coincides with the topology of the tree obtained in the previous work on eight genes.

Apparently, most modern plasmids found in clinical and veterinary isolates share a common ancestor. Nevertheless, judging by the topology of the tree, there are several variants of such plasmids, some of which are found in the clinic and some in nature. It is noteworthy that the environmental variants of the representatives of group III-4a are quite remote from all clinical variants, and the most remote of them is pALWED1.1, isolated from permafrost aged forty thousand years.

DISCUSSION

The role of plasmids as the main genetic elements involved in the process of horizontal gene transfer has been repeatedly demonstrated by various researchers (Stokes and Gillings, 2011; Martins et al., 2015; Da Silva and Domingues, 2016; Pagano et al., 2016). This is especially evident in acinetobacters, which are characterized by the presence of numerous plasmids in one strain (Feng et al., 2016; Brovedan et al., 2019; Veress et al., 2020). Recently, a novel family of mega-plasmids, designated group III-4a, was discovered, which are ubiquitous among various strains and species of the *Acinetobacter* genus (Ghaly et al., 2020; Mindlin et al., 2020). It turned out that these mega-plasmids are characterized by multiple drug resistance due to the presence of various transposons and integrons in their genomes, along with individual resistance genes. Various combinations of resistance determinants were observed in different members of the group, with a significant diversity in the composition of accessory regions in different plasmids (Ghaly et al., 2020). The role of these plasmids in the propagation of resistance genes among various species of *Acinetobacter* genus was also demonstrated (Ghaly et al., 2020).

In this work, we have filled important gaps left by the previous studies. In particular, a previously unknown replication initiator *rep* gene was in the region 228158–229948 bp of pALWED1.1. The identity of the *rep* gene is confirmed by: (1) the presence of almost identical genes in all mega-plasmids (2) the presence of iterons in the vicinity of the putative replicase gene; (3) the relationship of the putative Rep to the proteins members of the pfam01051, presumably including replicases. Obviously, further research is needed to definitively prove that the selected gene encodes a replication initiator protein.

Despite the fact that we were able to identify a number of genes of the conjugative complex, a relaxase gene related to the known ones was not found in mega-plasmids from the III-4a group. Since other plasmids are known, in which relaxases have not been found (Smillie et al., 2010; Hu et al., 2017; Hamidian et al., 2016), it can be assumed that a larger diversity of relaxases exists in nature that remain to be identified in future studies.

We performed comparative analysis of the structure of the accessory region in 28 sequenced mega-plasmids of III-4a group (**Supplementary Table 3**). Some of these were isolated from clinical specimens, others from waste water, and the rest from various animal and environmental sources. The main differences between modern plasmids from the III-4a group from the ancient plasmid pALWED1.1 are (1) the complete or partial absence of determinants of resistance to heavy metal salts, and (2) the presence of multiple determinants of resistance to antibiotics. At the same time, the backbone regions of these plasmids are highly homologous.

Analysis of *Acinetobacter* whole-genome shotgun contigs of clinical strains deposited in the Genbank showed that plasmids belonging to the group III-4a are present in 59 genomes. In the collection of environmental *Acinetobacter* strains, group III-4a plasmids are also found in more than 20% of the strains, including ancient isolates from permafrost. The discovery of this group of plasmids in the permafrost samples indicates their wide distribution long before the use of antibiotics. Most likely, similarly to pALWED1.1, ancient plasmids of this group contained various determinants of resistance to heavy metals, since such genes predominate in the composition of large plasmids of five *A. lwoffii* strains isolated from permafrost (Mindlin et al., 2016). After the beginning of the use of antibiotics, the selection of plasmid variants that already contained drug resistance genes or acquired them by horizontal gene transfer, with simultaneous loss of metal resistance genes, has begun. Subsequently, they repeatedly and independently acquired different versions of integrons, which facilitated the process of adaptation to the clinical conditions of the host strains.

CONCLUSION

In this work we studied the structure of basic region of multiply resistant mega-plasmids of acinetobacters belonging to the recently discovered group (lineage) named III-4a. A previously unknown gene encoding a replication initiator protein was identified, with 10 copies of 82–83 bp iterons next to it. A number of genes involved in the process of plasmid conjugation and belonging to the MOB_F family were also identified. The ability of mega-plasmids both to conjugate and to mobilize small *Acinetobacter* plasmids was demonstrated in mating experiments.

Our analysis showed that all sequenced mega-plasmids of this group have a common region of about 85 kb, which includes not only the genes responsible for replication, maintenance and conjugation transfer, but also additional genes not identified until now. It was shown that accessory regions of plasmids contain adaptive genes, including genes for antibiotic resistance, the set of which varies depending on the conditions of existence of the host strain.

Phylogenetic analysis revealed that all clinical and some modern environmental plasmids form one large branch, while most environmental plasmids, including ancient ones, are much more diverse. Our data clearly indicate that conjugative plasmids from group III-4a are widely distributed on all continents,

including Antarctica, not only in clinical but also in natural habitats. Such plasmids were also widely and universally distributed tens of thousands years ago. These data, in addition to those obtained earlier (Petrova et al., 2014; Mindlin et al., 2020) add new evidence of the origin of mobile elements of modern clinical bacteria from those of environmental bacteria.

DATA AVAILABILITY STATEMENT

The datasets presented in this study can be found in online repositories. The names of the repository/repositories and accession number(s) can be found in the article/ **Supplementary Material**.

AUTHOR CONTRIBUTIONS

SM had the initial idea, which was developed into a project together with MP. ZZ isolated the strain *A. wuhouensis* WCHAW010062 and SM, MP isolated the other strains used in the research. AM, AB, ZZ, and MP conducted the sequencing, assembly of plasmids, and genome annotation. OM conducted a plasmid screening among a collection of environmental *Acinetobacter* strains. OM and VN conducted the experiments on conjugation and mobilization. AM, AB, and MP performed the bioinformatic analysis. SM, OM, and MP designed the tables. AB and MP processed the figures. SM, MP, and AM wrote the manuscript. All authors approved the submitted version.

FUNDING

This research was supported by the Ministry of Education and Science of Russian Federation within the framework of the Kurchatov Genome Center development Program.

ACKNOWLEDGMENTS

We are grateful to Alexander Nemec for the provided strain *A. wuhouensis* WCHAW010062 and to A. Kulbachinskiy for helpful comments and suggestions.

SUPPLEMENTARY MATERIAL

The Supplementary Material for this article can be found online at: https://www.frontiersin.org/articles/10.3389/fmicb.2021.728644/full#supplementary-material

Supplementary Table 1 | Screening of pALWED1.1 plasmid among environmental *Acinetobacter* strains.

Supplementary Table 2 | Identification of backbone region genes in genomes of modern plasmids related to pALWED1.1 (summary information for 27 modern plasmids).

Supplementary Table 3 | Characteristics of *Acinetobacter* conjugative mega-plasmids.

Supplementary Table 4 | *rep* and *trbC* genes of pALWED1.1 in whole genome shotgun sequences.

REFERENCES

Altschul, S. F., Madden, T. L., Schäffer, A. A., Zhang, J., Zhang, Z., Miller, W., et al. (1997). Gapped BLAST and PSI-BLAST: a new generation of protein database search programs. *Nucleic Acids Res.* 25, 3389–3402. doi: 10.1093/nar/25.17.3389

Bertini, A., Poirel, L., Mugnier, P. D., Villa, L., Nordmann, P., and Carattoli, A. (2010). Characterization and PCR-based replicon typing of resistance plasmids in *Acinetobacter baumannii*. *Antimicrob. Agents Chemother.* 54, 4168–4177. doi: 10.1128/AAC.00542-10

Brasch, M. A., and Meyer, R. J. (1986). Genetic organization of plasmid R1162 DNA involved in conjugative mobilization. *J. Bacteriol.* 167, 703–710. doi: 10.1128/jb.167.2.703-710.1986

Brovedan, M., Repizo, G. D., Marchiaro, P., Viale, A. M., and Limansky, A. (2019). Characterization of the diverse plasmid pool harbored by the blaNDM-1- containing *Acinetobacter bereziniae* HPC229 clinical strain. *PLoS One* 14:e0220584. doi: 10.1371/journal.pone.0220584

Brovedan, M. A., Cameranesi, M. M., Limansky, A. S., Morán-Barrio, J., Marchiaro, P., and Repizo, G. D. (2020). What do we know about plasmids carried by members of the *Acinetobacter* genus? *World J. Microbiol. Biotechnol.* 36:109. doi: 10.1007/s11274-020-02890-7

Da Silva, G. J., and Domingues, S. (2016). Insights on the horizontal gene transfer of carbapenemase determinants in the opportunistic pathogen *Acinetobacter baumannii*. *Microorganisms.* 4:29. doi: 10.3390/microorganisms4030029

Domingues, S., Nielsen, K. M., and da Silva, G. J. (2011). The blaIMP-5-carrying integron in a clinical *Acinetobacter baumannii* strain is flanked by miniature inverted-repeat transposable elements (MITEs). *J. Antimicrob. Chemother.* 66, 2667–2668. doi: 10.1093/jac/dkr327

Domingues, S., Toleman, M. A., Nielsen, K. M., and da Silva, G. J. (2013). Identical miniature inverted repeat transposable elements flank class 1 integrons in clinical isolates of *Acinetobacter* spp. *J. Clin. Microbiol.* 51, 2382–2384. doi: 10.1128/JCM.00692-13

Feng, Y., Yang, P., Wang, X., and Zong, Z. (2016). Characterization of *Acinetobacter johnsonii* isolate XBB1 carrying nine plasmids and encoding NDM-1, OXA-58 and PER-1 by genome sequencing. *J. Antimicrob. Chemother.* 71, 71–75. doi: 10.1093/jac/dkv324

Francia, M. V., Varsaki, A., Garcillán-Barcia, M. P., Latorre, A., Drainas, C., and la Cruz, F. (2004). A classification scheme for mobilization regions of bacterial plasmids. *FEMS Microbiol. Rev.* 28, 79–100. doi: 10.1016/j.femsre.2003.09.001

Garcillán-Barcia, M. P., Francia, M. V., and de la Cruz, F. (2009). The diversity of conjugative relaxases and its application in plasmid classification. *FEMS Microbiol. Rev.* 33, 657–687. doi: 10.1111/j.1574-6976.2009.00168.x

Ghaly, T. M., Paulsen, I. T., Sajjad, A., Tetu, S. G., and Gillings, M. R. (2020). A novel family of *Acinetobacter* mega-plasmids are disseminating multi-drug resistance across the globe while acquiring location-specific accessory genes. *Front Microbiol.* 11:605952. doi: 10.3389/fmicb.2020.605952

Gillings, M. R., Labbate, M., Sajjad, A., Giguère, N. J., Holley, M. P., and Stokes, H. W. (2009). Mobilization of a Tn402-like class 1 integron with a novel cassette array via flanking miniature inverted-repeat transposable element-like structures. *Appl. Environ. Microbiol.* 75, 6002–6004. doi: 10.1128/AEM.01033-09

Gilmour, M. W., Thomson, N. R., Sanders, M., Parkhill, J., Diane, E., and Taylor, D. E. (2004). The complete nucleotide sequence of the resistance plasmid R478: defining the backbone components of incompatibility group H conjugative plasmids through comparative genomics. *Plasmid* 52, 182–202. doi: 10.1016/j.plasmid.2004.06.006

Göttig, S., Gruber, T. M., Higgins, P. G., Wachsmuth, M., Seifert, H., and Kempf, V. A. (2014). Detection of pan drug- resistant *Acinetobacter baumannii* in Germany. *J Antimicrob. Chemother.* 69, 2578–2579. doi: 10.1093/jac/dku170

Guzman-Herrador, D. L., and Llosa, M. (2019). The secret life of conjugative relaxase. *Plasmid* 104:102415. doi: 10.1016/j.plasmid.102415

Hamidian, M., Ambrose, S. J., and Hall, R. M. (2016). A large conjugative *Acinetobacter baumannii* plasmid carrying the sul2 sulphonamide and strAB

streptomycin resistance genes. *Plasmid.* 8, 43–50. doi: 10.1016/j.plasmid.2016.09.001

Hamidian, M., and Hall, R. M. (2014). pACICU2 is a conjugative plasmid of *Acinetobacter* carrying the aminoglycoside resistance transposon TnaphA6. *J. Antimicrob. Chemother.* 69, 1146–1148. doi: 10.1093/jac/dkt488

Hu, Y., Feng, Y., Zhang, X., and Zong, Z. (2017). *Acinetobacter defluvii* sp. nov., recovered from hospital sewage. *Int. J. Syst. Evol. Microbiol.* 67, 1709–1713. doi: 10.1099/ijsem.0.001847

Kholodii, G., Mindlin, S., Gorlenko, Z., Petrova, M., Hobman, J., and Nikiforov, V. (2004). Translocation of transposition-deficient (TndPKLH2-like) transposons in the natural environment: mechanistic insights from the study of adjacent DNA sequences. *Microbiology* 150(Pt 4), 979–992. doi: 10.1099/mic.0.26844-0

Koepsell, H., Schmitt, B. M., and Gorboulev, V. (2003). Organic cation transporters. *Rev. Physiol. Biochem. Pharmacol.* 150, 36–90. doi: 10.1007/s10254-003-0017-x

Konieczny, I., Bury, K., Wawrzycka, A., and Wegrzyn, K. (2014). Iteron Plasmids. *Microbiol. Spectr.* 2, doi: 10.1128/microbiolspec.PLAS-0026-2014

Kurakov, A., Mindlin, S., Beletsky, A., Shcherbatova, N., Rakitin, A., Ermakova, A., et al. (2016). The ancient small mobilizable plasmid pALWED1.8 harboring a new variant of the non-cassette streptomycin/spectinomycin resistance gene aadA27. *Plasmid* 84-85, 36–43. doi: 10.1016/j.plasmid.2016.02.005

Llosa, M., and Alkorta, I. (2017). Coupling proteins in type IV secretion. *Curr. Top. Microbiol. Immunol.* 413, 143–168. doi: 10.1007/978-3-319-75241-9_6

Martins, N., Picão, R. C., Adams-Sapper, S., Riley, L. W., and Moreira, B. M. (2015). Association of class 1 and 2 integrons with multidrug-resistant *Acinetobacter baumannii* international clones and *Acinetobacter nosocomialis* isolates. *Antimicrob. Agents Chemother.* 59, 698–701. doi: 10.1128/AAC.02415-14

Mindlin, S., Beletsky, A., Rakitin, A., Mardanov, A., and Petrova, M. (2020). *Acinetobacter* plasmids: diversity and development of classifications strategies. *Front. Microbiol.* 11:588410. doi: 10.3389/fmicb.2020.588410

Mindlin, S., Minakhin, L., Petrova, M., Minakhina, S., Gorlenko, Zh, and Nikiforov, V. (2005). Present-day mercury resistance transposons are common in bacteria preserved in permafrost grounds since the Upper Pleistocene. *Res. Microbiol.* 156, 994–1004. doi: 10.1016/j.resmic.2005.05.011

Mindlin, S., Petrenko, A., Kurakov, A., Beletsky, A., Mardanov, A., and Petrova, M. (2016). Resistance of ancient and modern *Acinetobacter lwoffii* strains to heavy metals and arsenic revealed by genome analysis. *Bio. Med. Res. Int.* 3970831. doi: 10.1155/2016/3970831

Nigro, S. J., and Hall, R. M. (2017). A large plasmid, pD46-4, carrying a complex resistance region in an extensively antibiotic-resistant ST25 *Acinetobacter baumannii*. *J Antimicrob Chemother.* 72, 3496–3498. doi: 10.1093/jac/dkx287

Nigro, S. J., Holt, K. E., Pickard, D., and Hall, R. M. (2015). Carbapenem and amikacin resistance on a large conjugative *Acinetobacter baumannii* plasmid. *J. Antimicrob. Chemother.* 70, 1259–1261. doi: 10.1093/jac/dku486

Pagano, M., Martins, A., and Barth, A. (2016). Mobile genetic elements related to carbapenem resistance in *Acinetobacter baumannii*. *Braz J Microbiol.* 47, 785–792. doi: 10.1016/j.bjm.2016.06.005

Page, D. T., Whelan, K. F., and Colleran, E. (2001). Characterization of two autoreplicative regions of the IncHI2 plasmid R478: rephi2a and RepHI1A (R478). *Microbiology* 147, 1591–1598. doi: 10.1099/00221287-147-6-1591

Peleg, A. Y., de Breij, A., Adams, M. D., Cerqueira, G. M., Mocali, S., Galardini, M., et al. (2012). The success of *Acinetobacter* species; genetic, metabolic and virulence attributes. *PLoS One* 7:e46984. doi: 10.1371/journal.pone.0046984

Petrova, M., Kurakov, A., Shcherbatova, N., and Mindlin, S. (2014). Genetic structure and biological properties of the first ancient multiresistance plasmid pKLH80 isolated from a permafrost bacteria. *Microbiology* 160, 2253–2263. doi: 10.1099/mic.0.079335-0

Petrova, M. A., Mindlin, S. Z., Gorlenko, Z. M., Kaliaeva, E. S., Soina, V. S., and Bogdanova, E. S. (2002). Mercury-resistant bacteria from permafrost sediments and prospects for their use in comparative studies of mercury resistance determinants. *Genetika* 38, 1569–1574.

Salgado-Camargo, A. D., Castro-Jaimes, S., Rosa-Maria Gutierrez-Rios, R.-M., Lozano, L. F., Altamirano-Pacheco, L., Silva-Sanchez, J., et al. (2020). Structure and evolution of *Acinetobacter baumannii* plasmids. *Front. Microbiol.* 11:1283. doi: 10.3389/fmicb.202001283

Sambrook, J., and Russell, D. W. (2001). *Molecular Cloning: A Laboratory Manual, Cold Spring Harbor Laboratory*, 3d Edn. New York NY: Cold Spring Harbor.

Silva, L., Mourão, J., Grosso, F., and Peixe, L. (2018). Uncommon carbapenemase-encoding plasmids in the clinically emergent *Acinetobacter pittii*. *J. Antimicrob. Chemother.* 73, 52–56. doi: 10.1093/jac/dkx364

Smillie, C., Garcillán-Barcia, M. P., Francia, M. V., Rocha, E. P., and de la Cruz, F. (2010). Mobility of plasmids. *Microbiol. Mol. Biol. Rev.* 74, 434–452. doi: 10.1128/MMBR.00020-10

Stokes, H. W., and Gillings, M. R. (2011). Gene flow, mobile genetic elements and the recruitment of antibiotic resistance genes into Gram-negative pathogens. *FEMS Microbiol. Rev.* 35, 790–819. doi: 10.1111/j.1574-6976.2011.00273.x

Sullivan, M. J., Petty, N. K., and Beatson, S. A. (2011). Easyfig: a genome comparison visualizer. *Bioinformatics* 27, 1009–1010. doi: 10.1093/bioinformatics/btr039

Thomas, C. M. (2000). Paradigms of plasmid organization. *Mol. Microbiol.* 37, 485–491. doi: 10.1046/j.1365-2958.2000.02006.x

Touchon, M., Cury, J., Yoon, E. J., Krizova, L., Cerqueira, G. C., Murphy, C., et al. (2014). The genomic diversification of the whole *Acinetobacter* genus: origins, mechanisms, and consequences. *Genome Biol Evol.* 6, 2866–2882. doi: 10.1093/gbe/evu225

Turton, J. F., Shah, J., Ozongwu, C., and Pike, R. (2010). Incidence of *Acinetobacter* species other than A. *baumannii* among clinical isolates of *Acinetobacter*: evidence for emerging species. *J. Clin. Microbiol.* 48, 1445–1449. doi: 10.1128/JCM.02467-09

Veress, A., Nagy, T., Wilk, T., Kömüves, J., Olasz, F., and Kiss, J. (2020). Abundance of mobile genetic elements in an *Acinetobacter lwoffii* strain isolated from Transylvanian honey sample. *Sci. Rep.* 10:2969. doi: 10.1038/s41598-020-59938-9

von Wintersdorff, C. J., Penders, J., van Niekerk, J. M., Mills, N. D., Majumder, S., van Alphen, L. B., et al. (2016). Dissemination of antimicrobial resistance in microbial ecosystems through horizontal gene transfer. *Front. Microbiol.* 7:173. doi: 10.3389/fmicb.2016.00173

Wibberg, D., Salto, I. P., Eikmeyer, F. G., Maus, I., Winkler, A., Nordmann, P., et al. (2018). Complete genome sequencing of *Acinetobacter baumannii* strain K50 discloses the large conjugative plasmid pK50a encoding carbapenemase OXA-23 and extended-spectrum β-lactamase GES-11. *Antimicrob. Agents Chemother.* 62, e212–e218. doi: 10.1128/AAC.00212-18

Zong, Z. (2014). The complex genetic context of blaPER-1 flanked by miniature inverted-repeat transposable elements in *Acinetobacter johnsonii*. *PLoS One.* 9:e90046. doi: 10.1371/journal.pone.0090046

Conflict of Interest: The authors declare that the research was conducted in the absence of any commercial or financial relationships that could be construed as a potential conflict of interest.

frontiers in Cellular and Infection Microbiology

ORIGINAL RESEARCH
published: 11 October 2021
doi: 10.3389/fcimb.2021.738706

LeuO, a LysR-Type Transcriptional Regulator, Is Involved in Biofilm Formation and Virulence of *Acinetobacter baumannii*

Md. Maidul Islam[†], *Kyeongmin Kim*[†], *Je Chul Lee and Minsang Shin*[*]

Department of Microbiology, School of Medicine, Kyungpook National University, Daegu, South Korea

Acinetobacter baumannii is an important nosocomial pathogen that can survive in different environmental conditions and poses a severe threat to public health due to its multidrug resistance properties. Research on transcriptional regulators, which play an essential role in adjusting to new environments, could provide new insights into *A. baumannii* pathogenesis. LysR-type transcriptional regulators (LTTRs) are structurally conserved among bacterial species and regulate virulence in many pathogens. We identified a novel LTTR, designated as LeuO encoded in the *A. baumannii* genome. After construction of LeuO mutant strain, transcriptome analysis showed that LeuO regulates the expression of 194 upregulated genes and 108 downregulated genes responsible for various functions and our qPCR validation of several differentially expressed genes support transcriptome data. Our results demonstrated that disruption of LeuO led to increased biofilm formation and increased pathogenicity in an animal model. However, the adherence and surface motility of the LeuO mutant were reduced compared with those of the wild-type strain. We observed some mutations on amino acids sequence of LeuO in clinical isolates. These mutations in the *A. baumannii* biofilm regulator LeuO may cause hyper-biofilm in the tested clinical isolates. This study is the first to demonstrate the association between the LTTR member LeuO and virulence traits of *A. baumannii*.

Keywords: ***Acinetobacter baumannii*, LeuO, transcriptome (RNA-seq), biofilm, virulence, adherence**

OPEN ACCESS

Edited by:
Paolo Visca,
Roma Tre University, Italy

Reviewed by:
Younes Smani,
Institute of Biomedicine of Seville (IBIS), Spain
Beate Jutta Averhoff,
Goethe University Frankfurt, Germany

***Correspondence:**
Minsang Shin
shinms@knu.ac.kr

[†]*These authors have contributed equally to this work*

Specialty section:
This article was submitted to Molecular Bacterial Pathogenesis, a section of the journal Frontiers in Cellular and Infection Microbiology

Received: *09 July 2021*
Accepted: *23 September 2021*
Published: *11 October 2021*

Citation:
Islam MM, Kim K, Lee JC and Shin M (2021) LeuO, a LysR-Type Transcriptional Regulator, Is Involved in Biofilm Formation and Virulence of Acinetobacter baumannii. Front. Cell. Infect. Microbiol. 11:738706. doi: 10.3389/fcimb.2021.738706

INTRODUCTION

Acinetobacter baumannii is a member of ESKAPE pathogens that primarily affect patients with compromised defense in hospitals (Rice, 2008). Hospital-acquired *A. baumannii* infection can cause bacteremia, urinary tract infection, traumatic skin, and pneumonia (McConnell et al., 2013). Because of the nature of multidrug resistance (MDR), the World Health Organization (WHO) has listed *A. baumannii* as the "top priority" pathogen that requires new therapeutic options (WHO, 2017). *A. baumanni* can survive and persist in harsh environmental conditions in hospital settings, an ability that helps prolong outbreaks of nosocomial infection (Jawad et al., 1998). Numerous virulence factors contribute to successful *A. baumannii* infection, including biofilm formation on biological and innate surfaces (Longo et al., 2014), adherence to and invasion

of host cells (Lee et al., 2006), efflux pumps that extrude different molecules and antibiotics (Kumar and Schweizer, 2005), outer membrane protein A (OmpA) that mediates interaction with epithelial cells (Lee et al., 2010), iron acquisition system (Gaddy et al., 2012), and capsular polysaccharide (Russo et al., 2010). *A. baumannii* pili are a key factor for biofilm formation, and *csuA/BABCDE* chaperone-usher secretion system-mediated pili help planktonic bacteria to adhere onto abiotic surfaces for biofilm formation (Tomaras et al., 2003). Besides abiotic surfaces, *A. baumannii* can attach onto biotic surfaces such as respiratory epithelial cells, which is another important virulence factor for infection (Lee et al., 2008). Quorum sensing in *A. baumannii* is another important pathway by which the pathogen senses extracellular signals and regulates biofilm formation and virulence (Bhargava et al., 2015). However, understanding the molecular mechanisms of virulence factors would help develop novel strategies to prevent multidrug-resistant *A. baumannii* infection.

Transcriptional regulatory proteins help prokaryotes to communicate between environmental conditions and DNA transcription to survive in different habitats (Santos et al., 2009). Bacterial genomes encode several transcriptional regulatory proteins required for adaptive cellular responses belonging to different families, such as ArsR, AsnC, DeoR, GntR, IclR, LacI, LuxR, XylS, MarR, MerR, NtrC, TetR, YedF, and YhdG. Among these, the family of LysR-type transcriptional regulators (LTTRs) is the largest and resemble approximately 16% of the overall transcriptional factors in bacteria (Srinivasan et al., 2013). A typical LTTR comprises an N-terminal DNA-binding helix-turn-helix (HTH) domain and a C-terminal coinducer-binding domain (also known as a regulatory domain). LTTRs can function as either an activator or repressor of single or operonic gene expression, which is why they have been recently termed as global transcriptional regulators (Schell, 1993). LTTRs are associated with the control of various cellular processes. For instance, VirR in *Rhodococcus equi* and MvfR and PA2206 in *Pseudomonas aeruginosa* are involved in virulence and quorum sensing (Russell et al., 2004; Deziel et al., 2005). Moreover, the proteins CidR in *Staphylococcus aureus* and OxyR in *Klebsiella pneumoniae* are involved in antibiotic resistance (Rice et al., 2005; Yang et al., 2005). In *Yersinia pseudotuberculosis*, RovM controls cell invasion, motility, and virulence (Heroven and Dersch, 2006).

LeuO is a member of the LysR family of transcriptional regulators, and members of this family have been investigated in several bacteria, including *Escherichia coli*, *Salmonella enterica*, *Vibrio cholerae*, *Yersinia enterocolitica*, and *Enterobacter cloacae* (Guadarrama et al., 2014). LeuO controls several biological functions such as biofilm formation and virulence in *V. cholerae* and *E. coli*, regulates the expression of OmpS1 and OmpS2, and downregulates the expression of OmpX, which alter the transport of hydrophobic compounds and virulence in *S. enterica* (Moorthy and Watnick, 2005; Hernández-Lucas et al., 2008; Shimada et al., 2011). LeuO regulates a wide variety of genes that are involved in amino acid biosynthesis, nitrogen fixation, quorum sensing, and virulence (Schell, 1993). It also regulates bile tolerance, antibiotic resistance, and promoter binding in *V. cholera* (Bina et al., 2016). However, LeuO has not yet been characterized in *A. baumannii* and its functions also remain unclear.

In this study, to further understand the role of LeuO in *A. baumannii*, we generated a knockout mutant of LeuO and conducted transcriptome analysis to compare the differentially expressed genes between ΔLeuO and wild-type strains. Transcriptome analysis showed that several biological and metabolic pathways are altered after the deletion of LeuO. Our experiments on biofilm formation, surface motility and adherence to epithelial cell suggested that some genes related to these features are directly or indirectly regulated by LeuO. Overall, our study results provide novel understanding about the regulatory role of LeuO and the pathogenesis of *A. baumannii*. This identification of the role of transcriptional regulators may help in the development of novel therapeutics against MDR *A. baumannii* strains.

MATERIALS AND METHODS

Bacterial Strains, Plasmids, and Culture Conditions

A. baumannii ΔLeuO and complementation strains were constructed using the homologous recombination method as described in the supplementary data. *A. baumannii* strains were grown in Luria–Bertani (LB) media at 37°C or 30°C, and agar was added at the indicated concentrations obtained from Difco or Eiken (Eiken Chemical, Tokyo, Japan). Chloramphenicol (20 μg/mL), kanamycin (50 μg/mL), and ampicillin (100 μg/mL) were added to LB broth or LB agar plates to maintain the plasmids in *E. coli*. The bacterial strains, plasmids, and primers used in this study are listed in **Supplementary Tables S3** and **S4**.

Isolation of Bacterial mRNA and RNA Sequencing

Overnight bacterial cultures of both *A. baumannii* ATCC 17978 wild-type and ΔLeuO strains were subcultured in 10 mL of LB by 1:100 dilution and grown at 37°C until OD_{600} reached 1.00 under shaking condition. Total RNA was extracted using Qiagen RNeasy Mini kits (Qiagen, Hilden, Germany) according to the manufacturer's instructions. The total RNA concentration was measured using the NanoDrop 2000 Spectrophotometer (Thermo Fisher Scientific). Two biological replicates of each were sent to Macrogen Inc. (Seoul, Republic of Korea), where mRNA quality control (QC), cDNA library preparation, library QC, template preparation, template QC, and RNA sequencing were performed on the Illumina NovoSeq 6000 platform. RNA-sequencing reads were aligned to the *A. baumanni* strain ATCC 17978 (GCF_ 0000 15 425.1 _ A S M1542v1). Bowtie 1.1.2 (http://bowtie-bio.sourceforge.net/index.shtml) and HTSeq version 0.10.0 software (http://www-huber.embl.de/users/anders/HTSeq/doc/overview.html) were used for analyzing the sequencing data. Any of the sequencing reads with a fold change of <2 and a p value of >0.05 were eliminated.

Quantitative Real-Time PCR for RNA-seq Data Validation

Total RNA from *A. baumannii* strains was isolated as described earlier, and cDNA was synthesized using the M-MLV cDNA Synthesis kit (Enzynomics). Real-time PCR amplification of cDNA was performed using the ABI Step One Plus Real-Time System (Applied Biosystems), and TOPreal^{TM} q-PCR 2X PreMIX (SYBR Green with high ROX, Enzynomics) was used. The internal forward and reverse primers used in this study for each gene are listed in **Supplementary Table S4**. The expression level was standardized relative to the transcription level of 16S rRNA expression level. The fold change was determined using the ΔΔCt method. Experiments were performed in three independent replicates.

Biofilm Formation Assay

Biofilm formation by *A. baumannii* strains was evaluated according to the method described by (Stepanovic et al. (2000) with some modifications using a crystal violet staining assay. Briefly, bacterial strains were cultured overnight, resuspended in fresh LB broth without salt, and adjusted to a turbidity of 1.0 at 600 nm using a spectrophotometer. After dilution, the bacterial suspensions were aliquoted as 2 ml each into 5-mL polystyrene tubes and incubated for 24 h at 30°C under static conditions in a dark room. After the removal of supernatants, the tubes were washed twice with 2 ml distilled water to remove planktonic or loosely adherent cells. After air-drying the tubes for 10 min, 2 mL of crystal violet (0.1% v/v) was added to each tube to stain the inner wall with biofilm for 15 min. The stained biofilms were solubilized with 2 mL of 95% ethanol for 10 min, and 200 μL of each sample was transferred to a 96-well plate to measure turbidity at 570 nm using a microplate reader (Molecular Devices, Sunnyvale, USA.). To compensate for growth differences, turbidity was also measured at 600 nm before staining the biofilm. Three independent experiments were performed, each in triplicate.

Biofilm formation assays using *A. baumannii* 17978 wild-type strain, ΔLeuO strain, and clinical isolates of various sequence types (ST-208, ST-229, ST-357, ST-451, ST-552, and ST-784) were also performed as described earlier with two independent experiments.

Pellicle Formation Assay

Pellicle formation assay was performed based on a method described by Martí et al. (2011). Bacterial strains were cultured overnight in LB broth without salt and diluted at 1:40 with the same media. The assay was performed in 5-ml polypropylene tubes, and 2 ml of bacterial suspensions was aliquoted into each tube with incubation at 30°C for 48 h without shaking. The pellicle film was isolated from the tube by adding 1 ml methanol. The pellicle biomass was measured (optical density at 600 nm [OD_{600}]) after resuspending the pellets in 1 ml PBS. Experiments were performed in triplicates.

Surface Motility Assay

Motility assays were performed as described previously (Clemmer et al., 2011) with some modifications. Modified LB agar containing Eiken agar 3 g/L, tryptone 10 g/L, and yeast extract 5 g/L was autoclaved and cooled at 60°C. Modified LB medium was poured into Petri dishes, dried for 8 h, and used on the same day of preparation. For testing motility, *A. baumannii* strains were grown overnight and adjusted to the same optical density (OD_{600} = 1.0) by adding modified LB broth, and then 2 μL of culture was inoculated onto the center of agar plates. The plates were incubated at 37°C for 10 h, after which the diameter of motility zones was measured. The plates were photographed using a digital imaging system. Assays were performed in triplicate with three biological replicates each time.

Adherence Assay

Bacterial adherence to A549 cells was evaluated as described previously (Lee et al., 2006). Briefly, A549 human alveolar epithelial cells were grown in RPMI 1640 medium (HyClone, Logan, UT) supplemented with 10% heat-inactivated fetal bovine serum (HyClone), 100 U/ml penicillin G, and 50 μg/ml streptomycin. Cultures with 80%–90% confluency were trypsinized and seeded at a density of 2×10^5 cells/ml in 6-well culture dishes to obtain a monolayer. After 24-h incubation, the cells were washed twice with PBS and incubated with RPMI 1640 medium without antibiotics. *A. baumannii* strains were grown to reach an OD A_{600} of 1.0 and suspended in the same media. Then, 2×10^7 CFU/ml of bacteria were added into each well to obtain a multiplicity of infection (MOI) of 1:100 and incubated for 2 h at 37°C. To determine bacterial adhesion, cells were washed five times with PBS and lysed with 0.1% Triton X-100 at 37°C for 20 min. Colony-forming units were counted after 10-fold serial dilution of lysate samples to determine the number of bacteria that had attached to or invaded the A549 cells. Adherence assays were performed in three independent replicates.

In Vivo Virulence Assay

All animal infection experimental procedures were approved by the Animal Care Committee of Kyungpook National University, South Korea (approval number: KNU-2019-178). Briefly, 8-week-old female BALB/c mice were maintained under conventional conditions at five mice per case and allowed access to food and water throughout the experiment. To promote infection, neutropenic mice were induced by intraperitoneal (IP) injection of cyclophosphamide (150 mg/kg) in PBS before bacterial infection (−4 and −1 day). *A. baumannii* 17978 WT, ΔLeuO, CP, and *A. baumannii* 1656-2 WT strains were grown overnight in LB broth at 37°C, washed with PBS, and the concentration was set to 2×10^9 CFU/ml. Mice were injected intraperitoneally with 100 μl PBS (control) and *A. baumannii* strains (1×10^8 CFU/ml) per mice (n = 5 per group). Animals were monitored every 12 h over a period of 4 days. The number of live and dead animals was input into GraphPad Prism, and survival curve was generated. Statistical analysis was conducted using the Kaplan–Meier test in GraphPad Prism.

RESULTS

A. baumannii A1S_1874 Is the LTTR LeuO

LTTRs are organized as an N-terminal HTH DNA-binding domain and a C-terminal effector-binding domain (EBD)

connected by a long linker helix (Muraoka et al., 2003). *A. baumannii A1S_1874* constitutes 306 amino acid residues, and an analysis of the amino acid sequence revealed a DNA-binding domain (HTH, 25–79) and a substrate-binding domain (112–304), indicating that A1S_1874 is a member of the LTTR family (**Figure 1A**). Blast search of the *A1S_1874* amino acid sequence (306 aa) was performed to identify the homology sequence of *A1S_1874* among other *Acinetobacter* strains and other bacterial species. The amino acid sequence was conserved among other sequenced *A. baumannii* strains. Predicted 3D structure of *A1S_1874* elucidated using the Phyre2 and PymoL software program clearly displayed two distinct domains (**Figure 1B**), which support that *A1S_1874* is a putative LTTR. Finally, we compared the amino acid sequence of *A. baumannii A1S_1874* and other gram-negative bacterial LeuO whose functions have already been characterized. The amino acid sequence of *A1S_1874* exhibited 25% sequence homology with *E. coli* LeuO, 24% sequence homology with *S. enterica* LeuO, and 25% sequence homology with *V. navarrensis* LeuO. *A. baumannii A1S_1874* demonstrated high sequence homology at the N-terminal region with other bacterial LeuO protein compared with that at the C-terminal region (**Figure 1C**). LTTRs exhibit low sequence identity among the family members, possibly due to distinct effector recognition. However, the N-terminal region displayed more sequence conservation than the C-terminal region (Schell, 1993). Considering these findings, we predict that *A1S_1874* is LeuO, an LTTR in *A. baumanni*, whose functions must be explored.

Transcriptome Analysis of LeuO Mutant Strain

To characterize LeuO regulation in *A. baumannii* ATCC 17978, we conducted transcriptome profiling of LeuO mutant strain and compared with wild-type strain to obtain insights into the global transcriptomic changes caused by LeuO deletion. The LeuO mutant strain was constructed as described by Jung et al. (2020) (Supplementary data section), and it was confirmed using PCR analysis (**Supplementary Figure S1**). For RNA sequencing, we extracted RNA from cells growing up to an OD_{600} = 1. Differentially expressed genes were selected when the fold change in expression was ≥2 with p values <0.05 (**Figure 2A**). We found that a total of 302 genes were differentially expressed, among which 194 were upregulated and 108 were downregulated compared with those of *A. baumannii* WT and LeuO mutant. The complete list of differentially expressed genes is shown in **Supplementary Table S1**. An acyl carrier protein (locus tag *A1S_0114*) was the highest upregulated differentially expressed gene (fold change 201.60), and a hypothetical protein (locus tag *A1S_0645*) was the highest downregulated gene (fold change −16.02). In *A. baumannii* ATCC 17978, the *A1S_0112-A1S_0119* cluster is the polycistronic operon responsible for biofilm formation and virulence. Our transcriptome data indicated that the *A1S_0112-A1S_0119* cluster was highly upregulated (9.5- to 201.60-fold) in the absence of LeuO. *Csu* operon (CsuA/BABCDE) genes (*A1S_2213-2218*) were also upregulated in the LeuO mutant strain (10.40- to 64.16-fold). Proteins encoded by the *csu* operon have been identified in pellicle and biofilm formation. Quorum sensing–related genes (*A1S_0109-A1S_0111*) were also upregulated after LeuO mutation. Several genes related to iron ion binding and transport such as *A1S_0242*, *A1S_0243*, *A1S_0980*, *A1S_0981*, *A1S_1063*, and *A1S_3369* were also upregulated after LeuO mutation. Some efflux pump–related genes such as the MFS family transporters *A1S_1440* and *A1S_1772* and the RND family transporters *A1S_1649* and *A1S_1773* were also upregulated. Transcriptional regulators of

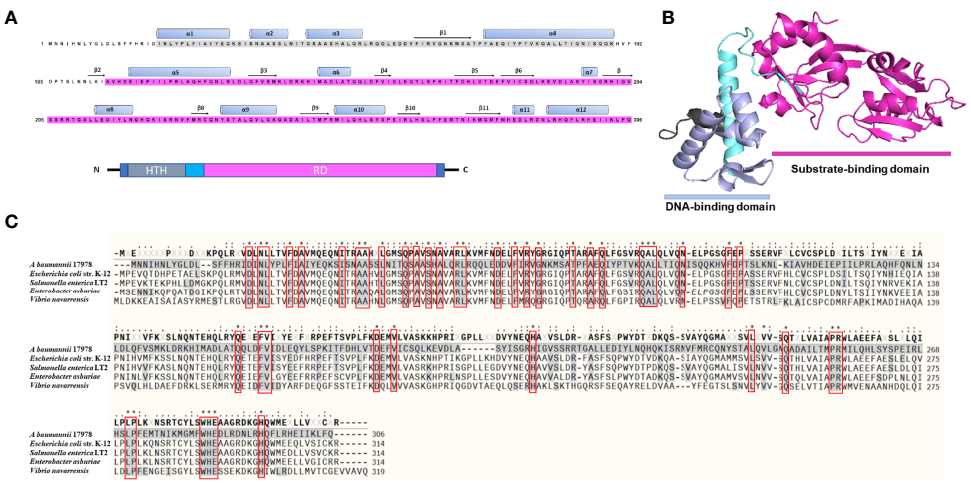

FIGURE 1 | Predicted three-dimensional structure and sequence alignment of LeuO. **(A)** Deduced amino acid sequence of *A1S_1874* where the ash box indicates the helix-turn-helix DNA-binding domain (25–79) and the purple box indicates the LysR family substrate-binding domain (112–304). **(B)** Predicted 3D structure of *A1S_1874* obtained using protein modeling server Phyre2 and PyMoL program. **(C)** Multiple sequence alignment using COBALT: Multiple Alignment Tool of *A. baumannii A1S_1874* with previously characterized LTTR member LeuO from *E. coli* strain *K-12*, *Salmonella enterica LT2*, *Enterobacter asburiae*, and *Vibrio navarrensis*. "*", ".", ":" indicate most conserved residues and semi-conserved sequence, respectively.

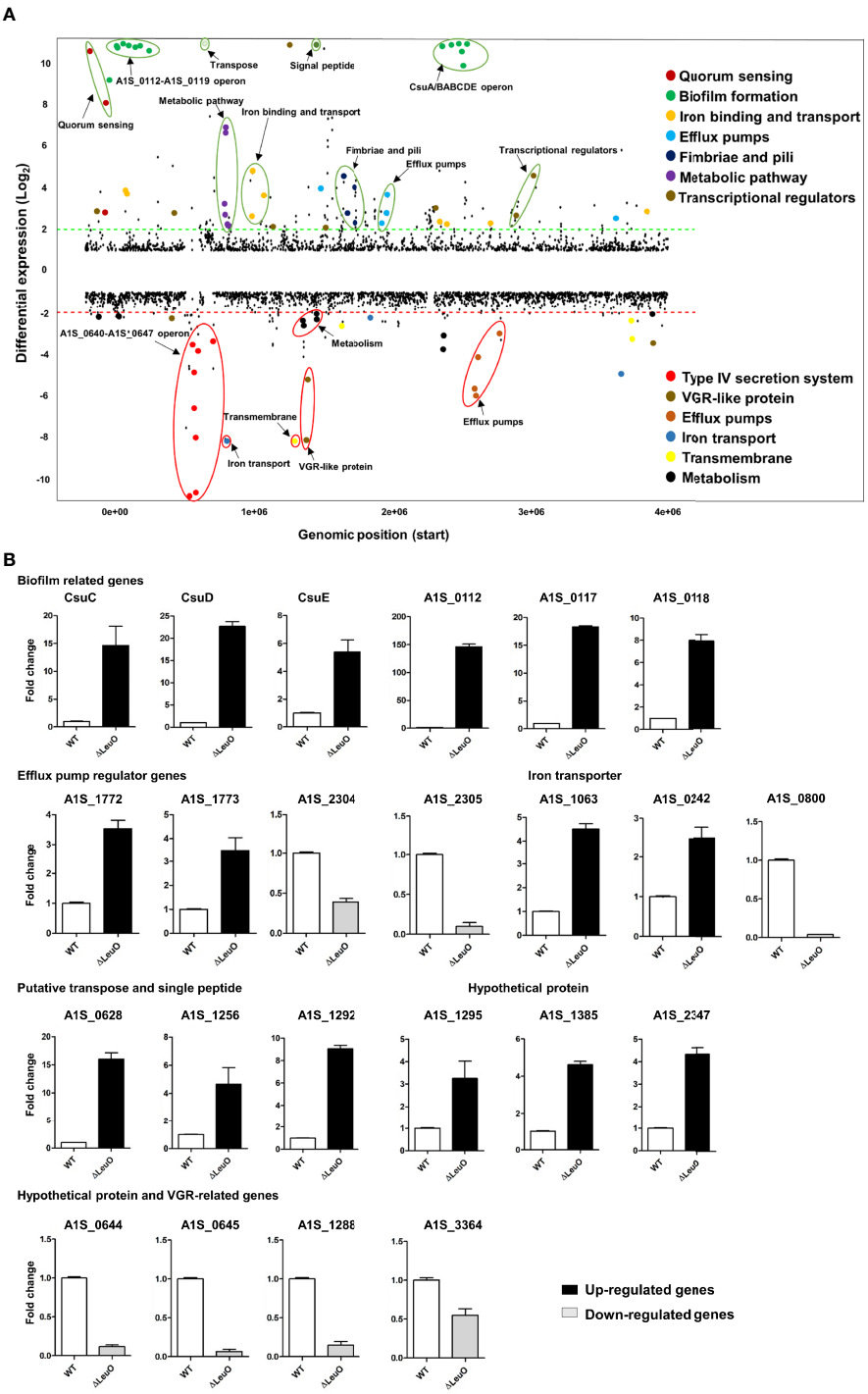

FIGURE 2 | Overview of transcriptional differences between ΔLeuO and ATCC 17978 wild-type *A. baumannii* strains and qRT-PCR validation. **(A)** Comparative transcriptomics of *A. baumannii* ATCC 17978 and ΔLeuO strain are displayed as the differential expression. Differential expression levels are presented as fold change (mutant/wild-type) in the Y-axis, and more than 10-fold expression levels are presented above the 10-scale. Each dot indicates the differential expression levels of all predicted open reading frames of the ATCC 17978 genome and sorted according to the locus tag on the X-axis. The dash lines indicate 2-fold differential expression; upregulated and downregulated genes are located above the green line and below the red line, respectively. Gene names or functions of various highly differentially expressed genes are indicated as colored dots and circles and grouped according to functions on the right side. **(B)** qRT-PCR analysis of selected differentially expressed genes categorized as different functional groups such as biofilm-related genes, efflux pump regulator genes, iron transporter, putative transpose and signal peptide, hypothetical protein genes and VGR-related genes. Upregulated genes are presented as black-colored bars, and ash-colored bars represent downregulated genes. The data represent mean ± standard deviation from three biological replicates.

different families such as the GntR family (*A1S_0072*), TetR family (*A1S_0548*), and AsnC family (*A1S_1090*) and another transcriptional regulator (*A1S_1256*) were also overexpressed. Interestingly, the gene cluster *A1S_0640-A1S_0647* (putative hypothetical protein) was highly downregulated (−3.53- to −16.02-fold) in the LeuO mutant strain. VGR-like proteins are putative T6SS effectors in *A. baumannii* that regulate cell invasion. The expression of several VGR-like protein genes (*A1S_1288*, *A1S_1289*, and *A1S_3364*) was downregulated. Iron-storing bacterioferritin (*A1S_0800* and *A1S_3175*) and several efflux pump transporters, especially RND efflux, were downregulated. Numerous genes involved in metabolism such as dehydrogenase, hydrolase, and hydratase were also downregulated. Several genes were classified as hypothetical proteins whose functions are unknown in *A. baumannii*.

We performed qPCR using the same RNA sample to validate differential gene expression levels obtained from RNA-seq. A total of 23 genes from different functional groups were selected for qPCR, including members of *A1S_0112-A1S-0119* operon, *csu* operon, efflux pump regulator, iron transporter, putative transpose and signal peptide, hypothetical proteins and VGR-like proteins (**Figure 2B**). The expression profiles were found to be consistent with data obtained from RNA-seq experiments. In some cases, there was a fold change difference in qPCR and RNA-seq data, which may be due to differences in sensitivity and specificity between the two technologies.

Contribution of LeuO to Biofilm Formation and Pellicle Formation

Biofilm formation is an important virulence factor for *A. baumannii* persistent infection. We conducted biofilm formation assay using the crystal violet staining method to determine the effect of LeuO deletion on the biofilm formation ability of *A. baumannii* on abiotic surfaces. The ΔLeuO strain produced significantly more biofilm than that produced by the wild-type strain. The LeuO-complemented (CP) strain yielded less biofilm than the mutant strain (**Figure 3A**). The biofilm mass formed by each strain was measured using absorbance at 570 nm of retained crystal violet, which was normalized relative to the growth of each strain using absorbance at 600 nm. The ΔLeuO strain demonstrated approximately 6-fold more biofilm than that of the wild-type strain, and CP restored the biofilm formation (**Figure 3B**). *A. baumannii* can form pellicles at the air–liquid interface. We analyzed the role of LeuO in pellicle formation using the *A. baumannii* strains in modified Luria-Bertani (LB) broth. During static culture, the ΔLeuO strain formed significantly more pellicles than the WT strain as photographed using a digital imaging system (**Figure 3C**). The pellicle biomass was measured at OD_{600} for quantification, wherein it was 0.51 for the ΔLeuO strain and 0.14 for the WT strain (**Figure 3D**). The complementation strain restored the pellicle formation to almost the same level as that of the wild-type strain.

Biofilm formation in *A. baumannii* is regulated by several specific genes, including *csuA/BABCDE*, *ompA*, *abaI*, and *pgaABCD* (Longo et al., 2014). We performed qPCR using the WT and ΔLeuO strains to determine the role of LeuO in the expression of *Csu* operon genes and thus in biofilm formation. Our results revealed that *CsuC*, *CsuD*, and *CsuE* showed 14-, 22-, and 5-fold higher expression levels, respectively, in the LeuO mutant strain than those in the wild-type strain (**Figure 2B**). We also conducted qPCR of several genes from the *A1S_0112-*

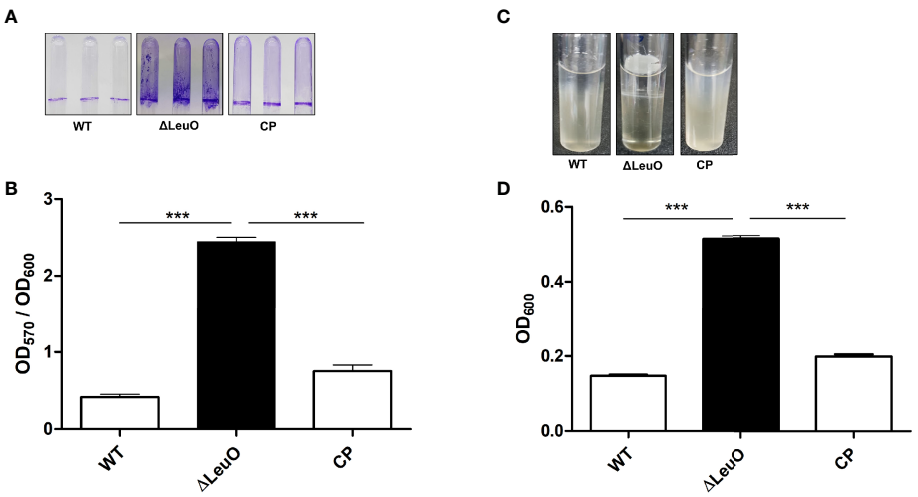

FIGURE 3 | Biofilm and air–liquid interface pellicle formed by *A. baumannii* 17978 WT, ΔLeuO, and complementation strains. *A. baumannii* ATCC 17978 WT, ΔLeuO, and its CP strains were cultured in 5-ml polystyrene tubes at 30°C for 24 h in LB broth without salt. **(A)** Biofilm formation on polystyrene tubes was photographed after staining with 0.1% crystal violet. **(B)** Biofilm values (OD_{570}) were normalized by growth levels (OD_{600}) to compensate for the levels of biofilm formation on the polystyrene surface. Biofilm formation assays were conducted in triplicate, and average values of three replicates were plotted with standard deviation. **(C)** *A. baumannii* strains were cultured at 30°C for 48 h in LB broth without salt, and the pellicle formed by each strain was photographed. **(D)** Pellicles were separated by adding methanol, and pellicle biomass was measured as OD_{600}. This experiment was performed in triplicate. Data are expressed as average values of three replicates with standard deviation. ***P < 0.001, significantly higher than that of the wild-type strain.

A1S_0119 cluster, which are responsible for biofilm formation. We observed that *A1S_0112*, *A1S_0117*, and *A1S_0118* exhibited 146-, 18-, and 8-fold higher expression levels, respectively, in the LeuO mutant strain than those in the wild-type strain (**Figure 2B**). These findings suggest that LeuO regulates the expression of biofilm-related genes and LeuO mutation results in high biofilm formation in *A. baumannii*.

Point Mutations in LeuO Contribute to Biofilm Formation of *A. baumannii* Clinical Isolates

Considering the significant regulatory role of LeuO in the biofilm formation of *A. baumannii* ATCC 17978 strain, we conducted biofilm formation assay using different clones of *A. baumannii* clinical isolates (ST-208, ST-229, ST-357, ST-451, ST-552, and ST-784). We observed that clinical *A. baumannii* isolates formed much more biofilm than ATCC 17978 strain and almost similar biofilm to that formed by the ΔLeuO strain in some cases (**Figure 4A** and **Supplementary Figure S3B**). We focused on the genetic analysis of LeuO locus (*A1S_1874*) in our tested strains to identify the cause of high biofilm formation. Sequencing analysis of LeuO locus revealed that each of the clinical isolates had 306 amino acid residues identical to those in the ATCC 17978 strain but carried several point mutations in the linker helix or in the EBD (**Supplementary Figure S3A**). In ST-208, ST-451, ST-357 and ST-784 isolates, D-to-E, K-to-R, and N-to-S point mutation changed the amino acid aspartic acid to glutamic acid, lysine to arginine, and asparagine to serine at positions 63, 99, and 109, respectively (**Figure 4B**). The isolate ST-229 exhibited a seven-point mutation at positions 109, 187, 194, 195, 198, 264, and 303 compared with that in the ATCC 17978 strain. The clinical isolate ST-552 shared two-point mutations in the regulatory domain at positions 198 and 264, which changed serine to asparagine and glutamic acid to lysine, respectively (**Figure 4B** and **Supplementary Figure S3A**). These mutations in the *A. baumannii* biofilm regulator LeuO may modulate LeuO stability and cause hyper-biofilm formation in the tested clinical isolates.

Contribution of LeuO to Surface Motility

We next determined whether there was any influence of LeuO on surface motility by comparing motility with that of wild-type parent strain, ΔLeuO strain, and complementation strain on semisolid motility agar plates. Bacterial migration from the center of agar plates was measured at a point of time. Migration distance of the ΔLeuO strain from its inoculating point was smaller than that of the wild-type strain (68 mm in the mutant and 89 mm in the wild-type strain; (**Figures 5A, B**). The impaired motility of the ΔLeuO strain was restored in the complementation strain. Comparative transcriptome analysis revealed that several type VI pili genes (VGR-like proteins) were downregulated in the LeuO mutant strain compared with those in the wild-type strain. VGR-like protein genes were validated by qPCR (**Figure 2B**), which illustrated decreased expression of those genes in the LeuO mutant strain. These results imply that LeuO is an important regulator of surface motility.

LeuO Contributes to *A. baumannii* Adherence and Invasion Onto A549 Cell Line

A. baumannii pathogenesis largely depends on cellular adhesion and invasion. For determining the importance of LeuO in adherence to human alveolar epithelial cells, we performed an adherence assay on A549 alveolar epithelial cells using *A. baumanni* ATCC 17978 wild-type strain, ΔLeuO strain, and its complementation strain. In contrast to the result of biofilm formation assay on the polystyrene surface, the ΔLeuO strain exhibited approximately 10-fold reduction in attachment compared with that in the wild-type strain (**Figure 6**). This difference in adherence to epithelial cells was statistically significant. The complementation strain exhibited partial recovery of adhesion properties similar to the wild-type strain.

LeuO Regulates Virulence in Murine Infection

Because of the differences in some virulence-related traits such as biofilm formation and surface motility, we investigated the *in vivo* virulence of *A. baumannii* WT strain, ΔLeuO strain, and CP strain in a mice infection model. Because *A. baumannii* commonly infected immunocompromised patients, neutropenic mice were infected intraperitonially (10^8 CFU/mouse) and monitored for 96 h postinfection. After bacterial challenge with the LeuO mutant strain, all of mice succumbed to infection within 18 h (**Figure 7**). However, mice exposed to wild-type strain infection survived at 40% till the end of experimental period and all mice (100%) injected with PBS survived during the experimental period. Complementation of LeuO disruption restored the ability of *A. baumannii* to survive during the experimental period. The highly virulent *A. baumannii* 1656-2 strain (Park et al., 2011) showed almost the same result as that of the LeuO mutant strain. The Kaplan–Meier survival curve of the tested strains revealed statistical significance between the strains. Altogether, these data suggested that LeuO was responsible for the virulence of *A. baumannii* in the mice model.

DISCUSSION

Despite the increasing prevalence of multidrug-resistant strains, the molecular mechanism underlying *A. baumannii* pathogenesis remains poorly defined. Prokaryotes have diverse transcription factors that regulate gene expression to adjust to new environments, among which the LTTR family is highly conserved in bacteria (Rivera-Gómez et al., 2011). In the present study, the predicted 3D structure of *A. baumannii A1S_1874* showed two domains, a DNA-binding domain and a substrate-binding domain, suggesting that *A1S_1874* belongs to the LTTR family (**Figure 1**). LeuO showed the highly conserved region at the N-terminal region compared with other bacterial LTTR family member protein. We suggested that *A1S_1874* encodes LeuO in *A. baumannii* and a new global transcriptional regulator controlled different gene expression and biological functions. In *S. enterica*, LeuO regulates virulence-related genes

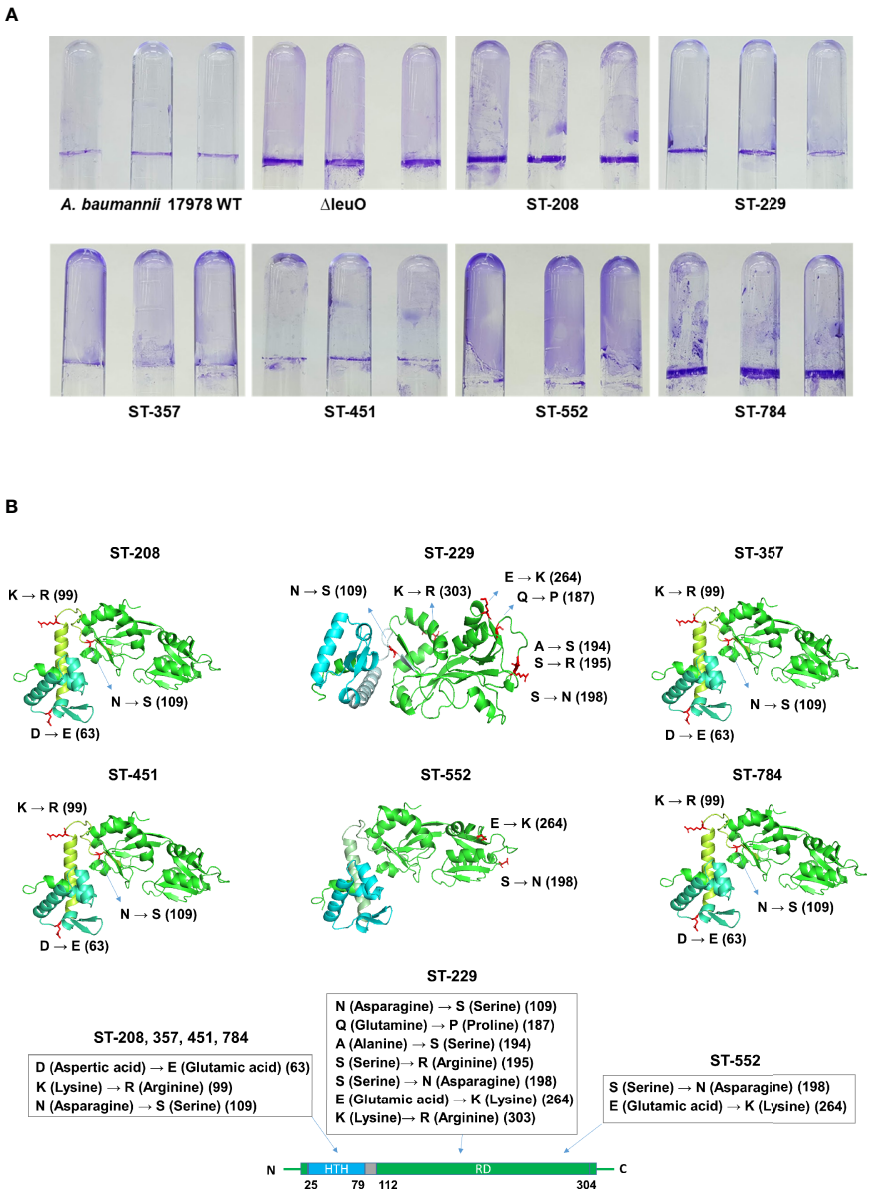

FIGURE 4 | Hyper-biofilm-forming clinical strains have point mutation in the LeuO gene locus. **(A)** *A. baumannii* ATCC 17978 WT, ΔLeuO, and clinical strains of different sequence type ST-208(011), ST-229(079), ST-357(004), ST-451(001), ST-552(015), and ST-784(001) were cultured in 5-ml polystyrene tubes at 30°C for 24 h in LB broth without salt. **(A)** Biofilm formation on polystyrene tubes was photographed after staining with 0.1% crystal violet. **(B)** Cartoon representations of predicted LeuO gene structures of the clinical strains ST-208, ST-229, ST-357, ST-451, ST-552, and ST-784, respectively, obtained using the PyMoL software. Blue color indicates the N-terminal HTH domain, and green color indicates the C-terminal regulatory domain. Mutated residues are shown in red sticks at different positions such as 63, 99, 109, 187, 194, 195, 198, 264, and 303 and are marked beside.

(Fernández-Mora et al., 2004). In this study, we observed that LeuO is involved in regulating several phenotypes of *A. baumannii*. Our initial identification of the LeuO mutation indicated that there is also no significant difference in the growth of *A. baumannii* strains after LeuO deletion (**Supplementary Figure S2**). This result is consistent with another finding of LTTR deletion in *Listeria monocytogenes* (Abdelhamed et al., 2020). The RND superfamily efflux pump member AdeABC is responsible for resistance to aminoglycoside antibiotics (Marchand et al., 2004). In this experiment, the LeuO mutant exhibited higher susceptibility to the aminoglycoside antibiotics tobramycin, amikacin and gentamicin and also to the widely used beta-lactam antibiotics imipenem and meropenem (**Supplementary Table S2**).

Our RNA-seq data showed that 194 genes were upregulated and 108 genes were downregulated in the LeuO mutant

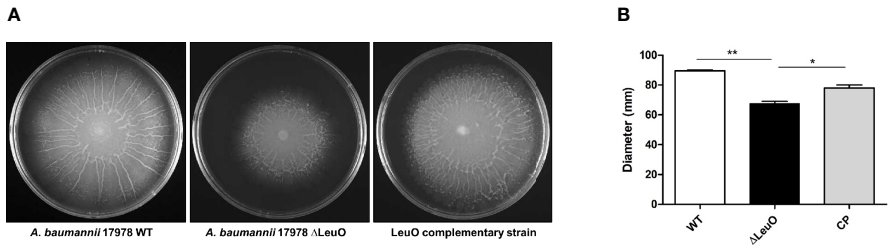

FIGURE 5 | Comparison of surface motility of *A. baumannii* 17978 WT, ΔLeuO, and complementation strains. **(A)** 0.3% Eiken soft agar plates were used to test the surface motility of *A. baumannii* strains. Migration of bacteria from the inoculation point was photographed after culturing at 37°C for 10 h. **(B)** Average area of migration (diameter in mm) of three biological replicates is presented with standard deviation. The experiment was performed in triplicates. *P < 0.05, **P < 0.01, significantly lower than that of the wild-type strain.

compared with those in the wild-type strain (**Supplementary Table S1**). Differentially expressed genes were further categorized into COG categories to elucidate the potential roles of LeuO in transcriptomic regulation in *A. baumannii* (**Figure 2A**). Transcriptomic data showed that the *csu* operon genes and the *A1S_0112-A1S_0119* cluster were highly upregulated, which are responsible for biofilm formation. The quorum sensing–related genes *A1S_0109* and *A1S_0111* (*AbaI* and *AbaR*) were also upregulated. We also observed that some putative transcriptional regulators of a different family were also upregulated. This could potentially affect different regulatory networks, and hence, further investigation would help understand the role of LeuO in these regulatory networks. We observed that the type VI secretion system-related genes were downregulated, which may play a role in surface motility. A large number of downregulated genes were hypothetical proteins with unknown functions. Further research is necessary to decipher the role of these genes in the *A. baumannii* genome. Previous studies have shown that the members of LTTRs regulate the expression of numerous genes involved in essential bacterial functions, including virulence, motility, metabolism, cell division, and oxidative stress response (Russell et al., 2004; Heroven and Dersch, 2006; Lu et al., 2007; O'Grady et al., 2011). Our transcriptomic data and observation of these LysR family members indicated almost the same effects of gene expression.

Biofilm formation by bacteria provides persistence and protects them from unfavorable conditions, including antimicrobial activity, and it is a major virulence factor (Costerton et al., 1999). A variety of transcriptional regulators have been identified to control biofilm formation in different

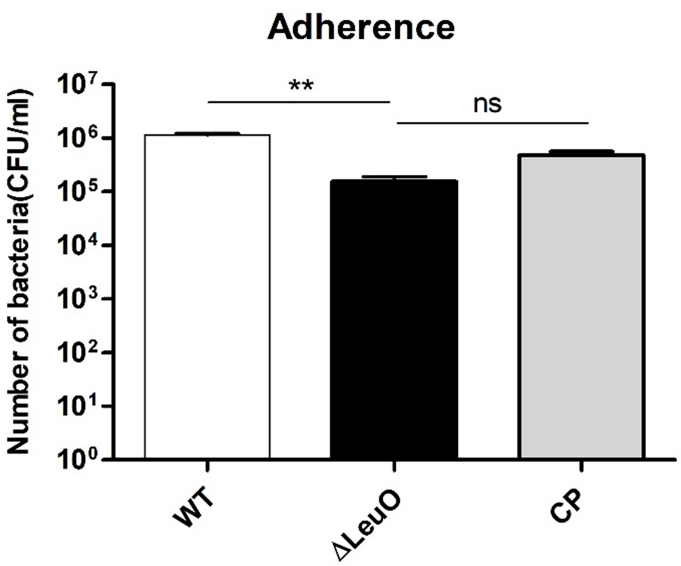

FIGURE 6 | Adherence of *A. baumannii* strains to A549 cells. A549 alveolar epithelial cells were infected with *A. baumannii* wild-type, ΔLeuO, .and CP strains at a MOI of 1:100 for 2 h. After lysis with Triton-X, cell lysates were diluted and plated onto LB agar plates for CFU counting. The experiment was performed with three replicates. Data are presented as mean ± SD. ns, non-significant; **P < 0.01, significantly lower than that of the wild-type strain.

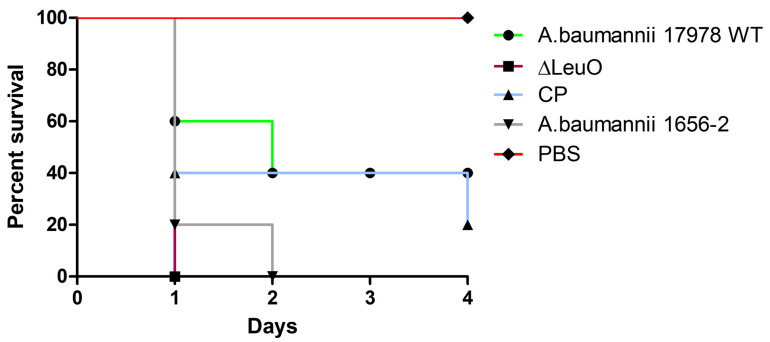

FIGURE 7 | Survival of mice infected with *A. baumannii* strains. Kaplan-Meier survival curves of the virulence of *A. baumannii* 17978 wild-type, ΔLeuO, CP strain and *A. baumannii* 1656-2 in mice were determined up to 4 days of infection. 8-week-old female BALB/c mice were injected intraperitoneally (IP) with 1×10^8 CFU/ml bacterial suspension of tested strains (n = 5 per group). PBS was administered as control group and survival of infected mice were monitored every 12h for 4 days. Survival curve was generated using GraphPad Prism software.

organisms, for example, the transcriptional regulator LrhA in *E. coli*, CytR in *V. cholerae*, Fur in *Yersinia pestis*, SinR in *Bacillus subtilis*, and LcrX in *Xanthomonas axonopodis* (Haugo and Watnick, 2002; Blumer et al., 2005; Kearns et al., 2005; Sun et al., 2012; Park et al., 2020). LeuO, a putative LTTR, was identified as a repressor of biofilm synthesis in *A. baumannii* for the first time in this study. Our results demonstrated that biofilm formation on abiotic surface was significantly increased in the LeuO mutant strain compared with that in the wild-type strain (**Figure 3**). The *csuA/BABCDE* chaperon-usher secretion system-mediated pili play an important role in biofilm formation (Gaddy and Actis, 2009). Our RNA transcriptomic data revealed that *csu* operon genes were highly upregulated in the LeuO mutant strain. Another gene cluster, *A1S_0112-A1S_0119*, was also highly upregulated. A previous study showed that the *A1S_0112-A1S_0119* cluster is critical for biofilm synthesis (Rumbo-Feal et al., 2017). These findings may explain the cause of high biofilm synthesis in the LeuO mutant strain. LeuO may be a transcriptional regulator that directly or indirectly controls genes that regulate biofilm formation. In contrast, several *A. baumannii* clinical isolates (ST-208, ST-229, ST-357, ST-451, ST-552, and ST-784) exhibited robust biofilm formation, which was almost similar to that of the LeuO mutant strain (**Figure 4A**). Sequence analysis of LeuO locus revealed several amino acid mutations in all the tested clinical strains compared with those in the wild-type strain in the linker helix and regulatory domain regions (**Figure 4B**). These mutations in amino acids may alter LeuO regulation in clinical strains and result in hyper-biofilm formation. It has been reported that mutation in the amino acids of the *B. subtilis* master biofilm regulator *sinR* modulated biofilm formation (Leiman et al., 2014).

A. baumannii displays surface-associated motility, which is an important virulence factor (Tomaras et al., 2003). We observed that the surface motility of the LeuO mutant was reduced compared with that in the wild-type strain (**Figure 5**). Extension and retraction of type IV pilus is required for motility (Clemmer et al., 2011). In our RNA-seq data, we observed that the type IV pilus genes *A1S_0646* (*IcmB*) and VGR-like protein (type VI secretion system) *A1S_1288* were downregulated by log 8.29- and 8.3-fold, respectively (**Supplementary Table S1**). Numerous transcriptional factors are known to be involved in the motility of other bacteria, such as ArcB, QseD, and RvoM (Heroven and Dersch, 2006; Habdas et al., 2010; Zhang et al., 2017). These results suggest that LeuO downregulates type IV and type VI pili genes and attenuates motility in the LeuO mutant strain. Surface motility is also controlled by quorum sensing in *A. baumannii*. Although abaRI genes were upregulated in LeuO mutant strain, surface motility was reduced. Further research will help to describe this discrepancy.

In the present study, we used alveolar epithelial cells (A549) to determine the role of LeuO in *A. baumannii* adherence. The LeuO mutant displayed significantly lower adherence to A549 epithelial cells than that shown by the wild-type strain (**Figure 6**). Our observations of the LeuO-mediated epithelial cell adherence and biofilm formation on abiotic surface are quite opposite, which suggests the presence of different mechanisms of adherence to either biotic or abiotic surface. Although *csu* operon is essential for biofilm formation, other studies have suggested that *A. baumannii* adherence to abiotic surfaces is independent of *csu*A/BABCDE-mediated pili and that *csu*-knockout strains showed no difference in binding to bronchial cells (de Breij et al., 2009; Gaddy and Actis, 2009). Our data corroborate with these findings. Further research is necessary to understand the exact molecular mechanisms involved in adherence to epithelial cells.

Several LTTRs are known to control the expression of virulence genes to maintain the host–pathogen interaction, such as ShvR in *B. cenocepacia*, MexT in *P. aeruginosa*, and LeuO in *S. enterica* serovar *Typhimurium* (Tropel and van der Meer, 2004; Tian et al., 2009; Espinosa and Casadesús, 2014). In this study, we observed that LeuO regulated several genes related to virulence. In our study, LeuO deletion increased lethal infection in the intraperitoneal mouse infection model (**Figure 7**). This increase in pathogenicity may be due to the result of increased virulence-related gene expression. Some previous studies have shown that disruption of LTTR

family members such as GigC, MvfR, and ShvR reduced virulence in mammalian and plant models of infection (Cao et al., 2001; Déziel et al., 2005; Gebhardt et al., 2020). This contrasting result requires further analysis to understand the actual role of LTTRs in *A. baumannii* pathogenicity.

In conclusion, LeuO (*A1S_1874*) was identified as an LTTR, and transcriptome analysis revealed that LeuO regulated divergent sets of genes with different biological functions that were altered after LeuO deletion. Altogether, LeuO is involved in the regulation of biofilm formation, adherence, motility, and virulence of *A. baumannii*. This study provides valuable information regarding the role of an LTTR in the pathogenesis of *A. baumannii.*

Statistical Analysis

All experiments in this study were performed independently, and data are expressed as mean and standard deviations (SDs). All raw data were saved in Excel files and imported to GraphPad Prism for statistical analysis. Statistical differences between groups of data were compared using Student's *t*-tests or one-way analysis of variance along with Turkey's multiple comparisons.

DATA AVAILABILITY STATEMENT

The findings of this study are available within this paper and its **Supplementary Material**. The transcriptomic data discussed in this publication have been deposited in the NCBI's gene expression omnibus database (http://www.ncbi.nlm.nih.gov/geo/) and can be accessed using the accession number GSE173626.

ETHICS STATEMENT

Animal experiments were conducted according to experimental procedures approved by the Animal Care Committee of Kyungpook National University, South Korea (approval number: KNU-2019-178).

AUTHOR CONTRIBUTIONS

MI, KK, and MS designed the study and MI wrote the manuscript. MI, KK, and MS performed the experiments. JL reviewed the manuscript. All authors contributed to the article and approved the submitted version.

FUNDING

This study was supported by a grant from the Korea Government National Research Foundation Grants 2016R1D1A1B01008960 (to MS).

SUPPLEMENTARY MATERIAL

The Supplementary Material for this article can be found online at: https://www.frontiersin.org/articles/10.3389/fcimb.2021.738706/full#supplementary-material

REFERENCES

Abdelhamed, H., Ramachandran, R., Narayanan, L., Ozdemir, O., Cooper, A., Olivier, A. K., et al. (2020). Contributions of a LysR Transcriptional Regulator to Listeria Monocytogenes Virulence and Identification of Its Regulons. *J. Bacteriol.* 202 (10), e00087–20. doi: 10.1128/JB.00087-20

Bhargava, N., Singh, S. P., Sharma, A., Sharma, P., and Capalash, N. (2015). Attenuation of Quorum Sensing-Mediated Virulence of Acinetobacter Baumannii by Glycyrrhiza Glabra Flavonoids. *Future Microbiol.* 10, 1953–1968. doi: 10.2217/fmb.15.107

Bina, X. R., Howard, M. F., Ante, V. M., and Bina, J. E. (2016). Vibrio Cholerae LeuO Links the ToxR Regulon to Expression of Lipid A Remodeling Genes. *Infect. Immun.* 84, 3161–3171. doi: 10.1128/IAI.00445-16

Blumer, C., Kleefeld, A., Lehnen, D., Heintz, M., Dobrindt, U., Nagy, G., et al. (2005). Regulation of Type 1 Fimbriae Synthesis and Biofilm Formation by the Transcriptional Regulator LrhA of Escherichia Coli. *Microbiology (Reading)* 151, 3287–3298. doi: 10.1099/mic.0.28098-0

Cao, H., Krishnan, G., Goumnerov, B., Tsongalis, J., Tompkins, R., and Rahme, L. G. (2001). A Quorum Sensing-Associated Virulence Gene of Pseudomonas Aeruginosa Encodes a LysR-Like Transcription Regulator With a Unique Self-Regulatory Mechanism. *Proc. Natl. Acad. Sci. U.S.A.* 98, 14613–14618. doi: 10.1073/pnas.251465298

Clemmer, K. M., Bonomo, R. A., and Rather, P. N. (2011). Genetic Analysis of Surface Motility in Acinetobacter Baumannii. *Microbiology (Reading)* 157, 2534–2544. doi: 10.1099/mic.0.049791-0

Costerton, J. W., Stewart, P. S., and Greenberg, E. P. (1999). Bacterial Biofilms: A Common Cause of Persistent Infections. *Science* 284, 1318–1322. doi: 10.1126/science.284.5418.1318

De Breij, A., Gaddy, J., van der Meer, J., Koning, R., Koster, A., Van Den Broek, P., et al. (2009). CsuA/BABCDE-Dependent Pili are Not Involved in the Adherence of Acinetobacter Baumannii ATCC19606(T) to Human Airway Epithelial Cells and Their Inflammatory Response. *Res. Microbiol.* 160, 213–218. doi: 10.1016/j.resmic.2009.01.002

Deziel, E., Gopalan, S., Tampakaki, A. P., Lepine, F., Padfield, K. E., Saucier, M., et al. (2005). The Contribution of MvfR to Pseudomonas Aeruginosa Pathogenesis and Quorum Sensing Circuitry Regulation: Multiple Quorum Sensing-Regulated Genes are Modulated Without Affecting lasRI, rhlRI or the Production of N-Acyl-L-Homoserine Lactones. *Mol. Microbiol.* 55, 998–1014. doi: 10.1111/j.1365-2958.2004.04448.x

Espinosa, E., and Casadesús, J. (2014). Regulation of Salmonella Enterica Pathogenicity Island 1 (SPI-1) by the LysR-Type Regulator LeuO. *Mol. Microbiol.* 91, 1057–1069. doi: 10.1111/mmi.12500

Fernández-Mora, M., Puente, J. L., and Calva, E. (2004). OmpR and LeuO Positively Regulate the Salmonella Enterica Serovar Typhi Omps2 Porin Gene. *J. Bacteriol.* 186, 2909–2920. doi: 10.1128/JB.186.10.2909-2920.2004

Gaddy, J. A., and Actis, L. A. (2009). Regulation of Acinetobacter Baumannii Biofilm Formation. *Future Microbiol.* 4, 273–278. doi: 10.2217/fmb.09.5

Gaddy, J. A., Arivett, B. A., Mcconnell, M. J., Lopez-Rojas, R., Pachon, J., and Actis, L. A. (2012). Role of Acinetobactin-Mediated Iron Acquisition Functions in the Interaction of Acinetobacter Baumannii Strain ATCC 19606T With Human Lung Epithelial Cells, Galleria Mellonella Caterpillars, and Mice. *Infect. Immun.* 80, 1015–1024. doi: 10.1128/IAI.06279-11

Gebhardt, M. J., Czyz, D. M., Singh, S., Zurawski, D. V., Becker, L., and Shuman, H. A. (2020). GigC, a LysR Family Transcription Regulator, Is Required for Cysteine Metabolism and Virulence in Acinetobacter Baumannii. *Infect. Immun.* 89 (1), e00180-20. doi: 10.1128/IAI.00180-20

Guadarrama, C., Villaseñor, T., and Calva, E. (2014). The Subtleties and Contrasts of the LeuO Regulator in Salmonella Typhi: Implications in the Immune Response. *Front. Immunol.* 5, 581–581. doi: 10.3389/fimmu.2014.00581

Habdas, B. J., Smart, J., Kaper, J. B., and Sperandio, V. (2010). The LysR-Type Transcriptional Regulator QseD Alters Type Three Secretion in Enterohemorrhagic Escherichia Coli and Motility in K-12 Escherichia Coli. *J. Bacteriol.* 192, 3699–3712. doi: 10.1128/JB.00382-10

Haugo, A. J., and Watnick, P. I. (2002). Vibrio Cholerae CytR is a Repressor of Biofilm Development. *Mol. Microbiol.* 45, 471–483. doi: 10.1046/j.1365-2958.2002.03023.x

Hernández-Lucas, I., Gallego-Hernández, A. L., Encarnación, S., Fernández-Mora, M., Martínez-Batallar, A. G., Salgado, H., et al. (2008). The LysR-Type Transcriptional Regulator LeuO Controls Expression of Several Genes in Salmonella Enterica Serovar Typhi. *J. Bacteriol.* 190, 1658–1670. doi: 10.1128/JB.01649-07

Heroven, A. K., and Dersch, P. (2006). RovM, a Novel LysR-Type Regulator of the Virulence Activator Gene Rova, Controls Cell Invasion, Virulence and Motility of Yersinia Pseudotuberculosis. *Mol. Microbiol.* 62, 1469–1483. doi: 10.1111/j.1365-2958.2006.05458.x

Jawad, A., Seifert, H., Snelling, A. M., Heritage, J., and Hawkey, P. M. (1998). Survival of Acinetobacter Baumannii on Dry Surfaces: Comparison of Outbreak and Sporadic Isolates. *J. Clin. Microbiol.* 36, 1938–1941. doi: 10.1128/JCM.36.7.1938-1941.1998

Jung, H. W., Kim, K., Islam, M. M., Lee, J. C., and Shin, M. (2020). Role of Ppgpp-Regulated Efflux Genes in Acinetobacter Baumannii. *J. Antimicrob. Chemother.* 75, 1130–1134. doi: 10.1093/jac/dkaa014

Kearns, D. B., Chu, F., Branda, S. S., Kolter, R., and Losick, R. (2005). A Master Regulator for Biofilm Formation by Bacillus Subtilis. *Mol. Microbiol.* 55, 739–749. doi: 10.1111/j.1365-2958.2004.04440.x

Kumar, A., and Schweizer, H. P. (2005). Bacterial Resistance to Antibiotics: Active Efflux and Reduced Uptake. *Adv. Drug Deliv. Rev.* 57, 1486–1513. doi: 10.1016/j.addr.2005.04.004

Lee, J. S., Choi, C. H., Kim, J. W., and Lee, J. C. (2010). Acinetobacter Baumannii Outer Membrane Protein A Induces Dendritic Cell Death Through Mitochondrial Targeting. *J. Microbiol.* 48, 387–392. doi: 10.1007/s12275-010-0155-1

Lee, J. C., Koerten, H., Van Den Broek, P., Beekhuizen, H., Wolterbeek, R., Van Den Barselaar, M., et al. (2006). Adherence of Acinetobacter Baumannii Strains to Human Bronchial Epithelial Cells. *Res. Microbiol.* 157, 360–366. doi: 10.1016/j.resmic.2005.09.011

Lee, H. W., Koh, Y. M., Kim, J., Lee, J. C., Lee, Y. C., Seol, S. Y., et al. (2008). Capacity of Multidrug-Resistant Clinical Isolates of Acinetobacter Baumannii to Form Biofilm and Adhere to Epithelial Cell Surfaces. *Clin. Microbiol. Infect.* 14, 49–54. doi: 10.1111/j.1469-0691.2007.01842.x

Leiman, S. A., Arboleda, L. C., Spina, J. S., and Mcloon, A. L. (2014). SinR is a Mutational Target for Fine-Tuning Biofilm Formation in Laboratory-Evolved Strains of Bacillus Subtilis. *BMC Microbiol.* 14, 301–301. doi: 10.1186/s12866-014-0301-8

Longo, F., Vuotto, C., and Donelli, G. (2014). Biofilm Formation in Acinetobacter Baumannii. *New Microbiol.* 37, 119–127.

Lu, Z., Takeuchi, M., and Sato, T. (2007). The LysR-Type Transcriptional Regulator YofA Controls Cell Division Through the Regulation of Expression of ftsW in Bacillus Subtilis. *J. Bacteriol.* 189, 5642–5651. doi: 10.1128/JB.00467-07

Marchand, I., Damier-Piolle, L., Courvalin, P., and Lambert, T. (2004). Expression of the RND-Type Efflux Pump AdeABC in Acinetobacter Baumannii is Regulated by the AdeRS Two-Component System. *Antimicrob. Agents Chemother.* 48, 3298–3304. doi: 10.1128/AAC.48.9.3298-3304.2004

Martí, S., Rodríguez-Baño, J., Catel-Ferreira, M., Jouenne, T., Vila, J., Seifert, H., et al. (2011). Biofilm Formation at the Solid-Liquid and Air-Liquid Interfaces by Acinetobacter Species. *BMC Res. Notes* 4, 5. doi: 10.1186/1756-0500-4-5

Mcconnell, M. J., Actis, L., and Pachon, J. (2013). Acinetobacter Baumannii: Human Infections, Factors Contributing to Pathogenesis and Animal Models. *FEMS Microbiol. Rev.* 37, 130–155. doi: 10.1111/j.1574-6976.2012.00344.x

Moorthy, S., and Watnick, P. I. (2005). Identification of Novel Stage-Specific Genetic Requirements Through Whole Genome Transcription Profiling of Vibrio Cholerae Biofilm Development. *Mol. Microbiol.* 57, 1623–1635. doi: 10.1111/j.1365-2958.2005.04797.x

Muraoka, S., Okumura, R., Ogawa, N., Nonaka, T., Miyashita, K., and Senda, T. (2003). Crystal Structure of a Full-Length LysR-Type Transcriptional Regulator, CbnR: Unusual Combination of Two Subunit Forms and Molecular Bases for Causing and Changing DNA Bend. *J. Mol. Biol.* 328, 555–566. doi: 10.1016/S0022-2836(03)00312-7

O'grady, E. P., Nguyen, D. T., Weisskopf, L., Eberl, L., and Sokol, P. A. (2011). The Burkholderia Cenocepacia LysR-Type Transcriptional Regulator ShvR Influences Expression of Quorum-Sensing, Protease, Type II Secretion, and Afc Genes. *J. Bacteriol.* 193, 163–176. doi: 10.1128/JB.00852-10

Park, H., Do, E., Kim, M., Park, H.-J., Lee, J., and Han, S.-W. (2020). A LysR-Type Transcriptional Regulator LcrX Is Involved in Virulence, Biofilm Formation, Swimming Motility, Siderophore Secretion, and Growth in Sugar Sources in Xanthomonas Axonopodis Pv. Glycines. *Front. Plant Sci.* 10, 1657–1657. doi: 10.3389/fpls.2019.01657

Park, J. Y., Kim, S., Kim, S. M., Cha, S. H., Lim, S. K., and Kim, J. (2011). Complete Genome Sequence of Multidrug-Resistant Acinetobacter Baumannii Strain 1656-2, Which Forms Sturdy Biofilm. *J. Bacteriol.* 193, 6393–6394. doi: 10.1128/JB.06109-11

Rice, L. B. (2008). Federal Funding for the Study of Antimicrobial Resistance in Nosocomial Pathogens: No ESKAPE. *J. Infect. Dis.* 197, 1079–1081. doi: 10.1086/533452

Rice, K. C., Nelson, J. B., Patton, T. G., Yang, S. J., and Bayles, K. W. (2005). Acetic Acid Induces Expression of the Staphylococcus Aureus cidABC and lrgAB Murein Hydrolase Regulator Operons. *J. Bacteriol.* 187, 813–821. doi: 10.1128/JB.187.3.813-821.2005

Rivera-Gómez, N., Segovia, L., and Pérez-Rueda, E. (2011). Diversity and Distribution of Transcription Factors: Their Partner Domains Play an Important Role in Regulatory Plasticity in Bacteria. *Microbiology (Reading)* 157, 2308–2318. doi: 10.1099/mic.0.050617-0

Rumbo-Feal, S., Pérez, A., Ramelot, T. A., Ãlvarez-Fraga, L., Vallejo, J. A., Beceiro, A., et al. (2017). Contribution of the A. Baumannii A1S_0114 Gene to the Interaction With Eukaryotic Cells and Virulence. *Front. Cell. Infect. Microbiol.* 7, 108–108. doi: 10.3389/fcimb.2017.00108

Russell, D. A., Byrne, G. A., O'connell, E. P., Boland, C. A., and Meijer, W. G. (2004). The LysR-Type Transcriptional Regulator VirR is Required for Expression of the Virulence Gene vapA of Rhodococcus Equi ATCC 33701. *J. Bacteriol.* 186, 5576–5584. doi: 10.1128/JB.186.17.5576-5584.2004

Russo, T. A., Luke, N. R., Beanan, J. M., Olson, R., Sauberan, S. L., Macdonald, U., et al. (2010). The K1 Capsular Polysaccharide of Acinetobacter Baumannii Strain 307-0294 is a Major Virulence Factor. *Infect. Immun.* 78, 3993–4000. doi: 10.1128/IAI.00366-10

Santos, C. L., Tavares, F., Thioulouse, J., and Normand, P. (2009). A Phylogenomic Analysis of Bacterial Helix-Turn-Helix Transcription Factors. *FEMS Microbiol. Rev.* 33, 411–429. doi: 10.1111/j.1574-6976.2008.00154.x

Schell, M. A. (1993). Molecular Biology of the LysR Family of Transcriptional Regulators. *Annu. Rev. Microbiol.* 47, 597–626. doi: 10.1146/annurev.mi.47.100193.003121

Shimada, T., Bridier, A., Briandet, R., and Ishihama, A. (2011). Novel Roles of LeuO in Transcription Regulation of E. coli Genome: Antagonistic Interplay With the Universal Silencer H-NS. *Mol. Microbiol.* 82, 378–397. doi: 10.1111/j.1365-2958.2011.07818.x

Srinivasan, V. B., Mondal, A., Venkataramaiah, M., Chauhan, N. K., and Rajamohan, G. (2013). Role of oxyRKP, a Novel LysR-Family Transcriptional Regulator, in Antimicrobial Resistance and Virulence in Klebsiella Pneumoniae. *Microbiology (Reading)* 159, 1301–1314. doi: 10.1099/mic.0.065052-0

Stepanovic, S., Vukovic, D., Dakic, I., Savic, B., and Svabic-Vlahovic, M. (2000). A Modified Microtiter-Plate Test for Quantification of Staphylococcal Biofilm Formation. *J. Microbiol. Methods* 40, 175–179. doi: 10.1016/S0167-7012(00)00122-6

Sun, F., Gao, H., Zhang, Y., Wang, L., Fang, N., Tan, Y., et al. (2012). Fur is a Repressor of Biofilm Formation in Yersinia Pestis. *PloS One* 7, e52392–e52392. doi: 10.1371/journal.pone.0052392

Tian, Z. X., Fargier, E., Mac Aogáin, M., Adams, C., Wang, Y. P., and O'gara, F. (2009). Transcriptome Profiling Defines a Novel Regulon Modulated by the LysR-Type Transcriptional Regulator MexT in Pseudomonas Aeruginosa. *Nucleic Acids Res.* 37, 7546–7559. doi: 10.1093/nar/gkp828

Tomaras, A. P., Dorsey, C. W., Edelmann, R. E., and Actis, L. A. (2003). Attachment to and Biofilm Formation on Abiotic Surfaces by Acinetobacter Baumannii: Involvement of a Novel Chaperone-Usher Pili Assembly System. *Microbiology (Reading)* 149, 3473–3484. doi: 10.1099/mic.0.26541-0

Tropel, D., and van der Meer, J. R. (2004). Bacterial Transcriptional Regulators for Degradation Pathways of Aromatic Compounds. *Microbiol. Mol. Biol. Rev.* 68, 474–500. doi: 10.1128/MMBR.68.3.474-500.2004

WHO (2017). WHO Publishes List of Bacteria for Which New Antibiotics Are Urgently Needed. *Saudi Med. J.* 38, 444–445.

Yang, S. J., Rice, K. C., Brown, R. J., Patton, T. G., Liou, L. E., Park, Y. H., et al. (2005). A LysR-Type Regulator, CidR, is Required for Induction of the Staphylococcus Aureus cidABC Operon. *J. Bacteriol.* 187, 5893–5900. doi: 10.1128/JB.187.17.5893-5900.2005

Zhang, X., Wu, D., Guo, T., Ran, T., Wang, W., and Xu, D. (2017). Differential Roles for ArcA and ArcB Homologues in Swarming Motility in Serratia Marcescens FS14. *Antonie van Leeuwenhoek* 111, 609–617. doi: 10.1007/s10482-017-0981-9

Conflict of Interest: The authors declare that the research was conducted in the absence of any commercial or financial relationships that could be construed as a potential conflict of interest.

Publisher's Note: All claims expressed in this article are solely those of the authors and do not necessarily represent those of their affiliated organizations, or those of the publisher, the editors and the reviewers. Any product that may be evaluated in this article, or claim that may be made by its manufacturer, is not guaranteed or endorsed by the publisher.

frontiers in Cellular and Infection Microbiology

ORIGINAL RESEARCH
published: 04 November 2021
doi: 10.3389/fcimb.2021.778331

A LysR-Type Transcriptional Regulator Controls Multiple Phenotypes in *Acinetobacter baumannii*

Aimee R. P. Tierney[1], *Chui Yoke Chin*[2,3,4,5], *David S. Weiss*[2,3,4,5,6] *and Philip N. Rather*[1,6]*

[1] Department of Microbiology and Immunology, Emory University School of Medicine, Atlanta, GA, United States, [2] Emory Vaccine Center, Atlanta, GA, United States, [3] Yerkes National Primate Research Center, Atlanta, GA, United States, [4] Division of Infectious Diseases, Department of Medicine, Emory University School of Medicine, Atlanta, GA, United States, [5] Emory Antibiotic Resistance Center, Atlanta, GA, United States, [6] Research Service, Department of Veterans Affairs, Atlanta Veterans Affairs (VA) Medical Center, Decatur, GA, United States

Acinetobacter baumannii is a multidrug-resistant, Gram-negative nosocomial pathogen that exhibits phenotypic heterogeneity resulting in virulent opaque (VIR-O) and avirulent translucent (AV-T) colony variants. Each variant has a distinct gene expression profile resulting in multiple phenotypic differences. Cells interconvert between the VIR-O and AV-T variants at high frequency under laboratory conditions, suggesting that the genetic mechanism underlying the phenotypic switch could be manipulated to attenuate virulence. Therefore, our group has focused on identifying and characterizing genes that regulate this switch, which led to the investigation of *ABUW_1132* (*1132*), a highly conserved gene predicted to encode a LysR-type transcriptional regulator. ABUW_1132 was shown to be a global regulator as the expression of 74 genes was altered ≥ 2-fold in an *1132* deletion mutant. The *1132* deletion also resulted in a 16-fold decrease in VIR-O to AV-T switching, loss of 3-OH-C_{12}-HSL secretion, and reduced surface-associated motility. Further, the deletion of *1132* in the AV-T background caused elevated capsule production, which increased colony opacity and altered the typical avirulent phenotype of translucent cells. These findings distinguish *1132* as a global regulatory gene and advance our understanding of *A. baumannii*'s opacity-virulence switch.

Keywords: *Acinetobacter baumannii*, AB5075, LysR-type transcriptional regulator, phenotypic heterogeneity, quorum sensing, motility, polysaccharide capsule, virulence

OPEN ACCESS

Edited by:
Paolo Visca,
Roma Tre University, Italy

Reviewed by:
Jerónimo Pachon,
Sevilla University, Spain
John Dallas Boyce,
Monash University, Australia

***Correspondence:**
Philip N. Rather
prather@emory.edu

Specialty section:
This article was submitted to Molecular Bacterial Pathogenesis, a section of the journal Frontiers in Cellular and Infection Microbiology

Received: *16 September 2021*
Accepted: *14 October 2021*
Published: *04 November 2021*

Citation:
Tierney ARP, Chin CY, Weiss DS and Rather PN (2021) A LysR-Type Transcriptional Regulator Controls Multiple Phenotypes in Acinetobacter baumannii. Front. Cell. Infect. Microbiol. 11:778331. doi: 10.3389/fcimb.2021.778331

INTRODUCTION

The Gram-negative pathogen *Acinetobacter baumannii* poses a major threat to hospitalized patients. Cases of ventilator-associated pneumonia are among the most common *A. baumannii* infections, but incidences of skin and soft tissue infections, urinary tract infections, and sepsis are on the rise (Davis et al., 2005; Dijkshoorn et al., 2007; Peleg et al., 2008; Peleg and Hooper, 2010; Doyle et al., 2011; Weiner et al., 2016; Wong et al., 2017). Of primary concern is *A. baumannii*'s increasing resistance to treatment with antimicrobials, with 63% of infections caused by multidrug-resistant

(MDR) strains (Clark et al., 2016; Lee et al., 2017; Centers for Disease Control and Prevention, 2019). In particular, *A. baumannii*'s rapidly growing resistance to carbapenem antibiotics and its ability to widely disseminate resistance *via* mobile genetic elements prompted the World Health Organization to name this organism as a critical priority for the research and development of new antimicrobial drugs in 2017 (World Health Organization, 2017). Further, its extreme resistance to desiccation and disinfectants makes it notoriously difficult to eradicate in hospital environments (Jawad et al., 1998; Chapartegui-Gonzalez et al., 2018; Rocha et al., 2018; Bravo et al., 2019; D'souza et al., 2019). In the face of such problematic phenotypes, an understanding of pathogenesis and virulence in this species is imperative. To meet this need, experiments conducted by our group have been carried out in the strain AB5075 (GenBank Accession Number CP008706.1), a highly virulent MDR clinical isolate that is genetically tractable (Jacobs et al., 2014; Gallagher et al., 2015).

Our group has sought to better understand the genetic mechanisms regulating *A. baumannii* virulence in light of our findings that clinical isolates of this species exhibit phenotypic heterogeneity resulting in virulent and avirulent colony opacity variants (Tipton et al., 2015; Chin et al., 2018). The virulent variant has a golden, opaque colony morphotype under oblique lighting and is termed VIR-O, while the avirulent variant is translucent and is termed AV-T (**Figure 1A**). In addition to differences in virulence, the VIR-O variant displays higher levels of capsule production, quorum sensing signal secretion, and surface-associated motility, while AV-T demonstrates greater production of biofilm and is able to utilize multiple carbon sources. Both variants switch back and forth at high frequency, with rates of approximately 4-13% conversion at 24 hours of

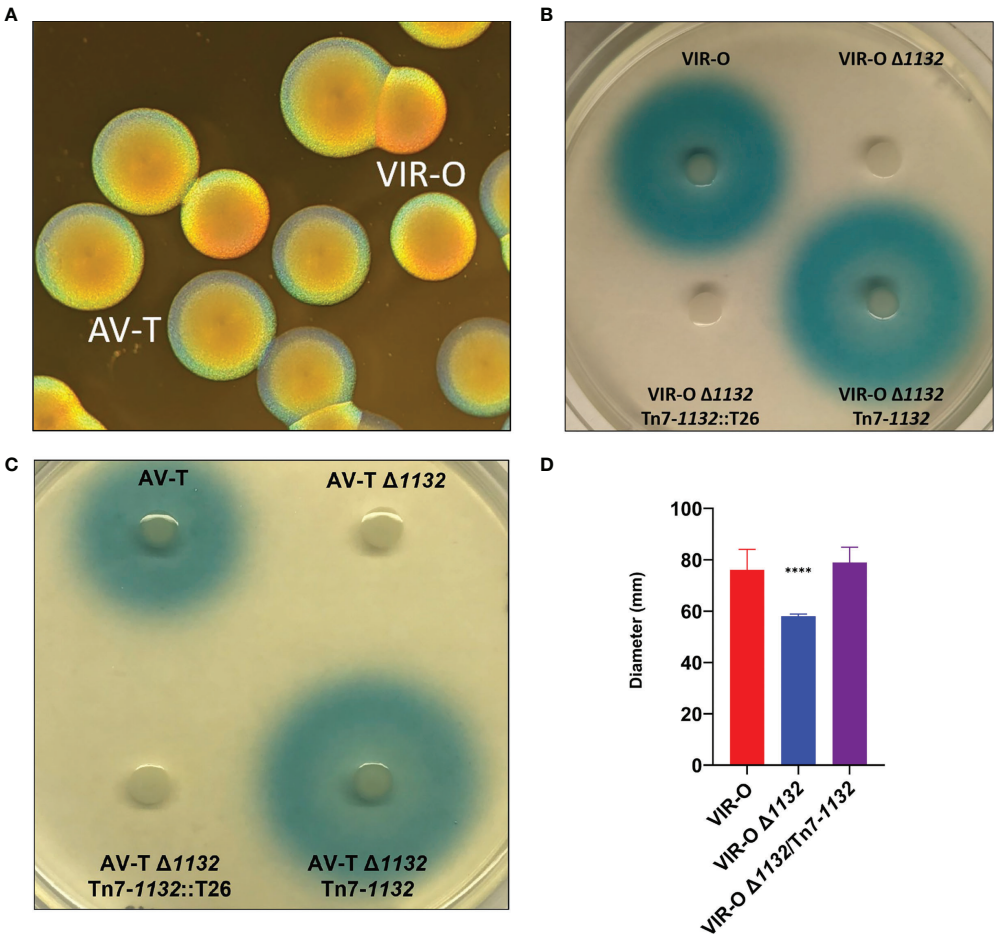

FIGURE 1 | **(A)** AB5075 Wild-type opaque (VIR-O) and translucent (AV-T) colonies, viewed under a dissecting microscope with oblique lighting from underneath. **(B)** Qualitative assay of AHL secretion in which cultures of the wild-type (VIR-O), the VIR-O Δ*1132* mutant, the complemented mutant (VIR-O Δ*1132*/Tn7-*1132*), and a version of the complemented mutant disrupted by transposon insertion (VIR-O Δ*1132*/Tn7-*1132*::T26) were spotted onto a soft agar lawn containing X-Gal and an *Agrobacterium tumefaciens traG*::*lacZ* biosensor that reacts to the presence of exogenous AHL by cleaving X-Gal, forming a blue halo. **(C)** Qualitative assay of AHL secretion in the wild-type (AV-T), the AV-T Δ*1132* mutant, the complemented mutant (AV-T Δ*1132*/Tn7-*1132*), and a version of the complemented mutant disrupted by transposon insertion (AV-T Δ*1132*/Tn7-*1132*::T26). Signal secretion was analyzed as in panel **(B)**, except the amount of X-gal was increased 2-fold. **(D)** Surface-associated motility of wild-type (VIR-O), the VIR-O Δ*1132* mutant, and the complemented mutant (VIR-O Δ*1132*/Tn7-*1132*) measured on 0.3% Eiken Agar plates. A Welch's ANOVA (****$p < 0.00005$) was carried out to assess **(D)** error bars indicate standard deviation of the mean.

colony growth and 20-40% at 48 hours (Chin et al., 2018). The two types have distinctly different genomic expression profiles as revealed by RNA sequencing, and a variety of gene products—including transcriptional regulators, a two-component system (OmpR/EnvZ), an efflux pump (ArpB), and a putative sRNA located upstream of a plasmid-encoded antibiotic resistance locus—appear to contribute to interconversion between VIR-O and AV-T (Tipton and Rather, 2016; Tipton et al., 2017; Chin et al., 2018; Anderson et al., 2020).

One such regulator, *ABUW_1645* (*1645*), is a TetR-type transcriptional regulator (TTTR) whose rate of expression is 150-fold higher in the AV-T state and whose overexpression in the VIR-O background drives conversion to the AV-T state (Chin et al., 2018). Although *1645* is crucial to the maintenance of the AV-T variant and is a key regulator of the VIR-O to AV-T switch, it does not appear to act in the same pathways as other previously discovered regulators of the switch such as *arpB* or *ompR* (Tipton and Rather, 2016; Tipton et al., 2017), a fact which emphasizes the complexity of the switching mechanism and the probable functional redundancy of many of the regulatory elements.

We continued to investigate additional genes to better understand the VIR-O and AV-T variants and the processes that regulate their interconversion. This led to the characterization of *ABUW_1132* (*1132*), a LysR-type transcriptional regulator (LTTR) that influences the VIR-O to AV-T switch. LTTRs are highly abundant in Proteobacteria (Reen et al., 2015) and are the most common type of transcriptional regulator in AB5075 at 24% (59/243) (Casella et al., 2017). They often function as global regulators and act in conjunction with a ligand molecule to repress and/or activate target genes (Maddocks and Oyston, 2008). Prototypical LTTRs are self-repressing and regulate gene(s) divergently transcribed from their own coding sequence, though these need not be the case.

A recent publication by our group detailed the identification of *1132* and its role in a *relA* mutant (*ΔrelA*), which exhibits increased quorum sensing signal secretion and hyper-motility (Perez-Varela et al., 2020). Quorum sensing in *A. baumannii* is carried out by a LuxI-LuxR type system composed of *abaI*, the autoinducer synthase, and *abaR*, the signal receptor and transcriptional regulator (Niu et al., 2008). We reported that the quorum sensing and motility phenotypes of *ΔrelA* were largely enacted through *1132*, which is overexpressed 14-fold in the absence of *relA* (Perez-Varela et al., 2020). Specifically, *1132* overexpression results in upregulation of the autoinducer synthase *abaI*, resulting in a large increase to secretion of the quorum sensing signal 3-OH-C_{12}-homoserine lactone. Expression of the *abaR* transcriptional regulator is also increased, resulting in strong upregulation of one of AbaR's targets: the *ABUW_3766-ABUW_3773* operon. This operon promotes production of the lipopeptide acinetin-505, which acts as a surfactant and gives rise to a hyper-motile phenotype.

This study builds on these findings and details multiple phenotypic changes resulting from the deletion of *1132;* including quorum sensing signal secretion, surface-associated motility, the virulence-opacity switch, capsule expression, and virulence in a mouse pneumonia model of infection.

RESULTS

ABUW *1132* Is a Global Regulator

To identify genes and pathways regulated by *1132*, we carried out genome-wide transcriptional profiling by RNA sequencing of VIR-O Δ*1132* vs. wild-type VIR-O, which revealed a total of 74 differentially regulated genes in VIR-O Δ*1132* (greater than 2-fold change, p value less than 0.05) (**Supplementary Table 1**). These results showed that *1132* impacts transcription of a variety of genes involved in regulation, metabolism, protein synthesis, and possibly the cell stress response. Genes that encode ribosomal proteins, RNA polymerase, translation initiation factors, and both transcriptional and translational elongation factors are among genes that are upregulated in VIR-O Δ*1132*. On the other hand, several genes that are downregulated in the absence of *1132* encode a variety of enzymes involved in oxidative stress protection including catalases, peroxidases and others that interact with glutathione.

Deletion of *1132* Impacts Quorum Sensing Signal Secretion and Motility

Deletion of *1132* results in loss of secretion of the quorum sensing signal 3-OH-C_{12}-HSL (AHL) (**Figure 1B**). This is based on the inability to activate an *Agrobacterium tumefaciens traG*::*lacZ* fusion when grown on a soft agar lawn containing this biosensor strain and X-Gal (Niu et al., 2008; Paulk Tierney and Rather, 2019). We utilized a Tn7 transposon system (Ducas-Mowchun et al., 2019a) to provide single-copy complementation of *1132* (VIR-O Δ*1132*-Tn7/*1132*), which restored AHL secretion. This restoration is lost again if the Tn7 copy of *1132* is disrupted (**Figure 1B**). The loss of AHL secretion also occurs in the AV-T Δ*1132* mutant (**Figure 1C**).

Considering our previously published findings that *1132* overexpression activates the *abaI-abaR* system (Perez-Varela et al., 2020), we hypothesized that loss of AHL secretion was due to downregulation of *abaI* when *1132* is deleted. Surprisingly, our RNA sequencing analysis indicated wild-type levels of *abaI* expression in VIR-O Δ*1132*, which we confirmed by qRT-PCR (**Supplementary Figure 1**). This result suggested that the mutant cells synthesize AHL, but do not secrete it. To investigate this possibility, we conducted an assay utilizing the *A. tumefaciens* biosensor in which 10% SDS was added to a well at the center of the plate (**Supplementary Figure 2**). Cultures of wild-type VIR-O, an *abaI* mutant (VIR-O *abaI*::T26), and VIR-O Δ*1132* were then added to the plate in lines going toward the SDS-containing well. As expected, we saw that the wild-type VIR-O cells uniformly activate the biosensor. However, the VIR-O Δ*1132* cells show activation of the biosensor only at the point where the VIR-O Δ*1132* cells have been lysed by the SDS in the presence of non-lysed biosensor cells, which confirmed our hypothesis that AHL is synthesized but cannot exit the cell. Since there is no activation by an *abaI* mutant near the SDS, the activating signal in the *1132* mutant is 3-OH-C_{12}-HSL and not a released metabolite. These results indicate a more complicated role for *1132* in quorum sensing than simple regulation of *abaI*, which is further considered in the *Discussion* section.

We previously reported that overexpression of *1132* increases surface-associated motility 3.8-fold and that this effect requires both *abaI* and the *ABUW_3766-ABUW_3773* operon (Perez-Varela et al., 2020). As expected, both VIR-O Δ*1132* and AV-T Δ*1132* demonstrate a significant decrease in motility compared to their wild-type counterparts, both which are complemented by the single-copy chromosomal insertion of *1132* (**Figure 1D**, only VIR-O results shown).

The *1132* deletion behaves in a manner opposite to *1132* overexpression with respect to motility, but the mechanism for this is unclear. As previously mentioned, *abaI* mRNA levels are unaffected by *1132* deletion, and although the RNA sequencing data shows a 1.5-fold downregulation of *abaR*, there are no transcriptional differences in the *ABUW_3766-ABUW_3773* operon (**Supplementary Table 1**). We also considered the possibility that AHL itself acts as a surfactant to some extent and that the loss of AHL secretion could reduce motility. To test this, we constructed a double mutant of *1132* and *abaR*—to control for quorum sensing-directed motility—and measured motility on 0.3% Eiken agar plates containing 1 μM synthetic 3-OH-C_{12}-HSL. However, motility was similar between the solvent control (38.75 mm ± 0.83) and the plate with AHL added (41.0 ± 1.73) p = 0.11.

Role of *1132* in Regulation of the VIR-O to AV-T Switch

VIR-O Δ*1132* exhibited lower levels of colony sectoring than observed for the wild-type VIR-O on 0.5X LB agar (**Figure 2A**). This lack of sectoring indicated a decreased rate of switching to the AV-T variant, and we subsequently quantified a 16.4-fold decrease in the switching frequency (**Figure 2B**). To confirm these effects were due to *1132* deletion, we provided single-copy complementation of *1132* using the Tn7 transposon system. This strain exhibited the wild-type phenotype of colony sectoring and restored VIR-O to AV-T switching to wild-type levels (**Figure 2B**).

Deletion of *1132* in the AV-T Background Increases Capsule

We further noted that AV-T Δ*1132* colonies are more opaque than wild-type AV-T colonies, although AV-T Δ*1132* is still translucent compared to the VIR-O Δ*1132* colonies (**Figures 3A, B**). Single-copy chromosomal complementation of the AV-T Δ*1132* mutant restored wild-type levels of translucence (**Figure 3A**). We first hypothesized that the increased opacity indicated hyper-switching from AV-T to VIR-O within the colony; however, the rate of switching was the same as the wild-type AV-T (**Supplementary Figure 3**). We then considered that the AV-T Δ*1132* mutant's increased opacity may be due to increased levels of capsule.

Previous work revealed that wild-type VIR-O cells exhibit a 2-fold increase in capsule compared with the wild-type AV-T (Chin et al., 2018). We utilized a Percoll density gradient, a method that was recently described as a method to separate *A.*

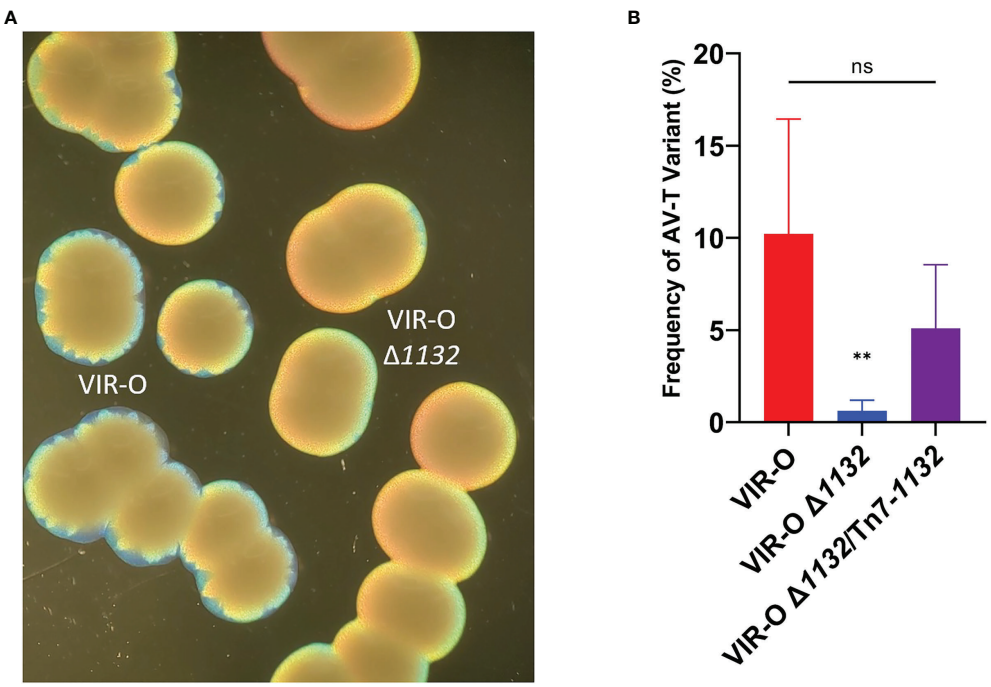

FIGURE 2 | The Reduced Switching Phenotypes in VIR-O Δ*1132*. **(A)** Micrograph showing the loss of sectoring in VIR-O Δ*1132* colonies compared to wild-type VIR-O colonies at 24 hours of growth. **(B)** Quantification of switching frequencies demonstrating restoration of normal switching of VIR-O Δ*1132* through single copy complementation (VIR-O Δ*1132*/Tn7-*1132*). The wild-type VIR-O and VIR-O Δ*1132* controls each have integrated an empty version of the pUC18T-mini-Tn7T-Apr-LAC insertion element into the attTn7 site. All micrographs were taken under a dissecting microscope illuminated from below the plate at an angle. All quantitative switching assays represent six colonies from each strain. A two-tailed Mann-Whitney test (**p < 0.005) was carried out for **(B)**, and error bars represent the standard deviation of the mean. ns, not significant. The p value represents a comparison of both wild-type to mutant and mutant to the complemented strain.

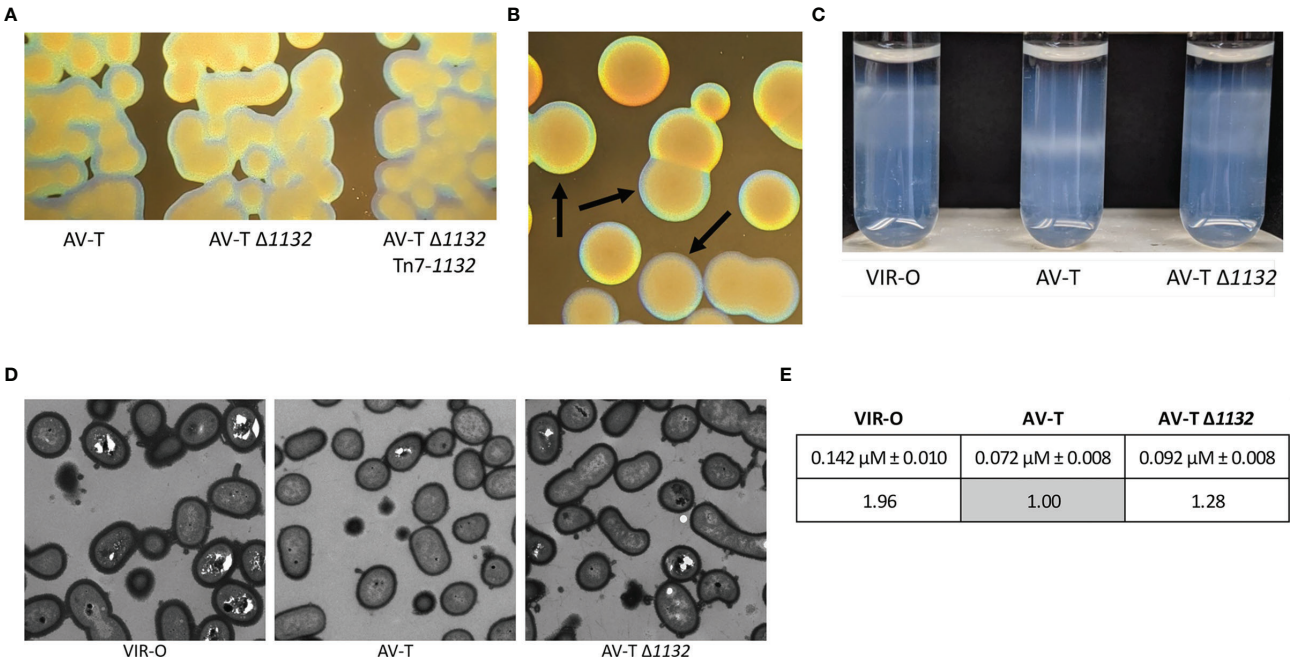

FIGURE 3 | Deletion of *1132* in the AV-T background alters the opacity phenotype and capsule expression. **(A)** Micrographs comparing representative colonies of AV-T, AV-T Δ*1132* and AV-T Δ*1132* Tn7-*1132*. **(B)** Micrographs comparing colonies of AV-T Δ*1132*, indicated by arrows, to VIR-O Δ*1132*. Micrographs were taken under a dissecting scope lit from underneath at an angle. **(C)** Wild-type VIR-O, wild-type AV-T, and AV-T Δ*1132* cells were layered onto a Percoll gradient (top layer 40%, bottom layer 50%) and centrifuged for 30 minutes at 3,000 xg. AV-T Δ*1132* cells migrate between the stopping points for VIR-O and AV-T wild-types, indicating intermediate capsular levels with high levels of heterogeneity in the AV-T Δ*1132* mutant. Photograph shown is one of six experimental replicates. **(D)** Transmission electron micrographs of representative wild-type VIR-O, wild-type AV-T, and AV-T Δ*1132* cells, stained with Ruthenium red. **(E)** Averages ± standard deviation of the mean of capsule widths of these three strains converted to ratios to the wild-type AV-T. The difference between the wild-type AV-T and AV-T Δ*1132* capsule widths is significant at $p < 0.0001$ as determined by a Student's two-tailed *t* test.

baumannii strains by capsule level (Kon et al., 2020), to compare capsular polysaccharide levels in AV-T Δ*1132* to wild-type VIR-O and AV-T cells. As seen in **Figure 3C**, the gradient is able to distinguish between capsule levels of the wild-type VIR-O and AV-T variants, with the AV-T cells migrating significantly further than the VIR-O cells. Intriguingly, AV-T Δ*1132* cells exhibited a high degree of heterogeneity and occupied a space in the gradient layer that was intermediate to that of the wild-type VIR-O and AV-T. We interpret this result as indication that deletion of *1132* causes a dysregulation and increase of capsule in the AV-T state, which imparts the more opaque appearance of AV-T Δ*1132*.

To confirm the effect of *1132* deletion on capsule, we next carried out TEM imaging of cell samples of wild-type VIR-O, wild-type AV-T, and AV-T Δ*1132* stained with Ruthenium red (**Figure 3D**). We used ImageJ to measure capsule width in 100 cells per strain with 3 measurements taken per cell, which revealed average capsule widths of 0.142 µM ± 0.010, 0.072 µM ± 0.008, and 0.092 µM ± 0.008 in VIR-O, AV-T, and AV-T Δ*1132*, respectively (**Figure 3E**). The resulting ratio of these values is 1.96:1.00:1.28, which demonstrates the 2-fold difference in capsule previously seen in the VIR-O vs. AV-T (Chin et al., 2018) and confirms a 28% increase in capsule in the AV-T background when *1132* is deleted. The difference between the wild-type AV-T and AV-T Δ*1132* is highly significant at $p < 0.0001$ as determined by a Student's two-tailed *t* test.

In light of these results, we considered that, in the AV-T state, *1132* may regulate the K locus genes that encode the proteins largely responsible for the biosynthesis and export of capsular polysaccharide (CPS). We assessed representative genes from the K locus—*manB, galE*, *ABUW_3818, ABUW_3820, ABUW_3821, ABUW_3830*, *wza, wzb*, and *wzc*—by qRT-PCR across three sets of samples (**Supplementary Figure 4**). These results indicated that *1132* did not transcriptionally regulate the K locus genes.

The Δ*1132* Mutation Increases Virulence in the AV-T Background

Capsule is a known virulence factor in *A. baumannii*, and presumably contributes to virulent phenotype of the VIR-O variant relative to AV-T (Russo et al., 2010; Chin et al., 2018; Singh et al., 2018; Tipton et al., 2018; Talyansky et al., 2021). The intermediate capsular levels of AV-T Δ*1132* therefore suggested that this deletion may increase virulence. Before initiating virulence studies, we first tested the growth rates of the AV-T and AV-T Δ*1132* strains and found no significant differences under laboratory conditions (**Supplementary Figure 5A**. Using the *Galleria mellonella* (waxworm) model of infection, a modest, but statistically significant increase in AV-T Δ*1132* virulence was

observed (**Figure 4A**). Waxworms injected with the wild-type AV-T control showed a 23.3% survival rate after five days, while only 10% of those injected with AV-T Δ*1132* survived. Complementation of AV-T Δ*1132* with the single-copy chromosomal insertion of *1132* (AV-T Δ*1132*/Tn7-*1132*) reversed the increase in virulence, bringing the rate of survival back up to 30%.

We next examined the virulence of AV-T Δ*1132* in a mouse pneumonia model of infection. In three experiments, mice were intranasally inoculated with 1 x 10^8 CFU/mL of VIR-O (n=10), AV-T (n=17), or AV-T Δ*1132* (n=17). At 24 hours post-inoculation, lungs were harvested, and the CFU/g for each tissue was calculated where a significant increase in CFU/g in AV-T Δ*1132* was observed compared to wild-type AV-T in the lungs (**Figure 4B**). Both strains exhibited a similar number of VIR-O variants recovered from the lungs (approximately 0.1%). The highly virulent VIR-O variant was unaffected by the Δ*1132* mutation in both a *Galleria mellonella* waxworm model and in a mouse pneumonia model (**Supplementary Figures 5B, C**) and both strains exhibited similar growth rates *in-vitro* (**Supplementary Figure 5A**).

DISCUSSION

This study confirms 1132 as a global transcriptional regulator that impacts multiple pathways: surface-associated motility, AHL secretion, regulation of the opacity-virulence switch, and capsule expression. Most importantly, our work demonstrates that an *1132* deletion, and possibly its natural downregulation, has the potential to increase virulence of the typically avirulent translucent colony variant in the clinical isolate AB5075. The *1132* gene was highly conserved in all completed *A. baumannii* genome sequences (n = 330), where at least 98.7% nucleotide homology was observed. The gene was also conserved in *A. nosocomialis* (91.7% or greater nucleotide identity), *A. seifertii* (89.8% or greater identity) and *A. pittii* (83.7% or greater identity). Given the high conservation of *1132* among *A. baumannii* strains, it is likely that the *1132*-associated phenotypes we have reported here and in a previous publication (Perez-Varela et al., 2020) will also be conserved in other strains.

Some questions remain regarding the mechanisms through which 1132 acts in the described phenotypes. As previously mentioned, in our earlier publication we determined that overexpression of *1132* causes large increases in AHL secretion and surface-associated motility. This occurs through activation of the *abaI-abaR* system and follows a well-defined downstream pathway ending with overproduction of the surfactant acinetin-505 (Perez-Varela et al., 2020) Perplexingly, although the deletion of *1132* results in phenotypes opposite to that of *1132* overexpression —loss of both AHL secretion and motility—our experiments show that neither of these phenotypes are due to transcriptional downregulation of the *abaI-abaR* system or the *ABUW_3766-ABUW_3773* operon. A post-transcriptional effect of *1132* on *abaI* also seems unlikely, as VIR-O Δ*1132* cells lysed in the presence of the AHL-detecting biosensor are able to activate the *traG*::*lacZ* fusion, indicating a functional AbaI protein (**Supplementary Figure 2**). It is possible that the length of the *N*-acyl chain of the AHL molecule is altered due to the global changes that occur when *1132* is deleted. Both shortened and elongated chains could affect the hydrophobicity of the AHL molecule and therefore have the potential to disrupt diffusion or export of the autoinducer across the membrane. Due to the trapping of signal within the cell, it is possible that the quorum sensing response is altered, possibly being activated earlier in cell density, or being constitutive. With respect to capsule, the effect of 1132 on capsule thickness did not involve transcriptional changes in representative genes within the capsule locus. Therefore, the *1132* mutation may alter biosynthetic pathways that impact precursors for capsule

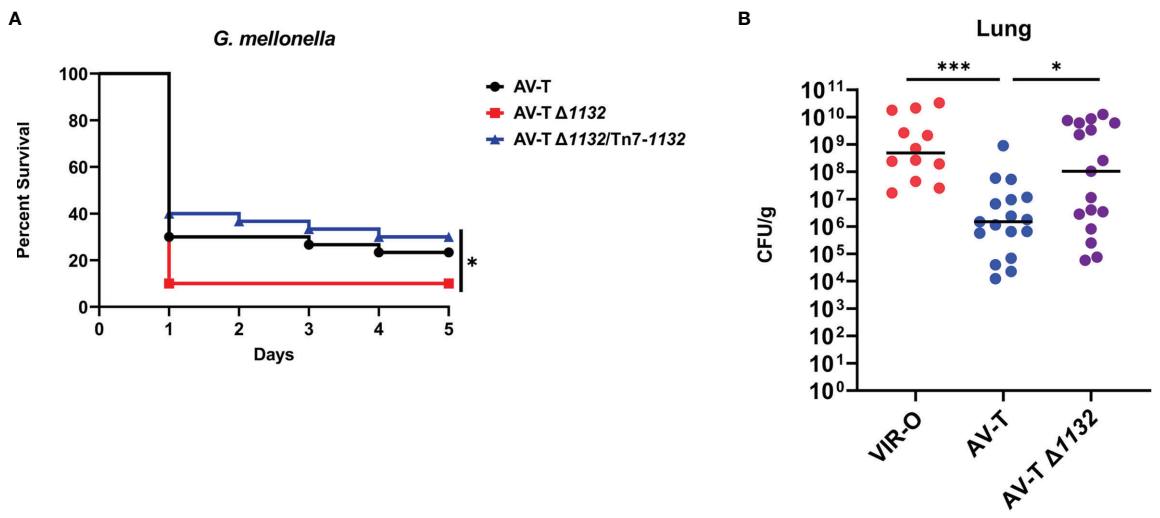

FIGURE 4 | Deletion of *1132* in AV-T background increases virulence. **(A)** *Galleria mellonella* infected with AV-T Δ*1132* are killed at higher rates compared with wild-type AV-T or the complemented mutant (AV-T Δ*1132*/Tn7-*1132*). **(B)** Bacterial CFU/g recovered from mice lungs 24 hours after intranasal inoculation with pure cultures of wild-type VIR-O, wild-type AV-T, or AV-T Δ*1132*. A Log-Rank (Mantel-Cox) test (*p < 0.05) was carried out for **(A)** and a two-tailed Mann-Whitney test (*p < 0.05; ***p < 0.0005) was carried out for **(B)**.

synthesis in a manner that increases their abundance and results in enhanced capsule thickness.

This work revealed that *1132* positively regulated the VIR-O to AV-T switch and experiments to address the mechanism for this increase are ongoing. It is possible that one or more of several regulatory genes revealed by the RNA sequencing as differentially regulated by 1132 is involved. However, it is intriguing that other known regulators of the switch, including the OmpR/EnvZ two-component system and the ArpB efflux pump, were not regulated by 1132. A possibility is that the *1132* deletion creates a cellular metabolome that withholds ligands or other molecules required by other known regulators of the switch, such as the TetR regulator *ABUW_1645* (Chin et al., 2018). It is important to note that the lack of AHL secretion is not expected to impact the switch, as deletion of *abaI* does not cause alteration of switching frequency (Tipton et al., 2015).

Our work here has important implications for the characterizations of VIR-O cells as virulent and AV-T cells as avirulent. While the increase in virulence in the AV-T variant caused by *1132* deletion was modest, this finding demonstrates that stochastic downregulation of *1132*—potentially mediated by RelA's repression of *1132*—may allow an AV-T cell to be moderately virulent in a mammalian host without necessitating a switch to the VIR-O state. We have previously hypothesized that AV-T cells possess an advantage in natural environments due to their versatility in utilization of carbon sources and their improved formation of biofilm (Chin et al., 2018). Combined, these observations suggest that AB5075, and possibly other *A. baumannii* strains, could survive in a natural environment while existing in a virulent state.

MATERIALS AND METHODS

Bacterial Strains and Growth Conditions

All experiments were conducted using the clinical isolate AB5075. For all experiments, cultures were started from frozen glycerol stocks containing at least 99.5% of the desired colony variant (VIR-O or AV-T). Cultures were grown in either broth or on solid media containing LB (10 g tryptone, 5 g yeast extract, and 5 g NaCl per liter) and 1.5% agar (Difco) ("1X" LB agar) or 0.8% agar ("0.5X" LB agar).

Methods to Distinguish Colony Variants

Cultures were plated or streaked on 0.5X LB agar and viewed under a dissecting microscope, illuminated from underneath at an oblique angle. Colonies must be viewed at high colony density (at least 100 colonies per plate) to effectively distinguish VIR-O and AV-T colonies.

Detection of 3-OH-C_{12}-HSL

Plates containing the *Agrobacterium tumefaciens traG*::*lacZ* biosensor and X-Gal were prepared as described in Paulk Tierney and Rather (2019). AB5075 cell cultures were grown in 2 mL LB to OD_{600} ~ 0.3, and 1 μL was spotted onto the soft agar lawn. Plates were incubated at 28°C overnight.

Quantification of VIR-O and AV-T Switching

Dilutions were plated from frozen pure stocks of the strains to be assessed, and plates were incubated at 37°C for a set number of growth hours. High density plates were used to verify the purity of the stock. Isolated colonies were extracted from the plate by cutting out a section of agar underlying the colony and then resuspended and dilutions plated. The percent variant was then determined for each set of resuspended colonies from each strain. All experiments were performed twice with three colonies each for a total of six colonies.

Electroporation

Cell cultures for competent cells were grown in 2 mL LB to OD_{600} ~ 0.5 (mid-log phase) at 37°C, shaking from frozen stocks. Cultures were pelleted and washed twice in sterile dH_2O, then resuspended to accommodate a volume of approximately 50 μL of cell per electroporation. Plasmid minipreps or ligation products mixed with cells were added to 2 mm cuvettes and electroporated at 2.5 kV. Cells were recovered in 1 mL LB at 37°C, shaking for one hour, then plated onto media containing selective antibiotics.

Construction of Deletion Mutations

In-frame deletion of *ABUW_1132* was generated using sucrose counterselection and a suicide vector containing the *sacB* marker (pEX18Tc) using methods previously described (Hoang et al., 1998). Briefly, PCR amplification (Phusion polymerase, Thermo-Fisher Scientific) was used to amplify the 2-kb regions upstream and downstream of the gene to be deleted, gel purified (UltraClean 15 DNA Purification Kit, MO BIO Laboratories), and ligated (Fast-Link DNA Ligation Kit, Epicentre Biotechnologies). The 4-kb ligation product was PCR amplified, gel purified, and ligated into the pEX18Tc vector MCS. The product vector was verified by sequencing and then transformed into competent *E. coli* Transformax EC100D cells (Epicentre Biotechnologies) by electroporation. The resulting suicide vector was confirmed by PCR and transformed by electroporation into AB5075, grown to OD_{600} of 0.5 in 2-mL LB and washed twice in 10% glycerol. Transformants were plated on 1X LB agar plus Tetracycline (5-μg/mL) to yield single-crossover mutants. Counterselection was carried out at room temperature on 1X LB plates with 10% sucrose and no NaCl, and colonies were screened by PCR for the deletion. Primer sequences are recorded in **Supplementary Table 2**.

To construct the Δ*1132*, *abaR*::T26 double mutant, genomic DNA was purified from an *abaR*::T26 mutant obtained from the University of Washington AB5075 transposon mutant library. Genomic DNA was then electroporated into VIR-O Δ*1132*. Transformants were selected on 1X LB plus Tetracycline (5-μg/mL) and confirmed by PCR.

Construction of Single-Copy Complementation in Deletion Mutants

We utilized a Tn7-based single-copy insertion element system (Ducas-Mowchun et al., 2019a; Ducas-Mowchun et al., 2019b) to reintroduce *1132* into the VIR-O Δ*1132* and AV-T Δ*1132* deletion mutants. We opted to use a segment of *1132* that

includes a large portion of the up and downstream regions (GenBank Accession NZ_CP008706.1:1152309-1156236). This is the portion of the genome contained within the original *1132*-containing fragment isolated from a high-copy AB5075 chromosomal library during the screen that led to our first discovery of *1132* (Perez-Varela et al., 2020), and previous experiments showed that this fragment allows for optimal expression of *1132*. A modified version of this construct containing a T26 transposon (tetracycline) in *1132* had also been made to confirm loss of the phenotypes presumably caused by *1132* overexpression. This was made by digestion of the plasmid with PmlI, which cuts once near the beginning of the *1132* ORF, and re-ligation with a PCR-amplified T26 transposon. The original *1132*-containing fragment and the modified version with *1132*::T26 were excised from these plasmids by digestion with XbaI, which flanks the site into which the library was cloned, and gel purified to be used in construction of the suicide vector.

The pUC18T-mini-Tn*7*T-Apr-LAC construct was digested with SpeI and ligated with the *1132*- or *1132*::T26-containing fragment (Fast-Link DNA Ligation Kit, Epicentre Biotechnologies). The ligation product was transformed into competent *E. coli* Transformax EC100D cells (Epicentre Biotechnologies) by electroporation. The resulting constructs—pUC18T-mini-Tn*7*T-Apr-LAC/*1132* and pUC18T-mini-Tn*7*T-Apr-LAC/*1132*::T26—were confirmed by PCR and sequencing then transformed into pure cultures of VIR-O Δ*1132* and AV-T Δ*1132* by electroporation along with the helper plasmid pTNS2. Transformant colonies were screened by PCR for insertion into the *att*Tn7 site and those containing the correct insertion were again verified by sequencing. Wild-type Tn7 and Δ*1132*-Tn7 control strains were also made in both VIR-O and AV-T backgrounds using the same methods with an empty pUC18T-mini-Tn*7*T-Apr-LAC construct. Primer sequences are recorded in **Supplementary Table 2**.

RNA Preparation and qRT-PCR Analysis

Strains for qRT-PCR analysis in **Supplementary Figure 1** were prepared for RNA isolation by growing them from pure frozen stocks to OD_{600} ~ 0.15 then plating 100 μL on a 1X LB plate. Plates were incubated at 37°C for 6 hours, then pooled with 3 mL ice cold LB. Resuspensions were normalized to within OD_{600} of 0.01, then 1 mL of the resuspension was pelleted, flash frozen in an ethanol-dry ice bath and stored at -80°C. The resuspension cultures were streaked on 0.5X LB to ensure sample purity.

Strains for qRT-PCR analysis in **Supplementary Figure 4** were grown up to match the growth conditions of the cells prepared for electron microscopy (see below). Samples were grown from pure frozen stocks in overnight cultures of 2 mL LB and were then shaken at 37°C to the same OD_{600} of 0.3. 20 μL of each culture was then plated as a line onto a 0.5X plate, allowed to incubate at 37°C for 4 hours, and then harvested off the plate. Scraped cells were resuspended to an OD_{600} of 0.6 in 2 mL LB. 1 mL of cells was pelleted, flash frozen in an ethanol-dry ice bath, then stored at -80°C. The resuspension cultures were streaked on 0.5X LB to ensure sample purity.

RNA was prepared using the Epicentre MasterPure RNA Purification kit according to the manufacturer's protocols. The resulting nucleic acid product was purified to remove DNA contamination using the Invitrogen TURBO DNA-*free* kit according to the manufacturer's instructions. Following quantification of RNA concentration using a NanoDrop ND-1000 spectrophotometer, cDNA was prepared from 1 μg of RNA using the High-Capacity cDNA Reverse Transcription Kit by Applied Biosystems and subsequently diluted 1:10 in nuclease-free water. qRT-PCR experiments were carried out on a Bio-Rad CFX Connect Real-Time PCR Detection System using iQ SYBR Green Supermix reverse transcriptase from Bio-Rad. RNA purity was confirmed by qRT-PCR through the inclusion of template controls made without reverse transcriptase. qRT-PCR data was analyzed by the delta-delta Ct method ($2^{-\Delta\Delta Ct}$) with comparison to *16S* as an internal control. This method was carried out for three biological replicates. Each biological replicate had three technical replicates for each primer set. Primer sequences are recorded in **Supplementary Table 2**.

RNA Sequencing and Analysis

Three independent sets of RNA were prepared from each of AB5075 strains VIR-O and VIR-O Δ*1132*. Cultures were grown in 2 mL LB from pure frozen stocks to OD_{600} ~ 0.5 (shaking, 37°C) and were streaked on 0.5X LB to ensure purity of samples. 1 mL of cells was pelleted and flash frozen in a dry ice bath before being stored at -80°C. RNA was prepared using the Epicentre MasterPure RNA Purification kit according to the manufacturer's protocols.

RNA quality control, sequencing, and analysis was carried out by the Yerkes Non-Human Primate Genomics Core at Emory University. RNA quantity and quality assessments were carried out using a Thermo Nanodrop2000 and Agilent 2100 Bioanalyzer, respectively. RNA sequencing was carried out using an Illumina HiSeq 3000, and reads were normalized and mapped using Cufflinks software. The RNA-Seq data discussed in this publication have been deposited in NCBI's Gene Expression Omnibus and are accessible through GEO Series accession number GSE185730 (https://www.ncbi.nlm.nih.gov/geo/query/acc.cgi?acc=GSE185730).

Percoll Density Gradient

Method slightly modified from Kon et al. (2020). Cell cultures of VIR-O, AV-T, and AV-T Δ*1132* were grown in 2 mL LB from pure frozen stocks to OD_{600} ~ 0.6 (shaking, 37°C). For each strain, 600 μL of cells was pelleted and washed in PBS 1X, then resuspended in 100 μL PBS 1X. Percoll solutions were prepared by first mixing 9 parts Percoll (Sigma Aldrich Cat. P4937) and 1 part 1.5 M NaCl, which was further diluted using 0.15 M NaCl to make 40% and 50% Percoll solutions. For each cell sample to be tested, 1 mL of 40% Percoll was added to a 12x75 mm glass tube (Fisherbrand 14958C), and 1 mL 50% Percoll was gently layered underneath using a 1cc syringe and a 1.5 in. 23G needle (BD 305194). 100 μL of cells were gently layered at the top of the gradient. Samples were spun at 3,000 xg for 30 minutes at room temperature and then visually assessed. This protocol was repeated 6 times.

Electron Microscopy

Ruthenium red-lysine fixation and cell staining and subsequent transmission electron microscopy were performed by the Robert P. Apkarian Integrated Electron Microscopy Core at Emory University using previously described techniques (Fassel et al., 1997; Fassel et al.,1998; Beaussart et al., 2014). Samples were provided to the EM Core as follows: cells grown from pure frozen stocks in overnight cultures were shaken at 37°C until OD ~ 0.30, and 20 µL of each culture was plated as a line onto the same 0.5X LB plate. Plates were then incubated at 37°C for 4 hours and stored overnight at 4°C before being transported to the EM Core.

Capsule widths in the electron micrographs were measured by ImageJ 1.53e (Rasband, W.S., ImageJ, U. S. National Institutes of Health, Bethesda, Maryland, USA, https://imagej.nih.gov/ij/, 1997-2018). Three measurements were taken for 100 cells of each strain at the same magnification, which were averaged and then converted to micrometers.

Galleria mellonella Larvae (Waxworm) Virulence Assays

Waxworms were purchased from Speedy Worm (www.speedyworm.com). Cultures of AV-T, AV-T Δ*1132*, and AV-T Δ*1132*/Tn7-*1132* were grown in 2 mL LB from pure frozen stocks to OD_{600} ~ 0.5 (shaking, 37°C). 5 µL of a LB control, AV-T, AV-T Δ*1132*, or AV-T Δ*1132*/Tn7-*1132* was injected into the hemolymph of a larvae of mass 150-200 mg (n=30 per condition; approximately 1.2 x 10^6 CFU were administered per strain). Larvae were then housed in petri dishes in a humidified incubator at 37°C for 5 days. Each day, dead larvae were removed and surviving larvae counted.

Mouse Virulence Assays

Approximately 1 × 10^8 CFU were administered per mouse for infections to quantify the bacterial load. For mouse infections, overnight standing bacterial cultures at room temperature were sub-cultured in LB broth and grown at 37°C with shaking to an OD600 ~0.15, washed and re-suspended in PBS. Each mouse was inoculated intranasally with 50 µL of bacteria. Mice were anesthetized with isoflurane immediately prior to intranasal inoculation. At 24 hours, the mice were sacrificed and the lungs were harvested, homogenized, and ten-fold serial dilutions plated for CFU on 0.5X LB plates. The mouse strain used was C57BL/6J (females at 8-10 weeks of age) from Jackson Laboratories (JAX stock #000664). Experiments were carried out under the Institutional Animal Care and Use Committee guidelines.

Statistics

Statistics were performed using GraphPad Prism 9.2.0 software for Windows (GraphPad Software, San Diego, California USA, www.graphpad.com). The following statistical tests were utilized: (1) Mann-Whitney test for the mouse experiments (two-tailed), two-sample switching assays (two-tailed), motility assays (two-tailed) and qRT-PCR experiments (two-tailed or multiple, as indicated); (2) Log-Rank (Mantel-Cox) test for the *Galleria mellonella* experiments; (3) Welch's ANOVA analysis for three-sample switching assays; and (4) Student's two-tailed *t* test for capsule width measurements from the TEM micrographs. The Mann-Whitney test was utilized instead of a Student's *t* test to allow for the possibility or reality of a non-Gaussian distribution. Welch's ANOVA was chosen over standard ANOVA to allow for unequal variance between samples.

DATA AVAILABILITY STATEMENT

The RNA-Seq data presented in this study have been deposited in NCBI's Gene Expression Omnibus and are accessible through GEO Series accession number GSE185730 (https://www.ncbi.nlm.nih.gov/geo/query/acc.cgi?acc=GSE185730).

ETHICS STATEMENT

The animal study was reviewed and approved by Emory University Institutional Animal Care and Use Committee.

AUTHOR CONTRIBUTIONS

PR and AT conceptualized and designed the study and experiments. AT carried out all of the experiments except the RNA sequencing, mouse experiments, and electron microscopy. CC performed the mouse experiments and subsequent data analysis. AT analysed all other data with guidance from PR. AT and CC wrote the original manuscript. All authors contributed to the article and approved the submitted version.

FUNDING

Research in the PNR Laboratory is supported by T32 AI106699 to AT and NIH R01 AI72219 and R21 AI115183 and Department of Veterans Affairs awards I01 BX001725 and IK6BX004470 to PR. Research in the DSW Laboratory is supported by a Department of Veteran's Affairs award BX002788. DW is also supported by a Burroughs Wellcome Fund Investigators in the Pathogenesis of Infectious Disease award. The content expressed herein is solely the responsibility of the authors and does not necessarily represent the official views of the NIH or the Department of Veterans Affairs.

ACKNOWLEDGMENTS

We thank Dr. M. Pérez-Varela for critical reading of this manuscript and Drs. K.A. Tipton, S.E. Anderson, J.M. Colquhoun, and M. Pérez-Varela for their valuable input. We are grateful to Dr. Ayush Kumar at the University of Manitoba for providing pUC18T-mini-Tn7T-Apr-LAC. This work was supported in part by the Robert P. Apkarian Integrated Electron Microscopy Core at Emory University, and we especially thank Jeannette Taylor and Dr. Ricardo C. Guerrero for conducting the electron microscopy.

SUPPLEMENTARY MATERIAL

The Supplementary Material for this article can be found online at: https://www.frontiersin.org/articles/10.3389/fcimb.2021.778331/full#supplementary-material

Supplementary Figure 1 | Deletion of *1132* does not affect *abaI* expression. qRT-PCR experiments comparing wild-type VIR-O and VIR-O Δ*1132* indicate no significant difference in the expression of *abaI*, using *16S* as an internal control (two-tailed Mann-Whitney test, ns, not significant). Results are the average of three biological replicates.

Supplementary Figure 2 | VIR-O Δ*1132* cells contain quorum sensing signal (AHL), but do not secrete it. Cultures of wild-type VIR-O, VIR-O Δ*1132*, and VIR-O Δ*abaI* were grown to the same OD_{600} and plated as a line onto a soft-agar lawn containing *Agrobacterium tumefaciens* (*traG*::*lacZ*) and X-Gal. 10% SDS was added to a well at the center of the plate, lysing the cells.

Supplementary Figure 3 | AV-T Δ*1132* switches to the VIR-O variant at the same frequency as wild-type AV-T. Bars represent averages of six colonies assayed for switching frequency at 18 hours of growth. Error bars indicate standard deviation of the mean, and there is no statistical significance as assessed by Welch's ANOVA.

Supplementary Figure 4 | K locus genes for capsule polysaccharide synthesis and export are not transcriptionally regulated by 1132. Bars for AV-T Δ*1132* and AV-T Δ*1132*/Tn*7*-*1132* represent averages of three biological replicates. Error bars indicate standard deviation of the mean, and there is no statistical significance in expression across strains as assessed by multiple Mann-Whitney tests.

Supplementary Figure 5 | (A) Growth curves for VIR-O, AV-T, VIR-O Δ*1132*, and AV-T Δ*1132* in LB media. Data represents two biological replicates, and error bars indicate standard deviation of the mean. **(B)** *Galleria mellonella* infected with VIR-O Δ*1132* show no significant difference in mortality compared with wild-type VIR-O (n=30 per strain) as assessed by a log-rank (Mantel-Cox) test. **(C)** Mice were infected intranasally with either VIR-O or VIR-O Δ*1132*. At 24 hours post-inoculation, bacteria were recovered from the lungs, spleen, and liver tissues and CFU/g quantified. There is no significant difference between the two strains in all tissues as assessed by a Mann-Whitney test. ns, not significant.

REFERENCES

Anderson, S. E., Chin, C. Y., Weiss, D. S., and Rather, P. N. (2020). Copy Number of an Integron-Encoded Antibiotic Resistance Locus Regulates a Virulence and Opacity Switch in Acinetobacter Baumannii AB5075. *mBio* 11. doi: 10.1128/mBio.02338-20

Beaussart, A., Péchoux, C., Trieu-Cuot, P., Hols, P., Mistou, M. Y., and Dufrêne, Y. F. (2014). Molecular Mapping of the Cell Wall Polysaccharides of the Human Pathogen Streptococcus Agalactiae. *Nanoscale* 6, 14820–14827. doi: 10.1039/C4NR05280C

Bravo, Z., Orruno, M., Navascues, T., Ogayar, E., Ramos-Vivas, J., Kaberdin, V. R., et al. (2019). Analysis of Acinetobacter Baumannii Survival in Liquid Media and on Solid Matrices as Well as Effect of Disinfectants. *J. Hosp. Infect.* 103, e42–e52. doi: 10.1016/j.jhin.2019.04.009

Casella, L. G., Weiss, A., Pérez-Rueda, E., Antonio Ibarra, J., and Shaw, L. N. (2017). Towards the Complete Proteinaceous Regulome of Acinetobacter Baumannii. *Microb. Genom.* 3, mgen000107. doi: 10.1099/mgen.0.000107

Centers for Disease Control and Prevention (2019). *Antibiotic Resistance Threats in the United States, 2019* (Atlanta, GA). Available at: https://www.cdc.gov/drugresistance/pdf/threats-report/2019-ar-threats-report-508.pdf (Accessed August 2 2021).

Chapartegui-Gonzalez, I., Lazaro-Diez, M., Bravo, Z., Navas, J., Icardo, J. M., and Ramos-Vivas, J. (2018). Acinetobacter Baumannii Maintains its Virulence After Long-Time Starvation. *PloS One* 13, e0201961. doi: 10.1371/journal.pone.0201961

Chin, C. Y., Tipton, K. A., Farokhyfar, M., Burd, E. M., Weiss, D. S., and Rather, P. N. (2018). A High-Frequency Phenotypic Switch Links Bacterial Virulence and Environmental Survival in Acinetobacter Baumannii. *Nat. Microbiol.* 3, 563–569. doi: 10.1038/s41564-018-0151-5

Clark, N. M., Zhanel, G. G., and Lynch, J. P.3rd (2016). Emergence of Antimicrobial Resistance Among Acinetobacter Species: A Global Threat. *Curr. Opin. Crit. Care* 22, 491–499. doi: 10.1097/MCC.0000000000000337

D'souza, A. W., Potter, R. F., Wallace, M., Shupe, A., Patel, S., Sun, X., et al. (2019). Spatiotemporal Dynamics of Multidrug Resistant Bacteria on Intensive Care Unit Surfaces. *Nat. Commun.* 10, 4569. doi: 10.1038/s41467-019-12563-1

Davis, K. A., Moran, K. A., Mcallister, C. K., and Gray, P. J. (2005). Multidrug-Resistant Acinetobacter Extremity Infections in Soldiers. *Emerg. Infect. Dis.* 11, 1218–1224. doi: 10.3201/1108.050103

Dijkshoorn, L., Nemec, A., and Seifert, H. (2007). An Increasing Threat in Hospitals: Multidrug-Resistant Acinetobacter Baumannii. *Nat. Rev. Microbiol.* 5, 939–951. doi: 10.1038/nrmicro1789

Doyle, J. S., Buising, K. L., Thursky, K. A., Worth, L. J., and Richards, M. J. (2011). Epidemiology of Infections Acquired in Intensive Care Units. *Semin. Respir. Crit. Care Med.* 32, 115–138. doi: 10.1055/s-0031-1275525

Ducas-Mowchun, K., De Silva, P. M., Crisostomo, L., Fernando, D. M., Chao, T. C., Pelka, P., et al. (2019a). Next Generation of Tn7-Based Single-Copy Insertion Elements for Use in Multi- and Pan-Drug-Resistant Strains of Acinetobacter Baumannii. *Appl. Environ. Microbiol.* 85. doi: 10.1128/AEM.00066-19

Ducas-Mowchun, K., De Silva, P. M., Patidar, R., Schweizer, H. P., and Kumar, A. (2019b). Tn7-Based Single-Copy Insertion Vectors for Acinetobacter Baumannii. *Methods Mol. Biol.* 1946, 135–150. doi: 10.1007/978-1-4939-9118-1_13

Fassel, T. A., Mozdziak, P. E., Sanger, J. R., and Edmiston, C. E. (1997). Paraformaldehyde Effect on Ruthenium Red and Lysine Preservation and Staining of the Staphylococcal Glycocalyx. *Microsc. Res. Tech.* 36, 422–427. doi: 10.1002/(SICI)1097-0029(19970301)36:5<422::AID-JEMT12>3.0.CO;2-U

Fassel, T. A., Mozdziak, P. E., Sanger, J. R., and Edmiston, C. E. (1998). Superior Preservation of the Staphylococcal Glycocalyx With Aldehyde-Ruthenium Red and Select Lysine Salts Using Extended Fixation Times. *Microsc. Res. Tech.* 41, 291–297. doi: 10.1002/(SICI)1097-0029(19980515)41:4<291::AID-JEMT2>3.0.CO;2-U

Gallagher, L. A., Ramage, E., Weiss, E. J., Radey, M., Hayden, H. S., Held, K. G., et al. (2015). Resources for Genetic and Genomic Analysis of Emerging Pathogen Acinetobacter Baumannii. *J. Bacteriol.* 197, 2027–2035. doi: 10.1128/JB.00131-15

Hoang, T. T., Karkhoff-Schweizer, R. R., Kutchma, A. J., and Schweizer, H. P. (1998). A Broad-Host-Range Flp-FRT Recombination System for Site-Specific Excision of Chromosomally-Located DNA Sequences: Application for Isolation of Unmarked Pseudomonas Aeruginosa Mutants. *Gene* 212, 77–86. doi: 10.1016/S0378-1119(98)00130-9

Jacobs, A. C., Thompson, M. G., Black, C. C., Kessler, J. L., Clark, L. P., Mcqueary, C. N., et al. (2014). AB5075, a Highly Virulent Isolate of Acinetobacter Baumannii, as a Model Strain for the Evaluation of Pathogenesis and Antimicrobial Treatments. *mBio* 5, e01076–e01014. doi: 10.1128/mBio.01076-14

Jawad, A., Seifert, H., Snelling, A. M., Heritage, J., and Hawkey, P. M. (1998). Survival of Acinetobacter Baumannii on Dry Surfaces: Comparison of Outbreak and Sporadic Isolates. *J. Clin. Microbiol.* 36, 1938–1941. doi: 10.1128/JCM.36.7.1938-1941.1998

Kon, H., Schwartz, D., Temkin, E., Carmeli, Y., and Lellouche, J. (2020). Rapid Identification of Capsulated Acinetobacter Baumannii Using a Density-Dependent Gradient Test. *BMC Microbiol.* 20, 285. doi: 10.1186/s12866-020-01971-9

Lee, C. R., Lee, J. H., Park, M., Park, K. S., Bae, I. K., Kim, Y. B., et al. (2017). Biology of Acinetobacter Baumannii: Pathogenesis, Antibiotic Resistance Mechanisms, and Prospective Treatment Options. *Front. Cell Infect. Microbiol.* 7, 55. doi: 10.3389/fcimb.2017.00055

Maddocks, S. E., and Oyston, P. C. F. (2008). Structure and Function of the LysR-Type Transcriptional Regulator (LTTR) Family Proteins. *Microbiology* 154, 3609–3623. doi: 10.1099/mic.0.2008/022772-0

Niu, C., Clemmer, K. M., Bonomo, R. A., and Rather, P. N. (2008). Isolation and Characterization of an Autoinducer Synthase From Acinetobacter Baumannii. *J. Bacteriol.* 190, 3386–3392. doi: 10.1128/JB.01929-07

Paulk Tierney, A. R., and Rather, P. N. (2019). Methods for Detecting N-Acyl Homoserine Lactone Production in Acinetobacter Baumannii. *Methods Mol. Biol.* 1946, 253–258. doi: 10.1007/978-1-4939-9118-1_23

Peleg, A. Y., and Hooper, D. C. (2010). Hospital-Acquired Infections Due to Gram-Negative Bacteria. *N. Engl. J. Med.* 362, 1804–1813. doi: 10.1056/NEJMra0904124

Peleg, A. Y., Seifert, H., and Paterson, D. L. (2008). Acinetobacter Baumannii: Emergence of a Successful Pathogen. *Clin. Microbiol. Rev.* 21, 538–582. doi: 10.1128/CMR.00058-07

Perez-Varela, M., Tierney, A. R. P., Kim, J., Vazquez-Torres, A., and Rather, P. N. (2020). Characterization of RelA in Acinetobacter Baumannii. *J. Bacteriol.* doi: 10.1128/JB.00045-20

Reen, F. J., Romano, S., Dobson, A. D., and O'gara, F. (2015). The Sound of Silence: Activating Silent Biosynthetic Gene Clusters in Marine Microorganisms. *Mar. Drugs* 13, 4754–4783. doi: 10.3390/md13084754

Rocha, I. V., Xavier, D. E., Almeida, K. R. H., Oliveira, S. R., and Leal, N. C. (2018). Multidrug-Resistant Acinetobacter Baumannii Clones Persist on Hospital Inanimate Surfaces. *Braz. J. Infect. Dis.* 22, 438–441. doi: 10.1016/j.bjid.2018.08.004

Russo, T. A., Luke, N. R., Beanan, J. M., Olson, R., Sauberan, S. L., Macdonald, U., et al. (2010). The K1 Capsular Polysaccharide of Acinetobacter Baumannii Strain 307-0294 Is a Major Virulence Factor. *Infect. Immun.* 78, 3993–4000. doi: 10.1128/IAI.00366-10

Singh, J. K., Adams, F. G., and Brown, M. H. (2018). Diversity and Function of Capsular Polysaccharide in Acinetobacter Baumannii. *Front. Microbiol.* 9, 3301. doi: 10.3389/fmicb.2018.03301

Talyansky, Y., Nielsen, T. B., Yan, J., Carlino-Macdonald, U., Di Venanzio, G., Chakravorty, S., et al. (2021). Capsule Carbohydrate Structure Determines Virulence in Acinetobacter Baumannii. *PloS Pathog.* 17, e1009291. doi: 10.1371/journal.ppat.1009291

Tipton, K. A., Chin, C. Y., Farokhyfar, M., Weiss, D. S., and Rather, P. N. (2018). Role of Capsule in Resistance to Disinfectants, Host Antimicrobials, and Desiccation in Acinetobacter Baumannii. *Antimicrob. Agents Chemother.* 62. doi: 10.1128/AAC.01188-18

Tipton, K. A., Dimitrova, D., and Rather, P. N. (2015). Phase-Variable Control of Multiple Phenotypes in Acinetobacter Baumannii Strain Ab5075. *J. Bacteriol.* 197, 2593–2599. doi: 10.1128/JB.00188-15

Tipton, K. A., Farokhyfar, M., and Rather, P. N. (2017). Multiple Roles for a Novel RND-Type Efflux System in Acinetobacter Baumannii AB5075. *Microbiologyopen* 6. doi: 10.1002/mbo3.418

Tipton, K. A., and Rather, P. N. (2016). An Ompr/envZ Two-Component System Ortholog Regulates Phase Variation, Osmotic Tolerance, Motility, and Virulence in Acinetobacter Baumannii Strain AB5075. *J. Bacteriol.* doi: 10.1128/JB.00188-15

Weiner, L. M., Webb, A. K., Limbago, B., Dudeck, M. A., Patel, J., Kallen, A. J., et al. (2016). Antimicrobial-Resistant Pathogens Associated With Healthcare-Associated Infections: Summary of Data Reported to the National Healthcare Safety Network at the Centers for Disease Control and Prevention 2011-2014. *Infect. Control Hosp. Epidemiol.* 37, 1288–1301. doi: 10.1017/ice.2016.174

Wong, D., Nielsen, T. B., Bonomo, R. A., Pantapalangkoor, P., Luna, B., and Spellberg, B. (2017). Clinical and Pathophysiological Overview of Acinetobacter Infections: A Century of Challenges. *Clin. Microbiol. Rev.* 30, 409–447. doi: 10.1128/CMR.00058-16

World Health Organization (2017) *Global Priority List of Antibiotic-Resistant Bacteria to Guide Research, Discovery, and Development of New Antibiotics*. Available at: https://www.who.int/medicines/publications/WHO-PPL-Short_Summary_25Feb-ET_NM_WHO.pdf (Accessed August 2 2021).

Conflict of Interest: The authors declare that the research was conducted in the absence of any commercial or financial relationships that could be construed as a potential conflict of interest.

Publisher's Note: All claims expressed in this article are solely those of the authors and do not necessarily represent those of their affiliated organizations, or those of the publisher, the editors and the reviewers. Any product that may be evaluated in this article, or claim that may be made by its manufacturer, is not guaranteed or endorsed by the publisher.

frontiers in Microbiology

ORIGINAL RESEARCH
published: 13 January 2022
doi: 10.3389/fmicb.2021.785161

MacAB-TolC Contributes to the Development of *Acinetobacter baumannii* Biofilm at the Solid–Liquid Interface

Brandon Robin[1†], Marion Nicol[1†], Hung Le[1], Ali Tahrioui[2], Annick Schaumann[1,3], Jean-Baptiste Vuillemenot[4], Delphine Vergoz[1], Olivier Lesouhaitier[2], Thierry Jouenne[1,3], Julie Hardouin[1,3], Anaïs Potron[4], Valérie Perrot[1] and Emmanuelle Dé[1]**

[1] Normandie Univ, UNIROUEN, INSA Rouen, CNRS, Polymers, Biopolymers, Surfaces Laboratory, Rouen, France, [2] Normandie Univ, UNIROUEN, LMSM EA4312, Evreux, France, [3] PISSARO Proteomic Facility, IRIB, Mont-Saint-Aignan, France, [4] UMR 6249 Chrono-Environnement, CNRS-Université de Bourgogne/Franche-Comté, Besançon, France

Acinetobacter baumannii has emerged as one of the most problematic bacterial pathogens responsible for hospital-acquired and community infections worldwide. Besides its high capacity to acquire antibiotic resistance mechanisms, it also presents high adhesion abilities on inert and living surfaces leading to biofilm development. This lifestyle confers additional protection against various treatments and allows it to persist for long periods in various hospital niches. Due to their remarkable antimicrobial tolerance, *A. baumannii* biofilms are difficult to control and ultimately eradicate. Further insights into the mechanism of biofilm development will help to overcome this challenge and to develop novel antibiofilm strategies. To unravel critical determinants of this sessile lifestyle, the proteomic profiles of two *A. baumannii* strains (ATTC17978 and SDF) grown in planktonic stationary phase or in mature solid–liquid (S-L) biofilm were compared using a semiquantitative proteomic study. Of interest, among the 69 common proteins determinants accumulated in the two strains at the S-L interface, we sorted out the MacAB-TolC system. This tripartite efflux pump played a role in *A. baumannii* biofilm formation as demonstrated by using Δ*macAB-tolC* deletion mutant. Complementary approaches allowed us to get an overview of the impact of *macAB-tolC* deletion in *A. baumannii* physiology. Indeed, this efflux pump appeared to be involved in the envelope stress response occurring in mature biofilm. It contributes to maintain wild type (WT) membrane rigidity and provides tolerance to high osmolarity conditions. In addition, this system is probably involved in the maintenance of iron and sulfur homeostasis. MacAB-TolC might help this pathogen face and adapt to deleterious conditions occurring in mature biofilms. Increasing our knowledge of *A. baumannii* biofilm formation will undoubtedly help us develop new therapeutic strategies to tackle this emerging threat to human health.

Keywords: solid–liquid interface, biofilm, efflux pump, eDNA, envelop stress response

OPEN ACCESS

Edited by:
Jian Li,
Monash University, Australia

Reviewed by:
Hua Zhou,
Zhejiang University, China
Kunihiko Nishino,
Osaka University, Japan
Faye Christina Morris,
Monash University, Australia
Jhih-Hang Jiang,
Monash University, Australia
Mohamad Yasmin,
Louis Stokes Cleveland VA Medical Center, United States

***Correspondence:**
Valérie Perrot
valerie.perrot@univ-rouen.fr
Emmanuelle Dé
emmanuelle.de@univ-rouen.fr

† These authors have contributed equally to this work and share first authorship

Specialty section:
This article was submitted to Antimicrobials, Resistance and Chemotherapy, a section of the journal Frontiers in Microbiology

Received: *28 September 2021*
Accepted: *22 November 2021*
Published: *13 January 2022*

Citation:
Robin B, Nicol M, Le H, Tahrioui A, Schaumann A, Vuillemenot J-B, Vergoz D, Lesouhaitier O, Jouenne T, Hardouin J, Potron A, Perrot V and Dé E (2022) MacAB-TolC Contributes to the Development of Acinetobacter baumannii Biofilm at the Solid–Liquid Interface. Front. Microbiol. 12:785161. doi: 10.3389/fmicb.2021.785161

1. INTRODUCTION

Over the last decades, *Acinetobacter baumannii* has emerged as one of the most problematic opportunistic pathogens involved in hospital-acquired infections and community infections worldwide (Lin and Lan, 2014). The pathogenicity of this member of the ESKAPE group of bacterial pathogens (*Enterococcus faecium*, *Staphylococcus aureus*, *Klebsiella pneumoniae*, *A. baumannii*, *Pseudomonas aeruginosa*, and *Enterobacter* spp.) (Boucher et al., 2009) and its success as an infective agent appear to be related to multiple factors, and especially its ability to form biofilms. Indeed, its high capacity to acquire antibiotic resistance mechanisms has led to the increasing occurrence of outbreaks of infection involving multi- or pan-drug-resistant *A. baumannii* (Lee et al., 2017; Nasr, 2020). Furthermore, it also presents remarkable adhesion abilities on inert and leaving surfaces, leading to biofilm development that allows it to survive desiccation (Gayoso et al., 2014), oxidative stress (Soares et al., 2010), or disinfectants (Peleg et al., 2008; Harding et al., 2018) and hence to persist for long periods in various hospital environments. This concerning public health threat was therefore ranked on the global priority pathogens list established by the World Health Organization (WHO) for which there is an urgent need for new antibiotic development.

Biofilms are structural communities of interface-associated bacteria organized as microcolonies embedded within a complex hydrated polymeric matrix composed of extracellular polymeric substances (EPSs), such as exopolysaccharides, proteins, nucleic acids, and other compounds (Monds and O'Toole, 2009). The regulatory process of biofilm formation is highly dynamic and influenced by environmental factors that allow the transition between free-floating cells and biofilm lifestyles. The sessile growth mode provides clear ecological and physiological advantages to microorganisms that inherently benefit of protection against adverse environments, host immune system clearance, antibiotics, and other antimicrobial agents and protection from starvation through carbon storage (Yan and Bassler, 2019; Zhang et al., 2020). In addition, bacterial biofilm appears also to be an ideal environment for the horizontal exchange of genetic material between microorganisms through genetic mutations and rearrangements and also integration of determinants carried by mobile genetic elements, thus reinforcing bacterial genetic plasticity (Soucy et al., 2015). It is now well established that bacterial biofilm is involved in lots of infectious diseases and in a variety of medical device-related infections (Zhang et al., 2020). Indeed, the pathogenic potential of sessile microorganisms is much higher than the one of planktonic cells.

The ability of *A. baumannii* to form a biofilm is one of the leading mechanisms that has largely contributed to its success as a human pathogen. This Gram-negative bacterium may cause severe nosocomial infections including hospital-acquired and ventilator-associated pneumonia, bacteremia, endocarditis, skin and soft tissue infections, urinary tract infections, or meningitis (Peleg et al., 2008; Nasr, 2020). Biofilms are commonly referred to as solid-attached structures, but they can develop on a wide variety of interfaces including solid–liquid (S-L), air–liquid (A-L), liquid–liquid, or air–solid interfaces. *A. baumannii* biofilms grow at S-L interfaces, e.g., between a biological or an abiotic surface and an aqueous medium, but this organism has also been characterized for its ability to develop A-L interface biofilms, also known as pellicles, which constitute more complex structures than classical surface-attached biofilms in terms of development, level of organization, and mechanics (Marti et al., 2011b). Some of our investigations have revealed that *Acinetobacter* species forming pellicles, such as *A. baumannii* and *A. nosocomialis*, are those mainly involved in nosocomial infections, suggesting a correlation between this sedentary lifestyle and bacterial pathogenicity (Marti et al., 2011a; Kentache et al., 2017).

Despite the abundant literature on biofilm lifestyles and their widespread distribution in diseases, some issues remain unclear. Owing to their increasing resilience to antimicrobial treatments, *A. baumannii* biofilms are difficult to control and ultimately eradicate. Our understanding of this pathogen is that biofilm formation rather facilitates and/or prolongs its survival in harsh conditions likely by adopting a "persist and resist" strategy as previously proposed (Harding et al., 2018). Therefore, it is urgently needed to decipher mechanisms involved in *A. baumannii* biofilm formation and thus to identify key determinants that can be potential targets, aiming at developing novel anti-biofilm strategies. In this context, efflux pumps constitute critical determinants of this sessile lifestyle and have emerged as promising targets, as their inhibition may allow to fight pathogens at various levels, antibiotic resistance, but also biofilm formation. Indeed, in some bacterial species, such as *Escherichia coli*, tripartite efflux pumps have been previously reported to be involved in biofilm formation (Alav et al., 2018). In *A. baumannii*, it was envisaged that the Pmt [putative major facilitator superfamily (MFS) transporter-like] protein could be associated with the release of eDNA and adhesion on biotic and abiotic surfaces (Sahu et al., 2012). Another MFS transporter, AbeF, involved in fosfomycin efflux, was also proposed to participate in the secretion of biofilm matrix (Sharma et al., 2017). The contribution of resistance-nodulation-division (RND)-efflux pumps, like AdeABC, to this growth mode was also demonstrated but especially in terms of adhesion (Richmond et al., 2016). Finally, deletion of the efflux pump genes *emrA/emrB* resulted in a decrease of biofilm formation in *A. baumannii*, even though their precise roles remained to be clarified (Lin et al., 2020).

In the current study, we have compared the biofilm-forming ability of two strains of *A. baumannii* harboring specific features. We used the SDF strain that interestingly produces an abundant biofilm, but not pellicle, without presenting the main classical determinants associated with virulence of biofilm (such as Csu pili, PgaABCD, and type IV pili) (Antunes et al., 2011; Eijkelkamp et al., 2014), and the *A. baumannii* ATCC 17978 strain as a reference strain. The proteome profiles of bacteria grown in planktonic stationary phase with those of bacteria grown in mature S-L biofilm were compared using a proteomic semiquantitative study. This analysis highlights adhesins that could contribute to initiation and development of the SDF biofilm. Of interest, among the 69 common protein determinants accumulated by the two *A. baumannii* strains at the S-L interface, we sorted out the MacAB-TolC system. This pump has been reported to actively extrude various substrates, including macrolide antibiotics and virulence factors in *E. coli* and other

Gram-negative bacteria. It was also involved in the transport of outer membrane glycolipids, lipopeptides, and protoporphyrin (reviewed in Fitzpatrick et al., 2017). Interestingly, this tripartite efflux pump appears to be a noteworthy determinant of *A. baumannii* mature biofilms as demonstrated by using *macAB-tolC* deletion mutant. Complementary approaches allowed us to suggest its contribution to iron and sulfur homeostasis and to demonstrate its involvement in cell wall rigidity and osmotic protection.

2. MATERIALS AND METHODS

2.1 Bacterial Strains and Growth Conditions

Strains and plasmids used in this study are listed in **Supplementary Table 1**. *A. baumannii* SDF strain was selected based on its failure to form pellicle and the lack of the main classically defined determinants of biofilm (Fournier et al., 2006). The ATCC 17978 strain, lacking the pAB3 plasmid (pAB3-) as checked by PCR amplification and sulfamethoxazole/trimethoprim (SXT) susceptibility testing (Weber et al., 2015), was chosen because of its high capacity to form biofilms compared to ATCC 17978 pAB3+ strain. The SDF strain was grown in Luria Bertani medium (LB, Difco; Antunes et al., 2011). ATCC 17978 and its derivative strains were grown in Mueller–Hinton broth (MHB, Difco). The mutant strains complemented with pWH1266 (ΔMac_e) or pWH1266::*macAB-tolC* (ΔMac_c) were selected on MHB supplemented with 10 μg/ml ticarcillin. *E. coli* DH5α (pCR-Blunt) and CC118λpir (pKNG101) were selected on MHB containing 50 μg/ml kanamycin and 50 μg/ml streptomycin, respectively.

2.2. Mutant and Complemented Strain Construction

Deletion mutant was constructed from *A. baumannii* ATCC 17978 using overlapping PCRs and recombination events according to the protocol of Richardot et al. (2016). Briefly, the 5′ region of *tolC* gene (ABYAL0571, 703 bp) and the 3′ region of *macA* gene (ABYAL0574, 816 bp) were amplified by PCR with specific primers (**Supplementary Table 2**). The resulting PCR products were used as templates for overlapping PCRs to generate the mutagenic DNA insert Δ*macAB-tolC*. The insert was cloned into pCR-Blunt plasmid, then digested with *Bam*HI/*Apa*I. The generated fragment was subcloned into pKNG101, then the resulting plasmid pKNG101::Δ*macAB-tolC* was transferred into *E. coli* CC118λpir. The suicide vector was introduced into *A. baumannii* strain by triparental mattings using *E. coli* HB101 (pRK2013) helper strain. *A. baumannii* with pKNG101::Δ*macAB-tolC* was selected on MH agar supplemented with 800 μg/ml streptomycin, and *E. coli* was counterselected with 30 μg/ml chloramphenicol. Suicide vector pKNG101 with the *macAB-tolC* genes was excised by selection on M9 medium agar plates supplemented with 5% sucrose. The plasmid loss was confirmed by negative selection on MH agar with 800 μg/ml streptomycin, and the deletion of 4,524 bp was checked by PCR and sequencing (**Supplementary Table 2**). The entire operon *macAB-tolC* from *A. baumannii* ATCC 17978 was amplified using specific primers containing a complemented sequence from the expression vector pWH1266 (**Supplementary Table 2**). The plasmid pWH1266 was linearized with *HindIII* enzyme and then reassembled with the *macAB-tolC* PCR product using NEBuilder DNA Hifi Assembly kit (New England Biolabs). The resulting plasmid pWH1266::*macAB-tolC* was transferred into *E. coli* DH5a by transformation and then into Δ*Mac* strain by electroporation.

2.3. Proteomic Analyses of Planktonic and Sessile Bacterial Cultures

Biofilms were grown on 30 g of glass wool in 800 ml of rich medium using 10^7 [Colony Forming Unit (CFU)/ml] as an inoculum (Crouzet et al., 2017). They were incubated at 37°C for 4 days with slight shaking (90 rpm) to avoid pellicle formation. Then, glass wool was washed three times with phosphate buffer saline (PBS) to remove unattached cells. Biofilm bacteria were recovered from glass wool by vigorous shaking with 30 g of glass beads and a subsequent centrifugation (6,000 × *g*, 15 min, 4°C). One-day-old planktonic cultures were performed similarly but with shaking at 140 rpm and without glass wool. Total protein extraction from planktonic and biofilm cells was performed as already described (Kentache et al., 2017). Protein samples were prepared at least in biological triplicate for each condition. Then, enzymatic digestion of protein extracts and quantitative analysis by mass spectrometry analyses were performed according to Kentache et al. (2017). Protein abundances in the wild type (WT) and ΔMac were compared using Progenesis LC-MS software for protein quantification. False discovery rates (FDRs) were calculated using a decoy-fusion approach in Mascot (version 2.6.0.0). Identified peptide spectrum matches with −10logP value higher than 14 were kept at an FDR threshold of 1%, and proteins identified with less than two peptides were discarded. The mass spectrometry proteomics data have been deposited to the ProteomeXchange Consortium *via* the PRIDE partner repository with the dataset identifier PXD028619.

2.4. Biofilm Assays

To compare *A. baumannii* ATCC 17978 and derivatives strains, biofilm formation and metabolic activity were measured using 2,3-bis(2-methoxy-4-nitro-5-sulfophenyl)-5-[(phenylamino)carbonyl]-2H-tetrazolium hydroxide (XTT) assays as previously described (Orsinger-Jacobsen et al., 2013) with some modifications. Briefly, MHB in a 96-well flat-bottomed polystyrene plate was inoculated with 150 μl per well at 5.10^7 CFU/ml of a fresh overnight culture. The plate was incubated at 37°C without shaking in darkness. After 24 h, the plate was read at 595 nm, and the medium and the pellicle were discarded. Biofilm was washed twice with 200 μl of ultrapure water. XTT solution was added, and samples were incubated for 3 h at 37°C. The optical density (OD) at 490 nm was then measured. Biomass quantification between the different strains was performed by crystal violet (CV) method using a 24-well flat-bottomed polystyrene plate inoculated with 1 ml per well at 5.10^7 CFU/ml. The plate was incubated at 37°C without shaking in darkness for 48 h. Then, OD at 600 nm of cultures was read. Biofilm was

washed once and stained with 1 ml of 0.1% CV for 15 min. After CV removal, wells were washed twice with 1 ml of ultrapure water. CV attached to biomass was solubilized by 1 ml of acetic acid at 30%. Wells were homogenized to measure OD at 580 nm. All assays were performed at least in triplicate in a minimum of three independent experiments.

2.5. Confocal Laser Scanning Microscopy

Biofilm formation at the S-L interface was achieved in glass coverslips as described (Le et al., 2021). Briefly, aliquots of 1 ml of bacteria in MHB (inoculum 5.10^7 CFU/ml) were transferred into each well (24-well flat-bottomed plate) containing a glass coverslip ø12 mm (**Supplementary Figure 1**). The plate was incubated at 37°C without shaking in darkness for 48 h. The medium was discarded, and biofilms were washed twice with PBS. Biofilms were finally stained with Syto9 (Thermo Fisher Scientific) for 30 min following the manufacturer's protocol prior to microscopy. Biofilm formation at the solid–liquid–air interface was prepared using a previously described protocol (Fulaz et al., 2019) with some modifications. A 10-ml volume of bacteria in MHB (inoculum 5.10^7 CFU/ml) was added to a sterile 50-ml Falcon centrifuge tube containing a glass coverslip (24 mm × 50 mm) (**Supplementary Figure 1**). Biofilm formation in the presence of DNase I from bovine pancreas (Sigma-Aldrich) was performed by supplementing medium with DNase I at 100 μg/ml (Tahrioui et al., 2019). After 24 h of incubation at 37°C without shaking, the coverslip was washed with PBS, and biofilms were stained with Syto9 (Filmtracer LIVE/DEAD Biofilm Viability Kit, Invitrogen). The coverslip was then assembled onto a glass microscope slide using Mowiol 4–88 mounting medium. Image acquisitions were performed using Leica TCS SP8 CFS confocal microscope with fixed stature (Leica Microsystems), equipped with diode laser (Coherent) at 488 nm for Syto9. Fluorescence emission was detected sequentially by a hybrid detector (Leica Microsystems) in photon counting mode with a specific band from 500 to 540 nm for Syto9. Image processing was performed with Imaris software.

2.6. Drug Susceptibility Assays

The minimum inhibitory concentrations (MICs) of antibiotics (azithromycin, erythromycin, spiramycin, ticarcillin, erythromycin, colistin, gentamicin, tobramycin, novobiocin, tetracycline, tigecycline, imipenem, and ciprofloxacin; Sigma-Aldrich) and antiseptic (chlorhexidine gluconate, Sigma-Aldrich) on ATCC 17978 WT and derivative strains were determined by the standard microdilution method in MH or MH-cation-adjusted broth using an initial inoculum of 5.10^5 CFU/ml, as recommended by the Clinical and Laboratory Standards Institute (CLSI) (2015). The minimum biofilm eradication concentration (MBEC), defined as the lowest concentration of an antibiotic that prevents visible growth in the recovery medium used to collect biofilm cells (Macia et al., 2014), was determined using Calgari Biofilm Device (Innovotech, Canada) as previously described (Ceri et al., 1999). Briefly, MH or MH-cation-adjusted broth was inoculated with 10^7 CFU/ml from an overnight culture in a 96-well plate and incubated at 37°C for 24 h with shaking. Biofilms grew around the plastic pegs on the lid of the plate. Pegs were washed with PBS at 10 mM and challenged with increasing concentrations of antimicrobial agents for an additional 24 h at 37°C. Then, biofilms were washed and removed from pegs by sonication (ultrasonic bath) for 20 min in fresh sterile MHB (recovery plate). The recovery plate was incubated for 24 h at 37°C. OD_{650} of each well was measured to determine MBEC values. MIC and MBEC experiments were performed in three independent assays.

2.7. Growth Assays

MHB was inoculated at 10^7 CFU/ml with fresh overnight cultures of *A. baumannii* ATCC 17978 WT or derivative strains. Strains were grown to mid-log phase and harvested by centrifugation (2,000 × *g* for 5 min). Spotting assay method on supplemented M9 agar plate (Harding et al., 2017) was then used to quantify the impact of 10 mM L-phenylalanine, 256 μg/ml phenylacetic acid (PAA), and 2,048 μg/ml gallic acid (GA) and tannic acid (TA) (Cerqueira et al., 2014; Lin et al., 2015). High-osmolarity adaptation was achieved by measuring for 24 h *A. baumannii* growth in MHB supplemented with 500 mM sucrose (Fluka). Conventional dilution series and plating techniques were carried out to evaluate bacterial survival. Three independent experiments were performed.

2.8. Fluorescence Anisotropy Assay

Planktonic or biofilm cultures of *A. baumannii* ATCC 17978 WT, ΔMac, and ΔMac_c were grown in MHB at 37°C for 24 or 48 h, respectively, and cell membrane fluidity was investigated as previously described (Tahrioui et al., 2020). Briefly, cell pellets were washed twice in 10 mM $MgSO_4$ and resuspended to reach 0.1 OD_{600}. Then, 1 ml of the resuspended cultures was incubated with 4 μM 1,6-diphenyl-1,3,5-hexatriene (DPH; Sigma-Aldrich) in the dark for 30 min at 37°C. Measurement of the fluorescence anisotropy was performed using the Spark 20 M multimode Microplate Reader (Tecan Group Ltd.). Excitation and emission wavelengths were set to 365 and 425 nm, respectively. The anisotropy was calculated according to Lakowicz (2006). The relationship between anisotropy and membrane fluidity is an inverse one, where decreasing anisotropy values correspond to a more fluid lipid membrane and *vice versa*. All values are reported as means of at least triplicate analyses for each experimental variable.

2.9. Chrome Azurol S Assay

Quantification of secreted siderophores was performed as previously described (Penwell and Actis, 2019). Briefly, 250 ml Erlenmeyer for preculture and 24-well plate for culture were both conditioned with 0.5 M HCl and then rinsed three times with MiliQ water before sterilization (autoclaving or 30-min UV treatment). For the preculture, 50 ml of the succinate medium (Penwell and Actis, 2019) was inoculated with three colonies and then incubated at 37°C during 48 h under 140 rpm agitation. For the culture, 2 ml of succinate medium were inoculated from the preculture at 0.01 OD_{600} and incubated for 48 h at 37°C without agitation. Then, 1 ml of the culture was centrifuged during 20 min at 10,000 × *g*, and 150 μl of the supernatant were transferred to a 96-well plate, at least in triplicate. Finally, 30 μl of the chrome

azurol S (CAS) reagent were added, and kinetic absorbance at 630 nm was performed for 60 min. All assays were repeated three times in triplicate.

2.10. Bacterial Adhesion to A549 Human Alveolar Epithelial Cells

A549 human lung adenocarcinoma cells from ATCC were grown as monolayer cultures in Dulbecco's modified Eagle's medium (DMEM) or in Ham's F-12 Nutrient Mixture for at least 20 days to allow differentiation to an alveolar type II (ATII)-like phenotype, as indicated, supplemented with 10% heat-inactivated fetal bovine serum and antibiotics (100 U/ml of penicillin G and 100 μg/ml of streptomycin) (Cooper et al., 2016). Cells were maintained at 37°C in a humidified atmosphere of 5% CO_2. All cell culture media and supplements were purchased from Thermo Fisher Scientific. Then, cells were trypsinized and transferred to 24-well plates to get a monolayer of 10^5 cells per well. After 24 h of incubation under the same conditions, A549 cells were washed twice with PBS and fresh medium without antibiotic was added. *A. baumannii* ATCC 17978 WT, ΔMac, and ΔMac_c strains were added to the cells at a ratio of bacteria to host cells of 20:1 [multiplicity of infection (MOI) of 20]. The cells infected with bacteria were incubated at 37°C under an atmosphere of 5% CO_2 for 5 or 24 h. To determine bacterial adhesion, they were washed five times with PBS, fixed with ice-cold methanol for 20 min, and stained with Giemsa solution. Routinely, 10 microscopic fields were examined along the length of the coverslip. In each field, 10 epithelial cells were examined. The adhesion index was calculated as the total bacterial count divided by 100. The cells were examined using a Nikon Eclipse Ci-S microscope. All assays were repeated three times in triplicate. Student's *t*-test was performed to evaluate the statistical significance of the observed differences.

2.11 Statistical Analysis

Proteomic data were statistically analyzed using Progenesis LC-MS software with ANOVA. Except for the proteomic data, the statistical analyses were carried out with the GraphPad Prism8 software. We used the non-parametric *t*-test, which is a Mann–Whitney test. Mean and standard deviation (SD) calculated from at least three independent experiments were presented.

3. RESULTS AND DISCUSSION

Biofilms are key microbial ecosystems. To highlight critical determinants of *A. baumannii* sessile lifestyle that can be potential targets against biofilms, we compared protein profiles of bacteria grown in mature S-L biofilms with those of their planktonic stationary phase counterparts. For this comparison, we used the SDF strain, since it does not present classical biofilm determinants (such as Csu pili, PgaABCD, and type IV pili) (Antunes et al., 2011; Eijkelkamp et al., 2014) and may therefore express less characterized and interesting protein systems involved in biofilm development. We compared its proteome with those of the well-studied ATCC 17978 strain that was cultivated in similar conditions.

3.1 Proteomic Study of Solid–Liquid Biofilms Formed by SDF and ATCC 17978 Strains

The S-L interface is not the favored interface to grow as biofilm for some *A. baumannii* strains (Marti et al., 2011b), and thus, for an optimized biomass–surface ratio, S-L biofilms were grown on glass wool (Crouzet et al., 2017). A slight shaking was performed to prevent the pellicle development that could happen with the ATCC 17978 strain (Kentache et al., 2017). The proteomic quantitative study revealed that among the 1,523 and 1,114 unique proteins identified in the overall samples (planktonic and biofilm) from ATCC 17978 and SDF, respectively (**Figure 1A**), 477 and 403 proteins showed a significant variation of abundance (fold $\geq$ 2) according to the mode of growth [**Supplementary Table 3** (ATCC) and **Supplementary Table 4** (SDF)]. Indeed, two protein populations were distinguished in S-L biofilms: (i) underrepresented and (ii) overrepresented proteins (**Figure 1B**). Among all the differentially represented proteins, 106 out of 143 proteins common to both analyses presented the same dynamics of variation. Taken together, *A. baumannii* S-L biofilms were characterized by decreased accumulation of proteins involved in bacterial fitness including metabolic proteins and in important surface remodeling such as membrane proteins belonging to transport systems. Indeed, underrepresented proteins were mainly distributed in four functional groups according to the kyoto encyclopedia of genes and genomes (KEGG) pathway: (1) amino acid metabolism (37/297 in ATCC 17978 and 29/171 in SDF), (2) carbohydrate metabolism (27/297 and 18/171, respectively), (3) genetic information processes corresponding to replication and repair, transcription, translation, folding, and sorting (87/297 of underrepresented population in ATCC 17978 and 41/171 in SDF), and (4) unknown functions (74/297 and 38/171 proteins, respectively). Even though in both strains overrepresented proteins were more heterogeneously distributed (**Figure 1B**), we were able to distinguish two main groups: (1) proteins involved in transport systems (39/180 in ATCC 17978 and 36/232 in SDF) and (2) proteins with unknown functions (37/180 of overrepresented proteins in ATCC 17978 and 54/232 overrepresented proteins in SDF).

3.2 Specific Determinants of SDF Solid-Liquid Biofilm

We looked for specific determinants of SDF S-L biofilm to understand how this strain could produce and maintain a biofilm as dense as the reference strain ATCC 17978, while lacking the main critical biofilm determinants. Of interest, SDF S-L biofilm was characterized by the accumulation of proteins involved in translation (**Figure 1B**). Indeed, the SDF strain accumulated 22 ribosomal subunits in S-L biofilm (with maximum fold changes ranging from 3.3 to 48; **Supplementary Table 4**). These proteins are usually characteristics of the physiological growing state (Bosdriesz et al., 2015) like in ATCC 17978 planktonic growth mode (Cabral et al., 2011; Kentache et al., 2017). However, analysis of *P. aeruginosa* PAO1 biofilms showed that the ribosomic mRNA expression level was stably maintained between dividing and slowly growing cells (Williamson et al., 2012). The importance of these ribosomal proteins was also

A

	ATCC 17978	SDF	Similar variation
Total unique proteins	1523	1114	-
Over-represented	180	232	69
Under-represented	297	171	37
Total variable	**477**	**403**	**106**

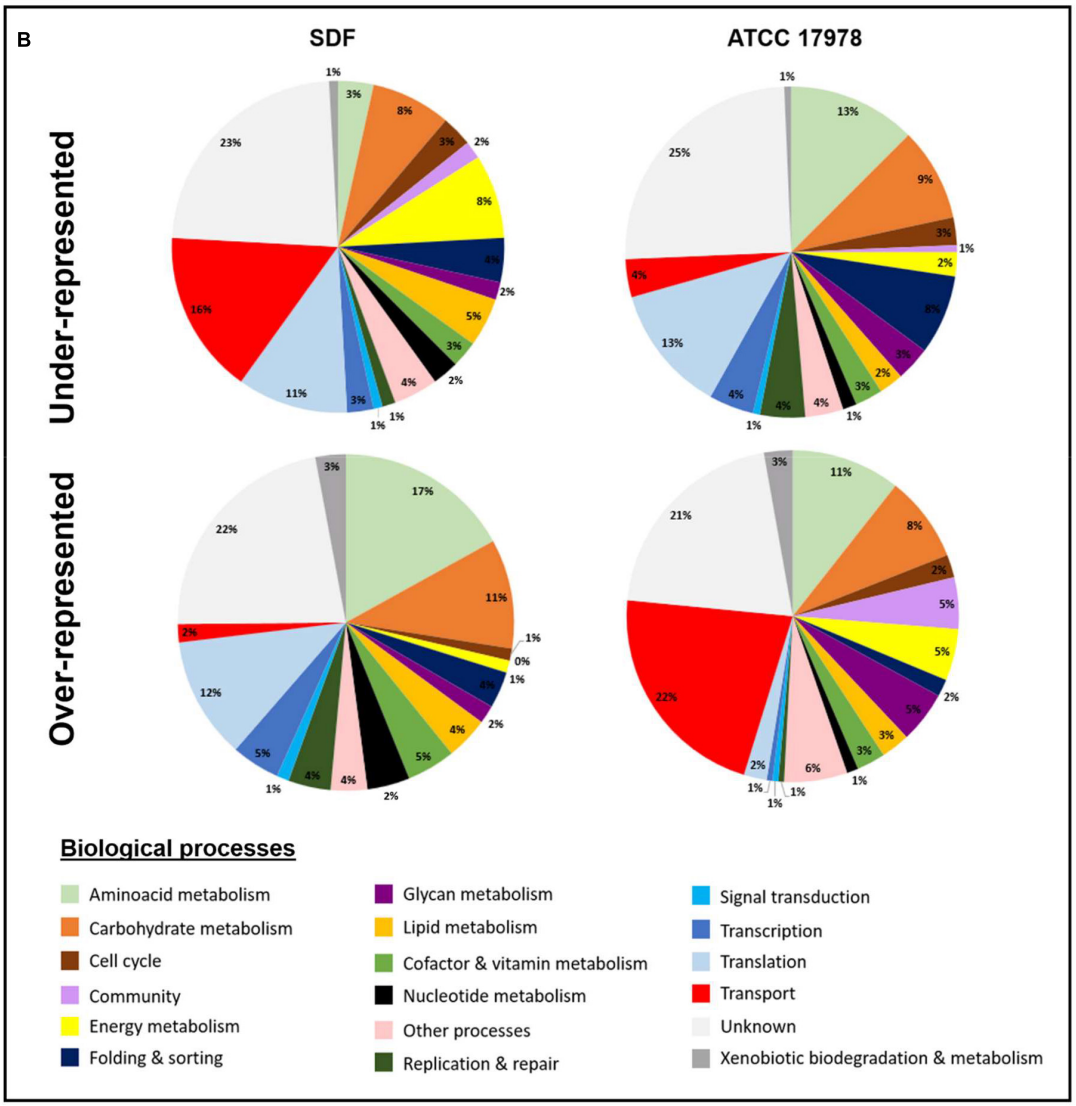

FIGURE 1 | Proteomic analyses of solid–liquid (S-L) biofilms formed by *A. baumannii* ATCC 17978 and SDF strains compared to their planktonic counterparts. **(A)** Number of proteins identified by proteomic analyses of *A. baumannii* ATCC 17978 and SDF strains and number of proteins with modified abundance in S-L biofilms compared to their planktonic counterparts. **(B)** Classification of these differentially represented proteins from *A. baumannii* SDF (left) and ATCC 17978 (right) according to their biological processes using the kyoto encyclopedia of genes and genomes (KEGG) pathway.

reported in *Bacillus subtilis* where the deletion of *rpsU* and *rpsK* genes highly decreased biofilm formation (Takada et al., 2014). Even though S-L biofilms were 4 days old, we cannot exclude that the SDF strain continues to divide, with a substantial part of ribosomes translating community determinants.

In addition, our analysis also revealed the accumulation of 20 proteins being part of the energy metabolism and that belong to the complex I (NuoABCDFGHI, 7.7- to 37-fold changes), the complex II (SdhCAB, 17- to 252-fold changes), the cytochrome b0 oxidase (CyoAB, 9- and 57-fold changes, respectively) or the F1F0 ATP synthase (3 proteins) and three ubiquinone biosynthesis proteins (UbiG, 10-fold; UbiB, 18-fold; and UbiE, fivefold), and the flavoprotein-ubiquinone oxidoreductase EftD (13-fold), indicating that the function of

the energetic respiratory chain was strongly exacerbated here. This suggests that a high ATP requirement and a potential redox regulation may increase the membrane potential to promote biofilm development (Qin et al., 2019).

Finally, we observed the overexpression of 11 proteins involved in the lipid metabolism, several of them being enzymes implicated in complex lipid biosyntheses. For example, PlsB (13-fold change) synthesizes phosphatidic acid precursors (Lehner and Kuksis, 1996), which are essential for the adaptation to environmental stresses through the modification of membrane composition and fluidity (Dubois-Brissonnet et al., 2016; Tao et al., 2021). As already reported, it may also contribute to modify the SDF adhesiveness character (Benamara et al., 2011; Lattif et al., 2011; Dubois-Brissonnet et al., 2016). Other enzymes, like Acr1 (54-fold change) and Wax-dgaT (fivefold change) are characteristics of environmental bacteria. The bifunctional acyltransferase Wax-dgaT is involved in the synthesis of triacylglycerols (TAGs) from diacylglycerols as well as in the synthesis of wax-ester (WE) (Lehner and Kuksis, 1996; Ishige et al., 2002). Accumulation of Wax-dgaT might so promote lipid storage as a carbon source to survive in nutrient deprivation. TAG storage could also contribute to bacterial desiccation tolerance (Alvarez et al., 2004; Alvarez, 2016).

This S-L biofilm proteomic quantitative analysis showed that SDF did not synthesize adhesion/community determinants known to be expressed in *A. baumannii*, like the Acinetin locus, the Csu pili or the P pilus or the PNAG polymer transporter PgaA, determinants detected in ATCC 17978 S-L biofilm. Interestingly, two systems may participate to the maintenance and the cohesion of the SDF S-L biofilm: (i) the type III *pilus* adhesion factors, FilC (71-fold change) and FilF (12-fold change), already described in ATCC 17978 pellicle communities (Marti et al., 2011b; Kentache et al., 2017), and (ii) a two-partner secretion system (TPS) FhaB/C. Indeed, we identified the protein ABSDF3544 (fourfold change), which is a hemagglutinin/hemolysin type protein. It may correspond to the secreted protein of a TPS system, with FhaB being the passenger domain and FhaC, the translocator (identified here with a 17.8-fold change). ABSDF3544 is not conserved between *A. baumannii* species, but it had two homologous in the SDF genome (not identified here). In *A. baumannii*, FhaB/C systems are involved in the adhesion to human epithelial and bronchial cells (Astaneh et al., 2014, 2017; Pérez et al., 2017). In AbH12O-A2 strain, the exoprotein AbFhaB (also called TpsA, 31.8% id. to ABSDF3544) contributes to the tridimensional *A. baumannii* aggregation (Pérez et al., 2017). Here, ABSDF3544 may participate in cell–cell interactions but also in SDF biofilm formation, as it was already shown for FhaB/C system in *Bordetella pertussis* (Serra et al., 2011).

3.3 Common Determinants of Solid–Liquid Biofilm Formation

Despite the small genome of SDF (3.2 Mb and 3,050 open reading frames) (Fournier et al., 2006), we highlighted 69 commonly overexpressed proteins in both ATCC 17978 and SDF S-L biofilm cells. Among them, we identified proteins belonging to already characterized metabolic pathways and several systems necessary for environmental exchanges in sessile bacteria such as: (*i*) arginine catabolism (Cabral et al., 2011; Kentache et al., 2017), (*ii*) some adhesion factors like OmpA (Gaddy et al., 2009), (*iii*) the polysaccharide export system (Wza-Wzc-Wzi) (Kenyon and Hall, 2013), (*iv*) the T6SS secretion system, and (*v*) transport systems for surface modulation (Bam, Tam) or environmental exchanges (OmpW, Omp25, OprD, CarO, and ABYAL0223 porins) and also the AdeIJK efflux pump (Kentache et al., 2017). Interestingly our comparative analysis revealed that both SDF and ATCC 17978 S-L biofilm cells overexpressed also two proteins of a tripartite efflux pump ABSDF2985 and ABSDF2983 (40- and 22-fold changes, respectively) and ABYAL0573-74 and ABYAL0571 (four and sixfold changes, respectively) that were annotated MacAB-TolC. The overexpression of the *A1S_0538* gene from this system was also highlighted in a transcriptomic approach of *A. baumannii* ATCC1978 24-h S-L biofilms (Rumbo-Feal et al., 2013).

In *A. baumannii*, the MacAB-TolC system is a tripartite efflux pump where MacB is an atypical ABC family transporter with a recently determined atomic structure (Okada et al., 2017), MacA is a membrane fusion protein, and TolC is an outer membrane protein. This well-conserved system was first identified in *E. coli* (Kobayashi et al., 2001). It handles the efflux of substrates either from the periplasm and/or from the cytoplasm to the extracellular environment of the bacterial cell (Crow et al., 2017; Fitzpatrick et al., 2017). For many species like *E. coli*, *Stenotrophomonas maltophilia*, or *K. pneumoniae*, it is involved in the resistance to macrolides, aminoglycosides, polymyxins, and cyclines (Lin Y. T. et al., 2014; Fitzpatrick et al., 2017; Zheng et al., 2018). In addition, MacAB was shown to extrude various compounds such as toxins (enterotoxin STII in *E. coli*; Yamanaka et al., 2008), protoporphyrin IX (Turlin et al., 2014), or lipopeptides and siderophores in *Pseudomonas* species (Imperi et al., 2009; Greene et al., 2018) and can be involved in virulence (Nishino et al., 2006). MacAB was recently described to protect *Salmonella enterica* serovar typhimurium from oxidative stress through linearized siderophore product secretion (Bogomolnaya et al., 2020). Thus, the MacAB system appears to fulfill numerous transport functions for a wide range of substrates. In addition, its contribution to biofilm formation has been described for *S. maltophilia* (Lin Y. T. et al., 2014). In *A. baumannii*, MacAB-TolC shares 83% of amino acid sequence similarity with its *E. coli* counterpart and, therefore, may be involved in the efflux of macrolides and novobiocin (Okada et al., 2017; Pérez-Varela et al., 2019). So far, to our knowledge, the function of the MacAB-TolC pump in *A. baumannii* biofilm cells has never been considered.

3.4 Involvement of MacAB-TolC in Biofilm Formation

To unravel the function of MacAB-TolC tripartite efflux system of *A. baumannii* in biofilm formation, we have attempted unsuccessfully to generate a Δ*macAB-tolC* deletion mutant in the SDF strain. We, however, succeeded to make this deletion mutant (ΔMac) in the ATCC 17978 strain and also generated

a complemented strain (ΔMac_c) harboring pWH1266::*macAB-tolC*. We checked that deletion of *macAB-tolC* did not affect growth of ΔMac mutant neither in planktonic nor in biofilm cultures (**Supplementary Figure 2**). For ΔMac_c strain, the cell metabolic activity was slightly decreased in biofilm probably due to the presence of the complementation plasmid, since the same phenotype was observed in the strain carrying the empty plasmid (**Supplementary Figure 2**).

Interestingly, our results showed that deletion of the Mac system negatively affected the biomass amount that was decreased by 33% ($p < 0.05$) after 48 h of biofilm growth (**Figure 2A**). Complementation did not, however, restore the phenotype to a level comparable to the level reached by the WT strain. Since the antibiotic selection pressure was not applied in our experiment owing to its influence on biofilm formation (Peleg et al., 2008; Penesyan et al., 2019), the complementation plasmid may have been lost within the time frame of the experiment. We, however, failed to demonstrate by numeration a difference between the ΔMac and the ΔMac_c strains (data not shown). In parallel, confocal laser scanning microscopy (CLSM) analysis of biofilms was performed using Syto9 staining. Again, the total biovolume subsequent to the ΔMac deletion was reduced by 23% after 48 h biofilm formation (**Figures 2B,C**). Our results are consistent with the study performed in *S. maltophilia*, where the deletion of the MacAB-TolC system induces a 48% decrease of biofilm formation (Lin Y. T. et al., 2014). Taken together, inactivation of genes encoding the MacAB-TolC tripartite efflux system of *A. baumannii* results in impaired biofilm formation.

3.5 Involvement of MacAB-TolC in Antibiotic Resistance

As the MacAB-TolC system was already shown to contribute to the antibiotic resistance in *A. baumannii* and various bacterial species (Greene et al., 2018; Pérez-Varela et al., 2019), we compared MICs of WT and ΔMac strains. In the present study, we did not observe any difference between both strains (**Supplementary Table 5**). The deletion of the MacB transporter was, however, shown to be associated with a slight decrease in erythromycin (from 4 to 2 μg/ml) and novobiocin MICs (from 8 to 2 μg/ml; Pérez-Varela et al., 2019). This discrepancy might be linked to the deletion of the entire system instead of *macB* alone. Here, MacAB-TolC does not seem to participate in the antibiotic efflux in *A. baumannii* in a planktonic growth mode or the expression of another efflux pump may counteract the deletion of the Mac system in the ΔMac strain. Regarding the antibiotic tolerance in biofilms, MBEC assays revealed that ΔMac was surprisingly more tolerant to aminoglycosides, such as gentamicin (128 μg/ml) and tobramycin (64 μg/ml), than the WT strain (32 μg/ml). ΔMac_c strain showed a restored phenotype with MBEC at 16 μg/ml for gentamicin and 32 μg/ml for tobramycin. Hence, to investigate this difference, a biofilm model at the solid–liquid–air interface (three-phase interface), similar to the one present in the Calgary biofilm device, was performed for CLSM imaging (**Supplementary Figure 1**). After 24 h of incubation, all bacteria (live and dead cells) and biofilm matrices were stained with Syto9. There was no difference in the biovolume at the three-phase interface (**Figure 3A**) contrary to the one observed at the S-L interface (**Figure 2B**). This is consistent with our proteomic data pointing out that the overexpression of MacAB-TolC happens essentially when *A. baumannii* grows at the S-L interface and not in pellicle (Kentache et al., 2017). However, ΔMac biofilm images at the three-phase interface showed a well-developed fiber-like network within the EPS matrix. These fibers are extracellular DNA (eDNA), since this component was labeled with Syto9 and was also degraded by DNAse I (**Figure 3**). Indeed, DNase I treatment led to a significant reduction of biofilm formation for both WT and ΔMac (72 and 95%, respectively) after 24-h incubation (**Figure 3A**). In *A. baumannii*, eDNA was shown to be released either by an active mode, in a free form or encapsulated in membrane vesicles during early biofilm growth phase, or by cell lysis contributing to the regrowth of freshly dispersed cells (Sahu et al., 2012). A kinetic profile of biofilm formation at the three-phase interface was also performed in our study. As these eDNA-containing fibers were mainly observed from 24 h of growth (data not shown), these eDNA fibers may mainly originate from cell lysis.

It has been largely reported that aminoglycosides could have an impaired penetration in *P. aeruginosa* biofilms due to their interaction with negative components of the matrix (alginate or eDNA; Alipour et al., 2009). In line with this observation, exogenous DNA addition to biofilm growth medium was shown to provide a shield effect against aminoglycosides (Chiang et al., 2013). Here, in the ΔMac mutant, it is likely that an excess of eDNA could promote divalent cation sequestration and block aminoglycoside antibiotic diffusion within the matrix, thus explaining the observed tobramycin and gentamicin tolerance increase (Tseng et al., 2013). Although colistin can interfere with the electrostatic network of the EPS matrix (Klinger-Strobel et al., 2017), eDNA does not seem here to induce a colistin biofilm tolerance.

3.6 MacAB-TolC Contributes to the Envelope Stress Response

Gram-negative bacteria possess a complex envelope to adapt their physiology to environmental conditions. This adaptation is highly controlled by two-component systems (TCSs) (De Silva and Kumar, 2019). In *A. baumannii*, MacAB-TolC is regulated by BaeSR, a TCS that detects environmental stresses, like specific envelope-damaging agents and high osmolarity conditions. Moreover, BaeSR modulates the expression of other efflux pumps such as AdeIJK and AdeABC, which are involved in cell detoxification and maintenance (Lin M. F. et al., 2014; Lin et al., 2015).

Lin et al. (2015) have demonstrated by phenotype microarray experiment the Δ*baeR* mutant susceptibility and an upregulation of *macB* (6.2-fold) in response to a tannic acid (TA) treatment. Herein, we determined TA MICs on WT and ΔMac deletion mutant and found accordingly that the WT strain was more resistant to TA (512 μg/ml) than the ΔMac strain (128 μg/ml). Complementation partially restored the resistance to this tannin

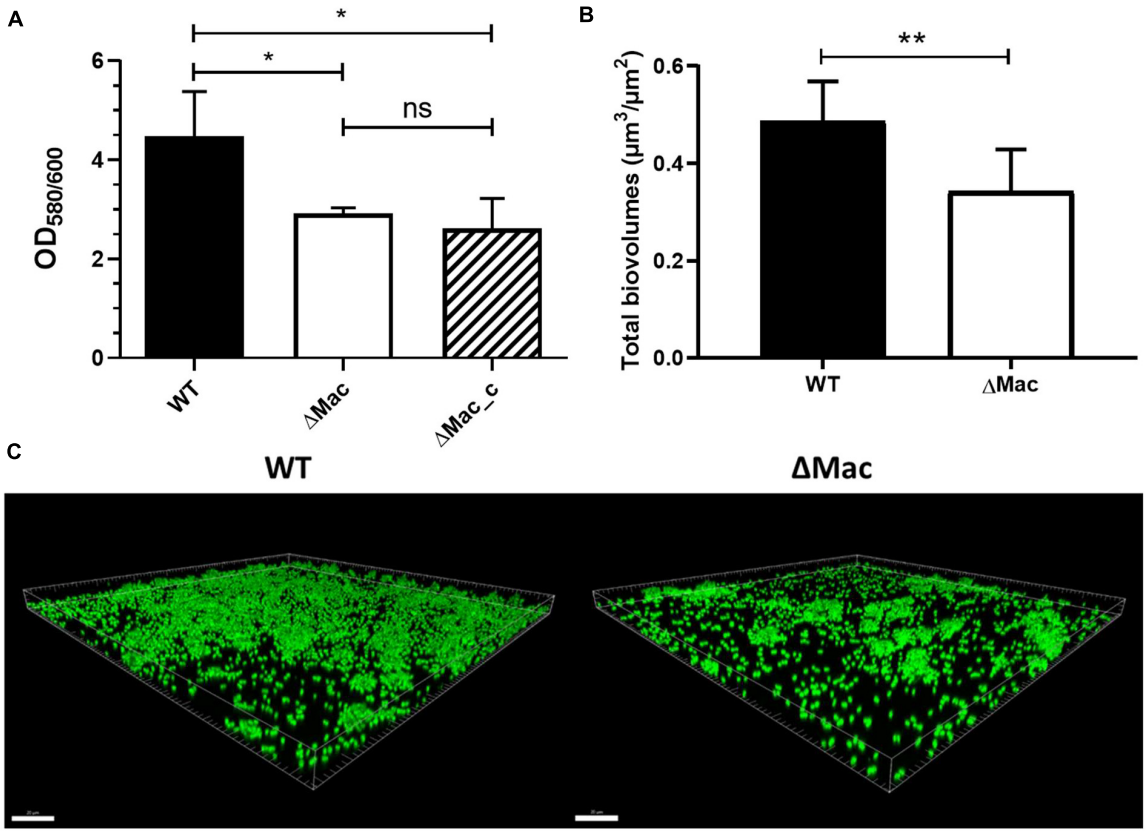

FIGURE 2 | Impact of the *macAB-tolC* deletion on *A. baumannii* biofilm formation at the solid–liquid interface. **(A)** Biomass quantification by crystal violet staining of *A. baumannii* ATCC 17978 wild type (WT), ΔMac, and ΔMac_c (ΔMac complemented strain). **(B)** Quantification of biovolume ($\mu m^3/\mu m^2$) of *A. baumannii* ATCC 17978 WT and ΔMac biofilms based on the confocal fluorescence images. **(C)** Representative confocal laser scanning microscopy (CLSM) images of *A. baumannii* ATCC 17978 WT (left) and ΔMac biofilms (right) labeled with Syto9. Data shown represent mean values (±SD) from at least three independent biological experiments (ns, not significant; $*p < 0.05$; $**p < 0.01$). Scale bar: 20 μm. OD, optical density.

(256 μg/ml in ΔMac_c). The ΔMac susceptibility to TA was confirmed using spot assay (**Supplementary Figure 3**). At least 10^8 CFU/ml of ΔMac were inhibited by 2,048 μg/ml of TA, whereas the same concentration of tannin inhibited only 10^5 CFU/ml of WT and 10^6 CFU/ml of the complemented strain. The same experiments were performed with GA, a degradation product of TA (Tahmourespour et al., 2016), but no significant difference between the WT and the ΔMac strains was observed (**Supplementary Figure 3**). Thus, MacAB-TolC may be required to allow *A. baumannii* survival in the presence of high doses of TA through either a TA efflux or a degradation process. Since TA is also an iron-chelating and antioxidant agent (Lin et al., 2015, 2020), the incapacity of the ΔMac strain to survive at high doses of TA could also be due to its impairment in maintaining iron homeostasis.

Moreover, we compared the tolerance to envelope stress of the WT, ΔMac, and ΔMac_c strains in high-osmolarity conditions. Interestingly, the ΔMac mutant was less tolerant to 500 mM sucrose after 24 h of growth as compared to the WT strain (**Figure 4A**). Susceptibility to this high-osmolarity condition was restored in ΔMac_c complemented mutant. These results are consistent with the study demonstrating that the expression of *baeR* was increased by twofold in response to 20% sucrose (Lin M. F. et al., 2014). To counteract high-osmolarity conditions and to survive this environmental stress, microorganisms may change their membrane composition, thus impacting membrane fluidity (Beney and Gervais, 2001). Accordingly, we measured the membrane fluidity of WT, ΔMac, and ΔMac_c strains by fluorescence anisotropy method (**Figure 4B**). The anisotropy index indicated that the ΔMac mutant presented a higher membrane fluidity than that in the WT strain, either in planktonic suspension or in biofilm. The membrane fluidity of ΔMac_c was partially and significantly restored as compared to the WT one, in planktonic but not in sessile lifestyle, probably due to the lack of antibiotic selection pressure.

These results demonstrated that MacAB-TolC contributes to maintain WT membrane rigidity and allow the tolerance to high-osmolarity conditions. This is in agreement with the study of Henry et al. (2012), highlighting that the rebuilding and rigidity maintenance of the membrane of a lipopolysaccharide (LPS)-deficient mutant is concomitant with the overexpression (28- to 39-fold) of the *macAB-tolC* system under the regulation of BaeS/R. In a similar manner, colistin treatment causing major membrane damages, i.e., an important envelope stress, induced

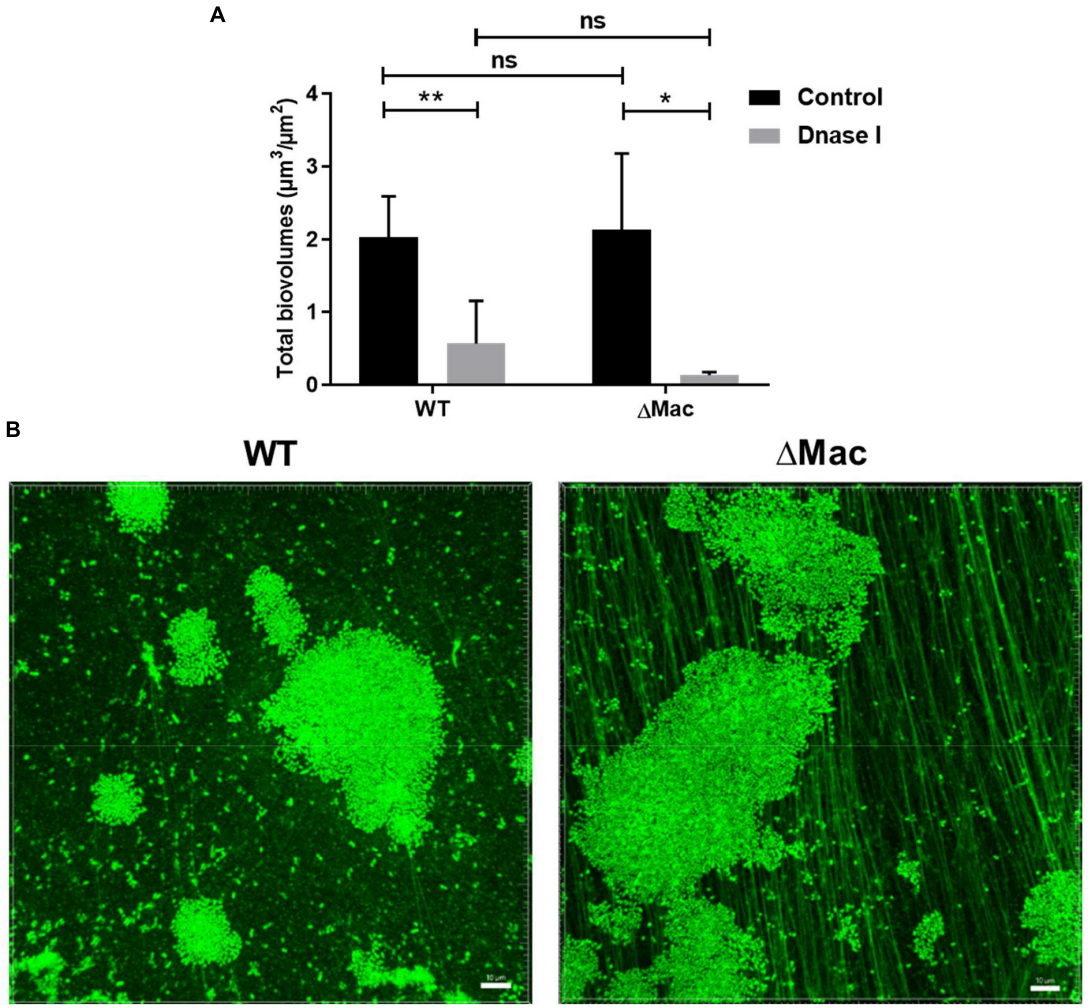

FIGURE 3 | Impact of *macAB-tolC* deletion on biofilm formation at the solid-liquid-air interface. **(A)** Total biovolume ($\mu m^3/\mu m^2$) of 24-h-old *A. baumannii* ATCC 17978 WT and ΔMac biofilms after exposure to DNase I (100 μg/ml) compared to untreated control biofilms. Quantification of biovolume was based on the confocal fluorescence images of Syto9 stained biofilms. Data shown represent mean values (±SD) from at least three independent biological experiments (ns, not significant; $^*p < 0.05$; $^{**}p < 0.01$). **(B)** Representative confocal fluorescence images of *A. baumannii* ATCC 17978 WT (left) and ΔMac biofilms (right) labeled with Syto9 at the solid–liquid–air interface (three-phase interface). Image construction was carried out using Imaris software. Scale bar: 10 μm.

the overexpression of *macAB-tolC* as a cell wall maintenance response (Henry et al., 2014). Of note, the *emrAB* efflux pump contributes in a similar manner to osmotic stress and colistin resistance in *A. baumannii* (Lin et al., 2017). Recently, it was also reported to be involved in biofilm formation (Lin et al., 2020). As mentioned above, BaeS/R positively regulates AdeIJK and AdeABC together with MacAB-TolC (Lin M. F. et al., 2014; Lin et al., 2015). In our proteomic data (**Supplementary Tables 3, 4**), these efflux pumps were overrepresented in biofilm and could therefore contribute to antibiotic tolerance in this mode of growth.

When the deletion of AdeB led to a significant decrease of biofilm formation similarly to what the deletion of MacAB-TolC did, the deletion of BaeR moderately impacted biofilm development (Lin et al., 2020). It is tempting to speculate that an effective antibiofilm strategy would be directed toward the design of a broad efflux pump inhibitor rather than to prevent a TCS activity.

3.7 Biofilm Proteome Reveals Disrupted Iron Homeostasis in ΔMac

To further understand the contribution of MacAB-TolC to *A. baumannii* biofilm formation, we proceeded to a large-scale proteomic analysis of WT and ΔMac strains in the conditions used to highlight MacAB-TolC overexpression (see *Proteomic Analyses of Planktonic and Sessile Bacterial Cultures* section). We analyzed intracellular and membrane compartments and identified 48 proteins with varying expression levels. Among them, 37 proteins were underexpressed (**Table 1**), whereas 11 were overexpressed in the ΔMac strain (**Table 2**).

All bacterial cells need iron and have thus developed iron-uptake pathways to scavenge iron from their host

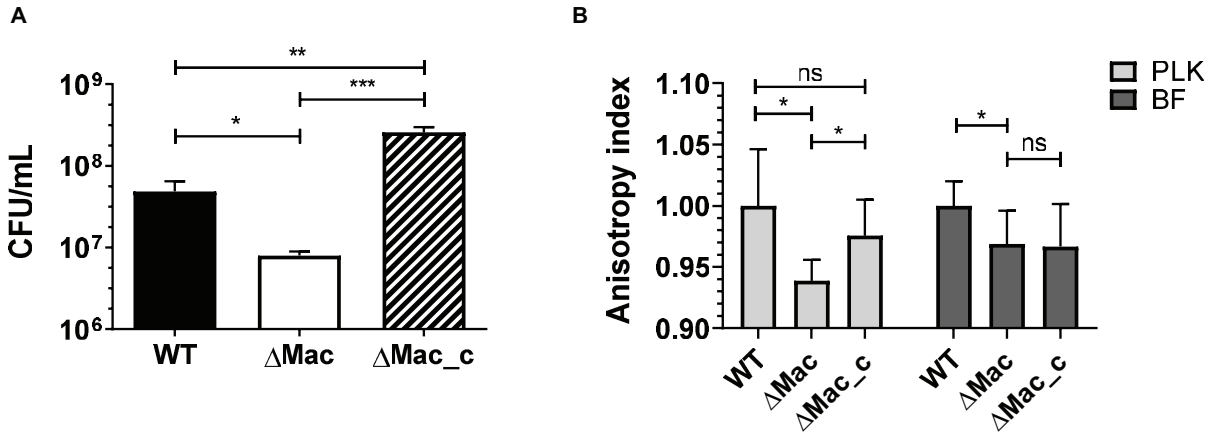

FIGURE 4 | Tolerance to sucrose and membrane fluidity analyses of WT vs. ΔMac and ΔMac_c derivative strains of *A. baumannii*. **(A)** The 24 h growth measurements in high-osmolarity condition (500 mM sucrose). **(B)** Fluorescence anisotropy measurements of planktonic (PLK) growth culture (24 h; clear gray) or biofilm (BF) growth culture (48 h; dark gray). Data shown represent mean values (±SD) from at least three independent experiments. The data were statistically analyzed using unpaired *t*-test to calculate *p*-values (ns, not significant; $*p < 0.05$; $**p < 0.01$; $***p < 0.001$). CFU/mL, colony-forming unit per ml.

during infection. *A. baumannii* ATCC 17978 produces up to 10 siderophores that chelate iron with high affinity from three different loci, named acinetobactin, baumannoferrin (A and B), and the fimsbactins (A–F) (Sheldon and Skaar, 2020). Acinetobactin and the fimsbactins are mixed catechol-hydroxamate-type siderophores, whereas baumannoferrin has solely a hydroxamate-type structure (Yamamoto et al., 1994; Proschak et al., 2013; Penwell et al., 2015). It was already reported that these siderophores and iron requirement were critical for the development of *A. baumannii* communities (Nait Chabane et al., 2014; Kentache et al., 2017). Accordingly, the ATCC 17978 S-L biofilm proteomic analysis pointed out the underexpression of the negative regulator Fur (Ferric uptake regulator). It inhibits the expression of siderophore synthesis and promoted iron storage (Cornelis et al., 2011). Consistently, BauA (10-fold) was involved in acinetobactin import, and proteins involved in baumannoferrin transport (BfnH, threefold; TonB-dependent receptor, 26-fold) were accumulated (**Supplementary Table 3**).

Interestingly, in the ΔMac proteome analysis, the BfnL protein, involved in the biosynthesis of the baumannoferrin, and five other proteins related to the acinetobactin locus (BasB, BasE, and BasF for biosynthesis; BauB for import; and BarB for export) were underexpressed compared to those in the WT strain (**Table 1**). However, a potential decrease of baumannoferrin biosynthesis in ΔMac should be considered with caution, since only the BfnL amount decreased (Sheldon and Skaar, 2020). Nevertheless, there was no doubt regarding the decrease of acinetobactin production. Likewise, in *P. aeruginosa*, a deletion mutant of PvdRT-OpmQ, an efflux pump sharing a high structural similarity with MacAB-TolC, presented a downregulation of pyoverdin biosynthesis (Imperi et al., 2009). This PvdRT-OpmQ system was proposed to be responsible for pyoverdin recycling and/or required for its secretion when newly synthesized (Imperi et al., 2009; Hannauer et al., 2010). It is thus tempting to propose that the MacAB-TolC system could participate in the secretion and/or recycling of acinetobactin from the periplasm to the extracellular medium. We performed CAS assays to examine this hypothesis, but as already mentioned (Sheldon and Skaar, 2020), we did not detect any variation of siderophore activity in ΔMac compared to WT in disrupting only the acinetobactin pathway (**Supplementary Figure 4A**).

In ΔMac, the sulfonate-sulfur utilization step of cysteine biosynthesis pathway was notably affected with the downregulation of five proteins (**Table 1**) with: (*i*) *and* (*ii*) SsuA involved in aliphatic sulfonate import and SsuD involved in desulfonation of aliphatic sulfonates, both are members of the SsuEADCB system; (*iii*) SsuR the regulator of this system; (*iv*) *and* (*v*) MsuE and MsuD also involved in desulfonation of other aliphatic sulfonate (Kertesz et al., 1999). Moreover, MetQ responsible for the methionine import, an organosulfur source other than sulfonates (Kertesz et al., 1999), was also underexpressed (**Table 1**). Altogether, these results showed a potential decrease of the cysteine biosynthesis. This particular amino acid is crucial for [Fe-S] cluster biosynthesis. Indeed, iron–sulfur cluster (ISC) and sulfur formation (SUF) pathways, directly regulated by cellular iron status, use free cysteine to liberate sulfur atoms for [Fe-S] cluster assembly (Guédon and Martin-Verstraete, 2006; Ayala-Castro et al., 2008). In ΔMac, iron homeostasis deregulation might compromise [Fe-S] cluster status. Of interest, IscR regulator of [Fe-S] cluster synthesis (Ayala-Castro et al., 2008) and two chaperones involved in this pathway, HscA (3-fold) and HscB (4-fold) were downregulated in ATCC 17978 S-L biofilm (**Supplementary Table 3**) consistently with an iron limitation in these growth conditions (Vickery and Cupp-Vickery, 2007).

Finally, the highest protein fold changes (up to 15-fold) in ΔMac were obtained for five proteins: PaaA, PaaG, PaaZ, PaaJ, and PaaH, which were highly underrepresented (**Table 1**). These proteins belong to the phenylacetate (PAA) catabolic pathway that allows the degradation of aromatic compounds to produce

TABLE 1 | Proteins under-represented in solid–liquid biofilm of ΔMac.

Label ABYAL	Label A1S_	Fold change	Gene	Description	Fraction	Peptides	Confidence	Anova (*p*)
				MacAB-TolC system				
ABYAL0571	A1S_0535	18.0	*tolC*	Outer membrane protein	M	2	89.64	1.1E-03
ABYAL0574	A1S_0538	12.9	*macA*	ABC tripartite efflux pump membrane fusion protein	M	5	216.38	1.5E-10
				Siderophore				
ABYAL1976	A1S_1657	2.6	*bfnL*	Baumannoferrin biosynthesis protein	I	3	137.34	5.1E-03
ABYAL2846	A1S_2375	3.1	*barB*	Siderophore ABC transporter	M	13	716.65	1.6E-03
ABYAL2852	A1S_2380	3.2	*basF*	Isochorismatase	I+M	3	109.43	3.8E-03
ABYAL2853	A1S_2381	2.8	*basE*	2,3-Dihydroxybenzoate-AMP ligase/S-dihydroxybenzoyltransferase	I	2	168.79	5.1E-03
ABYAL2858	A1S_2386	2.3	*bauB*	Acinetobactin periplasmic binding protein	M	7	389.76	7.5E-03
ABYAL2863	A1S_2390	2.3	*basB*	Acinetobactin biosynthesis protein	M	3	161.11	7.6E-03
				Sulfur				
ABYAL0038	A1S_0028	2.2	*ssuD*	$FMNH_{(2)}$-dependent alkanesulfonate monooxygenase	I+M	4	202.00	3.4E-03
ABYAL0039	A1S_0029	2.5	*ssuA*	Aliphatic sulfonate ABC transporter periplasmic	M	2	103.65	4.2E-04
ABYAL0040	A1S_0030	2.5	*ssuA*	Aliphatic sulfonate ABC transporter periplasmic	M	2	88.15	1.3E-03
ABYAL3025	A1S_2537	2.3	*ssuR*	DNA-binding transcriptional activator (LysR-family)	M	3	147.98	2.1E-04
ABYAL3888	A1S_3305	2.1	*msuE*	NADH-dependent FMN reductase	M	2	96.85	3.7E-03
ABYAL3889	A1S_3306	3.1	*msuD*	$FMNH_{(2)}$-dependent dimethylsulfone monooxygenase	I+M	4	259.99	3.8E-04
ABYAL1751	A1S_1485	2.4	*metQ*	Methionine ABC transporter permease	M	8	392.49	4.3E-04
				PAA degradation				
ABYAL1576	A1S_1335	15.2	*paaZ*	Oxepin-CoA hydrolase/dehydrosuberyl-CoA semialdehyde dehydrogenase	I+M	5	221.52	4.9E-03
ABYAL1577	A1S_1336	9.6	*paaA*	1,2-phenylacetyl-CoA epoxidase subunit A	I	3	113.1	7.7E-04
ABYAL1583	A1S_1342	9.2	*paaG*	2-(1,2-epoxy-1.2-dihydrophenyl)acetyl-CoA isomerase	I+M	8	394.61	3.1E-03
ABYAL1584	A1S_1343	9.6	*paaH*	3-hydroxybutyryl-CoA dehydrogenase	I	3	178.95	2.6E-03
ABYAL1585	A1S_1344	12.4	*paaJ*	Beta-ketoadipyl-CoA thiolase	I	2	123.36	6.4E-03
				Secretion system				
ABYAL1534	A1S_1296	2.5	*hcp1*	Type VI secretion system effector	M	14	1017.28	2.6E-07
ABYAL3106	A1S_2602	4.1	*rbtA*	Rhombotarget A	M	3	102.26	3.2E-04
				Others				
ABYAL0608	A1S_0569	2.0		Short-chain dehydrogenase/reductase	M	2	86.33	1.1E-03
ABYAL1300	A1S_1126	3.6		Baeyer–Villiger monooxygenase	M	3	149.25	1.5E-04
ABYAL1493	A1S_1264	2.2		Class A β-lactamase-related serine hydrolase	M	2	105.9	1.4E-03
ABYAL1530	A1S_1292	2.4		Conserved hypothetical protein	M	2	48.99	3.4E-05
ABYAL1698	A1S_1439	2.3		Luciferase-like monooxygenase	I	2	129.35	9.8E-05
ABYAL1742	A1S_1478	2.4		Conserved hypothetical protein	I	3	128.33	9.3E-05
ABYAL1831	A1S_1551	2.1	*parA*	ATPase chromosome partitioning protein	M	2	127.04	8.0E-05
ABYAL2029	A1S_1700	2.0	*acoB*	Acetoin:2,6-dichlorophenolindophenol oxidoreductase beta subunit	M	2	127.54	1.5E-03
ABYAL2289	A1S_1922	2.5		Ribokinase	M	2	96.2	3.3E-04
ABYAL2361		2.2		Conserved hypothetical protein	I	3	127.91	2.2E-03
ABYAL2518	A1S_2084	3.4	*pheA*	Secreted chorismate mutase	M	3	180.53	1.8E-05
ABYAL2931	A1S_2452	3.6	*styD*	Phenylacetaldehyde dehydrogenase	I+M	8	448.54	1.3E-04
ABYAL3342	A1S_2820	2.8		Conserved hypothetical protein	I	2	122.24	1.7E-03
ABYAL3515	A1S_2957	2.2		Zn-dependent hydrolase	M	2	101.57	2.3E-05
ABYAL4020	A1S_3418	2.7	*hpd*	4-hydroxyphenylpyruvate dioxygenase	I	4	210.88	6.0E-03

"M" for membrane fraction and "I" for intracellular fraction.

acetyl-coA and succinyl-coA for the trichloroacetic acid (TCA) cycle (Teufel et al., 2010; Cerqueira et al., 2014). Considering the function of this pathway, we investigated the capacity of ΔMac to grow on M9 agar plate with phenylacetic acid or phenylalanine. We did not observe a difference between the ΔMac and the WT strains (**Supplementary Figure 4B**). However,

TABLE 2 | Over-represented proteins in solid–liquid biofilm of ΔMac.

Label ABYAL	Label A1S_	Fold change	Gene	Description	Fraction	Peptides	Confidence	Anova (*p*)
				Quorum sensing				
ABYAL0138	A1S_0115	2.7		Non-ribosomal peptide synthetase (NRPS)	I	2	93.95	9.4E-04
ABYAL0139	A1S_0116	2.3		Resistance-nodulation-division (RND) transporter (Ac-505 secretion)	M	5	259.28	2.0E-03
				Others				
ABYAL1401	A1S_1191	2.1	*pyrX*	Aspartate carbamoyltransferase	M	4	214.67	1.6E-03
ABYAL1402	A1S_1192	2.3	*pyrX*	Aspartate carbamoyltransferase	M	2	169.65	4.2E-05
ABYAL1640	A1S_1387	2.0	*yhdF*	Short-chain dehydrogenase reductase	M	2	56.02	9.3E-03
ABYAL2806	A1S_2338	2.2	*maeB*	Malate dehydrogenase	M	20	1084.58	2.4E-05
ABYAL2984	A1S_2501	2.2	*gap*	Glyceraldehyde-3-phosphate dehydrogenase	I	2	97.82	1.3E-05
ABYAL3089	A1S_2586	2.0	*dgt2*	Deoxyguanosinetriphosphate triphosphohydrolase-like protein	M	2	92.13	6.3E-04
ABYAL3806	A1S_3231	2.7	*cat*	Succinyl-CoA coenzyme A transferase	I	2	97.74	4.1E-06
ABYAL3914	A1S_3327	2.2	*aceF*	Dihydrolipoamide acyltransferase (E2) component	M	10	587.81	2.8E-05
ABYAL4005	A1S_3403	2.0	*hutI*	Imidazolonepropionase	I	3	147.31	1.0E-04

"M" for membrane fraction and "I" for intracellular fraction.

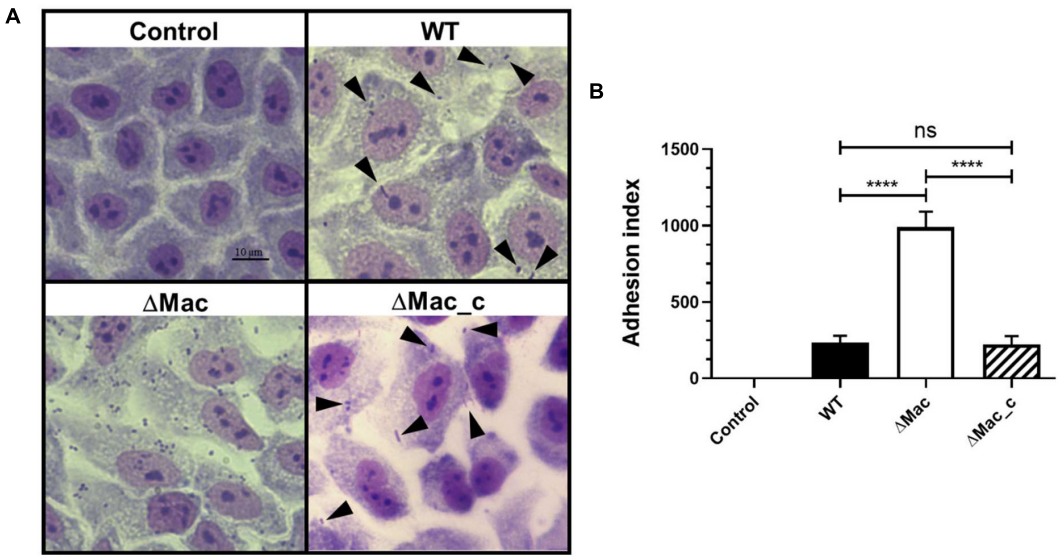

FIGURE 5 | Adhesion of *A. baumannii* to A549 human alveolar epithelial cells. **(A)** ATII-like phenotype A549 differentiated cells were infected with *A. baumannii* ATCC 17978 (WT), ΔMac, and ΔMac_c (ΔMac complemented) at a multiplicity of infection (MOI) of 20. Negative control corresponds to cells with no bacteria added. Black arrows indicate bacteria attached to A549 cells (magnification, ×400). **(B)** Quantification of the adherence of *A. baumannii* ATCC 17978 WT, ΔMac, and ΔMac_c strains to A549 cells. Index of attached bacteria after 24 h of infection. Data shown represent mean values (±SD) from at least three independent experiments performed at least in triplicate. Student's *t*-test was used to validate the experimental data (ns, not significant; ****$p < 0.0001$).

iron availability and/or the unbalanced cellular iron status of the ΔMac mutant may influence the synthesis of this operon as described (Nwugo et al., 2011). Here, the unbalanced cellular iron status on the ΔMac mutant may also influence the PAA expression. It is known that the PAA catabolic pathway, under the control of the global virulence regulator GacA, is involved in *A. baumannii* virulence (Cerqueira et al., 2014). Virulence assays conducted on the ΔMac strain in the model organism *Caenorhabditis elegans* model did not, however, allow us to observe attenuated virulence compared to WT (data not shown, Pérez-Varela et al., 2019). Similarly, in the ATCC 17978 S-L biofilm, five proteins of the PAA pathway and GacA were downregulated (**Supplementary Table 3**). This is remarkably different from our proteomic analysis of *A. baumannii* pellicle (Kentache et al., 2017) and suggests that *A. baumannii* virulence mediated by *paa* locus and GacA is strictly associated with pellicle formation (Marti et al., 2011a).

3.8 MacAB-TolC Limits Adhesion to Human Alveolar Epithelial Cells

Bacterial adherence to target cells is the first step of the infectious process. Interestingly, in our proteomic study, we identified two proteins, ABYAL0138 (A1S_0115, 2.7-fold) and ABYAL0139 (A1S_0116, 2.3-fold), overrepresented in the ΔMac mutant that are involved in the synthesis and transport of acinetin. They are part of the *A1S_0112-A1S_0119* operon already described to contribute to biofilm formation and potential acinetin secretion but also to the interaction with eukaryotic cells and in virulence

(Rumbo-Feal et al., 2017). The biological effect of the *macAB-tolC* deletion was therefore tested using A549 human alveolar epithelial cells as a model, since they represent a host cell that could be targeted by *A. baumannii* during respiratory infections. The ΔMac strain shows a remarkable ability (fivefold more) to attach to ATII-like phenotype A549 differentiated cells compared to the *A. baumannii* 17978 parental strain (**Figure 5**). The results obtained with the ATII-like phenotype A549 cells cultured in Ham's F-12 Nutrient Mixture for at least 20 days were also confirmed by infecting A549 cells cultured in DMEM with the *A. baumannii* WT or the ΔMac derivative strains (data not shown). When the mutant strain was complemented, the phenotype was restored. The observed increase of bacterial adherence to epithelial cells when *macAB-tolC* was deleted is presumably due to the fact that this strain produced more eDNA that is a cell–cell interconnecting compound (Whitchurch et al., 2002) and overexpressed the *A1S_0112-A1S_0119* operon contributing to the interaction with eukaryotic cells (Rumbo-Feal et al., 2017).

4. CONCLUSION

Even though a positive correlation between biofilm formation and antimicrobial resistance is still debated, clinical *A. baumannii* strains presenting concomitantly a biofilm-forming capacity and a multidrug resistance are currently isolated (Badave and Kulkarni, 2015; Qi et al., 2016; Wang et al., 2018). Indeed, increasing evidence demonstrated that efflux pumps are key actors of antibiotic resistance and also play a role in biofilm formation. They could efflux QS or quorum quenching molecules, as well as EPSs, but also harmful accumulated molecules and can thus promote or regulate biofilm formation (Alav et al., 2018). In *A. baumannii*, MFS and RND-efflux pumps may participate in eDNA release, transport of autoinducer molecules, or adhesion process, but this involvement was suggested to be strain-dependent (Sahu et al., 2012; He et al., 2015; Yoon et al., 2015; Richmond et al., 2016; Lin et al., 2020). Here, we demonstrated that the MacAB-TolC pump is commonly overexpressed in mature S-L biofilms of SDF and ATCC17978 strains. This system, being involved in osmotic protection and probably maintenance of iron homeostasis, may help *A. baumannii* not only to face deleterious conditions present in mature biofilms, where severe ionic gradients can develop. It could help to detoxify cell to persist and to fit in harsh environments, even though the precise substrates of this pump remain to be characterized. Its role in cell wall maintenance demonstrated here is in agreement with its overexpression when bacteria are facing membrane-targeted antibiotics such as colistin (Henry et al., 2014). Shedding some light on the roles of efflux pumps in the biofilm formation may help to develop therapeutic strategies and to improve treatments of biofilm-related infections as well. Design of broad-spectrum and safe efflux pump inhibitors would be valuable tools to both decrease the bacterial biofilm development and restore the activity of antimicrobials.

DATA AVAILABILITY STATEMENT

The datasets presented in this study can be found in online repositories. The names of the repositories and accession number(s) can be found in the "Materials and Methods" section.

AUTHOR CONTRIBUTIONS

AP, VP, and ED contributed to conception and design of the study. MN, BR, HL, AT, AS, J-BV, DV, OL, and VP performed the experiments. MN, BR, HL, AT, TJ, AP, VP, and ED wrote the article. All authors approved the submitted version.

FUNDING

This work was supported by the Normandie Region (SéSAD Research Network, France) and European Union. Europe gets involved in Normandie with European Regional Development Fund. BR was a recipient of a French fellowship of the Ministère de l'Enseignement Supérieur et de la Recherche.

ACKNOWLEDGMENTS

Images were obtained on PRIMACEN (https://primacen.crihan.fr), the Cell Imaging Platform of Normandy, IRIB, Faculty of Sciences, University of Rouen, 76821 Mont-Saint-Aignan.

SUPPLEMENTARY MATERIAL

The Supplementary Material for this article can be found online at: https://www.frontiersin.org/articles/10.3389/fmicb.2021.785161/full#supplementary-material

REFERENCES

Alav, I., Sutton, J. M., and Rahman, K. M. (2018). Role of bacterial efflux pumps in biofilm formation. *J. Antimicrob. Chemother.* 73, 2003–2020. doi: 10.1093/jac/dky042

Alipour, M., Suntres, Z. E., and Omri, A. (2009). Importance of DNase and alginate lyase for enhancing free and liposome encapsulated aminoglycoside activity against *Pseudomonas aeruginosa*. *J. Antimicrob. Chemother.* 64, 317–325. doi: 10.1093/JAC/DKP165

Alvarez, H. M. (2016). Triacylglycerol and wax ester-accumulating machinery in prokaryotes. *Biochimie* 120, 28–39. doi: 10.1016/J.BIOCHI.2015.08.016

Alvarez, H. M., Silva, R. A., Cesari, A. C., Zamit, A. L., Peressutti, S. R., Reichelt, R., et al. (2004). Physiological and morphological responses of the soil bacterium *Rhodococcus opacus* strain PD630 to water stress. *FEMS Microbiol. Ecol.* 50, 75–86. doi: 10.1016/j.femsec.2004.06.002

Antunes, L. C. S., Imperi, F., Carattoli, A., and Visca, P. (2011). Deciphering the multifactorial nature of *Acinetobacter baumannii* pathogenicity. *PLoS One* 6:e22674. doi: 10.1371/JOURNAL.PONE.0022674

Astaneh, S. D. A., Rasooli, I., and Gargari, S. L. M. (2017). Filamentous hemagglutinin adhesin FhaB limits *A baumannii* biofilm formation. *Front. Biosci. Elit.* 9:266–275. doi: 10.2741/e801

Astaneh, S. D. A., Rasooli, I., and Mousavi Gargari, S. L. (2014). The role of filamentous hemagglutinin adhesin in adherence and biofilm formation in *Acinetobacter baumannii* ATCC19606T. *Microb. Pathog.* 74, 42–49. doi: 10.1016/j.micpath.2014.07.007

Ayala-Castro, C., Saini, A., and Outten, F. W. (2008). Fe-S cluster assembly pathways in bacteria. *Microbiol. Mol. Biol. Rev.* 72, 110–125. doi: 10.1128/mmbr.00034-07

Badave, G. K., and Kulkarni, D. (2015). Biofilm producing multidrug resistant *Acinetobacter baumannii*: an emerging challenge. . *J. Clin. Diagnostic Res.* 9, DC08–DC10. doi: 10.7860/JCDR/2015/11014.5398

Benamara, H., Rihouey, C., Jouenne, T., and Alexandre, S. (2011). Impact of the biofilm mode of growth on the inner membrane phospholipid composition and lipid domains in *Pseudomonas aeruginosa*. *Biochim. Biophys. Acta Biomembr.* 1808, 98–105. doi: 10.1016/J.BBAMEM.2010.09.004

Beney, L., and Gervais, P. (2001). Influence of the fluidity of the membrane on the response of microorganisms to environmental stresses. *Appl. Microbiol. Biotechnol.* 57, 34–42. doi: 10.1007/s002530100754

Bogomolnaya, L. M., Tilvawala, R., Elfenbein, J. R., Cirillo, J. D., and Andrews-Polymenis, H. L. (2020). Linearized siderophore products secreted via MacAB efflux pump protect *Salmonella enterica* serovar *Typhimurium* from oxidative stress. *MBio* 11:e00528-20. doi: 10.1128/mBio.00528-20

Bosdriesz, E., Molenaar, D., Teusink, B., and Bruggeman, F. J. (2015). How fast-growing bacteria robustly tune their ribosome concentration to approximate growth-rate maximization. *FEBS J.* 282, 2029–2044. doi: 10.1111/FEBS.13258

Boucher, H. W., Talbot, G. H., Bradley, J. S., Edwards, J. E., Gilbert, D., Rice, L. B., et al. (2009). Bad bugs, no drugs: no ESKAPE! An update from the infectious diseases society of America. *Clin. Infect. Dis.* 48, 1–12. doi: 10.1086/595011

Cabral, M. P., Soares, N. C., Aranda, J., Parreira, J. R., Rumbo, C., Poza, M., et al. (2011). Proteomic and functional analyses reveal a unique lifestyle for *Acinetobacter baumannii* biofilms and a key role for histidine metabolism. *J. Proteome Res.* 10, 3399–3417. doi: 10.1021/pr101299j

Ceri, H., Olson, M. E., Stremick, C., Read, R. R., Morck, D., and Buret, A. (1999). The calgary biofilm device: new technology for rapid determination of antibiotic susceptibilities of bacterial biofilms. *J. Clin. Microbiol.* 37, 1771–1776.

Cerqueira, G. M., Kostoulias, X., Khoo, C., Aibinu, I., Qu, Y., Traven, A., et al. (2014). A global virulence regulator in *Acinetobacter baumannii* and its control of the phenylacetic acid catabolic pathway. *J. Infect. Dis.* 210, 46–55. doi: 10.1093/infdis/jiu024

Chiang, W. C., Nilsson, M., Jensen, P. Ø, Høiby, N., Nielsen, T. E., Givskov, M., et al. (2013). Extracellular DNA shields against aminoglycosides in *Pseudomonas aeruginosa* biofilms. *Antimicrob. Agents Chemother.* 57, 2352–2361. doi: 10.1128/AAC.00001-13

Clinical and Laboratory Standards Institute (CLSI) (2015). *M07-A10: Methods for Dilution Antimicrobial Susceptibility Tests for Bacteria That Grow Aerobically*. Wayne, PA: CLSI.

Cooper, J. R., Abdullatif, M. B., Burnett, E. C., Kempsell, K. E., Conforti, F., Tolley, H., et al. (2016). Long term culture of the a549 cancer cell line promotes multilamellar body formation and differentiation towards an alveolar type II pneumocyte phenotype. *PLoS One* 11:e0164438. doi: 10.1371/JOURNAL.PONE.0164438

Cornelis, P., Wei, Q., Andrews, S. C., and Vinckx, T. (2011). Iron homeostasis and management of oxidative stress response in bacteria. *Metallomics* 3, 540–549. doi: 10.1039/C1MT00022E

Crouzet, M., Claverol, S., Lomenech, A.-M., Le Sénéchal, C., Costaglioli, P., Barthe, C., et al. (2017). *Pseudomonas aeruginosa* cells attached to a surface display a typical proteome early as 20 minutes of incubation. *PLoS One* 12:e0180341. doi: 10.1371/journal.pone.0180341

Crow, A., Greene, N. P., Kaplan, E., and Koronakis, V. (2017). Structure and mechanotransmission mechanism of the MacB ABC transporter superfamily. *Proc. Natl. Acad. Sci. U.S.A.* 114, 12572–12577. doi: 10.1073/pnas.1712153114

De Silva, P. M., and Kumar, A. (2019). Signal transduction proteins in *Acinetobacter baumannii*: role in antibiotic resistance, virulence, and potential as drug targets. *Front. Microbiol.* 10, 1–12. doi: 10.3389/fmicb.2019.00049

Dubois-Brissonnet, F., Trotier, E., and Briandet, R. (2016). The biofilm lifestyle involves an increase in bacterial membrane saturated fatty acids. *Front. Microbiol.* 7:1673. doi: 10.3389/fmicb.2016.01673

Eijkelkamp, B. A., Stroeher, U. H., Hassan, K. A., Paulsen, I. T., and Brown, M. H. (2014). Comparative analysis of surface-exposed virulence factors of *Acinetobacter baumannii*. *BMC Genomics* 15:1020. doi: 10.1186/1471-2164-15-1020

Fitzpatrick, A. W. P., Llabrés, S., Neuberger, A., Blaza, J. N., Bai, X.-C., Okada, U., et al. (2017). Structure of the MacAB–TolC ABC-type tripartite multidrug efflux pump. *Nat. Microbiol.* 2:17070. doi: 10.1038/nmicrobiol.2017.70

Fournier, P. E., Vallenet, D., Barbe, V., Audic, S., Ogata, H., Poirel, L., et al. (2006). Comparative genomics of multidrug resistance in *Acinetobacter baumannii*. *PLoS Genet.* 2:e0020007. doi: 10.1371/journal.pgen.0020007

Fulaz, S., Hiebner, D., Barros, C. H. N., Devlin, H., Vitale, S., Quinn, L., et al. (2019). Ratiometric imaging of the in Situ pH distribution of biofilms by use of fluorescent mesoporous silica nanosensors. *ACS Appl. Mater. Interfaces* 11, 32679–32688. doi: 10.1021/ACSAMI.9B09978

Gaddy, J. A., Tomaras, A. P., and Actis, L. A. (2009). The *Acinetobacter baumannii* 19606 OmpA protein plays a role in biofilm formation on abiotic surfaces and in the interaction of this pathogen with eukaryotic cells. *Infect. Immun.* 77, 3150–3160. doi: 10.1128/IAI.00096-09

Gayoso, C. M., Mateos, J., Méndez, J. A., Fernández-Puente, P., Rumbo, C., Tomás, M., et al. (2014). Molecular mechanisms involved in the response to desiccation stress and persistence in *Acinetobacter baumannii*. *J. Proteome Res.* 13, 460–476. doi: 10.1021/pr400603f

Greene, N. P., Kaplan, E., Crow, A., and Koronakis, V. (2018). Antibiotic resistance mediated by the MacB ABC transporter family: a structural and functional perspective. *Front. Microbiol.* 9:950. doi: 10.3389/fmicb.2018.00950

Guédon, E., and Martin-Verstraete, I. (2006). "Cysteine metabolism and its regulation in bacteria," in *Amino Acid Biosynthesis ˜ Pathways, Regulation and Metabolic Engineering*, ed. V. F. Wendisch (Berlin: Springer), 195–218. doi: 10.1007/7171_2006_060

Hannauer, M., Yeterian, E., Martin, L. W., Lamont, I. L., and Schalk, I. J. (2010). An efflux pump is involved in secretion of newly synthesized siderophore by *Pseudomonas aeruginosa*. *FEBS Lett.* 584, 4751–4755. doi: 10.1016/j.febslet.2010.10.051

Harding, C. M., Hennon, S. W., and Feldman, M. F. (2018). Uncovering the mechanisms of *Acinetobacter baumannii* virulence. *Nat. Rev. Microbiol.* 16, 91–102. doi: 10.1038/nrmicro.2017.148

Harding, C. M., Pulido, M. R., Di Venanzio, G., Kinsella, R. L., Webb, A. I., Scott, N. E., et al. (2017). Pathogenic *Acinetobacter* species have a functional type I secretion system and contact-dependent inhibition systems. *J. Biol. Chem.* 292:90759087. doi: 10.1074/jbc.M117.781575

He, X., Lu, F., Yuan, F., Jiang, D., Zhao, P., Zhu, J., et al. (2015). Biofilm formation caused by clinical *Acinetobacter baumannii* isolates is associated with overexpression of the adefgh efflux pump. *Antimicrob. Agents Chemother.* 59, 4817–4825. doi: 10.1128/AAC.00877-15

Henry, R., Crane, B., Powell, D., Lucas, D. D., Li, Z., Aranda, J., et al. (2014). The transcriptomic response of *Acinetobacter baumannii* to colistin and doripenem alone and in combination in an in vitro pharmacokinetics/pharmacodynamics model. *J. Antimicrob. Chemother.* 70, 1303–1313. doi: 10.1093/jac/dku536

Henry, R., Vithanage, N., Harrison, P., Seemann, T., Coutts, S., Moffatt, J. H., et al. (2012). Colistin-resistant, lipopolysaccharide-deficient *Acinetobacter baumannii* responds to lipopolysaccharide loss through increased expression of genes involved in the synthesis and transport of lipoproteins, phospholipids, and poly-β-1,6-N-acetylglucosamine. *Antimicrob. Agents Chemother.* 56, 59–69. doi: 10.1128/AAC.05191-11

Imperi, F., Tiburzi, F., and Visca, P. (2009). Molecular basis of pyoverdine siderophore recycling in *Pseudomonas aeruginosa*. *Proc. Natl. Acad. Sci.U.S.A.* 106, 20440–20445. doi: 10.1073/pnas.0908760106

Ishige, T., Tani, A., Takabe, K., Kawasaki, K., Sakai, Y., and Kato, N. (2002). Wax ester production from n-alkanes by *Acinetobacter* sp. strain M-1: ultrastructure of cellular inclusions and role of acyl coenzyme a reductase. *Appl. Environ. Microbiol.* 68, 1192–1195. doi: 10.1128/AEM.68.3.1192-1195.2002

Kentache, T., Ben Abdelkrim, A., Jouenne, T., Dé, E., and Hardouin, J. (2017). Global dynamic proteome study of a pellicle-forming *Acinetobacter baumannii* strain. *Mol. Cell. Proteomics* 16, 100–112. doi: 10.1074/mcp.M116.061044

Kenyon, J. J., and Hall, R. M. (2013). Variation in the complex carbohydrate biosynthesis loci of *Acinetobacter baumannii* Genomes. *PLoS One* 8:e62160. doi: 10.1371/JOURNAL.PONE.0062160

Kertesz, M. A., Schmidt-Larbig, K., and Wüest, T. (1999). A novel reduced flavin mononucleotide-dependent methanesulfonate sulfonatase encoded by the sulfur-regulated msu operon of *Pseudomonas aeruginosa*. *J. Bacteriol.* 181, 1464–1473. doi: 10.1128/jb.181.5.1464-1473.1999

Klinger-Strobel, M., Stein, C., Forstner, C., Makarewicz, O., and Pletz, M. W. (2017). Effects of colistin on biofilm matrices of *Escherichia coli* and *Staphylococcus aureus*. *Int. J. Antimicrob. Agents* 49, 472–479. doi: 10.1016/j.ijantimicag.2017.01.005

Kobayashi, N., Nishino, K., and Yamaguchi, A. (2001). Novel macrolide-specific ABC-type efflux transporter in *Escherichia coli*. *J. Bacteriol.* 183, 5639–5644. doi: 10.1128/JB.183.19.5639-5644.2001

Lakowicz, J. R (ed) (2006). "Fluorescence anisotropy," in *Principles of Fluorescence Spectroscopy*, (Boston, MA: Springer), 353–382. doi: 10.1007/978-0-387-46312-4_10

Lattif, A. A., Mukherjee, P. K., Chandra, J., Roth, M. R., Welti, R., Rouabhia, M., et al. (2011). Lipidomics of *Candida albicans* biofilms reveals phase-dependent production of phospholipid molecular classes and role for lipid rafts in biofilm formation. *Microbiology* 157:3232. doi: 10.1099/MIC.0.051086-0

Le, H., Arnoult, C., Dé, E., Schapman, D., Galas, L., Le Cerf, D., et al. (2021). Antibody-conjugated nanocarriers for targeted antibiotic delivery: application in the treatment of bacterial biofilms. *Biomacromolecules* 22, 1639–1653. doi: 10.1021/ACS.BIOMAC.1C00082

Lee, C. R., Lee, J. H., Park, M., Park, K. S., Bae, I. K., Kim, Y. B., et al. (2017). Biology of *Acinetobacter baumannii*: pathogenesis, antibiotic resistance mechanisms, and prospective treatment options. *Front. Cell. Infect. Microbiol.* 7:55. doi: 10.3389/fcimb.2017.00055

Lehner, R., and Kuksis, A. (1996). Biosynthesis of triacylglycerols. *Prog. Lipid Res.* 35, 169–201. doi: 10.1016/0163-7827(96)00005-7

Lin, M.-F., and Lan, C.-Y. (2014). Antimicrobial resistance in *Acinetobacter baumannii*: from bench to bedside. *World J. Clin. Cases WJCC* 2:787. doi: 10.12998/WJCC.V2.I12.787

Lin, M. F., Lin, Y. Y., and Lan, C. Y. (2015). The role of the two-component system BaeSR in disposing chemicals through regulating transporter systems in *Acinetobacter baumannii*. *PLoS One* 10:e0132843. doi: 10.1371/journal.pone.0132843

Lin, M.-F., Lin, Y.-Y., and Lan, C.-Y. (2017). Contribution of EmrAB efflux pumps to colistin resistance in *Acinetobacter baumannii*. *J. Microbiol.* 55, 130–136. doi: 10.1007/s12275-017-6408-5

Lin, M.-F., Lin, Y.-Y., and Lan, C.-Y. (2020). Characterization of biofilm production in different strains of *Acinetobacter baumannii* and the effects of chemical compounds on biofilm formation. *PeerJ* 8:e9020. doi: 10.7717/peerj.9020

Lin, M.-F., Lin, Y.-Y., Yeh, H.-W., and Lan, C.-Y. (2014). Role of the BaeSR two-component system in the regulation of *Acinetobacter baumannii* adeAB genes and its correlation with tigecycline susceptibility. *BMC Microbiol.* 14:119. doi: 10.1186/1471-2180-14-119

Lin, Y.-T., Huang, Y.-W., Liou, R.-S., Chang, Y.-C., and Yang, T.-C. (2014). MacABCsm, an ABC-type tripartite efflux pump of *Stenotrophomonas maltophilia* involved in drug resistance, oxidative and envelope stress tolerances and biofilm formation. *J. Antimicrob. Chemother.* 69, 3221–3226. doi: 10.1093/jac/dku317

Macia, M. D., Rojo-Molinero, E., and Oliver, A. (2014). Antimicrobial susceptibility testing in biofilm-growing bacteria. *Clin. Microbiol. Infect.* 20, 981–990. doi: 10.1111/1469-0691.12651

Marti, S., Rodríguez-Bão, J., Catel-Ferreira, M., Jouenne, T., Vila, J., Seifert, H., et al. (2011b). Biofilm formation at the solid-liquid and air-liquid interfaces by *Acinetobacter* species. *BMC Res. Notes* 4:5. doi: 10.1186/1756-0500-4-5

Marti, S., Chabane, Y. N., Alexandre, S., Coquet, L., Vila, J., Jouenne, T., et al. (2011a). Growth of *Acinetobacter baumannii* in pellicle enhanced the expression of potential virulence factors. *PLoS One* 6:e0026030. doi: 10.1371/journal.pone.0026030

Monds, R. D., and O'Toole, G. A. (2009). The developmental model of microbial biofilms: ten years of a paradigm up for review. *Trends Microbiol.* 17, 73–87. doi: 10.1016/j.tim.2008.11.001

Nait Chabane, Y., Marti, S., Rihouey, C., Alexandre, S., Hardouin, J., Lesouhaitier, O., et al. (2014). Characterisation of pellicles formed by *Acinetobacter baumannii* at the air-liquid interface. *PLoS One* 9:e111660. doi: 10.1371/journal.pone.0111660

Nasr, P. (2020). Genetics, epidemiology, and clinical manifestations of multidrug-resistant *Acinetobacter baumannii*. *J. Hosp. Infect.* 104, 4–11. doi: 10.1016/j.jhin.2019.09.021

Nishino, K., Latifi, T., and Groisman, E. A. (2006). Virulence and drug resistance roles of multidrug efflux systems of *Salmonella enterica* serovar *Typhimurium*. *Mol. Microbiol.* 59, 126–141.

Nwugo, C. C., Gaddy, J. A., Zimbler, D. L., and Actis, L. A. (2011). Deciphering the iron response in *Acinetobacter baumannii*: a proteomics approach. *J. Proteomics* 74, 44–58. doi: 10.1016/j.jprot.2010.07.010

Okada, U., Yamashita, E., Neuberger, A., Morimoto, M., Van Veen, H. W., and Murakami, S. (2017). Crystal structure of tripartite-type ABC transporter MacB from *Acinetobacter baumannii*. *Nat. Commun.* 8, 1–11. doi: 10.1038/s41467-017-01399-2

Orsinger-Jacobsen, S. J., Patel, S. S., Vellozzi, E. M., Gialanella, P., Nimrichter, L., Miranda, K., et al. (2013). Use of a stainless steel washer platform to study *Acinetobacter baumannii* adhesion and biofilm formation on abiotic surfaces. *Microbiol. (United Kingdom)* 159, 2594–2604. doi: 10.1099/mic.0.068825-0

Peleg, A. Y., Seifert, H., and Paterson, D. L. (2008). *Acinetobacter baumannii*: emergence of a successful pathogen. *Clin. Microbiol. Rev.* 21, 538–582. doi: 10.1128/CMR.00058-07

Penesyan, A., Nagy, S. S., Kjelleberg, S., Gillings, M. R., and Paulsen, I. T. (2019). Rapid microevolution of biofilm cells in response to antibiotics. *NPJ Biofilms Microbiomes* 51, 1–14. doi: 10.1038/s41522-019-0108-3

Penwell, W. F., and Actis, L. A. (2019). "Isolation and Characterization of the acinetobactin and baumannoferrin siderophores produced by *Acinetobacter baumannii*," in *Acinetobacter baumannii* Methods and Protocols, eds I. Biswas and P. N. Rather (New York, NY: Humana Press), 259–270. doi: 10.1007/978-1-4939-9118-1_24

Penwell, W. F., DeGrace, N., Tentarelli, S., Gauthier, L., Gilbert, C. M., Arivett, B. A., et al. (2015). Discovery and characterization of new hydroxamate siderophores, baumannoferrin A and B, produced by *Acinetobacter baumannii*. *ChemBioChem* 16, 1896–1904. doi: 10.1002/cbic.201500147

Pérez, A., Merino, M., Rumbo-Feal, S., Álvarez-Fraga, L., Vallejo, J. A., Beceiro, A., et al. (2017). The FhaB/FhaC two-partner secretion system is involved in adhesion of *Acinetobacter baumannii* AbH12O-A2 strain. *Virulence* 8, 959–974. doi: 10.1080/21505594.2016.1262313

Pérez-Varela, M., Corral, J., Aranda, J., and Barbé, J. (2019). Roles of efflux pumps from different superfamilies in the surface-associated motility and virulence of *Acinetobacter baumannii* ATCC 17978. *Antimicrob. Agents Chemother.* 63, 1–11. doi: 10.1128/AAC.02190-18

Proschak, A., Lubuta, P., Grün, P., Löhr, F., Wilharm, G., De Berardinis, V., et al. (2013). Structure and biosynthesis of fimsbactins a-f, Siderophores from *Acinetobacter baumannii* and *Acinetobacter baylyi*. *ChemBioChem* 14, 633–638. doi: 10.1002/cbic.201200764

Qi, L., Li, H., Zhang, C., Liang, B., Li, J., Wang, L., et al. (2016). Relationship between antibiotic resistance, biofilm formation, and biofilm-specific resistance in *Acinetobacter baumannii*. *Front. Microbiol.* 7:483. doi: 10.3389/fmicb.2016.00483

Qin, Y., He, Y., She, Q., Larese-Casanova, P., Li, P., and Chai, Y. (2019). Heterogeneity in respiratory electron transfer and adaptive iron utilization in a bacterial biofilm. *Nat. Commun. 2019* 101, 1–12. doi: 10.1038/s41467-019-11681-0

Richardot, C., Juarez, P., Jeannot, K., Patry, I., Plésiat, P., and Llanes, C. (2016). Amino acid substitutions account for most mexS alterations in clinical nfxC mutants of *Pseudomonas aeruginosa*. *Antimicrob. Agents Chemother.* 60, 2302–2310. doi: 10.1128/AAC.02622-15

Richmond, G. E., Evans, L. P., Anderson, M. J., Wand, M. E., Bonney, L. C., Ivens, A., et al. (2016). The *Acinetobacter baumannii* two-component system aders regulates genes required for multidrug efflux, biofilm formation, and virulence in a strain-specific manner. *MBio* 7:e00430-16. doi: 10.1128/mBio.00430-16

Rumbo-Feal, S., Gómez, M. J., Gayoso, C., Álvarez-Fraga, L., Cabral, M. P., Aransay, A. M., et al. (2013). Whole transcriptome analysis of *Acinetobacter*

baumannii assessed by RNA-sequencing reveals different mrna expression profiles in biofilm compared to planktonic cells. *PLoS One* 8:e72968. doi: 10.1371/journal.pone.0072968

Rumbo-Feal, S., Pérez, A., Ramelot, T. A., Álvarez-Fraga, L., Vallejo, J. A., Beceiro, A., et al. (2017). Contribution of the *A. baumannii* A1S_0114 Gene to the Interaction with eukaryotic cells and virulence. *Front. Cell. Infect. Microbiol.* 7:108. doi: 10.3389/fcimb.2017.00108

Sahu, P. K., Iyer, P. S., Oak, A. M., Pardesi, K. R., and Chopade, B. A. (2012). Characterization of eDNA from the clinical strain *Acinetobacter baumannii* AIIMS 7 and Its role in biofilm formation. *Sci. World J.* 2012, 1–10. doi: 10.1100/2012/973436

Serra, D. O., Conover, M. S., Arnal, L., Sloan, G. P., Rodriguez, M. E., Yantorno, O. M., et al. (2011). FHA-mediated cell-substrate and cell-cell adhesions are critical for bordetella pertussis biofilm formation on abiotic surfaces and in the mouse nose and the trachea. *PLoS One* 6:e28811. doi: 10.1371/journal.pone.0028811

Sharma, A., Sharma, R., Bhattacharyya, T., Bhando, T., and Pathania, R. (2017). Fosfomycin resistance in *Acinetobacter baumannii* is mediated by efflux through a major facilitator superfamily (MFS) transporter—AbaF. *J. Antimicrob. Chemother.* 72, 68–74. doi: 10.1093/jac/dkw382

Sheldon, J. R., and Skaar, E. P. (2020). *Acinetobacter baumannii* can use multiple siderophores for iron acquisition, but only acinetobactin is required for virulence. *PLoS Pathog.* 16:e1008995. doi: 10.1371/journal.ppat.1008995

Soares, N. C., Cabral, M. P., Gayoso, C., Mallo, S., Rodriguez-Velo, P., Fernández-Moreira, E., et al. (2010). Associating growth-phase-related changes in the proteome of *Acinetobacter baumannii* with increased resistance to oxidative stress. *J. Proteome Res.* 9, 1951–1964. doi: 10.1021/pr901116r

Soucy, S. M., Huang, J., and Gogarten, J. P. (2015). Horizontal gene transfer: building the web of life. *Nat. Rev. Genet.* 168, 472–482. doi: 10.1038/nrg3962

Tahmourespour, A., Tabatabaee, N., Khalkhali, H., and Amini, I. (2016). Tannic acid degradation by *Klebsiella* strains isolated from goat feces. *Iran. J. Microbiol.* 8, 14–20.

Tahrioui, A., Duchesne, R., Bouffartigues, E., Rodrigues, S., Maillot, O., Tortuel, D., et al. (2019). Extracellular DNA release, quorum sensing, and PrrF1/F2 small RNAs are key players in *Pseudomonas aeruginosa* tobramycin-enhanced biofilm formation. *NPJ Biofilms Microbiomes* 5, 1–11. doi: 10.1038/s41522-019-0088-3

Tahrioui, A., Ortiz, S., Azuama, O. C., Bouffartigues, E., Benalia, N., Tortuel, D., et al. (2020). Membrane-interactive compounds from *Pistacia lentiscus* L. Thwart *Pseudomonas aeruginosa* virulence. *Front. Microbiol.* 11:1068. doi: 10.3389/FMICB.2020.01068

Takada, H., Morita, M., Shiwa, Y., Sugimoto, R., Suzuki, S., Kawamura, F., et al. (2014). Cell motility and biofilm formation in *Bacillus subtilis* are affected by the ribosomal proteins, S11 and S21. *Biosci. Biotechnol. Biochem.* 78, 898–907. doi: 10.1080/09168451.2014.915729

Tao, Y., Acket, S., Beaumont, E., Galez, H., Duma, L., and Rossez, Y. (2021). Colistin treatment affects lipid composition of *Acinetobacter baumannii*. *Antibiotics* 10:528. doi: 10.3390/antibiotics10050528

Teufel, R., Mascaraque, V., Ismail, W., Voss, M., Perera, J., Eisenreich, W., et al. (2010). Bacterial phenylalanine and phenylacetate catabolic pathway revealed. *Proc. Natl. Acad. Sci. U.S.A.* 107, 14390–14395. doi: 10.1073/pnas.1005399107

Tseng, B. S., Zhang, W., Harrison, J. J., Quach, T. P., Song, J. L., Penterman, J., et al. (2013). The extracellular matrix protects *Pseudomonas aeruginosa* biofilms by limiting the penetration of tobramycin. *Environ. Microbiol.* 15, 2865–2878. doi: 10.1111/1462-2920.12155

Turlin, E., Heuck, G., Simões Brandão, M. I., Szili, N., Mellin, J. R., Lange, N., et al. (2014). Protoporphyrin (PPIX) efflux by the MacAB-TolC pump in *Escherichia coli*. *Microbiologyopen* 3, 849–859. doi: 10.1002/mbo3.203

Vickery, L. E., and Cupp-Vickery, J. R. (2007). Molecular chaperones HscA/Ssq1 and HscB/Jac1 and their roles in iron-sulfur protein maturation. *Crit. Rev. Biochem. Mol. Biol.* 42, 95–111. doi: 10.1080/10409230701322298

Wang, Y.-C., Huang, T.-W., Yang, Y.-S., Kuo, S.-C., Chen, C.-T., Liu, C.-P., et al. (2018). Biofilm formation is not associated with worse outcome in *Acinetobacter baumannii* bacteraemic pneumonia. *Sci. Rep.* 8:7289. doi: 10.1038/s41598-018-25661-9

Weber, B. S., Ly, P. M., Irwin, J. N., Pukatzki, S., and Feldman, M. F. (2015). A multidrug resistance plasmid contains the molecular switch for type VI secretion in *Acinetobacter baumannii*. *Proc. Natl. Acad. Sci. U.S.A.* 112, 9442–9447. doi: 10.1073/pnas.1502966112

Whitchurch, C. B., Tolker-Nielsen, T., Ragas, P. C., and Mattick, J. S. (2002). Extracellular DNA required for bacterial biofilm formation. *Science* 295:1487. doi: 10.1126/science.295.5559.1487

Williamson, K. S., Richards, L. A., Perez-Osorio, A. C., Pitts, B., McInnerney, K., Stewart, P. S., et al. (2012). Heterogeneity in *Pseudomonas aeruginosa* biofilms includes expression of ribosome hibernation factors in the antibiotic-tolerant subpopulation and hypoxia-induced stress response in the metabolically active population. *J. Bacteriol.* 194, 2062–2073. doi: 10.1128/JB.00022-12

Yamamoto, S., Okujo, N., and Sakakibara, Y. (1994). Isolation and structure elucidation of acinetobactin., a novel siderophore from *Acinetobacter baumannii*. *Arch. Microbiol.* 162, 249–254. doi: 10.1007/BF00301846

Yamanaka, H., Kobayashi, H., Takahashi, E., and Okamoto, K. (2008). MacAB Is involved in the secretion of *escherichia coli* heat-stable enterotoxin II. *J. Bacteriol.* 190, 7693–7698. doi: 10.1128/JB.00853-08

Yan, J., and Bassler, B. L. (2019). Surviving as a community: antibiotic tolerance and persistence in bacterial biofilms. *Cell Host Microbe* 26, 15–21. doi: 10.1016/J.CHOM.2019.06.002

Yoon, E.-J., Nait Chabane, Y., Goussard, S., Snesrud, E., Courvalin, P., Dé, E., et al. (2015). Contribution of resistance-nodulation-cell division efflux systems to antibiotic resistance and biofilm formation in *Acinetobacter baumannii*. *MBio* 6:e00309-15. doi: 10.1128/mBio.00309-15

Zhang, K., Li, X., Yu, C., and Wang, Y. (2020). Promising therapeutic strategies against microbial biofilm challenges. *Front. Cell. Infect. Microbiol.* 10:359. doi: 10.3389/FCIMB.2020.00359

Zheng, J., Lin, Z., Sun, X., Lin, W., Chen, Z., Wu, Y., et al. (2018). Overexpression of OqxAB and MacAB efflux pumps contributes to eravacycline resistance and heteroresistance in clinical isolates of *Klebsiella pneumoniae*. *Emerg. Microbes Infect.* 7, 1–11. doi: 10.1038/s41426-018-0141-y

Conflict of Interest: The authors declare that the research was conducted in the absence of any commercial or financial relationships that could be construed as a potential conflict of interest.

Publisher's Note: All claims expressed in this article are solely those of the authors and do not necessarily represent those of their affiliated organizations, or those of the publisher, the editors and the reviewers. Any product that may be evaluated in this article, or claim that may be made by its manufacturer, is not guaranteed or endorsed by the publisher.

frontiers in Microbiology

ORIGINAL RESEARCH
published: 07 February 2022
doi: 10.3389/fmicb.2021.790263

Inhibition of AdeB, AcrI, and AmvA Efflux Pumps Restores Chlorhexidine and Benzalkonium Susceptibility in *Acinetobacter baumannii* ATCC 19606

Antonella Migliaccio[1†], Eliana Pia Esposito[1†], Maria Bagattini[1], Rita Berisio[2], Maria Triassi[1], Eliana De Gregorio[3] and Raffaele Zarrilli[1*]*

[1] Department of Public Health, University of Naples Federico II, Naples, Italy, [2] Institute of Biostructures and Bioimaging, National Research Council, Naples, Italy, [3] Department of Molecular Medicine and Medical Biotechnology, University of Naples Federico II, Naples, Italy

OPEN ACCESS

Edited by:
Henrietta Venter, University of South Australia, Australia

Reviewed by:
Karl Hassan, The University of Newcastle, Australia
William T. Doerrler, Louisiana State University, United States

***Correspondence:**
Eliana De Gregorio
edegrego@unina.it
Raffaele Zarrilli
rafzarri@unina.it

† These authors have contributed equally to this work and share first authorship

Specialty section:
This article was submitted to Antimicrobials, Resistance and Chemotherapy, a section of the journal Frontiers in Microbiology

Received: *06 October 2021*
Accepted: *23 December 2021*
Published: *07 February 2022*

Citation:
Migliaccio A, Esposito EP, Bagattini M, Berisio R, Triassi M, De Gregorio E and Zarrilli R (2022) Inhibition of AdeB, AcrI, and AmvA Efflux Pumps Restores Chlorhexidine and Benzalkonium Susceptibility in Acinetobacter baumannii ATCC 19606. Front. Microbiol. 12:790263. doi: 10.3389/fmicb.2021.790263

The management of infections caused by *Acinetobacter baumannii* is hindered by its intrinsic tolerance to a wide variety of biocides. The aim of the study was to analyze the role of different *A. baumannii* efflux pumps (EPs) in tolerance to chlorhexidine (CHX) and benzalkonium (BZK) and identify non-toxic compounds, which can restore susceptibility to CHX and BZK in *A. baumannii*. *A. baumannii* ATCC 19606 strain was tolerant to both CHX and BZK with MIC and MBC value of 32 mg/L. CHX subMIC concentrations increased the expression of *adeB* and *adeJ* (RND superfamily), *acrI* (PACE family) and *amvA* (MFS superfamily) EP genes. The values of CHX MIC and MBC decreased by eightfold in Δ*adeB* and twofold in Δ*amvA* or Δ*acrI* mutants, respectively, while not affected in Δ*adeJ* mutant; EPs double and triple deletion mutants showed an additive effect on CHX MIC. CHX susceptibility was restored in double and triple deletion mutants with inactivation of *adeB* gene. BZK MIC was decreased by fourfold in Δ*adeB* mutant, and twofold in Δ*amvA* and Δ*acrI* mutants, respectively; EPs double and triple deletion mutants showed an additive effect on BZK MIC. BZK susceptibility was recovered in Δ*adeB* Δ*acrI* Δ*adeJ* and Δ*amvA* Δ*adeB* Δ*adeJ* triple mutants. The structural comparison of AdeB and AdeJ protomers showed a more negatively charged entrance binding site and F-loop in AdeB, which may favor the transport of CHX. The carbonyl cyanide m-chlorophenylhydrazine protonophore (CCCP) EP inhibitor reduced dose-dependently CHX MIC in *A. baumannii* ATCC 19606 and in Δ*adeJ,* Δ*acrI,* or Δ*amvA* mutants, but not in Δ*adeB* mutant. Either piperine (PIP) or resveratrol (RV) at non-toxic concentrations inhibited CHX MIC in *A. baumannii* ATCC 19606 parental strain and EPs gene deletion mutants, and CHX-induced EP gene expression. Also, RV inhibited BZK MIC and EP genes expression in *A. baumannii* ATCC 19606 parental

strain and EPs mutants. These results demonstrate that tolerance to CHX and BZK in *A. baumannii* is mediated by the activation of AdeB, AceI and AmvA EPs, AdeB playing a major role. Importantly, inhibition of EP genes expression by RV restores CHX and BZK susceptibility in *A. baumannii.*

Keywords: *Acinetobacter baumannii*, chlorhexidine susceptibility, efflux pumps, AdeB, biofilm growth, resveratrol, piperine, benzalkonium

INTRODUCTION

Bacteria belonging to the genus *Acinetobacter* are glucose non-fermentative Gram-negative coccobacilli that are a frequent cause of health-care associated infections and hospital outbreaks. *A. baumannii* represents the most clinically relevant species among those belonging to the *A. baumannii-calcoaceticus* group (Wong et al., 2017). Global epidemiology of *A. baumannii* shows a clonal population structure dominated by two major international clonal lineages and few additional epidemic clones (Gaiarsa et al., 2019). The most successful *Acinetobacter* clones show resistance to a broad range of antimicrobials and tolerance to disinfectants and share virulence features such as biofilm formation on biotic and abiotic surfaces, resistance to desiccation and adherence to epithelial cells (Giannouli et al., 2013; Wong et al., 2017; Harding et al., 2018). *A. baumannii* strains responsible for nosocomial outbreaks are resistant to a wide range of antimicrobials, resistance to carbapenems being present in more than 90% of them and resistance to colistin emerging also (Wong et al., 2017).

A. baumannii persistence in the contaminated hospital environment is contributed also by reduced susceptibility of the bacteria to a broad range of biocides used as antiseptics or disinfectants, such as the bisphenol triclosan (TRI), the quaternary ammonium compounds benzalkonium chloride (BZK), dequalinium chloride (DQ), and cetrimide (CT), and the biguanide chlorhexidine (CHX) (McDonnell and Russell, 1999). CHX is a positively charged molecule able to react with the negatively charged microbial cell surface, thereby destroying the integrity of the cell membrane (McDonnell and Russell, 1999). CHX is a bactericidal agent, which is widely used for hand hygiene, skin antisepsis, oral care, and patient washing (Milstone et al., 2008). BZK has been widespread used as disinfectant in hospitals, food industry and commercial products, or antiseptic in antimicrobial soaps (Merchel Piovesan Pereira and Tagkopoulos, 2019). Reduced susceptibility to CHX and BZK is emerging in various nosocomial pathogens (Kampf, 2016; Merchel Piovesan Pereira and Tagkopoulos, 2019; Weber et al., 2019). Reduced susceptibility to CHX in *A. baumannii* has been correlated with activation of different efflux systems (Rajamohan et al., 2010a,b; Hassan et al., 2013; Tucker et al., 2014; Du et al., 2018; Harding et al., 2018; Kornelsen and Kumar, 2021). In particular, activation of AdeB and AdeJ resistance–nodulation–cell division (RND) efflux systems (Rajamohan et al., 2010a; Tucker et al., 2014), AmvA and CraA major facilitator superfamily (MFS) efflux systems (Rajamohan et al., 2010b; Foong et al., 2019) have been shown to induce tolerance to CHX and other disinfectants in clinical *A. baumannii* isolates. Reduced susceptibility to chlorhexidine has also been associated with activation of AceI proteobacterial antimicrobial compound efflux (PACE) system in *A. baumannii* ATCC17978 (Hassan et al., 2013; Tucker et al., 2014).

Non-toxic natural substances such as the alkaloid piperine (Haq et al., 2021) and the monomeric stilbenoid resveratrol (Mattio et al., 2020) are able to modulate the susceptibility to CHX in *A. baumannii* and other bacteria (Sharma et al., 2010; Mirza et al., 2011; Singkham-In et al., 2020).

The objectives of the present study were to: (i) study the contribution of efflux pump systems to and the molecular mechanisms responsible for tolerance to CHX and BZK in *A. baumannii*; (ii) identify non-toxic compounds, which can modulate and restore susceptibility to CHX and BZK in *A. baumannii.*

MATERIALS AND METHODS

Bacterial Strain, Growth Condition, Antibiotics, and Reagents

A. baumannii ACICU (Iacono et al., 2008), *A. baumannii* AYE (Poirel et al., 2003), *A. baumannii* ATCC 19606 (Janssen et al., 1997), *Escherichia coli* 25922 and *E. coli* S17 λpir (Simon et al., 1983) strains were used for this study. *E. coli* ATCC 25922 was purchased from LGC Standards S.r.l., Italy). All strains were cultured under aerobic conditions at 37°C in Luria-Bertani (LB) broth/agar. LB broth, cation-adjusted Mueller-Hinton broth (CAMHB) and Tryptic soy broth (TSB) were used to perform growth curves, susceptibility tests and biofilm assays. The chemical reagents were chlorhexidine digluconate (CHX), carbonyl cyanide m-chlorophenylhydrazine (CCCP), triclosan (5-chloro-2-(2,4-dichlorophenoxy) phenol (TRI), the quaternary ammonium compounds benzalkonium chloride (alkylbenzyldimethylammonium chloride (BZK), dequalinium chloride (DQ), and cetrimide (alkyltrimethylammonium bromide (CT), piperine (1-piperoyliperidine, PIP) and resveratrol (3,5,4'-trihydroxy-*trans*-stilbene, RV). The antimicrobials and chemical reagents were purchased from Sigma-Aldrich (Sigma, Milan, Italy).

Construction of *adeB*, *adeJ*, *acel,* and *amvA* Gene Knockouts

DNA and plasmid DNAs of *A. baumannii* ATCC 19606 and knockout mutants were extracted using the DNeasy Blood & Tissue Kit (Qiagen, Milan, Italy) and the Plasmid Mini/Midi Kits (Qiagen, Milan, Italy), respectively, according to the

manufacturer's instructions. *A. baumannii* ATCC 19606 was mutagenized as previously described (Amin et al., 2013; De Gregorio et al., 2015) with the following minor changes. The upstream and downstream fragments of target genes were amplified using the primers listed in **Supplementary Table 1** and inserted in the TA Cloning pCR2.1 vector (Invitrogen); 100 μL of competent *E. coli* DH5α were transformed with TA-cloning vector. The upstream fragments were digested with *Not*I-*Bam*HI and cloned into suicide vector pMo130-Tel^R, creating pMo130-TelR-Up. Next, the downstream fragments were digested with *Bam*HI–*Sph*I and inserted in pMo130-TelR-Up to obtain the plasmid pMo130-TelR-Up/Dw. The final plasmid was introduced into *E. coli* S17-1 λpir by $CaCl_2$ transformation and mobilized to the *A. baumannii* ATCC 19606 strain or single/double mutants via conjugation as described (Amin et al., 2013), to obtain single, double and triple mutants. Transconjugants were selected in LB agar containing 30 mg/L tellurite + 50 mg/L ampicillin and 50 mg/L kanamycin + 50 mg/L ampicillin, cultured in LB broth containing 14% sucrose. Serial dilutions were spread onto LB plates containing 14% sucrose. Colonies were screened for tellurite sensitivity to monitor excision of the suicide vector. The inactivation of *adeB*, *adeJ*, *aceI* and *amvA* genes were confirmed by PCR amplification using control primers (**Supplementary Table 1**).

Determination of Minimum Inhibitory Concentration and Minimum Bactericidal Concentration

A. baumannii ATCC 19606 was grown overnight at 37°C on LB broth, under shaking (200 rpm). The MIC and MBC of CHX was determined by a manual microdilution method according to the recommended procedures by the European Committee for Antimicrobial Susceptibility Testing (Eucast) of the European Society of Clinical Microbiology and Infectious Diseases (Escmid) (2000) and the Clinical and Laboratory Standards (CLSI, 2019). Susceptibility was assessed to MIC value < 4 mg/L as described (Rajamohan et al., 2010a). *A. baumannii* ATCC 19606 and deletion mutants were grown on CAMHB at 37°C for 24 h. Afterward, 50 μL of 1×10^6 CFU/mL bacterial cells were added to each well of the microtiter plate containing 50 μL of the CAMHB with twice the final concentration of molecules studied. Then the plates were incubated at 37°C for 18–24 h. Non-treated bacteria were used as controls. All tests were performed in triplicate and repeated three times.

In vitro Combination Studies

The tests were carried out using the checkerboard method according to the previously reported method (Hall et al., 1983). Serial dilutions of CHX (0.5–164 mg/L) were prepared and combined with serial dilutions of piperine (8–128 mg/L), resveratrol (32–128 mg/L), CCCP (0.5, 1, and 2 mg/L). Subsequently, 1×10^6 CFU/mL of either *A. baumannii* ATCC 19606 or deletion mutants were added to each well of the microtiter plate. Then the plates were incubated at 37°C for 18–24 h. All experiments were repeated three times.

Biofilm Assay

Biofilm formation was examined using a crystal violet (CV) staining assay according to the previously reported method (De Gregorio et al., 2020). Bacterial cell suspension was prepared at 0.5 McFarland standard and it was diluted 1:100 in TSB. Subsequently, 100 μL of 1×10^6 cells/mL was transferred into a 96-well flat-bottomed polystyrene microtiter plate containing 100 μL of scalar doses of CHX (164–0.5 g mg/L) and incubated at 37°C for 24 h. Non-treated bacteria were incubated with 100 μL of broth and used as the control. The culture supernatant was gently discarded, the wells were washed twice with phosphate-buffered saline (PBS) 1 × pH 7.4 and the biofilms were stained with 200 μL of 0.1% crystal violet for 20 min. The wells were washed twice with PBS 1X, and dye was re-eluted with 100% ethanol. The absorbance was measured at 595 nm using a microplate reader (Bio-Rad Laboratories S.r.l.). The OD595/OD600 ratio was used to normalize the amount of biofilm formed to the total cell content.

RNA Purification and Real-Time RT-PCR

A. baumannii ATCC 19606 cells were grown over night on LB broth at 37°C at 200 rpm. Subsequently, ATCC 19606 was diluted 1:100 in LB broth alone or LB broth with subMIC of CHX or RV or PIP or CHX plus RV or CHX plus PIP and grown at 37°C at 200 rpm for a further 3 h to reach the exponential phase (OD_{600} = 0.5). Total RNA was isolated from three independent cultures according to the previously reported method (De Gregorio et al., 2018). The cDNAs were synthesized using QuantiTect Reverse Transcription Kit (Qiagen, Milan, Italy), according to the manufacturer's protocol. Real-time RT-PCR assays were performed using SYBR Green master mix (Applied Biosystems) (Martinucci et al., 2016). The *rpoB* gene (the housekeeping gene) was used to normalize the expressions of target genes. The fold-change of the gene expression level was calculated using the $2^{-\Delta\Delta ct}$ method (Livak and Schmittgen, 2001). All experiments were performed three times in triplicate. The primers used in the qRT-PCR experiments were reported in **Supplementary Table 2**.

Statistical Analysis

All statistical analyses were carried out using GraphPad Prism version 8.0 for Windows (GraphPad Software, San Diego, CA, United States). All experiments were performed at least three times and the results are shown as means ± SD. Differences between mean values were tested for significance using ANOVA. A $P < 0.05$ was considered to be statistically significant.

Structural Analysis

Comparison of cryo EM structures of AdeB (PDB code 7 kgd) and AdeJ (PDB code 7 m4q) were conducted using the DALI platform for pairwise alignment (Holm, 2020) and the software Coot (Emsley and Cowtan, 2004) and PyMol (Seeliger and de Groot, 2010).

TABLE 1 | MIC (mg/L) and MBC (mg/L) values of CHX against *A. baumannii* strains and *E. coli* reference strain.

Strain	CHX		Interpretation
	MIC	MBC	
A. baumannii ATCC 19606	32	32	T
A. baumannii ACICU	32	32	T
A. baumannii AYE	32	64	T
E. coli ATCC 25922	2	2	S

T, tolerant; S, susceptible.

RESULTS

Effect of Chlorhexidine Digluconate on *A. baumannii* ATCC 19606

A. baumannii ATCC 19606, AYE, ACICU strains having different antimicrobial susceptibility profiles and classified as susceptible, multidrug-resistant (MDR) and extensively drug-resistant (XDR) as described (Magiorakos et al., 2012), respectively, invariably showed both CHX MIC and MBC values of 32 mg/L and were considered tolerant to CHX (**Table 1**). Instead, *E. coli* ATCC 25922 showed a CHX MIC/MBC value of 2 mg/L and was considered susceptible (**Table 1**). *A. baumannii* ATCC 19606 was able to grow and retain viability in the presence of 4–16 mg/L subMIC concentrations of CHX, while *A. baumannii* ATCC 19606 growth was abolished at 32 mg/L CHX (**Figure 1**). Also, CHX subMIC concentrations of 8 and 16 mg/L decreased stationary phase cell density of *A. baumannii* ATCC 19606 by three and fourfold, respectively (**Figure 1**).

Because it has been demonstrated that CHX increased the expression of *aceI* efflux pump (EP) gene in *A. baumannii* ATCC 17978 (Hassan et al., 2013), we asked if CHX was able to regulate the expression of EPs genes in ATCC 19606. Preliminary data showed that basal level of expression of *adeB, adeG*, *adeJ*, belonging to RND superfamily, *amvA* and *craA* belonging to MFS superfamily, *aceI*, belonging to PACE superfamily, and *abeS* and *abeM*, belonging to the SMR superfamily were different in *A. baumannii* ATCC 19606. In particular, *aceI*, *adeJ*, *adeB,* and *amvA* were expressed at high levels, with expression levels normalized on *rpoB* of 0.49, 0.34, 0.25, and 0.28, respectively, while *craA*, *abeS,* and *abeM* at low levels (**Supplementary Figure 1**). As shown in **Figure 2**, CHX at subMIC concentrations (4 and 8 mg/L) increased the expression of *adeB* and *adeJ* EPs genes by 6x and 2x, respectively, while the expression of *adeG* EP gene and *adeR* and *adeS* regulatory genes were not affected. Moreover, subMIC concentrations of CHX increased the expression of *aceI* EP gene and *amvA* EP gene 5x by 4 mg/mL and 9x by 8 mg/mL, and 2x by 4 mg/mL, respectively (**Figure 2**). *amvA* EP gene expression was not induced in the presence of 8 mg/mL CHX. On the other hand, subMIC concentrations of CHX decreased the expression of *craA* EP gene 4x by 4 mg/L and 8x by 8 mg/L (**Figure 2**). The above data indicated that *adeB*, *aceI* and to lesser extent *adeJ* and *amvA* EP genes are activated by CHX in *A. baumannii* ATCC 19606.

Effect of Efflux Pumps Inactivation on Chlorhexidine Minimum Inhibitory Concentration and Minimum Bactericidal Concentration, Planktonic and Sessile Growth in *A. baumannii* ATCC 19606

To study the molecular mechanisms responsible for tolerance to CHX in *A. baumannii*, we analyzed the effect of inactivation of AdeB and AdeJ, AceI, and AmvA EPs, which are abundantly expressed and positively regulated by CHX in *A. baumannii*

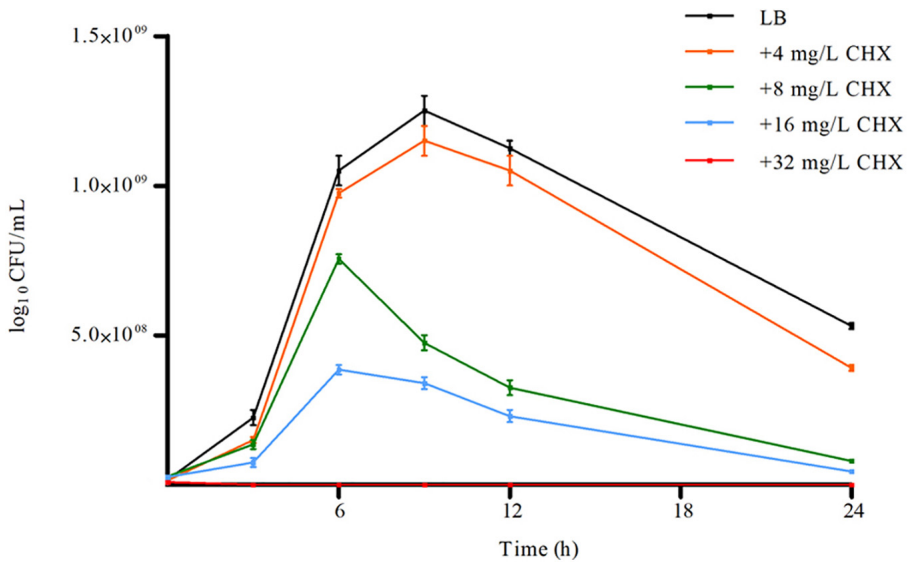

FIGURE 1 | Effect of increasing concentration of CHX on *A. baumannii* ATCC 19606 planktonic growth. Error bars represent standard deviations based on three independent experiments. CFU, colony-forming units.

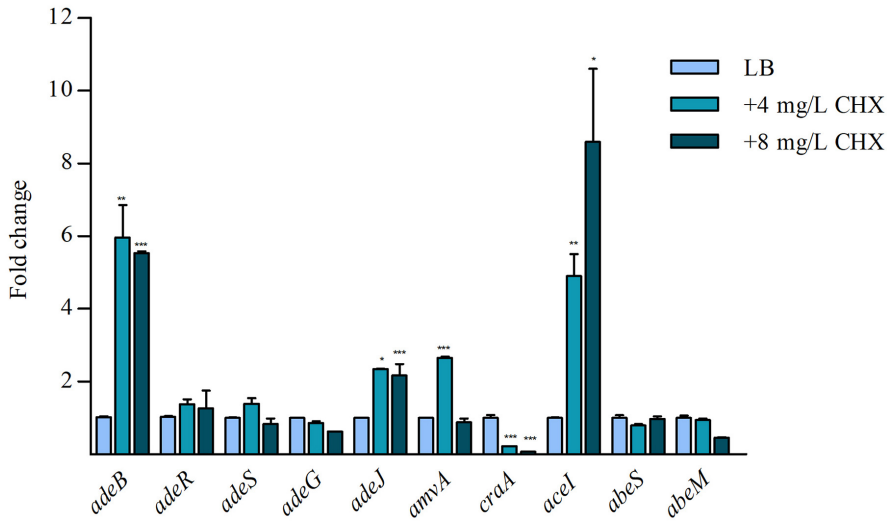

FIGURE 2 | RT-qPCR assay of *adeB, adeR*, *adeS*, *adeG*, *adeJ*, *amvA*, *craA*, *aceI*, *abeS,* and *abeM* expression in the presence of LB and 4 mg/L and 8 mg/L CHX. Relative number of transcripts of each gene was normalized in each condition and calculated using the $2^{-\Delta\Delta ct}$ method compared to the expression level in LB control. The mean + standard deviation of relative number of transcripts is shown for each gene. All experiments were performed in triplicate. *p*-values were calculated using ANOVA (*$p < 0.05$; **$p < 0.01$; ***$p < 0.001$).

ATCC19606, on susceptibility to CHX. To this aim, CHX MIC and MBC were analyzed in *A. baumannii* ATCC 19606 marker-less mutants of *adeB*, *adeJ*, *aceI* and *amvA* EPs genes. As shown in **Table 2**, CHX MIC and MBC values were decreased by eight and twofold in Δ*adeB* and in Δ*aceI* mutant, respectively, compared with *A. baumannii* ATCC19606; in Δ*amvA* mutant CHX MIC was also decreased by twofold but CHX MBC was not affected. Instead, CHX MIC and MBC in Δ*adeJ* mutant were similar to *A. baumannii* ATCC19606 (**Table 2**). Furthermore, CHX MIC and MBC values were decreased by 16-fold in Δ*adeB* Δ*aceI* and Δ*adeB* Δ*adeJ* double mutants, eightfold in Δ*amvA* Δ*adeB*, and fourfold in Δ*amvA* Δ*aceI* double mutant, while CHX MIC was decreased by two fold, but CHX MBC not affected in Δ*amvA* Δ*adeJ* and Δ*aceI* Δ*adeJ* double mutants. Moreover, CHX MIC and MBC were decreased by 32-fold in Δ*adeB* Δ*aceI* Δ*adeJ*, 16-fold in Δ*amvA* Δ*adeB* Δ*aceI* and Δ*amvA* Δ*adeB* Δ*adeJ*, and twofold in Δ*amvA* Δ*aceI* Δ*adeJ* triple mutants (**Table 2**). CHX susceptibility with MIC and MBC values of 2–1 was recovered in Δ*adeB* Δ*aceI* and Δ*adeB* Δ*adeJ* double mutants, and Δ*adeB* Δ*aceI* Δ*adeJ*, Δ*amvA* Δ*adeB* Δ*aceI,* and Δ*amvA* Δ*adeB* Δ*adeJ* triple mutants (**Table 2**). The above data indicated that CHX MIC and MBC in *A. baumannii* ATCC 19606 were mainly sustained by the expression of *adeB* and that *aceI*, *amvA* and to a lesser extent *adeJ* played an additive effect.

TABLE 2 | CHX MIC (mg/L) and MBC (mg/L) of *A. baumannii* ATCC 19606 parental strain and EP deletion mutants.

Strain	CHX MIC	
	MIC	MBC
ATCC 19606	32	32
Δ*amvA*	16	32
Δ*aceI*	16	16
Δ*adeB*	4	4
Δ*adeJ*	32	32
Δ*amvA* Δ*aceI*	8	8
Δ*amvA* Δ*adeB*	4	4
Δ*adeB* Δ*aceI*	2	2
Δ*amvA* Δ*adeJ*	16	32
Δ*aceI* Δ*adeJ*	16	32
Δ*adeB* Δ*adeJ*	2	2
Δ*amvA* Δ*adeB* Δ*aceI*	2	2
Δ*adeB* Δ*aceI* Δ*adeJ*	1	1
Δ*amvA* Δ*aceI* Δ*adeJ*	16	16
Δ*amvA* Δ*adeB* Δ*adeJ*	2	2

To further study the role of EPs on CHX susceptibility in *A. baumannii*, we analyzed the effect the EP inhibitor CCCP in *A. baumannii* ATCC 19606 and EPs marker-less mutants. As shown in **Table 3**, CCCP reduced dose-dependently CHX MIC in *A. baumannii* ATCC 19606 and in Δ*adeJ,* Δ*aceI,* or Δ*amvA* single, double or triple mutants. CCCP reduced CHX MIC in Δ*adeB*, single, double or triple mutants but the effect was not dose-dependent. This indicates that inhibition of efflux pump activity restores susceptibility to CHX in *A. baumannii* ATCC 19606 and in Δ*adeJ,* Δ*aceI,* or Δ*amvA,* but not in Δ*adeB* mutants.

We next asked whether EPs knockout gene inactivation might affect the *in vitro* planktonic and sessile growth of *A. baumannii* ATCC 19606. *A. baumannii* ATCC 19606 and single, double or triple Δ*adeJ,* Δ*aceI,* Δ*amvA,* Δ*adeB* mutants showed similar sigmoid growth curves and no difference in growth rates, despite Δ*amvA* Δ*adeB* Δ*aceI* and Δ*amvA* Δ*adeB* Δ*adeJ* triple mutants showed a longer lag phase than *A. baumannii* ATCC 19606 and other deletion mutants (**Supplementary Figure 2**). We analyzed also biofilm growth of *A. baumannii* ATCC 19606 and single, double or triple EP mutants. As shown in **Figure 3**,

TABLE 3 | MIC of CHX (mg/L) in combination with CCCP of *A. baumannii* ATCC 19606 parental strain and EP deletion mutants.

Strain	CCCP MIC	CHX MIC			
		CCCP			
		0	0.5	1	2
ATCC 19606	32	32	16	8	8
Δ*amvA*	32	16	8	8	4
Δ*acel*	32	16	16	8	4
Δ*adeB*	16	4	2	2	2
Δ*adeJ*	32	32	16	16	8
Δ*amvA* Δ*acel*	16	8	4	4	1
Δ*amvA* Δ*adeB*	32	4	2	2	2
Δ*adeB* Δ*acel*	16	2	2	2	1
Δ*amvA* Δ*adeJ*	32	16	8	4	1
Δ*acel* Δ*adeJ*	32	16	16	2	1
Δ*adeB* Δ*adeJ*	8	2	1	1	1
Δ*amvA* Δ*adeB* Δ*acel*	32	2	1	1	1
Δ*adeB* Δ*acel* Δ*adeJ*	8	1	1	1	0.5
Δ*amvA* Δ*acel* Δ*adeJ*	32	16	8	4	1
Δ*amvA* Δ*adeB* Δ*adeJ*	32	2	1	1	1

biofilm formation of single, double or triple Δ*adeJ,* Δ*aceI,* Δ*amvA,* Δ*adeB* mutants grown in the absence or in the presence of 1/2 MIC CHX was decreased by 30–50% compared with *A. baumannii* ATCC 19606 parental cells. On the other hand, 1/2 MIC CHX decreased biofilm growth in ATCC 19606 parental, Δ*adeJ,* Δ*aceI,* Δ*amvA,* Δ*adeB* single mutants, Δ*amvA* Δ*aceI*, Δ*amvA* Δ*adeB,* Δ*adeB* Δ*aceI,* and Δ*aceI* Δ*adeJ* double mutants and Δ*amvA* Δ*adeB* Δ*adeJ* triple mutants, while induced biofilm growth in Δ*adeB* Δ*adeJ* or Δ*amvA* Δ*adeJ* double mutants, and Δ*amvA* Δ*adeB* Δ*aceI*, Δ*adeB* Δ*aceI* Δ*adeJ,* or Δ*amvA* Δ*aceI* Δ*adeJ* triple mutants (**Figure 3**).

Susceptibility to Benzalkonium Chloride, Dequalinium Chloride, Cetrimide and Triclosan in *A. baumannii* ATCC 19606 Wild Type and Efflux Pump Deletion Mutants

The susceptibility to other biocides, which are used as antiseptics or disinfectants (McDonnell and Russell, 1999), was analyzed in *A. baumannii* ATCC 19606 wild type and EP deletion mutants. In accordance with previous findings (Chen et al., 2009), *A. baumannii* ATCC19606 and single EP deletion mutants showed TRI MIC and MBC of 0.06 and 0.125 mg/L, respectively, and were considered susceptible to TRI (**Supplementary Table 3**). On the contrary, *A. baumannii* ATCC19606 and single EP deletion mutants were tolerant to quaternary ammonium compounds DQ and CT, showing MIC and MBC values of 32–256 and 16–64 mg/L, respectively (**Supplementary Table 3**).

The mechanisms responsible for tolerance to BZK was studied in detail in *A. baumannii* ATCC 19606 parental strain and marker-less mutants of *adeB*, *adeJ*, *aceI* and *amvA* EPs genes. As shown in **Table 4**, BZK MIC and MBC values were decreased by four, two, and onefold in Δ*adeB*, Δ*amvA,* and Δ*aceI* mutants, respectively, compared with *A. baumannii* ATCC19606; BZK MIC and MBC were not affected in Δ*adeJ* mutant. Also, BZK MIC and MBC values were decreased by eightfold in Δ*amvA* Δ*adeB*, Δ*adeB* Δ*aceI,* and Δ*adeB* Δ*adeJ* double mutants, and

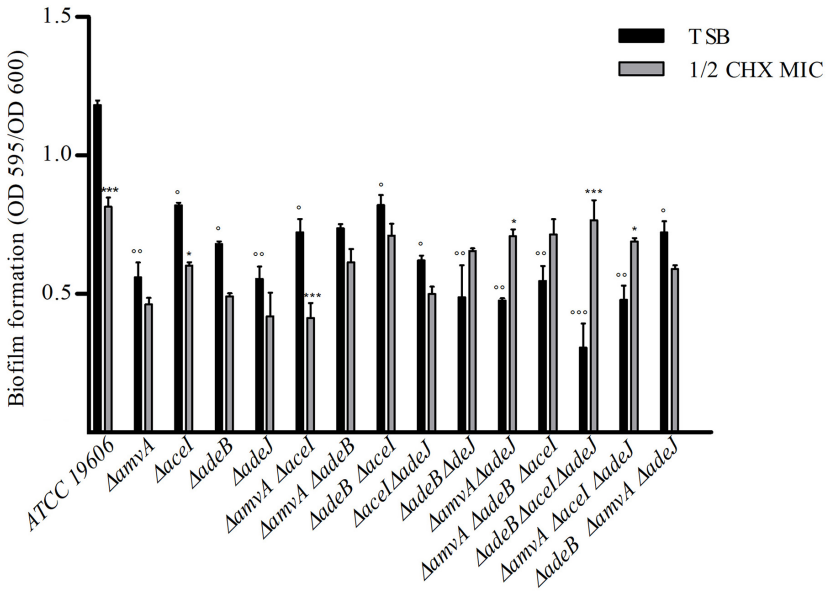

FIGURE 3 | Biofilm formation of A. *baumannii* ATCC 19606 parental strain and single, double and triple deletion mutants in the absence (TSB) or the presence of 1/2 CHX MIC. *P*-values were calculated using ANOVA (°$p < 0.05$, °°$p < 0.01$, or °°°$p < 0.001$ vs. *A. baumannii* ATCC 19606 parental strain; *$p < 0.05$ or ***$p < 0.001$ vs. 1/2 CHX MIC).

TABLE 4 | BZK MIC (mg/L) and MBC (mg/L) of *A. baumannii* ATCC 19606 parental strain and EP deletion mutants.

Strain	BZK	
	MIC	MBC
ATCC 19606	32	32
Δ*amvA*	16	16
Δ*acel*	16	16
Δ*adeB*	8	8
Δ*adeJ*	32	32
Δ*amvA* Δ*acel*	16	16
Δ*amvA* Δ*adeB*	4	4
Δ*adeB* Δ*acel*	4	4
Δ*amvA* Δ*adeJ*	16	16
Δ*acel* Δ*adeJ*	16	16
Δ*adeB* Δ*adeJ*	4	4
Δ*amvA* Δ*adeB* Δ*acel*	4	8
Δ*adeB* Δ*acel* Δ*adeJ*	2	2
Δ*amvA* Δ*acel* Δ*adeJ*	8	8
Δ*amvA* Δ*adeB* Δ*adeJ*	2	2

BZK, Benzalkonium chloride.

twofold in Δ*amvA* Δ*aceI*, Δ*amvA* Δ*adeJ,* and Δ*aceI* Δ*adeJ* double mutants. Moreover, BZK MIC and MBC were decreased by 16-fold in Δ*adeB* Δ*aceI* Δ*adeJ* and Δ*amvA* Δ*adeB* Δ*adeJ*, eightfold in Δ*amvA* Δ*adeB* Δ*aceI*, fourfold in Δ*amvA* Δ*aceI* Δ*adeJ* triple mutants (**Table 4**). BZK susceptibility with MIC and MBC values of 2 was recovered in Δ*adeB* Δ*aceI* Δ*adeJ* and Δ*amvA* Δ*adeB* Δ*adeJ* triple mutants (**Table 4**). The above data indicated that BZK MIC and MBC in *A. baumannii* ATCC 19606 were mainly regulated by the functioning of *adeB* and to a lesser extent *amvA, aceI,* and *adeJ* EPs.

Structural Comparison of AdeB and AdeJ Protomers

Overall, AdeB and AdeJ are two highly homologous proteins sharing a sequence identity of 49%. Both AdeB and AdeJ adopt a homotrimeric structure, with the typical RND-like fold (Su et al., 2019; Morgan et al., 2021; Zhang et al., 2021). Similar to AcrB of *E. coli* (seqid 50%), they are composed of a transmembrane domain formed by 12 transmembrane (TM) helices and a large periplasmic domain (**Figure 4A**). In this structural organization, the periplasmic domain harbors an entrance, a proximal and a distal substrate binding pockets (PBP and DBP, respectively). The PBP is separated from the DPB by a so-called "gate-loop" (or G-loop). Another conserved flexible loop (F-loop) connects the cleft entrance to the proximal drug-binding pocket. These loops are crucial to substrate discrimination in AcrB (Schuster et al., 2016). During substrate extrusion, AdeB and AcrB are thought to pass through a conformational change that forces the substrate to move from the PBP to the DBP for final extrusion (Schuster et al., 2016; Morgan et al., 2021).

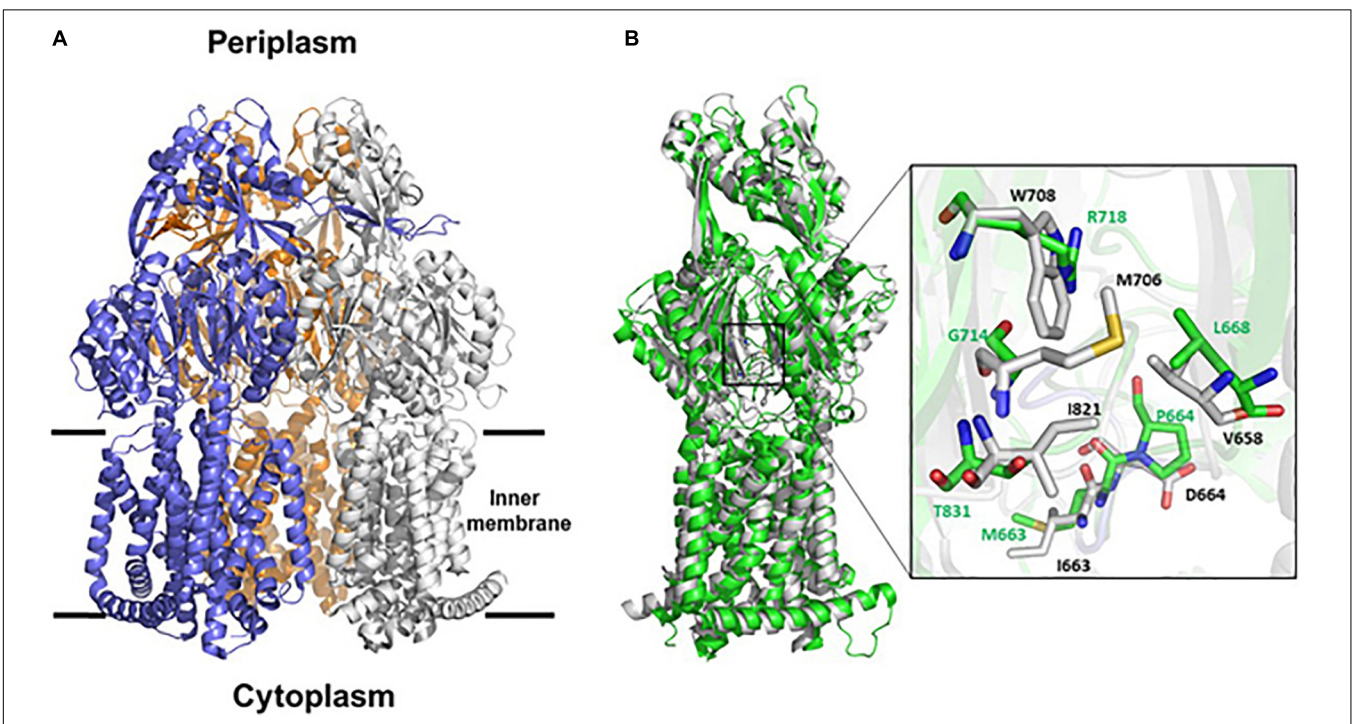

FIGURE 4 | Structural representation of AdeB and AdeJ pumps of *A. baumannii*. **(A)** Cartoon representation of AdeB heterotrimer (pdb code 7 kgd); the three protomers are represented in blue, white and orange. **(B)** Superposition between the structures of AdeB and AdeJ (pdb code 7m4q) protomers. The two structures superpose with a backbone root mean square deviations (rmsd) of 2.5, 2.9, 3.0 Å on chains A, B, and C, respectively. The inset shows a zoom of the entrance sites of AdeB (white) and AdeJ (green). AdeB residues are labeled black whereas corresponding AdeJ residues are labeled green.

TABLE 5 | MIC (mg/L) and MBC of CHX (mg/L) in combination with PIP in *A. baumannii* ATCC 19606 parental strain and EP deletion mutants.

Strain	PIP MIC	CHX MIC (MBC)					
		PIP					
		0	8	16	32	64	128
ATCC 19606	>1,024	32 (32)	32 (32)	16 (16)	8 (8)	8 (8)	8 (8)
Δ*amvA*	>1,024	16 (16)	16 (16)	8 (16)	8 (8)	8 (8)	8 (8)
Δ*acel*	>1,024	16 (16)	16 (16)	16 (16)	8 (16)	8 (16)	8 (8)
Δ*adeB*	>1,024	4 (4)	4 (4)	2 (4)	2 (4)	2 (2)	2 (2)
Δ*adeJ*	>1,024	32 (32)	32 (32)	16 (16)	16 (16)	8 (8)	4 (4)
Δ*amvA* Δ*acel*	>1,024	8 (8)	8 (8)	8 (8)	4 (8)	4 (4)	4 (4)
Δ*amvA* Δ*adeB*	>1,024	4 (4)	4 (4)	1 (4)	1 (2)	1 (2)	1 (2)
Δ*adeB* Δ*acel*	>1,024	2 (2)	2 (2)	1 (1)	1 (1)	1 (1)	1 (1)
Δ*amvA* Δ*adeJ*	>1,024	16 (16)	16 (16)	16 (16)	8 (16)	8 (8)	8 (8)
Δ*adeB* Δ*adeJ*	>1,024	2 (2)	2 (2)	1 (2)	1 (2)	1 (1)	1 (1)
Δ*acel* Δ*adeJ*	>1,024	16 (16)	16 (16)	16 (16)	8 (16)	8 (8)	8 (8)
Δ*amvA* Δ*adeB* Δ*acel*	>1,024	2 (2)	2 (2)	0.5 (2)	0.5 (1)	0.5 (1)	0.5 (1)
Δ*adeB* Δ*acel* Δ*adeJ*	>1,024	1 (1)	1 (1)	1 (1)	0.5 (0.5)	0.5 (0.5)	0.5 (0.5)
Δ*amvA* Δ*acel* Δ*adeJ*	>1,024	16 (16)	16 (16)	8 (8)	4 (8)	4 (4)	4 (4)
Δ*amvA* Δ*adeB* Δ*adeJ*	>1,024	2 (2)	2 (2)	1 (2)	0.5 (1)	0.5 (0.5)	0.5 (0.5)

A structural comparison of AdeB and AdeJ protomers was performed to analyze whether differences in the structural features of the two pumps may account for the major role observed for AdeB, compared to AdeJ, on CHX extrusion and susceptibility. As shown in **Figure 4B**, AdeB and AdeJ share a strictly conserved fold, with root mean square deviations (rmsd) ranging between 2.5 and 3.0 Å on the three chains. The analysis of the entrance binding sites of AdeB and AdeJ suggests different features that may explain a different involvement in CHX transport. Most relevant, the conserved W708 of AdeB is replaced by an arginine residue (R718) in AdeJ (**Figure 4B**). Other residues belonging to this cavity also differ. Specifically, V658, M706, I861 are replaced by L668, G714, and T831, respectively. These differences in the composition of the entrance site of AdeJ, compared to AdeB, make the pocked positively charged and not prone to bind the positively charged CHX. Significant differences are also observed in the F loops of the two pumps. In AdeB, the F-loop (661-PAIDELGT-668) resembles that of AcrB (669-PAIVELGT-676) of *E. coli*, in which residue I671 has been shown to be important for drug discrimination (Schuster et al., 2016). Differently, the F-loop of AdeJ does not contain this key isoleucine (669-PAMPELGV-676), which is thought to be part of a preferential small-drug entrance pathway. Additionally, a more negatively charged F-loop (due to the charge contribution of D664) in AdeB may also contribute to its stronger involvement in the transport of the positively charged CHX.

TABLE 6 | RV effect on CHX MIC (mg/L) and CHX MBC (mg/L) in *A. baumannii* ATCC 19606 parental strain and EP deletion mutants.

Strain	RV MIC	CHX MIC (MBC)			
		RV			
		0	32	64	128
ATCC 19606	>1,024	32 (32)	8 (16)	4 (8)	<0.5 (2)
Δ*amvA*	>1,024	16 (16)	8 (8)	4 (8)	<0.5 (2)
Δ*acel*	>1,024	16 (16)	8 (16)	4 (8)	<0.5 (2)
Δ*adeB*	>1,024	4 (4)	4 (4)	4 (4)	<0.5 (2)
Δ*adeJ*	>1,024	32 (32)	8 (16)	4 (16)	<0.5 (2)
Δ*amvA* Δ*acel*	>1,024	8 (8)	4 (4)	1 (4)	<0.5 (1)
Δ*amvA* Δ*adeB*	>1,024	4 (4)	2 (4)	1 (2)	<0.5 (2)
Δ*adeB* Δ*acel*	>1,024	2 (2)	2 (2)	1 (2)	<0.5 (1)
Δ*amvA* Δ*adeJ*	>1,024	16 (16)	4 (4)	1 (2)	<0.5 (1)
Δ*adeB* Δ*adeJ*	>1,024	2 (2)	1 (2)	<0.5 (1)	<0.5 (0.5)
Δ*acel* Δ*adeJ*	>1,024	16 (16)	4 (8)	1 (2)	<0.5 (0.5)
Δ*amvA* Δ*adeB* Δ*acel*	>1,024	2 (2)	0.5 (1)	0.5 (1)	<0.5 (0.5)
Δ*adeB* Δ*acel* Δ*adeJ*	>1,024	1 (1)	0.5 (1)	<0.5 (1)	<0.5 (0.5)
Δ*amvA* Δ*acel* Δ*adeJ*	>1,024	16 (16)	4 (8)	0.5 (1)	<0.5 (0.5)
Δ*amvA* Δ*adeB* Δ*adeJ*	>1,024	2 (2)	1 (1)	<0.5 (0.5)	<0.5 (0.5)

Effect of Piperine and Resveratrol on Chlorhexidine and Benzalkonium Susceptibility and Expression of Efflux Pumps Genes in *A. baumannii* ATCC 19606 Wild Type and Deletion Mutants

We next screened two natural compounds, RV and PIP, which have shown promising activity as EPs inhibitors (Sharma et al., 2010; Mirza et al., 2011; Singkham-In et al., 2020). We tested if these non-toxic compounds can decrease CHX MIC in *A. baumannii* ATCC 19606 and EPs gene knockout mutants and restore susceptibility to CHX. Both PIP and RV showed no antimicrobial activity against *A. baumannii* ATCC 19606 and Δ*adeJ,* Δ*aceI,* Δ*amvA,* Δ*adeB* mutants (MIC > 1,024 mg/L) (**Tables 5**, **6**). We then determined the antimicrobial activity of PIP in combination with CHX by *in vitro* combination

assay. As shown in **Table 5**, increasing doses of PIP up to 128 mg/L decreased CHX MIC and MBC by four fold in *A. baumannii* ATCC 19606 and by two to eightfold in Δ*adeJ,* Δ*aceI,* Δ*amvA,* Δ*adeB* mutants, being able to restore CHX susceptibility in single, double and triple mutants with inactivation of *adeB* gene. Furthermore, RV from 32 to 128 mg/L decreased dose-dependently CHX MIC and MBC and restored CHX susceptibility in *A. baumannii* ATCC 19606 and Δ*adeJ,* Δ*aceI,* Δ*amvA,* Δ*adeB* single, double and triple mutants. In particular, CHX susceptibility was restored by RV at 128 mg/L in *A. baumannii* ATCC 19606 and Δ*aceI,* Δ*amvA,* Δ*adeB*, or Δ*adeJ* single mutants, 64 mg/L in all double or EP triple mutants, 32 mg/L in double or triple EP mutants harboring deletion of *adeB* (**Table 6**).

To assess whether the effect of PIP and RV on CHX susceptibility was mediated by inhibition of EPs expression, we analyzed *amvA*, *aceI*, *adeB,* and *adeJ* expression in *A. baumannii* ATCC 19606 in the presence of 4 mg/L subMIC CHX in combination with 32 mg/L PIP or 32 mg/L RV. As shown in **Figure 5A**, PIP counteracted CHX-dependent increased expression of *amvA*, *aceI*, *adeB,* and *adeJ,* while it did not affect basal EP gene expression. On the other hand, resveratrol inhibited both basal and CHX-dependent increased expression of *amvA*, *aceI*, *adeB,* and *adeJ*, the highest effect found for *adeB* and *amvA* (**Figure 5B**). The above data suggested that different effects of PIP and RV on CHX MIC in *A. baumannii* ATCC 19606 were mediated by distinct regulation of *amvA*, *aceI*, *adeB,* and *adeJ* expression.

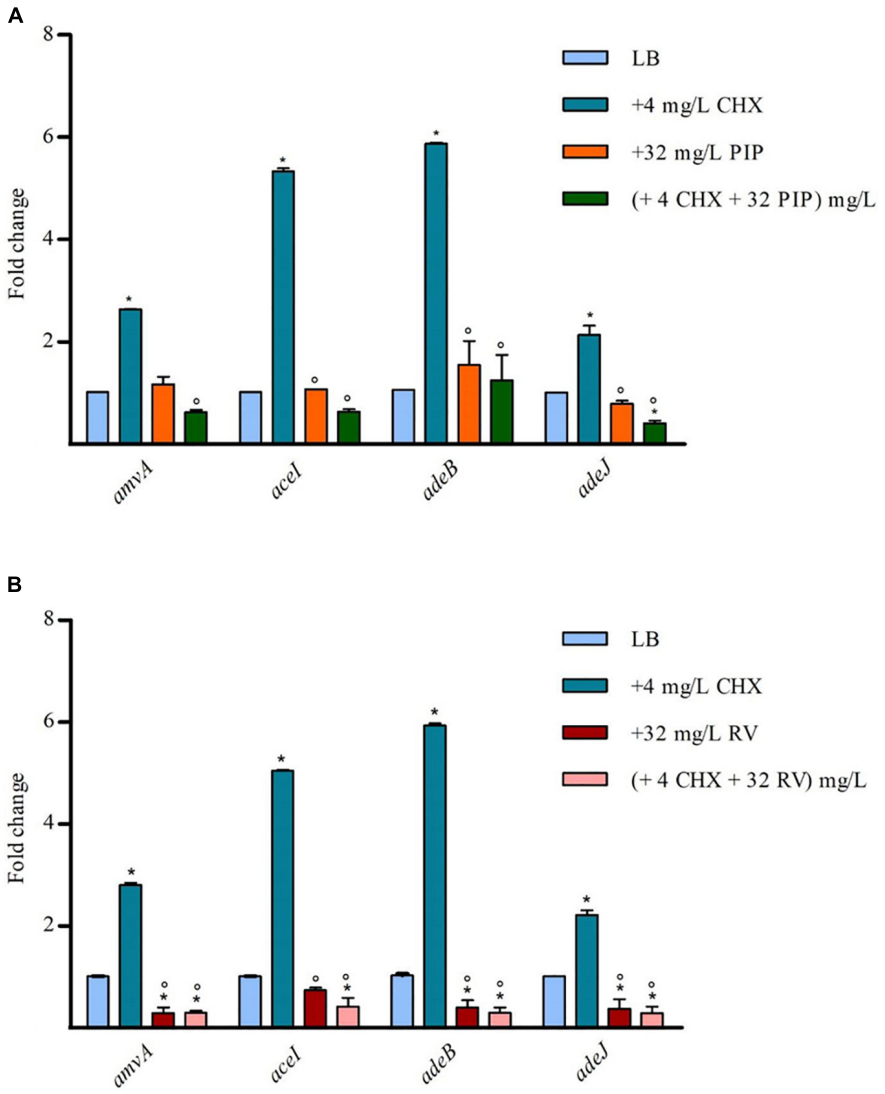

FIGURE 5 | RT-qPCR assay of *amvA*, *aceI*, *adeB,* and *adeJ* genes expression in the absence (LB) or presence of 4 mg/L CHX alone or in combination with 32 mg/L PIP **(A)** or 32 mg/L RV **(B)**. Relative number of transcripts of each gene was normalized in each condition and calculated using the $2^{-\Delta\Delta ct}$ method compared to the expression level in LB control. The mean ± standard deviation of relative number of transcripts is shown for each gene. All experiments were performed in triplicate. *P*-values were calculated using ANOVA (*$p < 0.01$ vs. LB;°$p < 0.01$ vs. 4 mg/L CHX).

TABLE 7 | RV effect on BZK MIC (mg/L) and MBC (mg/L) in *A. baumannii* ATCC 19606 parental strain and EP deletion mutants.

Strain	BZK MIC (MBC)			
	RV			
	0	32	64	128
ATCC 19606	32 (32)	16 (32)	4 (16)	0.5 (1)
Δ*amvA*	16 (16)	8 (8)	4 (4)	<0.5 (0.5)
Δ*acel*	16 (16)	16 (16)	4 (4)	<0.5 (0.5)
Δ*adeB*	8 (8)	2 (4)	1 (1)	<0.5 (0.5)
Δ*adeJ*	32 (32)	8 (16)	2 (4)	<0.5 (1)
Δ*amvA* Δ*acel*	16 (16)	2 (2)	1 (1)	<0.5 (0.5)
Δ*amvA* Δ*adeB*	4 (4)	1 (2)	0.5 (0.5)	<0.5 (0.5)
Δ*adeB* Δ*acel*	4 (4)	2 (2)	1 (2)	<0.5 (0.5)
Δ*amvA* Δ*adeJ*	16 (16)	4 (4)	1 (1)	<0.5 (0.5)
Δ*adeB* Δ*adeJ*	4 (4)	1 (1)	0.5 (0.5)	<0.5 (0.5)
Δ*acel* Δ*adeJ*	16 (16)	2 (2)	1 (1)	<0.5 (0.5)
Δ*amvA* Δ*adeB* Δ*acel*	4 (8)	0.5 (1)	0.5 (1)	<0.5 (0.5)
Δ*adeB* Δ*acel* Δ*adeJ*	2 (2)	0.5 (0.5)	0.5 (0.5)	<0.5 (0.5)
Δ*amvA* Δ*acel* Δ*adeJ*	8 (8)	2 (16)	1 (2)	<0.5 (0.5)
Δ*amvA* Δ*adeB* Δ*adeJ*	2 (2)	0.25 (1)	<0.5 (0.5)	<0.5 (0.5)

The effect of RV was also analyzed on BZK MIC and MBC in *A. baumannii* ATCC 19606 parental strain and EP deletion mutants. As shown in **Table 7**, RV from 32 mg/L to 128 mg/L decreased dose-dependently BZK MIC and MBC and restored BZK susceptibility in *A. baumannii* ATCC 19606 and single, double and triple EP deletion mutants. BZK susceptibility was restored by RV at 128 mg/L in *A. baumannii* ATCC 19606 and Δ*aceI* or Δ*amvA,* single mutants, 64 mg/L in Δ*adeB*, or Δ*adeJ* single mutants and in all double or EP triple mutants, 32 mg/L in Δ*adeB* single mutant and in all, but not Δ*amvA* Δ*adeJ*, double mutants (**Table 7**).

We analyzed also the effect of 2 mg/L BZK alone or in combination with 32 mg/L RV on *amvA*, *aceI*, *adeB,* and *adeJ* expression. As shown in **Figure 6**, two mg/L BZK alone inhibited in a non-significant way EP gene expression, and 2 mg/L BZK in combination with 32 mg/L RV significantly inhibited *amvA*, *adeB,* and *adeJ* expression by 10–15-fold and *aceI* expression by twofold respect to untreated cells. The above data indicated that the effect of RV on BZK susceptibility was mediated by inhibition of *amvA*, *adeB*, *adeJ,* and to a lesser extent *aceI* expression.

DISCUSSION

The present study analyzes the molecular mechanism responsible for adaptation and tolerance of *A. baumannii* to CHX and BZK. Our data demonstrate that *adeB*, *aceI* and to lesser extent *adeJ* and *amvA* EP genes are activated by CHX in *A. baumannii* ATCC 19606 and that inactivation of EP genes decreases CHX MIC and MBC and restores CHX susceptibility in *A. baumannii* ATCC 19606. We show that subMIC concentrations of CHX enhance the expression of *aceI* efflux pump gene five to nine-fold, whereas that of *adeB* is enhanced sixfold. Despite this observation, CHX MIC and MBC decrease is significantly higher (eightfold) in Δ*adeB* compared to Δ*amvA* or Δ*aceI* mutant (two fold), or Δ*adeJ* mutant (no decrease). Single, double and triple mutants with inactivation of *adeB* gene showed an additive effect on CHX MIC and MBC (**Table 2**). Our data are in agreement with and extend previous studies showing that resistance to CHX in *A. baumannii* ATCC 17978 is dependent on increased expression of *aceI* in *A. baumannii* ATCC17978 (Hassan et al., 2013) and that inactivation of AceI EP (Hassan et al., 2013), AdeB or AdeJ RND EPs (Rajamohan et al., 2010a) or AmvA MFS EP (Rajamohan et al., 2010b), AceI or AdeB (Tucker et al., 2014) restores susceptibility to CHX and other disinfectants in *A. baumannii*. In accordance with previous findings (Tucker et al., 2014), data

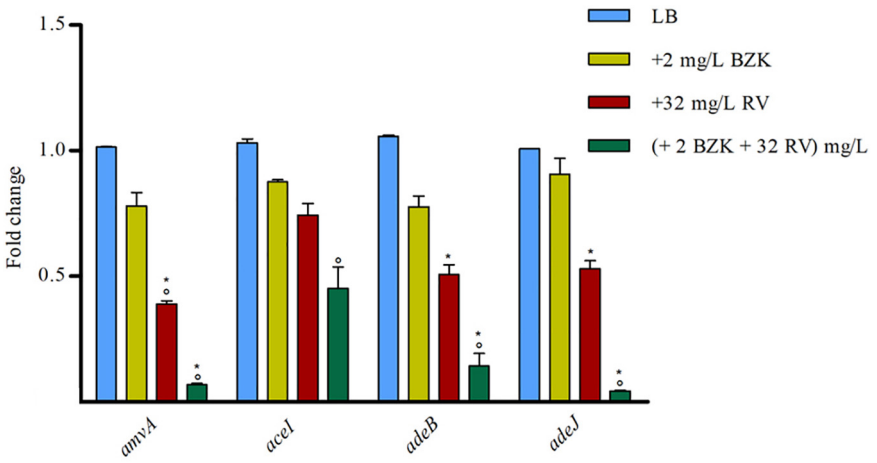

FIGURE 6 | RT-qPCR assay of *amvA*, *acel*, *adeB,* and *adeJ* genes expression in the absence (LB) or presence of 2 mg/L BZK alone or in combination with 32 mg/L RV. Relative number of transcripts of each gene was normalized in each condition and calculated using the $2^{-\Delta\Delta ct}$ method compared to the expression level in LB control. The mean ± standard deviation of relative number of transcripts is shown for each gene. All experiments were performed in triplicate. *P*-values were calculated using ANOVA (*$p < 0.01$ vs. LB; °$p < 0.01$ vs. 2 mg/L BZK).

reported herein suggest a major involvement of AdeB in CHX transport compared to AceI. Susceptibility to CHX suggests an even lower involvement of the other pumps (AdeJ, AmvA) in CHX efflux, with no effect on MIC nor on MBC observed upon Δ*adeJ* mutation. In accordance with previous study (Yoon et al., 2015), we showed that inactivation of either AmvA, AceI, AdeB, or AdeJ alone or in combination did not affect planktonic growth but reduced biofilm formation by 30–50% in the absence and in the presence of 1/2 MIC CHX. However, subMIC CHX concentrations increase biofilm formation in Δ*amvA* Δ*adeJ*, Δ*adeB* Δ*aceI* Δ*adeJ,* and Δ*amvA* Δ*aceI* Δ*adeJ* mutants compared to untreated cells, thus suggesting that CHX positively regulate the phenomenon. Overall, our data indicates that EPs have pleiotropic effect and regulate multiple functions in addition to tolerance to disinfectants (Yoon et al., 2015; Du et al., 2018; Kornelsen and Kumar, 2021).

Our data demonstrate that tolerance to BZK in *A. baumannii* ATCC 19606 is regulated by AdeB EP and that AmvA, AceI and AdeJ EPs play a role also. BZK MIC was decreased by fourfold in Δ*adeB* mutant, and twofold in Δ*amvA* and Δ*aceI* mutants, respectively; EPs double and triple deletion mutants showed an additive effect on BZK MIC (**Table 4**). BZK susceptibility is recovered in Δ*adeB* Δ*aceI* Δ*adeJ* and Δ*amvA* Δ*adeB* Δ*adeJ* triple mutants. This is in partial agreement with previous study showing that inactivation of AmvA MFS EP decreases BZK MIC by fourfold in *A. baumannii* but not restores full susceptibility to biocide (Rajamohan et al., 2010b). In keeping with this, the data shown herein demonstrate that simultaneous inactivation of AdeB, AmvA, and AdeJ or AceI is necessary to restore BZK susceptibility in *A. baumannii*.

Importantly, AdeB and AdeJ are two highly homologous proteins sharing a sequence identity of 49%. Both *adeB* and *adeJ* genes are abundantly expressed at basal level, showing normalized expression level of 0.25 and 0.34, respectively (**Supplementary Figure 1**), but *adeB* is 3x higher expressed than *adeJ* in the presence of CHX (**Figure 2**). Also, *A. baumannii* ATCC 19606 does not possess the *adeC* gene of the *adeABC* operon and may use an alternate outer membrane protein (OMP), likely AdeK, of the constitutive efflux pump, AdeIJK, as described in other *A. baumannii* strains (Sugawara and Nikaido, 2014). However, we observe a completely different involvement of the two RND-type efflux pumps in CHX extrusion and tolerance, with AdeABC playing a central role and AdeIJK being only marginal in this mechanism (**Table 2**) and we postulate that differences in the structure between AdeB and AdeJ protomers may be responsible for this. The structural comparison of AdeB and AdeJ shows different features at the entrance binding site, such as W708, V658, M706, I861 in AdeB, which are replaced by R718, L668, G714, and T831 in AdeJ, respectively. Overall, a more positive electrostatic potential surface at the entrance site of AdeJ, due to R817, may render this pump not prone to bind the positively charged CHX. Additionally, the F-loop of AdeB presents different features than that of AdeJ, as it is more negatively charged (due to the charge contribution of D664) and contains a key isoleucine residue, I671, which was shown to be important in AcrB (Schuster et al., 2016). These features may contribute to its stronger involvement in the transport of the positively charged CHX by AdeB (**Figure 4B**). Future experimental data will be necessary to validate the impact of specific residues in AdeB protomer on CHX efflux in *A. baumannii.*

In this work, we also searched for EP inhibitors that restore CHX susceptibility, to tackle *A. baumannii* tolerance to CHX and BZK induced by EP pumps. As a first compound, CCCP showed a significant effect on CHX MIC (**Table 3**). However, due to the toxicity of this compound, we analyzed the effects on CHX susceptibility of two antioxidant molecules, the non-toxic PIP and RV. As a result, both PIP and RV were able to decrease CHX MIC and MBC in *A. baumannii* ATCC 19606 and EP deletion mutants. In particular, PIP was able to restore CHX susceptibility only in single, double and triple mutants with inactivation of *adeB* gene. In partial agreement with our data, PIP inhibited rifampicin-induced expression of Rv1258c multidrug efflux pump and rifampicin MIC in *Mycobacterium tuberculosis* (Sharma et al., 2010). Similarly, PIP has been demonstrated to inhibit ethidium bromide efflux and mupirocin resistance in methicillin-resistant *S. aureus* (Mirza et al., 2011). Our data also demonstrated that RV has higher efficacy than PIP on CHX susceptibility, being resveratrol able to restore CHX susceptibility dose-dependently both in *A. baumannii* ATCC 19606 and in EP deletion mutants. Coherent with this finding, we show that PIP inhibits CHX-induced, though not basal, expression of EP genes. In addition, consistent with previous data (Singkham-In et al., 2020) we find that RV is able to inhibit both basal levels and CHX-induced expression of *amvA*, *aceI*, *adeB,* and *adeJ* genes in *A. baumannii* ATCC 19606. The differential effects of PIP and RV on CHX MIC is likely to be ascribed to their different ability to inhibit EPs gene expression.

Our data also demonstrated that RV restored BZK susceptibility both in *A. baumannii* ATCC 19606 and in EP deletion mutants. Although unlike CHX, BZK does not induce the expression of EPs genes, RV alone or in the presence of BZK inhibited *amvA*, *aceI*, *adeB* and *adeJ* expression, the effect of RV and BZK being synergic for *amvA*, *adeB*, *adeJ*. Based on this, we hypothesize that the effect of RV on BZK susceptibility in *A. baumannii* is mediated by the inhibition of expression of EPs.

CONCLUSION

The data reported in this study demonstrate that tolerance to CHX and BZK in *A. baumannii* is mediated by the activation of EPs. In particular, *adeB*, *adeJ*, *aceI,* and *amvA* expression is induced by CHX; EPs gene inactivation inhibits both CHX and BZK MIC in an additive manner, with AdeB EP playing a major role. We also identified PIP and RV as non-toxic compounds able to inhibit EPs gene expression and CHX or BZK tolerance in *A. baumannii*. Our data demonstrate that co-treatments of RV and CHX or RV and BZK restore susceptibility to biocides in *A. baumannii.*

A. baumannii ATCC19606 and EP inactivation mutants described herein may represent a useful model system to study the molecular mechanisms responsible for tolerance to biocides other than CHX and BZK in *A. baumannii* and to identify

innovative molecules and combination regimens, which are able to restore susceptibility to disinfectants in *A. baumannii*. The combination of RV may represent a useful strategy to maintain susceptibility to biocides in *A. baumannii* and other nosocomial pathogens.

DATA AVAILABILITY STATEMENT

The original contributions presented in the study are included in the article/**Supplementary Material**, further inquiries can be directed to the corresponding author/s.

AUTHOR CONTRIBUTIONS

ED and RZ conceived the study and participated in its design and coordination. AM, EE, and MB performed laboratory experiments. RB, MT, ED, and RZ performed data analyses. AM, EE, RB, ED, and RZ wrote the manuscript. All authors read and approved the final manuscript.

FUNDING

This work was supported in part by grant from the Italian Ministry of Education, University and Research (MIUR): PRIN2017 (Grant No. 2017SFBFER to RZ and RB).

ACKNOWLEDGMENTS

We thank all colleagues who generously provided strains included in the study: Alessandra Carattoli, Patrice Nordmann, and Paolo Visca.

SUPPLEMENTARY MATERIAL

The Supplementary Material for this article can be found online at: https://www.frontiersin.org/articles/10.3389/fmicb.2021.790263/full#supplementary-material

REFERENCES

Amin, I. M., Richmond, G. E., Sen, P., Koh, T. H., Piddock, L. J. V., and Chua, K. L. (2013). A method for generating marker-less gene deletions in multidrug-resistant *Acinetobacter baumannii*. *BMC Microbiol.* 13:158. doi: 10.1186/1471-2180-13-158

Chen, Y., Pi, B., Zhou, H., Yu, Y., and Li, L. (2009). Triclosan resistance in clinical isolates of *Acinetobacter baumannii*. *J. Med. Microbiol.* 58, 1086–1091. doi: 10.1099/jmm.0.008524-0

CLSI (2019). *Performance Standards for Antimicrobial Susceptibility Testing M100S*. Wayne, PA: Clinical and Laboratory Standards Institute.

De Gregorio, E., Del Franco, M., Martinucci, M., Roscetto, E., Zarrilli, R., and Di Nocera, P. (2015). Biofilm-associated proteins: news from Acinetobacter. *BMC Genomics*. 16:933. doi: 10.1186/s12864-015-2136-6

De Gregorio, E., Esposito, A., Vollaro, A., De Fenza, M., D'Alonzo, D., Migliaccio, A., et al. (2020). N-Nonyloxypentyl-l-Deoxynojirimycin inhibits growth, biofilm formation and virulence factors expression of *Staphylococcus aureus*. *Antibiotic (Basel)* 9, 362. doi: 10.3390/antibiotics9060362

De Gregorio, E., Esposito, E. P., Zarrilli, R., and Di Nocera, P. P. (2018). Contact-dependent growth inhibition proteins in *Acinetobacter baylyi* ADP1. *Curr. Microbiol.* 75, 1434–1440. doi: 10.1007/s00284-018-1540-y

Du, D., Wang-Kan, X., Neuberger, A., van Veen, H. W., Pos, K. M., Piddock, L. J. V., et al. (2018). Multidrug efflux pumps: structure, function and regulation. *Nat. Rev. Microbiol.* 16, 523–539. doi: 10.1038/s41579-018-0048-6

Emsley, P., and Cowtan, K. (2004). Coot: model-building tools for molecular graphics. *Acta Crystallogr. D Biol. Crystallogr.* 60(Pt 12 Pt 1), 2126–2132. doi: 10.1107/S0907444904019158

European Committee for Antimicrobial Susceptibility Testing (Eucast) of the European Society of Clinical Microbiology and Infectious Diseases (Escmid) (2000). Terminology relating to methods for the determination of susceptibility of bacteria to antimicrobial agents. *Clin. Microbiol. Infect.* 6, 503–508. doi: 10.1046/j.1469-0691.2000.00149.x

Foong, W. E., Tam, H. K., Crames, J. J., Averhoff, B., and Pos, K. M. (2019). The chloramphenicol/H+ antiporter CraA of *Acinetobacter baumannii* AYE reveals a broad substrate specificity. *J. Antimicrob. Chemother.* 74, 1192–1201. doi: 10.1093/jac/dkz024

Gaiarsa, S., Batisti Biffignandi, G., Esposito, E. P., Castelli, M., Jolley, K. A., Brisse, S., et al. (2019). Comparative analysis of the two *Acinetobacter baumannii* multilocus sequence typing (MLST) schemes. *Front Microbiol.* 10:930. doi: 10.3389/fmicb.2019.00930

Giannouli, M., Antunes, L. C. S., Marchetti, V., Triassi, M., Visca, P., and Zarrilli, R. (2013). Virulence-related traits of epidemic *Acinetobacter baumannii* strains belonging to the international clonal lineages I-III and to the emerging genotypes ST25 and ST78. *BMC Infect. Dis.* 13:282. doi: 10.1186/1471-2334-13-282

Hall, M., Middleton, R., and Westmacott, D. (1983). The fractional inhibitory concentration (FIC) index as a measure of synergy. *J. Antimicrob. Chemother.* 11, 427–433. doi: 10.1093/jac/11.5.427

Haq, I. U., Imran, M., Nadeem, M., Tufail, T., Gondal, T. A., and Mubarak, M. S. (2021). Piperine: a review of its biological effects. *Phytother. Res.* 35, 680–700. doi: 10.1002/ptr.6855

Harding, C. M., Hennon, S. W., and Feldman, M. F. (2018). Uncovering the mechanisms of *Acinetobacter baumannii* virulence. *Nat. Rev. Microbiol.* 16, 91–102. doi: 10.1038/nrmicro.2017.148

Hassan, K. A., Jackson, S. M., Penesyan, A., Patching, S. G., Tetu, S. G., Eijkelkamp, B. A., et al. (2013). Transcriptomic and biochemical analyses identify a family of chlorhexidine efflux proteins. *Proc. Natl. Acad. Sci. U.S.A.* 110, 20254–20259. doi: 10.1073/pnas.1317052110

Holm, L. (2020). Using dali for protein structure comparison. *Methods Mol. Biol.* 2112, 29–42. doi: 10.1007/978-1-0716-0270-6_3

Iacono, M., Villa, L., Fortini, D., Bordoni, R., Imperi, F., Bonnal, R. J., et al. (2008). Whole-genome pyrosequencing of an epidemic multidrug-resistant *Acinetobacter baumannii* strain belonging to the European clone II group. *Antimicrob. Agents Chemother.* 52, 2616–2625. doi: 10.1128/AAC.01643-07

Janssen, P., Maquelin, K., Coopman, R., Tjernberg, I., Bouvet, P., Kersters, K., et al. (1997). Discrimination of *Acinetobacter* genomic species by AFLP fingerprinting. *Int. J. Syst. Bacteriol.* 47, 1179–1187. doi: 10.1099/00207713-47-4-1179

Kampf, G. (2016). Acquired resistance to chlorhexidine - is it time to establish an 'antiseptic stewardship' initiative? *J. Hosp. Infect.* 94, 213–227. doi: 10.1016/j.jhin.2016.08.018

Kornelsen, V., and Kumar, A. (2021). Update on multidrug resistance efflux pumps in *Acinetobacter* spp. *Antimicrob. Agents Chemother.* 65, e514–e521. doi: 10.1128/AAC.00514-21 e00514-21,

Livak, K. J., and Schmittgen, T. D. (2001). Analysis of relative gene expression data using real-time quantitative PCR and the 2(-Delta Delta C(T)) method. *Methods* 25, 402–408. doi: 10.1006/meth.2001.1262

Magiorakos, A. P., Srinivasan, A., Carey, R. B., Carmeli, Y., Falagas, M. E., Giske, C. G., et al. (2012). Multidrug-resistant, extensively drug-resistant and pandrug-resistant bacteria: an international expert proposal for interim standard definitions for acquired resistance. *Clin. Microbiol. Infect.* 18, 268–281. doi: 10.1111/j.1469-0691.2011.03570.x

Martinucci, M., Roscetto, E., Iula, V. D., Votsi, A., Catania, M. R., and De Gregorio, E. (2016). Accurate identification of members of the *Burkholderia*

cepacia complex in cystic fibrosis sputum. *Lett. Appl. Microbiol.* 62, 221–229. doi: 10.1111/lam.12537

Mattio, L. M., Catinella, G., Dallavalle, S., and Pinto, A. (2020). Stilbenoids: a natural arsenal against bacterial pathogens. *Antibiotics (Basel)* 9:336. doi: 10.3390/antibiotics9060336

McDonnell, G., and Russell, A. D. (1999). Antiseptics and disinfectants: activity, action, and resistance. *Clin. Microbiol. Rev.* 12, 147–179. doi: 10.1128/CMR.12.1.147

Merchel Piovesan Pereira, B., and Tagkopoulos, I. (2019). Benzalkonium chlorides: uses, regulatory status, and microbial resistance. *Appl. Environ. Microbiol.* 85:e00377-19. doi: 10.1128/AEM.00377-19

Milstone, A. M., Passaretti, C. L., and Perl, T. M. (2008). Chlorhexidine: expanding the armamentarium for infection control and prevention. *Clin. Infect. Dis.* 46, 274–281. doi: 10.1086/524736

Mirza, Z. M., Kumar, A., Kalia, N. P., Zargar, A., and Khan, I. A. (2011). Piperine as an inhibitor of the MdeA efflux pump of *Staphylococcus aureus*. *J. Med. Microbiol.* 60(Pt 10), 1472–1478. doi: 10.1099/jmm.0.033167-0

Morgan, C. E., Glaza, P., Leus, I. V., Trinh, A., Su, C. C., Cui, M., et al. (2021). Cryoelectron microscopy structures of AdeB illuminate mechanisms of simultaneous binding and exporting of substrates. *mBio* 12:e03690–20. doi: 10.1128/mBio.03690-20

Poirel, L., Manuteau, O., Agoli, N., Cattoen, C., and Nordmann, P. (2003). Outbreak of extended-spectrum β-lactamase VEB-1-producing isolates of *Acinetobacter baumannii* in a French hospital. *J. Clin. Microbiol.* 41, 3542–3547. doi: 10.1128/JCM.41.8

Rajamohan, G., Srinivasan, V. B., and Gebreyes, W. A. (2010a). Novel role of *Acinetobacter baumannii* RND efflux transporters in mediating decreased susceptibility to biocides. *J. Antimicrob. Chemother.* 65, 228–232. doi: 10.1093/jac/dkp427

Rajamohan, G., Srinivasan, V. B., and Gebreyes, W. A. (2010b). Molecular and functional characterization of a novel efflux pump, AmvA, mediating antimicrobial and disinfectant resistance in *Acinetobacter baumannii*. *J. Antimicrob. Chemother.* 65, 1919–1925. doi: 10.1093/jac/dkq195

Schuster, S., Vavra, M., and Kern, W. V. (2016). Evidence of a substrate discriminating entrance channel in the lower porter domain of the multidrug resistance efflux pump AcrB. *Antimicrob. Agents Chemother.* 60, 4315–4323. doi: 10.1128/AAC.00314-16

Seeliger, D., and de Groot, B. L. (2010). Ligand docking and binding site analysis with PyMOL and Autodock/Vina. *J. Comput. Aided Mol. Des.* 24, 417–422. doi: 10.1007/s10822-010-9352-6

Sharma, S., Kumar, M., Sharma, S., Nargotra, A., Koul, S., and Khan, I. A. (2010). Piperine as an inhibitor of Rv1258c, a putative multidrug efflux pump of *Mycobacterium tuberculosis*. *J. Antimicrob. Chemother.* 65, 1694–1701. doi: 10.1093/jac/dkq186

Simon, R., Priefer, U., and Piihler, A. (1983). A broad host range mobilization system for in vivo genetic engineering: transposon mutagenesis in gram-negative bacteria. *Biotechnology* 1, 784–791.

Singkham-In, U., Higgins, P. G., Wannigama, D. L., Hongsing, P., and Chatsuwan, T. (2020). Rescued chlorhexidine activity by resveratrol against carbapenem-resistant *Acinetobacter baumannii* via down-regulation of AdeB efflux pump. *PLoS One* 15:e0243082. doi: 10.1371/journal.pone.0243082

Su, C. C., Morgan, C. E., Kambakam, S., Rajavel, M., Scott, H., Huang, et al. (2019). Cryo-electron microscopy structure of an *Acinetobacter baumannii* multidrug efflux pump. *mBio* 10:e01295-19. doi: 10.1128/mBio.01295-19

Sugawara, E., and Nikaido, H. (2014). Properties of AdeABC and AdeIJK efflux systems of *Acinetobacter baumannii* compared with those of the AcrAB-TolC system of *Escherichia coli*. *Antimicrob. Agents Chemother.* 58, 7250–7257. doi: 10.1128/AAC.03728-14

Tucker, A. T., Nowicki, E. M., Boll, J. M., Knauf, G. A., Burdis, N. C., Trent, M. S., et al. (2014). Defining gene-phenotype relationships in *Acinetobacter baumannii* through one-step chromosomal gene inactivation. *mBio* 5:e01313-14. doi: 10.1128/mBio.01313-14

Weber, D. J., Rutala, W. A., and Sickbert-Bennett, E. E. (2019). Use of germicides in health care settings-is there a relationship between germicide use and antimicrobial resistance: a concise review. *Am. J. Infect. Contr.* 47, A106–A109. doi: 10.1016/j.ajic.2019.03.023

Wong, D., Nielsen, T. B., Bonomo, R. A., Pantapalangkoor, P., Luna, B., and Spellberg, B. (2017). Clinical and pathophysiological overview of *Acinetobacter* infections: a century of challenges. *Clin. Microbiol. Rev.* 30, 409–447. doi: 10.1128/CMR.00058-16

Yoon, E. J., Chabane, Y. N., Goussard, S., Snesrud, E., Courvalin, P., Dé, E., et al. (2015). Contribution of resistance-nodulation-cell division efflux systems to antibiotic resistance and biofilm formation in *Acinetobacter baumannii*. *mBio* 6:e00309-15. doi: 10.1128/mBio.00309-15

Zhang, Z., Morgan, C. E., Bonomo, R. A., and Yu, E. W. (2021). Cryo-EM determination of eravacycline-bound structures of the ribosome and the multidrug efflux pump AdeJ of *Acinetobacter baumannii*. *mBio* 12:e0103121. doi: 10.1128/mBio.01031-21

Conflict of Interest: The authors declare that the research was conducted in the absence of any commercial or financial relationships that could be construed as a potential conflict of interest.

Publisher's Note: All claims expressed in this article are solely those of the authors and do not necessarily represent those of their affiliated organizations, or those of the publisher, the editors and the reviewers. Any product that may be evaluated in this article, or claim that may be made by its manufacturer, is not guaranteed or endorsed by the publisher.

frontiers | Frontiers in Microbiology

ORIGINAL RESEARCH
published: 19 May 2022
doi: 10.3389/fmicb.2022.869208

Identification of Promoter Region Markers Associated With Altered Expression of Resistance-Nodulation-Division Antibiotic Efflux Pumps in *Acinetobacter baumannii*

*Mireia López-Siles, Michael J. McConnell and Antonio J. Martín-Galiano**

Intrahospital Infections Laboratory, National Center for Microbiology, Instituto de Salud Carlos III (ISCIII), Madrid, Spain

OPEN ACCESS

Edited by:
Paolo Visca,
Roma Tre University, Italy

Reviewed by:
Ayush Kumar,
University of Manitoba, Canada
Karl Hassan,
The University of Newcastle, Australia

****Correspondence:***
Antonio J. Martín-Galiano
mgaliano@isciii.es

Specialty section:
This article was submitted to Antimicrobials, Resistance and Chemotherapy, a section of the journal Frontiers in Microbiology

Received: *04 February 2022*
Accepted: *27 April 2022*
Published: *19 May 2022*

Citation:
López-Siles M, McConnell MJ and Martín-Galiano AJ (2022) Identification of Promoter Region Markers Associated With Altered Expression of Resistance-Nodulation-Division Antibiotic Efflux Pumps in Acinetobacter baumannii. Front. Microbiol. 13:869208. doi: 10.3389/fmicb.2022.869208

Genetic alterations leading to the constitutive upregulation of specific efflux pumps contribute to antibacterial resistance in multidrug resistant bacteria. The identification of such resistance markers remains one of the most challenging tasks of genome-level resistance predictors. In this study, 487 non-redundant genetic events were identified in upstream zones of three operons coding for resistance-nodulation-division (RND) efflux pumps of 4,130 *Acinetobacter baumannii* isolates. These events included insertion sequences, small indels, and single nucleotide polymorphisms. In some cases, alterations explicitly modified the expression motifs described for these operons, such as the promoter boxes, operators, and Shine-Dalgarno sequences. In addition, changes in DNA curvature and mRNA secondary structures, which are structural elements that regulate expression, were also calculated. According to their influence on RND upregulation, the catalog of upstream modifications were associated with "experimentally verified," "presumed," and "probably irrelevant" degrees of certainty. For experimental verification, DNA of upstream sequences independently carrying selected markers, three for each RND operon, were fused to a luciferase reporter plasmid system. Five out of the nine selected markers tested showed significant increases in expression with respect to the wild-type sequence control. In particular, a 25-fold expression increase was observed with the IS*Aba*1 insertion sequence upstream the *adeABC* pump. Next, overexpression of each of the three multi-specific RND pumps was linked to their respective antibacterial substrates by a deep *A. baumannii* literature screen. Consequently, a data flow framework was then developed to link genomic upregulatory RND determinants to potential antibiotic resistance. Assignment of potential increases in minimal inhibitory concentrations at the "experimentally verified" level was permitted for 42 isolates to 7–8 unrelated antibacterial agents including tigecycline, which is overlooked by conventional resistome predictors. Thus, our protocol may represent a time-saving filter step prior to laborious confirmation experiments for efflux-driven resistance. Altogether, a computational-experimental pipeline containing all

components required for identifying the upstream regulatory resistome is proposed. This schema may provide the foundational stone for the elaboration of tools approaching antibiotic efflux that complement routine resistome predictors for preventing antimicrobial therapy failure against difficult-to-threat bacteria.

Keywords: resistome, promoter, repressor, insertion sequence, systems biology, nosocomial infection, operator

INTRODUCTION

Prompt and precise identification of genetic determinants that contribute to antibiotic resistance, the resistome, in difficult-to-treat bacteria can facilitate the administration of the most effective therapy. Cost decreases in DNA sequencing have further promoted the development of several computational protocols that predict antibiotic resistance at a whole-genome level (Gupta et al., 2014; de Man and Limbago, 2016; Alcock et al., 2020; Bortolaia et al., 2020) with a reported accuracy comparable to antibiograms determined using traditional microbiological techniques. Resistome identification often involves at least three elements: (a) a database of resistance determinants, either whole genes or specific mutations; (b) an algorithm that accurately detects the determinants in the genome sequence of interest; and (c) a controlled language that links genetic determinants of resistance to specific antibiotics (Alcock et al., 2020).

Isolates with identical predicted resistomes can, however, demonstrate different antibiograms and/or responses to antimicrobial therapy (Gerson et al., 2018). False predictions due to determinants that escape current algorithms can cause therapeutic failure, leading to increases in treatment cost and adverse outcomes. The identification of genetic markers underlying the constitutive upregulation of efflux pumps is considered the most significant challenge for future resistome predictors (Jeukens et al., 2017; Boolchandani et al., 2019; Mahfouz et al., 2020). Overexpression of otherwise repressed efflux pumps can reduce the cytoplasmic concentration of an antibiotic to ineffective levels (Kapp et al., 2018). Pump upregulation can be achieved by alterations in either repressor proteins (Gerson et al., 2018) or in upstream sequences of pump genes involved in gene expression (Olliver et al., 2005; Baylay and Piddock, 2015). Therefore, prediction of efflux-based resistance only by gene presence can lead to inaccurate interpretations. The multiplicity of DNA elements affecting gene transcription and translation makes the automated screening of upstream sequences for resistance traits a formidable task.

Efflux pump upregulation is a prominent resistance mechanism in *Acinetobacter baumannii* (Vila and Pachon, 2011; Cag et al., 2016), a nosocomial pathogen of high priority for international health organizations (Tacconelli et al., 2018; Rello et al., 2019). The resistance-nodulation-division (RND) system is the most relevant and extensively studied efflux pump family in this species (Lin et al., 2015). RND complexes demonstrate multi-specificity, and consequently single genetic events that produce their upregulation can increase resistance to several unrelated antibiotics (Nikaido and Pagès, 2012). Nearly, all *A. baumannii* isolates harbor three RND types encoded by the *adeABC* (Magnet et al., 2001), *adeFGH* (Coyne et al., 2010), and *adeIJK* (Damier-Piolle et al., 2008) operons. Their expression is tightly controlled by cognate regulatory repressors, namely AdeRS (Marchand et al., 2004; Chang et al., 2016), AdeL (Coyne et al., 2010), and AdeN (Rosenfeld et al., 2012), respectively, that bind to DNA operator motifs upstream of the operon. Regular and active repression of RND operon transcription prevents diminishment of bacterial fitness since high pump levels may lead to increased metabolic requirements, proton motive force exhaustion, and imbalances in the sessile-to-planktonic equilibrium (Leus et al., 2018). Nevertheless, genetic changes leading to dysregulation of this control can still be advantageous under the antibiotic- and disinfectant-rich environment of healthcare centers (Higgins et al., 2010; Machado et al., 2018). Mutations affecting full translation or DNA binding in repressor proteins of RND pump operons have been associated with MIC increases to several antibiotics (Gerson et al., 2018). Moreover, alterations have also been associated with resistance in upstream untranslated regions of *adeIJK* (Zang et al., 2021).

The substantial body of knowledge gained for *A. baumannii* RND regulation has not been transferred to automated resistome tools. The exclusion of untranslated upstream factors producing constitutive RND expression can lead to inappropriate therapy, in particular for some last-resort therapies, such as tigecycline. In this study, we provide several proofs of concept required for overcoming limiting steps prior to integrating resistome tools based on upstream and coding sequences.

MATERIALS AND METHODS

Sequence Identification and Management

The first gene of the three RND pump operons was screened by nBLAST, with ≥80% identity and ≥95% alignment length thresholds, in non-anomalous *A. baumannii* genomes stored in the Assembly database (Kitts et al., 2016). E5A70_10260 (*adeA*), A1S_2304 (*adeF*), and A1S_2735 (*adeI*) ORFs from *A. baumannii* ATCC17978 were used as reference query sequences for the nBLAST search. Then, 500 nt upstream sequences were extracted for each gene and isolate, if not discontinued by contig-limits, and subjected to clustering by CD-HIT (Fu et al., 2012) on the stringent 100% identity and 100% alignment length basis to detect allelicity. All alleles were aligned to their respective wild type (WT) sequences with Muscle v3.8.31 (Edgar, 2004). Insertion sequences (ISs) were detected with ISFinder (Siguier et al., 2012). For alleles alignable with the whole WT sequence but showing >20 SNPs to the WT sequence, the species carrying the most significant hit was searched by nBLAST against the whole *Acinetobacter* genus in the NCBI nucleotide collection (nr/nt) database. If not explicitly reported in the

literature, the most probable −35 and −10 promoter box sequences were predicted by Pattern locator (Mrazek and Xie, 2006) applying the {TTGACA}[2](N)[15–20]{TATAAT}[2] motif. Shine-Dalgarno sequences were those located between −15 and −3 positions with respect to the start codon that showed the lowest free energy of the pairing with respect to the consensus anti-ribosome binding site sequence (CCTCCT) using the RNAcofold algorithm, available in the Vienna RNA 2.0 suite (Lorenz et al., 2011). If more than one candidate Shine-Dalgarno sequence was identified, the one closest to the optimal 7 nt spacer to the start codon was selected. DNA bending was calculated using Bend-it (Vlahovicek et al., 2003), applying a curvature window size of 31 nt. The minimum free energy (MFE) of RNA secondary structures of both whole alleles and WT sequences containing SNPs in isolation was calculated by the RNA-fold program of the Vienna RNA 2.0 suite (Lorenz et al., 2011). For MFE calculation, only the sequence section from the experimental (*adeABC*, −403) (Kröger et al., 2018) or theoretical (*adeFGH*, −188; *adeIJK*, −31) start transcription site to the −1 position, i.e., the transcribed zone, was considered.

Sequence types (STs) were assigned using the Oxford scheme (Bartual et al., 2005) by identification of perfect matches (100% identity over 100% aligned length) by nBLAST using allelic information from the official MultiLocus Sequence Typing (MLST) site.[1] Spatial and time isolate metadata were collected from the Biosample database (Barrett et al., 2012). Average nucleotide identity (ANI) at genome level was calculated with OrthoANI (Yoon et al., 2017).

Construction of Chimeras and Experimental Activity Assessment

Selected upstream sequences were synthetized *ab initio* by Thermo Fisher Scientific Inc. (Massachusetts, United States) flanked by *BamHI* and *NotI* target sequences. Synthesized DNA fragments and the pLPV1Z plasmid (Lucidi et al., 2019) were cleaved with appropriate restriction enzymes and, after ligation, electroporated into *Escherichia coli* DH5α. Constructions were verified by Sanger sequencing and then introduced into *A. baumannii* ATCC 17978 by electroporation as previously reported (Lucidi et al., 2019). To test the promoter activity of individual alleles, *A. baumannii* cells were grown overnight at 37°C in LB medium with gentamycin, then cultures were diluted 1:100, and incubated under the same conditions but without gentamycin for 6 h. The OD_{620} and luminescence were measured at this point. Relative luminescence units (RLUs) for each sample were normalized to OD_{620}, the background (culture with no plasmid) subtracted, and then divided by the same value obtained for the intra-experiment WT control.

Conventional Resistome Prediction

The conventional resistome, involving coding sequences, was determined by CARD2020 (Alcock et al., 2020). Only "perfect" and "strict" hits were considered. Sequence quality "high quality/coverage" was applied. Nudge loose hits to strict were excluded.

[1]https://pubmlst.org

RESULTS

Analysis of the Allelic Variability of RND Upstream Sequences

The sequence variability of upstream regions of operons coding the three principal RND pumps of *A. baumannii* (AdeABC, AdeFGH, and AdeIJK) was screened. For that, full sections of 500 bp upstream of these operons were identified for 89%–99% of *A. baumannii* genomes in a sample of 4,130 isolates. These isolates represented 352 STs previously reported by PubMLST (Jolley et al., 2018). Identical upstream sequences were unified into "upstream alleles." For the three operons considered, there was a dominant upstream allele (covering 52%–64% of the total of isolates) that involved a large number of STs and was therefore considered the WT sequence. There was large disparity for a number of upstream alleles and their average genetic distance to the WT between the three operons (*adeABC* > *adeFGH* > *adeIJK*; **Table 1**). This suggests the existence of different intensities for selective pressure acting on the regulation of *A. baumannii* RND pumps.

Within alleles, a total of 487 non-redundant genetic alterations (termed here determinants, markers, or tags) were identified with respect to the reference WT sequence in the three datasets (**Supplementary Table S1**). Up to 54% of the isolates evaluated carried at least one determinant for one of the three RND pumps. Determinants showed a wide value range for parameters, such as isolate occurrence, predictable degree of severity, distance to start codon, and type of genetic event (**Figures 1A,B**).

Of note, 19 alleles involving 30 isolates and six official STs showed >20 SNPs. These alleles were more similar to sequences from *Acinetobacter nosocomialis* or *Acinetobacter pittii* (**Supplementary Table S2**), two species considered less pathogenic than *A. baumannii*. Most of these alleles corresponded to original species misassignation. Only one allele involving four

TABLE 1 | Resistance-nodulation-division (RND) gene coverage in sequenced genomes and allelicity data.

Property	*adeABC*	*adeFGH*	*adeIJK*
% isolates in which the first operon gene were detected	92.1	99.2	99.3
% isolates in which 500 nt upstream the first operon gene were available	89.3	98.6	98.2
Number of upstream alleles	213	110	80
Average (±SD) allelic SNPs	9.3 ± 8.2	7.1 ± 9.7	4.6 ± 7.4
% isolates showing the WT allele	62.4	52.3	62.6
Number of identified tags	203	172	87
Number of alleles (isolates) with ISs	17 (40)	1 (1)	7 (7)
% alleles with a bending peak ≥2°/turn with respect to WT[a]	61	18	88
MFE mRNA secondary structure of WT (Kcal/mol)	−61.0	−41.2	−3.6
% alleles with mRNA mfe ≥ 5% with respect to WT[b]	71.6	13.9	6.9

[a]*Only alleles showing no indels respect to the WT sequence. Maximal bending differences between equivalent positions respect to WT were considered.*
[b]*Only alleles showing no indels respect to the WT sequence in the transcribed section were considered.*

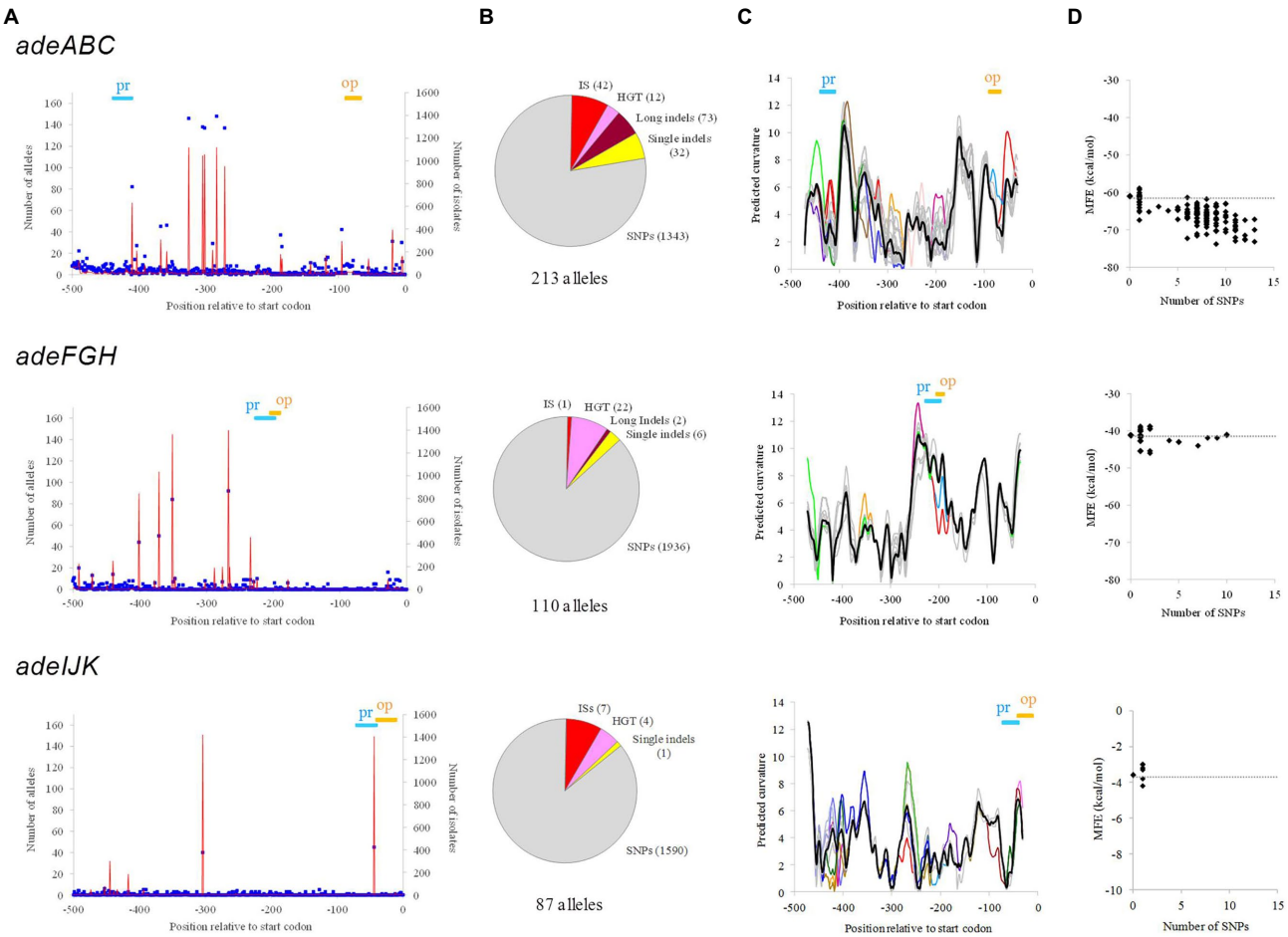

FIGURE 1 | Genetic and structural properties of upstream alleles of *Acinetobacter baumannii* RND-encoding operons. **(A)** Location of RND upstream positions showing SNPs. Polymorphisms due to ISs were not included. Allelic occurrence (blue points) and the number of isolates involved (red line) are shown. The positioning of promoter (Pr) and operator (Op) motifs is indicated. **(B)** Number of alleles and raw genetic events observed for each operon. If more than one type of genetic event pertained the same position, only the most relevant was considered applying the following prevalence: ISs > horizontal gene transfer (HGT) > long indels > single indels > SNPs. **(C)** DNA bending calculations for all allelic sequences showing no indels respect to the WT. Curvature is expressed in degrees per helical turn. Thick black line: allelic average (nearly identical to the WT values); superimposed alleles are in grey except for those showing maximal divergences of ≥2 degrees/turn with respect to the allelic average or ≥1 degree/turn in key motifs, which were color-highlighted. The positioning of promoter (Pr) and operator (Op) motifs is also indicated. **(D)** Minimum free energy (MFE) of the mRNA structure for all allelic sequences showing no indels respect to the WT. Black dots indicate MFE values and the number of SNPs respect to the WT for each allele. The MFE value for the WT is indicated (grey line).

isolates appeared to be from an *A. baumannii* isolate according to whole genome ANI analysis. These four isolates were collected in Thailand in 2018 and were nearly identical (all-against-all ANI ≥ 99.8%), which indicates outbreak or intra-patient microevolution sampling. These isolates were closer to the *A. baumannii* reference sequence (ab736 strain, ANI = 97.6%, where ANI > 95% is accepted as same species) than to *A. nosocomialis* and *A. pittii* isolates (ANI < 92%). In these isolates, two similarity swaps between *A. nosocomialis* and *A. baumannii* sequences, i.e., 5′ and 3′ potential recombination points were detected. These located at 502-GGCGTTTTT AAAC-514 of the *adeS* ORF and the 941-GAGCC-945 nucleotides of the *adeA* ORF (**Supplementary Figure S1A**). Thus, the genetic exchange affected both translated and untranslated elements. On the one hand, the resulting hybrid AdeS, AdeR, and AdeA polypeptides shared 98%–99% similarity with the *A. baumannii* reference homolog. Whether these scarce residue changes suffice to affect protein activity of the mosaic protein should be assessed. On the other hand, in contrast, the impact on expression in the recombinants appears more explicit since *A. nosocomialis* genuine mutations affected key motifs and nucleic acid structure of the *adeABC* upstream sequence (**Supplementary Figures S1B**,**C**). This suggests different AdeABC regulation in the inter-species recombinant *A. baumannii* isolates, which may have clinical consequences.

To assess the potential effect of the identified tags on pump overexpression, their context with respect to 16 key motifs explicitly associated with pump expression was evaluated. These motifs included promoter boxes, repressor operators, and Shine-Dalgarno sequences (**Table 2**). Interestingly, at least for those markers affecting key motifs, genetic tags involved a fraction of isolates from different STs and unrelated geotemporal

TABLE 2 | Upstream motifs associated to RND pump expression.

Operon	Motif	Start	End	Length	WT sequence	Identification method[a]	Reference
adeABC	Promoter-35 box	−438	−433	6	TTATCA	Primer extension	Marchand et al., 2004
	Promoter-10 box	−415	−411	5	CGTCA	Primer extension	Marchand et al., 2004
	Start transcription site	−403	−403	1	C	Primer extension	Marchand et al., 2004
	AdeR binding operator repeat 1	−88	−79	10	CTCCACACTT	EMSA	Chang et al., 2016
	AdeR binding operator repeat 2	−77	−68	10	CTCCACACTT	EMSA	Chang et al., 2016
	Shine-Dalgarno region	−8	−3	5	TGGACA	RNAcofold	This work
adeFGH	Promoter-35 box	−226	−221	6	TTGTTA	Bprom	Coyne et al., 2010
	Promoter-10 box	−205	−198	8	TGTTATCA	Bprom	Coyne et al., 2010
	AdeL binding operator	−203	−191	13	TTATCAAATTTAA	Presence of LTTR box	Coyne et al., 2010
	Shine-Dalgarno region	−13	−8	6	CGGTGG	RNAcofold	This work
adeIJK	Promoter-35 box	−70	−65	6	ATTACA	TSSs, PatLoc	This work, Kröger et al., 2018
	Promoter-10 box	−46	−41	6	TAAAAA	TSSs, PatLoc	This work, Kröger et al., 2018
	AdeN binding operator	−39	−12	28	CAAATATATTTTTAGATTTTATCTAAAC	Manual inspection	Rosenfeld et al., 2012
	Shine-Dalgarno region	−13	−8	6	ACGAGG	RNAcofold	This work

[a]*EMSA, electrophoretic mobility shift assay.*

sampling data. The global absence of a clear clonal origin for these determinants suggests convergent evolution and/or horizontal transfer rather than pure vertical inheritance. However, it is unknown whether maintenance of tags that involve constitutive RND expression is favored by some specific genetic backgrounds.

Some upstream alleles showed abrupt mismatching to the WT, which were due to the presence of ISs. These events differed with respect to (i) the distance between the IS insertion site and the start codon, where ISs can cause complete removal of central elements such as promoters and/or operators; and (ii) the IS family involved, either IS*Aba*1 or IS*Aba*4. Both IS family sequences carry strong promoters: TTAGAA-N_{16}-TTATTT and TAACTA-N_{17}-TTTCTT, respectively.

DNA bending and mRNA secondary structure of alleles were also analyzed. DNA bending can alter expression (Agustiandari et al., 2011) by modifying DNA accessibility and/or recognition by the RNA polymerase and repressors. A substantial fraction of upstream alleles that could be aligned to the WT allele over the full length (<20 SNPs, no indels) showed maximal bending differences over 2° per turn (**Table 1**; **Figure 1C**). In some cases, these high curvature difference peaks affected the promoter and operator zones. The stability of the mRNA secondary structure can also modulate expression (Del Campo et al., 2015) by changing transcription rate, translation efficiency, and hydrolysis by RNases. WT alleles from the three genes showed distant predicted values for maximum free energy at the mRNA level that in some alleles was altered by more than 10% (**Table 1**; **Figure 1D**).

Experimental Verification of DNA Marker-to-Phenotype Relationships

Based on findings from previous studies, the effect of some of the markers above on pump expression, and likely on resistance, can be theoretically presumed. However, certainty on upregulation caused by these markers can only be obtained by experimental corroboration under an isogenic background. Given the high technical difficulty in introducing chromosomal modifications in *A. baumannii*, a plasmid mid-throughput screening was developed with the aim of validating markers that result in gene upregulation. An illustrative schema for such screening that contains the procedural steps, expertise required, and expected timescale is provided in **Figure 2A**. Our method involved the fusion between synthesized DNA carrying the marker to a luciferase report system.

This plasmid reporter system has been previously validated for characterizing gene expression dynamics under multiple experimental conditions (Lucidi et al., 2019) and used to assess expression changes in RND pumps from *A. baumannii* reference strains (Prieto Martin Gil et al., 2021). In our hands, the series of steps from DNA design to measurement of expression activity can be accomplished with an average cost of 150€ per marker in a turnaround time of 28–36 working days.

Since the experimental evaluation of the whole determinant catalog is not feasible, the protocol was evaluated using three selected markers per operon. The selected genetic tags were prioritized in order to optimize coverage of different ranges of the nature of the genetic changes, type of DNA motif affected, DNA curvature and mRNA structural alterations, isolate occurrence, and clonal distribution (**Figure 2B**).

Significant differences of up to 25-fold between the expression of five genetic tags, out of nine, and both promoterless plasmid cells and their respective WT controls were observed (**Figure 2C**). The most active markers for *adeABC* and *adeIJK* corresponded to IS insertions. Notably, the results obtained with ISs allowed us to verify our plasmid-luciferase experimental model, after observations of similar genomic arrangements involving upregulation of other resistance determinants such as carbapenemases (Corvec et al., 2003, 2007; Turton et al., 2006; Adams et al., 2010). Besides, selected mutations in the repressor-binding operator and the Shine-Dalgarno sequence of *adeFGH* produced notable increments in the expression of the reporter gene downstream. Altogether, 42 isolates in the dataset harbor at least one of these experimentally validated upregulating determinants (**Supplementary Table S3**).

A

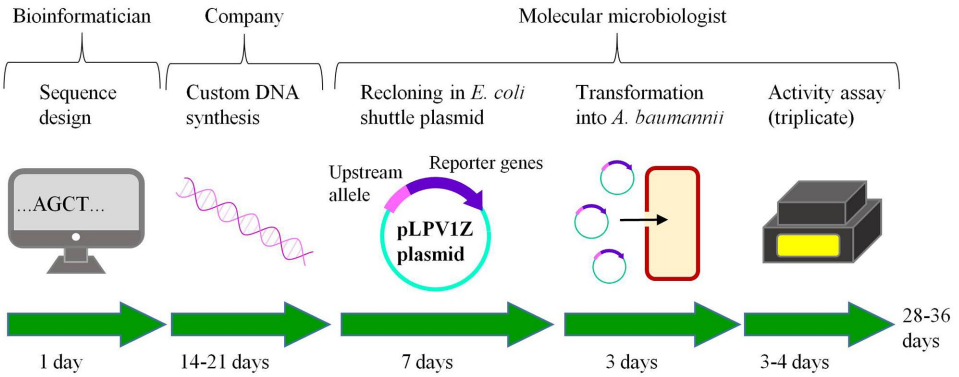

B

Operon	Tag	Genetic event	Elements affected	Number of isolates	ST spread	DNA bending	RNA MFE	S-D pairing
adeABC	adeA_is-28	IS (-45/-28)	pr / op	19	6	NC	NC	0.0
	adeA_op_del-8	Deletion (1-8)	op	18	9	NC	NC	0.0
	adeA_op_C4T	SNP (C4T)	op	2	1	0.246	0.0	0.0
adeFGH	adeF_op_A6G	SNP (A6G)	op	11	6	0.839	0.0	0.0
	adeF_op_A8T	SNP (A8T)	op	9	3	0.073	0.0	0.0
	adeF_sd-C1A/T4A	SNPs (C1A, T4A)	sd	3	3	0.499	+1.0	-4.23
adeIJK	adeI_is-43	IS (-43)	pr	2	2	NC	NC	0.0
	adeI_pr10_A3G	SNP (A3G)	pr	1396	292	2.138	0.0	0.0
	adeI_op_C28G	SNP (C28G)	op	16	6	0.711	-1.2	0.0

C

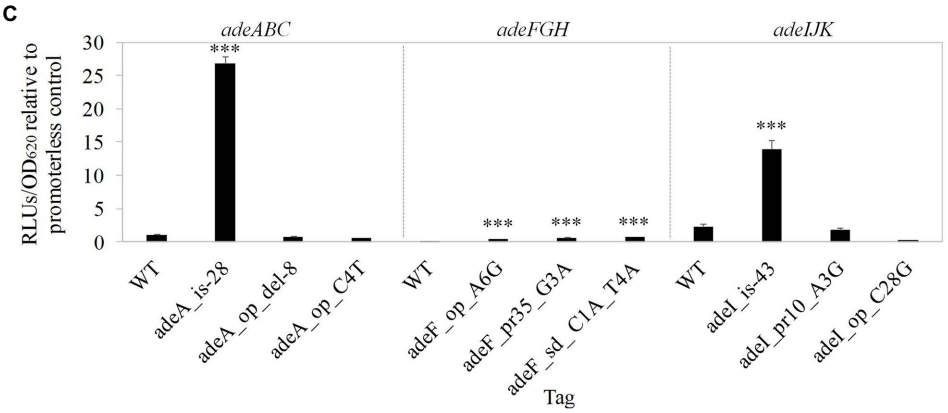

FIGURE 2 | Experimental validation of selected tags. **(A)** Timeline schema of the experimental validation pipeline. Stages, human staff involved, and their estimated time duration are shown. **(B)** Tags selected for experimental evaluation. Tag nomenclature include the first gene of the pump operon followed by either the label "-is" plus the insertion distance to start codon (for ISs), or the element affected (op: operator; pr: promoter; and sd: Shine-Dalgarno sequence) plus the "del" label plus the length of the removed section (for deletions) or the nucleotide change (for point mutations). For clarity, values for parameter criteria utilized for tag prioritization are highlighted in red when deemed relevant: deletions or IS (genetic event); opt, pr, and sd (elements affected); ≥5 isolates carrying the tag (number of isolates); ≥5 different STs with isolates carrying the tag (ST spread); ≥0.5 degrees per turn difference respect to the WT (DNA bending); ≥1 Kcal/mol differences in RNA MFE (RNA MFE); and ≥1 Kcal/mol differences in Shine-Dalgarno (S-D) and anti-S-D ribosomal sequence pairing (S-D pairing). IS alleles were clustered if the insertion point was so proximal that the same motifs were affected. The number of isolates that harbor the tag is shown together with the number of alleles involved under brackets. Isolates not included in formal STs were considered together as a single unit for the ST count estimation. DNA bending, RNA MFE, and S-D pairing columns indicate maximal differences of the tag-carrying sequence respect to the WT in degrees per turn for the former, and Kcal/mol for the rest parameters. NC, non-comparable. **(C)** Expression activity of prioritized alleles measured by luminometry. Fold-changes of normalized RLUs associated to the alleles respect to the promoterless cells are shown. Cells containing plasmids with WT upstream sequences for *adeABC*, *adeFGH*, and *adeIJK* pumps showed 103 ± 9%, 5 ± 2%, and 220 ± 46% expression values, with respect to the original promoterless plasmid, respectively. Data are the averages ± SDs of four independent experiments. Statistical significance was calculated using the two-tailed Student's *t*-test. Significant differences are indicated: ***$p < 0.001$.

Analysis of RND Regulatory Resistance in Testing Isolates: Algorithm Flowchart and Ontology

The results described above would find their utility in clinical practice as an automated resistome tool that identifies genetic tags resulting in increased expression of RND pumps in *A. baumannii*. For that, a procedural flowchart that processes all the upstream sequence information in a sequential order compatible with data structure is proposed (**Figure 3A**). Briefly, if known markers are detected in the upstream RND sequences of a query genome using this protocol, potential upregulation and subsequently reduced response to antimicrobial therapy may be assigned to the isolate. In these cases, upregulation would be suggested at three certainty levels ("Verified," "Presumed," and "Probably irrelevant"), according to the genetic tag identified.

The corresponding response to precise antimicrobial therapy of a clinical isolate based on the detected determinants would be carried out using a controlled vocabulary. For that, the efflux-pump upregulation ontology was completed with a list of antibacterial agents expelled by each upregulated RND pump considered here. This information was exhaustively collected from clinical *A. baumannii* isolates and laboratory studies reported in the literature (**Supplementary Table S4**). The search accounted for 115 pump-to-phenotype causal associations revealed in 16 articles involving 40 antibacterial agents from 12 classes (**Figure 3B**). These associations between RND pump and expelled antibacterial agents involved at least 4-fold increases in MIC with respect to their susceptible counterpart. RND efflux pumps are linked to several unrelated antibiotics due to their multi-specificity.

A question in point is what degree of novelty can our approach provide with respect to standard, coding sequence-oriented, resistome tools. For that, results concerning the 42 isolates showing verified RND upregulating markers described above were compared to outcomes of CARD2020,

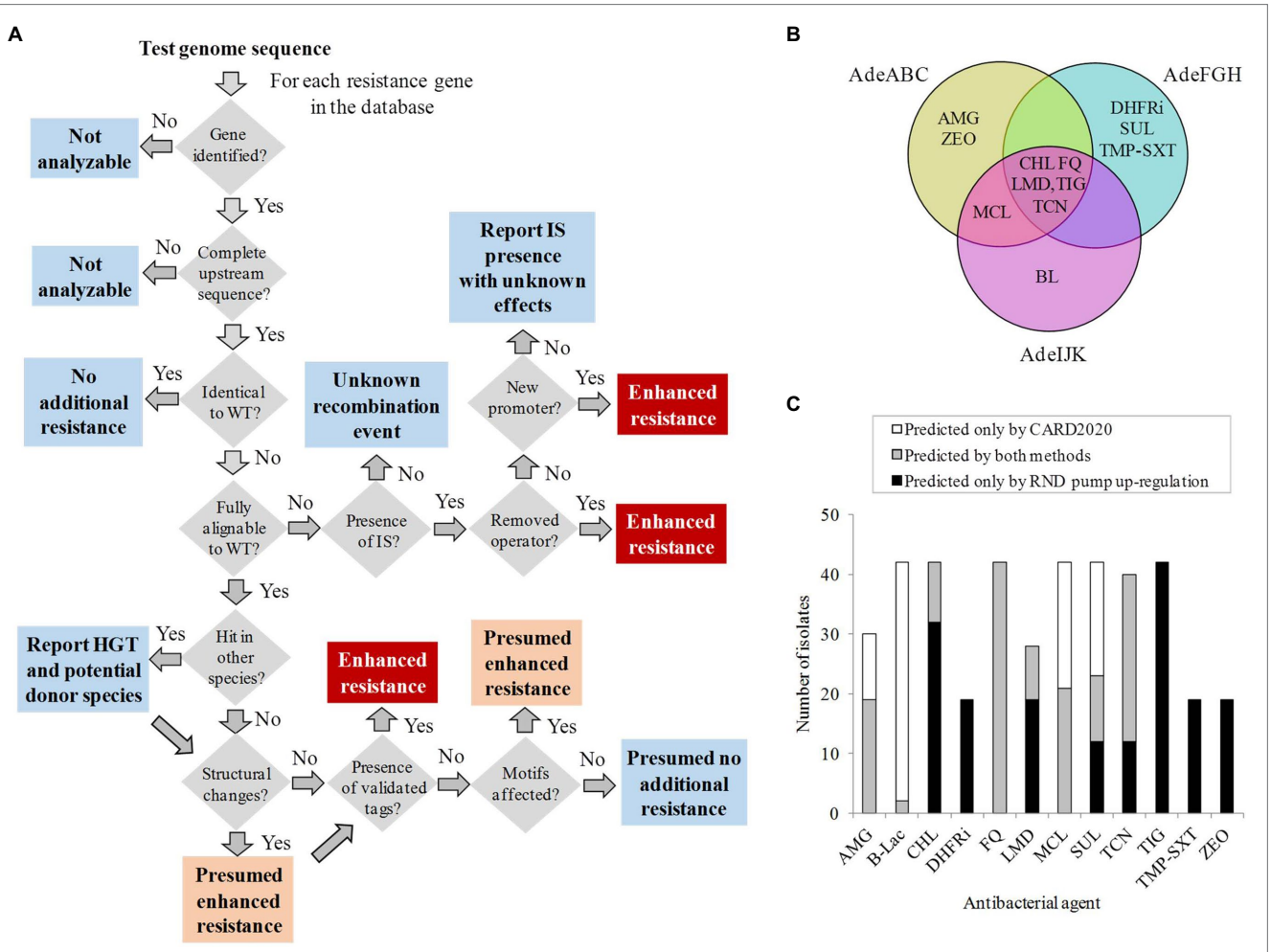

FIGURE 3 | Prediction of the non-coding regulatory resistome. **(A)** Information management flowchart built with decision (grey), warning (light blue), presumed resistance (orange), and verified resistance (red) boxes. **(B)** Venn diagram with the antibacterial class descriptors associated with resistance for each RND pump. AMG, aminoglycosides; BL, beta-lactams; CHL, chloramphenicol; DHFRi, dihydrofolate reductase inhibitors; FQ, fluoroquinolones; LMD, lincosamides; MCL, macrolides; SUL, sulfonamides; TCN, tetracyclines; TIG, tigecycline; TMP-SXT, trimethoprim sulfamethoxazole; and ZEO, zeocin. **(C)** Exclusivity and concordance between CARD2020 and regulatory resistome predictions for 12 antibacterial agents in the 42 isolates at the "Verified" level of our system.

a very complete and frequently updated resistome protocol for these isolates (Alcock et al., 2020). Resistance to tigecycline to all 42 isolates was not detected by CARD2020 but associated through RND upstream determinants (**Figure 3C**). Likewise, new potential resistance to dihydrofolate reductase inhibitors and trimethoprim sulfamethoxazole was assigned to 23 isolates and to zeocin to 19 isolates with verified RND pump upregulation markers. In contrast, several degrees of exclusivity and isolate coverage by validated RND upregulating determinants respect to CARD2020 predictions were obtained for the remaining antibiotic classes, including aminoglycosides and macrolides. Notably, all 42 isolates considered showed co-existing fluoroquinolone efflux prediction and resistance by other mechanisms, suggesting step-wise increases in resistance through several mechanisms for this antibacterial agent class.

Finally, our protocol was applied to 100 phylogenetically unrelated isolates with well-annotated antibiotic resistance and resistome profiles (Galac et al., 2020). Although tigecycline resistance data was not included in this work, we identified that six isolates in the dataset were simultaneously non-susceptible to ciprofloxacin and tetracycline, without a conventional resistome support provided by the curators that justifies these phenotypes. Since ciprofloxacin and tetracycline are substrates of the three principal RND pumps (Yoon et al., 2015), upstream RND sequences of these inconsistent isolates were analyzed in detail. In five of these six cases, isolates carried unusual minor upstream alleles for at least one of the pumps with nucleotide substitutions overlapping or adjacent (<10 positions) to operator and/or promoter elements. All these mutations involved AT::GC changes that modified the DNA bending by 1.5–2.5 degrees per turn on these expression meaning motifs (**Supplementary Table S5**). These mutations were not experimentally validated but, due to their properties, would be classified in a "Presumed" status according to our scoring system. Notably, four of these mutants harbor the A(-44)G mutation in the −10 promoter box of the *adeIJK* operon. These findings suggest these five isolates are candidate to undergo altered RND efflux, which warrants further experimental investigation.

DISCUSSION

There is a dramatic lack of bioinformatic strategies that properly approach the regulatory resistome with regard to efflux pumps in multidrug resistant bacteria. This may be explained by the cumbersome regulatory circuitry, involving many heterogeneous aspects that converge into augmented expression of these pumps. Therefore, the identification of clinical isolates carrying efflux-related antibiotic resistance by conventional resistome predictors is prone to either over- or under-detection.

In this study, we provide a catalog of pre-analyzed determinants in upstream regions of the principal RND pumps found in a large genome dataset of *A. baumannii*; in addition to an experimental protocol to screen the influence of the most relevant ones in expression in a timely and cost effective manner; and, finally, a data flowchart that includes a controlled vocabulary between pumps and expelled antibiotics. These three layers may constitute a framework for mature genome-based routine tools. Such tools would predict, with different degrees of certainty, which antibiotic ligands may not achieve clinically-relevant intracytoplasmic levels in a query isolate.

A number of upstream alleles containing a large variety of genetic determinants were found. Different types of genetic events (ISs, indels, and SNPs) were identified, which in some cases may affect expression by directly overlapping key motifs (promoters, operators, and Shine-Dalgarno sequences) and/or nucleic acid structural alterations (DNA curvature and mRNA structure). These markers can be prioritized for experimental validation according to several factors such as the motif/s affected and the prevalence of the marker in the genome dataset. In this regard, the elements with the highest upregulatory confirmed influence for *adeABC* and *adeIJK* operons were ISs. ISs in non-coding upstream sequences have been associated with resistance by overexpression of beta-lactamases/carbapenemases in *A. baumannii* (Corvec et al., 2003; Turton et al., 2006; Adams et al., 2010) and efflux pumps in *Salmonella enterica* (Olliver et al., 2005). ISs are thus versatile genetic elements for *A. baumannii* to modify the efflux response to antibiotics in two different possible ways. Namely, first, by negating repressor loci through intra-gene insertion (Gerson et al., 2018) and, second, by providing potent new promoters to pump genes downstream. However, it should be confirmed whether the same will apply to multidrug bacterial species other than *A. baumannii* or, instead, SNPs in promoter boxes and/or operators are more frequent. This was also the case for *A. baumannii adeFGH*. Upregulation of this operon was proved for mutations in the operator motif and in the Shine-Dalgarno sequence that predictably increase the binding stability to the ribosome. The later result indicates that our protocol may not only be valid for screening enhanced expression markers acting on transcription but also at a translational level. Of note, horizontal transfer of upstream zones from less-pathogenic *Acinetobacter* species showing evidence of different regulation was detected. However, interspecies mosaics produced by recombination potentially affecting pump regulation were extremely rare.

Although some upstream alleles contained several identified determinants, a single-tag classification schema eases analysis, in particular when pertaining to key motifs. However, the combination of several determinants may cooperate to determine the expression phenotype. Thus, a legitimate question is: what should be the subject of study, the single genetic tag or the whole allele, in the upstream sequence resistome? The later could be justified to globally calculate structural properties of nucleic acids that affect expression.

Conventional resistome methods are oriented to the analysis of coding sequences, either gene presence or gene mutations, and in some cases they do not cover pumps. Moreover, genes coding for these RND efflux pumps are present in most *A. baumannii* isolates, irrespective of the efflux-related resistance of the isolate. Therefore, mere gene detection does

not suffice for inferring enhanced expression and corresponding resistance, resulting in false positives in isolates that can still be treatable (Grkovic et al., 2001). In our protocol, markers would be labeled as "Verified" if experimentally confirmed as upregulating; "Presumed" if they were not experimentally verified affect key expression motifs; and "Probably irrelevant" for the rest. This escalated certainty assignment of resistance is reminiscent of the BLAST-based "Perfect," "Strict," and "Loose" degrees used by formal resistome protocols (Alcock et al., 2020). Likewise, our method resembles the "variant model" (i.e., mutations) rather than the "gene model" (i.e., gene presence) of resistome predictors since it approaches genetic changes that switch the expression modality of core genome genes.

Importantly, and in contrast to other kinds of resistance modes, the upregulating-linked markers concerning RND overexpression may be associated with extended resistance due to the broad range of expelled substrates by RND pumps. However, predictions based on increased RND expression must be interpreted with caution since it may be either (a) as relevant as mutations in primary targets (Lari et al., 2018); (b) be synergic with other mechanisms to quantitatively increase resistance (e.g., from low- to mid- or high-resistance levels; Suh et al., 2010; Schmalstieg et al., 2012); or (c) not or barely contributing to resistance. In particular, our protocol would play a relevant role in the prediction of resistance to tigecycline and of high-level synergistic resistance for fluoroquinolones.

Regarding potential limitations, the relevance of the markers found is interpreted according to current knowledge of expression for the RND pumps analyzed, which may be incomplete. A further technical drawback is that the actual resistance phenotype was not confirmed by introducing the markers directly into the chromosome. Unfortunately, this limitation reflects the scarcity of scalable molecular tools for *A. baumannii*, in particular, for scalable mutation screening in practice. Instead, we have used a state-of-the-art reporter plasmid to detect upregulation since a robust direct correlation between the level of upregulation of the RND genes and the MIC for the antibiotics the pumps expel has been reported (Ruzin et al., 2010). However, our protocol would greatly benefit from ideal high-throughput genome mutagenesis and direct MIC measurement of the resulting strains. Nevertheless, the global schema presented here is dynamic in nature. Thus, future versions of the schema will incorporate additional RND promoters/operators reported in the literature and novel molecular manipulating tools when available for this difficult-to-handle microorganism. Despite the drawbacks, our protocol could be instrumental to check batches of tens of markers associated with irregular enhanced RND expression. This may be a filter step prior to undertake laborious experiments that confirm or rule out antibacterial resistance of the pertaining isolates. We recommend that the plasmid-based screening should be restricted to those markers showing theoretical evidence using the comprehensive catalog of computationally pre-analyzed determinants built here.

In summary, our protocol provides a conceptual predictive upgrade of the resistome tailored to the nature of efflux pump upregulation. The initial *A. baumannii* RND model proposed lays the foundation for knowledge-based identification of efflux pump upregulation. We envisage that it can be broadened to cover more genetic alterations, other prioritized multi-resistant microorganisms and key residue changes in regulators to build a public resource that universally addresses the non-coding regulatory resistome. When applied in combination with regular resistome predictors, this information may help to support genome-guided treatment to prevent ineffective therapy involving fatal consequences. This information may even guide the design of complex synergic therapies that combine canonical antibiotics and anti-efflux drugs (Verma and Tiwari, 2018). In particular, it may be particularly useful for outbreak emerging lineages for which formal resistomes do not match the antibiogram or the therapeutic response.

DATA AVAILABILITY STATEMENT

The original contributions presented in the study are included in the article/**Supplementary Material**, further inquiries can be directed to the corresponding author.

AUTHOR CONTRIBUTIONS

AM-G conceived the study and performed the computational analyses. AM-G and MM supervised the study, drafted the manuscript, and granted funding. ML-S performed the plasmid constructions and the quantitative analysis of expression. AM-G, MM, and ML-S revised the final version of the manuscript. All authors contributed to the article and approved the submitted version.

FUNDING

This research was supported by grants MPY 380/18 and MPY 509/19 from the Instituto de Salud Carlos III (ISCIII). ML-S is the recipient of a Sara Borrell contract by the ISCIII. AM-G is the recipient of a Miguel Servet contract by the ISCIII.

ACKNOWLEDGMENTS

We thank Paolo Visca (University Roma Tre) for donating pLPV1Z plasmid.

SUPPLEMENTARY MATERIAL

The Supplementary Material for this article can be found online at: https://www.frontiersin.org/articles/10.3389/fmicb.2022.869208/full#supplementary-material

REFERENCES

Adams, M. D., Chan, E. R., Molyneaux, N. D., and Bonomo, R. A. (2010). Genomewide analysis of divergence of antibiotic resistance determinants in closely related isolates of *Acinetobacter baumannii*. *Antimicrob. Agents Chemother.* 54, 3569–3577. doi: 10.1128/AAC.00057-10

Agustiandari, H., Peeters, E., de Wit, J. G., Charlier, D., and Driessen, A. J. M. (2011). LmrR-mediated gene regulation of multidrug resistance in *Lactococcus lactis*. *Microbiol. Read. Engl.* 157, 1519–1530. doi: 10.1099/mic.0.048025-0

Alcock, B. P., Raphenya, A. R., Lau, T. T. Y., Tsang, K. K., Bouchard, M., Edalatmand, A., et al. (2020). CARD 2020: antibiotic resistome surveillance with the comprehensive antibiotic resistance database. *Nucleic Acids Res.* 48, D517–D525. doi: 10.1093/nar/gkz935

Barrett, T., Clark, K., Gevorgyan, R., Gorelenkov, V., Gribov, E., Karsch-Mizrachi, I., et al. (2012). BioProject and BioSample databases at NCBI: facilitating capture and organization of metadata. *Nucleic Acids Res.* 40, D57–D63. doi: 10.1093/nar/gkr1163

Bartual, S. G., Seifert, H., Hippler, C., Luzon, M. A. D., Wisplinghoff, H., and Rodriguez-Valera, F. (2005). Development of a multilocus sequence typing scheme for characterization of clinical isolates of *Acinetobacter baumannii*. *J. Clin. Microbiol.* 43, 4382–4390. doi: 10.1128/JCM.43.9.4382-4390.2005

Baylay, A. J., and Piddock, L. J. V. (2015). Clinically relevant fluoroquinolone resistance due to constitutive overexpression of the PatAB ABC transporter in *Streptococcus pneumoniae* is conferred by disruption of a transcriptional attenuator. *J. Antimicrob. Chemother.* 70, 670–679. doi: 10.1093/jac/dku449

Boolchandani, M., D'Souza, A. W., and Dantas, G. (2019). Sequencing-based methods and resources to study antimicrobial resistance. *Nat. Rev. Genet.* 20, 356–370. doi: 10.1038/s41576-019-0108-4

Bortolaia, V., Kaas, R. S., Ruppe, E., Roberts, M. C., Schwarz, S., Cattoir, V., et al. (2020). ResFinder 4.0 for predictions of phenotypes from genotypes. *J. Antimicrob. Chemother.* 75, 3491–3500. doi: 10.1093/jac/dkaa345

Cag, Y., Caskurlu, H., Fan, Y., Cao, B., and Vahaboglu, H. (2016). Resistance mechanisms. *Ann. Transl. Med.* 4:326. doi: 10.21037/atm.2016.09.14

Chang, T.-Y., Huang, B.-J., Sun, J.-R., Perng, C.-L., Chan, M.-C., Yu, C.-P., et al. (2016). AdeR protein regulates *adeABC* expression by binding to a direct-repeat motif in the intercistronic spacer. *Microbiol. Res.* 183, 60–67. doi: 10.1016/j.micres.2015.11.010

Corvec, S., Caroff, N., Espaze, E., Giraudeau, C., Drugeon, H., and Reynaud, A. (2003). AmpC cephalosporinase hyperproduction in *Acinetobacter baumannii* clinical strains. *J. Antimicrob. Chemother.* 52, 629–635. doi: 10.1093/jac/dkg407

Corvec, S., Poirel, L., Naas, T., Drugeon, H., and Nordmann, P. (2007). Genetics and expression of the carbapenem-hydrolyzing oxacillinase gene blaOXA-23 in *Acinetobacter baumannii*. *Antimicrob. Agents Chemother.* 51, 1530–1533. doi: 10.1128/AAC.01132-06

Coyne, S., Guigon, G., Courvalin, P., and Perichon, B. (2010). Screening and quantification of the expression of antibiotic resistance genes in *Acinetobacter baumannii* with a microarray. *Antimicrob. Agents Chemother.* 54, 333–340. doi: 10.1128/AAC.01037-09

Damier-Piolle, L., Magnet, S., Bremont, S., Lambert, T., and Courvalin, P. (2008). AdeIJK, a resistance-nodulation-cell division pump effluxing multiple antibiotics in *Acinetobacter baumannii*. *Antimicrob. Agents Chemother.* 52, 557–562. doi: 10.1128/AAC.00732-07

de Man, T. J. B., and Limbago, B. M. (2016). SSTAR, a stand-alone easy-to-use antimicrobial resistance gene predictor. *mSphere* 1, e00050–e00015. doi: 10.1128/mSphere.00050-15

Del Campo, C., Bartholomaus, A., Fedyunin, I., and Ignatova, Z. (2015). Secondary structure across the bacterial transcriptome reveals versatile roles in mRNA regulation and function. *PLoS Genet.* 11:e1005613. doi: 10.1371/journal.pgen.1005613

Edgar, R. C. (2004). MUSCLE: multiple sequence alignment with high accuracy and high throughput. *Nucleic Acids Res.* 32, 1792–1797. doi: 10.1093/nar/gkh340

Fu, L., Niu, B., Zhu, Z., Wu, S., and Li, W. (2012). CD-HIT: accelerated for clustering the next-generation sequencing data. *Bioinforma* 28, 3150–3152. doi: 10.1093/bioinformatics/bts565

Galac, M. R., Snesrud, E., Lebreton, F., Stam, J., Julius, M., Ong, A. C., et al. (2020). A diverse panel of clinical *Acinetobacter baumannii* for research and development. *Antimicrob. Agents Chemother.* 64, e00840–e00820. doi: 10.1128/AAC.00840-20

Gerson, S., Nowak, J., Zander, E., Ertel, J., Wen, Y., Krut, O., et al. (2018). Diversity of mutations in regulatory genes of resistance-nodulation-cell division efflux pumps in association with tigecycline resistance in *Acinetobacter baumannii*. *J. Antimicrob. Chemother.* 73, 1501–1508. doi: 10.1093/jac/dky083

Grkovic, S., Brown, M. H., and Skurray, R. A. (2001). Transcriptional regulation of multidrug efflux pumps in bacteria. *Semin. Cell Dev. Biol.* 12, 225–237. doi: 10.1006/scdb.2000.0248

Gupta, S. K., Padmanabhan, B. R., Diene, S. M., Lopez-Rojas, R., Kempf, M., Landraud, L., et al. (2014). ARG-ANNOT, a new bioinformatic tool to discover antibiotic resistance genes in bacterial genomes. *Antimicrob. Agents Chemother.* 58, 212–220. doi: 10.1128/AAC.01310-13

Higgins, P. G., Schneiders, T., Hamprecht, A., and Seifert, H. (2010). In vivo selection of a missense mutation in adeR and conversion of the novel blaOXA-164 gene into blaOXA-58 in carbapenem-resistant *Acinetobacter baumannii* isolates from a hospitalized patient. *Antimicrob. Agents Chemother.* 54, 5021–5027. doi: 10.1128/AAC.00598-10

Jeukens, J., Kukavica-Ibrulj, I., Emond-Rheault, J. G., Freschi, L., and Levesque, R. C. (2017). Comparative genomics of a drug-resistant *Pseudomonas aeruginosa* panel and the challenges of antimicrobial resistance prediction from genomes. *FEMS Microbiol. Lett.* 364:fnx161. doi: 10.1093/femsle/fnx161

Jolley, K. A., Bray, J. E., and Maiden, M. C. J. (2018). Open-access bacterial population genomics: BIGSdb software, the PubMLST.org website and their applications. *Wellcome Open Res.* 3:124. doi: 10.12688/wellcomeopenres.14826.1

Kapp, E., Malan, S. F., Joubert, J., and Sampson, S. L. (2018). Small molecule efflux pump inhibitors in *mycobacterium tuberculosis*: a rational drug design perspective. *Mini-Rev. Med. Chem.* 18, 72–86. doi: 10.2174/1389557517666170510105506

Kitts, P. A., Church, D. M., Thibaud-Nissen, F., Choi, J., Hem, V., Sapojnikov, V., et al. (2016). Assembly: a resource for assembled genomes at NCBI. *Nucleic Acids Res.* 44, D73–D80. doi: 10.1093/nar/gkv1226

Kröger, C., MacKenzie, K. D., Alshabib, E. Y., Kirzinger, M. W. B., Suchan, D. M., Chao, T.-C., et al. (2018). The primary transcriptome, small RNAs and regulation of antimicrobial resistance in *Acinetobacter baumannii* ATCC 17978. *Nucleic Acids Res.* 46, 9684–9698. doi: 10.1093/nar/gky603

Lari, A. R., Ardebili, A., and Hashemi, A. (2018). AdeR-AdeS mutations & overexpression of the AdeABC efflux system in ciprofloxacin-resistant *Acinetobacter baumannii* clinical isolates. *Indian J. Med. Res.* 147, 413–421. doi: 10.4103/ijmr.IJMR_644_16

Leus, I. V., Weeks, J. W., Bonifay, V., Smith, L., Richardson, S., and Zgurskaya, H. I. (2018). Substrate specificities and efflux efficiencies of RND efflux pumps of *Acinetobacter baumannii*. *J. Bacteriol.* 200, e00049–e00018. doi: 10.1128/JB.00049-18

Lin, M.-F., Lin, Y.-Y., and Lan, C.-Y. (2015). The role of the two-component system BaeSR in disposing chemicals through regulating transporter systems in *Acinetobacter baumannii*. *PLoS One* 10:e0132843. doi: 10.1371/journal.pone.0132843

Lorenz, R., Bernhart, S. H., Honer Zu Siederdissen, C., Tafer, H., Flamm, C., Stadler, P. F., et al. (2011). ViennaRNA Package 2.0. *Algorithms Mol. Biol.* 6:26. doi: 10.1186/1748-7188-6-26

Lucidi, M., Visaggio, D., Prencipe, E., Imperi, F., Rampioni, G., Cincotti, G., et al. (2019). New shuttle vectors for real-time gene expression analysis in multidrug-resistant *Acinetobacter* species: in vitro and in vivo responses to environmental stressors. *Appl. Environ. Microbiol.* 85, e01334–e01319. doi: 10.1128/AEM.01334-19

Machado, D., Antunes, J., Simoes, A., Perdigao, J., Couto, I., McCusker, M., et al. (2018). Contribution of efflux to colistin heteroresistance in a multidrug resistant *Acinetobacter baumannii* clinical isolate. *J. Med. Microbiol.* 67, 740–749. doi: 10.1099/jmm.0.000741

Magnet, S., Courvalin, P., and Lambert, T. (2001). Resistance-nodulation-cell division-type efflux pump involved in aminoglycoside resistance in *Acinetobacter baumannii* strain BM4454. *Antimicrob. Agents Chemother.* 45, 3375–3380. doi: 10.1128/AAC.45.12.3375-3380.2001

Mahfouz, N., Ferreira, I., Beisken, S., von Haeseler, A., and Posch, A. E. (2020). Large-scale assessment of antimicrobial resistance marker databases for genetic

phenotype prediction: a systematic review. *J. Antimicrob. Chemother.* 75, 3099–3108. doi: 10.1093/jac/dkaa257

Marchand, I., Damier-Piolle, L., Courvalin, P., and Lambert, T. (2004). Expression of the RND-type efflux pump AdeABC in *Acinetobacter baumannii* is regulated by the AdeRS two-component system. *Antimicrob. Agents Chemother.* 48, 3298–3304. doi: 10.1128/AAC.48.9.3298-3304.2004

Mrazek, J., and Xie, S. (2006). Pattern locator: a new tool for finding local sequence patterns in genomic DNA sequences. *Bioinforma* 22, 3099–3100. doi: 10.1093/bioinformatics/btl551

Nikaido, H., and Pagès, J.-M. (2012). Broad-specificity efflux pumps and their role in multidrug resistance of gram-negative bacteria. *FEMS Microbiol. Rev.* 36, 340–363. doi: 10.1111/j.1574-6976.2011.00290.x

Olliver, A., Valle, M., Chaslus-Dancla, E., and Cloeckaert, A. (2005). Overexpression of the multidrug efflux operon acrEF by insertional activation with IS1 or IS10 elements in *salmonella enterica* serovar typhimurium DT204 acrB mutants selected with fluoroquinolones. *Antimicrob. Agents Chemother.* 49, 289–301. doi: 10.1128/AAC.49.1.289-301.2005

Prieto Martin Gil, S., Tajuelo, A., López-Siles, M., and McConnell, M. J. (2021). Subinhibitory concentrations of clinically-relevant antimicrobials affect resistance-nodulation-division family promoter activity in *Acinetobacter baumannii*. *Front. Microbiol.* 12:780201. doi: 10.3389/fmicb.2021.780201

Rello, J., Kalwaje Eshwara, V., Lagunes, L., Alves, J., Wunderink, R. G., Conway-Morris, A., et al. (2019). A global priority list of the TOp TEn resistant microorganisms (TOTEM) study at intensive care: a prioritization exercise based on multi-criteria decision analysis. *Eur. J. Clin. Microbiol. Infect. Dis.* 38, 319–323. doi: 10.1007/s10096-018-3428-y

Rosenfeld, N., Bouchier, C., Courvalin, P., and Perichon, B. (2012). Expression of the resistance-nodulation-cell division pump AdeIJK in *Acinetobacter baumannii* is regulated by AdeN, a TetR-type regulator. *Antimicrob. Agents Chemother.* 56, 2504–2510. doi: 10.1128/AAC.06422-11

Ruzin, A., Immermann, F. W., and Bradford, P. A. (2010). RT-PCR and statistical analyses of adeABC expression in clinical isolates of *Acinetobacter calcoaceticus-Acinetobacter baumannii* complex. *Microb. Drug Resist.* 16, 87–89. doi: 10.1089/mdr.2009.0131

Schmalstieg, A. M., Srivastava, S., Belkaya, S., Deshpande, D., Meek, C., Leff, R., et al. (2012). The antibiotic resistance arrow of time: efflux pump induction is a general first step in the evolution of mycobacterial drug resistance. *Antimicrob. Agents Chemother.* 56, 4806–4815. doi: 10.1128/AAC.05546-11

Siguier, P., Varani, A., Perochon, J., and Chandler, M. (2012). Exploring bacterial insertion sequences with ISfinder: objectives, uses, and future developments. *Methods Mol. Biol.* 859, 91–103. doi: 10.1007/978-1-61779-603-6_5

Suh, B., Bae, I. K., Kim, J., Jeong, S. H., Yong, D., and Lee, K. (2010). Outbreak of meropenem-resistant *Serratia marcescens* comediated by chromosomal AmpC beta-lactamase overproduction and outer membrane protein loss. *Antimicrob. Agents Chemother.* 54, 5057–5061. doi: 10.1128/AAC.00768-10

Tacconelli, E., Carrara, E., Savoldi, A., Harbarth, S., Mendelson, M., Monnet, D. L., et al. (2018). Discovery, research, and development of new antibiotics: the WHO priority list of antibiotic-resistant bacteria and tuberculosis. *Lancet Infect. Dis.* 18, 318–327. doi: 10.1016/S1473-3099(17)30753-3

Turton, J. F., Ward, M. E., Woodford, N., Kaufmann, M. E., Pike, R., Livermore, D. M., et al. (2006). The role of ISAba1 in expression of OXA carbapenemase genes in *Acinetobacter baumannii*. *FEMS Microbiol. Lett.* 258, 72–77. doi: 10.1111/j.1574-6968.2006.00195.x

Verma, P., and Tiwari, V. (2018). Targeting outer membrane protein component AdeC for the discovery of efflux pump inhibitor against AdeABC efflux pump of multidrug resistant *Acinetobacter baumannii*. *Cell Biochem. Biophys.* 76, 391–400. doi: 10.1007/s12013-018-0846-5

Vila, J., and Pachon, J. (2011). *Acinetobacter baumannii* resistant to everything: what should we do? *Clin. Microbiol. Infect.* 17, 955–956. doi: 10.1111/j.1469-0691.2011.03566.x

Vlahovicek, K., Kajan, L., and Pongor, S. (2003). DNA analysis servers: plot. It, bend.It, model.It and IS. *Nucleic Acids Res.* 31, 3686–3687. doi: 10.1093/nar/gkg559

Yoon, E.-J., Chabane, Y. N., Goussard, S., Snesrud, E., Courvalin, P., Dé, E., et al. (2015). Contribution of resistance-nodulation-cell division efflux systems to antibiotic resistance and biofilm formation in *Acinetobacter baumannii*. *MBio* 6, e00309–e00315. doi: 10.1128/mBio.00309-15

Yoon, S.-H., Ha, S.-M., Lim, J., Kwon, S., and Chun, J. (2017). A large-scale evaluation of algorithms to calculate average nucleotide identity. *Antonie Van Leeuwenhoek* 110, 1281–1286. doi: 10.1007/s10482-017-0844-4

Zang, M., Adams, F. G., Hassan, K. A., and Eijkelkamp, B. A. (2021). The impact of Omega-3 fatty acids on the evolution of *Acinetobacter baumannii* drug resistance. *Microbiol. Spectr.* 9:e0145521. doi: 10.1128/Spectrum.01455-21

Conflict of Interest: MM is a founder and shareholder in the biotechnology company Vaxdyn, S.L.

The remaining authors declare that the research was conducted in the absence of any commercial or financial relationships that could be construed as a potential conflict of interest.

Publisher's Note: All claims expressed in this article are solely those of the authors and do not necessarily represent those of their affiliated organizations, or those of the publisher, the editors and the reviewers. Any product that may be evaluated in this article, or claim that may be made by its manufacturer, is not guaranteed or endorsed by the publisher.

frontiers | Frontiers in Microbiology

ORIGINAL RESEARCH
published: 15 June 2022
doi: 10.3389/fmicb.2022.869653

Genomic Characterization of Mobile Genetic Elements Associated With Carbapenem Resistance of *Acinetobacter baumannii* From India

*Saranya Vijayakumar[1], Jobin John Jacob[1], Karthick Vasudevan[1], Purva Mathur[2], Pallab Ray[3], Ayyanraj Neeravi[1], Ashtawarthani Baskaran[1], Agilandeeswari Kirubananthan[1], Shalini Anandan[1], Indranil Biswas[4], Kamini Walia[5] and Balaji Veeraraghavan[1]**

[1] Christian Medical College & Hospital, Vellore, India, [2] Jai Prakash Narayan Apex Trauma Center, All India Institute of Medical Sciences, New Delhi, India, [3] Post Graduate Institute of Medical Education and Research (PGIMER), Chandigarh, India, [4] Microbiology Department, Molecular Genetics and Immunology, University of Kansas, Lawrence, KS, United States, [5] Indian Council of Medical Research (ICMR), New Delhi, National Capital Territory of Delhi, New Delhi, India

OPEN ACCESS

Edited by:
Raffaele Zarrilli,
University of Naples Federico II, Italy

Reviewed by:
Santiago Castillo Ramírez,
National Autonomous University of Mexico, Mexico
Mehrad Hamidian,
University of Technology Sydney, Australia

***Correspondence:**
Balaji Veeraraghavan
vbalaji@cmcvellore.ac.in

Specialty section:
This article was submitted to Antimicrobials, Resistance and Chemotherapy, a section of the journal Frontiers in Microbiology

Received: 04 February 2022
Accepted: 20 May 2022
Published: 15 June 2022

Citation:
Vijayakumar S, Jacob JJ, Vasudevan K, Mathur P, Ray P, Neeravi A, Baskaran A, Kirubananthan A, Anandan S, Biswas I, Walia K and Veeraraghavan B (2022) Genomic Characterization of Mobile Genetic Elements Associated With Carbapenem Resistance of Acinetobacter baumannii From India. Front. Microbiol. 13:869653. doi: 10.3389/fmicb.2022.869653

With the excessive genome plasticity, *Acinetobacter baumannii* can acquire and disseminate antimicrobial resistance (AMR) genes often associated with mobile genetic elements (MGEs). Analyzing the genetic environment of resistance genes often provides valuable information on the origin, emergence, evolution, and spread of resistance. Thus, we characterized the genomic features of some clinical isolates of carbapenem-resistant *A. baumannii* (CRAb) to understand the role of diverse MGEs and their genetic context responsible for disseminating carbapenem resistance genes. For this, 17 clinical isolates of *A. baumannii* obtained from multiple hospitals in India between 2018 and 2019 were analyzed. AMR determinants, the genetic context of resistance genes, and molecular epidemiology were studied using whole-genome sequencing. This study observed an increased prevalence of bla_{OXA-23} followed by dual carbapenemases, bla_{OXA-23}, and bla_{NDM}. This study identified three novel Oxford MLST sequence types. The majority of the isolates belonged to the dominant clone, IC2, followed by less prevalent clones such as IC7 and IC8. This study identified variations of AbaR4 and AbGRI belonging to the IC2 lineage. To the best of our knowledge, this is the first study that provides comprehensive profiling of resistance islands, their related MGEs, acquired AMR genes, and the distribution of clonal lineages of CRAb from India.

Keywords: CRAb, OXA–23, Tn*2006*, IC2, AbGRI1 variant, AbaR4

INTRODUCTION

Acinetobacter baumannii is a member of the ESKAPE group of pathogens and is considered to be one of the major global causes of hospital-acquired infections (HAIs) (Lee et al., 2017). *A. baumannii* is responsible for causing a wide range of infections, with pneumonia being the most commonly observed infection among critically ill patients (Dexter et al., 2015). This pathogen has

a propensity to rapidly acquire antibiotic resistance genes and to develop resistance to multiple classes of antimicrobials (Lee et al., 2017). Carbapenems are one of the most commonly used antibiotics for the treatment of *Acinetobacter* infections. Carbapenem resistance in *A. baumannii* ranges between 70 and 85% in the Asia-Pacific region (O'Donnell et al., 2021). A study from SENTRY surveillance reported carbapenem resistance rates ranging from 55 to 90% in India (Gales et al., 2019). Both the Center for Disease Control (CDC) and the World Health Organization (WHO) categorized carbapenem-resistant *A. baumannii* (CRAb) under "Urgent Threat" and as Priority 1: Critical pathogen, respectively. Recently, the WHO Country Office for India developed the Indian Priority Pathogen List (IPPL) and categorized carbapenem-resistant, colistin-resistant *A. baumannii* under "Critical Priority."[1]

With excessive genome plasticity, *A. baumannii* can acquire and disseminate antimicrobial resistance (AMR) genes that are often associated with various mobile genetic elements (MGEs) (Roca et al., 2012). Carbapenem resistance in *A. baumannii* is mainly due to genes encoding class D oxacillinases, $bla_{OXA-23-like}$, $bla_{OXA-51-like}$, and $bla_{OXA-58-like}$ (Poirel and Nordmann, 2006). The bla_{OXA-23} gene is the most predominant and is carried on many MGEs, including transposons, plasmids, and resistance islands (RIs) (Pagano et al., 2016). The association of insertion sequence (IS) elements with $bla_{OXA-51-like}$, $bla_{OXA-23-like}$, $bla_{NDM-like}$, and $bla_{OXA-58-like}$ genes was reported earlier (Poirel et al., 2005, 2012; Turton et al., 2006a). Typically, bla_{OXA-23} is associated with transposons such as Tn*2006*, Tn*2008*, and Tn*2009*, while bla_{NDM-1} was mobilized by the Tn*125*-like composite transposon (Pagano et al., 2016). Recent studies have also indicated the role of conjugative plasmids as vehicles for disseminating resistance determinants such as bla_{OXA-23} in *A. baumannii* (Salto et al., 2018). Additionally and most importantly, the emergence of *A. baumannii* RIs carrying clusters of horizontally transferred genes is considered a significant contributor to the multidrug-resistant (MDR) phenotype of *A. baumannii* (Cameranesi et al., 2020). RIs in *A. baumannii* are made of transposons and are known to carry genes that confer resistance to multiple antibiotics and heavy metals (Hamidian and Hall, 2018). The AbaR3-type elements are confined to the International Clone 1 (IC1) and represented by ST1, ST19, ST20, and ST81. AbaR3 comprises a Tn*6019* backbone and is consistently linked with Tn*6018* or its components with multiple antimicrobial resistance regions (MARRs) (Hamidian and Hall, 2011). Similarly, studies have shown that Tn*6022* can acquire bla_{OXA-23} transposon Tn*2006* and form AbaR4 islands (Hamidian and Hall, 2017). **Table 1** outlines the genomic and epidemiological features of different clones of CRAb.

Although the endemic burden of CRAb is a significant public health problem within Indian hospitals, the lack of genomic information makes it difficult to track its persistence (Mancilla-Rojano et al., 2019). Studying the genetic environment of resistance genes often provides valuable information on the origin, emergence, evolution, and spread of resistance in bacterial populations (Hamidian and Nigro, 2019).

We aimed to characterize the prevalent genomic features of clinical isolates of CRAb in India. We also compared the structural configuration of RIs with the complete genetic information and observed structural variations within the genetic environment of resistance genes. We found that the backbone of MGEs and their associated AMR genes among this study isolates were similar to that of the global context.

MATERIALS AND METHODS

Bacterial Isolates

A total of 17 clinical isolates of *A. baumannii* collected as a part of a surveillance study were used. Of the 17 isolates included in this study, 13 were from Christian Medical College (CMC), Vellore, three from All India Institute of Medical Sciences (AIIMS) Trauma Center, New Delhi, and one from Post Graduate Institute of Medical Education & Research (PGIMER), Chandigarh (**Supplementary Figure 1**). Among the isolates, ten isolates were from blood (B; $n = 10$), six from endotracheal aspirate (ETA; $n = 6$), and one from pus (P; $n = 1$). Phenotypic characterization of all the isolates as *A. baumannii calcoaceticus* (*Acb*) complex was determined using standard biochemical tests. Confirmation of the *Acb* complex at the species level was performed by Vitek-MS (Database v2.0, bioMerieux, France) as described earlier and by identifying chromosomally encoded $bla_{OXA-51-like}$ gene by PCR (Turton et al., 2006b).

Antimicrobial Susceptibility Testing

All the isolates were characterized for susceptibility to ceftazidime (30 μg), cefepime (30 μg), piperacillin-tazobactam (100/10 μg), cefoperazone-sulbactam (75/30 μg), imipenem (10 μg), meropenem (10 μg), levofloxacin (5 μg), amikacin (30 μg), netilmicin (30 μg), tobramycin (10 μg), aztreonam (30 μg), tetracycline (30 μg), minocycline (30 μg), and tigecycline (15 μg) using the Kirby Bauer's disk diffusion (DD) method.

For colistin, broth microdilution (BMD) was performed. Isolates identified as carbapenem-resistant by DD were further subjected to BMD to determine the minimum inhibitory concentration (MIC) for imipenem and meropenem. The susceptibility was interpreted as per the criteria defined by CLSI guidelines (Weinstein et al., 2018, 2019). *Escherichia coli* (ATCC 25922) and *Pseudomonas aeruginosa* (ATCC 27853) were included in every batch for quality control (QC). For colistin susceptibility testing, in addition to QC strains, an *mcr-1* positive *E. coli* isolate and two *Klebsiella pneumoniae* strains (BA38416 and BA25425) were also included for QC.

Whole-Genome Sequencing and Assembly

The isolates were recovered overnight on blood agar, and genomic DNA was extracted from pure cultures using a QIAamp DNA mini kit (Qiagen, Germany) following the

[1]https://dbtindia.gov.in

TABLE 1 | Genomic and epidemiological features of different clones of carbapenem-resistant *Acinetobacter baumannii*–Indian vs. global scenario.

International clone (IC)	IC1		IC2		IC7		IC8	
	Indian	**Global**	**Indian**	**Global**	**Indian**	**Global**	**Indian**	**Global**
Antimicrobial resistance (AMR) genes	bla_{OXA-23}, bla_{NDM-1}	bla_{OXA-23}, bla_{OXA-58}	bla_{OXA-23}, bla_{OXA-58}, bla_{NDM-1}	bla_{OXA-23}, bla_{OXA-24}, bla_{OXA-58}, bla_{NDM-1}	bla_{OXA-23}	bla_{OXA-23}, bla_{NDM-1}	bla_{OXA-23}	bla_{OXA-23}, bla_{OXA-58}, bla_{NDM-1}
Insertion sequence ISAba1								
Transposon	Tn*6022*, Tn*2006*, Tn*125*	Tn*6018*, Tn*6019*, Tn*6022*, Tn*6172* Tn*2006*	Tn*6022*, Tn*6172*, Tn*2006*, Tn*6706*, Tn*6708*, Tn*125*	Tn*6022*, Tn*6172*, Tn*2006*, Tn*2007*, Tn*2008*, Tn*125*	Tn*6022*, Tn*2006*	Tn*6022*, Tn*6172*, Tn*6183*	Tn*6022*, Tn*2006*	Tn*6022*, Tn*6172*
Resistance Island	AbaR4	AbaR1, AbaR3, AbaR4, AbaR5 AbaR6, AbaR7, AbaR8, AbaR21, AbaR23, AbaR24	AbaR4, Novel AbGRIs	AbaR4, AbaR26, AbaR27, AbGRI1, AbGRI2, AbGRI3	AbaR4	AbGRI2	AbaR4	NA
Predominant STs (Oxford MLST)	ST231	ST109, ST207, ST231, ST405, ST441, ST491, ST781, ST945, ST947	ST848, ST208, ST195, ST451, ST218, ST369, ST349, ST1052	ST92, ST848, ST208, ST195, ST451, ST218, ST369	ST229, ST691, ST993	ST229, ST691	ST447, ST391, ST1390	ST447
Predominant STs (Pasteur MLST)	ST1	ST1	ST2	ST1	ST25	ST25	ST10	ST10
Level of spread	Low	Medium	High	High	Low	Low and region-specific	Low	Low and region-specific

manufacturers' instructions. DNA was quantified by NanoDrop spectrophotometry (Thermo Fisher Scientific, United States) and Qubit 3.0 fluorometry (Life Technologies, United States) and stored at −20°C until further characterization.

Short read sequencing of the 17 isolates was carried out using the Ion Torrent PGM™ platform using 400-bp chemistry (Life Technologies, United States) or 150-bp paired-end sequencing using HiSeq 2500 platform (Illumina, United States). The PHRED quality score was checked on the sequences, and reads with a score below 20 were discarded. Adapters were trimmed using cutadapt v. 1.8.1[2] and assessed with FastQC version 0.11.4.[3]

All genomic DNA was further subjected to Oxford Nanopore MinION sequencing (Oxford Nanopore Technologies, United Kingdom) to obtain long-read sequences. For this, the DNA library was prepared as per the manufacturer's protocol using the SQK-LSK108 ligation sequencing kit (version R9) and the ONT EXP-NBD103 Native Barcode Expansion Kit (Oxford Nanopore Technologies, United Kingdom). The library was loaded onto the FLO-MIN106 R9 flow cell and run for 48 h using the standard MinKNOW software. The Fast5 files from MinION sequencing were subjected to base calling using Guppy.[4]

Complete circular genomes for the 17 isolates were obtained using the *de novo* hybrid assembly of Illumina and Oxford nanopore sequences as described earlier (Wick et al., 2017a). The long reads were error-corrected using the standalone Canu tool (version 1.7) and filtered using Filtlong version 0.2.0[5] with parameters set at *min_length 1000* −90 %. The short reads generated using ion torrent were error-corrected using Ionhammer (Ershov et al., 2019) available in SPAdes, and the default FastA output was converted to FastQ with custom scripts. Additionally, genomes were assembled using the Unicycler hybrid assembly pipeline (version 0.4.6) with the default settings (Wick et al., 2017b). The obtained genome sequence was polished using high-quality Illumina/Ion torrent reads to reduce the base level errors with multiple rounds of Pilon (version 1.22) (Walker et al., 2014). The assembly quality was assessed for completeness, correctness, and contiguity using CheckM version 1.0.5 (Parks et al., 2015). The genome sequences of the chromosomes and plasmids have been deposited in GenBank under the accession numbers–AB01 (CP040080–CP040083), AB02

[2]https://github.com/marcelm/cutadapt

[3]http://www.bioinformatics.babraham.ac.uk/projects/fastqc

[4]https://github.com/gnetsanet/ONT-GUPPY

[5]https://github.com/rrwick/Filtlong

(CP035672–CP035675), AB03 (CP050388–CP050389), AB06 (CP040050–CP040052), AB10 (CP040053–CP040055), AB11 (CP040056–CP040057), AB13 (CP040087–CP040088), AB14 (CP040259–CP040262), AB15 (CP050385–CP050387), AB16 (CP050523–CP050525), AB18 (CP050390–CP050391), AB19 (CP050410–CP050411), AB20 (CP050412–CP050414), AB23 (CP050432–CP050435), AB26 (CP050401–CP050402), AB27 (CP050421–CP050423), and AB28 (CP050403–CP050409).

Genome Analysis

Further downstream analysis of the 17 complete genome sequences was performed using tools available at the Center for Genomic Epidemiology (CGE).[6] AMR genes were identified from the genome sequences using the BLASTn-based ABRicate (version 0.8.10) program[7] to query the ResFinder database.[8] The Capsular Polysaccharide loci (KL) and the Outer Core Lipooligosaccharide loci (OCL) types were identified using the Kaptive database.[9]

The presence of ISs was identified using ISFinder.[10] Using BLAST analysis, the plasmid rep*Aci* types from the complete genomes were identified and characterized. The PHASTER server was used to determine the prophages.[11] The prophage regions identified were analyzed for the presence of any AMR genes using the ABRicate (version 0.8.10) program(see text footnote 7). A BLAST similarity search was performed on the individual genomes to identify the *comM* region that flanks AbaR type genomic islands. Based on the known AbaR sequences collected from published literature, the precise boundary of AbaRs and the respective backbone were curated manually. The sequence types were identified with MLST Finder 2.0 using Oxford MLST and Pasteur MLST schemes.[12]

Phylogenetic Analysis

The assembled genome sequences were mapped to the reference genome ATCC 17978 (CP012004) using the BWA MEM[13] algorithm, and the variants were filtered with FreeBayes available in Snippy (Seemann, 2015). The core SNP genome alignment of all the genomes was generated with Snippy-core. The recombination regions within the core genome alignment were further filtered and removed using the Gubbins (version 2.4.1) algorithm (Croucher et al., 2015). The maximum likelihood (ML) phylogeny was constructed using FastTree version 2.1.8 (Price et al., 2010) using the GTR model with 100 bootstrap replicates. The phylogenetic tree was rooted in the reference genome and labeled using the Interactive Tree of Life software (iTOL v3) (Letunic and Bork, 2021).

[6]http://www.genomicepidemiology.org/services/

[7]https://github.com/tseemann/abricate

[8]https://cge.food.dtu.dk/services/ResFinder/

[9]https://kaptive-web.erc.monash.edu/

[10]https://www-is.biotoul.fr/blast.php

[11]https://phaster.ca/

[12]https://cge.food.dtu.dk/services/MLST/

[13]https://github.com/lh3/bwa

RESULTS

Varied Resistance Profile of *Acinetobacter baumannii* Strains With bla_{OXA-51} and bla_{OXA-23} Variants

All 17 isolates were phenotypically identified as *Acb*-complex and further reconfirmed as *A. baumannii* using Vitek-MS (Data not shown). Among the 17 isolates, AB01 was pan-susceptible (PSAB), AB23 was multidrug-resistant (MDRAB) but susceptible to carbapenem (CSAB), 12 isolates (AB10, AB11, AB13, AB14, AB15, AB16, AB18, AB19, AB20, AB26, AB27, and AB28) were CRAb, and the remaining three isolates (AB02, AB03, and AB06) were pan-drug resistant (PDRAB). **Table 2** outlines the presence of resistance genes among the 17 isolates against different classes of antimicrobials. All the study isolates carried the intrinsic $bla_{OXA-51-like}$ and $bla_{ADC-25-like}$ genes. Whole-genome sequencing (WGS) identified seven different variants of bla_{OXA-51} (bla_{OXA-66}, bla_{OXA-68}, bla_{OXA-64}, $bla_{OXA-144}$, $bla_{OXA-203}$, $bla_{OXA-337}$, and $bla_{OXA-371}$), a single variant of bla_{OXA-23} ($bla_{OXA-169}$), and a single variant of $bla_{NDM-like}$ gene (bla_{NDM-1}). Among the 17 study isolates, ten carried $bla_{OXA-23-like}$ alone, one isolate carried bla_{NDM-1} alone, and four isolates co-harbored $bla_{OXA-23-like}$ and bla_{NDM-1}. No acquired carbapenemase genes were identified in the remaining two isolates. More than one copy of bla_{OXA-23} was observed in thirteen isolates (**Table 2**). As expected, none of our isolates carried $bla_{OXA-24-like}$ or $bla_{OXA-58-like}$ genes. The *A. baumannii* isolates in this study belonged to diverse sequence types (STs) representing four International clones, ICs (IC1/CC1, IC2/CC2, IC7/CC25, and IC8/CC10), one clonal complex, i.e., CC862, and one singleton (**Table 2**). Although genes that confer resistance to different antimicrobials were identified across all clonal lineages, the majority of the genes that encode for aminoglycoside modifying enzymes, RMTases, macrolide resistance, sulfonamide resistance, chloramphenicol, and rifampicin resistance were confined to isolates belonging to IC2 (Rodrigues et al., 2021; Hernández-González et al., 2022).

IC2–the Predominant and Endemic Lineage With Novel Structural Variations

Nine isolates belonged to IC2, and all had either XDR or PDR phenotypes. Six Oxford MLST STs (ST^{Oxf}) were identified, ST195 (2), ST451 (2), ST848 (2), ST208 (1), ST218 (1), and ST349 (1), but there was a single Pasteur MLST $ST2^{Pas}$. IC2 isolates predominantly carried either bla_{OXA-23} alone (7/9) or coproduced bla_{OXA-23} and bla_{NDM-1} (2/9). All had bla_{OXA-23} in Tn*2006*, an IS*Aba1*-bounded composite transposon in the chromosome (**Figure 1**). Of the nine isolates, AB03, AB13, and AB16 carried the bla_{NDM-1} gene on the chromosome with two different structural variations in the genetic context. AB03 and AB16 were associated with the most commonly reported transposon, Tn*125* (**Figure 2A**), while a truncated form of Tn*125* (Tn*125*-like) was identified in AB13, where the genome harbors a single copy of IS*Aba125* and an incomplete transposase at the left-hand and right-hand extremities of Tn*125*, respectively (**Figure 2B**). One to three plasmids were

TABLE 2 | Presence of antimicrobial resistance (AMR) genes, mobile genetic elements, and resistance islands among the 17 complete genomes of *Acinetobacter baumannii*.

Isolate ID (Accession number)	Specimen ID (ST Oxford/ Pasteur)	Susceptibility	AMR gene profile	IS*Aba1*-bla_{OXA-51} like	bla_{ADC} allele* / IS*Aba1*-ADC	IS*Aba1*-bla_{OXA-23} like transposon	IS*Aba3*-bla_{OXA-58} like	IS*Aba125*-bla_{NDM-1} like transposon	Integron	Resistance Island (RI)
AB01 (CP040080)	SP304 (2439/285)	Pan-susceptible	$bla_{OXA-337}$	–	bla_{ADC-33} (closest match) / Absent	–	–	–	–	Absent
AB02 (CP035672)	VB23193 (848/2)	PDR	*aac(6′)-Ib3*, *aadA1*, *aph(3″)-Ib*, *aph(6)-Id*, *armA*, $bla_{OXA-169}$, bla_{OXA-23}, bla_{OXA-66}, bla_{PER-7} (2 copies), *mphE*, *msrE*, *catB8*, *cmlA1*, *aac(6′)-Ib-cr*, *ARR-2*, *sul1*, *sul2*, *tet(B)*	–	bla_{ADC-1} (closest match) / Present	Present–Tn*2006*	–	–	–	AbGRI-variant
AB03 (CP050388)	VB473 (848/2)	PDR	*aph(3″)-Ib*, *aph(3′)-Ia*, *aph(6)-Id*, *armA*, bla_{NDM-1}, bla_{OXA-23} (2 copies), bla_{OXA-66}, *mph(E)*, *msrE*, *sul2*, *tet(B)*	–	bla_{ADC-1} (closest match) / Present	Present–Tn*2006*	–	Present–Tn*125*	–	AbGRI1-variant
AB06 (CP040050)	VB16141 (2440/622)	PDR	bla_{NDM-1}, $bla_{OXA-203}$, bla_{OXA-23} (2 copies)	–	bla_{ADC-23} (closest match) / Absent	Present–Tn*2006*	–	Incomplete Tn*125*	–	AbaR4
AB10 (CP040053)	VB35179 (2392/586)	XDR	bla_{OXA-23} (2 copies), bla_{OXA-68}	–	bla_{ADC-29} (closest match) / Present	Present–Tn*2006*	–	–	–	AbaR4
AB11 (CP040056)	VB35435 (2441/575)	XDR	$bla_{OXA-144}$, bla_{OXA-23} (2 copies)	–	bla_{ADC-29} (Exact match) / Absent	Present–Tn*2006*	–	–	–	AbaR4
AB13 (CP040087)	VB35575 (349/2)	XDR	*aac(6′)-Ib3*, *aadA1*, *aph(3″)-Ib*, *aph(6)-Id*, *armA*, bla_{NDM-1}, bla_{OXA-23} (2 copies), bla_{OXA-66}, *mphE*, *msrE*, *catB8*, *cmlA1*, *aac(6′)-Ib-cr*, *ARR-2*, *sul1*, *sul2*, *tet(B)*	–	bla_{ADC-1} (closest match) / Present	Present–Tn*2006*	–	Present–Tn*125* like)	–	AbGRI- variant
AB14 (CP040259)	P7774 (1388/25)	XDR	bla_{OXA-23} (2 copies), bla_{OXA-64}	–	bla_{ADC-23} (closest match) / Absent	Present–Tn*2006*	–	–	–	AbaR4
AB15 (CP050385)	VB82 (691/25)	XDR	bla_{OXA-23}, bla_{OXA-64}, bla_{TEM-1D}, *mphE*, *msrE*, *tet(B)*	–	bla_{ADC-23} (closest match) / Absent	Present–Tn*2006*	–	–	–	AbaR4

(Continued)

TABLE 2 | (Continued)

Isolate ID (Accession number)	Specimen ID (ST Oxford/ Pasteur)	Susceptibility	AMR gene profile	IS*Aba1*-bla_{OXA-51} like	bla_{ADC} allele* / IS*Aba1*-ADC	IS*Aba1*-bla_{OXA-23} like transposon	IS*Aba3*-bla_{OXA-58} like	IS*Aba125*-bla_{NDM-1} like transposon	Integron	Resistance Island (RI)
AB16 (CP050523)	VB7036 (218/2)	XDR	*aph(3″)-Ib*, *aph(3′)-Ia*, *aph(6)-Id*, *armA*, bla_{NDM-1}, bla_{OXA-23} (2 copies), bla_{OXA-66}, *mphE*, *msrE*, *sul2*, *tet(B)*	–	bla_{ADC-1} (closest match) / Present	Present–Tn*2006*	–	Present–Tn*125* like	–	AbGRI1-variant
AB18 (CP050390)	VB723 (208/2)	XDR	*aph(3″)-Ib*, *armA*, *aph(3′)-Ia*, *aph(6′)-Id*, bla_{OXA-23} (2 copies), bla_{OXA-66}, bla_{TEM-1D}, *mphE*, *msrE*, *sul2*, *tet(B)*	–	bla_{ADC-1} (closest match) / Present	Present–Tn*2006*	–	–	–	AbGRI- variant
AB19 (CP050410)	PM2235 (451/2)	XDR	*aph(3″)-Ib*, *aph(3′)-Ia*, bla_{OXA-23} (2 copies), bla_{OXA-66}, bla_{TEM-1D}, *mphE*, *msrE*, *tet(B)*	–	bla_{ADC-1} (closest match) / Present	Present–Tn*2006*	–	–	–	AbGRI1-variant
AB20 (CP050412)	PM2696 (195/2)	XDR	*aph(3″)-Ib*, *aph(6′)-Id*, bla_{OXA-23} (2 copies), bla_{OXA-66}, *mphE*, *msrE*, *sul2*, *tet(B)*	–	bla_{ADC-1} (closest match) / Present	Present–Tn*2006*	–	–	–	AbGRI- variant
AB23 (CP050432)	PM4229 (447/10)	MDR	*aph(3″)-Ib*, *aph(6)-Id*, bla_{OXA-68}, *sul2*	–	bla_{ADC-29} (Exact match) / Absent	–	–	–	–	–
AB26 (CP050401)	VB2181 (195/2)	XDR	*aph(3″)-Ib*, *armA*, *aph(3′)-Ia*, *aph(6′)-Id*, bla_{OXA-23} (2 copies), bla_{OXA-66}, bla_{TEM-1D}, *mphE*, *msrE*, *tet(B)*	–	bla_{ADC-1} (closest match) / Present	Present–Tn*2006*	–	–	–	AbGRI1-variant
AB27 (CP050421)	VB2200 (451/2)	XDR	*aph(3″)-Ib*, *armA*, *aph(3′)-Ia*, *aph(6′)-Id*, bla_{OXA-23} (2 copies), bla_{OXA-66}, bla_{TEM-1D}, *mphE*, *msrE*, *tet(B)*	–	bla_{ADC-1} (closest match) / Present	Present–Tn*2006*	–	–	–	AbGRI- variant
AB28 (CP050403)	VB2486 (231/1)	XDR	*aph(3″)-Ib*, *aph(6′)-Id*, $bla_{OXA-371}$, bla_{NDM-1}, *sul2*	IS*Aba16* present but no insertional inactivation	bla_{ADC-27} (closest match) / Present	–	–	Present–Tn*125*	–	Tn*6022* derived elements

PDR, pan drug-resistant; XDR, extensively drug-resistant; repAci, replicase type of Acinetobacter; IS, insertion sequence; Tn, transposon; tra, transfer genes; Mob, mobility genes.
**The blaADC allele was identified using the ampC database incorporated in the PubMLST website: https://pubmlst.org/bigsdb?db=pubmlst_abaumannii_seqdef&page=sequenceQuery.*

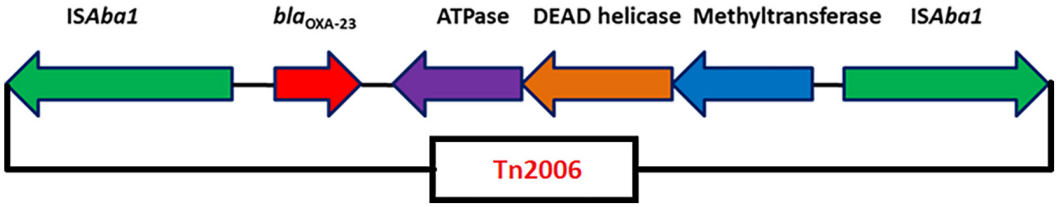

FIGURE 1 | Genetic arrangement of bla_{OXA-23} identified in this study. The bla_{OXA-23} gene was flanked by two copies of an insertion sequence, IS*Aba1* in opposite orientations, forming a composite transposon, Tn*2006*.

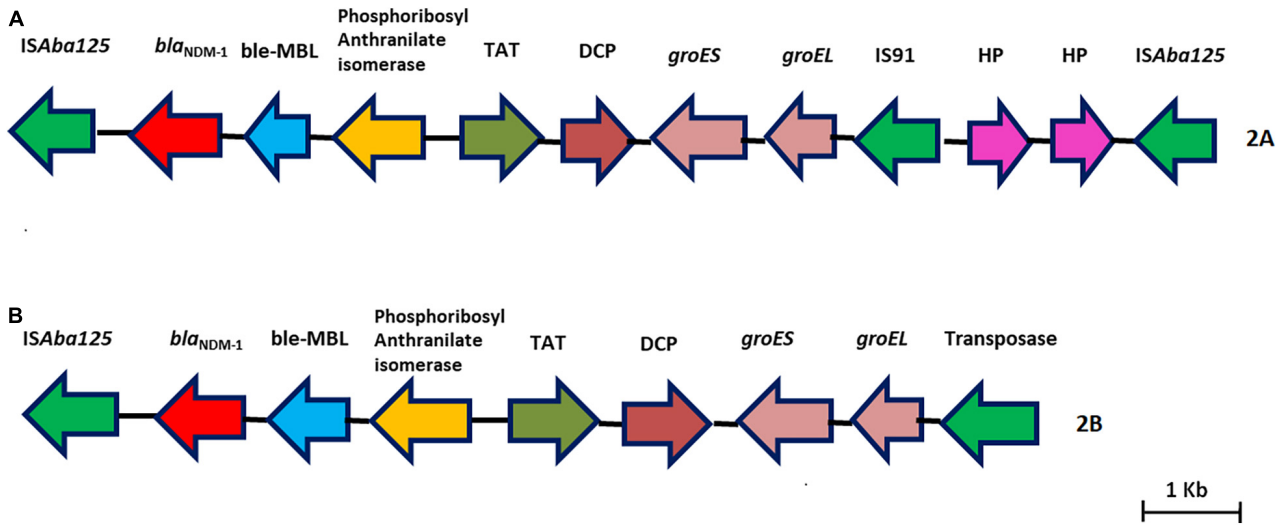

FIGURE 2 | (A,B) Representative genomes showing the genetic environment of the bla_{NDM-1} gene characterized in this study. **(A)** Tn*125*–bla_{NDM-1} with two copies of IS*Aba125*. **(B)** Tn*125*-like–bla_{NDM-1} with one copy of IS*Aba125* and a truncated transposase.

present among the nine genomes (**Table 3**). The p1AB20 belongs to the plasmid family which encodes *rep*Aci6 and was found to carry the *aphA6* gene within Tn*aphA6* that was bounded by two copies of IS*Aba125* in direct orientation. The most commonly observed prophage elements among the nine IC2 genomes include PHAGE_Acinet_Bphi_B1251_NC_019541, PHAGE_Psychr_Psymv2_NC_023734, and PHAGE_Acinet_YMC11/11/R3177_NC_041866.

Based on the genetic configurations, three different variants of RIs were identified among the nine genomes. Of which, AB03, AB16, AB19, and AB26 carried variants of AbGR1, which included the presence of a partial region of Tn*6172* with the aminoglycoside resistance genes; *aph*(6) and *aph*(3)-I, mobilization gene; *mobL*, transposable element; CR2, phosphoglucosamine mutase; *pgm*, arsenic resistance encoding gene; *arsR*, tetracycline efflux protein; *tet(B)*, and tetracycline resistance transcriptional repressor gene; *tetR*(B) along with △Tn*6022* and Tn*2006* (**Figure 3**). AB18, AB20, and AB27 carried AbGRI variants with complex, diverse structures (**Figure 4**). AB18 and AB20 had a single copy of an IS*Aba1* element, *sul2*, *rcr2*, and a hypothetical protein inserted at the *tni*CA element on the Tn*6172* backbone. Two copies of Tn*2006* were observed in both the genomes but differed at the insertion site. In AB18, one copy of Tn*2006* was inserted at *orf4* while the second copy was inserted between *orf*BA and the tetracycline resistance transcriptional repressor gene, *tetR*(B). In AB20, one copy of Tn*2006* was observed between the Tn*6022* element and the plasmid linker, whereas another Tn*2006* was inserted near *orf*BA. AB27 had two copies of IS*Aba1*, one copy inserted at the *tniE* on the Tn*6022* backbone and the second copy inserted at *tniA* of Tn*6172*. Two copies of Tn*2006* were seen, one present on Tn*6022* at *orf4* with the second adjacent to *orf*BA on Tn*6172*. Insertion of *sul2*, *rcr2*, and hypothetical protein at the left inverted repeat of the Tn*6172* element was also observed. Additionally, insertion of the arsenic resistance encoding gene, *arsR*, and the mobilization gene, *mobL*, was present on the Tn*6172* element of all three genomes (**Figure 4**).

Interestingly, AB02 and AB13 carried the novel Tn*6022*-derived, plasmid linker, and Tn*6172*-derived elements. Insertion of a single copy of Tn*2006* and △CR2-△Tn10-MARR-like region in Tn*6172* was observed in both the genomes (**Figures 5A,B**). However, one minor difference was identified between the genomes, where AB02 carried bla_{PER-7} within the class 1 integron of the Tn*6172*-derived element (**Figure 5A**), while

TABLE 3 | Characteristic features of plasmids among the 17 complete genomes of *Acinetobacter baumannii.*

Isolate ID	Specimen ID (ST Oxford/ Pasteur)	Susceptibility	Number of plasmids	Plasmid ID (Accession number)	*repAci* type	AMR gene profile	Virulence genes	Insertion sequence (IS) family	Integron	Others
AB01	SP304 (2439/285)	Pan-susceptible	3	p1AB01 (CP040081)	Frameshifted replication initiation protein	–	Sel1	–	–	–
				p2AB01 (CP040082)	Frameshifted replication initiation protein	–	Sel1	–	–	–
				p3AB01 (CP040083)	repAci3-97.89%	–	Sel1	–	–	–
AB02	VB23193 (848/2)	PDR	3	p1AB02 (CP035673)	RepM-Aci9	–	Septicolysin	–	–	–
				p2AB02 (CP035674)	RepM-Aci9-99.4%	–	Septicolysin	–	–	–
				p3AB02 (CP035675)	RepM-Aci9-99.79%	–	Septicolysin	–	–	–
AB03	VB473 (848/2)	PDR	1	p1AB03 (CP050389)	repAci4	–	Septicolysin	IS3	–	–
AB06	VB16141 (2440/622)	PDR	2	p1AB06 (CP040051)	Aci7-89.75%	aph(3″)-Ib, aph(6)-Id, armA, blaPER-7, mph€, msr€, cmlA1, ARR-2, sul1, sul2	–	IS4, IS91, IS6-like, IS5-like, Tn3-like	Class 1 (Int I1)	–
				p2AB06 (CP040052)	–	aph(3′)-VI				–
AB10	VB35179 (2392/586)	XDR	2	p1AB10 (CP040054)	–	aph(3″)-Ib, aph(6)-Id, armA, blaPER-7, mph€, msr€, cmlA1, ARR-2, sul1, sul2, tet(B)	–	IS5, IS6-like, Tn3-like, IS3, IS91-like, IS4-like	Class 1 (Int I1)	–
				p2AB10 (CP040055)	Aci4	–	Septicolysin	IS3	–	–
AB11	VB35435 (2441/575)	XDR	1	p1AB11 (CP040057)	–	aph(3′)-*via*, blaCARB-2, blaPER-7, sul1	–	IS6, IS91, IS30	–	–
AB13	VB35575 (349/2)	XDR	1	p1AB13 (CP040088)	repMAci9	–	Septicolysin	–	–	–
AB14	P7774 (1388/25)	XDR	3	p1AB14 (CP040260)	–	aac(6′)-Ian, aph(3″)-Ib, aph(6)-Id, armA, blaPER-7, mph€, msr€, cmlA1, ARR-2, sul1, sul2, tet(B)	–	IS5, IS4, IS70-like, IS91, IS6, IS30	Class 1 (Int I1)	–
				p2AB14 (CP040261)	A1S_3472	–	Septicolysin	IS3	–	–
				p3AB14 (CP040262)	–	–	–	–	–	–

(Continued)

TABLE 3 | (Continued)

Isolate ID	Specimen ID (ST Oxford/ Pasteur)	Susceptibility	Number of plasmids	Plasmid ID (Accession number)	*repAci* type	AMR gene profile	Virulence genes	Insertion sequence (IS) family	Integron	Others
AB15	VB82 (691/25)	XDR	2	p1AB15 (CP050386)	RepB family plasmid replication initiator protein (incomplete; partial on complete genome)	aac(6′)-Ian, aph(3″)-Ib, aph(6)-Id, armA, blaOXA-23, blaPER-7, mph€, msr€, cmlA1, ARR-2, sul1, sul2, tet(B)	MobL like, septicolysin	IS5, IS6, IS91, IS3, IS4, IS701-like	Class 1 (Int I1)	–
				p2AB15 (CP050387)	A1S_3472	–	–	–	–	–
AB16	VB7036 (218/2)	XDR	2	p1AB16 (CP050524)	RepA_AB	–	Sel1, Septicolysin			–
				p2AB16 (CP050525)	–	–	–			–
AB18	VB723 (208/2)	XDR	1	P1AB18 (CP050391)	AB57_3921	–	Sel1, Septicolysin			–
AB19	PM2235 (451/2)	XDR	1	P1AB19 (CP050411)	–	–	Sel1, Septicolysin			–
AB20	PM2696 (195/2)	XDR	2	p1AB20 (CP050413)	rep*Aci6*	aph(3′)-*via*	–	IS30 like		T4SS, type 4 *TraL*, *TraE*, *TraK*, *TraB*, *TraV*, *TraC*, *TraW*, *TraU*, *TrbC*, *TraN*, *TraF*, *TraH*, *TraG*
				p2AB20 (CP050414)	AB57_3921	–	Sel1, Septicolysin	–		–
AB23	PM4229 (447/10)	MDR	3	p1AB23 (CP050433)	–	aph(3″)-Ib, aph(6)-Id, armA, blaPER-7, mph€, msr€, cmlA1, ARR-2, sul1, sul2, tet(B)	MobL-like	IS4-like, IS5, IS91, IS26	Class 1 (Int I1)	Mercury operon, T6S protein, Conjugal transfer protein, TrbI, T4SS
				p2AB23 (CP050434)	Aci2-99.89%	–	MobA, MobL, Sel1, Septicolysin	–	–	–
				p3AB23 (CP050435)	repAci3	–	Sel1	–	–	–

(Continued)

TABLE 3 | (Continued)

Isolate ID	Specimen ID (ST Oxford/ Pasteur)	Susceptibility	Number of plasmids	Plasmid ID (Accession number)	*repAci* type	AMR gene profile	Virulence genes	Insertion sequence (IS) family	Integron	Others
AB26	VB2181 (195/2)	XDR	1	P1AB26 (CP050402)	AB57_3921	–	Sel1, Septicolysin			–
AB27	VB2200 (451/2)	XDR	2	p1AB27 (CP050422)	repAci1	–	Sel1, Septicolysin			–
				p2AB27 (CP050423)	–	aph(3′)-VI	MobA, mobL			–
AB28	VB2486 (231/1)	XDR	6	p1AB28 (CP050404)	plasmid replicase (rep*Aci6*) (PriCT_1" = "Primase C terminal 1 (PriCT-1)	blaOXA-23	IS21, IS256, IS66, IS4, IS30 like			T4SS, type 4 *TraL*, *TraE*, *TraK*, *TraB*, *TraV*, *TraC*, *TraW*, *TraU*, *TrbC*, *TraN*, *TraF*, *TraH*, *TraG* (Presence of repAci6 carrying AbaR4 with Tn2006-OXA-23)
				p2AB28 (CP050405)	repAci4	–	–			–
				p3AB28 (CP050406)	–	mph€, msr€	–			–
				p4AB28 (CP050407)	–	aph(3′)-VI	–			–
				p5AB28 (CP050408)	–	–	–			–
				p6AB28 (CP050409)	–	–	–			–

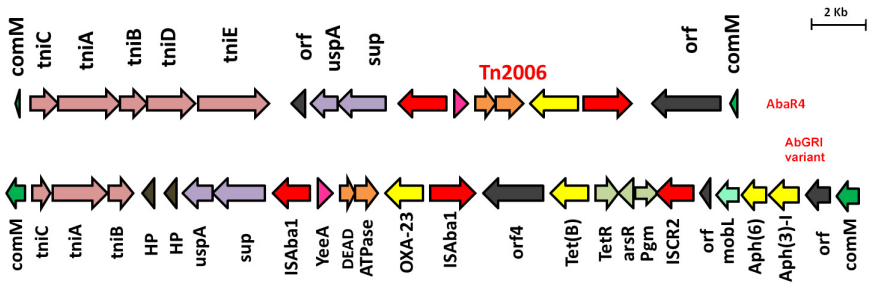

FIGURE 3 | Structures of AbaR4 and variants of AbGRI1 identified in this study. The top figure depicts the typical AbaR4 island, while the bottom figure indicates the AbGRI1 variant due to additional *mobL* (light green arrow) and arsenic resistance gene, *arsR* (light gray arrow). The yellow arrow indicates antimicrobial resistance genes, and the red arrow depicts insertion elements.

AB13 was found to carry a class 1 integron but was devoid of bla_{PER-7} (**Figure 5B**).

IC7 and IC8–the Emerging Lineage of CRAb Isolates in India

Two genomes, namely, AB14 and AB15, belonged to IC7 and were represented by ST1388 ^{Oxf}/ST25^{Pas} and ST691 ^{Oxf}/ST25^{Pas}, and both were XDR. AB14 and AB15 carried three and two plasmids, respectively. AB14 harbored bla_{OXA-23} in Tn*2006* on the chromosome alone, whereas AB15 had it in both the chromosome (bla_{OXA-23} in Tn*2006*) and on an incomplete RepB family plasmid (bla_{OXA-23} in △Tn*2006*). Both AB14 and AB15 showed the presence of two prophage regions, namely, PHAGE_Mannhe_vB_MhM_3927AP2_NC_028766 and PHAGE_Acinet_YMC11/11/R3177_NC_041866. AbaR4 that were mapped to Tn*6022* backbone and Tn*2006* linked bla_{OXA-23} locus was present in both the genomes (**Figure 3**).

AB10, AB11, and AB23 belonged to IC8. Of the three, AB10 and AB11 were XDR and corresponded to novel STs: ST2392 ^{Oxf}/ST586^{Pas} (AB10) and ST2441 ^{Oxf}/ST575^{Pas} (AB11), whereas AB23 corresponded to ST447^{Oxf}/ST10^{Pas} and had an MDR phenotype. AB10 and AB11 were bla_{OXA-23} producers, while AB23 was found to be a non-carbapenemase producer. Two, one, and three plasmids were identified in AB10, AB11, and AB23, respectively. Three intact prophages such as PHAGE_Pelagi_HTVC010P_NC_020481, PHAGE_Acinet_Bphi_B1251_NC_019541, and PHAGE_Acinet_vB_AbaS_TRS1_NC_031098 were seen in AB10. In AB11, PHAGE_Acinet_YMC11/11/R3177_NC_041866, PHAGE_Acinet_Bphi_B1251_NC_019541, and PHAGE_Mannhe_vB_MhM_3927AP2_NC_028766 were observed. A single prophage, PHAGE_Acinet_Bphi_B1251_NC_019541, was present in AB23. Similar to IC7, both XDR isolates carried AbaR4 on the chromosome but were absent in the MDR isolate, AB23 (**Figure 3**).

IC1 Lineage With Tn6022-Derived Elements

AB28 had an XDR phenotype that corresponded to ST231 ^{Oxf}/ST1^{Pas} and belonged to IC1. Interestingly, in AB28, which carried a variant of bla_{OXA-51} ($bla_{OXA-371}$), an insertion of IS*Aba16*, TnpB, and an IS66 transposase, there was no upstream presence or insertional inactivation (**Figure 6**). AB28 carried Tn*125* linked bla_{NDM-1} on the chromosome (**Figure 2A**). AB28 harbored six plasmids. Of which, p1AB28 carried bla_{OXA-23} on *rep*Aci6 family plasmid and several plasmid transfer (*tra*) genes. When we analyzed and compared the p1AB28 plasmid sequence with the reference plasmid, pA85-3 (accession number–KJ493819), we found the presence of a complete bla_{OXA-23} gene with one complete and an incomplete copy of an IS*Aba1* locus. However, some transposon-related genes such as *uspA* and *sulP* were intact. IS66 family transposase with its accessory protein, *tnpB*, was also encoded within the p1AB28 plasmid but was absent in the pA85-3 reference plasmid. The plasmid, p1AB28, also carried putative *tra* genes that are required for mating pair formation and *trwC* and *trwB* genes that are needed for plasmid mobilization (**Figure 7**). AB28 carried five different prophages as follows: PHAGE_Stx2_c_Stx2a_F451_NC_049924, PHAGE_Acinet_Bphi_B1251_NC_019541, PHAGE_Psychr_pOW20_A_NC_020841, PHAGE_Escher_SH2026Stx1_NC_049919, and PHAGE_Acinet_vB_AbaS_TRS1_NC_031098. Notably, AB28 encoded Tn*6022*-derived elements in which the insertion of an IS256 family transposase, IS*Aba42*, was observed between *tniE* and *orf* [Tn*6022* (*tniE-orf*)::IS*Aba42*] (**Figure 8**).

Pan-Susceptible Singleton and Pan-Drug Resistant CC862

The PSAB, AB01 represented as a singleton and belonged to the novel ST, ST2439 ^{Oxf}/ST285^{Pas}, while the PDRAB, AB06 belonged to CC862 and was represented by another novel ST, ST2440 ^{Oxf}/ST622^{Pas}. As expected, AB01 did not harbor any of the AMR determinants except $bla_{ADC-25-like}$, $bla_{OXA-337}$. Three plasmids were present with no AMR genes. No intact prophage and RI were present.

AB06 carried dual carbapenemases, bla_{OXA-23} and bla_{NDM-1}, on the chromosome, and they were found to be carried on transposon, Tn*2006*, and Tn*125*, respectively. Two plasmids were observed with genes encoding resistance to β-lactamases, aminoglycosides, macrolides, and sulfonamides. Three intact prophages, PHAGE_Pseudo_phiCTX_NC_003278, PHAGE_Acinet_Bphi_B1251_NC_019541, and PHAGE_

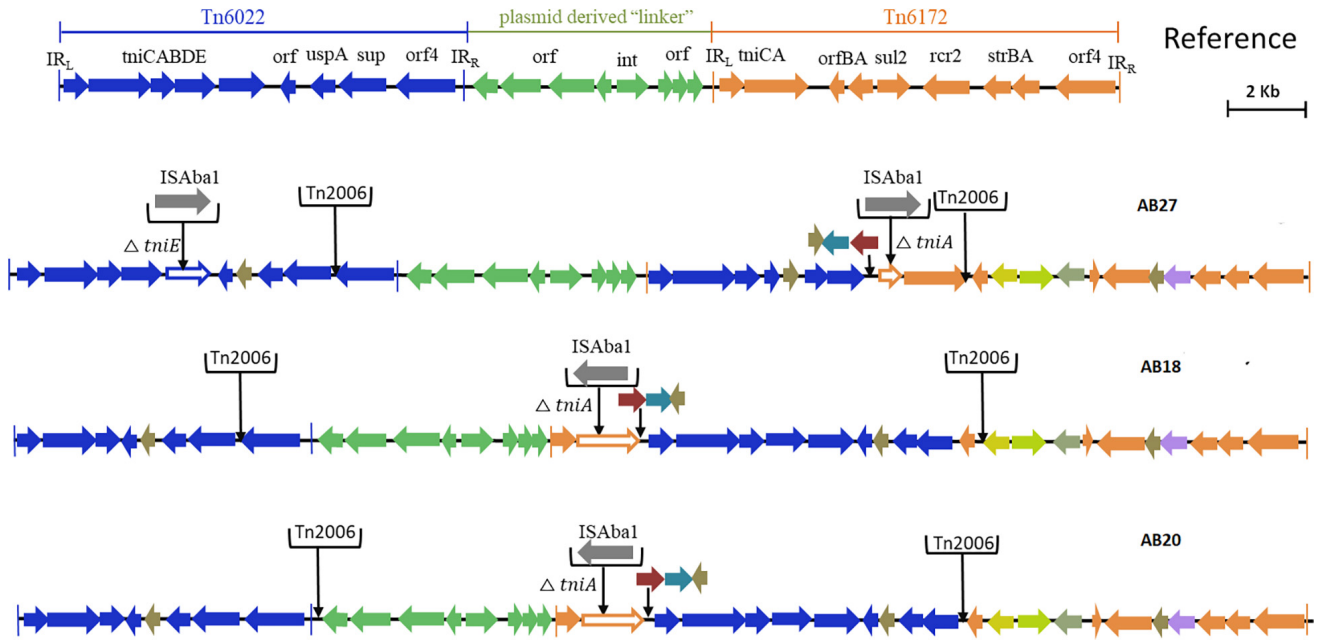

FIGURE 4 | Structures of variants of AbGRI resistance island identified in this study. The typical AbGRI1 structure with an intact "Tn*6022*-linker-Tn*6172*" backbone is shown as a reference. The Tn*6022* or Tn*6022*-derived part is shown in blue, the Tn*6172* part or its partial segments are shown in orange, and the linker region is shown in green. The black arrows shown downward indicate the insertion of insertion sequence (IS) element or transposon or additional genes.

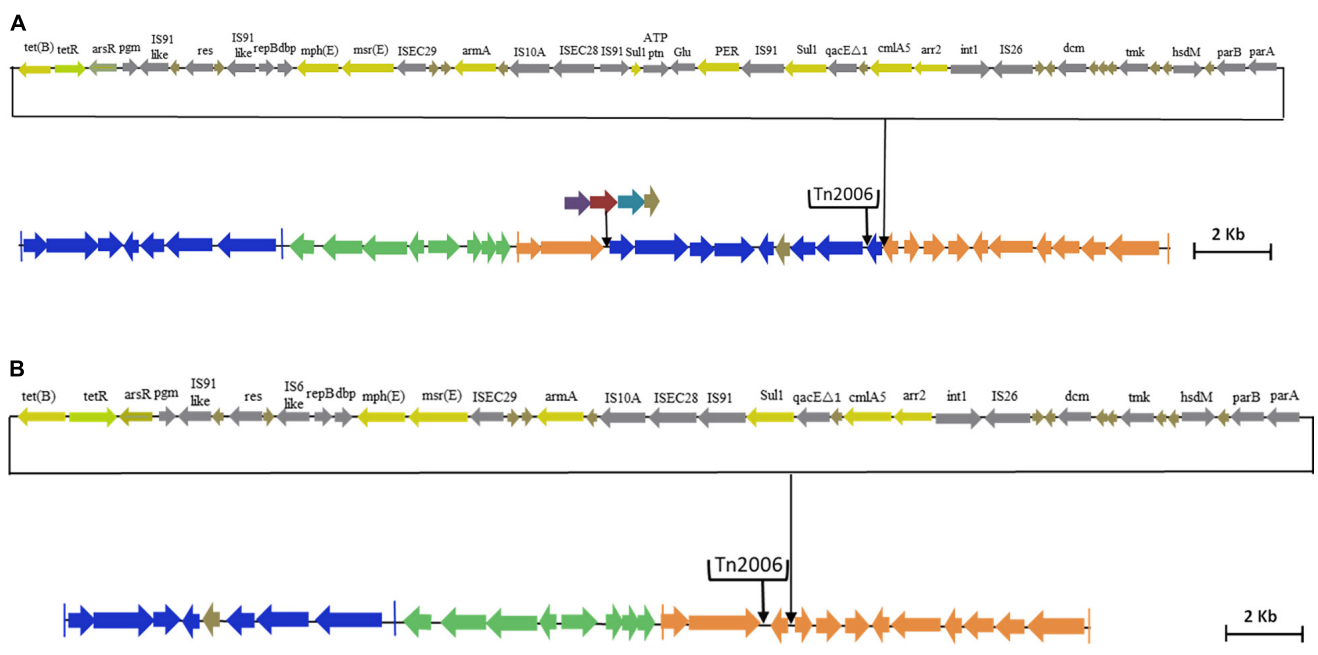

FIGURE 5 | (A) Genetic backbone of AB13 carrying AbGRI variant identified in this study. The Tn*6022* or Tn*6022*-derived part is shown in blue, the Tn*6172* part or its partial segments are shown in orange, and the linker region is shown in green. The black arrows in the downward direction indicate the insertion of IS element, transposon, or additional genes. The pale yellow arrow indicates AMR genes, the light green arrow represents the tetracycline repressor gene, the gray arrow represents insertion elements, and the brown arrow indicates hypothetical protein. **(B)** Genetic backbone of AB02 carrying AbGRI variant identified in this study. The Tn*6022* or Tn*6022*-derived part is shown in blue, the Tn*6172* part or its partial segments are shown in orange, and the linker region is shown in green. The black arrows shown downward indicate the insertion of IS element or transposon or additional genes. The pale yellow arrow indicates AMR genes, the light green arrow represents the tetracycline repressor gene, the gray arrow represents insertion elements, and the brown arrow indicates hypothetical protein.

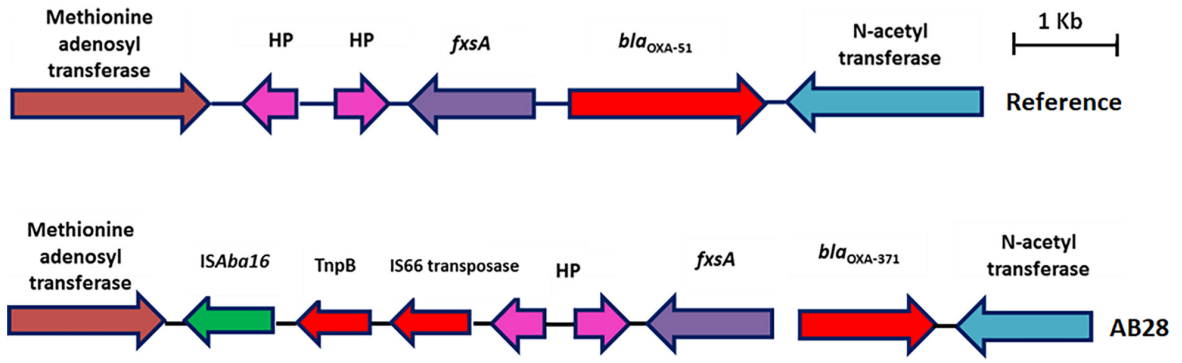

FIGURE 6 | Genetic backbone of bla_{OXA-51}. Two types of genetic structures were identified in this study. Sixteen isolates were identified with typical backbone, whereas one isolate with $bla_{OXA-371}$ was identified with insertion sequence, IS*Aba16*, TnpB, and IS66 family transposase.

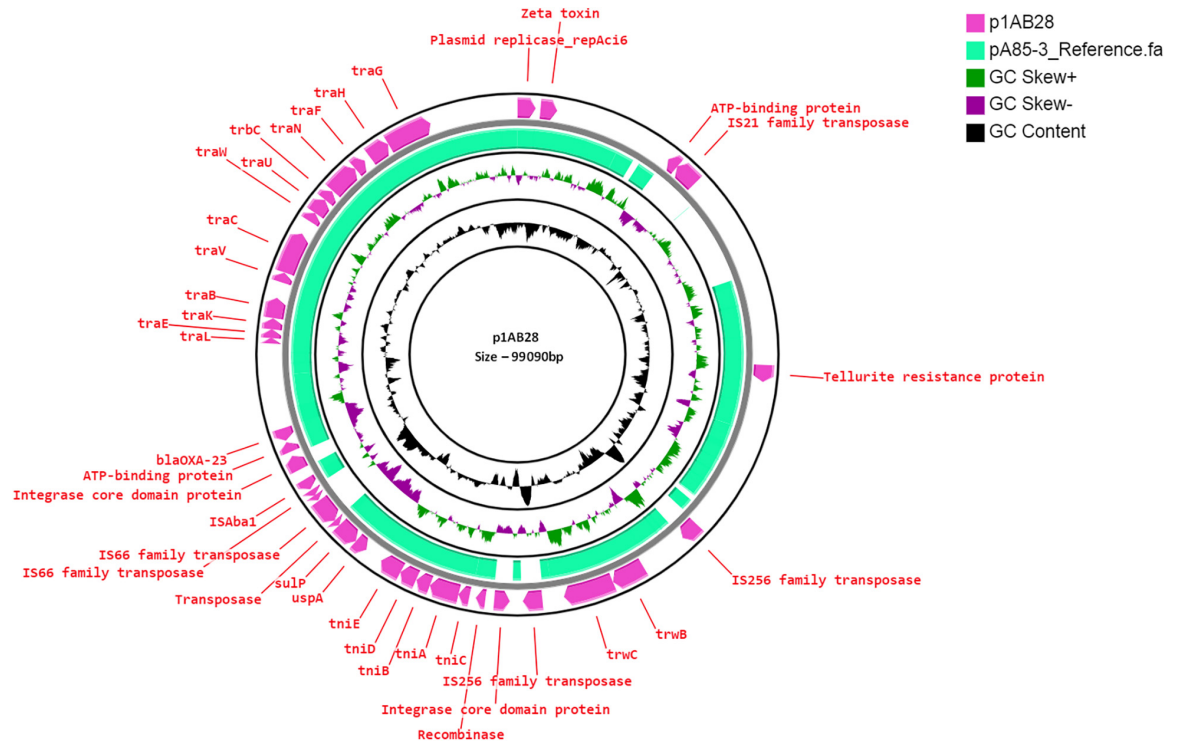

FIGURE 7 | Circular representation of *rep*Aci6 plasmid (pink arrow), p1AB28, of *Acinetobacter baumannii* displayed using CG view server with the reference plasmid pA85-3 (accession number–KJ493819) (green-colored region). The two inner circles represent GC content and GC skew. The pink-colored arrow represents the presence of the OXA-23 gene along with the plasmid replication gene, repAci6, *tra* genes, and plasmid mobilization genes in p1AB28.

Acinet_YMC11/11/R3177_NC_041866, were present. In addition, AB06 possesses the commonly reported AbaR4 RI (**Figure 3**).

Phylogenetic Analysis of Core Genomes of CRAb

Analysis of core genomes of CRAb revealed the presence of multiple AMR genes among the IC2 isolates. Clone-specific OCL types such as OCL1 to IC2, OCL5 to IC7, and OCL2 to IC8 were observed. Diverse KL types were identified among the study isolates, and the tree showed the presence of ST-specific KL types within a specific clonal lineage. AbaR4 was present among the IC1, IC7, and IC8 isolates, while AbaR4 and AbGRI variants were observed only among the IC2 isolates (**Figure 9**).

DISCUSSION

Acinetobacter baumannii has become an important hospital-acquired pathogen and is of major concern due to the rapid

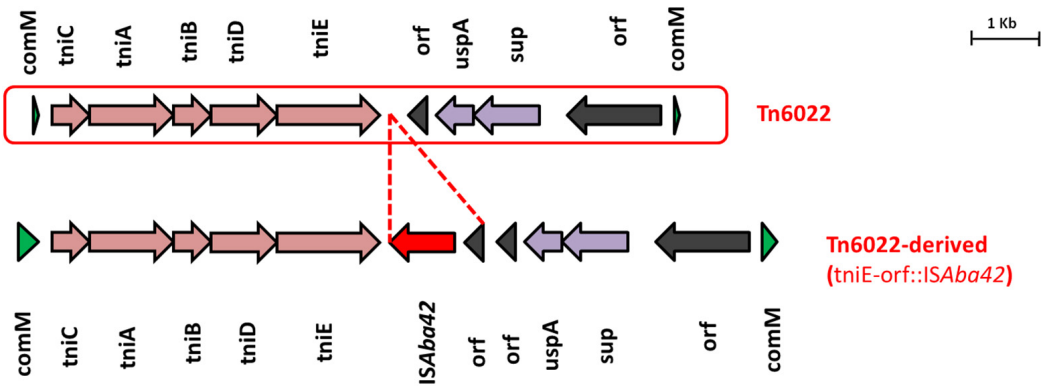

FIGURE 8 | Structures of Tn*6022* and Tn*6022*-like elements. The typical Tn*6022* backbone is shown at the top of the figure. Tn*6022*-derived element observed in this study is displayed at the bottom of the figure and showed the insertion of IS*Aba42* (red arrow) with an additional *orf*. Appropriate names of the elements found within the genetic configurations are given. Dotted lines in red are used to depict the insertion of genetic elements.

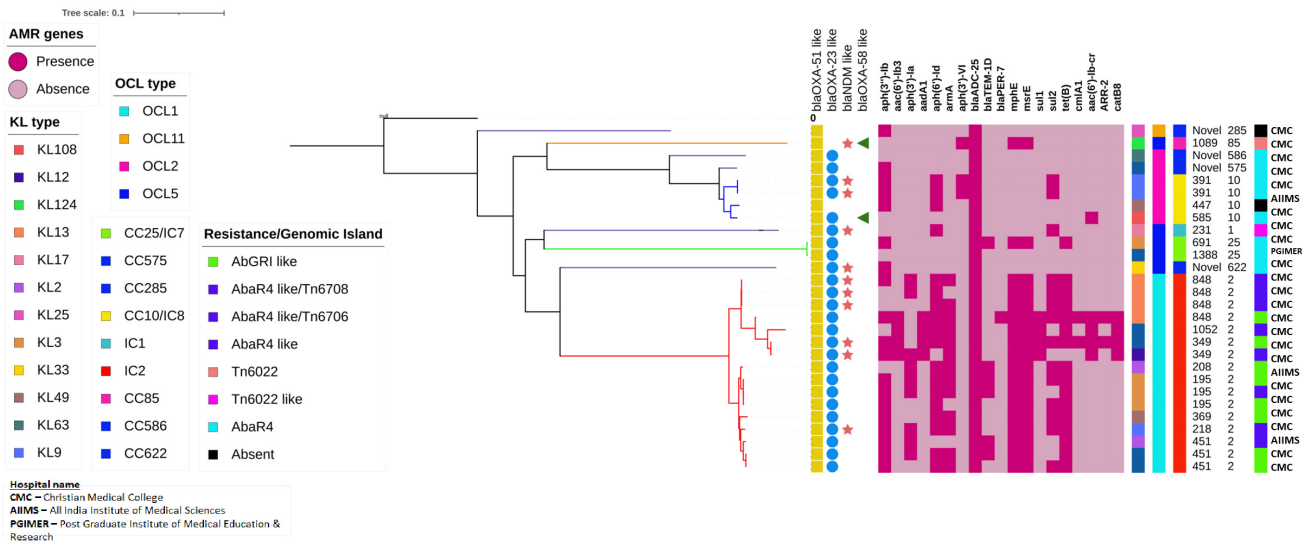

FIGURE 9 | Single nucleotide polymorphism (SNP)-based phylogenetic tree of carbapenem-resistant *Acinetobacter baumannii* sequenced in this study. The color-filled shape denoted presence, while the empty shape denoted the absence of the respective traits. The heat map represents the presence or absence of AMR genes; Dark red indicates the presence of the respective gene, while light red indicates the lack of the respective gene. The capsular types (KL), outer core lipopolysaccharide types (OCL), International clones/clonal complexes, and resistance/genomic islands of the CRAb isolates were represented by color-coded boxes as given in the legend. The Oxford and Pasteur scheme sequence types (STs) were given as text labels.

emergence of MDR, XDR, and PDR strains (Agoba et al., 2018; Havenga et al., 2019). Carbapenem resistance rates of more than 85% in *A. baumannii* have been reported from previous studies in India and are typically associated with isolates carrying either bla_{OXA-23} alone or both bla_{OXA-23} and bla_{NDM-1}, which concurs with this study (Vijayakumar et al., 2016; Vijayakumar et al., 2019; Vijayakumar et al., 2020). The majority of the isolates (13/17) in this study encoded more than one copy of the bla_{OXA-23} gene. However, we could not find any high-level carbapenem resistance genes in these isolates. Earlier, Hua et al. (2016) reported the presence of multiple copies of bla_{OXA-23} among CRAb as a common phenomenon without an increase in carbapenem resistance.

This study showed the endemicity of IC2 along with the emergence of sporadic clones, such as IC7 and IC8. Although previous studies from India reported the predominance of IC2, the presence of isolates that belongs to IC7 and IC8 indicates the dissemination of CRAb and reinforces the fact that the International clones of CRAb isolates are widespread among hospitals in India.

Several studies have reported that the bla_{OXA-23} gene has relocated to chromosomes and plasmids with the help of transposons (Hamidian and Nigro, 2019; Graña-Miraglia et al., 2020). Fourteen CRAb isolates were identified with Tn*2006*-linked bla_{OXA-23} in this study. Although experimental observations were not performed, carbapenem resistance

in these isolates could be due to the IS*Aba1*-mediated overexpression of the bla_{OXA-23} gene in Tn*2006*. Occasionally, carbapenem resistance in *A. baumannii* could happen due to the overexpression of bla_{OXA-51} variants by insertion of IS*Aba1* (Wong et al., 2019). In this study, the presence of IS*Aba16* was observed in one genome; however, insertional inactivation of $bla_{OXA-51-like}$ was not seen.

In *A. baumannii*, *the* bla_{NDM-1} gene can be encoded by either chromosomes or plasmids (Bonnin et al., 2012). However, this study observed *A. baumannii* isolates harboring bla_{NDM-1} only in chromosomes. Unlike *Enterobacteriaceae*, in which bla_{NDM-1} is often observed with a single copy of truncated IS*Aba125* on plasmids, the dissemination of bla_{NDM-1} in *A. baumannii* is always associated with a complete Tn*125* (Poirel et al., 2012; Dortet et al., 2014). In contrast with the above statement, one genome in this study was identified with Tn*125-*$_{like}$ linked bla_{NDM-1}, suggesting that it could have acquired bla_{NDM-1} from other species.

The presence of *rep*Aci6 harboring bla_{OXA-23} and belonging to IC1 was identified in the p1AB28 plasmid. Comparative analysis revealed that AB28 carries a plasmid closely related to the reference, as it harbors *the* bla_{OXA-23} gene in a different context (Hamidian et al., 2016). The p1AB28 plasmid is conjugative and can spread carbapenem resistance by disseminating the bla_{OXA-23} gene into diverse clones. However, further studies are warranted to confirm the same. Another genome, AB20, belonged to IC2 and carried a *rep*Aci6 conjugative plasmid. This plasmid harbors the *aphA6* gene on the Tn*aphA6* transposon which encodes an aminoglycoside (3′) phosphotransferase and confers resistance to amikacin. Previous studies from European and Asian countries have reported isolates of *A. baumannii* with large conjugative plasmid such as rep*Aci6*, carrying both the bla_{OXA-23} and *aphA6* genes, which contribute to the dissemination of resistance to carbapenems and amikacin, respectively (Towner et al., 2011; Nigro and Hall, 2016). Earlier studies by Costa et al. (2018) reported the presence of AMR and virulence genes within the prophage regions of *A. baumannii* genomes. This study showed at least one prophage region in all the genomes except the PSAB. However, no prophages with AMR genes were detected.

Genomic analysis of AbaRs in this study unveiled novel genetic configurations specific to backbones, which involve either insertion of MGEs or structural modifications driven by known MGEs. For example, insertion of IS*Aba42* within the Tn*6022* backbone leads to a truncated form of the *tniE* transposition gene, thereby forming the Tn*6022* derived element. Furthermore, in this study, we identified an isolate (AB28) that belonged to IC1 but lacked an AbaR3 type island. Instead, it carried an IC2-specific Tn*6022*-derived backbone, which indicates the possibility of independent acquisition. Tn*6022*-derived elements and AbaR4 and AbGRI variants are typically confined to IC2. In this study, we also found that none of the IC2 isolates carried AbaR4; instead, it was present among isolates belonging to other ICs such as IC7 and IC8. All the study isolates belonging to IC2 possessed either the AbGRI1 variant or the AbGRI variant with complex chimeric structures. Although the genetic events behind this process are unclear, such complex structural variation in the AbaR backbones might have resulted either due to the target sequences favorable for MGE insertion or due to the exposure of AbaRs with different MGEs in different clones. These findings indicate that AbaRs with diverse backbones might have evolved separately.

CONCLUSION

Overall, to the best of our knowledge, this study is the first that provides comprehensive profiling of RIs together with the MGEs, acquired AMR genes, and the distribution of clonal lineages among CRAb from India. Although this study provides a clear picture of the Indian scenario, further comparative analysis with an extensive collection of global isolates is required to understand the structural diversity and the evolution of these MGEs that drive the genome plasticity of *A. baumannii*.

DATA AVAILABILITY STATEMENT

The datasets presented in this study can be found in online repositories. The names of the repository/repositories and accession number(s) can be found in the article/**Supplementary Material**.

AUTHOR CONTRIBUTIONS

SV: laboratory methods, data analysis and interpretation, and manuscript writing. JJ: data analysis, interpretation, and manuscript writing. KV: hybrid genome assembly and other bioinformatics methods. PM, PR, SA, IB, and KW: manuscript correction. AN and AB: data analysis. BV: study design and supervising, manuscript writing, and manuscript correction. All authors contributed to the article and approved the submitted version.

ACKNOWLEDGMENTS

We would like to acknowledge Ms. Catherine Truman, Clinical Pharmacist, Christian Medical College and Hospital, India, for her valuable input in language editing.

SUPPLEMENTARY MATERIAL

The Supplementary Material for this article can be found online at: https://www.frontiersin.org/articles/10.3389/fmicb.2022.869653/full#supplementary-material

Supplementary Figure 1 | A map of India showing the location of three hospitals from where the samples were collected as a part of the study. The red color represents PGIMER, Chandigarh, the green color represents AIIMS-Trauma, New Delhi, and the light red color represents CMC, Vellore. Map outline was created using mapchart.net. Republished from mapchart.net under a CC BY license, with permission from MapChart, original copyright 2021.

REFERENCES

Agoba, E. E., Govinden, U., Peer, A. K., Osei Sekyere, J., and Essack, S. Y. (2018). IS Aba1 regulated OXA-23 carbapenem resistance in *Acinetobacter baumannii* strains in Durban, South Africa. *Microb. Drug Resist.* 24, 1289–1295. doi: 10.1089/mdr.2017.0172

Bonnin, R. A., Poirel, L., Naas, T., Pirs, M., Seme, K., Schrenzel, J., et al. (2012). Dissemination of New Delhi metallo-β-lactamase-1-producing *Acinetobacter baumannii* in Europe. *Clin. Microbiol. Infect.* 18, E362–E365.

Cameranesi, M. M., Paganini, J., Limansky, A. S., Moran-Barrio, J., Salcedo, S. P., Viale, A. M., et al. (2020). Acquisition of plasmids conferring carbapenem and aminoglycoside resistance and loss of surface-exposed macromolecule structures as strategies for the adaptation of *Acinetobacter baumannii* CC104O/CC15P strains to the clinical setting. *Microbial Genom.* 6:mgen000360. doi: 10.1099/mgen.0.000360

Costa, A. R., Monteiro, R., and Azeredo, J. (2018). Genomic analysis of *Acinetobacter baumannii* prophages reveals remarkable diversity and suggests profound impact on bacterial virulence and fitness. *Sci. Rep.* 8:15346.

Croucher, N. J., Page, A. J., Connor, T. R., Delaney, A. J., Keane, J. A., Bentley, S. D., et al. (2015). Rapid phylogenetic analysis of large samples of recombinant bacterial whole genome sequences using Gubbins. *Nucleic Acids Res.* 43:e15. doi: 10.1093/nar/gku1196

Dexter, C., Murray, G. L., Paulsen, I. T., and Peleg, A. Y. (2015). Community-acquired *Acinetobacter baumannii*: clinical characteristics, epidemiology, and pathogenesis. *Expert Rev. Anti-infective Therapy* 13, 567–573. doi: 10.1586/14787210.2015.1025055

Dortet, L., Poirel, L., and Nordmann, P. (2014). Worldwide dissemination of the NDM-type carbapenemases in Gram-negative bacteria. *BioMed Res. Int.* 2014:249856. doi: 10.1155/2014/249856

Ershov, V., Tarasov, A., Lapidus, A., and Korobeynikov, A. (2019). IonHammer: homopolymer-space hamming clustering for IonTorrent read error correction. *J. Comput. Biol.* 26, 124–127. doi: 10.1089/cmb.2018.0152

Gales, A. C., Seifert, H., Gur, D., Castanheira, M., Jones, R. N., and Sader, H. S. (2019). Antimicrobial susceptibility of Acinetobacter calcoaceticus–*Acinetobacter baumannii* complex and *Stenotrophomonas* maltophilia clinical isolates: results from the SENTRY antimicrobial surveillance program (1997–2016). *Open Forum Infectious Dis.* 6, S34–S46.

Graña-Miraglia, L., Evans, B. A., López-Jácome, L. E., Hernández-Durán, M., Colín-Castro, C. A., Volkow-Fernández, P., et al. (2020). Origin of OXA-23 variant OXA-239 from a recently emerged lineage of *Acinetobacter baumannii* international clone V. *mSphere* 5:e00801-19. doi: 10.1128/mSphere.00801-19

Hamidian, M., Ambrose, S. J., and Hall, R. M. (2016). A large conjugative *Acinetobacter baumannii* plasmid carrying the sul2 sulphonamide and strAB streptomycin resistance genes. *Plasmid* 87, 43–50. doi: 10.1016/j.plasmid.2016.09.001

Hamidian, M., and Hall, R. M. (2017). Origin of the AbGRI1 antibiotic resistance island found in the comM gene of *Acinetobacter baumannii* GC2 isolates. *J. Antimicrobial Chemotherapy* 72, 2944–2947. doi: 10.1093/jac/dkx206

Hamidian, M., and Hall, R. M. (2011). AbaR4 replaces AbaR3 in a carbapenem-resistant *Acinetobacter* baumannii isolate belonging to global clone 1 from an Australian hospital. *J. Antimicrob. Chemother.* 1, 2484–2491. doi: 10.1093/jac/dkr356

Hamidian, M., and Hall, R. M. (2018). The AbaR antibiotic resistance islands found in *Acinetobacter baumannii* global clone 1–structure, origin and evolution. *Drug Resist. Updat* 41, 26–39.

Hamidian, M., and Nigro, S. J. (2019). Emergence, molecular mechanisms and global spread of carbapenem-resistant *Acinetobacter baumannii*. *Microbial Genom.* 5:e000306. doi: 10.1099/mgen.0.000306

Havenga, B., Ndlovu, T., Clements, T., Reyneke, B., Waso, M., and Khan, W. (2019). Exploring the antimicrobial resistance profiles of WHO critical priority list bacterial strains. *BMC Microbiol.* 19:303. doi: 10.1186/s12866-019-1687-0

Hernández-González, I. L., Mateo-Estrada, V., and Castillo-Ramirez, S. (2022). The promiscuous and highly mobile resistome of *Acinetobacter baumannii*. *Microbial Genom.* 8:000762. doi: 10.1099/mgen.0.000762

Hua, X., Shu, J., Ruan, Z., Yu, Y., and Feng, Y. (2016). Multiplication of blaOXA-23 is common in clinical *Acinetobacter baumannii*, but does not enhance carbapenem resistance. *J. Antimicrobial Chemotherapy* 71, 3381–3385. doi: 10.1093/jac/dkw310

Lee, C. R., Lee, J. H., Park, M., Park, K. S., Bae, I. K., Kim, Y. B., et al. (2017). Biology of *Acinetobacter baumannii*: pathogenesis, antibiotic resistance mechanisms, and prospective treatment options. *Front. Cell. Infect. Microbiol.* 7:55. doi: 10.3389/fcimb.2017.00055

Letunic, I., and Bork, P. (2021). Interactive Tree Of Life (iTOL) v5: an online tool for phylogenetic tree display and annotation. *Nucleic Acids Res.* 49, W293–W296. doi: 10.1093/nar/gkab301

Mancilla-Rojano, J., Castro-Jaimes, S., Ochoa, S. A., Bobadilla, del Valle, M., Luna-Pineda, V. M., et al. (2019). Whole-genome sequences of five *Acinetobacter baumannii* strains from a child with leukemia M2. *Front. Microbiol.* 10:132. doi: 10.3389/fmicb.2019.00132

Nigro, S. J., and Hall, R. M. (2016). Structure and context of Acinetobacter transposons carrying the OXA-23 carbapenemase gene. *J. Antimicrobial Chemotherapy* 71, 1135–1147.

O'Donnell, J. N., Putra, V., and Lodise, T. P. (2021). Treatment of patients with serious infections due to carbapenem-resistant *Acinetobacter baumannii*: how viable are the current options? *Pharmacotherapy: J. Hum. Pharmacol. Drug Therapy* 41, 762–780. doi: 10.1002/phar.2607

Pagano, M., Martins, A. F., and Barth, A. L. (2016). Mobile genetic elements related to carbapenem resistance in *Acinetobacter baumannii*. *Braz. J. Microbiol.* 47, 785–792. doi: 10.1016/j.bjm.2016.06.005

Parks, D. H., Imelfort, M., Skennerton, C. T., Hugenholtz, P., and Tyson, G. W. (2015). CheckM: assessing the quality of microbial genomes recovered from isolates, single cells, and metagenomes. *Genome Res.* 25, 1043–1055. doi: 10.1101/gr.186072.114

Poirel, L., and Nordmann, P. (2006). Carbapenem resistance in *Acinetobacter baumannii*: mechanisms and epidemiology. *Clin. Microbiol. Infect.* 12, 826–836.

Poirel, L., Bonnin, R. A., Boulanger, A., Schrenzel, J., Kaase, M., and Nordmann, P. (2012). Tn125-related acquisition of blaNDM-like genes in *Acinetobacter baumannii*. *Antimicrob. Agents Chemother.* 56, 1087–1089. doi: 10.1128/AAC.05620-11

Poirel, L., Marqué, S., Héritier, C., Segonds, C., Chabanon, G., and Nordmann, P. (2005). OXA-58, a novel class D β-lactamase involved in resistance to carbapenems in *Acinetobacter baumannii*. *Antimicrob. Agents Chemother.* 49, 202–208.

Price, M. N., Dehal, P. S., and Arkin, A. P. (2010). FastTree 2–approximately maximum-likelihood trees for large alignments. *PLoS One* 5:e9490. doi: 10.1371/journal.pone.0009490

Roca, J., Subirà, I., Espinal, P., Vila-Farrés, X., and Vila Estapé, J. (2012). The *Acinetobacter baumannii* oxymoron: commensal hospital dweller turned pan-drug-resistant menace. *Front. Microbiol.* 3:148. doi: 10.3389/fmicb.2012.00148

Rodrigues, D. L., Morais-Rodrigues, F., Hurtado, R., Dos Santos, R. G., Costa, D. C., Barh, D., et al. (2021). Pan-resistome insights into the multidrug resistance of *Acinetobacter baumannii*. *Antibiotics* 10:596. doi: 10.3390/antibiotics10050596

Salto, I. P., Tejerizo, G. T., Wibberg, D., Pühler, A., Schlüter, A., and Pistorio, M. (2018). Comparative genomic analysis of *Acinetobacter spp*. plasmids originating from clinical settings and environmental habitats. *Sci. Rep.* 8:7783. doi: 10.1038/s41598-018-26180-3

Seemann, T. (2015). *Snippy: Fast Bacterial Variant Calling from NGS Reads*. San Francisco, CA: GitHub.

Towner, K. J., Evans, B., Villa, L., Levi, K., Hamouda, A., Amyes, S. G., et al. (2011). Distribution of intrinsic plasmid replicase genes and their association with carbapenem-hydrolyzing class D β-lactamase genes in European clinical isolates of *Acinetobacter baumannii*. *Antimicrob. Agents Chemother.* 55, 2154–2159. doi: 10.1128/AAC.01661-10

Turton, J. F., Ward, M. E., Woodford, N., Kaufmann, M. E., Pike, R., Livermore, D. M., et al. (2006a). The role of ISAba1 in expression of OXA carbapenemase genes in *Acinetobacter baumannii*. *FEMS Microbiol. Lett.* 258, 72–77. doi: 10.1111/j.1574-6968.2006.00195.x

Turton, J. F., Woodford, N., Glover, J., Yarde, S., Kaufmann, M. E., and Pitt, T. L. (2006b). Identification of *Acinetobacter baumannii* by detection of the blaOXA-51-like carbapenemase gene intrinsic to this species. *J. Clin. Microbiol.* 44, 2974–2976. doi: 10.1128/JCM.01021-06

Vijayakumar, S., Anandan, S., Prabaa, D., Kanthan, K., Vijayabaskar, S., Kapil, A., et al. (2019). Insertion sequences and sequence types profile of clinical isolates

of carbapenem-resistant *A. baumannii* collected across India over four year period. *J. Infect. Public Health* 23, 1022–1028. doi: 10.1016/j.jiph.2019.11.018

Vijayakumar, S., Gopi, R., Gunasekaran, P., Bharathy, M., Walia, K., Anandan, S., et al. (2016). Molecular characterization of invasive carbapenem-resistant *Acinetobacter baumannii* from a tertiary care hospital in South India. *Infect. Dis. Therapy* 5, 379–387. doi: 10.1007/s40121-016-0125-y

Vijayakumar, S., Wattal, C., Oberoi, J. K., Bhattacharya, S., Vasudevan, K., Anandan, S., et al. (2020). Insights into the complete genomes of carbapenem-resistant *Acinetobacter baumannii* harbouring blaOXA-23, blaOXA-420 and blaNDM-1 genes using a hybrid-assembly approach. *Access Microbiol.* 2:acmi000140. doi: 10.1099/acmi.0.000140

Walker, B. J., Abeel, T., Shea, T., Priest, M., Abouelliel, A., Sakthikumar, S., et al. (2014). Pilon: an integrated tool for comprehensive microbial variant detection and genome assembly improvement. *PLoS One* 9:e112963. doi: 10.1371/journal.pone.0112963

Weinstein, M. P., Patel, J. B., and Bobenchik, A. M. (2018). *Performance Standards for Antimicrobial Susceptibility Testing*. Wayne, PA: Clinical, and Laboratory Standards Institute.

Weinstein, M. P., Patel, J. B., Bobenchik, A. M., Campeau, S., Cullen, S. K., and Gallas, M. F. (2019). *Performance Standards for Antimicrobial Susceptibility Testing*. Wayne, PA: Clinical and laboratory standards institute.

Wick, R. R., Judd, L. M., Gorrie, C. L., and Holt, K. E. (2017a). Completing bacterial genome assemblies with multiplex MinION sequencing. *Microbial Genom.* 3:e000132. doi: 10.1099/mgen.0.000132

Wick, R. R., Judd, L. M., Gorrie, C. L., and Holt, K. E. (2017b). Unicycler: resolving bacterial genome assemblies from short and long sequencing reads. *PLoS Comp. Biol.* 13:e1005595. doi: 10.1371/journal.pcbi.1005595

Wong, M. H., Chan, B. K., Chan, E. W., and Chen, S. (2019). Over-expression of ISAba1-linked intrinsic and exogenously acquired OXA type carbapenem-hydrolyzing-class D-ß-lactamase-encoding genes is key mechanism underlying carbapenem resistance in *Acinetobacter baumannii*. *Front. Microbiol.* 10:2809. doi: 10.3389/fmicb.2019.02809

Conflict of Interest: The authors declare that the research was conducted in the absence of any commercial or financial relationships that could be construed as a potential conflict of interest.

Publisher's Note: All claims expressed in this article are solely those of the authors and do not necessarily represent those of their affiliated organizations, or those of the publisher, the editors and the reviewers. Any product that may be evaluated in this article, or claim that may be made by its manufacturer, is not guaranteed or endorsed by the publisher.

frontiers | Frontiers in Microbiology

ORIGINAL RESEARCH
published: 22 July 2022
doi: 10.3389/fmicb.2022.878912

Genetic Configuration of Genomic Resistance Islands in *Acinetobacter baumannii* Clinical Isolates From Egypt

Samira M. Hamed[1], *Amira F. A. Hussein*[2], *Mohamed H. Al-Agamy*[3,4], *Hesham H. Radwan*[3] *and Mai M. Zafer*[5]*

[1] Department of Microbiology and Immunology, Faculty of Pharmacy, October University for Modern Sciences and Arts (MSA), Giza, Egypt, [2] Department of Clinical and Chemical Pathology, Faculty of Medicine, Cairo University, Cairo, Egypt, [3] Department of Pharmaceutics, College of Pharmacy, King Saud University, Riyadh, Saudi Arabia, [4] Department of Microbiology and Immunology, Faculty of Pharmacy, Al-Azhar University, Cairo, Egypt, [5] Department of Microbiology and Immunology, Faculty of Pharmacy, Ahram Canadian University, Cairo, Egypt

In *Acinetobacter baumannii* (*A. baumannii*), a wide repertoire of resistance genes is often carried within genomic resistance islands (RIs), particularly in high-risk global clones (GCs). As the first in Egypt, the current study aimed at exploring the diversity and genetic configuration of RIs in the clinical isolates of *A. baumannii*. For this purpose, draft genomes of 18 isolates were generated by Illumina sequencing. Disk diffusion susceptibility profiling revealed multidrug resistance (MDR) and extensive drug resistance (XDR) phenotypes in 27.7 and 72.2%, respectively. The highest susceptibility was noted for tigecycline (100.0%) followed by colistin (94.4%), for which an MIC_{50} of 0.25 μg/ml was recorded by the broth microdilution assay. Sequence typing (ST) showed that the majority of the isolates belonged to high-risk global clones (GC1, GC2, and GC9). A novel Oxford sequence type (ST2329) that also formed a novel clonal complex was submitted to the PubMLST database. A novel bla_{ADC} variant ($bla_{ADC-258}$) was also identified in strain M18 ($ST85^{Pas}/1089^{Oxf}$). In addition to a wide array of resistance determinants, whole-genome sequencing (WGS) disclosed at least nine configurations of genomic RIs distributed over 16/18 isolates. GC2 isolates accumulated the largest number of RIs (three RIs/isolate) followed by those that belong to GC1 (two RIs/isolate). In addition to Tn*6022* (44.4%), the *comM* gene was interrupted by AbaR4 (5.5%) and three variants of *A. baumannii* genomic resistance island 1(AbGRI)-type RIs (44.4%), including AbaR4b (16.6%) and two novel configurations of AbGRI1-like RIs (22.2%). Three of which (AbaR4, AbaR4b, and AbGRI1-like-2) carried bla_{OXA-23} within Tn*2006*. With less abundance (38.8%), IS*26*-bound RIs were detected exclusively in GC2 isolates. These included a short version of AbGRI2 (AbGRI2-15) carrying the genes bla_{TEM-1} and *aphA1* and two variants of AbGRI3 RIs carrying up to seven resistance genes [*mphE-msrE-armA-sul1-aadA1-catB8-aacA4*]. Confined to GC1 (22.2%), sulfonamide resistance was acquired by an IS*Aba1* bracketed GIsul2 RI. An additional RI (RI-PER-7) was also identified on a plasmid carried by strain M03. Among others, RI-PER-7 carried

OPEN ACCESS

Edited by:
Raffaele Zarrilli,
University of Naples Federico II, Italy

Reviewed by:
Sara Domingues,
University of Coimbra, Portugal
Agnese Lupo,
ANSES Site de Lyon, France

***Correspondence:**
Mai M. Zafer
maizafer@acu.edu.eg

Specialty section:
This article was submitted to Antimicrobials, Resistance and Chemotherapy, a section of the journal Frontiers in Microbiology

Received: *18 February 2022*
Accepted: *22 June 2022*
Published: *22 July 2022*

Citation:
Hamed SM, Hussein AFA, Al-Agamy MH, Radwan HH and Zafer MM (2022) Genetic Configuration of Genomic Resistance Islands in Acinetobacter baumannii Clinical Isolates From Egypt. Front. Microbiol. 13:878912. doi: 10.3389/fmicb.2022.878912

the resistance genes *armA* and bla_{PER-7}. Here, we provided a closer view of the diversity and genetic organization of RIs carried by a previously unexplored population of *A. baumannii*.

Keywords: *Acinetobacter baumannii*, whole genome sequencing, resistance islands, AbaR4, AbGRI1, AbGRI2, AbGRI3, RI-PER-7

INTRODUCTION

In the last decades, *Acinetobacter baumannii* infections have moved to the forefront of challenges encountered by clinicians worldwide. It is mainly recognized for causing a wide range of difficult-to-treat hospital-acquired infections, particularly in critically ill patients (Morris et al., 2019). Working in concert, the remarkable capacity for upregulating intrinsic resistance mechanisms and acquisition of foreign resistance genes contributed to an ever-expanding spectrum of antimicrobial resistance in *A. baumannii*. Leaving behind limited or no antimicrobial treatment options, extensively drug-resistant (XDR) and pandrug-resistant strains have been increasingly reported from different parts of the world (Hsueh et al., 2002; Leite et al., 2016; Hamidian and Nigro, 2019). Most of them are members of the high-risk global clones (GCs) 1 and 2 (also known as international clones; ICs) (Karah et al., 2012). Genome sequencing of the earliest strains of the high-risk GCs uncovered a wide repertoire of resistance genes being associated with genomic resistance islands (RIs) (Hamidian and Hall, 2017b). These are genomic regions encompassing variable assortments of transposons and integrons loaded with specific resistance genes (Fournier et al., 2006). They are one of the hallmarks of the horizontal transfer of resistance genes (Carraro et al., 2017).

The first known genomic RI, designated AbaR1 (*A. baumannii* Resistance 1), was identified in *A. baumannii* strain AYE from France carrying antimicrobial and heavy metal resistance genes within transposon fragments (Fournier et al., 2006). With a wide variability in size, genetic structure, and insertion sites (Bi et al., 2020), at least seven families of genomic RIs are currently known. These include AbaR-type islands (Post et al., 2010), AbaR4 (Hamidian and Hall, 2011), and *A. baumannii* genomic resistance islands (AbGRIs) types 1 to 5 (Nigro and Hall, 2012b; Nigro et al., 2013; Wright et al., 2014; Blackwell et al., 2017; Chan et al., 2020; Hua et al., 2021). Any or more than one RIs may be carried by MDR *A. baumannii* strains (Chan et al., 2015; Hamidian and Hall, 2017b). In addition to the Tn*6019* backbone, AbaR contains multiple antibiotic resistance regions (MARRs) enclosed by two copies of Tn*6018*. AbaR-type RIs are commonly inserted within the ATPase-coding gene *comM* (Hamidian and Hall, 2018) often in GC1 strains. In the same location, two other RIs were identified. These include AbaR4, in which Tn*2006* is inserted in a Tn*6022* backbone (Hamidian and Hall, 2011), and AbGRI1, identified in GC2 strains (Nigro and Hall, 2012a,b; Hamidian and Hall, 2017b). AbGRI1 consists of Tn*6022* (or its deletion derivatives) and Tn*6172* joined by a plasmid-derived linker (Hamidian and Hall, 2017b). AbGRI1 variants often carry the resistance genes *sul2*, *tet(B)*, *strA*, *strB,* and sometimes bla_{OXA-23} (Bi et al., 2020). The three RIs, AbaR, AbaR4, and AbGRI1, are complex class III transposons carrying the transposition genes *tniCABDE* that target the *comM* gene for insertion (Hamidian and Hall, 2017b). The other four types of AbGRIs are IS*26*-bound transposons harboring variable combinations of resistance genes that are characteristic for each type. They are commonly identified in the chromosomes of *A. baumannii* strains that belong to GC2. They include AbGRI2 (Nigro et al., 2013), AbGRI3 (Blackwell et al., 2017), AbGRI4 (Chan et al., 2020), and AbGRI5 (Hua et al., 2021). AbGRI2 characteristically carries all or some of the resistance genes bla_{TEM}, *aphA1, catA1*, and a class I integron carrying *sul1*, *aacC1,* and *aadA1* (Nigro et al., 2013). AbGRI3 commonly inserts within a putative GNAT family N-acetyltransferase gene. In addition to *armA* conferring resistance to all clinically useful aminoglycosides, AbGRI3 also carries *msrE* and *mphE*, with or without class I integron carrying the resistance genes *aacA4*, *catB8*, *aadA*, and *sul1*. In some cases, IS*26*-bracketed *aphA1* also integrates into AbGRI3 (Blackwell et al., 2017). Recently, AbGRI4 was identified in GC2 and non-GC2 strains carrying the resistance genes *aadB*, *aadA2*, and *sul1* in a class I integron. AbGRI4 uniquely targets an α/β-hydrolase gene (Chan et al., 2020). AbGRI5 is the latest RI to be identified in *A. baumanni* that resembles AbGRI3 in harboring *armA, msrE-mphE, sul1,* and class I integron that carries a different array of resistance genes [bla_{PER-1}-bla_{CARB-2}-*aadA2-cmlA1-aadA1*] compared to AbGRI3. In addition, AbGRI5 distinctively carries the macrolide resistance gene *ere(B)* (Hua et al., 2021).

Even though reports about the structure of RIs carried by strains of this extremely problematic pathogen were published from several parts of the world (Lee et al., 2016; Blackwell et al., 2017; Kim et al., 2017; Chan et al., 2020; Leal et al., 2020; Hua et al., 2021), little is known about those circulating in Egyptian hospitals. Here, we used whole-genome sequencing (WGS) to analyze the diversity and configuration of RIs carried by 18 strains of *A. baumannii* isolated from patients admitted to one of the largest tertiary university hospitals in Cairo, Egypt, in 2020.

MATERIALS AND METHODS

Clinical Isolates

The current study included 20 non-duplicate clinical isolates of carbapenem-resistant *A. baumannii* from patients admitted to Kasr Al-Ainy University Hospital, Cairo, Egypt. The isolates were recovered from clinical specimens received by the clinical pathology laboratory for bacteriological analysis in the period from July to October 2020. They were identified to species level using the VITEK®2 automated identification system (bioMérieux, Marcy l'Etoile, France) before polymerase chain reaction (PCR) amplification of the $bla_{OXA-51-like}$ genes, as

described before (Turton et al., 2006). Identification was further confirmed by WGS using the Speciesfinder tool hosted by the Center of Genomic Epidemiology (http://www.genomicepidemiology.org/).

Antimicrobial Susceptibility Testing

Broth microdilution assay was used for the determination of the minimum inhibitory concentrations (MICs) of colistin (Sigma-Aldrich, St Louis, MO, USA) in a concentration range of 128-0.125 μg/ml. Susceptibility to other antimicrobial agents was inferred by Kirby–Bauer disc diffusion test. These included amikacin (30 μg), amoxicillin/clavulanic acid (20/10 μg), ampicillin (10 μg), cefepime (30 μg), cefotaxime (30 μg), cefoxitin (30 μg), ceftriaxone (30 μg), imipenem (10 μg), levofloxacin (5 μg), meropenem (10 μg), piperacillin/tazobactam (10/100 μg), tetracycline (30 μg), tigecycline (15 μg), and trimethoprim/sulfamethoxazole (1.25/23.75 μg). Both susceptibility tests were performed and interpreted according to the Clinical and Laboratory Standards Institute (CLSI) guidelines (CLSI, 2020) for all antimicrobial agents except tigecycline for which susceptibility breakpoints recommended by EUCAST v11.0 for *Enterobacterales* were used (EUCAST, 2021). For quality control purposes, *Escherichia coli* ATCC 25922 and *Pseudomonas aeruginosa* ATCC 27853 were used.

Whole-Genome Sequencing

After DNA extraction using the QIAGEN DNA purification kit (Qiagen, Valencia, CA) and library preparation using the Nextera DNA Sample Preparation kit (Nextera, USA), WGS was performed on an Illumina MiSeq platform (Illumina Inc., San Diego, CA, USA). Pre-assembly processing of the generated reads was carried out by FastQC (Andrews, 2010) for quality assessment and Trimmomatic v0.32 (Bolger et al., 2014) for the trimming of low-quality reads. *De novo* assembly of trimmed reads was carried out using SPAdes 3.14.1 (Bankevich et al., 2012). Post-assembly metrics were generated by QUAST v5.0.2 (Gurevich et al., 2013). Draft genomes were annotated using the NCBI Prokaryotic Genome Annotation Pipeline (PGAP) (Tatusova et al., 2016). Plasmids were assembled from Illumina reads using PlasmidSPAdes (Antipov et al., 2016), a software for reading coverage-assisted plasmid identification. Assembly graphs (Fastg files) generated by PlasmidSPAdes were visualized on a bandage (Wick et al., 2015). Plasmid sequences were extracted from circular contigs or groups of contigs forming circular paths containing plasmid replication and/or mobilization genes. Contigs forming circular but overlapping paths were BLASTed for closest plasmids that were subsequently used for reference mapping using the short reads mapping tool BWA-MEM (Li and Durbin, 2010).

Epidemiology Analysis

Two sequence-based typing methods were used for the epidemiology analysis of the isolates. These included multilocus sequence typing (MLST) and single-nucleotide polymorphism (SNP)-based phylogeny analysis.

The draft genomes were uploaded to the PubMLST server (https://pubmlst.org/abaumannii/) for assigning STs for the isolates according to both Pasteur (Diancourt et al., 2010) and Oxford schemes (Bartual et al., 2005). Allocation of the isolates into clonal complexes (CCs) was done by goeBURST analysis. For this purpose, all allelic profiles defined by both schemes were retrieved from the PubMLST database (accessed on 30 April 2021). Together with the allelic profiles of the isolates studied here, they were used as inputs for Phyloviz software for the generation of minimum spanning trees using the goeBURST algorithm (Ribeiro-Goncalves et al., 2016).

Using the default setting parameters, the CSI phylogeny 1.4 online tool (https://cge.cbs.dtu.dk/services/CSIPhylogeny/) was employed in inferring the phylogeny of the isolates based on the concatenated alignment of the high-quality SNPs. *A. baumannii* ATCC17978 was used as a reference for the analysis. The analysis initially included 44 complete and draft genomes of *A. baumannii* strains that belong to STs identified here obtained from the NCBI and PubMLST databases. For easier visualization, the final phylogenetic tree was constructed using a smaller number of genomes of *A. baumannii* strains that were clustered with our isolates. Interactive tree of life (iTOL) v3 software (https://itol.embl.de/) (Letunic and Bork, 2016) was used for visualization and editing of the phylogenetic tree.

Antimicrobial Resistance Determinants and Resistance Island Analyses

Genes with a minimum of 80% coverage and 95% identity to known resistance genes were identified using the Comprehensive Antibiotic Resistance Database (CARD) server (https://card.mcmaster.ca/analyze/rgi) (Alcock et al., 2020). Point mutations of the genes relevant to fluoroquinolones (*gyrA* and *parC*) and colistin (*lpxACD* and *pmrABC*) resistance were extracted from the assemblies for pairwise comparison to the corresponding genes of the reference strain *A. baumannii* ATCC 19606 (GenBank accession: CP045110.1).

The context of resistance genes was examined by visualizing the annotated contigs using SnapGene software v5.1.3.1 by Insightful Science (http://www.snapgene.com). Insertion sequences (ISs) were identified by BLAST analysis against the nucleotide database of the NCBI and novel ISs were named by the ISFinder database team (http://www-is.biotoul.fr). Resistance islands were predicted using the webserver IslandViewer4 webtool (http://www.pathogenomics.sfu.ca/islandviewer/) (Bertelli et al., 2017), through which the draft genomes were mapped against different reference genomes. For RIs fragmented into multiple contigs, assembly gaps were filled by mapping raw reads against the closest RI using BWA (Li and Durbin, 2010).

Accession Numbers

The Whole Genome Shotgun project including Fastq files generated by the Illumina sequencer and the assembled draft genomes were submitted to GenBank database under the BioProject number PRJNA690827. The nucleotide sequence of the novel $bla_{ADC-258}$ variant was submitted to the NCBI GenBank database under the accession number (MZ224612.1).

RESULTS

Bacterial Strains and Clinical Data

Twenty carbapenem-resistant *A. baumannii* isolates were received by the clinical pathology laboratory of Kasr Al-Ainy University Hospital, Cairo, Egypt, during the study period. All were preserved with the purpose of a WGS-based analysis of RIs. Having successfully passed the post-assembly quality control criteria, only 18 strains were selected for further analysis. Post-assembly and annotation metrics of the generated draft genomes are shown in **Supplementary Table 1**. Half of the strains selected for the study were isolated from patients in critical care units and at least 22.2% were from pediatric patients. Clinical data of all isolates are shown in **Table 1**.

Molecular Epidemiology

The MLST analysis revealed that the isolates belonged to six Pasteur and nine Oxford STs (**Figure 1**). GoeBURST analysis (**Supplementary Figure 1**) showed that the majority of the isolates belonged to the high-risk global clones 1, 2, and 9. Predominantly, seven isolates (38.8%) belonged to GC2 distributed over two CCs (CC208 and CC546) according to the Oxford scheme. GC9 ($CC464^{Pas}/1078^{Oxf}$) and GC1 ($CC1^{Pas}/231^{Oxf}$) were represented by three and two isolates, respectively. M14 had a novel Oxford ST (2329) that also formed a novel clonal complex to which 11 STs including that of M03 ($ST2246^{Oxf}$) belonged. The SNP-based phylogenetic analysis generated a seven-cluster phylogenetic tree (**Figure 1**). Notably, isolates that shared an Oxford ST were clustered together. The isolates M06 and M09 with undetermined STs were found to be phylogenetically related to GC1 isolates. The tree also showed that our isolates were clustered with other strains isolated in different parts of the world.

Antimicrobial Susceptibility Profiles and Resistance Determinants

Based on the definitions proposed by Magiorakos et al. (2012) for MDR and XDR, the majority of the isolates were XDR (13/18, 72.2%), and only five isolates (27.7%) showed an MDR phenotype. All GC2 and GC9 isolates were XDR, while MDR isolates belonged to GC1 as well as STs that do not belonging to high-risk clones. Susceptibility to tigecycline was retained by all isolates. Except for one isolate (5.5%), all were susceptible to colistin with an MIC_{50} of 0.25 μg/ml. Only five isolates (27.7%) were susceptible to amikacin, and one isolate (5.5%) was susceptible to trimethoprim/sulfamethoxazole. All isolates were nonsusceptible to all other tested antimicrobials. A wide repertoire of resistance genes was identified in our isolates, most of which were associated with mobile elements. As many as 38 resistance determinants were identified in combinations of up to 28 determinants per isolate. These included genes coding for antibiotic inactivation, target protection, target alteration, target replacement, and antibiotic efflux. The largest number of co-existing resistance genes was found in GC2 isolates (25-28 determinants/isolate), followed by those that belonged to GC9 (21–23 determinants/isolate). Antimicrobial susceptibility profiles and resistance determinants of all isolates are shown in **Figure 2**.

Resistance to β-Lactams

In addition to the intrinsic resistance genes (bla_{ADC} and $bla_{OXA-51-like}$) to β-lactams, five acquired β-lactamase-coding

TABLE 1 | Demographic data.

Strain	Specimen	Age	Gender	Diagnosis	Hospital Unit
M01	Endotracheal tube	5 Ds	Male	Chest infection	NICU
M02	Wound swab	28 Ys	Female	Sub ovarian abscess removal	ICU
M03	Blood	48 Ys	Male	Fever	Internal Medicine
M04	Sputum	NA	Female	Chest infection	ER
M05	Blood	NA	Female	Ventilator-associated pneumonia	Chest ICU
M06	Sputum	NA	Male	Pneumonia	ER
M09	Blood	NA	Female	Fever	ER
M10	Blood	24 Ds	Female	Pneumonia	NICU
M11	Pleural fluid	20 Ds	Female	Pneumonia	NICU
M12	Blood	50 Ys	Female	Fever of unknown origin	ER
M13	Wound swab	34 Ys	Male	Fever	ICU
M14	Urine	60 Ys	Male	Fever	ER
M15	Wound swab	NA	Male	Burn	Burns
M16	Blood	NA	Male	Fever	ER
M17	Sputum	56 Ys	Female	Pneumonia	ICU
M18	Blood	55 Ys	Female	Fever and disturbed consciousness level	ER
M19	Blood	20 Ds	Female	Fever of unknown origin	ICU
M20	Blood	65 Ys	Male	Splenectomy and fever	ICU

Ds, days; Ys, years; NA, not available; NICU, neonatal intensive care unit; ICU, intensive care unit; ER, emergency department.

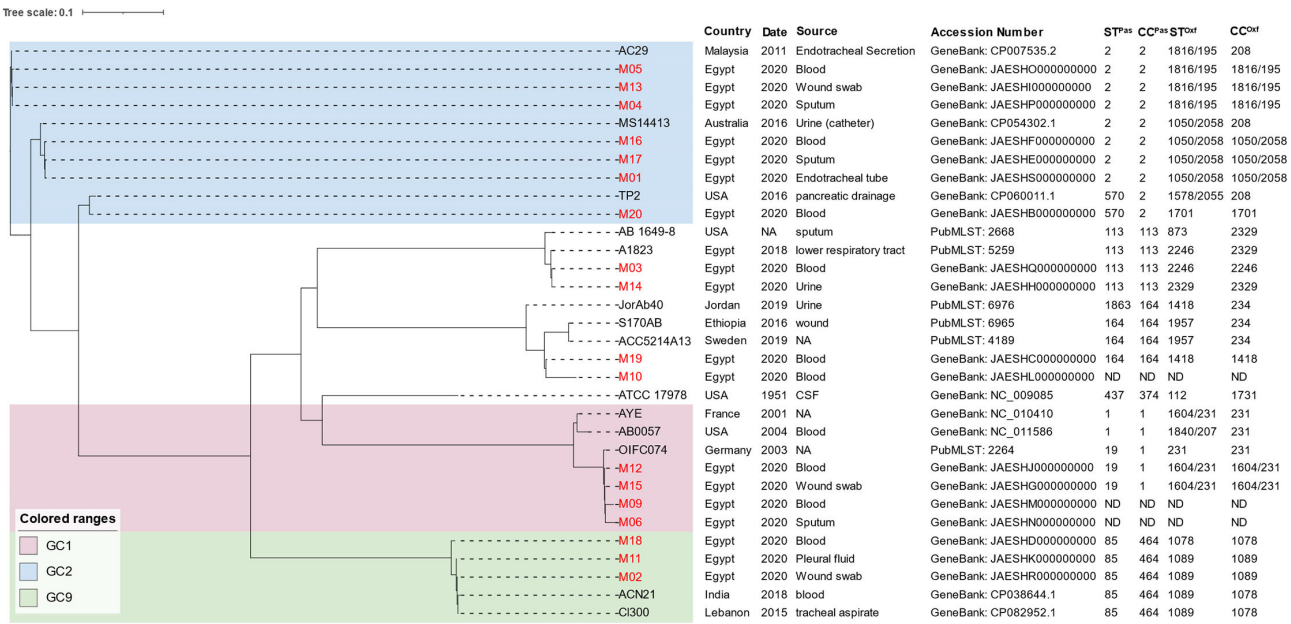

	Country	Date	Source	Accession Number	ST^{Pas}	CC^{Pas}	ST^{Oxf}	CC^{Oxf}
AC29	Malaysia	2011	Endotracheal Secretion	GeneBank: CP007535.2	2	2	1816/195	208
M05	Egypt	2020	Blood	GeneBank: JAESHO000000000	2	2	1816/195	1816/195
M13	Egypt	2020	Wound swab	GeneBank: JAESHI000000000	2	2	1816/195	1816/195
M04	Egypt	2020	Sputum	GeneBank: JAESHP000000000	2	2	1816/195	1816/195
MS14413	Australia	2016	Urine (catheter)	GeneBank: CP054302.1	2	2	1050/2058	208
M16	Egypt	2020	Blood	GeneBank: JAESHF000000000	2	2	1050/2058	1050/2058
M17	Egypt	2020	Sputum	GeneBank: JAESHE000000000	2	2	1050/2058	1050/2058
M01	Egypt	2020	Endotracheal tube	GeneBank: JAESHS000000000	2	2	1050/2058	1050/2058
TP2	USA	2016	pancreatic drainage	GeneBank: CP060011.1	570	2	1578/2055	208
M20	Egypt	2020	Blood	GeneBank: JAESHB000000000	570	2	1701	1701
AB 1649-8	USA	NA	sputum	PubMLST: 2668	113	113	873	2329
A1823	Egypt	2018	lower respiratory tract	PubMLST: 5259	113	113	2246	2329
M03	Egypt	2020	Blood	GeneBank: JAESHQ000000000	113	113	2246	2246
M14	Egypt	2020	Urine	GeneBank: JAESHH000000000	113	113	2329	2329
JorAb40	Jordan	2019	Urine	PubMLST: 6976	1863	164	1418	234
S170AB	Ethiopia	2016	wound	PubMLST: 6965	164	164	1957	234
ACC5214A13	Sweden	2019	NA	PubMLST: 4189	164	164	1957	234
M19	Egypt	2020	Blood	GeneBank: JAESHC000000000	164	164	1418	1418
M10	Egypt	2020	Blood	GeneBank: JAESHL000000000	ND	ND	ND	ND
ATCC 17978	USA	1951	CSF	GeneBank: NC_009085	437	374	112	1731
AYE	France	2001	NA	GeneBank: NC_010410	1	1	1604/231	231
AB0057	USA	2004	Blood	GeneBank: NC_011586	1	1	1840/207	231
OIFC074	Germany	2003	NA	PubMLST: 2264	19	1	231	231
M12	Egypt	2020	Blood	GeneBank: JAESHJ000000000	19	1	1604/231	1604/231
M15	Egypt	2020	Wound swab	GeneBank: JAESHG000000000	19	1	1604/231	1604/231
M09	Egypt	2020	Blood	GeneBank: JAESHM000000000	ND	ND	ND	ND
M06	Egypt	2020	Sputum	GeneBank: JAESHN000000000	ND	ND	ND	ND
M18	Egypt	2020	Blood	GeneBank: JAESHD000000000	85	464	1078	1078
M11	Egypt	2020	Pleural fluid	GeneBank: JAESHK000000000	85	464	1089	1089
M02	Egypt	2020	Wound swab	GeneBank: JAESHR000000000	85	464	1089	1089
ACN21	India	2018	blood	GeneBank: CP038644.1	85	464	1089	1078
CI300	Lebanon	2015	tracheal aspirate	GeneBank: CP082952.1	85	464	1089	1078

FIGURE 1 | SNP-based phylogenetic tree of *A. baumannii* draft genomes sequenced in the current study compared to other strains obtained from the NCBI and PubMLST databases. Labels of the *A. baumannii* strains sequenced in the current study are written in red. ST^{Pas}, sequence type according to Pasteur scheme; ST^{Oxf}, sequence type according to Oxford scheme; GC, global clone.

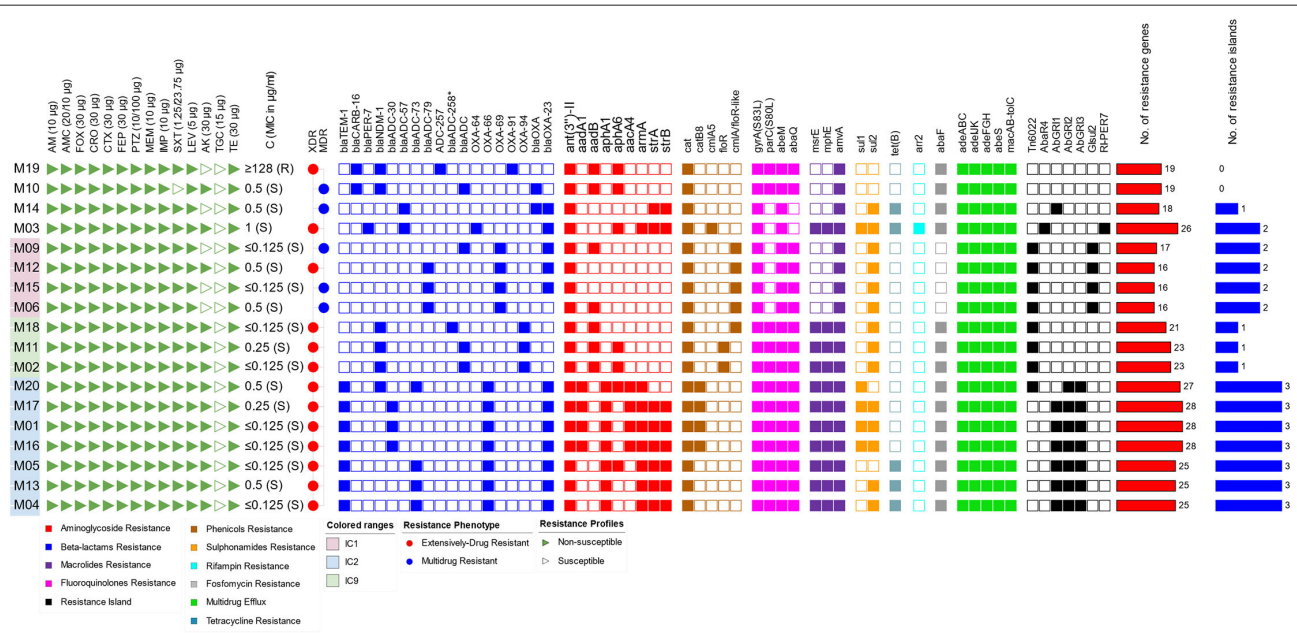

FIGURE 2 | Overview of the antimicrobial susceptibility profiles and resistance determinants. The isolates were ordered according to their SNP-based phylogenetic relationship. Labels of GC1 isolates (together with their phylogenetically related isolates) are highlighted in pink and those of GC2 and GC9 are highlighted in blue and green, respectively. The map is divided into panels corresponding to susceptibility to antimicrobial agents (triangular icons), resistance phenotypes (circular icons), resistance determinants (square icons), and the number of resistance determinants and islands (bars). AM, ampicillin; AMC, amoxicillin/clavulanic acid; FOX, cefoxitin; CRO, ceftriaxone; CTX, cefotaxime; FEP, cefepime; PTZ, piperacillin/tazobactam; MEM, meropenem; IMP, imipenem; SXT, sulfamethoxazole/trimethoprim; LEV, levofloxacin; AK, amikacin; TGC, tigecycline; TE, tetracycline; C, colistin; XDR, extensive drug resistance; MDR, multidrug resistance.

genes, encompassing bla_{TEM-1}, $bla_{CARB-16}$, bla_{NDM-1}, bla_{PER-7}, and bla_{OXA-23}, were identified. Up to five β-lactamase coding genes co-existed in the tested isolates. At least six bla_{ADC} variants were identified, including a novel variant ($bla_{ADC-258}$) carried by M18. $bla_{ADC-258}$ showed 99.74% similarity to $bla_{ADC-176}$ with the amino acid alterations Q2R and D24G. Meanwhile,

bla_{ADC} variants carried by four isolates could not be identified due to insertion sequence (IS) interruption (M02 and M11) or assembly gaps (M09 and M10). The N terminus of the bla_{ADC-73} carried by M20 was interrupted by an unknown sequence, as described before (Zafer et al., 2021). Interestingly, isolates of the same Oxford ST carried the same bla_{ADC} variants. An upstream IS*Aba1* was confirmed for only eight isolates (M01, M04, M06, M12, M13, M15, M16, and M17), all belonging to GCs 1 and 2. On their chromosomes, the isolates also carried five alleles of the intrinsic β-lactamase-coding gene $bla_{OXA-51-like}$. Isolates of the same clonal complex (Pasteur or Oxford) shared the same $bla_{OXA-51-like}$ variant. Of all acquired β-lactamase-coding genes, bla_{OXA-23} (class D β-lactamase-coding gene) was the most prevalent (12/18, 66.6%) either within RIs (5/18, 27.7%) or more frequently bracketed by IS*Aba1* in Tn*2006* (7/18, 38.8%). The bla_{OXA-23}-positive isolates belonged to GC2 and GC1, and two isolates (M03 and M14) belonged to the novel $CC113^{Pas}/2329^{Oxf}$ The gene bla_{OXA-23} was carried within Tn*2006* in GC1 isolates and GC2 isolates that belonged to the Oxford STs ST1050/2058 and ST1701. Meanwhile, in GC2 isolates of the $ST1816/195^{Oxf}$, bla_{OXA-23} was hosted by AbaR4b. M03 and M14 carried bla_{OXA-23} within AbaR4 and an AbGRI1-like-2 RI, respectively. Harbored by an AbGRI2-15 and exclusively in GC2, the class A β-lactamase-coding gene bla_{TEM-1} was found in seven isolates (38.8%). Among our isolates were six (33.3%) NDM-1 producers. These included all GC9 isolates, one GC2 isolate (M20), as well as M19 ($ST164^{Pas}/1418^{Oxf}$) and its phylogenetically related isolate M10. The genetic environment of bla_{NDM-1} was described in our previous study (Zafer et al., 2021). We reported, for the first time, a novel transposon in which both bla_{NDM-1} and *aphA6* were enclosed by two direct copies of IS*Aba14*. The transposition potential of the transposon was later demonstrated using bioinformatic tools (unpublished data). This environment was described only for GC9 isolates that belonged to $ST1089^{Oxf}$ as well as M10. While the right arm of the IS*Aba14*-bracketed transposon carrying bla_{NDM-1} was found in other NDM producers, the full sequence of the transposon could not be spotted.

The isolates M19 and M10 also carried $bla_{CARB-16}$ in contigs showing 100% similarity to a 63,650 kb plasmid carried by *A. baumannii* strain DT01139C (GenBank accession: CP053220.1) isolated in Tanzania in 2017. However, $bla_{CARB-16}$-positive plasmids could not be identified either by PlasmidSPAdes *de novo* assembly or by mapping the raw reads against the DT01139C plasmid. Finally, with the lowest prevalence, bla_{PER-7} was identified only in M03. Together with six more resistance genes, bla_{PER-7} was carried within RI-PER-7.

Resistance to Aminoglycosides

Resistance genes to aminoglycosides were found in abundance in our collection. Of them, *armA,* conferring resistance to all clinically relevant aminoglycosides, was the most prevalent and was carried by 8/18 (44.4%) isolates. These included all GC2 isolates in which it was carried on AbGRI3 and M03 in which *armA* was hosted by RI-PER-7. The amikacin resistance gene *aphA6* was carried by 7/18 (38.8%) isolates that belonged to different STs. Most commonly, *aphA6* was bracketed by IS*Aba14* and IS*Aba125* in the bla_{NDM-1}-positive isolates either within the composite IS*Aba14* bracketed transposon described above (M02, M10, and M11) or not (M19 and M20). In M05, *aphA6* was carried on a 70,101-bp RepAci6 plasmid closely similar to pACICU2 (GenBank accession: CP031382.1). The context of *aphA6* in M03 could not be defined. On pRAY plasmid derivatives, *aadB* was carried by 7/18 (38.8%) isolates that belonged to different sequence types except for those of GC2. Within AbGRI3, GC2 isolates of the STs $ST1050/2058^{Oxf}$ and $ST1701^{Oxf}$ carried *aacA4* and *aadA1* that were undetectable in other GC2 strains carrying a shorter version of AbGRI3. Other detected aminoglycoside resistance genes included the intrinsic gene *ant(3")-II* (Zhang et al., 2017) and other acquired resistance genes, such as *aphA1*(38.8%%), *strA* (44.4%), *strB* (44.4%), and *aadA1* (22.2%). In all *aphA1*-positive isolates that all belonged to GC2, the gene was carried on AbGRI2-15 together with bla_{TEM-1}. The genes *strA* and *strB* co-existed in all GC2 isolates that belonged to $CC208^{Oxf}$ in which they were carried on variants of AbGRI1. They also co-existed in $CC113^{Pas}/2329^{Oxf}$ isolates (M03 and M14) but within different environments. In M14, *strA* and *strB* were carried on AbGRI1-type RI. In M03, they were harbored by a transposon (∼ 24 Kb) also carrying *sul2* and *tet(B)* and bracketed by IS*Aba1* and IS*26* that were shared with an adjacent RI-PER-7. The whole genetic structure showed 99.9% similarity to a 226,394-bp plasmid pPM194229_1 (GenBank accession: CP050433.1). Using the plasmid sequence as a reference for mapping produced a sequence with 99.99% identity to the reference plasmid with a coverage of 90.0%. Although the full sequence of the plasmid could not be identified, the *de novo* assembled fragment revealed genetic rearrangement compared to the closely matched plasmid. This included insertion of [*tet(B)-tetR(B)*] downstream to *sul2* through homologous recombination that was also associated with IS*Vsa3*-mediated deletion, as shown in **Figure 3**. The context of β-lactams and aminoglycoside resistance determinants in all isolates are summarized in **Table 2**.

Isolates carrying single mutations (*gyrA*; S83L) belonged to $ST113^{Oxf}$ (M03 and M14) and $ST231^{Oxf}$ (M12 and M15) and their phylogenetically related strains (M06 and M09). Genes coding the quinolone efflux pumps *abeM* and *abaQ* were found in 100.0% and 88.8% of the isolates, respectively.

The chloramphenicol acetyltransferase-coding gene *cat* was carried in the chromosomes of all isolates not associated with any mobile elements. Meanwhile, *catB8* was identified in GC2 isolates within AbGRI3 except those carrying the short version of the island (M04, M05, and M13). Genes coding the chloramphenicol efflux pumps FloR and CmlA5 were also identified. FloR efflux pump-coding gene was carried by M02 and M11 (2/18, 11.1%) in association with *sul2* gene and ISs, as described before (Zafer et al., 2021). A novel *cmlA/floR*-like gene variant was identified in five isolates (27.7%). These included GC1 isolates M06, M09, M12, and M15 and the GC9 isolate M18. The gene was associated with a novel downstream 1,206-bp long IS designated IS*Aba61*. Together with the passenger *cmlA/floR*-like gene, IS*Aba61* was distinctively inserted within a molybdopterin-dependent oxidoreductase-coding gene, as shown in **Supplementary Figure 2**. As a transposition signature,

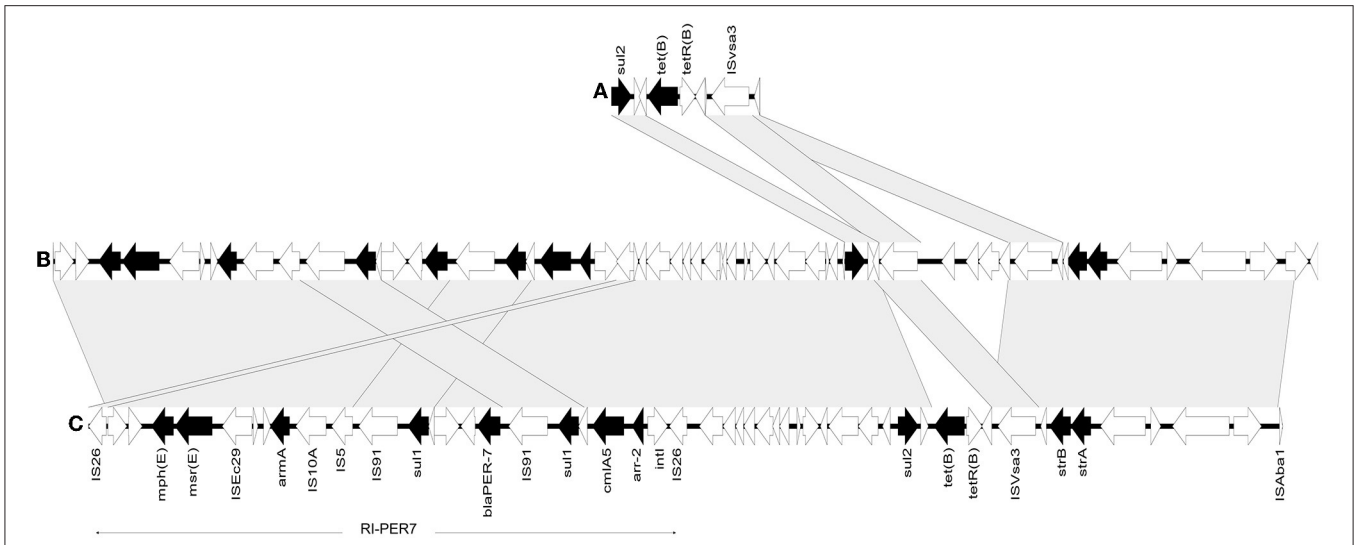

FIGURE 3 | Comparative genomic analysis of the partial sequence of M03 plasmid and the closely similar plasmid pPM194229_1(CP050433.1). **(A)** pPM194229_1 plasmid sequence region [218446-224334 bp]. **(B)** pPM194229_1 plasmid sequence region [1-50187 bp]. **(C)** M03 plasmid partial sequence. Arrows correspond to open reading frames, and black ones denote resistance genes. Gray shadings highlight regions of 99% or more nucleotide identity.

the insertion of IS*Aba61* generated an 8-bp TGAAAATA duplication in the target site. Only one isolate (M03) carried *cmlA5* within RI-PER-7.

In addition to the efflux pump gene *amvA*, macrolide resistance was coded by *msrE* and *mphE* that co-existed in 61.1% of the isolates. They were associated with the resistance islands AbGRI3 and RI-PER-7 in GC2 isolates and M03, respectively. In GC9 isolates, *msrE* and *mphE* were located outside the RIs enclosed by the insertion sequences ISNCY and IS*Aba1* in the upstream and downstream regions, respectively.

As many as 15 isolates (83.3%) carried at least one sulfonamide resistance gene. More frequently, the isolates carried *sul2*, which was identified in 14 isolates with no clonal bias. The gene was hosted by two types of RIs, namely, GIsul2 in GC1 (M12 and M15) and phylogenetically related isolates (M06 and M09) and AbGRI1-type RIs in M01, M14, M16, and M17. Only five isolates carried *sul1* that was associated with AbGRI3 in GC2 isolates (Oxford STs ST1050/2058 and ST1701) and RI-PER-7 in M03.

Resistance to Other Antimicrobial Classes

Resistance to levofloxacin was associated with *gyrA* mutations encoding S83L amino acid alterations in all isolates. Meanwhile, missense mutations (S80L) in the topoisomerase-coding gene (*parC*) were identified in only 12 (66.6%) isolates.

The gene *tet(B)* was the only tetracycline resistance gene identified in the isolates (5/18, 27.7%). In association with the resistance genes *strA*, *strB,* and bla_{OXA-23}, it was located within AbGRI1 in all GC1 isolates and M14. A different environment was found for *tet(B)* in M03 in which it was carried on a plasmid whose sequence was partially identified, as described above. Except for GC1 isolates, genes coding the fosfomycin major facilitator superfamily (MFS) transporter AbaF were carried on the chromosomes of all isolates not associated with any mobile elements. Within RI-PER-7, the rifampin resistance gene *arr-2* was only carried by M03. Colistin resistance in M19 was found to be associated with mutations in *pmrB* (H89L), *pmrC* (I42V, I212V, R323K, A354S, and V470I), *IpxA* (Y131H and Y231H), *IpxC* (C120R, N287D, and K130T), and *lpxD* (V631 and E117K), as described before (Zafer et al., 2021).

Resistance Islands (RIs)

Whole-genome sequencing of the isolates disclosed at least nine configurations of genomic RIs. An additional RI, RI-PER-7, was found to be carried on a plasmid whose structure was only partially identified. GC2 isolates accumulated the largest number of RIs (three RIs/isolate) followed by GC1 isolates in which two genomic RIs co-existed.

For the detection of AbaR-, AbaR4-, and AbGRI-type RIs, *comM* gene integrity was checked in all isolates. The gene was found to be interrupted in 16/18 (88.8%) isolates (all except M10 and M19) most frequently by Tn*6022* (the backbone of AbaR4). Lacking any resistance genes, Tn*6022* was carried by eight isolates (44.4%), including all GC1 and GC9 isolates as well as M20 that belonged to GC2. Less often, *comM* was interrupted by AbGRI1-type RIs carrying resistance genes exclusively within GC2 isolates (except M20), while AbaR4 was only found in M03 that belongs to the $ST113^{Pas}/2246^{Oxf}$. AbGRI1 was found in three variant structures shown in **Figure 4**. The first variant was AbaR4b, also called AbGRI1-1/*Tn2006* and Tn6166/*Tn2006*, that lacked the typical AbGRI1 structure [*Tn6022*-plasmid linker-*Tn6172*]. Instead, AbaR4b was formed of Tn*6166* in which Tn*6022Δ1* was interrupted by Tn*2006*. AbaR4b was identified in the chromosomes of GC2 isolates of the Oxford ST 1816/195. Another AbGRI1 variant, named here AbGRI1-like-1, was similar to AbGRI1-0, but Tn*6022* was replaced by Tn*6022Δ1,* and

TABLE 2 | β-lactam and aminoglycoside resistance determinants and their context.

Isolate No.	Resistance to β-lactams		Resistance to aminoglycosides	
	Intrinsic resistance genes (An upstream IS*Aba1*)	**Acquired resistance genes (associated MGEs)**	**Intrinsic resistance genes**	**Acquired resistance genes (associated MGEs)**
M01	*bla*$_{ADC-30}$ (present) *bla*$_{OXA-66}$ (ND)	*bla*$_{OXA-23}$ (Tn*2006*) *bla*$_{TEM-1}$ (AbGRI2-15)	*ant(3")-II*	*aacA4* (AbGRI3-1) *aadA1* (AbGRI3-1) *aphA1* (AbGRI2-15) *armA* (AbGRI3-1) *strA* (AbGRI1-like-1) *strB* (AbGRI1-like-1)
M02	*bla*$_{ADC}$ (interrupted by IS*1008*) *bla*$_{OXA-94}$ (present)	*bla*$_{NDM-1}$ (IS*Aba14* bracketed transposon also carrying *aphA6*)		*aadB* (pRAY*, JQ904627.1) *aphA6* (IS*Aba14* bracketed transposon also carrying *bla* $_{NDM-1}$)
M03	*bla*$_{ADC-57}$ (ND) *bla*$_{OXA-64}$ (ND)	*bla*$_{OXA-23}$ (AbaR4) *bla*$_{PER-7}$ (RI-PER-7, in an undetermined plasmid closely similar to pPM194229_1)		*aphA6* (ND) *armA* (RI-PER-7, in a plasmid closely similar to pPM194229_1) *strA* (plasmid closely similar to pPM194229_1) *strB* (plasmid closely similar to pPM194229_1)
M04	*bla*$_{ADC-73}$ (present) *bla*$_{OXA-66}$ (absent)	*bla*$_{OXA-23}$ (AbaR4b) *bla*$_{TEM-1}$ (AbGRI2-15)		*aphA1* (AbGRI2-15) *armA* (AbGRI3-1) *strA* (AbaR4b) *strB* (AbaR4b)
M05	*bla*$_{ADC-73}$ (ND) *bla*$_{OXA-66}$ (absent)	*bla*$_{OXA-23}$ (AbaR4b) *bla*$_{TEM-1}$ (AbGRI2-15)		*aphA1* (AbGRI2-15) *aphA6* (RepAci6 plasmid 99.9% similar to pACICU2) *armA* (AbGRI3-1) *strA* (AbaR4b) *strB* (AbaR4b)
M06	*bla*$_{ADC-79}$ (present) *bla*$_{OXA-69}$ (ND)	None		*aadB* (pRAY*-like,99.98% similarity)
M09	*bla*$_{ADC}$ (ND) *bla*$_{OXA-69}$ (ND)	*bla*$_{OXA-23}$ (Tn*2006*)		*aadB* (pRAY*, JQ904627.1)
M10	*bla*$_{ADC}$ (ND) *bla*$_{OXA}$ (ND)	*bla*$_{NDM-1}$ (IS*Aba14* bracketed transposon also carrying *aphA6*) *bla*$_{CARB-16}$ (ND)		*aadB* (pRAY*-V1, JF343536.2) *aphA6* (IS*Aba14* bracketed transposon also carrying *bla* $_{NDM-1}$)
M11	*bla*$_{ADC}$ (interrupted by IS*1008*) *bla*$_{OXA-94}$ (present)	*bla*$_{NDM-1}$ (IS*Aba14* bracketed transposon also carrying *aphA6*)		*aadB* (pRAY*, JQ904627.1) *aphA6* (IS*Aba14* bracketed transposon also carrying *bla* $_{NDM-1}$)
M12	*bla*$_{ADC-79}$ (present) *bla*$_{OXA-69}$ (absent)	*bla*$_{OXA-23}$ (Tn*2006*)		None
M13	*bla*$_{ADC-73}$ (present) *bla*$_{OXA-66}$ (ND)	*bla*$_{OXA-23}$ (AbaR4b) *bla*$_{TEM-1}$ (AbGRI2-15)		*aphA1* (AbGRI2-15) *armA* (AbGRI3-1) *strA* (AbaR4b) *strB* (AbaR4b)
M14	*bla*$_{ADC-57}$ (ND) *bla*$_{OXA-51-like}$ (ND)	*bla*$_{OXA-23}$ (AbGRI1-like-2)		*strA* (AbGRI1-like-2) *strB* (AbGRI1-like-2)
M15	*bla*$_{ADC-79}$ (present) *bla*$_{OXA-69}$ (absent)	*bla*$_{OXA-23}$ (Tn*2006*)		None
M16	*bla*$_{ADC-30}$ (present) *bla*$_{OXA-66}$ (absent)	*bla*$_{OXA-23}$ (Tn*2006*) *bla*$_{TEM-1}$ (AbGRI2-15)		*aacA4* (AbGRI3-1) *aadA1* (AbGRI3-1) *aphA1* (AbGRI2-15) *armA* (AbGRI3-1) *strA* (AbGRI1-like-1) *strB* (AbGRI1-like-1)
M17	*bla*$_{ADC-30}$ (present) *bla*$_{OXA-66}$ (absent)	*bla*$_{OXA-23}$ (Tn*2006*) *bla*$_{TEM-1}$ (AbGRI2-15)		*aacA4* (AbGRI3-1) *aadA1* (AbGRI3-1) *aphA1* (AbGRI2-15)

(Continued)

TABLE 2 | Continued

Isolate No.	Resistance to β-lactams		Resistance to aminoglycosides	
	Intrinsic resistance genes (An upstream IS*Aba1*)	Acquired resistance genes (associated MGEs)	Intrinsic resistance genes	Acquired resistance genes (associated MGEs)
				armA (AbGRI3-1) *strA* (AbGRI1-like-1) *strB* (AbGRI1-like-1)
M18	$bla_{ADC-258}$[a] (absent) bla_{OXA-94} (absent)	bla_{NDM-1} (IS*Aba14* interrupted Tn*125*)		*aadB* (pRAY*, JQ904627.1)
M19	$bla_{ADC-257}$ (absent) bla_{OXA-91} (absent)	bla_{NDM-1} (IS*Aba14* interrupted Tn*125*) $bla_{CARB-16}$ (ND)		*aadB* (pRAY*-V1, JF343536.2) *aphA6* (IS*Aba14-aphA6*-IS*Aba125*)
M20	bla_{ADC-73} (absent) bla_{OXA-66} (absent)	bla_{NDM-1} (IS*Aba14* interrupted Tn*125*) bla_{TEM-1} (AbGRI2-15) bla_{OXA-23} (Tn*2006*)		*aphA1* (AbGRI2-15) *aphA6* (IS*Aba14-aphA6*-IS*Aba125*) *aadA1*(AbGRI3-4) *aacA4* (AbGRI3-4) *armA* (AbGRI3-4)

[a]*novel variant; ND, could not be determined; MGEs, mobile genetic elements. The symbol * is part of the plasmid's name.*

the integrase-coding gene (*int*) of the plasmid linker was uniquely interrupted by and IS*Aba125* element. The island carried three resistance genes (*sul2*, *strA*, and *strB*). Of all abGRI1-type RIs, AbGRI1-like-2 carried the largest number of resistance genes (bla_{OXA-23}, *tet(B)*, *sul2*, *strA*, and *strB*). Compared to AbGRI1-0, this version distinctively carried Tn*6022* in which *sup* gene was interrupted by Tn*2006*. In addition, [*tet(B)-tetR(B)*] element was also inserted within Tn*6172*.

Two types of IS*26*-bound genomic RIs were also identified. These included AbGRI2- and AbGRI3-type RIs that coexisted in all GC2 isolates. Only one version of AbGRI2 (AbGRI2-15) (Liepa et al., 2021) was identified. It harbored the two resistance genes bla_{TEM-1} and *aphA1*. While two versions of AbGRI3 were identified, an expanded form (designated before AbGRI3-1) was the dominant one (Blackwell et al., 2017). AbGRI3-1 carried seven resistance genes [*mphE-msrE-armA-sul1-aadA1-catB8-aacA4]*. A shorter version, designated before as AbGRI3-4 (Blackwell et al., 2017), was confined to GC2 isolates of the ST1816/195^{Oxf} with only three resistance genes onboard [*mphE*, *msrE*, and *armA*]. Bracketed by two inversely oriented copies of IS*Aba1*, GIsul2 RI carrying *sul2* as a sole resistance gene co-existed with Tn*6022* in all GC1 isolates and their phylogenetically related isolates M06 and M09.

As described above, RI-PER-7 was identified on a plasmid carried by M03 whose sequence was partially identified. The island hosted the largest combination of resistance genes compared to other RIs identified in the current study. These included *arr-2*, *cmlA5*, bla_{PER-7}, *armA*, *msrE*, *mphE*, and two copies of *sul1*. RIs correlated to different STs are shown in **Table 3**.

DISCUSSION

Updates on the genetic background of MDR and XDR *A. baumannii* are continuously being published from different parts of the world (Hamidian and Nigro, 2019; Gheorghe et al., 2021; Wareth et al., 2021) and from Egypt as well (Hassan et al., 2021; Jalal et al., 2021; Wasfi et al., 2021). However, reports about the association of resistance genes with RIs are relatively scarce. This is in part due to the need for multistep PCR mapping or whole-genome sequencing. To the best of our knowledge, this is the first report about the diversity and the genetic configuration of genomic RIs carried by *A. baumannii* isolates from Egypt. For this purpose, draft genomes of 18 non-duplicate MDR and XDR isolates were generated. Mostly from ICUs, the isolates were recovered from patients with bloodstream, respiratory tract, and wound infections. Very few treatment options were available. Draft genomes were employed for MLST analysis using both Pasteur and Oxford schemes. Oxford scheme-based analysis revealed the co-existence of two different alleles of the *gdhB* locus in 7/18 isolates generating two STs per isolate, a previously reported drawback for the scheme (Tomaschek et al., 2016). Nevertheless, MLST profiles generated by the Oxford scheme showed superior discrimination and concordance with the SNP-based phylogeny results. This was in line with other reports as well (Tomaschek et al., 2016; Gaiarsa et al., 2019). As reported before (Karah et al., 2012), most of the MDR and XDR *A. baumannii* strains belong to the Pasteur CCs 1 and two widely known as GC1 and GC2. In agreement with other studies (Al-Hassan et al., 2019; Fam et al., 2020; Wasfi et al., 2021), MLST analysis revealed the predominance of GC2 isolates in our collection (38.8%). Nevertheless, GC1 strains outweighed those that belonged to GC2 studied by others in our region (Ghaith et al., 2017; Jalal et al., 2021). Less representation (16.6%) was noted for the recently described GC9 (Müller et al., 2019) known to be endemic in Middle East countries (Al-Hassan et al., 2013, 2021; Bonnin et al., 2013; Ghaith et al., 2017; Jaidane et al., 2018; Salloum et al., 2018). Notably, a low prevalence of high-risk GCs was reported by older studies in Egypt (Al-Hassan et al., 2013; El Bannah et al., 2018), reflecting the progressive expansion of high-risk global clones in Egyptian hospitals over years. The emergence of successful STs not assigned to any high-risk GCs was also evident in the current study. These included the novel clonal complex CC2329^{Oxf} (CC113^{Pas}) represented

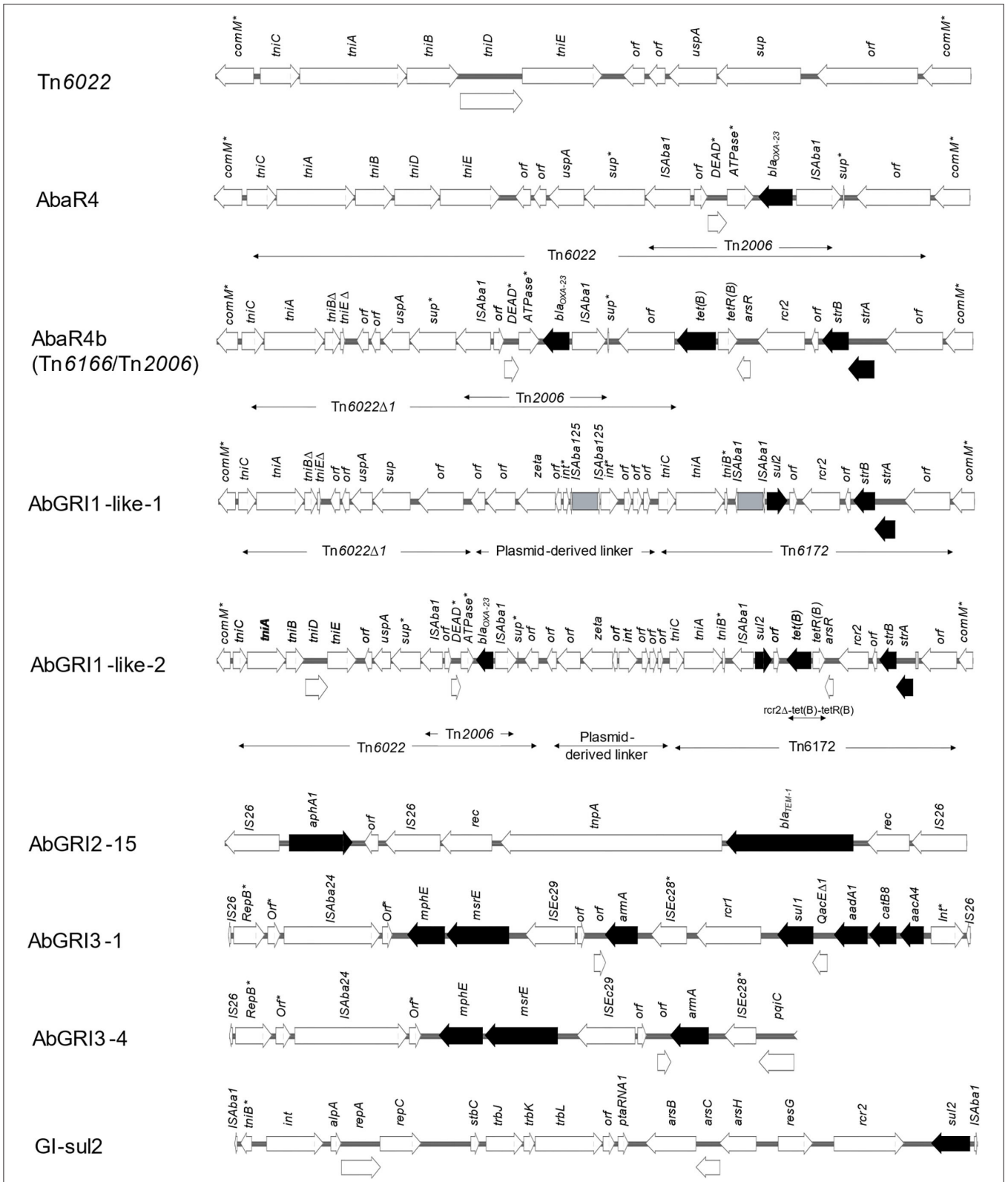

FIGURE 4 | Structures of resistance islands identified in the current study. Nine types of genomic RIs were identified in the isolates. These included Tn*6022*, AbaR4, three AbGRI1 variants, one AbGRI2, two variants of AbGRI3, and GIsul2. Arrows denote open reading frames. Antimicrobial resistance genes are represented by black arrows. Asterisks indicate interrupted genes.

TABLE 3 | Correlation between genomic resistance islands and STs.

GC	CC^{Pas}	CC^{Oxf}	ST^{Pas}	ST^{Oxf}	Isolate No.	RI	Resistance genes	References
1	1	231	19	1,604/231	M12	Tn*6022*	None	Hamidian and Hall, 2011
					M15	GIsul2	*sul2*	Nigro and Hall, 2011
2	2	208	2	1,050/2,058	M01	AbGRI1-like-1	*sul2-strA-strB*	Hamidian and Hall, 2017b
				1,050/2,058	M16	AbGRI2-15	bla_{TEM-1}-*aphA1*	Liepa et al., 2021
				1,050/2,058	M17	AbGRI3-1	*mphE-msrE-armA-sul1-aadA1-catB8-aacA4*	Blackwell et al., 2017
				1,816/195	M04	AbaR4b	*strA-strB-tet(B)-*bla_{OXA-23}	Seputiene et al., 2012
				1,816/195	M05	AbGRI2-15	bla_{TEM-1}-*aphA1*	Liepa et al., 2021
				1,816/195	M13	AbGRI3-4	*mphE-msrE-armA*	Blackwell et al., 2017
		546	570	1,701	M20	Tn*6022*	None	Hamidian and Hall, 2011
						AbGRI2-15	bla_{TEM-1}-*aphA1*	Liepa et al., 2021
						AbGRI3-1	*mphE-msrE-armA-sul1-aadA1-catB8-aacA4*	Blackwell et al., 2017
9	464	1,078	85	1,089	M02	Tn*6022*	None	Hamidian and Hall, 2011
					M11			
				1,078	M18			
-[a]	113	2,329	113	2,246	M03	AbaR4	bla_{OXA-23}	Hamidian and Hall, 2011
						RI-PER-7	*arr-2-cmlA5-sul1* (2 copies) - bla_{PER-7}-*armA-msrE-mphE*	Adams et al., 2020
				2,329	M14	AbGRI1-like-2	*strA-strB-tet(B)-sul2-*bla_{OXA-23}	Bi et al., 2020
	164	234	164	1,418	M19	-	-	-
ND[b]	ND	ND	ND	ND	M06[c]; M09[c]	Tn*6022*	None	Hamidian and Hall, 2011
						GIsul2	*sul2*	Nigro and Hall, 2011
					M10[d]	-	-	-

GC, international clone; CC, clonal complex; ST, sequence type; superscript Pas, Pasteur scheme; superscript Oxf, Oxford scheme; RI, resistance island; [a]not belonging to any GC; [b]could not be determined; [c]phylogenetically related to GC1 isolates; [d]phylogenetically related to M19 ($ST164^{Pas}$/$ST1418^{Oxf}$).

by M03 ($ST113^{Pas}/2246^{Oxf}$) and M14 ($ST113^{Pas}/ST2329^{Oxf}$). Isolates that belong to this CC were reported from Egypt (Jalal et al., 2021), Saudi Arabia (Lopes et al., 2015), and Brazil (Leal et al., 2020). Another ST identified here, $ST164^{Pas}/1418^{Oxf}$ was reported in the isolates from Myanmar (Tada et al., 2020), Vietnam (Wareth et al., 2021), Brazil (Coelho-Souza et al., 2013), Kenya (Musila et al., 2021), and as a major clone in Thailand (Khuntayaporn et al., 2021). SNP-based phylogenetic analysis showed that our isolates were clustered with others from different parts of the world. Transmission of genetically related strains over continents might be facilitated by travel-associated fecal colonization (Ostholm-Balkhed et al., 2013) and medical tourism (Benenson et al., 2018). Together with international strains with similar STs, our isolates were distributed over seven clusters in a pattern that fully matched the Oxford scheme-based STs.

The detailed profiling of the resistance determinants and correlation to STs and resistance phenotypes was presented in the current study with special emphasis on resistance to β-lactams and aminoglycosides. The epidemiological linkage between specific $bla_{OXA-51-like}$ variants and certain GCs was reported before (Zander et al., 2012; Karah et al., 2016; Jaidane et al., 2018) and was also evident in our isolates. This was noted for bla_{OXA-64}, bla_{OXA-66}, and bla_{OXA-94} that were linked to GC1, GC2, and GC9, respectively. In agreement with others (Jalal et al., 2021), bla_{ADC-79} was linked to GC1. Except for those that belonged to $ST1050/2058^{Oxf}$ which carried bla_{ADC-30}, GC2 isolates carried bla_{ADC-73}, a single-nucleotide variant of bla_{ADC-30} (Karah et al., 2016). IS*Aba1*-amplified ADC-type β-lactamases, previously coupled to high-level cephalosporin resistance (Corvec et al., 2003), were confined to GC1 and GC2 isolates. Carbapenem resistance in our collection was mediated by two carbapenem-hydrolyzing enzymes, namely, OXA-23 and NDM-1. OXA-23 was the most common of all acquired β-lactamases produced by our isolates. It is also the most frequently described carbapenemase globally (Hamidian and Nigro, 2019). The gene bla_{OXA-23} existed in Tn*2006* that, in turn, was sometimes embedded in RIs. Despite the variety of the genetic platforms known to harbor bla_{OXA-23}, Tn*2006* is the dominant vehicle for the acquisition of the gene worldwide (Nigro and Hall, 2016; Hamidian and Nigro, 2019). Less frequently, carbapenem resistance was mediated by NDM-1 (class B β-lactamases). In addition to one GC2 isolate (M20) and the phylogenetically related isolates M10 and M19, bla_{NDM-1} was carried by all GC9 ($ST85^{Pas}$) isolates. GC9 was claimed to act as a reservoir for bla_{NDM-1} in our region (Bonnin et al., 2013; Jaidane et al., 2018; Salloum et al., 2018; Al-Hassan et al., 2021). As described in our previous study (Zafer et al., 2021), bla_{NDM-1} laid within an IS*Aba14*-bracketed transposon also carrying *aphA6* in M02, M11, and M10. However, the transposon could not be identified in other NDM-producer strains in our collection.

Large-scale screening of this novel transposon is, therefore, recommended. Although reported in a higher prevalence in Egypt (El-Sayed-Ahmed et al., 2015; Abouelfetouh et al., 2019; Wasfi et al., 2021), a combination of the carbapenemase-coding genes bla_{OXA-23} and bla_{NDM-1} was found in only one isolate (M20). Class A β-lactamases, including TEM-1, CARB-16, and PER-7, had a considerable share in our collection too. While the exact environment of $bla_{CARB-16}$ could not be identified, both bla_{TEM-1} and bla_{PER-7} were exclusively carried within RIs, including AbGRI2 and RI-PER-7, respectively. The latter was first described as Tn*1548*-like-2 transposon by Karah et al. (2016) and later designated RI-PER-7 by Adams et al. (2020). Both reported the island in isolates that had Pasteur ST25, a double-locus variant of ST113^{Pas} in which RI-PER-7 was identified here. Shorter versions of the island were also reported to be carried by members of the family *Enterobacteriaceae* (Adams et al., 2020). WGSs of four isolates of the ST ST2246^{Oxf} were generated in a recent study in Egypt (Jalal et al., 2021). While the authors did not report the RI-PER-7 in their isolates, the signature genes of the island [*mphE*, *msrE*, *armA*, *sul1*, bla_{PER-7}, *cmlA5*, and *arr2*] were identified in 3/4 (75%) isolates. This newly emerging ST might thus serve as a reservoir for RI-PER-7. While the RI-PER-7-positive contig of M03 showed the highest similarity to a plasmid sequence and was thus anticipated to be plasmid-mediated, the exact location of the island in ST2246^{Oxf} is yet to be confirmed.

Of all the aminoglycoside resistance genes identified here, those conferring resistance to the clinically relevant aminoglycosides, amikacin, gentamicin, and tobramycin, were of much concern. Most importantly, the broad-spectrum *armA* gene conferring high-level resistance to all aminoglycosides (Galimand et al., 2003) was carried by all GC2 isolates. A high prevalence of *armA* has been previously reported in Egypt (El-Sayed-Ahmed et al., 2015). In addition, co-existing bla_{OXA-23}, bla_{NDM-1}, and *armA* were found in one GC2 isolate (M20). This combination was identified on plasmids of 8/25 (32%) isolates in an older study in Egypt (El-Sayed-Ahmed et al., 2015). Amikacin resistance in our isolates was also coded by *aphA6* in 38.8% of the isolates. The gene is commonly identified in *A. baumannii* within the composite transposon Tn*aphA6* in which it is bracketed by two directly oriented IS*Aba125* elements (Nigro et al., 2011). Nevertheless, here it was most commonly identified within a bracket of an upstream IS*Aba14* element and a downstream IS*Aba125* element that was sometimes part of a composite transposon also carrying bla_{NDM-1}, as described above. Given that the IS*Aba125* elements are thought to drive the overexpression of *aphA6* imparting high-level amikacin resistance, the effect of the upstream IS*Aba14* insertion is questionable. Notably, this unusual environment was associated with unrelated STs. While frequently found on plasmids (Nigro and Hall, 2012b; Hamidian and Hall, 2014; Hamidian et al., 2014), plasmid-associated *aphA6* was found in one isolate (M05) in our collection. Encoding resistance to both gentamicin and tobramycin, *aadB* was spotted in 7/18 isolates on pRAY plasmid derivatives. In *A. baumannii*, *aadB* was identified within a class 1 integron or more commonly on the globally distributed pRAY plasmid derivatives (Hamidian et al., 2012). While the GC1 isolates M12 and M15 did not carry any pRAY plasmids or *aadB*, such plasmids were carried by their phylogenetically related isolates M06 and M09. Other pRAY-positive STs included ST85^{Pas} and ST164^{Pas}. In addition to *armA*, the long version of AbGRI3-1 RIs also carried *aac4* that encodes the aminoglycoside modifying enzyme AAC(6')-Ib', conferring resistance to gentamicin rather than amikacin modified by AAC(6')-Ib (Ramirez and Tolmasky, 2010). In agreement with a recent study from Egypt, *aac4* was merely carried by a subset of GC2 strains, perhaps carrying the same version of AbGRI3 (Jalal et al., 2021). In addition, a wide array of resistance genes to other antimicrobial classes including multidrug efflux pumps was abundantly identified in our collection.

The advances in the next-generation sequencing technology made possible the genome-wide resistome analysis of different bacterial species and the investigation of the association of resistance genes with mobile genetic elements. Despite the difficulties imparted by the fragmented nature of contigs assembled from the short-read sequencer output, we used a combined approach of *de novo* assembly and reference mapping to uncover the configurations of RIs carried by our isolates. Examining the integrity of the *comM* gene, the hotspot for insertion of AbaR, AbaR4, and AbGRI1-type islands was the first step in RI analysis. The gene was found to be interrupted in the majority of the isolates (16/18) equally by the resistance genes-free transposon Tn*6022* and either AbaR4 or AbGRI1-like RIs (44.4%). A similar prevalence (46.7%) was reported for Tn*6022* in *A. baumannii* isolates from Korea (Kim et al., 2017). Tn*6022*, the backbone of AbaR4, comprises five transposition genes (*tniCABDE*), a universal stress protein-encoding gene (*uspA*), and a sulfate permease-coding gene (*sup*) (Hamidian and Hall, 2011). It has been widely identified in lineage 2 GC1 isolates (Hamidian and Hall, 2011). Here, the transposon was carried by GC1 isolates and their phylogenetically related ones (M06 and M09). In addition, the transposon interrupted the *comM* gene in all GC9 isolates and only one GC2 isolate (M20). In Tn*6022*, the gene *sup* is a hotspot for insertion of Tn*2006* with an embedded bla_{OXA-23} generating AbaR4. While widely described in GC2 isolates (Kim et al., 2012, 2013), AbaR4 was identified here within the chromosome of M03 only. Interestingly, co-existing chromosomal and plasmid copies of AbaR4 were recently reported in *Proteus mirabilis* (Octavia et al., 2020). While not self-transmissible (Bi et al., 2019), AbaR4 mobility to the chromosome of *P. mirabilis* was proposed to be mediated by plasmids (Octavia et al., 2020). This demonstrates the impending threat of interspecies plasmid-mediated transfer of AbaR4.

Twenty-two AbGRI1 configurations with different backbones were characterized by Bi et al. (2020). Here, we identified three variant structures of AbGRI1. Of them, two variants had the typical AbGRI1 backbone [Tn*6022* (or the deletion derivative, Tn*6022*Δ)-linker-Tn*6172*]. Despite their unique configurations, they were named here as AbGRI1-like-1 and AbGRI1-like-2 due to the lack of a universal nomenclature system for *A. baumannii* genomic RIs (Hamidian and Hall, 2018). AbGRI1-like-1 was identified in ST1050/2058^{Oxf} GC2 isolates. It was made up of Tn*6022*Δ, a plasmid-derived linker with *int* gene uniquely interrupted by an IS*Aba125* element and Tn*6172*. The

IS*Aba125* element interrupting the *int* gene might act as a hotspot for the insertion of resistance elements flanked by two direct copies of IS*Aba125* (such as Tn*aphA6*) by homologous recombination. The second variant AbGRI1-like-2 was formed of AbaR4, plasmid-derived linker, and Tn*6172* to which a ΔIS*CR2*-ΔTn*10* fragment carrying *tet(B)* gene was inserted (Hamidian and Hall, 2017b). This configuration resembled that of an unnamed RI identified by Bi et al. (2020) that also carried a second copy of AbaR4 inserted within *tet(B)* gene. AbGRI1-like-2 was solely carried by M14. The third variant of AbGRI1 was a Tn*2006*-interrupted AbGRI1-1. It had an atypical AbGRI1 structure lacking the plasmid-derived linker. Even though AbaR4 was reported not to have any variants (Hamidian and Hall, 2018), the Tn*2006*-interrupted AbGRI1-1 was named by Seputiene et al. (2012) as AbaR4b. For convenience, this name was used in the context of this study. In addition to conferring resistance to carbapenems, AbaR4b confers resistance to tetracycline and streptomycin/spectinomycin and was first identified in *A. baumannii* strains from Lithuania (Seputiene et al., 2012). In Korea, AbaR4b was found in 22.4% of the tested isolates, and all belonged to GC2 (Kim et al., 2017).

The IS*26*-bracketed RIs AbGRI2 and AbGRI3 co-existed in all GC2 isolates. While AbGRI2 occurred in only one configuration (AbGRI2-15), two variants of AbGRI3 with different resistance spectra were found. AbGRI2 has been reported most commonly in GC2 isolates carrying all or some of the resistance genes bla_{TEM}, *aphA1*, *catA1,* and [*sul1*, *aadA1,* and *aacC1*] within a class I integron (Nigro et al., 2013). AbGRI2-15 was first identified by Liepa et al. (2021) in *A. baumannii* strain collected from a patient in Lebanon. The island is a short version of AbGRI2 in which only *aphA1* and $bla_{\mathrm{TEM-1}}$ remained after IS*26*-mediated deletion and recombination events, as reported by the author. Each of the GC2 isolates carried either of the two variants AbGRI3-1 or AbGRI3-4. AbGRI3-1, also known as Tn*6180*, was first identified in *A. baumannii* strains MDR-TJ (GenBank accession: CP003500.1) and TYTH-1 (GenBank accession: CP003856.1) conferring resistance to four classes of antimicrobial agents (Blackwell et al., 2017). It was the least frequently identified among AbGRI3-type islands identified in a collection of *A. baumannii* isolates from Singapore in a study by Blackwell et al. (2017). In the same study, AbGRI3-4 was the dominant one identified in 46.6% of isolates. AbGRI3-4 is a short version of AbGRI3, most importantly, retaining *armA*. Blackwell et al. (2017) also highlighted the successful dispersion of AbGRI3-4 in isolates from India and Sweden.

Genomic island sul2 (GIsul2) is an integrating element first described by Nigro and Hall (2011) in the chromosome of *A. baumannii* strain ATCC 17978 isolated in France in 1951. Within GIsul2 is located a dihydropteroate synthase type 2-coding gene (*sul2*) preceded by an IS*Aba1*. While thought to provide a promotor for *sul2* (Nigro and Hall, 2011), high-level sulfonamide resistance in ATCC 19606 conferred by *sul2* was not accompanied by an upstream IS*Aba1* (Hamidian and Hall, 2017a). GIsul2 was reported as the main vehicle for the mobilization of the *sul2* gene (Hamidian and Hall, 2017a). It is also the donor of [CR2-*sul2*] elements in AbGRI1-type RIs integrated through homologous recombination. Here, GIsul2 was solely identified in GC1 isolates and those found to be phylogenetically related.

CONCLUSION

Beyond merely defining the resistance genes standing behind MDR and XDR in *A. baumannii*, WGS was used in the current study for defining the genomic RIs carried by clinical isolates of *A. baumannii* from Egypt. Epidemiology analysis of the isolates showed a significant representation of the high-risk GCs, particularly GC2. Novel ST ($\mathrm{ST2329^{Oxf}}$), resistance gene ($bla_{\mathrm{ADC-258}}$), and IS (IS*Aba61*) were identified. RIs were carried by the majority of the isolates most frequently co-existing in GC2. They were loaded with several genes conferring resistance to various antimicrobial classes and hotspots for the acquisition of more resistance genes. AbGRI1-type RIs showed up with the widest diversity, including two novel configurations.

DATA AVAILABILITY STATEMENT

The datasets presented in this study can be found in online repositories. The names of the repository/repositories and accession number(s) can be found in the article/**Supplementary Material**.

ETHICS STATEMENT

The study was performed in accordance with relevant guidelines and regulations, and no experiments were performed on humans and/or human tissue samples. The study was approved by the local Ethical Committee of the Clinical and Chemical Pathology Department, Kasr Al-Ainy Hospital, Cairo University. Bacterial isolates were only collected as part of the routine patient care, and informed consent was not required.

AUTHOR CONTRIBUTIONS

MZ, AH, MA-A, HR, and SH contributed to the study design, performance of experiments, and data analysis. SH performed the genome assembly, bioinformatics analysis, and wrote the first draft of the manuscript. All authors read and approved the final version of the manuscript.

FUNDING

The authors thank the Deanship of Scientific Research at King Saud University for funding this work through Project No. RGP-038.

SUPPLEMENTARY MATERIAL

The Supplementary Material for this article can be found online at: https://www.frontiersin.org/articles/10.3389/fmicb.2022.878912/full#supplementary-material

REFERENCES

Abouelfetouh, A., Torky, A. S., and Aboulmagd, E. (2019). Phenotypic and genotypic characterization of carbapenem-resistant Acinetobacter baumannii isolates from Egypt. *Antimicrob. Resist. Infect. Control* 8, 185. doi: 10.1186/s13756-019-0611-6

Adams, M. D., Pasteran, F., Traglia, G. M., Martinez, J., Huang, F., Liu, C., et al. (2020). Distinct mechanisms of dissemination of NDM-1 metallo-beta-lactamase in acinetobacter species in argentina. *Antimicrob. Agents Chemother.* 64. doi: 10.1128/AAC.00324-20

Alcock, B. P., Raphenya, A. R., Lau, T. T. Y., Tsang, K. K., Bouchard, M., Edalatmand, A., et al. (2020). CARD 2020: antibiotic resistome surveillance with the comprehensive antibiotic resistance database. *Nucleic Acids Res.* 48, D517–D525. doi: 10.1093/nar/gkz935

Al-Hassan, L., El Mehallawy, H., and Amyes, S. G. (2013). Diversity in Acinetobacter baumannii isolates from paediatric cancer patients in Egypt. *Clin. Microbiol. Infect.* 19, 1082–1088. doi: 10.1111/1469-0691.12143

Al-Hassan, L., Elbadawi, H., Osman, E., Ali, S., Elhag, K., Cantillon, D., et al. (2021). Molecular epidemiology of carbapenem-resistant acinetobacter baumannii from Khartoum State, Sudan. *Front. Microbiol.* 12, 628736. doi: 10.3389/fmicb.2021.628736

Al-Hassan, L., Zafer, M. M., and El-Mahallawy, H. (2019). Multiple sequence types responsible for healthcare-associated Acinetobacter baumannii dissemination in a single centre in Egypt. *BMC Infect. Dis.* 19, 829. doi: 10.1186/s12879-019-4433-1

Andrews, S. (2010). *FastQC: A Quality Control Tool for High Throughput Sequence Data*. Available online at: http://www.bioinformatics.babraham.ac.uk/projects/fastqc. (accessed December 27, 2020).

Antipov, D., Hartwick, N., Shen, M., Raiko, M., Lapidus, A., and Pevzner, P. A. (2016). plasmidSPAdes: assembling plasmids from whole genome sequencing data. *Bioinformatics.* 32, 3380–3387. doi: 10.1093/bioinformatics/btw493

Bankevich, A., Nurk, S., Antipov, D., Gurevich, A. A., Dvorkin, M., Kulikov, A. S., et al. (2012). SPAdes: a new genome assembly algorithm and its applications to single-cell sequencing. *J. Comput. Biol.* 19, 455–477. doi: 10.1089/cmb.2012.0021

Bartual, S. G., Seifert, H., Hippler, C., Luzon, M. A., Wisplinghoff, H., and Rodriguez-Valera, F. (2005). Development of a multilocus sequence typing scheme for characterization of clinical isolates of Acinetobacter baumannii. *J. Clin. Microbiol.* 43, 4382–4390. doi: 10.1128/JCM.43.9.4382-4390.2005

Benenson, S., Nir-Paz, R., Golomb, M., Schwartz, C., Amit, S., Moses, A. E., et al. (2018). Carriage of multi-drug resistant bacteria among foreigners seeking medical care. *Sci. Rep.* 8, 9471. doi: 10.1038/s41598-018-27908-x

Bertelli, C., Laird, M. R., Williams, K. P., Simon Fraser University Research Computing, G., Lau, B. Y., Hoad, G., et al. (2017). IslandViewer 4: expanded prediction of genomic islands for larger-scale datasets. *Nucleic Acids Res.* 45, W30–W35. doi: 10.1093/nar/gkx343

Bi, D., Xie, R., Zheng, J., Yang, H., Zhu, X., Ou, H. Y., et al. (2019). Large-scale identification of AbaR-Type genomic islands in acinetobacter baumannii reveals diverse insertion sites and clonal lineage-specific antimicrobial resistance gene profiles. *Antimicrob. Agents Chemother.* 63. doi: 10.1128/AAC.02526-18

Bi, D., Zheng, J., Xie, R., Zhu, Y., Wei, R., Ou, H. Y., et al. (2020). Comparative analysis of AbaR-type genomic islands reveals distinct patterns of genetic features in elements with different backbones. *mSphere.* 5. doi: 10.1128/mSphere.00349-20

Blackwell, G. A., Holt, K. E., Bentley, S. D., Hsu, L. Y., and Hall, R. M. (2017). Variants of AbGRI3 carrying the armA gene in extensively antibiotic-resistant Acinetobacter baumannii from Singapore. *J. Antimicrob. Chemother.* 72, 1031–1039. doi: 10.1093/jac/dkw542

Bolger, A. M., Lohse, M., and Usadel, B. (2014). Trimmomatic: a flexible trimmer for Illumina sequence data. *Bioinformatics* 30, 2114–2120. doi: 10.1093/bioinformatics/btu170

Bonnin, R. A., Cuzon, G., Poirel, L., and Nordmann, P. (2013). Multidrug-resistant Acinetobacter baumannii clone, France. *Emerging Infect. Dis.* 19, 822–823. doi: 10.3201/eid1905.121618

Carraro, N., Rivard, N., Burrus, V., and Ceccarelli, D. (2017). Mobilizable genomic islands, different strategies for the dissemination of multidrug resistance and other adaptive traits. *Mob. Genet. Elements* 7, 1–6. doi: 10.1080/2159256X.2017.1304193

Chan, A. P., Choi, Y., Clarke, T. H., Brinkac, L. M., White, R. C., Jacobs, M. R., et al. (2020). AbGRI4, a novel antibiotic resistance island in multiply antibiotic-resistant Acinetobacter baumannii clinical isolates. *J. Antimicrob. Chemother.* 75, 2760–2768. doi: 10.1093/jac/dkaa266

Chan, A. P., Sutton, G., Depew, J., Krishnakumar, R., Choi, Y., Huang, X. Z., et al. (2015). A novel method of consensus pan-chromosome assembly and large-scale comparative analysis reveal the highly flexible pan-genome of Acinetobacter baumannii. *Genome Biol.* 16, 143. doi: 10.1186/s13059-015-0701-6

CLSI (2020). "Performance standards for antimicrobial susceptibility testing; 30th edition," in *CLSI supplement M100*. Wayne, PA: Clinical and Laboratory Standards Institute.

Coelho-Souza, T., Reis, J. N., Martins, N., Martins, I. S., Menezes, A. O., Reis, M. G., et al. (2013). Longitudinal surveillance for meningitis by Acinetobacter in a large urban setting in Brazil. *Clin. Microbiol. Infect.* 19, E241–244. doi: 10.1111/1469-0691.12145

Corvec, S., Caroff, N., Espaze, E., Giraudeau, C., Drugeon, H., and Reynaud, A. (2003). AmpC cephalosporinase hyperproduction in Acinetobacter baumannii clinical strains. *J. Antimicrob. Chemother.* 52, 629–635. doi: 10.1093/jac/dkg407

Diancourt, L., Passet, V., Nemec, A., Dijkshoorn, L., and Brisse, S. (2010). The population structure of Acinetobacter baumannii: expanding multiresistant clones from an ancestral susceptible genetic pool. *PLoS ONE.* 5, e10034. doi: 10.1371/journal.pone.0010034

El Bannah, A. M. S., Nawar, N. N., Hassan, R. M. M., and Salem, S. T. B. (2018). Molecular epidemiology of carbapenem-resistant acinetobacter baumannii in a tertiary care hospital in Egypt: clonal spread of blaOXA-23. *Microb. Drug Resist.* 24, 269–277. doi: 10.1089/mdr.2017.0057

El-Sayed-Ahmed, M. A., Amin, M. A., Tawakol, W. M., Loucif, L., Bakour, S., and Rolain, J. M. (2015). High prevalence of bla(NDM-1) carbapenemase-encoding gene and 16S rRNA armA methyltransferase gene among Acinetobacter baumannii clinical Isolates in Egypt. *Antimicrob. Agents Chemother.* 59, 3602–3605. doi: 10.1128/AAC.04412-14

EUCAST (2021). *Breakpoint tables for interpretation of MICs and zone diameters, version 11.0*. Available online at: http://www.eucast.org (accessed May 1, 2021).

Fam, N. S., Gamal, D., Mohamed, S. H., Wasfy, R. M., Soliman, M. S., El-Kholy, A. A., et al. (2020). Molecular characterization of carbapenem/colistin-resistant acinetobacter baumannii clinical isolates from Egypt by whole-genome sequencing. *Infect. Drug Resist.* 13, 4487–4493. doi: 10.2147/IDR.S288865

Fournier, P. E., Vallenet, D., Barbe, V., Audic, S., Ogata, H., Poirel, L., et al. (2006). Comparative genomics of multidrug resistance in Acinetobacter baumannii. *PLoS Genet.* 2, e7. doi: 10.1371/journal.pgen.0020007

Gaiarsa, S., Batisti Biffignandi, G., Esposito, E. P., Castelli, M., Jolley, K. A., Brisse, S., et al. (2019). Comparative analysis of the two acinetobacter baumannii multilocus sequence typing (MLST) schemes. *Front. Microbiol.* 10, 930. doi: 10.3389/fmicb.2019.00930

Galimand, M., Courvalin, P., and Lambert, T. (2003). Plasmid-mediated high-level resistance to aminoglycosides in Enterobacteriaceae due to 16S rRNA methylation. *Antimicrob. Agents Chemother.* 47, 2565–2571. doi: 10.1128/AAC.47.8.2565-2571.2003

Ghaith, D. M., Zafer, M. M., Al-Agamy, M. H., Alyamani, E. J., Booq, R. Y., and Almoazzamy, O. (2017). The emergence of a novel sequence type of MDR Acinetobacter baumannii from the intensive care unit of an Egyptian tertiary care hospital. *Ann. Clin. Microbiol. Antimicrob.* 16, 34. doi: 10.1186/s12941-017-0208-y

Gheorghe, I., Barbu, I. C., Surleac, M., Sarbu, I., Popa, L. I., Paraschiv, S., et al. (2021). Subtypes, resistance and virulence platforms in extended-drug resistant Acinetobacter baumannii Romanian isolates. *Sci. Rep.* 11, 13288. doi: 10.1038/s41598-021-92590-5

Gurevich, A., Saveliev, V., Vyahhi, N., and Tesler, G. (2013). QUAST: quality assessment tool for genome assemblies. *Bioinformatics.* 29, 1072–1075. doi: 10.1093/bioinformatics/btt086

Hamidian, M., and Hall, R. M. (2011). AbaR4 replaces AbaR3 in a carbapenem-resistant Acinetobacter baumannii isolate belonging to global clone 1 from an Australian hospital. *J. Antimicrob. Chemother.* 66, 2484–2491. doi: 10.1093/jac/dkr356

Hamidian, M., and Hall, R. M. (2014). pACICU2 is a conjugative plasmid of Acinetobacter carrying the aminoglycoside resistance transposon TnaphA6. *J. Antimicrob. Chemother.* 69, 1146–1148. doi: 10.1093/jac/dkt488

Hamidian, M., and Hall, R. M. (2017a). Acinetobacter baumannii ATCC 19606 carries GIsul2 in a genomic island located in the Chromosome. *Antimicrob. Agents Chemother.* 61. doi: 10.1128/AAC.01991-16

Hamidian, M., and Hall, R. M. (2017b). Origin of the AbGRI1 antibiotic resistance island found in the comM gene of Acinetobacter baumannii GC2 isolates. *J. Antimicrob. Chemother.* 72, 2944–2947. doi: 10.1093/jac/dkx206

Hamidian, M., and Hall, R. M. (2018). The AbaR antibiotic resistance islands found in Acinetobacter baumannii global clone 1 - structure, origin and evolution. *Drug Resist. Updat.* 41, 26–39. doi: 10.1016/j.drup.2018.10.003

Hamidian, M., Holt, K. E., Pickard, D., Dougan, G., and Hall, R. M. (2014). A GC1 Acinetobacter baumannii isolate carrying AbaR3 and the aminoglycoside resistance transposon TnaphA6 in a conjugative plasmid. *J. Antimicrob. Chemother.* 69, 955–958. doi: 10.1093/jac/dkt454

Hamidian, M., and Nigro, S. J. (2019). Emergence, molecular mechanisms and global spread of carbapenem-resistant Acinetobacter baumannii. *Microb Genom.* 5. doi: 10.1099/mgen.0.000306

Hamidian, M., Nigro, S. J., and Hall, R. M. (2012). Variants of the gentamicin and tobramycin resistance plasmid pRAY are widely distributed in Acinetobacter. *J. Antimicrob. Chemother.* 67, 2833–2836. doi: 10.1093/jac/dks318

Hassan, R. M., Salem, S. T., Hassan, S. I. M., Hegab, A. S., and Elkholy, Y. S. (2021). Molecular characterization of carbapenem-resistant Acinetobacter baumannii clinical isolates from Egyptian patients. *PLoS ONE.* 16, e0251508. doi: 10.1371/journal.pone.0251508

Hsueh, P. R., Teng, L. J., Chen, C. Y., Chen, W. H., Yu, C. J., Ho, S. W., et al. (2002). Pandrug-resistant Acinetobacter baumannii causing nosocomial infections in a university hospital, Taiwan. *Emerging Infect. Dis.* 8, 827–832. doi: 10.3201/eid0805.020014

Hua, X., Moran, R. A., Xu, Q., He, J., Fang, Y., Zhang, L., et al. (2021). Acquisition of a genomic resistance island (AbGRI5) from global clone 2 through homologous recombination in a clinical Acinetobacter baumannii isolate. *J. Antimicrob. Chemother.* 76, 65–69. doi: 10.1093/jac/dkaa389

Jaidane, N., Naas, T., Oueslati, S., Bernabeu, S., Boujaafar, N., Bouallegue, O., et al. (2018). Whole-genome sequencing of NDM-1-producing ST85 Acinetobacter baumannii isolates from Tunisia. *Int. J. Antimicrob. Agents* 52, 916–921. doi: 10.1016/j.ijantimicag.2018.05.017

Jalal, D., Elzayat, M. G., Diab, A. A., El-Shqanqery, H. E., Samir, O., Bakry, U., et al. (2021). Deciphering multidrug-resistant acinetobacter baumannii from a pediatric cancer hospital in Egypt. *mSphere* 6, e0072521. doi: 10.1128/mSphere.00725-21

Karah, N., Dwibedi, C. K., Sjostrom, K., Edquist, P., Johansson, A., Wai, S. N., et al. (2016). Novel aminoglycoside resistance transposons and transposon-derived circular forms detected in carbapenem-resistant acinetobacter baumannii clinical isolates. *Antimicrob. Agents Chemother.* 60, 1801–1818. doi: 10.1128/AAC.02143-15

Karah, N., Sundsfjord, A., Towner, K., and Samuelsen, O. (2012). Insights into the global molecular epidemiology of carbapenem non-susceptible clones of Acinetobacter baumannii. *Drug Resist. Updat.* 15, 237–247. doi: 10.1016/j.drup.2012.06.001

Khuntayaporn, P., Kanathum, P., Houngsaitong, J., Montakantikul, P., Thirapanmethee, K., and Chomnawang, M. T. (2021). Predominance of international clone 2 multidrug-resistant Acinetobacter baumannii clinical isolates in Thailand: a nationwide study. *Ann. Clin. Microbiol. Antimicrob.* 20, 19. doi: 10.1186/s12941-021-00424-z

Kim, D. H., Choi, J. Y., Kim, H. W., Kim, S. H., Chung, D. R., Peck, K. R., et al. (2013). Spread of carbapenem-resistant Acinetobacter baumannii global clone 2 in Asia and AbaR-type resistance islands. *Antimicrob. Agents Chemother.* 57, 5239–5246. doi: 10.1128/AAC.00633-13

Kim, D. H., Jung, S. I., Kwon, K. T., and Ko, K. S. (2017). Occurrence of diverse AbGRI1-type genomic islands in acinetobacter baumannii global clone 2 isolates from South Korea. *Antimicrob. Agents Chemother.* 61. doi: 10.1128/AAC.01972-16

Kim, D. H., Park, Y. K., and Ko, K. S. (2012). Variations of AbaR4-type resistance islands in Acinetobacter baumannii isolates from South Korea. *Antimicrob. Agents Chemother.* 56, 4544–4547. doi: 10.1128/AAC.00880-12

Leal, N. C., Campos, T. L., Rezende, A. M., Docena, C., Mendes-Marques, C. L., De Sa Cavalcanti, F. L., et al. (2020). Comparative genomics of acinetobacter baumannii clinical strains from brazil reveals polyclonal dissemination and selective exchange of mobile genetic elements associated with resistance genes. *Front. Microbiol.* 11, 1176. doi: 10.3389/fmicb.2020.01176

Lee, Y., D'souza, R., Yong, D., and Lee, K. (2016). Prediction of putative resistance islands in a carbapenem-resistant acinetobacter baumannii global clone 2 clinical isolate. *Ann. Lab. Med.* 36, 320–324. doi: 10.3343/alm.2016.36.4.320

Leite, G. C., Oliveira, M. S., Perdigao-Neto, L. V., Rocha, C. K., Guimaraes, T., Rizek, C., et al. (2016). Antimicrobial combinations against pan-resistant acinetobacter baumannii isolates with different resistance mechanisms. *PLoS ONE.* 11, e0151270. doi: 10.1371/journal.pone.0151270

Letunic, I., and Bork, P. (2016). Interactive tree of life (iTOL) v3: an online tool for the display and annotation of phylogenetic and other trees. *Nucleic Acids Res.* 44, W242–245. doi: 10.1093/nar/gkw290

Li, H., and Durbin, R. (2010). Fast and accurate long-read alignment with Burrows-Wheeler transform. *Bioinformatics* 26, 589–595. doi: 10.1093/bioinformatics/btp698

Liepa, R., Mann, R., Osman, M., Hamze, M., Gunawan, C., and Hamidian, M. (2021). Cl415, a carbapenem-resistant Acinetobacter baumannii isolate containing four AbaR4 and a new variant of AbGRI2, represents a novel global clone 2 strain. *J. Antimicrob. Chemother.* 77, 345–350. doi: 10.1093/jac/dkab399

Lopes, B. S., Al-Agamy, M. H., Ismail, M. A., Shibl, A. M., Al-Qahtani, A. A., Al-Ahdal, M. N., et al. (2015). The transferability of blaOXA-23 gene in multidrug-resistant Acinetobacter baumannii isolates from Saudi Arabia and Egypt. *Int. J. Med. Microbiol.* 305, 581–588. doi: 10.1016/j.ijmm.2015.07.007

Magiorakos, A. P., Srinivasan, A., Carey, R. B., Carmeli, Y., Falagas, M. E., Giske, C. G., et al. (2012). Multidrug-resistant, extensively drug-resistant and pandrug-resistant bacteria: an international expert proposal for interim standard definitions for acquired resistance. *Clin. Microbiol. Infect.* 18, 268–281. doi: 10.1111/j.1469-0691.2011.03570.x

Morris, F. C., Dexter, C., Kostoulias, X., Uddin, M. I., and Peleg, A. Y. (2019). The Mechanisms of disease caused by Acinetobacter baumannii. *Front. Microbiol.* 10, 1601. doi: 10.3389/fmicb.2019.01601

Müller, C., Stefanik, D., Wille, J., Hackel, M., Higgins, P. G., and Siefert, H. (2019). "Molecular epidemiology of carbapenem-resistant Acinetobacter baumannii clinical isolates and identification of the novel international clone IC9: results from a worldwide surveillance study (2012–2016)", in *Paper presented at the ECCMID 2019: Proceeding of the 29th European Congress of Clinical Microbiology & Infectious Diseases.* Amsterdam, Netherlands.

Musila, L., Kyany'a, C., Maybank, R., Stam, J., Oundo, V., and Sang, W. (2021). Detection of diverse carbapenem and multidrug resistance genes and high-risk strain types among carbapenem non-susceptible clinical isolates of target gram-negative bacteria in Kenya. *PLoS ONE.* 16, e0246937. doi: 10.1371/journal.pone.0246937

Nigro, S. J., Farrugia, D. N., Paulsen, I. T., and Hall, R. M. (2013). A novel family of genomic resistance islands, AbGRI2, contributing to aminoglycoside resistance in Acinetobacter baumannii isolates belonging to global clone 2. *J. Antimicrob. Chemother.* 68, 554–557. doi: 10.1093/jac/dks459

Nigro, S. J., and Hall, R. M. (2011). GIsul2, a genomic island carrying the sul2 sulphonamide resistance gene and the small mobile element CR2 found in the Enterobacter cloacae subspecies cloacae type strain ATCC 13047 from 1890, Shigella flexneri ATCC 700930 from 1954 and Acinetobacter baumannii ATCC 17978 from 1951. *J. Antimicrob. Chemother.* 66, 2175–2176. doi: 10.1093/jac/dkr230

Nigro, S. J., and Hall, R. M. (2012a). Antibiotic resistance islands in A320 (RUH134), the reference strain for Acinetobacter baumannii global clone 2. *J. Antimicrob. Chemother.* 67, 335–338. doi: 10.1093/jac/dkr447

Nigro, S. J., and Hall, R. M. (2012b). Tn6167, an antibiotic resistance island in an Australian carbapenem-resistant Acinetobacter baumannii GC2, ST92 isolate. *J. Antimicrob. Chemother.* 67, 1342–1346. doi: 10.1093/jac/dks037

Nigro, S. J., and Hall, R. M. (2016). Structure and context of Acinetobacter transposons carrying the oxa23 carbapenemase gene. *J. Antimicrob. Chemother.* 71, 1135–1147. doi: 10.1093/jac/dkv440

Nigro, S. J., Post, V., and Hall, R. M. (2011). Aminoglycoside resistance in multiply antibiotic-resistant Acinetobacter baumannii belonging to global

clone 2 from Australian hospitals. *J. Antimicrob. Chemother.* 66, 1504–1509. doi: 10.1093/jac/dkr163

Octavia, S., Xu, W., Ng, O. T., Marimuthu, K., Venkatachalam, I., Cheng, B., et al. (2020). Identification of AbaR4 Acinetobacter baumannii resistance island in clinical isolates of blaOXA-23-positive Proteus mirabilis. *J. Antimicrob. Chemother.* 75, 521–525. doi: 10.1093/jac/dkz472

Ostholm-Balkhed, A., Tarnberg, M., Nilsson, M., Nilsson, L. E., Hanberger, H., Hallgren, A., et al. (2013). Travel-associated faecal colonization with ESBL-producing Enterobacteriaceae: incidence and risk factors. *J. Antimicrob. Chemother.* 68, 2144–2153. doi: 10.1093/jac/dkt167

Post, V., White, P. A., and Hall, R. M. (2010). Evolution of AbaR-type genomic resistance islands in multiply antibiotic-resistant Acinetobacter baumannii. *J. Antimicrob. Chemother.* 65, 1162–1170. doi: 10.1093/jac/dkq095

Ramirez, M. S., and Tolmasky, M. E. (2010). Aminoglycoside modifying enzymes. *Drug Resist. Updat.* 13, 151–171. doi: 10.1016/j.drup.2010.08.003

Ribeiro-Goncalves, B., Francisco, A. P., Vaz, C., Ramirez, M., and Carrico, J. A. (2016). PHYLOViZ Online: web-based tool for visualization, phylogenetic inference, analysis and sharing of minimum spanning trees. *Nucleic Acids Res.* 44, W246–251. doi: 10.1093/nar/gkw359

Salloum, T., Tannous, E., Alousi, S., Arabaghian, H., Rafei, R., Hamze, M., et al. (2018). Genomic mapping of ST85 blaNDM-1 and blaOXA-94 producing Acinetobacter baumannii isolates from Syrian Civil War Victims. *Int. J. Infect. Dis.* 74, 100–108. doi: 10.1016/j.ijid.2018.07.017

Seputiene, V., Povilonis, J., and Suziedeliene, E. (2012). Novel variants of AbaR resistance islands with a common backbone in Acinetobacter baumannii isolates of European clone II. *Antimicrob. Agents Chemother.* 56, 1969–1973. doi: 10.1128/AAC.05678-11

Tada, T., Uchida, H., Hishinuma, T., Watanabe, S., Tohya, M., Kuwahara-Arai, K., et al. (2020). Molecular epidemiology of multidrug-resistant Acinetobacter baumannii isolates from hospitals in Myanmar. *J Glob Antimicrob Resist* 22, 122–125. doi: 10.1016/j.jgar.2020.02.011

Tatusova, T., Dicuccio, M., Badretdin, A., Chetvernin, V., Nawrocki, E. P., Zaslavsky, L., et al. (2016). NCBI prokaryotic genome annotation pipeline. *Nucleic Acids Res.* 44, 6614–6624. doi: 10.1093/nar/gkw569

Tomaschek, F., Higgins, P. G., Stefanik, D., Wisplinghoff, H., and Seifert, H. (2016). Head-to-head comparison of two multi-locus sequence typing (MLST) schemes for characterization of acinetobacter baumannii outbreak and sporadic isolates. *PLoS ONE.* 11, e0153014. doi: 10.1371/journal.pone.0153014

Turton, J. F., Woodford, N., Glover, J., Yarde, S., Kaufmann, M. E., and Pitt, T. L. (2006). Identification of Acinetobacter baumannii by detection of the blaOXA-51-like carbapenemase gene intrinsic to this species. *J. Clin. Microbiol.* 44, 2974–2976. doi: 10.1128/JCM.01021-06

Wareth, G., Linde, J., Nguyen, N. H., Nguyen, T. N. M., Sprague, L. D., Pletz, M. W., et al. (2021). WGS-based analysis of carbapenem-resistant Acinetobacter baumannii in Vietnam and molecular characterization of antimicrobial determinants and MLST in Southeast Asia. *Antibiotics (Basel)* 10. doi: 10.3390/antibiotics10050563

Wasfi, R., Rasslan, F., Hassan, S. S., Ashour, H. M., and Abd El-Rahman, O. A. (2021). Co-Existence of Carbapenemase-Encoding GeJ. Clin. Microbiol.nes in Acinetobacter baumannii from Cancer Patients. *Infect Dis Ther.* 10, 291–305. doi: 10.1007/s40121-020-00369-4

Wick, R. R., Schultz, M. B., Zobel, J., and Holt, K. E. (2015). Bandage: interactive visualization of de novo genome assemblies. *Bioinformatics.* 31, 3350–3352. doi: 10.1093/bioinformatics/btv383

Wright, M. S., Haft, D. H., Harkins, D. M., Perez, F., Hujer, K. M., Bajaksouzian, S., et al. (2014). New insights into dissemination and variation of the health care-associated pathogen Acinetobacter baumannii from genomic analysis. *MBio.* 5, e00963–e00913. doi: 10.1128/mBio.00963-13

Zafer, M. M., Hussein, A. F. A., Al-Agamy, M. H., Radwan, H. H., and Hamed, S. M. (2021). Genomic characterization of extensively drug-resistant NDM-producing acinetobacter baumannii clinical isolates with the emergence of novel bla ADC-257. *Front. Microbiol.* 12, 736982. doi: 10.3389/fmicb.2021.736982

Zander, E., Nemec, A., Seifert, H., and Higgins, P. G. (2012). Association between beta-lactamase-encoding bla(OXA-51) variants and DiversiLab rep-PCR-based typing of Acinetobacter baumannii isolates. *J. Clin. Microbiol.* 50, 1900–1904. doi: 10.1128/JCM.06462-11

Zhang, G., Leclercq, S. O., Tian, J., Wang, C., Yahara, K., Ai, G., et al. (2017). A new subclass of intrinsic aminoglycoside nucleotidyltransferases, ANT(3")-II, is horizontally transferred among Acinetobacter spp. by homologous recombination. *PLoS Genet.* 13, e1006602. doi: 10.1371/journal.pgen.1006602

Conflict of Interest: The authors declare that the research was conducted in the absence of any commercial or financial relationships that could be construed as a potential conflict of interest.

Publisher's Note: All claims expressed in this article are solely those of the authors and do not necessarily represent those of their affiliated organizations, or those of the publisher, the editors and the reviewers. Any product that may be evaluated in this article, or claim that may be made by its manufacturer, is not guaranteed or endorsed by the publisher.

frontiers | Frontiers in Microbiology

TYPE Original Research
PUBLISHED 17 August 2022
DOI 10.3389/fmicb.2022.909886

OPEN ACCESS

EDITED BY
Remy A. Bonnin,
Université Paris-Saclay, France

REVIEWED BY
Duolong Zhu,
Baylor College of Medicine,
United States
Richa Misra,
University of Delhi, India

*CORRESPONDENCE
Ruchi Singh
ruchisp@gmail.com;
ruchisingh.nip@gov.in

SPECIALTY SECTION
This article was submitted to Antimicrobials, Resistance and Chemotherapy, a section of the journal Frontiers in Microbiology

RECEIVED 31 March 2022
ACCEPTED 25 July 2022
PUBLISHED 17 August 2022

CITATION
Yadav G and Singh R (2022) *In silico* analysis reveals the co-existence of CRISPR-Cas type I-F1 and type I-F2 systems and its association with restricted phage invasion in *Acinetobacter baumannii*. *Front. Microbiol.* 13:909886. doi: 10.3389/fmicb.2022.909886

In silico analysis reveals the co-existence of CRISPR-Cas type I-F1 and type I-F2 systems and its association with restricted phage invasion in *Acinetobacter baumannii*

Gulshan Yadav[1,2] and Ruchi Singh[1]*

[1]Indian Council of Medical Research (ICMR)—National Institute of Pathology, Safdarjung Hospital Campus, New Delhi, India, [2]Manipal Academy of Higher Education (MAHE), Manipal, Karnataka, India

Introduction: *Acinetobacter baumannii*, an opportunistic pathogen, rapidly acquires antibiotic resistance, thus compelling researchers to develop alternative treatments at utmost priority. Phage-based therapies are of appreciable benefit; however, CRISPR-Cas systems are a major constraint in this approach. Hence for effective implementation and a promising future of phage-based therapies, a multifaceted understanding of the CRISPR-Cas systems is necessary.

Methods: This study investigated 4,977 RefSeq genomes of *A. baumannii* from the NCBI database to comprehend the distribution and association of CRISPR-Cas systems with genomic determinants.

Results: Approximately 13.84% (n = 689/4,977) isolates were found to carry the CRSIPR-Cas system, and a small fraction of isolates, 1.49% (n = 74/4,977), exhibited degenerated CRISPR-Cas systems. Of these CRISPR-Cas positive (+) isolates, 67.48% (465/689) isolates harbored type I-F1, 28.59% (197/689) had type I-F2, and 3.7% (26/689) had co-existence of both type I-F1 and type I-F2 systems. Co-existing type I-F1 and type I-F2 systems are located distantly (~1.733 Mb). We found a strong association of CRISPR-Cas systems within STs for type I-F1 and type I-F2, whereas the type I-F1 + F2 was not confined to any particular ST. Isolates with type I-F1 + F2 exhibited a significantly high number of mean spacers (n = 164.58 ± 46.41) per isolate as compared to isolates with type I-F2 (n = 82.87 ± 36.14) and type I-F1 (n = 54.51 ± 26.27) with majority targeting the phages. Isolates with type I-F1 ($p < 0.0001$) and type I-F2 ($p < 0.0115$) displayed significantly larger genome sizes than type I-F1 + F2. A significantly reduced number of integrated phages in isolates with co-existence of type I-F1 + F2 compared with other counterparts was observed (p = 0.0041). In addition, the isolates carrying type I-F1 + F2 did not exhibit reduced resistance and virulence genes compared to CRISPR-Cas(−)

and CRISPR-Cas (+) type I-F1 and type I-F2, except for *bap, abaI*, and *abaR*.

Conclusion: Our observation suggests that the co-existence of type I-F1 and F2 is more effective in constraining the horizontal gene transfer and phage invasion in *A. baumannii* than the isolates exhibiting only type I-F1 and only type I-F2 systems.

KEYWORDS

***Acinetobacter baumannii*, CRISPR-Cas, co-existence, type I-F1, type I-F2**

Introduction

Acinetobacter baumannii, an opportunistic pathogen, is of great clinical relevance and is associated with hospital-acquired infections in immunocompromised patients (Munoz-Price and Weinstein, 2008). It rapidly develops resistance against all classes of antibiotics. Multidrug-resistant, extensively drug-resistant, and pan-drug-resistant strains of *A. baumannii* have now been prominently reported worldwide (Zarrilli et al., 2009; Tal-Jasper et al., 2016; Joshi et al., 2017; Bassetti et al., 2018; Leungtongkam et al., 2018) and obligated the World Health Organization to classify this pathogen as a critical priority pathogen for developing novel antibiotics (World Health Organization, 2017). In addition to novel antibiotics, alternative treatment strategies are also being explored (Baptista et al., 2018; Merker et al., 2020; Pires et al., 2020; Kumar et al., 2021; Micoli et al., 2021).

Clustered regularly interspaced short palindromic repeats (CRISPR) and CRISPR-associated (Cas) genes provide immunity against phages and other foreign genetic elements through the incorporation of spacers (Pourcel et al., 2005; Barrangou et al., 2007; Brouns et al., 2008). Approximately 36–42% of completely sequenced bacteria possess CRISPR-Cas systems (Makarova et al., 2020; Pourcel et al., 2020). The distribution of CRISPR-Cas systems in bacterial phyla is found to have differential representation across the taxonomic levels, where some groups and species are nearly devoid (< 1%) of CRISPR-Cas systems while some carry in almost all (> 95%) genomes (Burstein et al., 2016; Shehreen et al., 2019). The biological significance and basis of the irregular phyletic distribution of CRISPR–Cas systems are not yet proved.

CRISPR-Cas systems have been classified into two Classes (Class 1 and Class 2) and six types (Type I–VI) (Koonin et al., 2017; Makarova et al., 2020). Class 1 includes types I, III, and IV CRISPR-Cas systems, where type I systems are the most prevalent (~60%) in the bacterial population (Burstein et al., 2017; Hidalgo-Cantabrana et al., 2019). Contrary to Class 2, the Class 1 type I CRISPR-Cas system depends on a multi-subunit CRISPR-associated complex for antiviral defense (Cascade), which further employs Cas3 to degrade the foreign DNA (Westra et al., 2012). Based on the signature gene type I, CRISPR-Cas systems were further divided into seven subtypes (I–A to I–G) (Makarova et al., 2020). Being present in the clinically important (i.e., *Pseudomonas aeruginosa, A. baumannii*) and model bacterial species (i.e., *E. coli*), type I-F CRISPR-Cas is one of the most extensively studied systems. Because type I-F CRISPR-Cas system was first discovered in *Yersinia pestis* (Haft et al., 2005; Cady et al., 2011), its Cascade components were also named Csy (CRISPR subtype Ypest). An updated classification of type I-F CRISPR-Cas system defines type I-F1 loci consisting of four genes: *csy1* (*cas8f1*), *csy2* (*cas5f1*), *csy3* (*cas7f1*), and *csy4* (*cas6f*) while type I-F2 derived from type I-F1 consists of only three genes: *cas5fv* (*cas5f2*), *cas6f*, and *cas7fv* (*cas7f2*), along with the universal adaptation modules (*cas1* and *cas2-3* gene) (**Figure 1**). In addition, type I-F3, the minimal variant of type I-F1, is associated with Tn7-like transposons, has *cas8f3*/*cas5f3* fused, and lacks *cas1* and *cas2-3* genes (Makarova et al., 2020). Generally, only a single CRISPR-Cas system is present in the majority of the bacterial isolates. However, the co-existence of different types and subtypes was also reported in the single bacterial cell (Carte et al., 2014; Majumdar et al., 2015; Pinilla-Redondo et al., 2020). Type I-F was positively associated with the type IV-A1/2 CRISPR-Cas system and is proposed to compensate for the absence of adaptation modules in type IV (Pinilla-Redondo et al., 2020). Divisive evidence regarding the functional significance of co-occurrence of distinct CRISPR-Cas loci indicates that it can function either independently (Carte et al., 2014) or share components of the process (Deng et al., 2013).

Along with phages, the CRISPR-Cas system can restrict horizontal gene transfer (HGT) occurring through mobile genetic elements (MGEs), thereby limiting the acquisition of potentially beneficial antibiotic-resistant genes (ARGs) (Bikard et al., 2012; Jiang et al., 2013; O'Meara and Nunney, 2019). However, during strong antibiotic selection pressure, the bacterial population often involves loss or inactivation of the CRISPR-Cas system (Jiang et al., 2013; Watson et al., 2018). As the CRISPR-Cas system is

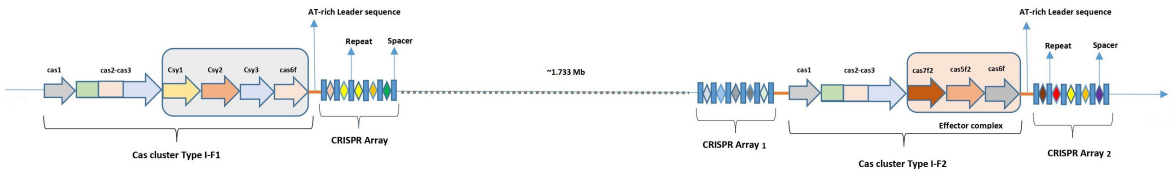

FIGURE 1
Diagrammatic representation of locus structure of CRISPR-Cas in isolates with co-existence of type I-F1 and type I-F2 systems.

present on MGEs (Koonin and Makarova, 2017), it can be attained back through HGT and generalized transduction (García-Martínez et al., 2018; Watson et al., 2018). However, there are some species where the CRISPR-Cas system can co-exist with resistance determinants indicating that a simple rule of selection pressure cannot be universal (Shehreen et al., 2019). The trade-off between retention of CRISPR-Cas system and HGT of beneficial MGEs is being explored to design novel treatments (Lin et al., 2017; Pursey et al., 2018; Pires et al., 2020). Being the natural predators of bacteria, phages can bypass their immune system through anti-CRISPR (ACR) genes. ACR inactivates the CRISPR-Cas system and can facilitate the successful integration of phage into the bacterial genome (Pawluk et al., 2018; Zhu et al., 2018), thereby making them an ideal tool to be used against antibiotic-resistant bacterial communities.

Genome-wide association studies with resistance, virulence, and other genomic determinants are proved to be beneficial to understand the behavior of CRISPR-Cas systems. This study involves the *in silico* analysis of a large set of genome data (n = 4,977) available in the public domain to reveal the distribution of CRISPR-Cas in *A. baumannii* and to validate the hypothesis that the presence of co-existing CRISPR-Cas systems may confer a fitness advantage in *A. baumannii* by impacting the dynamics of HGT.

Materials and methods

Genomic data

A total of 4,977 genome sequences of *A. baumannii* were downloaded from the NCBI RefSeq database as per availability on 18 January 2021. These genomes are either complete or assembled to different levels; complete genome (245) (containing 535 complete plasmid sequences), chromosome (23), scaffold (1,690), or contig (3,019). These sequences may also contain contigs or scaffolds from episomes. NCBI Annotation (Li et al., 2021) file and genome metadata (genome size, isolation source, host, host disease, submitter, geographic location of the sample) was collected for each isolate (**Supplementary Table 1**). Guanine–cytosine (GC) percentage was calculated using the pearl script available on git hub.[1] Multi-locus sequence typing (MLST) was performed using Pasture PubMLST typing scheme[2] (Jolley and Maiden, 2010).

Prediction of clustered regularly interspaced short palindromic repeats (CRISPR) arrays, Cas, anti- clustered regularly interspaced short palindromic repeats genes, and phages

The presence of CRISPR array/s was determined using a standalone command-line version of CRISPRCasFinder (v4.2.20), CRISPRDetect (v2.4), and CRISPR Recognition Tool (CRT) (v1.2) (Bland et al., 2007; Biswas et al., 2016; Couvin et al., 2018). CRISPRCasFinder, NCBI-BLASTn (v2.6.0), and NCBI RefSeq genome annotation GFF files were used to determine the presence of *cas* genes (McGinnis and Madden, 2004) and were classified according to the recent classification (Makarova et al., 2011, 2015, 2020). Final interpretations were made based on the same value given by any two out of the three software used. Manual interpretations were made wherever necessary (**Supplementary Table 1**). Anti-CRISPR (ACR) genes were identified by screening genomes against type I-F anti-CRISPRdb (Dong et al., 2018) using NCBI-tBLASTn with stringent cut-off to avoid false positives, that is, e-value $\leq 10^{-10}$ and bit score ≥ 200 (Shehreen et al., 2019). Integrated phages were discovered by ProphET, a phage estimation tool (Reis-Cunha et al., 2019).

Phylogenetic tree construction and annotation

The RealPhy (v1.13), a reference alignment-based phylogeny builder (Bertels et al., 2014) was used to construct a phylogenetic tree using whole-genome data of CRISPR-Cas (+) isolates. It directly maps short reads to a reference sequence. It extracts the single nucleotide polymorphisms (SNPs) to

1 https://github.com/rpotozky/GC-Content-Calculator
2 https://pubmlst.org/organisms/acinetobacter-baumannii

infer the phylogenetic tree using the maximum likelihood method for the aligned SNPs positions. We have used the merge option that combines alignments from mapping to multiple reference sequences to remove bias raised due to the alignment to a single reference genome. To visualize and annotate the phylogenetic tree, Interactive Tree Of Life (iTOL)[3] was used. The phylogenetic tree was uploaded as a Newick file and annotated using tools available on the iTOL website. Data of CRISPR-Cas systems, number of spacers, and MLST groups were overlaid on the phylogenetic tree as multi-value bars and color strips, respectively (Letunic and Bork, 2021). Genome alignment for variability visualization was performed using Mauve v2.4.0 (Darling et al., 2004).

Prediction of spacer target

A unique non-redundant spacer set for each class was obtained by clustering spacer sequences identified by CRISPRCasFinder with an array-quality score $\geq$ 4.0, using CD-HIT-EST (v4.8.1) (Huang et al., 2010) with an identity-cutoff of 0.95. Spacers with Ns were removed. NCBI-BLASTn (v2.6.0) was used to predict spacer targets against phage genomes, integrative conjugative elements (ICEs), plasmids, resistance genes, and virulence genes. BLASTn hits with at least 95% sequence identity and coverage were accepted as valid targets (Shehreen et al., 2019). Representative sequences of 99 phages that show interaction with *A. baumannii* were downloaded from the Microbe Vs. Phage (MVP) database (Gao et al., 2018). The life cycle (i.e., temperate, virulent) for these phages was predicted with PHAGEAI (Tynecki et al., 2020). ICEs sequences were downloaded from ICEberg 2.0 database (Liu M. et al., 2019). Plasmid sequences were downloaded from a curated database of plasmid sequences containing 10,892 complete plasmids (Brooks et al., 2019). Acquired resistance gene sequences were downloaded from the ResFinder database of acquired antimicrobial resistance genes (Zankari et al., 2012). Virulence genes were downloaded from the Virulence Factor Database (Chen et al., 2005; Liu B. et al., 2019).

Prediction of antibiotic resistance and virulence genes

ResFinder (v3.0), with a default minimum threshold and coverage of 0.9 and 0.6, respectively, were used to identify acquired antibiotic resistance genes (ARGs) (Camacho et al., 2009; Zankari et al., 2012, 2017; Bortolaia et al., 2020). ResFinder identifies ARGs from 15 antibiotic drug classes where a complete gene confers resistance. The virulence gene database was obtained from Virulence Finder Database (VFDB) for *Acinetobacter* spp. (Chen et al., 2005; Liu B. et al., 2019).

Statistical analysis

The presence of the CRISPR-Cas system, virulence, and ARGs are coded as binary variables for each genome. An unpaired two-tailed *t*-test (using GraphPad Prism v6.0.1) was used to determine the association of CRISPR-Cas systems with genome size, number of spacers, and phages. One-tailed paired *t*-test was used to compare the differences between CRISPR-Cas (−) and CRISPR-Cas (+) genomes of the same ST type. Chi-square (χ^2) test was used to determine the association of the virulence and ARGs with the CRISPR-Cas systems as described earlier (Shehreen et al., 2019).

Results and discussion

Clustered regularly interspaced short palindromic repeats (CRISPR)-Cas system in *Acinetobacter baumannii*

A total of 4,977 *A. baumannii* genomes from the NCBI Refseq database were analyzed to determine the frequency and distribution of CRISPR, Cas, and anti-CRISPRs among *A. baumannii*. Based on their source of origin at the time of isolation, genomes were classified into three major categories: clinical (n = 4,015), environmental (n = 185), and other (in case of unavailability of data) (n = 777). Among all, only 13.84% (n = 689/4,977) isolates harbored a functional CRISPR-Cas system and were distributed across the globe (**Figure 2**). These results are in concordance with previous studies that showed the presence of CRISPR-Cas systems in ∼14% of *A. baumannii* isolates (Shehreen et al., 2019; Pursey et al., 2022). Genomes with CRISPR-Cas systems were further analyzed and classified into three categories based on their type: 67.48% (465/689) CRISPR-Cas positive (+) genomes carried only type I-F1, 28.59% (197/689) carried only type I-F2, and 3.7% (26/689) were found to have co-existence of both type I-F1 and type I-F2 (herein after referred as type I-F1 + F2) (**Figure 3**). Although co-localization of different types of CRISPR-Cas systems is common in bacteria (Carte et al., 2014; Majumdar et al., 2015; Pinilla-Redondo et al., 2020) and are proposed to cooperate to counteract viral escape (Silas et al., 2017), co-localization of variants of type I-F (i.e., I-F1 and I-F2) is rare and not reported to date. A single isolate (strain MRSN7153, United States) was found to harbor a type III-B CRISPR-Cas system and was excluded from downstream analysis. A very low proportion of ACR genes (0.68%; n = 34/4,977) were found in *A. baumannii* (**Figure 3**). Hence, further correlational studies with ACR genes were not performed. Isolates with environmental niches were categorized

3 http://itol.embl.de

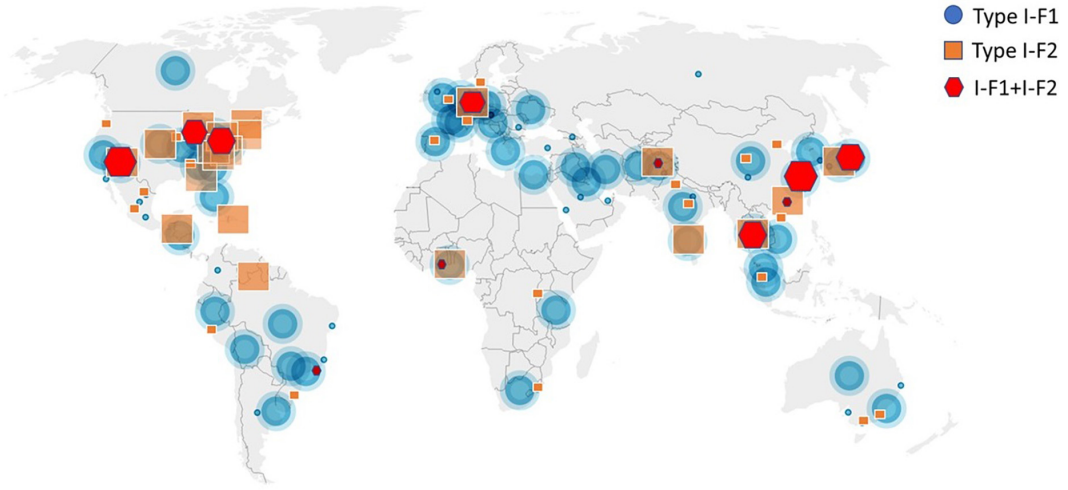

FIGURE 2
Geographical distribution of CRISPR-Cas (+) isolates across the world. Symbols are merged where two or more isolates coincide.

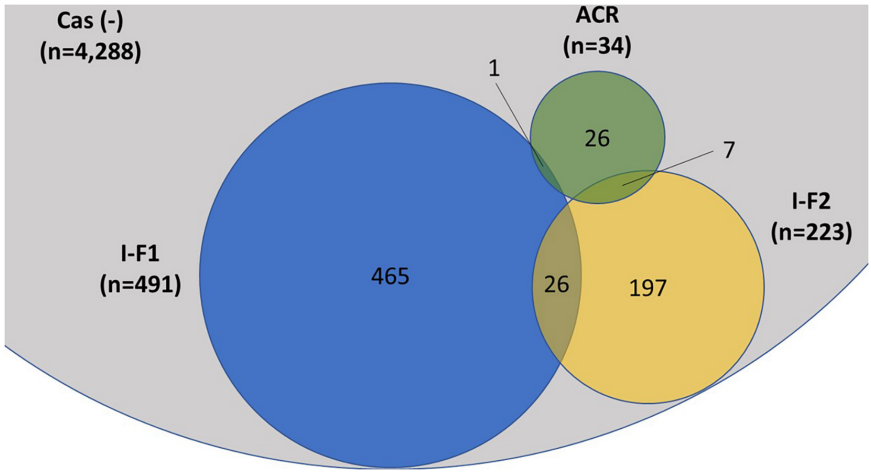

FIGURE 3
Distribution of CRISPR-Cas type I-F1, type I-F2, and anti-CRISPR (ACR) in the complete (n = 4,977) set of *A. baumannii* genomes. A single isolate was found to carry a type III-B system (data not shown). The proportions of degenerated systems (i.e., having either CRISPR or Cas cluster gene/s) are provided in **Supplementary Table 2**.

into hospital and natural environments categories. As expected, a significantly higher percentage (∼56%) of CRISPR-Cas presence was observed in isolates with natural environmental niche compared to clinical (∼15%) and hospital environment niche (∼9%) (**Supplementary Table 2**), indicating that CRISPR-Cas-mediated immunity provides a clear advantage during defense against phages (Barrangou et al., 2007).

Organization of type I-F1 + F2 locus

Recent classification based on the multiparametric analysis describes type I loci with *cas3* as a signature gene and type I-F with fused *cas3* and *cas2* genes (Makarova et al., 2011, 2015, 2020; Koonin et al., 2017). On exploring the genomes with type I-F1 + F2 Cas gene clusters, we found that both the systems follow the same organization and features of CRISPR-Cas type I-F1 and I-F2 systems as visualized individually and are distantly (∼1.733 Mb) located in the genome (**Figure 1**). Interestingly, type I-F2 systems are associated with two CRISPR arrays where one is very well-adapted and spacer rich, compared to the other. In contrast, type I-F1 is only associated with a single CRISPR array. The average spacer size for arrays associated with both type I-F1 and F2 systems is ∼29 bp and belongs to the medium spacers (28–32 bp) category (Pourcel et al., 2020).

Degenerated clustered regularly interspaced short palindromic repeats (CRISPR)-Cas systems

Under substantial antibiotic exposure, bacterial cells often suppress the function of the CRISPR-Cas system either by partial or complete loss of the CRISPR or Cas genes resulting in a degenerate system (Jiang et al., 2013). We found that 1.49% (74/4,977) isolates exhibited degenerated CRISPR-Cas systems, lacking either CRISPR (n = 15) or the complete set of Cas genes (n = 59) (**Supplementary Table 2**). We analyzed 545 plasmids from complete-level genome assemblies for the presence of the CRISPR-Cas systems and found that only 0.18% (1/545) plasmids carried a valid CRISPR array. This accounts for a very low proportion as compared to the average prevalence of 3.4% (546/15,938) across sequenced bacterial plasmids encoding the CRISPR-Cas system (Pourcel et al., 2020). None of the Cas cluster genes were found on the plasmid in *A. baumannii*.

A very low proportion of degenerated CRISPR-Cas systems and plasmids carrying CRISPR arrays suggest that these phenomena are rare but may occur in *A. baumannii*. However, a comparatively very low proportion of clinical isolates (∼15%) harboring CRISPR-Cas compared to environmental isolates (∼56%) suggests that antibiotics may exert selection pressure to lose out or selectively propagate isolates without CRISPR-Cas. Nevertheless, one can infer that the high prevalence of CRISPR-Cas among environmental isolates may be due to the abundance of phages in the environment and not the absence of antibiotics in the case of *A. baumannii*.

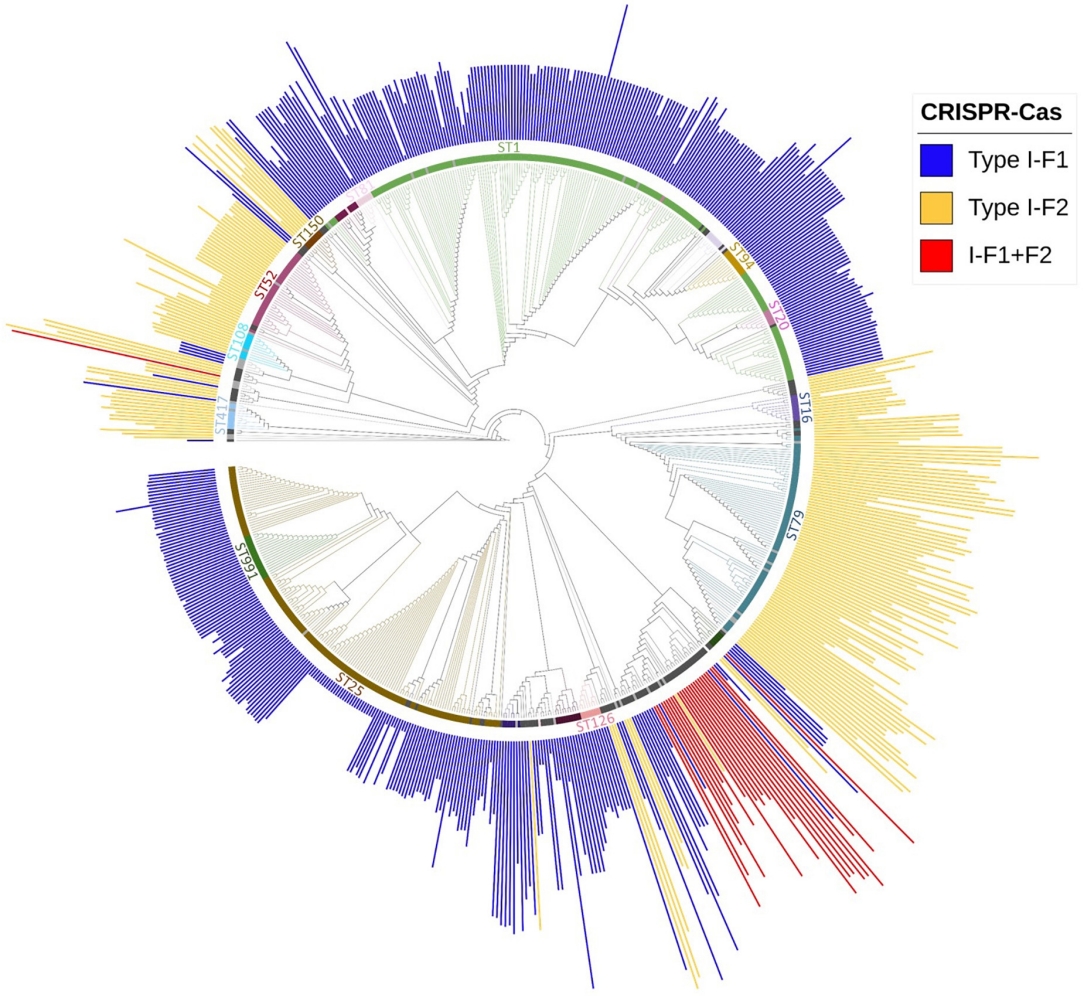

FIGURE 4
Phylogenetic distribution of different categories of CRISPR-Cas (+) isolates found in *A. baumannii* (n = 688). Major STs groups were labeled and are depicted with different colors, while lineages with ≤ 2 and ≤ 5 number of isolates with identical STs were colored with light gray and black, respectively. The height of the bars is proportionate to the total number of identified spacers in CRISPR array/s belonging to that isolate.

Association of sequence type and clustered regularly interspaced short palindromic repeats (CRISPR)-Cas

Multi-locus sequence typing relies on comparing the sequences of evolutionary conserved but polymorphism-harboring genes (Jolley and Maiden, 2010) and can be employed to compare the phylogenetic diversity among bacterial isolates (van Belkum et al., 2015). Sequence type of all *A. baumannii* isolates was determined using whole-genome sequence following the Pasture scheme and 4,841 isolates belonging to 314 different STs were found, 136 isolates did not belong to any defined ST. We observed that 60.63% (n = 3,018/4,977) isolates belonged to ST2 and were devoid of CRISPR-Cas except for 1 isolate which showed type I-F1. Analyzing the distribution of three classes of CRISPR-Cas system among STs, we observed that each class (type I-F1 or type I-F2) predominates within any particular ST with ST138 as an exception which showed the equivalent occurrence of both classes (**Supplementary Table 3**). Class I-F1 type was entirely observed in isolates with ST1 (n = 176/216), ST25 (n = 134/140), ST991 (n = 18/18), and ST20 (n = 9/10). Class I-F2 type was entirely observed in isolates with ST79 (n = 77/141), ST52 (n = 33/33), and ST16 (n = 10/25). However, type I-F1 + F2 were distributed in low frequencies across 12 different ST types, thereby not showing association toward any particular ST (**Figure 4**).

Relationship between genome size, phage, and clustered regularly interspaced short palindromic repeats (CRISPR)-Cas

The presence of an active CRISPR-Cas system constrains the HGT and phage genome integration, which can limit genome expansion in bacteria and may result in comparatively smaller genome size (Ochman et al., 2000; Lerat et al., 2005; van Belkum et al., 2015; Wheatley and MacLean, 2021; Pursey et al., 2022). Nevertheless, we found that CRISPR-Cas (+) *A. baumannii* isolates were ∼48,982 ± 34,462 bp lengthier than CRISPR-Cas (–) isolates. These results are consistent with the previous study on *A. baumannii* (Pursey et al., 2022). However, categorical observations differentiate skewed data among different types of CRISPR-Cas systems. The isolates harboring only type I-F1 and only type I-F2 CRISPR-Cas systems have unusually larger genomes ∼71,461 ± 29,915 bp ($p < 0.0001$) and ∼21,621 ± 252,021 bp ($p < 0.0115$) than CRISPR-Cas (–) isolates, respectively. However, the genome size of isolates having a type I-F1 + F2 system was smallest (∼1,45,733 ± 23,750 bp smaller ($p < 0.0001$) in comparison with Cas (–) isolates) as compared to other classes (**Figure 5A**).

Intra-ST analysis among prominent ST types harboring specific types of CRISPR-Cas systems confirmed the same trend (**Figure 5B**). The similarity in different isolates within an ST enables the identification of differential genomic determinants with relatively lower possibilities of discordant variables causing indeterminate effects of CRISPR-Cas systems (Wheatley and MacLean, 2021). Genome alignment of CRSIPR-Cas (+) and (–) isolates belonging to ST1 revealed the presence of phage, ICEs, and ARGs as the contributing factors for genome expansion, thus indicating the redundant function of CRISPR-Cas type I-F1 system (**Figure 5C**).

Because the active CRISPR-Cas system restricts phages, the observed genome size data were correlated with the integrated phage genome. Average number of phages incorporated (average phage genome size) in each category, Cas (–), type I-F1, type I-F2, and type I-F1 + F2 are 3.17 ± 1.55 (41,613 ± 26,878 bp), 3.91 ± 1.88 (36,789 ± 33,141 bp), 3.91 ± 2.27 (44,580 ± 42,515 bp), and 2.80769 ± 2.1357 (27,823 ± 15,807 bp), respectively. The mean number of integrated phages in CRISPR-Cas (+) isolates of both ST1 (type I-F1) and ST79 (type I-F2) was significantly higher than CRISPR-Cas (–) isolates (type I-F1 –4.73 + 1.86 vs. 3.92 + 0.98; $p = 0.005$; type I-F2– 5.04 ± 1.88 and 3.87 ± 2.54; $p = 0.000288$). Intra-ST comparative analysis of type I-F1 + F2 in CRISPR-Cas (+) and CRISPR-Cas (–) was not performed due to the limited data set available for the associated ST types.

Although a clear decline in the average number of phages in isolates with type I-F1 + F2 was found (p = 0.0041), to confirm the activity of the CRISPR-Cas system in restricting the incorporation of phage sequences, we also substantiated the results with phage genome size incorporated in each class, which demarcated a reduction in the size of the phage genome incorporated into the *A. baumannii* isolates with type I-F1 + F2 (**Figure 6**). The unusually high genome size and integrated phage genomes in isolates with either CRISPR-Cas type I-F1 or I-F2 compared with Cas (-) isolates needs further in-depth studies. We did not find any significant difference in the number of integrated phages in type I-F1 or type I-F2; indeed, their co-existence was more efficient in limiting phage entry, as evidenced by a significantly low number of integrated phages. However, co-occurrence may be associated with the synergistic/additive activity and improving the CRISPR-Cas system's efficacy but requires more deep, comprehensive, and experimental support.

Association with resistance and virulence genes

Antimicrobial resistance and virulence are important bacterial traits that help survive and infect the host. Bacteria develop antibiotic resistance either by acquiring resistance genes or through mutations in their genome. It is believed that the

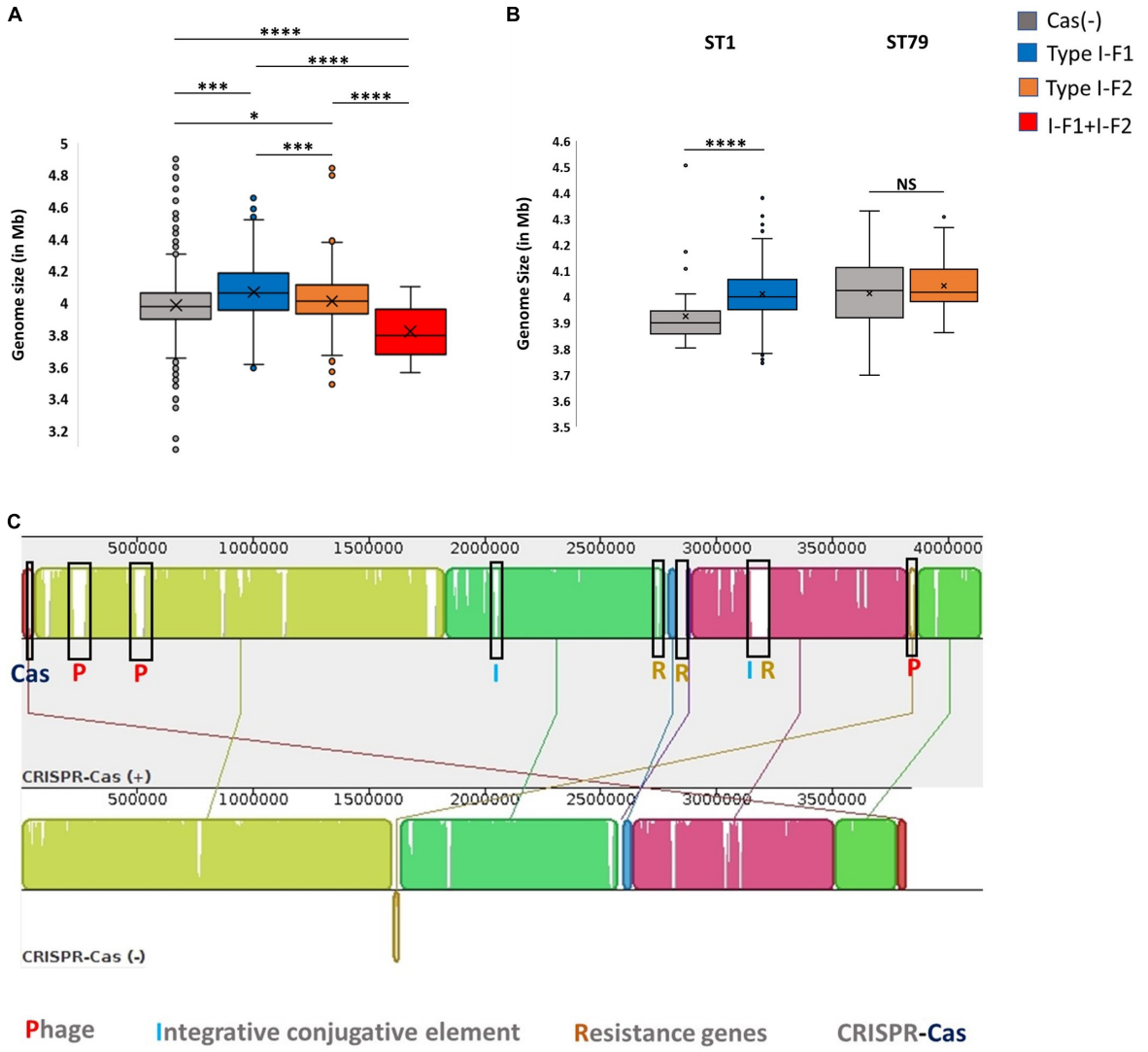

FIGURE 5
CRISPR-Cas and genome size. **(A)** Genome size comparison of CRISPR-Cas (−) and different categories of CRISPR-Cas (+) isolates. **(B)** Intra-ST analysis of genome size among CRISPR-Cas (−) and (+) isolates in ST1 and ST79. **(C)** Mauve alignment of CRISPR-Cas (+) and (−) ST1 isolates with extreme genome sizes. Where *($p < 0.05$), ***($p < 0.001$), ****($p < 0.0001$) and NS (Not Significant).

CRISPR-Cas system inhibits the acquisition of resistance genes but does not affect the emergence of mutations mediating antibiotic resistance. We investigated the impact of CRISPR-Cas affecting the acquisition of virulence genes and ARGs. In line with previous studies (Shehreen et al., 2019), our extensive analysis did not find an association of CRISPR-Cas (+) isolates with any particular antibiotic class (log frequency ratios ranged from −0.2 to + 0.2) (**Supplementary Figure 1A**). This suggests that CRISPR-Cas systems do not hinder the dissemination of resistance genes in *A. baumannii*. Similarly, we did not find an association of virulence genes with CRISPR-Cas (+) isolates. However, on analyzing the virulence gene frequencies among three CRISPR-Cas types, we found a strong negative association among isolates with type I-F1 + F2 for biofilm-associated protein (bap) and quorum-sensing genes, *abaI* and *abaR*, with a log frequency ratio of −0.8826, −1.0828, and −1.3767, respectively (**Supplementary Figure 1B**). The complete gene pool and their respective frequencies for each class of antibiotics and virulence genes found in *A. baumannii* are listed in **Supplementary Table 4**.

Overall, these results suggest that CRISPR-Cas in *A. baumannii* is not associated with limiting resistance and virulence gene uptake except among type I-F1 + F2 isolates for *bap* and quorum-sensing genes (*abaI* and *abaR*). Our results are consistent with previous studies showing a negative association among CRISPR-Cas (+) isolates for these genes with some modalities (Mangas et al., 2019; Leungtongkam et al., 2020; Tyumentseva et al., 2021).

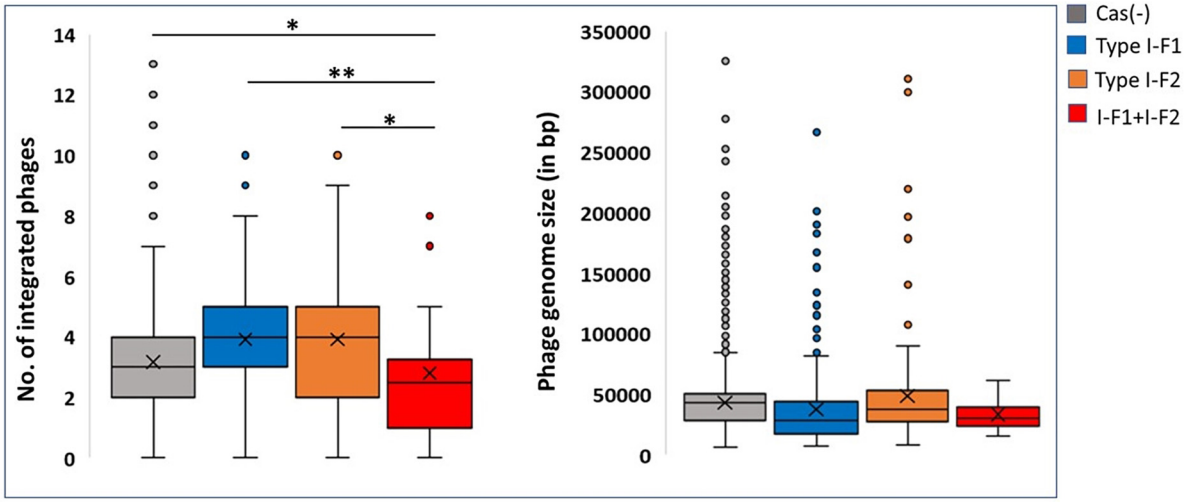

FIGURE 6
CRISPR and phages: Number of incorporated phages in genomes **(left side)** and the total genome size of the incorporated phage **(right side)**. Where *($p < 0.05$) and **($p < 0.01$).

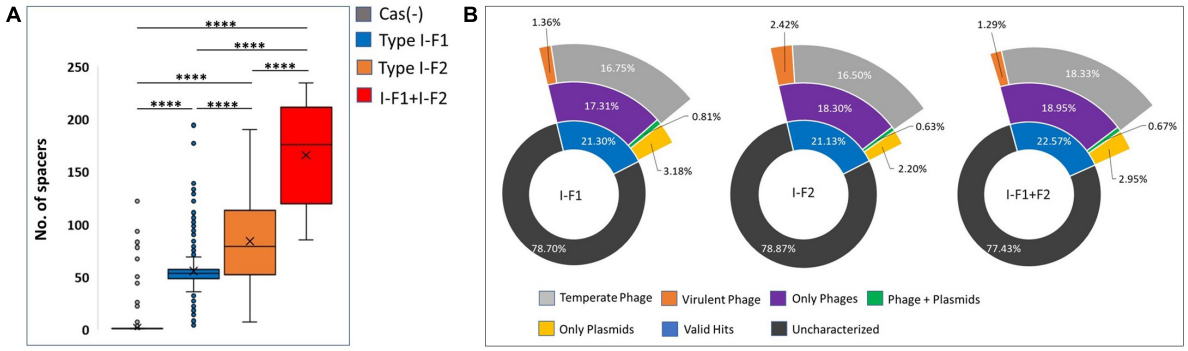

FIGURE 7
(A) Number of spacers incorporated in CRISPR array/s. **(B)** The predicted targets of unique spacers in CRISPR-Cas (+) genomes across different categories of isolates harboring CRISPR-Cas systems. Where ****($p < 0.0001$).

What are clustered regularly interspaced short palindromic repeats (CRISPR)-Cas loci spacers targeting?

CRISPR arrays consist of repeats and spacers where repeats were driven intrinsically, while spacers are proved to be acquired from bacteriophages and other mobile genetic MGEs that can provide memory-based immunity to the bacterium. We identified and counted incorporated spacers from each CRISPR-Cas (+) isolate within a valid (evidence level 4) CRISPR array/s. We found a significantly high number of mean spacers (n = 164.58 ± 46.41) per isolate in type I-F1 + F2 as compared to isolates with type I-F2 (n = 82.87 ± 36.14) and type I-F1 (n = 54.51 ± 26.27) (**Figure 7A**). Hyperactivity of type I-F2 CRISPR-Cas (+) isolates than type I-F1 in acquiring spacers may be correlated with the absence of *csy1* gene (in type I-F2) involved in the formation of Csy complex that negatively regulates Cas1/2-3 complex which functions in adaptation of the CRISPR arrays (Rollins et al., 2017). While in isolates with type I-F1 + F2, a synergistic effect could explain the observed higher spacers per isolate.

Spacerome with unique spacers from each category, that is, type I-F1 + F2 (n = 1,338), I-F2 (n = 2,224), and I-F1 (n = 2,094), were clustered. The number of unique spacers was higher in isolates with type I-F1 + F2 (31.26%), compared to type I-F2 (13.6%) and type I-F1 (8.28%), however, the high number of unique spacers in a population of isolates with CRISPR-Cas type I-F1 + F2 could not be correlated with the higher number of unique spacers per isolate and may be due to small number of isolates belonging to different ST types.

The unique spacers from each defined category were assessed for their potential targets, namely, phages, ICEs, plasmids, virulence factors, and resistance genes. We found that only approximately 21.67% of spacers had valid target hits. Also, it was evident that a single spacer can have a target for an element category, that is, either phage or plasmids. Only a few (∼0.70%) spacers were found to target both phage and plasmids (**Figure 7B**). The highest proportion of spacers was predicted to target phages in each class. The targeted phage type was further classified based on temperate and virulent groups. Temperate phages are the most common targets for spacers in each category. The limited number of spacers targeting the virulent phages could be attributed to their low abundance (n = 5/99) (**Figure 7B**). In-depth analysis revealed that a single spacer could have multiple targets (a range of 1–37 targets for phages). Spacers that have more than one target against phages are comparatively high in isolates with type I-F1 + F2 (64%), followed by type I-F2 (60%) and type I-F1 (56%). No valid hit was found to target ICEs, resistance, or virulence gene against spacers sets. Maximum remaining spacers had no identifiable target and were designated as dark matter, representing an uncharacterized microbial element (Shmakov et al., 2020).

The presence of spacers with multiple targets reflects the effective management of spacers with remarkable plasticity in *A. baumannii*.

Conclusion

Broad-scale comparisons across the diversity of *A. baumannii* revealed the distribution (**Figure 3**) and presence of co-existing CRISPR-Cas systems associated with a higher number of spacers, smaller genome size, and reduced number of integrated phages. It is well reported that CRISPR-Cas systems provide bacteria with an edge against phages. However, it can also target MGEs and may be simply a by-product of the system. We did not find any spacer that can directly target resistance or virulence genes, whereas spacers targeting plasmids that can facilitate the horizontal transfer of resistance and virulence-related genes were observed. However, neither negative nor positive association in CRISPR-Cas (+) isolates with resistance and virulence genes were found, with few exceptions for *bap*, *abaI,* and *abaR* only in type I-F1 + F2 isolates. These contrasting results indicate the existence of cryptic mechanisms for regulating spacers that can target plasmids to acquire and maintain resistance and virulence genes without compromising the phage-based memory in *A. baumannii*. *In silico* data analysis suggested that the co-existence of CRISPR-Cas type I-F1 and F2 systems in *A. baumannii* imparts the hyperactivity against phages without affecting the presence of resistance genes that may significantly hinder the potential of phage-based therapies and the trade-off capabilities. Further research regarding novel treatment strategies should be driven considering the co-existence of CRISPR-Cas systems in *A. baumannii*.

Limitations and future perspectives

The outcomes of this study correspond to the sequenced *A. baumannii* genomes, including scaffold-level assemblies available in the public domain assessed on 18 January 2021, and oversight newly added and un-sequenced *A. baumannii* population. Notably, the data are inclined toward clinical isolates due to under-represented environmental isolates. Our study shows that type I-F1 and I-F2 CRISPR-Cas systems in co-existence are distantly located; however, this distance may vary on incorporating more complete-level genome assemblies in the dataset. Understanding of complex and diverse CRISPR-Cas systems is rapidly evolving; our analysis does not account for unidentified types and subtypes of the CRISPR-Cas system and anti-CRISPR genes originating from phages. Hence the effect of anti-CRISPR genes is underestimated due to unknown anti-CRISPR proteins associated with the type I-F CRISPR-Cas system. Restricted phage entry as evidenced by a significantly low number of integrated phages in isolates with type I-F1 + F2 was determined *in silico* and requires experimental validation. This study identified maximum spacers with unknown targets, which depict the underrepresented or uncharacterized microbial community. Discovering such new elements may change the dynamics of targets corresponding to spacers being incorporated.

Data availability statement

The original contributions presented in this study are included in the article/**Supplementary material**, further inquiries can be directed to the corresponding author.

Author contributions

GY and RS conceived the idea and designed the study. GY collected and analyzed the data and wrote the manuscript draft. RS reviewed and edited the final manuscript. Both authors contributed to the article and approved the submitted version.

Funding

This work received Intramural support from the ICMR-National Institute of Pathology, New Delhi.

Acknowledgments

GY was grateful to University Grants Commission (UGC), India, for providing the research fellowship.

Conflict of interest

The authors declare that the research was conducted in the absence of any commercial or financial relationships that could be construed as a potential conflict of interest.

Publisher's note

All claims expressed in this article are solely those of the authors and do not necessarily represent those of their affiliated organizations, or those of the publisher, the editors and the reviewers. Any product that may be evaluated in this article, or claim that may be made by its manufacturer, is not guaranteed or endorsed by the publisher.

Supplementary material

The Supplementary Material for this article can be found online at: https://www.frontiersin.org/articles/10.3389/fmicb.2022.909886/full#supplementary-material

References

Baptista, P. V., Mccusker, M. P., Carvalho, A., Ferreira, D. A., Mohan, N. M., Martins, M., et al. (2018). Nano-strategies to fight multidrug resistant bacteria—"A Battle of the Titans". *Front. Microbiol.* 9:1441. doi: 10.3389/fmicb.2018.01441

Barrangou, R., Fremaux, C., Deveau, H., Richards, M., Boyaval, P., Moineau, S., et al. (2007). CRISPR provides acquired resistance against viruses in prokaryotes. *Science* 315, 1709–1712. doi: 10.1126/science.1138140

Bassetti, M., Righi, E., Vena, A., Graziano, E., Russo, A., and Peghin, M. (2018). Risk stratification and treatment of ICU-acquired pneumonia caused by multidrug-resistant/extensively drug-resistant/pandrug-resistant bacteria. *Curr. Opin. Crit. Care* 24, 385–393. doi: 10.1097/MCC.0000000000000534

Bertels, F., Silander, O. K., Pachkov, M., Rainey, P. B., and Van Nimwegen, E. (2014). Automated reconstruction of whole-genome phylogenies from short-sequence reads. *Mol. Biol. Evol.* 31, 1077–1088. doi: 10.1093/molbev/msu088

Bikard, D., Hatoum-Aslan, A., Mucida, D., and Marraffini, L. A. (2012). CRISPR interference can prevent natural transformation and virulence acquisition during in vivo bacterial infection. *Cell Host Microb.* 12, 177–186. doi: 10.1016/j.chom.2012.06.003

Biswas, A., Staals, R. H., Morales, S. E., Fineran, P. C., and Brown, C. M. (2016). CRISPRDetect: a flexible algorithm to define CRISPR arrays. *BMC Genomics* 17:356. doi: 10.1186/s12864-016-2627-0

Bland, C., Ramsey, T. L., Sabree, F., Lowe, M., Brown, K., Kyrpides, N. C., et al. (2007). CRISPR recognition tool (CRT): a tool for automatic detection of clustered regularly interspaced palindromic repeats. *BMC Bioinform.* 8:209. doi: 10.1186/1471-2105-8-209

Bortolaia, V., Kaas, R. S., Ruppe, E., Roberts, M. C., Schwarz, S., Cattoir, V., et al. (2020). ResFinder 4.0 for predictions of phenotypes from genotypes. *J. Antimicrob. Chemother.* 75, 3491–3500. doi: 10.1093/jac/dkaa345

Brooks, L., Kaze, M., and Sistrom, M. (2019). A curated, comprehensive database of plasmid sequences. *Microbiol. Resour. Announc.* 8, e1325–e1318. doi: 10.1128/MRA.01325-18

Brouns, S. J., Jore, M. M., Lundgren, M., Westra, E. R., Slijkhuis, R. J., and Snijders, A. P. (2008). Small CRISPR RNAs guide antiviral defense in prokaryotes. *Science* 321, 960–964. doi: 10.1126/science.1159689

Burstein, D., Harrington, L. B., Strutt, S. C., Probst, A. J., Anantharaman, K., Thomas, B. C., et al. (2017). New CRISPR–Cas systems from uncultivated microbes. *Nature* 542, 237–241. doi: 10.1038/nature21059

Burstein, D., Sun, C. L., Brown, C. T., Sharon, I., Anantharaman, K., Probst, A. J., et al. (2016). Major bacterial lineages are essentially devoid of CRISPR-Cas viral defence systems. *Nat. Commun.* 7:10613. doi: 10.1038/ncomms10613

Cady, K., White, A., Hammond, J., Abendroth, M., Karthikeyan, R., Lalitha, P., et al. (2011). Prevalence, conservation and functional analysis of Yersinia and *Escherichia* CRISPR regions in clinical *Pseudomonas aeruginosa* isolates. *Microbiology* 157:430. doi: 10.1099/mic.0.045732-0

Camacho, C., Coulouris, G., Avagyan, V., Ma, N., Papadopoulos, J., Bealer, K., et al. (2009). BLAST+: architecture and applications. *BMC Bioinform.* 10:421. doi: 10.1186/1471-2105-10-421

Carte, J., Christopher, R. T., Smith, J. T., Olson, S., Barrangou, R., Moineau, S., et al. (2014). The three major types of CRISPR-Cas systems function independently in CRISPR RNA biogenesis in *S treptococcus thermophilus*. *Mol. Microbiol.* 93, 98–112. doi: 10.1111/mmi.12644

Chen, L., Yang, J., Yu, J., Yao, Z., Sun, L., Shen, Y., et al. (2005). VFDB: a reference database for bacterial virulence factors. *Nucleic Acids Res.* 33, D325–D328. doi: 10.1093/nar/gki008

Couvin, D., Bernheim, A., Toffano-Nioche, C., Touchon, M., Michalik, J., Néron, B., et al. (2018). CRISPRCasFinder, an update of CRISRFinder, includes a portable version, enhanced performance and integrates search for Cas proteins. *Nucleic Acids Res.* 46, W246–W251. doi: 10.1093/nar/gky425

Darling, A. C., Mau, B., Blattner, F. R., and Perna, N. T. (2004). Mauve: multiple alignment of conserved genomic sequence with rearrangements. *Genome Res.* 14, 1394–1403. doi: 10.1101/gr.2289704

Deng, L., Garrett, R. A., Shah, S. A., Peng, X., and She, Q. (2013). A novel interference mechanism by a type IIIB CRISPR-Cmr module in S ulfolobus. *Mol. Microbiol.* 87, 1088–1099. doi: 10.1111/mmi.12152

Dong, C., Hao, G.-F., Hua, H.-L., Liu, S., Labena, A. A., Chai, G., et al. (2018). Anti-CRISPRdb: a comprehensive online resource for anti-CRISPR proteins. *Nucleic Acids Res.* 46, D393–D398.

Gao, N. L., Zhang, C., Zhang, Z., Hu, S., Lercher, M. J., Zhao, X.-M., et al. (2018). MVP: a microbe–phage interaction database. *Nucleic Acids Res.* 46, D700–D707. doi: 10.1093/nar/gkx1124

García-Martínez, J., Maldonado, R. D., Guzmán, N. M., and Mojica, F. J. (2018). The CRISPR conundrum: evolve and maybe die, or survive and risk stagnation. *Microb. Cell* 5:262. doi: 10.15698/mic2018.06.634

Haft, D. H., Selengut, J., Mongodin, E. F., and Nelson, K. E. (2005). A guild of 45 CRISPR-associated (Cas) protein families and multiple CRISPR/Cas subtypes exist in prokaryotic genomes. *PLoS Comput. Biol.* 1:e60. doi: 10.1371/journal.pcbi.0010060

Hidalgo-Cantabrana, C., Goh, Y. J., and Barrangou, R. (2019). Characterization and repurposing of type I and type II CRISPR–Cas systems in bacteria. *J. Mol. Biol.* 431, 21–33. doi: 10.1016/j.jmb.2018.09.013

Huang, Y., Niu, B., Gao, Y., Fu, L., and Li, W. (2010). CD-HIT Suite: a web server for clustering and comparing biological sequences. *Bioinformatics* 26, 680–682. doi: 10.1093/bioinformatics/btq003

Jiang, W., Maniv, I., Arain, F., Wang, Y., Levin, B. R., and Marraffini, L. A. (2013). Dealing with the evolutionary downside of CRISPR immunity: bacteria and beneficial plasmids. *PLoS Genet.* 9:e1003844. doi: 10.1371/journal.pgen.1003844

Jolley, K. A., and Maiden, M. C. (2010). BIGSdb: scalable analysis of bacterial genome variation at the population level. *BMC Bioinform.* 11:595. doi: 10.1186/1471-2105-11-595

Joshi, P. R., Acharya, M., Kakshapati, T., Leungtongkam, U., Thummeepak, R., and Sitthisak, S. (2017). Co-existence of bla OXA-23 and bla NDM-1 genes of *Acinetobacter baumannii* isolated from Nepal: antimicrobial resistance and clinical significance. *Antimicrob. Resist. Infect. Control* 6:21. doi: 10.1186/s13756-017-0180-5

Koonin, E. V., and Makarova, K. S. (2017). Mobile genetic elements and evolution of CRISPR-Cas systems: all the way there and back. *Genome Biol. Evol.* 9, 2812–2825.

Koonin, E. V., Makarova, K. S., and Zhang, F. (2017). Diversity, classification and evolution of CRISPR-Cas systems. *Curr. Opin. Microbiol.* 37, 67–78. doi: 10.1093/gbe/evx192

Kumar, M., Sarma, D. K., Shubham, S., Kumawat, M., Verma, V., Nina, P. B., et al. (2021). Futuristic non-antibiotic therapies to combat antibiotic resistance: a review. *Front. Microbiol.* 12:609459. doi: 10.3389/fmicb.2021.609459

Lerat, E., Daubin, V., Ochman, H., and Moran, N. A. (2005). Evolutionary origins of genomic repertoires in bacteria. *PLoS Biol.* 3:e130. doi: 10.1371/journal.pbio.0030130

Letunic, I., and Bork, P. (2021). Interactive Tree Of Life (iTOL) v5: an online tool for phylogenetic tree display and annotation. *Nucleic Acids Res.* 49, W293–W296. doi: 10.1093/nar/gkab301

Leungtongkam, U., Thummeepak, R., Kitti, T., Tasanapak, K., Wongwigkarn, J., and Styles, K. M. (2020). Genomic analysis reveals high virulence and antibiotic resistance amongst phage susceptible *Acinetobacter baumannii*. *Sci. Rep.* 10, 1–11. doi: 10.1038/s41598-020-73123-y

Leungtongkam, U., Thummeepak, R., Wongprachan, S., Thongsuk, P., Kitti, T., and Ketwong, K. (2018). Dissemination of bla OXA-23, bla OXA-24, bla OXA-58, and bla NDM-1 Genes of *Acinetobacter baumannii* Isolates from Four Tertiary Hospitals in Thailand. *Microb. Drug Resist.* 24, 55–62. doi: 10.1089/mdr.2016.0248

Li, W., O'neill, K. R., Haft, D. H., Dicuccio, M., Chetvernin, V., Badretdin, A., et al. (2021). RefSeq: expanding the prokaryotic genome annotation pipeline reach with protein family model curation. *Nucleic Acids Res.* 49, D1020–D1028. doi: 10.1093/nar/gkaa1105

Lin, D. M., Koskella, B., and Lin, H. C. (2017). Phage therapy: an alternative to antibiotics in the age of multi-drug resistance. *World J. Gastrointest. Pharmacol. Therapeut.* 8:162. doi: 10.4292/wjgpt.v8.i3.162

Liu, B., Zheng, D., Jin, Q., Chen, L., and Yang, J. (2019). VFDB 2019: a comparative pathogenomic platform with an interactive web interface. *Nucleic Acids Res.* 47, D687–D692. doi: 10.1093/nar/gky1080

Liu, M., Li, X., Xie, Y., Bi, D., Sun, J., Li, J., et al. (2019). ICEberg 2.0: an updated database of bacterial integrative and conjugative elements. *Nucleic Acids Res.* 47, D660–D665. doi: 10.1093/nar/gky1123

Majumdar, S., Zhao, P., Pfister, N. T., Compton, M., Olson, S., Glover, C. V., et al. (2015). Three CRISPR-Cas immune effector complexes co-exist in *Pyrococcus furiosus*. *RNA* 21, 1147–1158. doi: 10.1261/rna.049130.114

Makarova, K. S., Haft, D. H., Barrangou, R., Brouns, S. J., Charpentier, E., Horvath, P., et al. (2011). Evolution and classification of the CRISPR–Cas systems. *Nat. Rev. Microbiol.* 9, 467–477. doi: 10.1038/nrmicro2577

Makarova, K. S., Wolf, Y. I., Alkhnbashi, O. S., Costa, F., Shah, S. A., Saunders, S. J., et al. (2015). An updated evolutionary classification of CRISPR–Cas systems. *Nat. Rev. Microbiol.* 13, 722–736. doi: 10.1038/nrmicro3569

Makarova, K. S., Wolf, Y. I., Iranzo, J., Shmakov, S. A., Alkhnbashi, O. S., Brouns, S. J., et al. (2020). Evolutionary classification of CRISPR–Cas systems: a burst of class 2 and derived variants. *Nat. Rev. Microbiol.* 18, 67–83. doi: 10.1038/s41579-019-0299-x

Mangas, E. L., Rubio, A., Álvarez-Marín, R., Labrador-Herrera, G., Pachón, J., and Pachón-Ibáñez, M. E. (2019). Pangenome of *Acinetobacter baumannii* uncovers two groups of genomes, one of them with genes involved in CRISPR/Cas defence systems associated with the absence of plasmids and exclusive genes for biofilm formation. *Microb. Genomics* 5:e000309. doi: 10.1099/mgen.0.000309

McGinnis, S., and Madden, T. L. (2004). BLAST: at the core of a powerful and diverse set of sequence analysis tools. *Nucleic Acids Res.* 32, W20–W25. doi: 10.1093/nar/gkh435

Merker, M., Tueffers, L., Vallier, M., Groth, E. E., Sonnenkalb, L., Unterweger, D., et al. (2020). Evolutionary approaches to combat antibiotic resistance: opportunities and challenges for precision medicine. *Front. Immunol.* 11:1938. doi: 10.3389/fimmu.2020.01938

Micoli, F., Bagnoli, F., Rappuoli, R., and Serruto, D. (2021). The role of vaccines in combatting antimicrobial resistance. *Nat. Rev. Microbiol.* 19, 287–302. doi: 10.1038/s41579-020-00506-3

Munoz-Price, L. S., and Weinstein, R. A. (2008). *Acinetobacter* infection. *New Engl. J. Med.* 358, 1271–1281. doi: 10.1056/NEJMra070741

Ochman, H., Lawrence, J. G., and Groisman, E. A. (2000). Lateral gene transfer and the nature of bacterial innovation. *Nature* 405, 299–304. doi: 10.1038/35012500

O'Meara, D., and Nunney, L. (2019). A phylogenetic test of the role of CRISPR-Cas in limiting plasmid acquisition and prophage integration in bacteria. *Plasmid* 104:102418. doi: 10.1016/j.plasmid.2019.102418

Pawluk, A., Davidson, A. R., and Maxwell, K. L. (2018). Anti-CRISPR: discovery, mechanism and function. *Nat. Rev. Microbiol.* 16, 12–17.

Pinilla-Redondo, R., Mayo-Muñoz, D., Russel, J., Garrett, R. A., Randau, L., Sørensen, S. J., et al. (2020). Type IV CRISPR–Cas systems are highly diverse and involved in competition between plasmids. *Nucleic Acids Res.* 48, 2000–2012. doi: 10.1093/nar/gkz1197

Pires, D. P., Costa, A. R., Pinto, G., Meneses, L., and Azeredo, J. (2020). Current challenges and future opportunities of phage therapy. *FEMS Microbiol. Rev.* 44, 684–700. doi: 10.1093/femsre/fuaa017

Pourcel, C., Salvignol, G., and Vergnaud, G. (2005). CRISPR elements in *Yersinia pestis* acquire new repeats by preferential uptake of bacteriophage DNA, and provide additional tools for evolutionary studies. *Microbiology* 151, 653–663. doi: 10.1099/mic.0.27437-0

Pourcel, C., Touchon, M., Villeriot, N., Vernadet, J.-P., Couvin, D., Toffano-Nioche, C., et al. (2020). CRISPRCasdb a successor of CRISPRdb containing CRISPR arrays and cas genes from complete genome sequences, and tools to download and query lists of repeats and spacers. *Nucleic Acids Res.* 48, D535–D544. doi: 10.1093/nar/gkz915

Pursey, E., Dimitriu, T., Paganelli, F. L., Westra, E. R., and Van Houte, S. (2022). CRISPR-Cas is associated with fewer antibiotic resistance genes in bacterial pathogens. *Philos. Trans. R. Soc. B* 377:20200464. doi: 10.1098/rstb.2020.0464

Pursey, E., Sünderhauf, D., Gaze, W. H., Westra, E. R., and Van Houte, S. (2018). CRISPR-Cas antimicrobials: challenges and future prospects. *PLoS Pathogens* 14:e1006990. doi: 10.1371/journal.ppat.1006990

Reis-Cunha, J. L., Bartholomeu, D. C., Manson, A. L., Earl, A. M., and Cerqueira, G. C. (2019). ProphET, prophage estimation tool: a standalone prophage sequence prediction tool with self-updating reference database. *PLoS One* 14:e0223364. doi: 10.1371/journal.pone.0223364

Rollins, M. F., Chowdhury, S., Carter, J., Golden, S. M., Wilkinson, R. A., and Bondy-Denomy, J. (2017). Cas1 and the Csy complex are opposing regulators of Cas2/3 nuclease activity. *Proc. Natl Acad. Sci. U.S.A.* 114, E5113–E5121. doi: 10.1073/pnas.1616395114

Shehreen, S., Chyou, T.-Y., Fineran, P. C., and Brown, C. M. (2019). Genome-wide correlation analysis suggests different roles of CRISPR-Cas systems in the acquisition of antibiotic resistance genes in diverse species. *Philos. Trans. R. Soc. B* 374:20180384. doi: 10.1098/rstb.2018.0384

Shmakov, S. A., Wolf, Y. I., Savitskaya, E., Severinov, K. V., and Koonin, E. V. (2020). Mapping CRISPR spaceromes reveals vast host-specific viromes of prokaryotes. *Commun. Biol.* 3, 1–9. doi: 10.1038/s42003-020-1014-1

Silas, S., Lucas-Elio, P., Jackson, S. A., Aroca-Crevillen, A., Hansen, L. L., Fineran, P. C., et al. (2017). Type III CRISPR-Cas systems can provide redundancy to counteract viral escape from type I systems. *Elife* 6:e27601.

Tal-Jasper, R., Katz, D. E., Amrami, N., Ravid, D., Avivi, D., Zaidenstein, R., et al. (2016). Clinical and epidemiological significance of carbapenem resistance in *Acinetobacter baumannii* infections. *Antimicrob. Agents Chemother.* 60, 3127–3131. doi: 10.1128/AAC.02656-15

Tynecki, P., Guziński, A., Kazimierczak, J., Jadczuk, M., Dastych, J., and Onisko, A. (2020). PhageAI-bacteriophage life cycle recognition with machine learning and natural language processing. *BioRxiv*[preprint] doi: 10.1101/2020.07.11.198606

Tyumentseva, M., Mikhaylova, Y., Prelovskaya, A., Tyumentsev, A., Petrova, L., Fomina, V., et al. (2021). Genomic and phenotypic analysis of multidrug-resistant *Acinetobacter baumannii* clinical isolates carrying different types of CRISPR/Cas systems. *Pathogens* 10:205. doi: 10.3390/pathogens10020205

van Belkum, A., Soriaga, L. B., Lafave, M. C., Akella, S., Veyrieras, J.-B., Barbu, E. M., et al. (2015). Phylogenetic distribution of CRISPR-Cas systems in antibiotic-resistant *Pseudomonas aeruginosa*. *MBio* 6, e1796–e1715. doi: 10.1128/mBio.01796-15

Watson, B. N., Staals, R. H., and Fineran, P. C. (2018). CRISPR-Cas-mediated phage resistance enhances horizontal gene transfer by transduction. *MBio* 9, e02406–e02417. doi: 10.1128/mBio.02406-17

Westra, E. R., Van Erp, P. B., Künne, T., Wong, S. P., Staals, R. H., Seegers, C. L., et al. (2012). CRISPR immunity relies on the consecutive binding and degradation of negatively supercoiled invader DNA by Cascade and Cas3. *Mol. Cell* 46, 595–605. doi: 10.1016/j.molcel.2012.03.018

Wheatley, R. M., and MacLean, R. C. (2021). CRISPR-Cas systems restrict horizontal gene transfer in *Pseudomonas aeruginosa*. *ISME J.* 15, 1420–1433. doi: 10.1038/s41396-020-00860-3

World Health Organization (2017). *Guidelines for the prevention and control of carbapenem-resistant Enterobacteriaceae, Acinetobacter baumannii* and *Pseudomonas aeruginosa* in health care facilities. Geneva: World Health Organization.

Zankari, E., Allesøe, R., Joensen, K. G., Cavaco, L. M., Lund, O., and Aarestrup, F. M. (2017). PointFinder: a novel web tool for WGS-based detection of antimicrobial resistance associated with chromosomal point mutations in bacterial pathogens. *J. Antimicrob. Chemother.* 72, 2764–2768. doi: 10.1093/jac/dkx217

Zankari, E., Hasman, H., Cosentino, S., Vestergaard, M., Rasmussen, S., Lund, O., et al. (2012). Identification of acquired antimicrobial resistance genes. *J. Antimicrob. Chemother.* 67, 2640–2644.

Zarrilli, R., Giannouli, M., Tomasone, F., Triassi, M., and Tsakris, A. (2009). Carbapenem resistance in *Acinetobacter baumannii*: the molecular epidemic features of an emerging problem in health care facilities. *J. Infection Dev. Count.* 3, 335–341. doi: 10.3855/jidc.240

Zhu, Y., Zhang, F., and Huang, Z. (2018). Structural insights into the inactivation of CRISPR-Cas systems by diverse anti-CRISPR proteins. *BMC Biol.* 16:562–573. doi: 10.1080/15476286.2021.1985347

frontiers | Frontiers in Cellular and Infection Microbiology

TYPE Original Research
PUBLISHED 13 January 2023
DOI 10.3389/fcimb.2022.1064053

OPEN ACCESS

EDITED BY
Paolo Visca,
Roma Tre University, Italy

REVIEWED BY
Chelsie Armbruster,
University at Buffalo, United States
Alessandra Polissi,
University of Milan, Italy

*CORRESPONDENCE
Mireia López-Siles
mireia.lopezs@udg.edu

†The authors have contributed equally to this work and share senior authorship

SPECIALTY SECTION
This article was submitted to Molecular Bacterial Pathogenesis, a section of the journal Frontiers in Cellular and Infection Microbiology

RECEIVED 07 October 2022
ACCEPTED 13 December 2022
PUBLISHED 13 January 2023

CITATION
Tajuelo A, Terrón MC, López-Siles M and McConnell MJ (2023) Role of peptidoglycan recycling enzymes AmpD and AnmK in *Acinetobacter baumannii* virulence features. *Front. Cell. Infect. Microbiol.* 12:1064053.
doi: 10.3389/fcimb.2022.1064053

Role of peptidoglycan recycling enzymes AmpD and AnmK in *Acinetobacter baumannii* virulence features

Ana Tajuelo[1,2], María C. Terrón[3], Mireia López-Siles[1,4*†] and Michael J. McConnell[1†]

[1]Intrahospital Infections Laboratory, Instituto de Salud Carlos III (ISCIII), National Centre for Microbiology, Madrid, Spain, [2]Universidad Nacional de Educación a Distancia (UNED), Madrid, Spain, [3]Electron Microscopy Unit, Scientific-Technical Central Units, Instituto de Salud Carlos III (ISCIII), Madrid, Spain, [4]Serra Húnter Fellow, Microbiology of Intestinal Diseases, Biology Department, Universitat de Girona, Girona, Spain

Acinetobacter baumannii is an important causative agent of hospital acquired infections. In addition to acquired resistance to many currently-available antibiotics, it is intrinsically resistant to fosfomycin. It has previously been shown that AmpD and AnmK contribute to intrinsic fosfomycin resistance in *A. baumannii* due to their involvement in the peptidoglycan recycling pathway. However, the role that these two enzymes play in the fitness and virulence of *A. baumannii* has not been studied. The aim of this study was to characterize several virulence-related phenotypic traits in *A. baumannii* mutants lacking AmpD and AnmK. Specifically, cell morphology, peptidoglycan thickness, membrane permeability, growth under iron-limiting conditions, fitness, resistance to disinfectants and antimicrobial agents, twitching motility and biofilm formation of the mutant strains *A. baumannii* ATCC 17978 Δ*ampD*::Kan and Δ*anmK*::Kan were compared to the wild type strain. Our results demonstrate that bacterial growth and fitness of both mutants were compromised, especially in the Δ*ampD*::Kan mutant. In addition, biofilm formation was decreased by up to 69%, whereas twitching movement was reduced by about 80% in both mutants. These results demonstrate that, in addition to increased susceptibility to fosfomycin, alteration of the peptidoglycan recycling pathway affects multiple aspects related to virulence. Inhibition of these enzymes could be explored as a strategy to develop novel treatments for *A. baumannii* in the future. Furthermore, this study establishes a link between intrinsic fosfomycin resistance mechanisms and bacterial fitness and virulence traits.

KEYWORDS

***Acinetobacter baumannii*, peptidoglycan recycling, biofilm formation, twitching motility, disinfectants, fosfomycin resistance**

1 Introduction

Acinetobacter baumannii (*A. baumannii*) is a Gram-negative pathogen that causes different types of nosocomial infections. Most commonly, it can cause central line-associated bloodstream infections or ventilator-associated pneumonia, but it is also responsible for infections in soft tissues, the skin, and the urinary tract (Lee et al., 2017; Harding et al., 2018). *A. baumannii* is intrinsically resistant to several antimicrobial agents, and since the late 20th century increasing acquired resistance to other antibiotics has been reported (Rolain et al., 2013). Therefore, the emergence of multidrug-resistant (MDR) strains of *A. baumannii* is now recognized as a major global health problem due to the limited options for antibiotic therapy, prompting the World Health Organization (WHO) to declare *A. baumannii* a pathogen of critical priority for which new antimicrobials are urgently needed (Jiang et al., 2021). This can include both discovery of novel antibiotics or potentiating the activity of those currently in use.

Fosfomycin is a broad spectrum antibiotic widely used in clinical practice for treating a range of infections, such as meningitis, otitis, cystitis, respiratory infections, endocarditis or bacteremia (Candel et al., 2019). This is in part due to its high penetration, which allows efficient distribution into many tissues (Sastry and Doi, 2016; Múñez Rubio et al., 2019). In addition, fosfomycin has a favorable safety profile (Iarikov et al., 2015), and lower toxicity compared to other antibiotics such as colistin, whose use has increased over the past years due to its activity against many multidrug resistant bacteria (Spapen et al., 2011; Karaiskos and Giamarellou, 2014; Carretero-Ledesma et al., 2018). Furthermore, fosfomycin has been shown to reduce toxicity caused by nephrotoxic drugs (Karaiskos and Giamarellou, 2014; Sastry and Doi, 2016). However, intrinsic resistance to this antibiotic in *A. baumannii* has hampered its use in treating infections caused by this pathogen (Doi, 2019; Aghamali et al., 2019).

Fosfomycin acts by inhibiting the UDP-*N*-acetylglucosamine enolpyruvyl transferase (MurA). This enzyme is responsible to catalyze the reaction between UDP-*N*-acetylglucosamine (UDP-GlcNAc) with phosphoenolpyruvate (PEP) to form UDP-GlcNAc-enoyl pyruvate plus inorganic phosphate, which is one of the first steps in peptidoglycan synthesis (Silver, 2017). This antibiotic competes with PEP to bind covalently to the enzyme, acting as a PEP analog, which finally results in bacterial cell lysis and death (Silver, 2017; Doi, 2019; Aghamali et al., 2019). It is known that functional MurA is present in *A. baumannii* (Sonkar et al., 2017). In addition, mechanisms associated with fosfomycin resistance in other Gram-negative bacteria, such as the presence of a *fosA* homolog (encoding a glutathione S-transferase that conjugates glutathione to fosfomycin for its inactivation) or changes in the drug transporters GlpT and UhpT have not been described in *A. baumannii* (Gil-Marqués et al., 2018; Aghamali et al., 2019). In contrast, in *A. baumannii* a salvage pathway within the peptidoglycan recycling system has been reported. Specifically, homologs for some of the enzymes involved in the bypass of the enzymatic step catalyzed by MurA have been found in this species (Gil-Marqués et al., 2018). This pathway, present in many Gram-negative species, has been demonstrated to be responsible for resistance to fosfomycin in *Pseudomonas putida* (Gisin et al., 2013), which supports this as the most plausible mechanism resulting in intrinsic resistance to fosfomycin in *A. baumannii*.

In a previous study by our group (Gil-Marqués et al., 2018), we demonstrated that knockout strains of *A. baumannii* lacking *N*-acetyl-anhydromuramyl-L-alanine amidase (AmpD) and anhydro-*N*-acetylmuramic acid kinase (AnmK) enzymes, both acting in the initial steps of the peptidoglycan recycling salvage pathway, featured increased susceptibility to fosfomycin. However, how these mutations affect other pathogenic characteristics of this species has not been studied. Peptidoglycan is an essential component of the bacteria cell wall (Vollmer et al., 2008), so the disruption of its recycling pathway in *A. baumannii* could affect the fitness and virulence of this bacteria. *A. baumannii* presents different virulence factors that contribute to produce the infection in the host, including adherence and biofilm formation that confers to it the ability to survive in the environment and also host cells, surface motility that contributes to stablish the infection, acquisition systems for essential nutrients such as iron or stress resistance (McConnell et al., 2013; Lin and Lan, 2014; Harding et al., 2018). In this context, the aim of this study was to evaluate the role of these two enzymes in some of these traits related to virulence and fitness of *A. baumannii*.

2 Materials and methods

2.1 Bacterial strains

All bacterial strains used in this study and the assay in which they were used are listed in Table 1. Mutant strains and their complemented counterparts were obtained in a previous study by our group (Gil-Marqués et al., 2018). Briefly, the Δ*ampD*::Kan and Δ*anmK*::Kan mutants were constructed in the *A. baumannii* ATCC 17978 strain replacing the wild type genes with a kanamycin resistance cassette through homologous recombination. The pUCp24 plasmid (gentamicin resistance) was used to complement *ampD* and *anmK* mutant strains.

A. baumannii strains were routinely cultured in Mueller Hinton broth (MHB), supplemented, if required, with 10 μg/ml kanamycin (mutant strains) or with 10 μg/ml kanamycin plus 10 μg/ml gentamicin (complemented mutant strains). For long-term storage, strains were kept in Luria Bertani (LB) media containing 20% glycerol (v/v) and stored at -80 °C. Bacteria were freshly plated from stocks for each experiment.

2.2 Transmission electron microscopy

For TEM ultrastructural analysis, pellets of the *A. baumannii* ATCC 17978 wild type strain, mutants and complemented strains

TABLE 1 *Acinetobacter baumannii* (*A. baumannii*) strains used and experiments in which they were engaged.

Strain	Assay*	Reference
A. baumannii ATCC 17978	BF, CI, CP, GC, MIC, TEM, TW	ATCC, USA
A. baumannii ATCC 19606^T	TW	ATCC, USA
A. baumannii Δ*ampD*::Kan	BF, CI, CP, GC, MIC, TEM, TW	(Gil-Marqués et al., 2018)
A. baumannii Δ*ampD*::Kan/pUCp24-*ampD*	BF, CI, CP, GC, MIC, TEM, TW	(Gil-Marqués et al., 2018)
A. baumannii Δ*ampD*::Kan/pUCp24	BF, GC, MIC, TW	(Gil-Marqués et al., 2018)
A. baumannii Δ*anmK*::Kan	BF, CI, GC, MIC, TEM, TW	(Gil-Marqués et al., 2018)
A. baumannii Δ*anmK*::Kan/pUCp24-*anmK*	BF, CI, CP, GC, MIC, TEM, TW	(Gil-Marqués et al., 2018)
A. baumannii Δ*anmK*::Kan/pUCp24	BF, GC, MIC, TW	(Gil-Marqués et al., 2018)

*BF, biofilm; CI, Competition index; CP, Cell permeability; GC, Growth curves; MIC, Minimum inhibitory concentration; TW, Twitching; TEM, Transmission electron microscopy.

harvested during exponential growth (OD_{600} = 0.5) were chemically fixed in 0.1 M Na_2HPO_4 buffer pH 7.4, 3% glutaraldehyde and 4% paraformaldehyde for 150 min at 4 °C. Cells were centrifuged and washed in Na_2HPO_4 buffer three times. Postfixation was performed with a mixture of 1% osmium tetroxide and 1.5% potassium ferrocyanide for 1.75 h at 4 °C. Subsequent treatments consisted of 0.15% tannic acid for 1 min at room temperature and 2% uranyl acetate for 1 h at room temperature in the dark. Dehydration was carried out in increasing concentrations of ethanol (50, 75, 90, 95, and three times with 100%) for 10 min each at 4 °C. Infiltration was performed at room temperature and agitation, using increasing concentrations of epoxy-resin (25, 50, 75 and 100%). Polymerization was performed at 60 °C for 48 h. Ultrathin sections of the samples (50-70 nm) were obtained with a Leica EM UC6 ultramicrotome and harvested on 100 mesh Formvar coated copper grids. Staining was carried out following standard procedures with saturated uranyl acetate and 2% lead citrate. Images were captured at nominal magnifications of 15,000 × to 67,000 × with a CCD (Charged Coupled Device) FEI Ceta camera on a Tecnai 12 electron microscope (FEI) operated at 120 kV.

For measurement of the cell wall dimensions, bacteria were selected with the outer and inner membrane, and the peptidoglycan layer unequivocally visible to ensure the structures were perpendicular to the surface section. Images were recorded at a nominal magnification of 67,000 ×, corresponding to a pixel size of 0.15 nm. Images were opened in Fiji (Schindelin et al., 2012) software and a line profile was drawn from the innermost part of the inner membrane to the outermost part of the outer membrane, perpendicular to the peptidoglycan layer with the length of the line representing the dimensions of the cell wall as described in Bleck et al. (2010).

2.3 Cell permeability assay

To determine membrane permeability of *A. baumannii* strains, SYTOX green (S7020, Thermo Fisher) and 1-N-phenylnaphthylamine (NPN, 104043, Sigma-Aldrich) stains were used. Strains were grown until the exponential phase and adjusted to a final OD_{600} = 0.5 in PBS supplemented with 1 µM SYTOX green. 100 µl of each bacterial suspension were placed into the appropriate well of a black microtiter plate (clear bottom) (353219, Falcon). Fluorescence (λex = 504 nm, λem = 523 nm) was measured using an automated plate reader (M200 Infinite Pro, Tecan). For NPN assay, 150 µl of the bacterial suspensions grown until the exponential phase and adjusted to OD_{600} = 0.5 in 5 mM HEPES (pH = 7.2) were transferred to the wells of a plate as indicated previously. 50 µl of a 40 µM NPN solution in 96% ethanol were added and fluorescence (λex = 350 nm, λem = 420 nm) was measured immediately as indicated above. Permeability in the presence of 5mg/ml of the detergent SDS was carried out as a positive control of compound uptake.

2.4 *In vitro* growth curves

Growth in iron-rich media, iron-limiting conditions and serum was tested. *A. baumannii* strains were cultured in 5 ml of MHB overnight at 37 °C and then adjusted as appropriate as previously reported (Gil-Marqués et al., 2018), with slight modifications. Specifically, to elaborate *in vitro* growth curves in MHB (iron-rich condition) or inactivated human serum (SLCC3239, Sigma-Aldrich), 100 µl of bacteria at a concentration of 10^6 CFU/ml were used. As growth curves were performed without antibiotic pressure, a higher inoculum was used to minimize plasmid loss effect. To monitor growth in iron-limiting conditions, 200 µl of the overnight cultures adjusted to a concentration of 10^5 CFU/ml in MHB were supplemented with the iron chelator 2, 2'-bipyridyl (Bip) at a final concentration of 150 µM, following a previously reported method (Carretero-Ledesma et al., 2018). All experiments were carried out in 96-well flat bottom polystyrene microplates (351172, Falcon). Growth at 37 °C was assessed by measuring the OD_{600} every 30 min over 24 h using an automated reader (M200 Infinite Pro, Tecan). All assays were performed at least in duplicate.

2.5 *In vitro* competition indices

Four different strain combinations were analyzed in separate experiments: *A. baumannii* ATCC 17978 and *A. baumannii* Δ*ampD*::Kan; *A. baumannii* ATCC 17978 and *A. baumannii* Δ*anmK*::Kan; *A. baumannii* ATCC 17978 and *A. baumannii* Δ*ampD*::Kan/pUCp24-*ampD*; *A. baumannii* ATCC 17978 and *A. baumannii* Δ*anmK*::Kan/pUCp24-*anmK*.

In vitro competition experiments were carried out using a protocol from a previous study (Carretero-Ledesma et al., 2018). Overnight cultures of bacterial strains were diluted to a final concentration of 10^5 CFU/ml and mixed in 1:1 ratio in MHB. After 24 h, aliquots from the cultures were plated on MH agar plates and MH plates containing 10 μg/ml of kanamycin to select for *A. baumannii* mutant strains or MH plates containing 10 μg/ml of kanamycin and 10 μg/ml of gentamicin to select for *A. baumannii* complemented mutant strains. Competition indices (CI) were obtained from the following formula:

$$CI = \frac{\frac{CFU_{mut}}{CFU_{wt}}}{\frac{CFU_{mut0}}{CFU_{wt0}}},$$

where the number of CFU recovered from the mutant strain (CFU_{mut}) with respect to the number of CFU recovered from the wild type *A. baumannii* ATCC 17978 strain (CFU_{wt}), is divided by the number of CFU in the mutant inoculum (CFU_{mut0}) with respect to the number of CFU in the wild type inoculum (CFU_{wt0}). CI < 1 represents an increased growth of the wild type strain, C = 1 a similar growth of both strains and CI > 1 an increased growth of the mutant strain. All assays were performed in triplicate.

2.6 Susceptibility to disinfectants and other antimicrobial agents

The broth microdilution method was used to determine the minimum inhibitory concentration (MIC) values for disinfectants chlorhexidine (282227-1G, Sigma) and ethanol (141086.1212, Panreac), for deoxycholate (30970-25G, Sigma), a secondary bile acid that emulsify fats and alters the permeability of lipid membranes being considered a natural antimicrobial agent (Begley et al., 2005; Urdaneta and Casadesús, 2017), the chelating agent EDTA (A2937, Panreac) and the detergent SDS (A2263, Panreac). MHB II was used according to the Clinical and Laboratory Standards Institute for antimicrobials (CLSI) recommendations (CLSI, 2017). A culture of the corresponding *A. baumannii* strain adjusted to 10^6 CFU/ml was added to wells of a 96-well U-shaped bottom polystyrene microplate (140935, Biotech) containing two-fold serial dilutions of each disinfectant (0.06 - 0.0001 mM for chlorhexidine, 8.6 - 0.02 mM for ethanol, 120 - 2.4 mM for deoxycholate and 0.014 - 0.000027 mM for EDTA and SDS). Microplates were incubated at 37 °C for 24 h. The MIC was established as the lowest disinfectant concentration at which no growth was observed. MIC analyses were performed in triplicate for each strain.

2.7 Biofilm formation

Biofilm formation was determined following previously described protocols (Carretero-Ledesma et al., 2018; Domenech and García, 2020) with some modifications. Overnight cultures of each strain were adjusted to a final concentration of 10^8 CFU/ml in Mueller Hinton II broth. Each bacterial suspension (200 μl) was added into a well of a U-shaped polystyrene 96-well plate (140935, Biotech) and incubated without shaking at 37 °C for 24 h. After incubation, media was discarded and the adherent cells were washed with PBS. Biofilm staining was performed with a 1% crystal violet solution for 15 min at room temperature. The crystal violet solution in excess was removed, and the plates were washed twice as indicated previously. The stain was eluted from the adherent cells by adding 200 μl of 70% ethanol (v/v) to each well. Then, the absorbance at 595 nm was measured on a microplate reader (Epoch 2, BioTek). Percentages of biofilm formation were calculated by comparing the absorbance of mutant and complemented strains with respect to the absorbance of the wild type strain. The assay was performed six times.

2.8 Twitching motility assay

To analyze twitching motility, a previously reported protocol (Carretero-Ledesma et al., 2018) was used with minor modifications. Each strain was grown overnight in MHB. Prior to initiate the twitching motility assay, cultures were adjusted by dilution with PBS to a final concentration of 10^9 CFU/ml. LB plates containing 0.3% agarose (801000, Pronadisa) were prepared and inoculated the same day with 2 μl of the adjusted bacterial suspension placed in the interphase between the medium and the bottom of the Petri dish. Plates were allowed to dry for 5 min and then incubated at 37 °C with a humidity saturated atmosphere. The diameter of culture surface extension was measured after 32 h of incubation. *A. baumannii* ATCC 19606^T, a non-motile strain (Eijkelkamp et al., 2011), was used as a negative control. For each isolate, the assay was performed three times on separate days.

2.9 Statistical analyses

All analyses and data plotting were performed using SPSS (IBM) and Prism 5 v.5.01 (GraphPad Software). Given the normal distribution of the data, as assessed by Shapiro-Wilks

10.3389/fcimb.2022.1064053

test, parametric statistical tests were used. Growth in different conditions were compared using the Student t-test for pairwise analyses. Competition indices were compared to an expected value of 1 using the Wilcoxon signed rank test and differences between groups were also determined using the Student t-test. Cell permeability, biofilm production, and twitching motility were compared using a one-way ANOVA, and differences between groups were determined using the Tukey post-hoc test. p-values < 0.05 were considered statistically significant.

3 Results

3.1 Effect of *ampD* and *anmK* deletion in cell morphology and cell wall thickness

To determine whether *ampD* or *anmK* deletion affects peptidoglycan structure, *A. baumannii* strains were visualized by TEM (Figure 1A). All strains presented similar morphology and cell wall thickness (Table 2), indicating that the absence of AmpD and AnmK enzymes does not result in gross changes in membrane ultrastructure. Interestingly TEM images revealed the presence of outer membrane vesicles (OMV) in all strains analysed (Figure 1B), indicating that *A. baumannii* strains lacking AmpD or AnmK are still able to release OMV.

3.2 Effect of AmpD and AnmK on cell permeability

To evaluate if *ampD* and *anmK* deletion affected membrane permeability of *A. baumannii*, accumulation assays were carried out using the fluorescent stains NPN and SYTOX Green, neutral and positively charged compounds, respectively (Figure 2). There were no significant differences in intracellular accumulation of NPN and SYTOX Green in the mutant strains compared to the wild type strain ($p > 0.05$), indicating that the absence of AmpD or AnmK does not result in increased membrane permeability to these compounds. The presence of SDS, that disrupts the cell membrane, resulted in an almost two-fold significant increase in membrane permeability of ATCC 17978 ($p = 0.038$, Supplementary Figure 1).

3.3 *In vitro* growth of *A. baumannii* strains

The effect of *ampD* and *anmK* absence on *A. baumannii* growth in rich media (MHB) and in iron limiting conditions was assessed over 24 h (Figure 3). The *ampD* deletion resulted in reduced growth compared to the parental strain ATCC 17978 (Figure 3A). Complementation of the mutation with a wild type copy of the gene (Δ*ampD*::Kan/pUCp24-*ampD*) completely restored the growth defect observed, whereas the Δ*ampD*::Kan mutant containing an empty plasmid did not restore growth. A different result was obtained with the Δ*anmK*::Kan mutant, which grew similarly to the parental strain, as did the complemented strain and the strain containing an empty plasmid.

Under iron limiting conditions strains lacking AmpD or AnmK both demonstrated reduced growth compared to the wild type parental strain (Figure 3B). This difference was observed at both exponential (38 and 40% of growth, respectively) and stationary phase (35 and 50% of growth, respectively) time points (Figures 3C, D). Moreover, under this situation complementation with a wild type copy of the genes did not re-establish growth to the parental strain level in either case at exponential phase, showing a similar growth to the strain containing an empty plasmid. In the stationary phase, a partially restored wild type phenotype was only observed when the Δ*ampD*::Kan mutant was complemented, although significant differences compared to wild type strain were maintained. In addition, we assessed growth in human serum, and all strains including ATCC 17978 showed a marked growth defect with an OD_{600}< 0.4 after 24 h (Supplementary Figure 2).

3.4 Effect of *ampD* and *anmK* deletion on fitness of *A. baumannii*

To further characterize changes in fitness as a consequence of *ampD* and *anmK* deletion, competition indices were determined at 24 h in MHB by comparing the growth of the Δ*ampD*::Kan, Δ*anmK*::Kan and their complemented strains, Δ*ampD*::Kan/pUCp24-*ampD* and Δ*anmK*::Kan/pUCp24-*anmK*, to ATCC 17978 when grown together (Figure 4). Despite difference to 1 was not statistically significant in neither case according to the Wilcoxon test due to the low number of replicates, *A. baumannii* Δ*ampD*::Kan demonstrated a marked loss of fitness compared to ATCC 17978 (CI = 0.017), whereas the complemented strain Δ*ampD*::Kan/pUCp24-*ampD* showed a significant restoration of this fitness (CI = 0.59) ($p = 0.0042$). Fitness loss was less reduced in *A. baumannii* Δ*anmK*::Kan, (CI = 0.16) compared to Δ*ampD*::Kan mutant which was partly restored by its complemented counterpart (CI = 0.25).

3.5 Effect of AmpD and AnmK on susceptibility to disinfectants and other antimicrobial agents

The MIC for chlorhexidine, ethanol, deoxycholate, EDTA and SDS was determined to assess if deletion of *ampD* or *anmK* genes in *A. baumannii* affected susceptibility to different antimicrobial agents (Table 3). The absence of AmpD and AnmK did not affect susceptibility to chlorhexidine, ethanol,

EDTA or SDS. In contrast, ATCC 17978 Δ*ampD*::Kan strain was slightly more susceptible to deoxycholate than the wild type strain and complementing the mutation returned susceptibility to wild type levels.

3.6 Effect of *ampD* and *anmK* deletion on biofilm production

Biofilm production in the ATCC 17978, Δ*ampD*::Kan and Δ*anmK*::Kan mutants and their complemented counterpart strains was assessed (Figure 5). Absence of AmpD reduced the ability to form biofilm to 69% after 24 h compared to the parental strain, while a more marked phenotype was observed for *anmK* deletion, reducing biofilm formation to 41%.

TABLE 2 Dimensions of the cell wall of *Acinetobacter baumannii* (*A. baumannii*) strains.

Strain	OM-IM*
A. baumannii ATCC 17978	32.5 ± 3.9 nm
A. baumannii Δ*ampD*::Kan	33.1 ± 2.2 nm
A. baumannii Δ*ampD*::Kan/pUCp24-*ampD*	31.8 ± 2.8 nm
A. baumannii Δ*anmK*::Kan	31.7 ± 2.4 nm
A. baumannii Δ*anmK*::Kan/pUCp24-*anmK*	32.5 ± 2.9 nm

*Measurement of the cell wall from the outer membrane (OM) to the inner membrane (IM). Mean ± standard deviation of at least 20 cells.

Complementation with a wild type copy of the gene only resulted in a restoration of biofilm production in the Δ*ampD*::

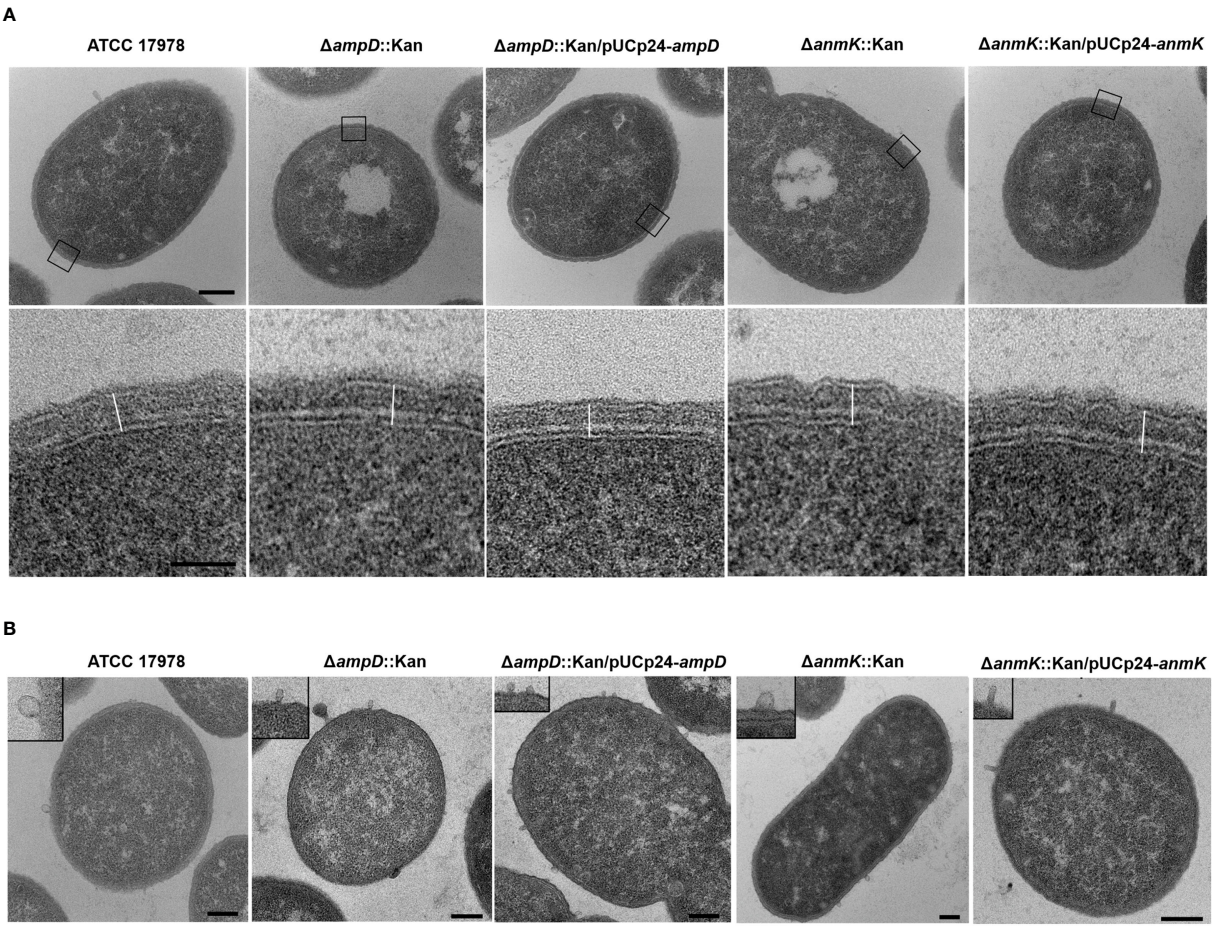

FIGURE 1
Morphology of the cell wall of *Acinetobacter baumannii* strains by TEM. **(A)** TEM images show an overview of a cell from the wild type strain and the respective mutants or complemented strains (upper row). The box marks areas used for cell wall measurement, which are shown in detail in the lower row. The outermost structure is the outer membrane with a thin electrone dense layer of lipopolysaccharide facing the exterior. The inner membrane separates the cell wall from the cytoplasm. Between outer and inner membrane the peptidoglycan layer is seen as an electron dense layer. The line used for measurements is represented. Scale bars: upper row = 200 nm, lower row = 50 nm. **(B)** TEM images show the presence of outer membrane vesicles (OMV) around a cell of each bacteria strain with the insert in each panel showing a detail of them. Scale bar: 200 nm.

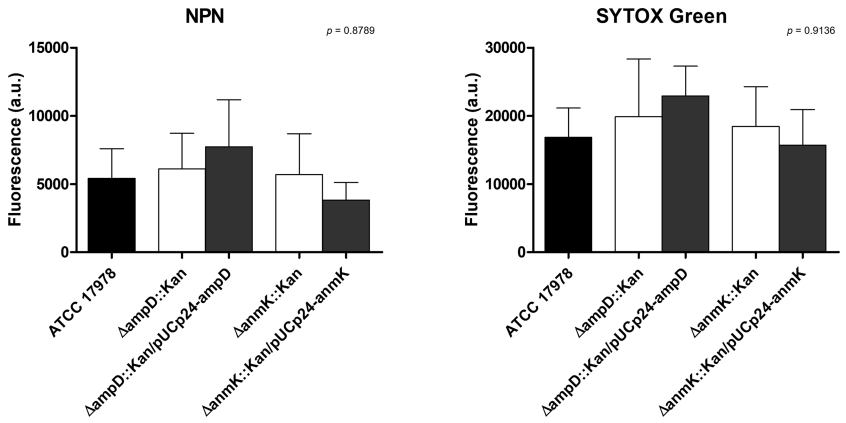

FIGURE 2
Cell permeability of *Acinetobacter baumannii* strains. Effect of *ampD* and *anmK* deletion on the membrane permeability as measured by the 1-N-phenylnaphthylamine (NPN) (left) and SYTOX Green (right) uptake assays. Bars represent the average of three separate assays, with error bars representing the standard deviation. No significant differences were found between replicates (p = 0.8789 and p = 0.9136 for NPN and SYTOX Green, respectively), as assessed by ANOVA followed by Tukey's Multiple Comparison Test.

Kan mutant, whereas complement with an empty plasmid produced similar biofilm to mutant strain, indicating that the decreased biofilm production was due to AmpD absence. These differences were not statistically supported (p = 0.082) because of the dispersion of data between the six replicates.

3.7 Effect of *ampD* and *anmK* deletion on twitching motility

Lastly, to determine if the lack of *ampD* and *anmK* affected *A. baumannii* surface motility, we determined twitching motility, based on the ability of the bacteria to translocate on the surface of a semisolid media over 32 h of incubation (Figure 6). Δ*ampD*::Kan and Δ*anmK*::Kan mutants showed an important loss in twitching motility (78 and 76% reduction, respectively) compared to *A. baumannii* ATCC 17978 (p< 0.001). Complementation of Δ*anmK*::Kan mutant totally restored surface motility to parental level. In contrast, a mild increase in surface motility was observed when complementing Δ*ampD*::Kan mutant. Strains complemented with an empty plasmid displayed the same twitching as the negative control strain and knockout mutants.

4 Discussion

A. baumannii resistance to fosfomycin has been linked to the presence of a functional peptidoglycan recycling pathway, as its disruption has been shown to increase susceptibility to this antibiotic (Gil-Marqués et al., 2018). However, how mutations in enzymes involved in this pathway affect bacterial physiology and virulence features has not been characterized. In the present study we have explored the role of the peptidoglycan recycling pathway enzymes AmpD and AnmK in multiple virulence associated traits. Since they are involved in an early and late step of the recycling route, respectively, this has allowed us to elucidate mild and more severe effects in virulence traits that result when altering the peptidoglycan recycling pathway at different enzymatic steps.

In addition to maintaining cell shape, the peptidoglycan is responsible for imparting strength and resistance to osmotic pressure (Cava et al., 2011). Therefore, we first explored if mutations in enzymes in the peptidoglycan recycling pathway affected cell morphology. TEM images demonstrate that *A. baumannii* strains lacking AmpD or AnmK showed no differences in morphology or cell wall thickness compared to the wild type strain. This could be because in our experimental setting, *de novo* synthesis of peptidoglycan is not interrupted and the UDP-MurNAc is supplied by this route in mutant strains. In addition, we observed that OMV were produced in both mutants. Production of OMV has been observed in several strains of *A. baumannii* (Kwon et al., 2009; Jin et al., 2011; Rumbo et al., 2011; McConnell et al., 2011). Reduced levels of crosslinks between the peptidoglycan and the outer membrane, which is modulated through the peptidoglycan recycling (Schwechheimer and Kuehn, 2015; Kim et al., 2021), have been shown to influence OMV release. However, our results indicate that altering AmpD and AnmK in peptidoglycan recycling pathway do not eliminate this process, although further analyses to quantify the OMVs produced for these strains will be of interest to compare with the wild type levels.

Deletion of *ampD* and *anmK* did not affect membrane permeability as observed when we analyzed the ability of NPN

10.3389/fcimb.2022.1064053

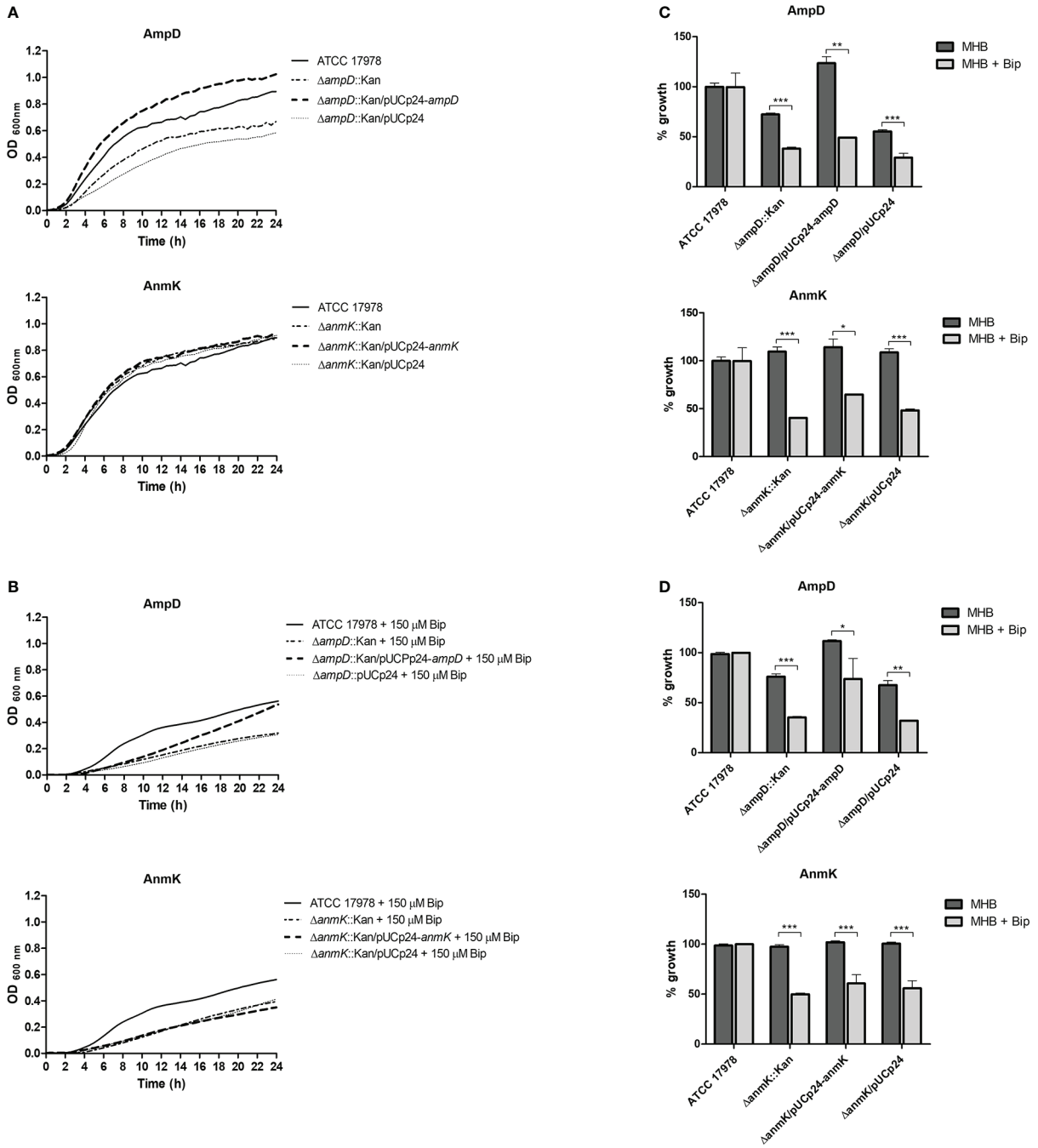

FIGURE 3
In vitro growth of *Acinetobacter baumannii* strains in Mueller Hinton broth (MHB). **(A)** Growth curves over 24 h of *A. baumannii* strains in media MHB. **(B)** Growth curves over 24 h of *A. baumannii* strains in MHB supplemented with 150 μM of the iron chelator 2, 2'-bipyridil (Bip). **(C)** Percentage of growth with respect to the *A. baumannii* ATCC 17978 strain in MHB or MHB + Bip at exponential growth phase (6 h). **(D)** Percentage of growth with respect to the *A. baumannii* ATCC 17978 strain in MHB or MHB + Bip at stationary growth phase (24h). * $p< 0.05$, ** $p< 0.01$ and *** $p< 0.001$, Student's t-test.

and SYTOX Green, neutral and positively charged fluorescent stains, respectively, to penetrate into the cell. These findings are in line with those reported in a previous study by our group (Gil-Marqués et al., 2018) in which we observed that there were no differences in permeability to ethidium bromide, another positively charged stain, in the same strains. Bacterial cells normally exclude these stains, which can only penetrate into the cell when membrane damage has occurred. Taken together, the

10.3389/fcimb.2022.1064053

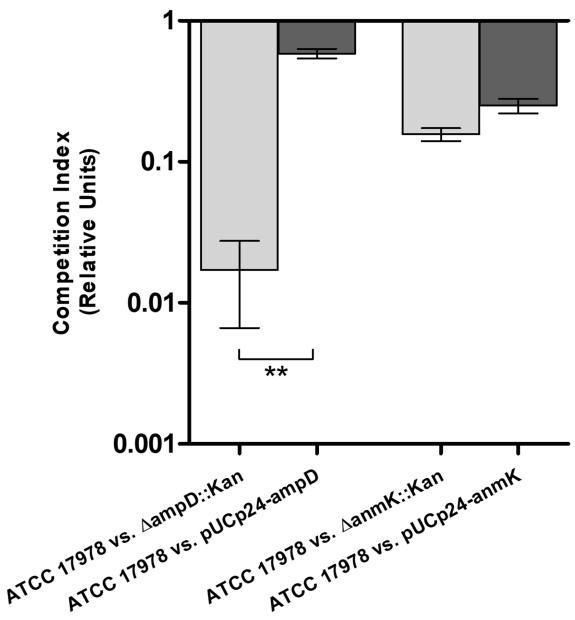

FIGURE 4
Fitness of mutant and complemented strains of *Acinetobacter baumannii* with its wild type counterpart in Mueller Hinton broth. Competition indices comparing ATCC 17978 and Δ*ampD*::Kan, ATCC 17978 and Δ*ampD*::Kan/pUCp24-*ampD*, ATCC 17978 and Δ*anmK*::Kan, and ATCC 17978 and Δ*anmK*::Kan/pUCp24-*anmK* in MHB. Bars represent the mean ± standard deviation of three independent assays. ** p = 0.0042 compared to mutant strain, Student's t-test.

results obtained with the different stains demonstrated that lack of AmpD and AnmK does not significantly alter the permeability of cell membrane with respect to these dyes.

Although no structural differences were observed, we wanted to analyze how bacterial fitness was affected by loss of AmpD and AnmK. Peptidoglycan recycling is not essential for *in vitro* growth, but provides metabolites that can be reused to synthesize more peptidoglycan and also as an energy source (Park and Uehara, 2008; Fisher and Mobashery, 2014). In fact, many bacteria remodel as much as half of their peptidoglycan per generation, and cell wall recycling and synthesis are tightly coordinated to preserve bacterial integrity (Johnson et al., 2013; Dhar et al., 2018). We demonstrate that, under laboratory conditions, loss of AmpD is associated with a more marked reduction in fitness than absence of AnmK, as we observed a marked defect in growth relative to the parental strain, both in iron-rich and iron-limiting conditions. In addition, this was confirmed with the lower competition index obtained for the Δ*ampD*::Kan mutant. Differences in inoculum between growth curves and competition experiments may explain why fitness loss is more evident in the latter. The differences in fitness found in this study between both mutants could be due to the fact that the amidase AmpD participates in an initial step of peptidoglycan recycling and thus its absence results in a more complete blockage of peptidoglycan recycling (Gil-Marqués et al., 2018). In addition, AmpD hydrolyzes anhydromuropeptides in the cytoplasm yielding not only products that are involved in the recycling pathway (anhMurNAc), but also Ala-Glu-DAP, that can be incorporated to *de novo* pathway of peptidoglycan (Gil-Marqués et al., 2018). On the other hand, AnmK is involved in the conversion of anhMurNAc to MurNAc-P. This is an enzymatic step that takes place after the hydrolysis of the anhydromuropeptide by AmpD (Gisin et al., 2013). Thus, lack of AnmK function likely only alters the yield of UDP-MurNAc obtained from anhMurNAc affecting the recycling pathway but not peptidoglycan *de novo* synthesis. Similar results were observed in other species such as *Pseudomonas aeruginosa* which has three closely related AmpD enzymes (Rivera et al., 2016), and the triple knockout mutant presented a marked decrease in fitness (Moya et al., 2008). Reduced fitness has also been observed in a *Salmonella typhimurium ampD* mutant in a murine model of infection (Folkesson et al., 2005). We observed that complementation with a plasmid encoding the deleted genes did not always restore the wild type phenotype in the experiments

TABLE 3 Minimum inhibitory concentration (MIC) of *Acinetobacter baumannii* (*A. baumannii*) strains to disinfectants and antimicrobial agents.

Strain	Chlorhexidine (mM)	Ethanol (mM)	Deoxycholate* (mM)	EDTA (mM)	SDS (mM)
A. baumannii ATCC 17978	0.03	1	> 120	0.007	0.002
A. baumannii Δ*ampD*::Kan	0.03	1	120	0.007	0.002
A. baumannii Δ*ampD*::Kan/pUCp24-*ampD*	0.03	1	> 120	0.007	0.002
A. baumannii Δ*ampD*::Kan/pUCp24	0.03	1	> 120	0.007	0.002
A. baumannii Δ*anmK*::Kan	0.03	1	> 120	0.007	0.002
A. baumannii Δ*anmK*::Kan/pUCp24-*anmK*	0.03	1	> 120	0.007	0.002
A. baumannii Δ*anmK*::Kan/pUCp24	0.03	1	> 120	0.007	0.002

*The exact MIC for deoxycholate could not be established because it was not soluble at concentrations above 120 mM.

10.3389/fcimb.2022.1064053

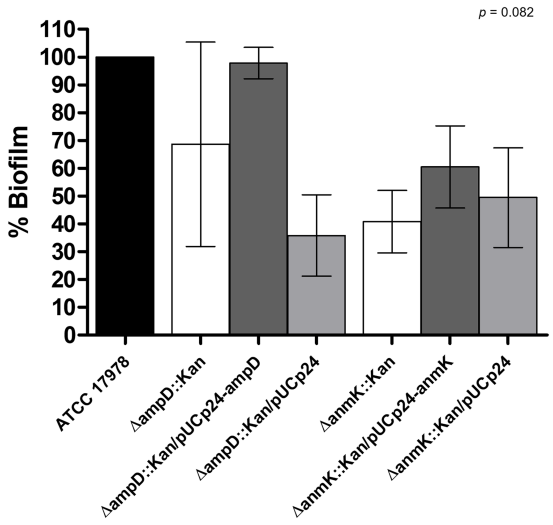

FIGURE 5
Effect of Δ*ampD* and Δ*anmK* deletion on biofilm production. Percentage of biofilm production was determined for mutants strains (Δ*ampD*::Kan and Δ*anmK*::Kan), their complemented strains (Δ*ampD*::Kan/pUCp24-*ampD* and Δ*anmK*::Kan/pUCp24-*anmK*), and the complemented strains with an empty plasmid (Δ*ampD*::Kan/pUCp24 and Δ*anmK*::Kan/pUCp24) respect to the wild type ATCC 17978 strain. Bars represent the average of six separate assays, with error bars representing the standard deviation. No significant differences were found between replicates (p = 0.082), as assessed by ANOVA followed by Tukey's Multiple Comparison Test.

carried out in this work, especially when complementing *anmK* mutant. Because carrying a plasmid has a fitness cost in the bacterium (San Millan and MacLean, 2017; Alonso-Del Valle et al., 2021), we hypothesize that the bacteria could prefer to maintain fitness rather than express the plasmid gene considering that AnmK plays a less important role in the peptidoglycan integrity maintenance. Lastly, we observed some differences in growth curves compared to previous data (Gil-Marqués et al., 2018) as in the present study more efficient complementation is observed by ectopic expression of AmpD and AnmK. This may be due to the higher inoculum used in the present study to minimizing plasmid loss during growth curve experiments.

In addition, it is interesting to note that peptidoglycan recycling also has a regulatory role in resistance mechanisms, for example *ampD* gene inactivation has been associated to an increased expression of AmpC β-lactamase, which results in an increased β-lactam resistance (Schmidtke and Hanson, 2006), although this has not been shown in *A. baumannii* (Gil-Marqués et al., 2018). In fact, except for fosfomycin, higher susceptibility of Δ*ampD*::Kan and Δ*anmK*::Kan mutant strains to most clinically relevant antibiotics was not observed (Gil-Marqués et al., 2018). Our data showed that deletion of *ampD* and *anmK* also does not affect susceptibility to the disinfectants chlorhexidine and ethanol, the chelating agent EDTA, that disrupts the lipopolysaccharide of the cell wall (Umerska et al., 2018) or the detergent SDS that also acts on the cell wall (Shehadul Islam et al., 2017), and only a small increase in susceptibility to deoxycholate was observed in Δ*ampD*::Kan mutant. This is in line with the idea that resistance to some disinfectants in Gram-negative bacteria is not mediated directly by peptidoglycan, but rather by the presence of efflux pumps in the outer membrane, as previously described (Venter et al., 2015). For example, expression of the

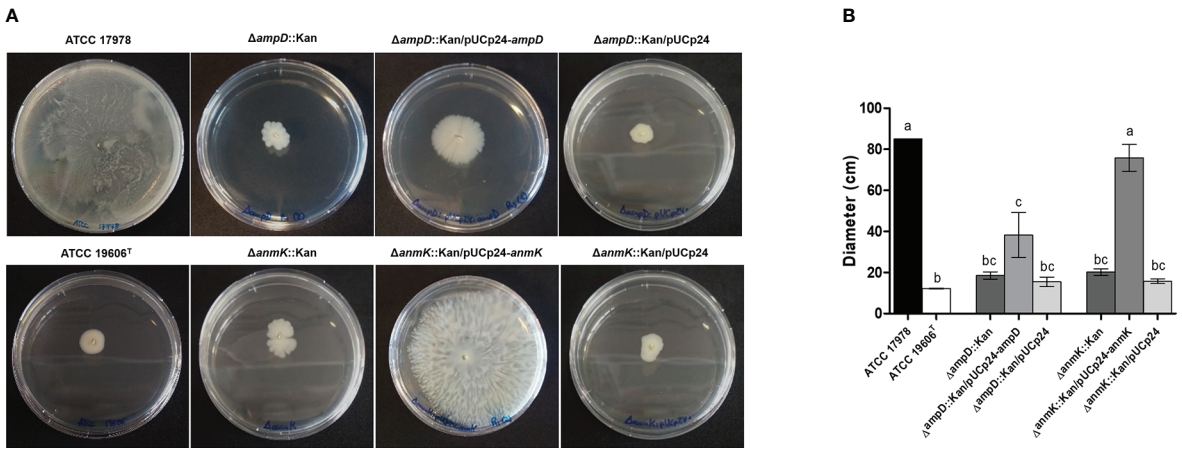

FIGURE 6
Twitching motility displayed by *Acinetobacter baumannii* strains. **(A)** Surface motility on semisolid media of wild type strain, the respective mutants and complemented strains after 32 h of incubation. **(B)** Measurement of surface extension for each bacterial strain. Error bars represent the standard deviation of triplicate experiments. Different superscript letters indicate significant difference (p< 0.05) between the strains as assessed by ANOVA followed by Tukey's Multiple Comparison Test.

multidrug efflux pump AceI has been associated with resistance to chlorhexidine in *A. baumannii* (Bolla et al., 2020). While AcrAB and CmeABC efflux pumps have been associated with resistance to deoxycolate in *Escherichia coli* and *Campylobacter jejuni*, respectively (Thanassi et al., 1997; Lin et al., 2003), for *A. baumannii* it remains to be elucidated if this occurs or it is associated to modifications on lipopolysaccharide. If so, our data points to hypothesise that AmpD may be partly involved, as a restructuring of bacterial envelope may take place. In contrast, the effects of ethanol on bacteria are due to colligative effects instead of damage in a specific receptor, but again mainly affect the integrity of the outer cell membrane (Ingram, 1989; Horinouchi et al., 2018).

Finally, in order to determine how AmpD and AnmK loss affects virulence traits in *A. baumannii*, we characterized biofilm formation and twitching motility, both involved in pathogenesis and transmission of this species (McConnell et al., 2013). *A. baumannii* survival on surfaces is enhanced due to its ability to form biofilms, contributing to its persistence in the hospital environment and increasing the chance of producing infections in the hospital setting (Lin et al., 2020). For the first time, we demonstrate that absence of either AmpD or AnmK results in a tendency towards decreased biofilm formation compared to the wild type strain. The defect on adherence and biofilm formation when peptidoglycan remodelling is altered could be due to alterations in large macromolecular structures needed for biofilm formation, such as pili or protein secretion systems. Those must pass through the peptidoglycan layer of the cell wall to be correctly displayed on the surface of the cell, and often have a large size that typically exceeds the mesh size of peptidoglycan. Therefore, to allow their transit, localized remodelling is required (Gallant et al., 2005). In fact, cell wall remodelling has been shown to be relevant for the assembly of flagella and for type III and type VI secretion systems (Pérez-Gallego et al., 2016). This could also explain the reduced twitching motility in Δ*anmK*::Kan and Δ*ampD*::Kan mutants observed in this work, since type IV pili are necessary for this surface movement (Wall and Kaiser, 1999; Piepenbrink et al., 2016). On the other hand, released peptidoglycan fragments can act as signalling molecules that could also affect motility and biofilm formation (Vermassen et al., 2019; Irazoki et al., 2019). Furthermore, studies carried out in *P. aeruginosa* linked twitching motility to formation and maintenance of biofilm (O'Toole and Kolter, 1998; Chiang and Burrows, 2003), so both virulence traits are related. Although little is known, this relationship has also been observed in *A. baumannii* (Luo et al., 2015), which could explain the defects observed in both virulence traits in the mutant strains used in this study. In addition, biofilm formation has also been related with desiccation tolerance in *A. baumannii* (Espinal et al., 2012) which may facilitate the survival of bacteria in a hospital setting, so it would be of interest to perform further assays to determine if the lack of AmpD and AnmK, also has an effect on resistance to desiccation.

5 Conclusion

In this study we demonstrate that the enzymes AmpD and AnmK, both involved in the peptidoglycan recycling pathway, go beyond intrinsic fosfomycin resistance in *A. baumannii*. Different traits related to fitness and virulence are affected when these enzymes are absent, especially AmpD. However, most of the molecular mechanisms that produce these phenotypic changes are still unknown and further analysis are needed to corroborate that these results occur *in vivo*. The findings presented here could be useful for the development of new strategies to fight *A. baumannii* infections. For example, *anmK* and especially *ampD* inhibition could be used in combination with fosfomycin to treat *A. baumannii* infections. In addition, these findings establish a link between fosfomycin resistance and bacterial fitness/virulence in *A. baumannii*.

Data availability statement

The raw data supporting the conclusions of this article will be made available by the authors upon request, without undue reservation.

Author contributions

AT: Performed growth curves, MIC, competition, biofilm formation, cell permeability and twitching studies. Analyzed data, drafted the manuscript and revised the final version. MT: Performed microscopy analyses and revised the final version of the manuscript. ML-S: Assisted in experimental procedures, supervised the study, drafted the manuscript and revised the final version. MM: Conceived and supervised the study, revised the manuscript and granted funding. All authors contributed to the article and approved the submitted version.

Funding

ML-S was supported by the Sara Borrell Program of the Instituto de Salud Carlos III (CD17CIII/00017), and AT was supported by the Garantía Juvenil Program of the Comunidad Autónoma de Madrid (PEJ2018-004820-A -MPY 387/19), is currently supported by a FPU grant (FPU20/03261) and PhD student in Biomedical Sciences and Public Health, Universidad Nacional de Educación a Distancia (UNED), Madrid, Spain (atajuelo11@alumno.uned.es). MM is supported by grants from the Instituto de Salud Carlos III (MP 516/19 and MPY 380/18).

Acknowledgments

We are grateful to Dr. Miriam Domenech (Bacterial infections Unit, National Center for Microbiology, Instituto de Salud Carlos III) for helping with the setting up of the biofilm

assay and Dr. Daniel Luque and Dr. Martin Sachse from the Electron Microscopy Unit (Instituto de Salud Carlos III) for assistance in microscopy analyses.

Conflict of interest

MM is founder and stockholder of the biotechnology spin-off company Vaxdyn, which develops vaccines for infections caused by MDR bacteria. Vaxdyn had no role in the elaboration of this manuscript.

The remaining authors declare that the research was conducted in the absence of any commercial or financial relationships that could be construed as a potential conflict of interest.

Publisher's note

Supplementary material

The Supplementary Material for this article can be found online at: https://www.frontiersin.org/articles/10.3389/fcimb.2022.1064053/full#supplementary-material

References

Aghamali, M., Sedighi, M., Zahedi Bialvaei, A., Mohammadzadeh, N., Abbasian, S., Ghafouri, Z., et al. (2019). Fosfomycin: Mechanisms and the increasing prevalence of resistance. *J. Med. Microbiol.* 68 (1), 11–25. doi: 10.1099/jmm.0.000874

Alonso-Del Valle, A., León-Sampedro, R., Rodríguez-Beltrán, J., Dela Fuente, J., Hernández-García, M., Ruiz-Garbajosa, P., et al. (2021). Variability of plasmid fitness effects contributes to plasmid persistence in bacterial communities. *Nat. Commun.* 12 (1), 2653. doi: 10.1038/s41467-021-22849-y

Begley, M., Gahan, C. G. M., and Hill, C. (2005). The interaction between bacteria and bile. *FEMS Microbiol. Rev.* 29 (4), 625–651. doi: 10.1016/j.femsre.2004.09.003

Bleck, C. K., Merz, A., Gutierrez, M. G., Walther, P., Dubochet, J., Zuber, B., et al. (2010). Comparison of different methods for thin section EM analysis of mycobacterium smegmatis. *J. Microsc.* 237 (1), 23–38. doi: 10.1111/j.1365-2818.2009.03299.x

Bolla, J. R., Howes, A. C., Fiorentino, F., and Robinson, C. V. (2020). Assembly and regulation of the chlorhexidine-specific efflux pump AceI. *Proc. Natl. Acad. Sci. U.S.A.* 117 (29), 17011–17018. doi: 10.1073/pnas.2003271117

Candel, F. J., Matesanz David, M., and Barberán, J. (2019). New perspectives for reassessing fosfomycin: Applicability in current clinical practice. *Rev. Esp. Quimioter* 32 (Suppl 1), 1–7.

Carretero-Ledesma, M., García-Quintanilla, M., Martín-Peña, R., Pulido, M. R., Pachón, J., and McConnell, M. J. (2018). Phenotypic changes associated with colistin resistance due to lipopolysaccharide loss in *Acinetobacter baumannii*. *Virulence* 9 (1), 930–942. doi: 10.1080/21505594.2018.1460187

Cava, F., Lam, H., de Pedro, M. A., and Waldor, M. K. (2011). Emerging knowledge of regulatory roles of d-amino acids in bacteria. *Cell. Mol. Life Sci.* 68 (5), 817–831. doi: 10.1007/s00018-010-0571-8

Chiang, P., and Burrows, L. L. (2003). Biofilm formation by hyperpiliated mutants of *Pseudomonas aeruginosa*. *J. Bacteriol.* 185 (7), 2374–2378. doi: 10.1128/JB.185.7.2374-2378.2003

CLSI (2017). "Performance standards for antimicrobial susceptibility testing; twenty-seventh informational supplement," in *CLSI document M100-S27* (Wayne, PA., USA: Clinical Laboratory Standards Institute).

Dhar, S., Kumari, H., Balasubramanian, D., and Mathee, K. (2018). Cell-wall recycling and synthesis in *Escherichia coli* and *Pseudomonas aeruginosa* - their role in the development of resistance. *J. Med. Microbiol.* 67 (1), 1–21. doi: 10.1099/jmm.0.000636

Doi, Y. (2019). Treatment options for carbapenem-resistant gram-negative bacterial infections. *Clin. Infect. Dis.* 69 (Suppl 7), S565–S575. doi: 10.1093/cid/ciz830

Domenech, M., and García, E. (2020). The n-acetylglucosaminidase LytB of *Streptococcus pneumoniae* is involved in the structure and formation of biofilms. *Appl. Environ. Microbiol.* 86 (10), e00280–20. doi: 10.1128/AEM.00280-20

Eijkelkamp, B. A., Stroeher, U. H., Hassan, K. A., Papadimitrious, M. S., Paulsen, I. T., Brown, M. H., et al. (2011). Adherence and motility characteristics of clinical *Acinetobacter baumannii* isolates. *FEMS Microbiol. Lett.* 323 (1), 44–51. doi: 10.1111/j.1574-6968.2011.02362.x

Espinal, P., Martí, S., and Vila, J. (2012). Effect of biofilm formation on the survival of *Acinetobacter baumannii* on dry surfaces. *J. Hosp. Infect.* 80 (1), 56–60. doi: 10.1016/j.jhin.2011.08.013

Fisher, J. F., and Mobashery, S. (2014). The sentinel role of peptidoglycan recycling in the β-lactam resistance of the gram-negative enterobacteriaceae and *Pseudomonas aeruginosa*. *Bioorg. Chem.* 56, 41–48. doi: 10.1016/j.bioorg.2014.05.011

Folkesson, A., Eriksson, S., Andersson, M., Park, J. T., and Normark, S. (2005). Components of the peptidoglycan-recycling pathway modulate invasion and intracellular survival of *Salmonella enterica* serovar *Typhimurium*. *Cell Microbiol.* 7 (1), 147–155. doi: 10.1111/j.1462-5822.2004.00443.x

Gallant, C. V., Daniels, C., Leung, J. M., Ghosh, A. S., Young, K. D., Kotra, L. P., et al. (2005). Common beta-lactamases inhibit bacterial biofilm formation. *Mol. Microbiol.* 58 (4), 1012–1024. doi: 10.1111/j.1365-2958.2005.04892.x

Gil-Marqués, M. L., Moreno-Martínez, P., Costas, C., Pachón, J., Blázquez, J., McConnell, M. J., et al. (2018). Peptidoglycan recycling contributes to intrinsic resistance to fosfomycin in *Acinetobacter baumannii*. *J. Antimicrob. Chemother.* 73 (11), 2960–2968. doi: 10.1093/jac/dky289

Gisin, J., Schneider, A., Nägele, B., Borisova, M., and Mayer, C. (2013). A cell wall recycling shortcut that bypasses peptidoglycan de novo biosynthesis. *Nat. Chem. Biol.* 9 (8), 491–493. doi: 10.1038/nchembio.1289

Harding, C. M., Hennon, S. W., and Feldman, M. F. (2018). Uncovering the mechanisms of *Acinetobacter baumannii* virulence. *Nat. Rev. Microbiol.* 16 (2), 91–102. doi: 10.1038/nrmicro.2017.148

Horinouchi, T., Maeda, T., and Furusawa, C. (2018). Understanding and engineering alcohol-tolerant bacteria using OMICS technology. *World J. Microbiol. Biotechnol.* 34 (11), 157. doi: 10.1007/s11274-018-2542-4

Iarikov, D., Wassel, R., Farley, J., and Nambiar, S. (2015). Adverse events associated with fosfomycin use: Review of the literature and analyses of the FDA adverse event reporting system database. *Infect. Dis. Ther.* 4 (4), 433–458. doi: 10.1007/s40121-015-0092-8

Ingram, L. O. (1989). Ethanol tolerance in bacteria. *Crit. Rev. Biotechnol.* 9 (4), 305–319. doi: 10.3109/07388558909036741

Irazoki, O., Hernandez, S. B., and Cava, F. (2019). Peptidoglycan muropeptides: Release, perception, and functions as signaling molecules. *Front. Microbiol.* 10, 500. doi: 10.3389/fmicb.2019.00500

Jiang, M., Chen, X., Liu, S., Zhang, Z., Li, N., Dong, C., et al. (2021). Epidemiological analysis of multidrug-resistant *Acinetobacter baumannii* isolates in a tertiary hospital over a 12-year period in China. *Front. Public Health*. 9 (1113). doi: 10.3389/fpubh.2021.707435

Jin, J. S., Kwon, S. O., Moon, D. C., Gurung, M., Lee, J. H., Kim, S. I., et al. (2011). *Acinetobacter baumannii* secretes cytotoxic outer membrane protein a *via* outer membrane vesicles. *PloS One* 6 (2), e17027. doi: 10.1371/journal.pone.0017027

Johnson, J. W., Fisher, J. F., and Mobashery, S. (2013). Bacterial cell-wall recycling. *Ann. N Y Acad. Sci.* 1277, 54–75. doi: 10.1111/j.1749-6632.2012.06813.x

Karaiskos, I., and Giamarellou, H. (2014). Multidrug-resistant and extensively drug-resistant gram-negative pathogens: Current and emerging therapeutic

approaches. *Expert Opin. Pharmacother.* 15 (10), 1351–1370. doi: 10.1517/14656566.2014.914172

Kim, N., Kim, H. J., Oh, M. H., Kim, S. Y., Kim, M. H., Son, J. H., et al. (2021). The role of zur-regulated lipoprotein a in bacterial morphology, antimicrobial susceptibility, and production of outer membrane vesicles in *Acinetobacter baumannii*. *BMC Microbiol.* 21 (1), 27. doi: 10.1186/s12866-020-02083-0

Kwon, S. O., Gho, Y. S., Lee, J. C., and Kim, S. I.. (2009). Proteome analysis of outer membrane vesicles from a clinical *Acinetobacter baumannii* isolate. *FEMS Microbiol. Lett.* 297 (2), 150–156. doi: 10.1111/j.1574-6968.2009.01669.x

Lee, C. R., Lee, J. H., Park, M., Park, K. S., Bae, I. K., Kim, Y. B., et al. (2017). Biology of *Acinetobacter baumannii*: Pathogenesis, antibiotic resistance mechanisms, and prospective treatment options. *Front. Cell Infect. Microbiol.* 7, 55. doi: 10.3389/fcimb.2017.00055

Lin, J., Sahin, O., Michel, L. O., and Zhang, Q. (2003). Critical role of multidrug efflux pump CmeABC in bile resistance and *in vivo* colonization of *Campylobacter jejuni*. *Infect. Immun.* 71 (8), 4250–4259. doi: 10.1128/IAI.71.8.4250-4259.2003

Lin, M. F., and Lan, C. Y. (2014). Antimicrobial resistance in *Acinetobacter baumannii*: From bench to bedside. *World J. Clin. cases* 2 (12), 787–814. doi: 10.12998/wjcc.v2.i12.787

Lin, M. F., Lin, Y. Y., and Lan, C. Y. (2020). Characterization of biofilm production in different strains of *Acinetobacter baumannii* and the effects of chemical compounds on biofilm formation. *PeerJ* 8, e9020. doi: 10.7717/peerj.9020

Luo, L. M., Wu, L. J., Xiao, Y. L., Zhao, D., Chen, Z. X., Kang, M., et al. (2015). Enhancing pili assembly and biofilm formation in *Acinetobacter baumannii* ATCC19606 using non-native acyl-homoserine lactones. *BMC Microbiol.* 15, 62. doi: 10.1186/s12866-015-0397-5

McConnell, M. J., Actis, L., and Pachón, J. (2013). *Acinetobacter baumannii*: human infections, factors contributing to pathogenesis and animal models. *FEMS Microbiol. Rev.* 37 (2), 130–155. doi: 10.1111/j.1574-6976.2012.00344.x

McConnell, M. J., Rumbo, C., Bou, G., and Pachón, J. (2011) Outer membrane vesicles as an acellular vaccine against *Acinetobacter baumannii*. *Vaccine* 29 (34), 5705–5710. doi: 10.1016/j.vaccine.2011.06.001

Moya, B., Juan, C., Albertí, S., Pérez, J. L., and Oliver, A. (2008). Benefit of having multiple *ampD* genes for acquiring beta-lactam resistance without losing fitness and virulence in *Pseudomonas aeruginosa*. *Antimicrob Agent Chemother* 52 (10), 1098–6596.

Múñez Rubio, E., Ramos Martínez, A., and Fernández Cruz, A. (2019). Fosfomycin in antimicrobial stewardship programs. *Rev. Esp. Quimioter* 32 (Suppl 1), 62–66.

O'Toole, G. A., and Kolter, R. (1998). Flagellar and twitching motility are necessary for *Pseudomonas aeruginosa* biofilm development. *Mol. Microbiol.* 30 (2), 295–304. doi: 10.1046/j.1365-2958.1998.01062.x

Park, J. T., and Uehara, T. (2008). How bacteria consume their own exoskeletons (Turnover and recycling of cell wall peptidoglycan). *Microbiol. Mol. Biol. Rev.* 72 (2), 211–227. doi: 10.1128/MMBR.00027-07

Pérez-Gallego, M., Torrens, G., Castillo-Vera, J., Moya, B., Zamorano, L., Cabot, G., et al. (2016). Impact of AmpC derepression on fitness and virulence: The mechanism or the pathway? *mBio* 7 (5), e01783-16. doi: 10.1128/mBio.01783-16

Piepenbrink, K. H., Lillehoj, E., Harding, C. M., Labonte, J. W., Zuo, X., Rapp, C. A., et al. (2016). Structural diversity in the type IV pili of multidrug-resistant *Acinetobacter*. *J. Biol. Chem.* 291 (44), 22924–22935. doi: 10.1074/jbc.M116.751099

Rivera, I., Molina, R., Lee, M., Mobashery, S., and Hermoso, J. A. (2016). Orthologous and paralogous AmpD peptidoglycan amidases from gram-negative bacteria. *Microb. Drug Resist.* 22 (6), 470–476. doi: 10.1089/mdr.2016.0083

Rolain, J. M., Diene, S. M., Kempf, M., Gimenez, G., Robert, C., Raoult, D., et al. (2013). Real-time sequencing to decipher the molecular mechanism of resistance of a clinical pan-drug-resistant *Acinetobacter baumannii* isolate from Marseille, France. *Antimicrob. Agents Chemother.* 57 (1), 592–596. doi: 10.1128/AAC.01314-12

Rumbo, C., Fernández-Moreira, E., Merino, M., Poza, M., Mendez, J. A., Soares, N. C., et al. (2011). Horizontal transfer of the OXA-24 carbapenemase gene via outer membrane vesicles: A new mechanism of dissemination of carbapenem resistance genes in *Acinetobacter baumannii*. *Antimicrob. Agents Chemother.* 55 (7), 3084–3090. doi: 10.1128/AAC.00929-10

San Millan, A., and MacLean, R. C. (2017). Fitness costs of plasmids: a limit to plasmid transmission. *Microbiol. Spectr.* 5 (5), 5.5.02. doi: 10.1128/microbiolspec.MTBP-0016-2017

Sastry, S., and Doi, Y. (2016). Fosfomycin: Resurgence of an old companion. *J. Infect. Chemother.* 22 (5), 273–280. doi: 10.1016/j.jiac.2016.01.010

Schindelin, J., Arganda-Carreras, I., Frise, E., Kaynig, V., Longair, M., Pietzsch, T., et al. (2012). Fiji: An open-source platform for biological-image analysis. *Nat. Methods* 9 (7), 676–682. doi: 10.1038/nmeth.2019

Schmidtke, A. J., and Hanson, N. D. (2006). Model system to evaluate the effect of *ampD* mutations on AmpC-mediated beta-lactam resistance. *Antimicrob. Agents Chemother.* 50 (6), 2030–2037. doi: 10.1128/AAC.01458-05

Schwechheimer, C., and Kuehn, M. J. (2015). Outer-membrane vesicles from gram-negative bacteria: Biogenesis and functions. *Nat. Rev. Microbiol.* 13 (10), 605–619. doi: 10.1038/nrmicro3525

Shehadul Islam, M., Aryasomayajula, A., and Selvaganapathy, P. R. (2017). A review on macroscale and microscale cell lysis methods, in *Micromachines (Basel)* 8 (3), 83.

Silver, L. L. (2017). Fosfomycin: Mechanism and resistance. *Cold Spring Harb. Perspect. Med.* 7 (2), a025262. doi: 10.1101/cshperspect.a025262

Sonkar, A., Shukla, H., Shukla, R., Kalita, J., Pandey, T., Tripathi, T., et al. (2017). UDP-N-Acetylglucosamine enolpyruvyl transferase (MurA) of *Acinetobacter baumannii* (AbMurA): Structural and functional properties. *Int. J. Biol. Macromol.* 97, 106–114. doi: 10.1016/j.ijbiomac.2016.12.082

Spapen, H., Jacobs, R., Van Gorp, V., Troubleyn, J., and Honoré, P. M. (2011). Renal and neurological side effects of colistin in critically ill patients. *Ann. Intensive Care* 1 (1), 14. doi: 10.1186/2110-5820-1-14

Thanassi, D. G., Cheng, L. W., and Nikaido, H. (1997). Active efflux of bile salts by *Escherichia coli*. *J. Bacteriol.* 179 (8), 2512–2518. doi: 10.1128/jb.179.8.2512-2518.1997

Umerska, A., Strandh, M., Cassisa, V., Matougui, N., Eveillard, M., and Saulnier, P. (2018). Synergistic effect of combinations containing EDTA and the antimicrobial peptide AA230, an arenicin-3 derivative, on gram-negative bacteria. *Biomolecules* 8 (4), 122. doi: 10.3390/biom8040122

Urdaneta, V., and Casadesús, J. (2017). Interactions between bacteria and bile salts in the gastrointestinal and hepatobiliary tracts. *Front. Med. (Lausanne)* 4, 163. doi: 10.3389/fmed.2017.00163

Venter, H., Mowla, R., Ohene-Agyei, T., and Ma, S. (2015). RND-type drug efflux pumps from gram-negative bacteria: Molecular mechanism and inhibition. *Front. Microbiol.* 6 (377). doi: 10.3389/fmicb.2015.00377

Vermassen, A., Leroy, S., Talon, R., Provot, C., Popowska, M., and Desvaux, M.. (2019). Cell wall hydrolases in bacteria: Insight on the diversity of cell wall amidases, glycosidases and peptidases toward peptidoglycan. *Front. Microbiol.* 10, 331. doi: 10.3389/fmicb.2019.00331

Vollmer, W., Blanot, D., and de Pedro, M. A. (2008). Peptidoglycan structure and architecture. *FEMS Microbiol. Rev.* 32 (2), 149–167. doi: 10.1111/j.1574-6976.2007.00094.x

Wall, D., and Kaiser, D. (1999). Type IV pili and cell motility. *Mol. Microbiol.* 32 (1), 1–10. doi: 10.1046/j.1365-2958.1999.01339.x

frontiers | Frontiers in Microbiology

TYPE Original Research
PUBLISHED 09 February 2023
DOI 10.3389/fmicb.2023.1057608

OPEN ACCESS

EDITED BY
Raffaele Zarrilli,
University of Naples Federico II, Italy

REVIEWED BY
Filipa Grosso,
University of Porto,
Portugal
German Matias Traglia,
Universidad de la República, Uruguay

*CORRESPONDENCE
Jorgelina Morán-Barrio
✉ moran@ibr-conicet.gov.ar
Alejandro M. Viale
✉ viale@ibr-conicet.gov.ar

†These authors have contributed equally to this work and share first authorship

‡PRESENT ADDRESS
M. Marcela Cameranesi,
Department of Biochemistry and Molecular Pharmacology, New York University School of Medicine, New York, NY, United States

SPECIALTY SECTION
This article was submitted to Antimicrobials, Resistance and Chemotherapy, a section of the journal Frontiers in Microbiology

RECEIVED 29 September 2022
ACCEPTED 04 January 2023
PUBLISHED 09 February 2023

CITATION
Giacone L, Cameranesi MM, Sanchez RI, Limansky AS, Morán-Barrio J and Viale AM (2023) Dynamic state of plasmid genomic architectures resulting from XerC/D-mediated site-specific recombination in *Acinetobacter baumannii* Rep_3 superfamily resistance plasmids carrying bla_{OXA-58}- and Tn*aphA6*-resistance modules. *Front. Microbiol.* 14:1057608. doi: 10.3389/fmicb.2023.1057608

Dynamic state of plasmid genomic architectures resulting from XerC/D-mediated site-specific recombination in *Acinetobacter baumannii* Rep_3 superfamily resistance plasmids carrying bla_{OXA-58}- and Tn*aphA6*-resistance modules

Lucía Giacone†, M. Marcela Cameranesi†‡, Rocío I. Sanchez, Adriana S. Limansky, Jorgelina Morán-Barrio*and Alejandro M. Viale*

Departamento de Microbiología, Facultad de Ciencias Bioquímicas y Farmacéuticas, CONICET, Instituto de Biología Molecular y Celular de Rosario (IBR), Universidad Nacional de Rosario (UNR), Rosario, Argentina

The acquisition of bla_{OXA} genes encoding different carbapenem-hydrolyzing class-D β-lactamases (CHDL) represents a main determinant of carbapenem resistance in the nosocomial pathogen *Acinetobacter baumannii*. The bla_{OXA-58} gene, in particular, is generally embedded in similar resistance modules (RM) carried by plasmids unique to the *Acinetobacter* genus lacking self-transferability. The ample variations in the immediate genomic contexts in which bla_{OXA-58}-containing RMs are inserted among these plasmids, and the almost invariable presence at their borders of non-identical 28-bp sequences potentially recognized by the host XerC and XerD tyrosine recombinases (pXerC/D-like sites), suggested an involvement of these sites in the lateral mobilization of the gene structures they encircle. However, whether and how these pXerC/D sites participate in this process is only beginning to be understood. Here, we used a series of experimental approaches to analyze the contribution of pXerC/D-mediated site-specific recombination to the generation of structural diversity between resistance plasmids carrying pXerC/D-bounded bla_{OXA-58}- and Tn*aphA6*-containing RM harbored by two phylogenetically- and epidemiologically-closely related *A. baumannii* strains of our collection, Ab242 and Ab825, during adaptation to the hospital environment. Our analysis disclosed the existence of different *bona fide* pairs of recombinationally-active pXerC/D sites in these plasmids, some mediating reversible intramolecular inversions and others reversible plasmid fusions/resolutions. All of the identified recombinationally-active pairs shared identical GGTGTA sequences at the cr spacer separating the XerC- and XerD-binding regions. The fusion of two Ab825 plasmids mediated by a pair of recombinationally-active pXerC/D sites displaying sequence differences at the cr spacer could be inferred on the basis of sequence comparison analysis, but no evidence of reversibility could be obtained in this case. The reversible plasmid genome rearrangements mediated by recombinationally-active pairs of pXerC/D sites reported here probably represents an ancient mechanism of generating structural diversity in the *Acinetobacter* plasmid pool. This recursive process could facilitate a rapid adaptation of an eventual bacterial host to changing environments, and has certainly contributed to the evolution of

Acinetobacter plasmids and the capture and dissemination of bla_{OXA-58} genes among *Acinetobacter* and non-*Acinetobacter* populations co-residing in the hospital niche.

KEYWORDS

***Acinetobacter baumannii*, carbapenem resistance, resistance plasmids, OXA-58 carbapenemase, XerC/D site-specific recombination, multiple pXerC/D sites, plasmid shuffling, plasmid dynamics and evolution**

Introduction

The main cause of carbapenem resistance among multidrug-resistant (MDR) clinical strains of the opportunistic pathogen *Acinetobacter baumannii* and its phylogenetically-related species of the *A. calcoaceticus-A. baumannii* (ACB) complex is represented by acquired bla_{OXA} genes encoding carbapenem-hydrolyzing class-D β-lactamases (CHDL) of the OXA-23, OXA-40/24, OXA-58, OXA-143, and OXA-235 groups (Roca et al., 2012; Carattoli, 2013; Evans and Amyes, 2014; Zander et al., 2014; Da Silva and Domingues, 2016; Hamidian and Nigro, 2019). The bla_{OXA-58} gene, in particular, is generally found in iteron plasmids endowed with replication initiation protein genes (*repAci*) encoding members of the Rep_3 (PF01051) superfamily (Rep_3 plasmids) unique to the *Acinetobacter* genus (Zarrilli et al., 2008; Roca et al., 2012; Carattoli, 2013; Evans and Amyes, 2014; Fu et al., 2014; Zander et al., 2014; Da Silva and Domingues, 2016; Cameranesi et al., 2017, 2018; Lean and Yeo, 2017; Salto et al., 2018; Hamidian and Nigro, 2019; Wang et al., 2020; Hamidian et al., 2021; Liu et al., 2021; Brito et al., 2022; Jones et al., 2022). A number of remarkable features distinguish the bla_{OXA-58}-containing structures carried by these plasmids, including the different genetic contexts in which they are inserted and the almost invariable presence at their borders of a variable number of short sequences displaying homology to the 28-bp chromosomal *dif* site recognized by the XerC and XerD tyrosine recombinases which have been alternatively designated Re27, p*dif*, or pXerC/D sites. This has led to suggestions that these pXerC/D-bounded structures could constitute modules endowed with horizontal mobilization abilities, but how these pXerC/D sites participate in the lateral mobilization of the structures they encircle is only beginning to be understood (Cameranesi et al., 2018).

The XerC/D SSR system, ubiquitous among bacteria, serves primary physiological roles in the separation of circular chromosomes prior to cell division by resolving dimers generated by homologous recombination during DNA replication (Cornet et al., 1994; Colloms et al., 1996; Rajeev et al., 2009; Crozat et al., 2014; Ramirez et al., 2014; Balalovski and Grainge, 2020). This system is unique among other SSR systems in that it employs two homologous tyrosine recombinases, XerC and XerD, which recognize a core 28-bp sequence known as *dif* organized in an imperfect palindrome composed of 11-bp each XerC- and XerD-binding regions, separated by a central spacer region (cr) of 6 bp where recombination occurs. Some ColE1-type plasmids of the *Enterobacteriaceae* use the XerC/D SSR system of their hosts to resolve their own multimeric forms, thus avoiding segregational instability. *Acinetobacter* plasmids, on the contrary, are unique in the sense that they contain not a single but several pXerC/D-like sites not necessarily located in direct orientations, which even display some sequence differences between them (Cameranesi et al., 2018). These features suggested functions other than participating only in the resolution of multimers and, in this context, sequence comparison analyses of a number of *Acinetobacter* plasmids provided evidence of their participation in DNA inversions and fusions/resolutions (Cameranesi et al., 2018; Balalovski and Grainge, 2020; Wang et al., 2020; Alattraqchi et al., 2021; Hamidian et al., 2021; Jones et al., 2022). Yet, experimental evidence supporting their role in SSR events is still scarce, and many questions remain including whether all the pXerC/D sites inferred in *Acinetobacter* plasmids are active in recombination, the kind of exchanges they can mediate, the factors that govern these reactions, and their effects on the evolutionary dynamics of the plasmids in which they are embedded and the hosts that eventually carry them.

We previously reported first empirical evidences indicating the existence of a recombinationally-active pair mediating the fusion of two plasmids into a co-integrate in *A. baumannii* cells of our collection (Cameranesi et al., 2018). Moreover, we observed that this co-integrate could also resolve in these cells, following an intramolecular SSR event now mediated by the pair of hybrid pXerC/D sites resulting from the previous intermolecular fusion. More recently, reconstructions of the evolutionary history of the bla_{OXA-58}-containing *A. baumannii* plasmid pA388 (Jones et al., 2022) also showed the existence of intramolecular inversions mediated by recombinationally active pairs of pXerC/D sites. The overall observations indicated that at least some of the pXerC/D sites inferred in *Acinetobacter* plasmids can constitute *bona fide* recombinationally active pairs, supporting roles in the evolution of the plasmid molecules in which they are embedded.

We recently characterized by whole genome sequencing (WGS) a number of phylogenetically- and epidemiologically-related MDR *A. baumannii* strains belonging to the clonal complex CC15 (Pasteur scheme) prevalent in South America (Matos et al., 2019; Cameranesi et al., 2020; Brito et al., 2022). Comparative genome analysis among two carbapenem-resistant strains of this collection, Ab242 and Ab825, indicated extensive chromosomal synteny between them but also disclosed a much larger number of acquired mobile elements in the Ab825 genome resulting in the inactivation of many exposed cell structures, including protective systems against external aggressors, effectors of the innate immune system, and outer membrane proteins related to carbapenem resistance and virulence, in a process most probably associated to the adaptation of this strain to the hospital environment (Mussi et al., 2005; Cameranesi et al., 2020; Labrador-Herrera et al., 2020). Assembly of the predominant plasmid forms based on WGS data indicated that Ab825 and Ab242 harbored plasmids endowed with almost identical bla_{OXA-58}- and Tn*aphA6*-containing resistance modules (RMs) bounded with pXerC/D sites, but disclosed differences between strains in the structural organization of these resistance plasmids.

We sought to analyze in this work whether and how pXerC/D-mediated recombination contributed to the generation of structural diversity between Ab242 and Ab825 plasmids. By developing a series of experimental approaches (see Supplementary Figure S2 for details),

we disclosed the existence of *bona fide* pairs of recombinationally-active pXerC/D sites among them, some mediating reversible intramolecular inversions and others reversible plasmid fusions/resolutions. This reversible remodeling of *Acinetobacter* plasmid structures mediated by different pairs of pXerC/D sites significantly impacts the possibilities of adaptation of an eventual host to varying and/or challenging environments, the evolutionary dynamics of the plasmids involved in this process, and the consequent dissemination of bla_{OXA-58} genes and other adaptive determinants among the bacterial community.

Materials and methods

Bacterial strains and growth conditions

The MDR, carbapenem-resistant *A. baumannii* clinical strains Ab242 and Ab825 were isolated from hospitalized patients in a public healthcare center (HECA) of Rosario, Argentina. These two strains were assigned to the clonal complex CC15 (Pasteur MLST scheme), and were characterized recently by WGS and comparative genome sequence analysis (Cameranesi et al., 2020).

The *A. nosocomialis* strain M2 (AnM2) is an antimicrobial susceptible ACB strain lacking indigenous plasmids (Carruthers et al., 2013), and was used as recipient for electrotransformation assays with plasmid mixtures extracted from the *A. baumannii* clinical strains analyzed (see below, and also Supplementary Figure S2). Similarly, the collection *A. baumannii* ATCC17978 strain (Ab17978) was also used for the same purpose.

All bacterial cells were grown in Lysogeny Broth (LB) liquid medium at 37°C under aerobic conditions with vigorous shaking, or in LB solid medium prepared by supplementing the LB liquid medium with 1.5% Difco Agar. When necessary, culture media were supplemented with the antimicrobials indicated at the concentrations stated in the text or in the legends to figures.

Growth of clonal populations of *Acinetobacter* strains and plasmid isolation

We used the general scheme described previously (Cameranesi et al., 2018). In short, isolated colonies of the clinical strains Ab242 or Ab825, or the selected IPM-resistant AnM2 or Ab17978 strains generated in this work, were independently obtained after streaking frozen stocks of the corresponding cells on LB agar media supplemented with 2 μg/ml IPM, followed by incubation at 37°C overnight. Then, clonal populations of each of these strains were generated by inoculating 10 ml of liquid LB medium supplemented with 2 μg/ml IPM with cells picked up from an isolated colony, followed by incubation at 37°C under gentle aeration until confluence. Plasmid extraction was performed from these cultures using the Wizard® Plus SV Minipreps DNA Purification Systems (Promega, WI, USA) and their quality was routinely analyzed by 0.7% agarose gel electrophoresis/ethidium bromide staining.

PCR identification of recombination events mediated by active sister pairs of pXerC/D sites in *Acinetobacter* plasmids

The plasmid mixtures obtained from the clonal cultures of the different *Acinetobacter* strains were independently used as templates in PCR assays aimed to detect recombination events mediated by particular pairs of pXerC/D sites (Supplementary Figures S1, S2). The primers employed were used in adequate combinations to detect the different pXerC/D sites and corresponding genetic contexts (see Supplementary Table S1). Primer pair H was additionally employed to detect the presence of plasmids containing the bla_{OXA-58} carbapenemase gene in isolated colonies of the Ab242 or Ab825 strains, as well as in IPM-resistant AnM2 or Ab17978 colonies obtained after transformation with Ab242 or Ab825 plasmids (see below). The amplification mixtures were analyzed by agarose gel electrophoresis, and the obtained amplicons were subsequently cloned into pGEM-T Easy (Promega) for further sequence analysis. Plasmids containing cloned DNA were analyzed by restriction mapping, and selected inserts were sequenced and subjected to comparative sequence analysis with the different predominant plasmid structures assembled from WGS data in the Ab242 or Ab825 strains to identify recombination events mediated by active pairs of pXerC/D sites (see Supplementary Figure S2 for details).

Transformation of AnM2 and *Acinetobacter baumannii* Ab17978 cells

Plasmid mixtures extracted from clonal cultures of the Ab242 or Ab825 strains were used for transformation assays employing electrocompetent AnM2 or Ab17978 cells as receptors, following previously described procedures (Ravasi et al., 2011). The rationale here was to obtain separate clonal lineages, in which each lineage originated from an individual cell initially transformed with a single plasmid structural variant carrying the RM from those present in the plasmid mixture (Supplementary Figure S2D). The transformed cells were plated on LB agar supplemented with 2 μg/ml IPM, and incubated 24–48 h at 37°C. Different IPM-resistant AnM2 or Ab17978 colonies developing during this period were analyzed by PCR for the presence of plasmids bearing the bla_{OXA-58} gene. Stocks of AnM2 or Ab17978 pure cultures generated from cells testing positive for bla_{OXA-58} were stored at −80° C and routinely used to regenerate the independent cultures (clonal populations) used in this work. Plasmids extracted from these clonal cultures were used in turn as templates in PCR reactions aimed to detect structural variants resulting from recombination events mediated by particular sister pairs of pXerC/D sites.

DNA sequencing, plasmid assembly, and comparative sequence analyses

The assembly of Ab242 plasmids was described previously (Cameranesi et al., 2018). Ab825 genomic DNA was isolated using the DNeasy Blood and Tissue kit (Qiagen), and its genomic sequence was obtained using a paired-end strategy using an Illumina MiSeq sequencer at the National Institute of Health (Lisbon, Portugal). Reads were subjected to quality assessment and further assembly using Velvet version 1.2.10. The *de novo* assembly process was optimized using the Velvet Optimiser script version 2.2.5. Gaps remaining in contigs corresponding to Ab825 plasmid sequences were closed using PCR with specifically designed primers employing Ab825 plasmid extracts as templates (Supplementary Figure S3).

The Rapid Annotation using Subsystem Technology standard operating procedures (RAST; http://rast.nmpdr.org/seedviewer.cgi; Aziz et al., 2008) and the National Center for Biotechnology

Information database (NCBI, U.S. National Library of Medicine, Bethesda MD, USA) were used to annotate the open reading frames (ORFs) found in the different plasmids. Insertion sequence (IS) elements were detected using IS Finder (Siguier et al., 2006; https://www-is.biotoul.fr/) and ISSaga (Varani et al., 2011). Plasmid pXerC/D-like core sequences were detected as described previously (Cameranesi et al., 2018).

The DNA sequences of the PCR fragments cloned into pGem-T were conducted at the Sequencing Facilities of Maine University, Orono (ME, U.S.A.) or at Macrogen (Seoul, Korea).

Results

Comparative analysis of *Acinetobacter baumannii* Ab242 and Ab825 carbapenem resistance plasmids

Detailed comparative sequence analysis of sequence-related plasmids found in different *A. baumannii* strains represents a useful tool to detect the recombination mechanism (s) that could account for any observed structural heterogeneity (Cameranesi et al., 2018; Wang et al., 2020; Alattraqchi et al., 2021; Hamidian et al., 2021; Jones et al., 2022). In the case of SSR events mediated by sister pairs of pXerC/D sites, these comparisons are also pivotal for the design of specific PCR primers hybridizing at the immediate neighboring regions associated to each of the pXerC/D-like half-sites that provided for the sister pair (Supplementary Figure S1). PCR analysis using appropriate combinations of primers and as template a plasmid mixture extracted from a clonal population of the studied strain (s), followed by sequence analysis of the obtained amplicons, could then verify whether plasmid structural variants (PSVs) carrying the inferred pXerC/D-mediated inversions and/or fusions are simultaneously present in the analyzed plasmid population (Supplementary Figure S2). This coexistence, in turn, signals the possible operation of a dynamic interconversion state of PSVs resulting from pXerC/D-mediated reversible SSR events in the analyzed cell populations.

WGS data analysis followed by gap closure strategies resulted in the assembly of two predominant circular plasmid forms in the Ab825 strain (Supplementary Figure S3). One of these plasmids of 11,891 bp in size was identical to pAb242_12 previously reported in the Ab242 strain (Cameranesi et al., 2018). Assembly of the second plasmid indicated a circular tri-replicon of 35,743 bp which was designated pAb825_36, and which carried a bla_{OXA-58}- and Tn*aphA6*-containing RM almost identical to that described in pAb242_25 including its associated pXerC/D sites (Figure 1). These two plasmids also showed additional regions of sequence similarity including two of the replication modules, a *mobA*- and *trbL*-containing mobilization region, and an IS*26* element. However, notorious differences were also found between them. First, the inversion of the DNA region that contains the bla_{OXA-58}- and Tn*aphA6*-containing RM, which was limited in pAb242_25 by the pXerC/D sites C2/D2 and C7/D7 (Figure 1B) and in pAb825_36 by C2/D7 and C7/D2 (Figure 1D). A detailed comparative analysis of the 28-bp core regions of these pXerC/D sites (Table 1) showed identical GGTGTA cr spacers as well as identical XerD-binding half sites for all of them, but some nucleotide differences at the XerC-binding half-sites. These comparisons, the relative orientations of these sites in the corresponding molecules, and the evidence provided by PCR assays (see Table 2; Supplementary Figure S4 below), indicated that C2/D7 and C7/D2 are in fact hybrid products of a SSR event mediated by an active sister pair composed of C2/D2 and C7/D7, and vice versa. Secondly, other main difference between pAb242_25 and pAb825_36 was represented by an extra DNA region of 9,284 bp in the latter plasmid, which is identical in sequence to a linearized form of plasmid pAb242_9. In pAb825_36 this pAb242_9-like region is bordered by two directly-oriented pXerC/D-like sites, namely C4/D14 and C14/D4, which share identical XerC and XerD sequences but differ in the cr region in two out of six nucleotides (Table 1). Detailed sequence comparisons between these plasmids strongly suggested that pAb825_36 resulted from an intermolecular fusion between a plasmid identical to pAb242_9 and a pAb242_25 structural variant, an event mediated by a pXerC/D pair formed by C14/D14 and C4/D4 (Figure 1D). Third, another difference between the carbapenem-resistance plasmid forms found in Ab242 and Ab825 is the presence in pAb825_36 of an IS*26*-bounded composite transposon-like structure carrying an *aac (3)*-IIa aminoglycoside acetyltransferase gene, designated here Tn*aac(3)*-IIa (Figure 1D). Since a single IS*26* copy was found in a similar location in pAb242_25 (Figure 1B), this resistance structure most probably resulted from an IS*26*-mediated recombination event that incorporated, next to this pre-existing IS*26*, a translocatable unit composed of another IS*26* copy (Harmer et al., 2014) carrying in this case a *aac(3)*-IIa-containing DNA fragment.

In summary, the comparative sequence analysis of the plasmids housed by the Ab242 and A825 strains assembled from WGS data analysis indicated that they shared extensive sequence identity as a whole, but also disclosed significant differences between strains including variations in the structural organization of their carbapenem-resistance plasmids and a complete IS*26*-based Tn*aac(3)*-IIa transposon-like structure in pAb825_36 (Figure 1). Moreover, these comparisons pointed to pXerC/D-mediated SSR as one of the main agents behind these structural differences.

Reversible DNA inversions mediated by recombinationally-active pairs of pXerC/D sites in Ab825 and Ab242 carbapenem-resistance plasmids

The presence of the pXerC/D sites predicted in the carbapenem resistance plasmids harbored by the Ab825 and Ab242 strains (Figure 1) was confirmed by PCR procedures using as templates whole plasmid mixtures extracted from clonal cultures of these strains (see Table 2 for a summary and Supplementary Figure S4 for details). These assays indicated the expected presence of plasmids containing C2/D7 and C7/D2 sites among Ab825 plasmids, and C2/D2 and C7/D7 sites among Ab242 plasmids. Notably, the use of appropriate primer combinations indicated the presence also of plasmid variants containing C2/D2 and C7/D7 sites among Ab825 plasmids, and variants containing C2/D7 and C7/D2 sites in Ab242 plasmid extracts (Table 2). These results indicated that PSVs containing inversions of the DNA region delimited by the recombinationally active pair C2/D2||C7/D7 (or the pair C2/D7||C7/D2) coexisted in the corresponding plasmid extracts. Based on these results, we define here as pAb242_25 In (Xer2/7; Figure 1C) the pAb242_25 structural variant detected in Ab242 clonal cultures that resulted from an Inversion mediated by the recombinationally-active pair composed of the oppositely-oriented sites C2/D2 and C7/D7 (Xer2/7).

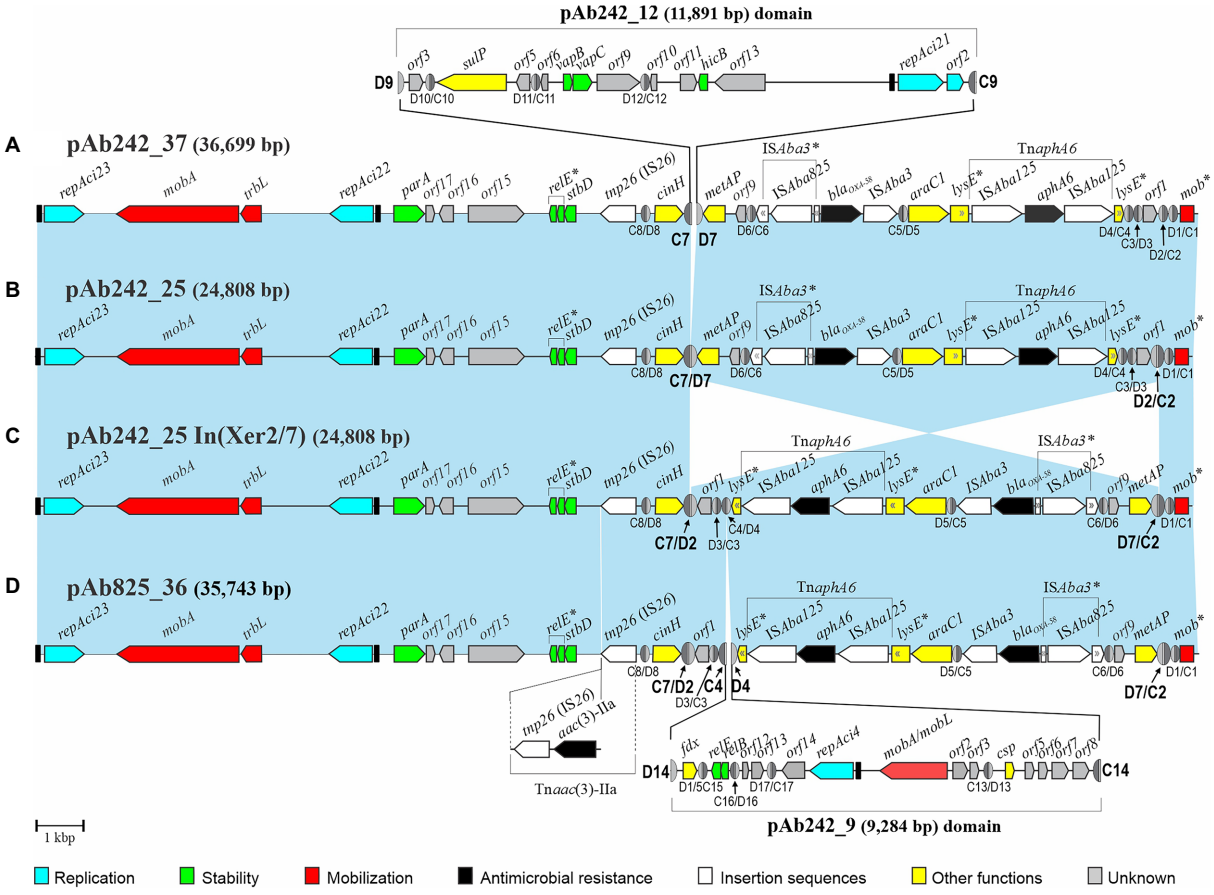

FIGURE 1
Comparisons of the genetic structures of four plasmid structural variants carrying identical bla_{OXA-58}- and Tn*aphA6*-containing resistance modules bordered by multiple pXerC/D sites identified among related *Acinetobacter baumannii* clinical strains studied in this work. Linear representations of four Rep_3-based multi-replicon resistance plasmids characterized in the Ab242 and Ab825 strains. For comparison purposes all plasmids were drawn starting from the iteron sequences region located immediately upstream of the *repAci23* replication initiation protein gene (black rectangle at the left), with the orientations and extents of the different genes and open reading frames also shown. The genes containing premature termination codons, insertions, and pseudogenes are labeled with asterisks. The genes encoding the different replication initiation proteins belonging to the Rep_3 superfamily are denoted as *repAci* followed by their assigned denominations, with their preceding iteron sequences indicated as black rectangles. The carbapenem- and aminoglycoside-resistance module (RM) encompassing the bla_{OXA-58}- and *aphA6* resistant genes and accompanying elements is found in all plasmids associated to multiple pXerC/D sites located in different orientations. The light-blue shaded background interconnecting the structures of the different plasmids denote homologous regions displaying nucleotide sequence identity ≥99%, the cross sectors indicate the inverted regions found between plasmids. Antimicrobial resistance genes are labeled in black and IS elements in white, with their corresponding denominations indicated above each plasmid structure. The extension of the IS*Aba125*-based composite transposon Tn*aphA6* inserted within the *lysE* gene is also indicated. The different pXerC/D-like sites inferred in these plasmids are shown as ovals (not drawn to scale), with the XerC (C) and XerD (D) recognition sequences depicted as dark and light gray semi-ovals, respectively. Their designations (see Cameranesi et al., 2018 for numbering and sequence details) and corresponding polarities are indicated below the structures. The pXerC/D sites identified as involved in SSR have been enlarged, and their designations highlighted in bold letters. **(A)** pAb242_37 structure. This tri-replicon resulted from an intermolecular fusion mediated by the pXerC/D pair C7/D7 and C9/D9 sites located in pAb242_25 and pAb242_12, respectively (Cameranesi et al., 2018). The structure of pAb242_12 and its insertion site into pAb242_25 are indicated above the structure, and resulted in the generation of a directly-oriented pair of (hybrid) sites formed by C7/D9 and C9/D7. **(B)** pAb242_25. This bi-replicon was assembled from WGS data analysis obtained from the Ab242 strain. **(C)** pAb242_25 In(Xer2/7). Plasmid structural variant of pAb242_25 described in this work, in which the region located between the oppositely-oriented sites C7/D7 and D2/C2 is inverted. As the result, a novel pair of oppositely-oriented (hybrid) sites, C7/D2 and D7/C2, was generated. **(D)** pAb825_36. Plasmid assembled from WGS data analysis of the Ab825 strain followed by gap closure using PCR with specifically-designated primers (see Supplementary Figure S3). Sequence analysis indicated that this tri-replicon was formed by the fusion of a plasmid much similar in structure to pAb242_25 In(Xer2/7) and another plasmid identical to pAb242_9, mediated by the pair of pXerC/D sites C4/D4 and C14/D14 located in pAb242_25 In(Xer2/7) and pAb242_9, respectively. This fusion resulted in the generation of a directly-oriented pair of (hybrid) sites, C4/D14 and C14/D4. A complete IS*26*-based composite transposon, Tn*aac(3)*-IIa, was also found in pAb825_36 and its location is also indicated below the plasmid structure. GenBank accession numbers: pAb242_25, KY984047; pAb242_12, KY984046; pAb242_9, KY984045, pAb825_36, MG100202.

The overall results suggested that a dynamic interconversion of PSVs resulting from reversible SSR events mediated by specific sister pairs of oppositely-oriented pXerC/D sites, in this case C2/D2||C7/D7 and C2/D7||C7/D2 (Figure 2), is in operation in both Ab825 and Ab242 cells.

We next used a transformation approach to verify the existence of the dynamic interconversion of PSVs postulated above. The rationale behind (see Supplementary Figure S2) consisted in the generation of clonal lineages of a model *Acinetobacter* strain (e.g., *A. nosocomialis* M2, AnM2). Each clonal lineage is derived from an individual cell transformed with a single PSV carrying the bla_{OXA-58}-containing RM, from the different structural variants present in a plasmid mixture extracted from a clonal population of the *A. baumannii* strain under study. The replication of a single

TABLE 1 pXerC/D core sequences found in the Ab825 and Ab242 plasmids studied in this work.

Plasmid	pXerC/D site[a]	Nucleotide sequence (5′→3′)			Relative orientation in the plasmid structure[b]
		XerC domain	cr	XerD domain	
pAb825_36	C7/D2	ATTACGTATAA	GGTGTA	TTATGTTAATT	C→D
	C2/D7	ATTTCGCATAA	GGTGTA	TTATGTTAATT	D→C
	C4/D14	ATTTCGTATAA	CAGCCA	TTATGTTAAAT	C→D
	C14/D4	ATTTCGTATAA	CGCCCA	TTATGTTAAAT	C→D
pAb242_25	C2/D2	ATTTCGCATAA	GGTGTA	TTATGTTAATT	D→C
	C7/D7	ATTACGTATAA	GGTGTA	TTATGTTAATT	C→D
	C4/D4	ATTTCGTATAA	CAGCCA	TTATGTTAAAT	D→C
pAb242_25 In(Xer2/7)	C7/D2	ATTACGTATAA	GGTGTA	TTATGTTAATT	C→D
	C2/D7	ATTTCGCATAA	GGTGTA	TTATGTTAATT	D→C
	C4/D4	ATTTCGTATAA	CAGCCA	TTATGTTAAAT	C→D
pAb242_12 (pAb825_12)	C9/D9	ATTTCGTATAA	GGTGTA	TTATGTTATTT	-
pAb242_9	C14/D14	ATTTCGTATAA	CGCCCA	TTATGTTAAAT	-
pAb242_37	C7/D9	ATTACGTATAA	GGTGTA	TTATGTTATTT	C→D
	C9/D7	ATTTCGTATAA	GGTGTA	TTATGTTAATT	C→D
Ab242	Chromosomal *dif*	AGTTCGCATAA	TGTATA	TTATGTTAAAT	-
Ab825	Chromosomal *dif*	ATGACGCATAA	TGTATA	TTATGTTAAAT	-

[a]The numbering and sequences of the different pXerC/D core regions are those assigned previously to the sites inferred in *A. baumannii* Ab242 plasmids (Cameranesi et al., 2018). All sequences are drawn in the C→D direction, and encompass the 11-bp left half-site recognized by the XerC recombinase, the 11-bp right half-site recognized by the XerD recombinase, and the 6-bp cr spacer separating them. The relative orientations (polarity) between sites found in a same plasmid molecule are indicated in the last column. The designation of hybrid pXerC/D sites product of SSR between pairs indicates the sources of the C- and D- half-sites on each novel site. For comparison purposes the nucleotide differences between sites are highlighted in red to facilitate the visualization of the SSR. The core sequences of the chromosomal *dif* sites of the Ab242 and Ab825 strains, retrieved from WGS data, are shown in the last two lanes.
[b]See Figure 1.

incoming plasmid in the new host cell would allow growth in selective medium and the subsequent generation of a clonal population derived from this original event. If a dynamic interconversion of PSVs resulting from reversible SSR events mediated by specific sister pairs of oppositely-oriented pXerC/D sites existed in the cells of the *A. baumannii* strain analyzed, this state could be re-established in a clonal population of the new *Acinetobacter* host and the different co-existing PSVs could therefore be detected by PCR assays.

Competent AnM2 cells were thus transformed with whole plasmids extracted from the Ab825 strain (AnM2/pAb825) or the Ab242 strain (AnM2/pAb242), followed by selection on LB solid medium containing IPM. Individual colonies of AnM2/pAb825 or AnM2/pAbAb242 testing positive for the bla_{OXA-58} gene were then used to generate clonal cultures, from which plasmids were extracted and subjected to PCR analysis as indicated above. Using these procedures, we could systematically reproduce in these transformants the PCR results obtained above using plasmids extracted from clonal cultures of Ab825 or Ab242 cells, that is, the co-existence of PSVs containing C2/D2||C7/D7 and C2/D7||C7/D2 sites also in AnM2/pAb825 and in AnM2/pAb242 cells (Table 2; Supplementary Figure S4). Moreover, similar results were obtained for Ab17978 cells transformed with Ab242 plasmid extracts (Ab17978/pAb242). This indicated that a dynamic interconversion of PSVs containing inversions of the DNA regions delimited by the pairs C2/D7||C7/D2 and C2/D2||C7/D7 and resulting from reversible SSR events mediated by these sites could be reproduced in clonal populations of the new hosts (Figure 2).

Detection of reversible plasmid fusions in Ab825 and Ab242 cells mediated by recombinationally-active pairs of pXerC/D sites

We experimentally verified previously (Cameranesi et al., 2018) the fusion of two Ab242 plasmids, pAb242_25 and pAb242_12, into a co-integrate designated pAb242_37 as the result of a SSR event mediated by the pXerC/D sites C7/D7 and C9/D9 (see Figure 1A for the corresponding structure). Moreover, we found that pAb242_37 could also resolve in the new host by employing a recombinationally active pair now formed by the C7/D9 and C9/D7 hybrid sites formed during the previous fusion.

We designed different PCR primers based on these results (Supplementary Table S1) aimed to test the presence of similar co-integrates (and their resolution products) in the plasmid extracts of AnM2/pAb242 and AnM2/pAb825 cells employed above. Hybrid C9/D7 and C7/D9 sites were both detected in AnM2/pAb242 plasmid extracts (Table 2; Supplementary Figure 4F, first two lines at the left), indicating the presence of the pAb242_37 co-integrate in these cells. Moreover, PSVs containing the C9/D9 site (Supplementary Figure 4F, third line at the left) and the C7/D7 site (Supplementary Figure 4F, second lane) were also detected in the same plasmid extracts. The coexistence of both the co-integrate and its resolution products in these cells reinforced the notion (Supplementary Figure S2) that the pAb242_37 co-integrate represented the incoming plasmid form with the ability to replicate and establish in a new AnM2 host cell, and that this co-integrate could also undergo resolution in these cells *via* an intramolecular SSR event mediated now by the directly-oriented hybrid

TABLE 2 Summary of the PCR evidence for the coexistence of different plasmid structural variants containing inversions and fusions resulting from SSR mediated by active pairs of pXerC/D sites in clonal populations of the different *Acinetobacter* strains analyzed.[a]

	Acinetobacter baumannii strain or *Acinetobacter* transformant				
XerC/D site	Ab825	Ab242	AnM2/ pAb825[b]	AnM2/ pAb242[c]	Ab17978/pAb242[d]
D2/D2	+	+	+	+	+
C7/D7	w	+	+	+	+
C2/D7	+	+	+	+	+
C7/D2	+	+	+	+	+
C9/D7	+	+	+	+	n.a.
C7/D9	+	+	+	+	n.a.
C9/D9	+	+	+	+	n.a.

+, detected amplification fragment containing the indicated site. n.a., not assayed. [a]See Supplementary Figure S4 for PCR details and analysis of the amplification fragments.
[b]*A. nosocomialis* M2 transformed with Ab825 plasmids.
[c]*A. nosocomialis* M2 transformed with Ab242 plasmids.
[d]*A. baumannii* ATCC17978 transformed with Ab242 plasmids.

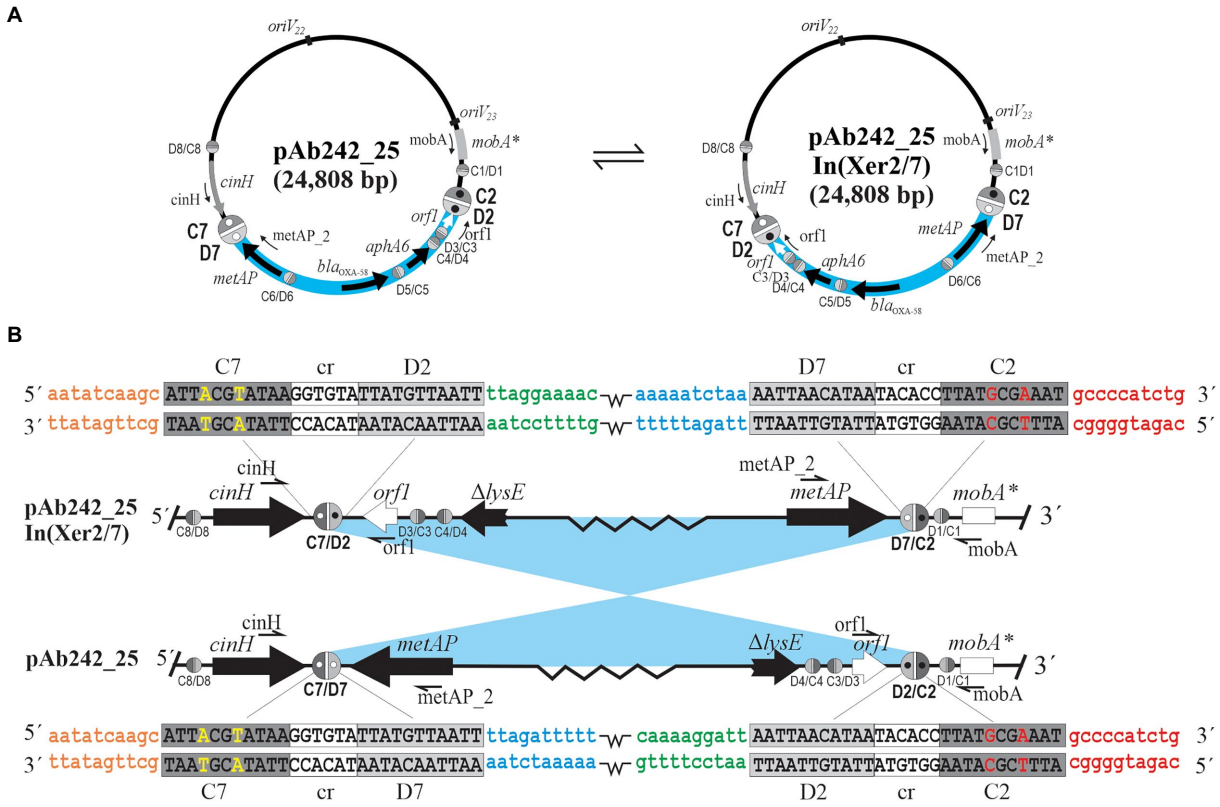

FIGURE 2
DNA inversions resulting from site-specific recombination between oppositely-oriented sister pairs of pXerC/D sites located at the borders of bla_{OXA-58}-and *aphA6*-containing adaptive modules in *Acinetobacter* plasmids. **(A)** SSR between the oppositely-oriented sister pair formed by the C2/D2 and C7/D7 sites located in plasmid pAb242_25 mediate the reversible inversion of the intervening sequences between them, thus generating a structural variant designated here as pAb242_25 In(Xer2/7). In turn, the reverse SSR reaction between the resulting oppositely-oriented C2/D7 and C7/D2 "hybrid" sites can regenerate the original pAb242_25 structure. These two structural variants co-exist in clonal populations of the *A. baumannii* strains analyzed, as well as in clonal populations of other *Acinetobacter* strains transformed with plasmids carrying the adaptive module present in these *A. baumannii* strains. The DNA region carrying the bla_{OXA-58}- and *aphA6*-containing RM is highlighted in pale blue, with the orientation of the genes indicated in each case. The different pXerC/D-like recognition sites are indicated as ovals (not drawn to scale), with the C and D binding regions depicted as dark and light gray semi-ovals, respectively. The active sister pairs mediating inversions have been arbitrarily enlarged, and additional open and closed inner circles within have been incorporated to facilitate visualization of the recombinatorial events. The PCR primers used to identify the presence of specific pXerC/D sites (see Supplementary Table S1 for details) are indicated. The *oriV22* and *oriV23* rectangles denote the location of the iteron regions of the two different replication modules predicted in these plasmids. **(B)** Enlarged vision of the SSR reactions conducing to the reversible inversions described above. The lowercase colored letters show the DNA sequences located at the immediate vicinities of each specific half-site forming the pXerC/D core (10bp each), and have been included to facilitate visualization of the SSR events. Note that the sequences of the cr and the XerD binding regions are identical for all recombining sites, while the XerC binding regions show some differences between sites (highlighted in uppercase colored letters). The figure is not drawn to scale.

pair C9/D7||C7/D9 (Supplementary Figure S5). Similar observations were made using AnM2/pAb825 plasmid extracts, indicating the co-existence in these extracts of PSVs that included a co-integrate variant containing the C9/D7 and C7/D9 hybrid sites as well as individual plasmids carrying the C9/D9 and C7/D7 sites product of the resolution of this co-integrate (Table 2; Supplementary Figures S4F, S4C, respectively). Again, these observations support the existence of a dynamic state of resolution and re-synthesis of similar co-integrates in both Ab825 and Ab242 cells (Supplementary Figure S5).

Contrary to the above results, PCR assays aimed to detect the presence of the C14/D14 site and neighboring regions using Ab825 plasmid extracts as templates (Supplementary Table S1) consistently failed, in sharp contrast with the amplification bands obtained for the C4/D14 and C14/D4 sites using the same extracts and different combinations of the same primers (Supplementary Figures S3, S4G). A successful detection of the C14/D14 site in Ab825 plasmid mixtures would have implicated the presence of a pAb242_9 circular plasmid structure, and therefore that pAb825_36 (Figure 1D) could be resolved in these cells into its putative plasmid constituents in a SSR event mediated by the directly-oriented C4/D14 and C14/D4 sites. It is worth noting that these sites contain identical XerC- and identical XerD- half-sites, but differed in 2 out of 6 positions in the cr spacer sequence (Table 1). This resolution, if taking place, probably occurs at a very low rate as compared to the other SSR events described above which could be reproducibly detected by the PCR assays employed.

The overall observations thus support the existence of a dynamic interconversion state of PSVs involving reversible intramolecular inversions and fusions/resolutions mediated by recombinationally active pairs of pXerC/D sites sharing identical GGTGTA cr spacers in both Ab825 and Ab242 cells. Moreover, this dynamic interconversion of PSVs could be reinstalled in the cells of other *A. baumannii* strains or other *Acinetobacter* species after transformation with a PSV carrying the bla_{OXA-58}-containing RM and possessing the capability to establish in the new host.

Structural comparisons between *A. baumannii* Ab242 and Ab825 plasmids with similar plasmids described in other Acinetobacter strains provide clues on the evolution of novel Rep_3 replicons endowed with blaOXA58-containing resistance modules

A BlastN search against the nucleotide GenBank database (as of August 15, 2022) using as query the Ab242_25 sequence (KY984047) identified a similar plasmid, pAs1069_a (accession number MK323040) housed by a carbapenem-resistant *Acinetobacter seifertii* clinical strain isolated in Brazil (Matos et al., 2019). pAb242_25 and pAs1069_a share 95% total sequence identity, including the presence and orientation of the bla_{OXA-58}- and Tn*aphA6*-containing RM in the corresponding molecules (Figure 3A). However, one remarkable difference between these two plasmids is the number of pXerC/D sites found at the Tn*aphA6*-proximal end of the corresponding RMs, which were reduced to two sites in pAs1069_a as compared to the four sites located in the equivalent region of pAb242_25. It is worth noting that pAs1069_a contains in this region an IS*Ajo2*-like element, and sequence comparison analysis indicated that the acquisition of this element was concomitant with the deletion of a fragment of around 490 bp that in pAb242_25 encompasses the C2/D2 and C3/D3 sites (Figure 3A). Among the seven pXerC/D sites located at the borders of the bla_{OXA-58}- and Tn*aphA6*-containing RM in pAb242_25, only the C7/D7 and C2/D2 sites share identical GGTGTA cr sequences (Table 1, see also Cameranesi et al., 2018). The selection of the insertion of this IS*Ajo2* element at this region in pAs1069_a, by removing the C2/D2 site, is most probably associated then with an impairment of the reversible inversion ability of the DNA fragment encompassing the carbapenem RM.

The use of pAb242_12 (KY984046) as a query retrieved no *repAci21*-containing plasmids carrying bla_{OXA-58} genes, with the exception of the pAb242_37 multi-replicon in which a pXerC/D-bounded pAb242_12 domain is inserted (Figure 1). On the contrary, the use of pAb242_9 (KY984045) identified, besides the pXerC/D-bounded pAb242_9 domain carried by the pAb825_36 tri-replicon (Figure 1), a series of plasmids sharing backbones also composed of a *repAci4*-based replicon and a *mobA*/*mobL* module (Figures 3B,C). It is worth noting that these plasmids were carried by *A. baumannii* CC15 strains isolated in Argentina, Brazil, and Chile (Matos et al., 2019; Cameranesi et al., 2020; Brito et al., 2022). Among them pAb244_7, the smallest plasmid of this group, differs from pAb242_9 in an approximately 1.3 kbp DNA region carrying genes for a *relBE* system and ferredoxin (*fd*; Figure 3B). This region is bordered by two directly-oriented pXerC/D sites, C14/D14 and C16/D16, which differ in 2 out of 11 positions in their XerC-binding regions and in 3 out of 6 positions in their cr spacers (Figure 3C). Yet, the identification of a hybrid C14/D16 site in pAb244_7 strongly suggests that a XerC/D-mediated resolution event occurring in pAb242_9 could be responsible for the loss of this pXerC/D-bounded module.

pAb45063_a, another member of this group, present in an *A. baumannii* CC15 strain isolated in Brazil (Matos et al., 2019), carries an IS*26*-based composite-like transposon endowed with bla_{TEM-1} and *aacC*(3)-IIa resistance genes and, most relevantly for this work, a pXerC/D-bounded bla_{OXA58}-containing RM (Figure 3B). Differences in mobile elements content between the RMs found in pAb45063_a and Ab242/Ab825 plasmids (Figure 1), such as the IS*Aba825* element found upstream of the bla_{OXA-58} gene and the Tn*aphA6* transposon inserted within the *lysE* gene in the latter plasmids as compared to the single IS*Aba125* copy interrupting *lysE* in pAb45063_a (Figure 3B), are commonly observed among *Acinetobacter* Rep_3 plasmids carrying similar adaptive modules, and most probably result from the collection of different ISs and transposons during plasmid transit through different bacterial hosts (Cameranesi et al., 2018). Most importantly however, these comparisons provide clues on how the generation of complex multi-replicon co-integrates such as pAb825_36 could also supply the substrates for subsequent XerC/D-mediated structural rearrangements that eventually evolve in novel replicon structures carrying bla_{OXA-58}-containing RMs. In principle, a SSR resolution event involving the directly-oriented C6/D6 and C16/D16 sites located in pAb825_36 as a sister pair (Figure 3D) could have generated two separate plasmids, one *repAci23*- and *repAci22*-containing bi-replicon and another replicon containing a *repAci4*- and *mobA*/*mobL*-backbone now carrying a bla_{OXA-58}-containing RM similar in structure to pAb45063_a (Figure 3B).

Discussion

We sought to analyze in this work whether and how pXerC/D-mediated recombination contributed to the generation of structural

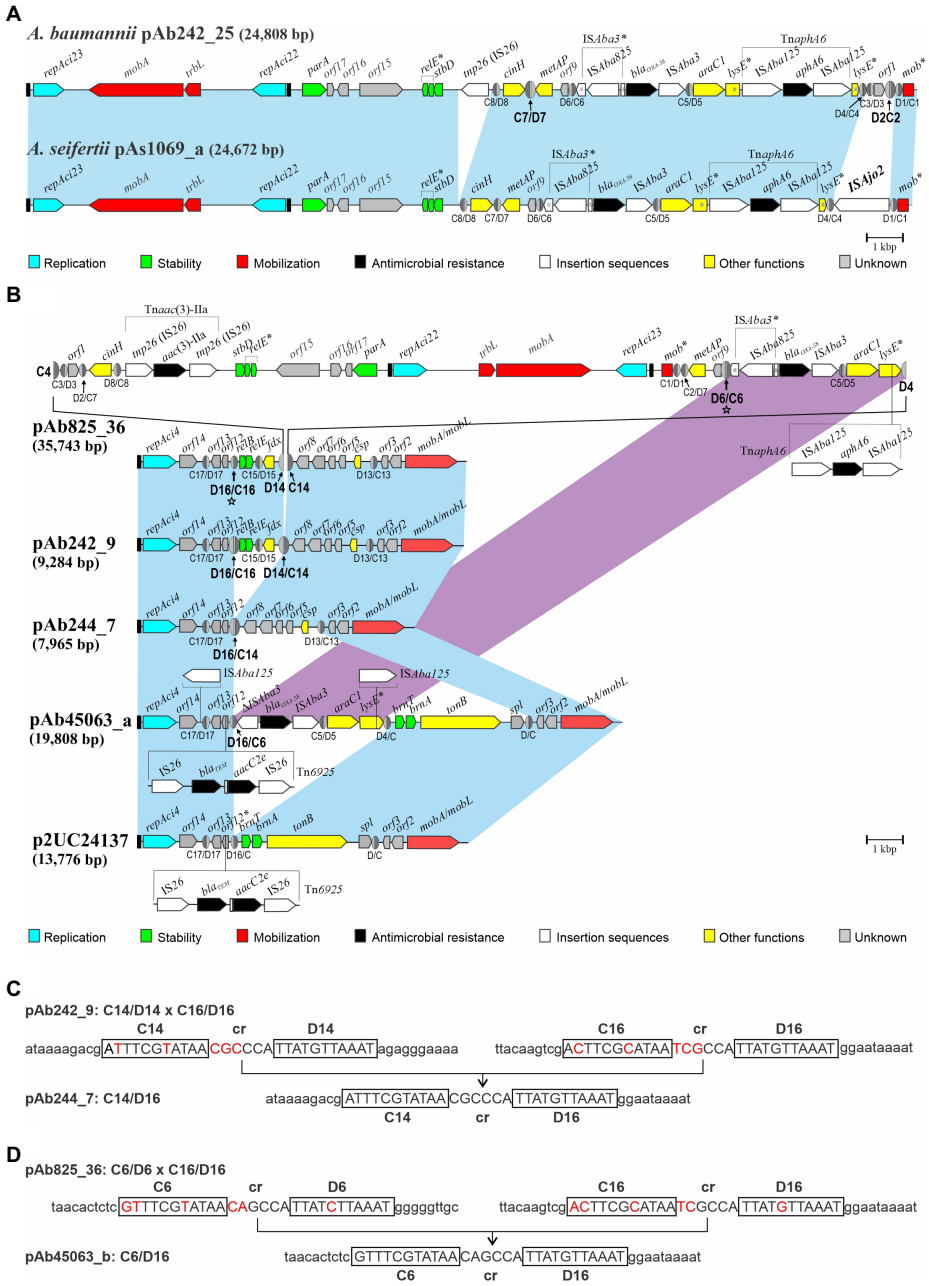

FIGURE 3
Structural comparisons between bla_{OXA-58}-containing Rep_3 plasmids carried by *Acinetobacter baumannii* Ab242/Ab825 strains with sequence-related plasmids deposited in databases described in other *Acinetobacter* strains. **(A)** Comparisons of bla_{OXA-58}-containing pAb242_25 with a similar *repAci23*- and *repAci22*-containing bi-replicon carried by the *Acinetobacter seifertii* 1,069 strain isolated in Brazil, pAs1069_a (GenBank accession number MK323040). The plasmids share 95% total sequence identity, all containing almost identical RMs encompassing bla_{OXA-58}- and *aphA6*-resistant genes which show the same orientation in pAs1069_a as compared to pAb242_25. However, pAs1069_a contains an extra IS*Ajo2*-like element at the Tn*aphA6*-proximal end of the RM (1,482bp; nucleotide positions 22,311 to 23,792), an insertion that is concomitant with the deletion of around 490bp containing the C2/D2 and C3/D3 sites in pAb242_25. For other details on plasmid structures see the legend to Figure 1. **(B)** Comparisons of the pAb825_36 tri-replicon structure characterized in this work with different plasmids containing backbones endowed with a *repAci4* replication module and *mobA*/*mobL* genes described in other *A. baumannii* CC15 strains. The light-blue shaded background interconnecting the different plasmid structures denote shared regions of sequence homology between plasmids. ISs or IS-based transposons found in a given plasmid but not in others within these otherwise homologous regions were represented either above or below the corresponding structures. The magenta-shaded background denotes homologous regions carrying similar pXerC/D-bounded bla_{OXA-58}-containing RMs between pAb825_36 and pAb45063_a. The pXerC/D sites constituting sister pairs mediating SSR events, or resulting from these events, have been arbitrarily enlarged. The directly-oriented C6/D6 and C16/D16 sites in pAb825_36 (labeled with stars ★), proposed here to mediate an intramolecular SSR event conducing to a pAb45063_a-like plasmid as one of the resolution products, have been also arbitrarily enlarged. GenBank accession numbers: pAb244_7: MG520098; pAb45063_a: MK323042. For other details on plasmid structures see the legend to Figure 1. **(C)** Sequence comparison evidence indicating the existence of an intramolecular SSR resolution event in pAb242_9 mediated by the directly-oriented C14/D14 and C16/D16 sites conducing to the generation of pAb244_7 containing a C14/D16 (hybrid) site. The pXerC/D core sequences of each site are displayed in uppercase letters, where the XerC and XerD half-sites have been additionally boxed. For a better visualization of the SSR event the nucleotide differences between core sites on the substrate plasmid have been highlighted in red, and additional sequences (10bp in each case) at the immediate vicinities of each specific half-site have been included. **(D)** Same, indicating an intramolecular SSR resolution event in a pAb825_36-like substrate plasmid mediated by the directly-oriented C6/D6 and C16/D16 sites resulting in the generation of a pAb45063_a-like plasmid containing a C6/D16 (hybrid) site.

diversity between carbapenem resistance plasmids harbored by the *A. baumannii* strains Ab242 and Ab825, two phylogenetically- and epidemiologically-closely related CC15 strains isolated from hospitalized patients in the same public healthcare center in Argentina. These two strains harbored similar Rep_3 plasmids carrying almost identical RM endowed with a bla_{OXA-58} gene accompanied with a Tn*aphA6* composite transposon, a structure associated to seven non-identical pXerC/D sites at their borders. Comparative sequence analysis of Ab242 and Ab825 plasmids assembled on the basis of WGS data (Figure 1) indicated significant structural variations between them, and pointed to XerC/D-mediated SSR as the main agent behind these differences.

We developed a series of methodologies to experimentally verify that SSR events mediated by pXerC/D sites represented the cause of the structural differences observed between Ab242 and Ab825 plasmids carrying the above-described RM. These procedures allowed us to disclose the existence of *bona fide* pairs of recombinationally-active pXerC/D sites in these plasmids, some mediating reversible intramolecular inversions and others reversible plasmid fusions/resolutions. Among them, the pair formed by the oppositely-oriented C2/D2 and C7/D7 sites, and its SSR products the (hybrid) C2/D7 and C7/D2 pair, mediated reversible intramolecular inversions of the RM in both strains. In turn, the pair formed by the C7/D7 and C9/D9 sites mediated intermolecular fusions, and that formed by its SSR products the (hybrid) C7/D9 and C9/D7 sites mediated intramolecular resolutions. These events strongly suggested that a dynamic interconversion of sequence-related PSVs is in operation in clonal populations of the Ab242 and Ab825 strains analyzed. Moreover, this reversible shuffling of plasmid structures could be reproduced in cells of model *Acinetobacter* strains including *A. nosocomialis* M2 and *A. baumannii* ATCC17978 in laboratory transformation assays. All of the *A. baumannii* pXerC/D pairs identified here as mediating reversible SSR events contained identical GGTGTA cr sequences separating the XerC from the XerD half-sites (Table 1), sharing characteristics with pairs classified as relaxed or unconstrained in other models (Cornet et al., 1994).

The findings that *Acinetobacter* plasmids contain pXerC/D sites capable of conforming recombinationally active pairs mediating reversible remodeling of their structures significantly impact the possibilities of rapid adaptation of their eventual hosts to varying environments, the evolution of plasmid structures, and the dissemination of bla_{OXA-58} genes among both *Acinetobacter* and non-*Acinetobacter* populations. In principle, this dynamic shuffling of plasmid structures could provide an eventual *Acinetobacter* host fitness advantage to confront the different selective pressures that the population may encounter during growth. In this context, a number of other bacterial species have been found capable of generating genetically- and phenotypically- heterogeneous subpopulations by employing reversible SSR mechanisms (Didelot et al., 2016; Andam, 2019; García-Pastor et al., 2019; Jiang et al., 2019; Trzilova and Tamayo, 2021). The degree of diversity in these cases solely depends on the number of phase-variable loci, and this process has a profound impact on the survival or fitness capacity of the population as a whole. A valuable asset of reversibility is the ability to rapidly restore genotypic and phenotypic heterogeneity after a bottleneck, a common situation for a bacterial pathogen such as *A. baumannii* that frequently transits from the human host to the environment and vice versa, especially in the highly selective conditions of the clinical setting.

The dynamic interconversion of plasmid structural variants could be also viewed as a trial- and-error game for the long-term adaptation of an eventual *Acinetobacter* host to a specific niche or to long-term exposures to particularly challenging conditions. The majority of bacterial genes are encoded on the leading strand of DNA replication such that transcription is co-directional with fork movement, preventing the deleterious consequences of head-on replication-transcription conflicts (Schroeder et al., 2020). Inversions that result in head-on conflicts promote the selection of mutations, including insertions/deletions and base substitutions depending on genetic context, leading to proposals that the generation of such conflicts potentiates bacterial evolvability (Merrikh and Merrikh, 2018). The dynamic state of DNA inversions and fusions/resolutions reported here in *Acinetobacter* plasmids, by promoting temporary head-on conflicts, could then accelerate the mutation rate in certain plasmid regions with lasting consequences for the evolution of these mobile elements. For instance, and depending on host and environmental pressures, mutational events could be selected that "freeze" a given structural variant thus allowing, for instance, continuous expression of a gene whose product is in extended demand. In this context, the several pXerC/D sites located at the borders of the plasmid-borne bla_{OXA58}-containing RM studied here (Figure 1) provide different alternatives for selection, which may range from complete deletions that abolish the possibilities of recombination (and thus shuffling) to subtle mutations that impede (or increase) the activity of a given pXerC/D pair. The comparisons shown in Figure 3A indicating the IS*Ajo2*-mediated elimination in *A. seifertii* plasmid pAs1069_a of a site composing a recombinationally active pXerC/D pair in Ab242/Ab825 plasmids (Figure 1), provide an example of the above. These observations additionally suggest that the position (or orientation) of the bla_{OXA-58}-containing RM in the *Acinetobacter* plasmid molecule is subjected to selection pressures, and that the selection of a particular orientation most probably depend on the fitness provided to a particular plasmid or plasmid/host partnership in a given environment.

The reversible SSR events mediated by pXerC/D sites reported here may have played important roles in facilitating the wide dissemination of bla_{OXA-58} genes among plasmids carried by *Acinetobacter* species, and also among other bacterial populations (Zarrilli et al., 2008; Carattoli, 2013; Evans and Amyes, 2014; Fu et al., 2014; Zander et al., 2014; Da Silva and Domingues, 2016; Hamidian and Nigro, 2019; Bonnin et al., 2020; Wang et al., 2020; Alattraqchi et al., 2021; Hamidian et al., 2021; Liu et al., 2021; Brito et al., 2022; Jones et al., 2022). It is noteworthy in this context the generation of multi-replicons resulting from pXerC/D-mediated SSR events in both the Ab242 and Ab825 strains (Figure 1). Multi-replicon plasmids have been described in many *Acinetobacter* members by different authors, suggesting selective advantage(s) for these ensembles (Carattoli, 2013; Shintani et al., 2015; Cameranesi et al., 2018, 2020; Hamidian and Hall, 2018; Dionisio et al., 2019; Mindlin et al., 2020; Salgado-Camargo et al., 2020; Alattraqchi et al., 2021; Jones et al., 2022). A reversible fusion of different replicons, by expanding the host range or by providing stability (or other functions) to the ensemble, could play important roles in the establishment of the different plasmid components in a given host (Dionisio et al., 2019). In this context, we observed that a co-integrate between pAb242_25 (or a pAb242_25-related plasmid) and pAb242_12 was the form that could successfully establish in different *Acinetobacter* hosts including *A. nosocomialis* M2 and *A. baumannii* ATCC17978 in laboratory transformation assays (Table 2). The presence of pXerC/D sites in bla_{OXA-58}-containing resident plasmids also opens the possibility of reversible co-integrate formation with newly incoming conjugative plasmid(s) endowed with pXerC/D sites, thus allowing the transfer of the cargo plasmid by conduction. Moreover, a rapid resolution of the co-integrate in the new host by the

reverse SSR reaction may facilitate the rapid segregational loss of the conjugative, energy-demanding counterpart in the progeny especially under antimicrobial selection pressure for the cargo plasmid (Dionisio et al., 2019).

The generation of complex multi-replicon structures endowed with bla_{OXA-58}-containining RMs, by generating new potential pairs of recombinationally active pXerC/D sites capable of mediating further intramolecular resolution events, can also facilitate the evolution of novel replicons carrying bla_{OXA-58}-containing RMs (Figure 3B). This mechanism, added to structural rearrangements generated by subsequent pXerC/D-mediated SSR events and the insertions of different ISs and transposons, could explain the evolution of novel carbapenem-resistance plasmids in the local *A. baumannii* CC15 population.

The different pXerC/D sites inferred in Ab242/Ab825 plasmids show some sequence differences between them at the level of the XerC- and also the XerD-half sites on the core, as well as in the cr spacer separating these regions (Cameranesi et al., 2018). The importance of homology between the core regions of the two recombining sites has not been clearly established for the *E. coli* XerC/D system (Rajeev et al., 2009), and little information exists on the *A. baumannii* XerC/D system. However, recent studies (Lin et al., 2020) indicated similar functions for this SSR system as compared to its *E. coli* counterpart. Our results (Table 2) indicated that reversible recombination could occur between pairs of sites sharing identical GGTGTA cr spacer sequences, even when these recombining sites display some nucleotide differences at the level of the XerC- and also XerD- half-sites. On the contrary, reversible recombination could not be detected for the C4/D14 and C14/D4 sites found in pAb825_36, which contained identical XerC- and identical XerD- half-sites but differed in 2 out of 6 positions in the cr spacer sequence (Table 2). This suggests that the reversibility potential of SSR reactions mediated by pXerC/D sites depends on the cr sequences of the pair involved. In this context, XerC/D-mediated recombination between plasmids containing *dif* and *psi* core sites sharing almost identical XerC- and also XerD- half-sites but differing in their cr sequences in 4 out of 6 positions occurred in *E. coli* cells at very low rates, as judged by the low frequency of colonies carrying plasmids with *dif*/*psi* hybrid sites obtained (Cornet et al., 1994). It was proposed that the XerC/D recombinases could mediate in these cases first strand exchanges but not the subsequent resolutions of the Holliday junction intermediate (HJ) formed, which would then be processed by XerC/D-independent cellular mechanisms (Cornet et al., 1994; Rajeev et al., 2009; Ramirez et al., 2014; Lin et al., 2020). Similarly, it remains possible that in the absence of complete cr identity between sites the *A. baumannii* XerC/XerD recombinases could mediate only first strand exchanges followed by HJ resolution by other mechanisms, making the reaction essentially irreversible. The selection of these infrequent events probably depends on the fitness provided by the resulting plasmid ensemble.

How far in time could we trace the existence of pXerC/D sites in *A. baumannii*? Although environmental *A. baumannii* strains of non-clinical origin are extremely rare (Antunes et al., 2014), we could recently reclassify as *A. baumannii* (Repizo et al., 2017, 2020) a collection strain, *Acinetobacter* sp. NCIMB8209, isolated before 1944 from the enriched microbiota responsible for the aerobic decomposition of the desert shrub guayule in a process aimed for the industrial production of natural latex (Allen et al., 1944). Expectedly from an environmental isolate obtained around or before 1944, WGS analysis of the NCIMB8209 genome indicated a general absence of antimicrobial resistance genes. Most relevantly for this work, however, this analysis also indicated the presence of a large Rep_3 plasmid of 133,709 bp designated pAbNCIMB8209_134 (GenBank accession CP028139.1) in which we detected a pair of directly-oriented pXerC/D sites, namely ATTTCGTATAAGGTGTATTATGTTAATT (positions 48,301 to 48,328) and ATTTCATATAAGGTGTATTATGTTAATT (positions 49,996 to 50,016), flanking a gene cluster composed of a toxin-antitoxin gene cluster (C4X49_18715/C4X49_18720) accompanied by an exonuclease subunit gene (C4X49_18710). Notably, these two sites also shared identical GGTGTA cr sequences. Multiple pXerC/D sites have also been identified in the pAB1 and pAB2 Rep_3 plasmids (Balalovski and Grainge, 2020) present in the *A. baumannii* ATCC17978 collection strain isolated from a clinical source around 1950 (Piechaud and Second, 1951). These inferences indicated that Rep_3 plasmids carrying pXerC/D-bounded genes were already present in the *A. baumannii* population before the massive anthropogenic introduction of antimicrobials by the middle of last century (Antunes et al., 2014; Baquero et al., 2021). GGTGTA cr sequences can also be found among 6 out of the 17 non-identical pXerC/D sites identified by us among Ab242/Ab825 plasmids (Cameranesi et al., 2018), and between many of the multiple pXerC/D sites described in other plasmids of many *Acinetobacter* (and even non-*Acinetobacter*) strains isolated in different periods and from different sources, both clinical and environmental (Fu et al., 2014; Blackwell and Hall, 2017; Brovedan et al., 2019; Matos et al., 2019; Mindlin et al., 2019; Balalovski and Grainge, 2020; Bonnin et al., 2020; Salgado-Camargo et al., 2020; Wang et al., 2020; Alattraqchi et al., 2021; Hamidian et al., 2021; Liu et al., 2021; Jones et al., 2022). Although it remains to be established what other factors influence the feasibility (or reversibility) of SSR events between sites sharing identical cr sequences, it is likely that some of these sites participate in the remodeling and evolution of *Acinetobacter* plasmids in the eventuality that they collide in the same cell, with the concomitant accelerated dissemination of the resistance determinants they bound. The whole process could probably be viewed then more adequately from the units-of-evolution perspective (Baquero et al., 2021).

Further work is in progress to address many of the interrogates posed above, including the influences of the different *Acinetobacter* pXerC/D core sequences and genetic context on the feasibility and directionality of the recombination reaction, as well as the detailed roles of the XerC and XerD recombinases in the recombination process.

Author's Note

Part of the results of this work have been previously presented in the following International Meetings:

1. A. M. Viale, M. Cameranesi, A. Limansky, G. Repizo, and J. Morán-Barrio. Site-specific recombination at XerC/D sites as mediators of plasticity among *Acinetobacter baumannii* plasmids carrying carbapenem- and aminoglycoside-resistance genetic modules. Plasmid Biology Symposium, Seattle, USA, August 2018.
2. M. M. Cameranesi, J. Morán-Barrio, A. S. Limansky, G. D. Repizo, A. M. Viale. Detection of active pairs of XerC/D recognition sites mediating fusions and inversions in *Acinetobacter baumannii* plasmids carrying OXA-58 carbapenemase adaptive modules. 12th International Symposium on the Biology of Acinetobacter, Frankfurt, Germany, September 2019.

Data availability statement

The datasets presented in this study can be found in online repositories. The names of the repository/repositories and accession number(s) are as follows. GenBank accession numbers for the Ab242 and Ab825 plasmids included in this work are: pAb242_25, KY984047; pAb242_12, KY984046; pAb242_9, KY984045; pAb825_36, MG100202; pAb25_12, MG100203. GenBank accession number for plasmid pAb244_7 is MG520098. GenBank accession numbers for the sequences of different PCR amplification fragments containing the particular pXerC/D sites and corresponding genetic contexts presented in this study (Supplementary Table S1) are as follows: C2/D2 site, ON060992; C2/D7 site, ON060990; C7/D2 site, ON060991; C9/D7 site, OM876186; C7/D7 site, ON060993; C7/D9 site, OM876185; C9/D9 site, ON060994.

Author contributions

AV, MC, JM-B, and AL conceived and designed the work. MC, LG, and RS performed the experimental work. MC, AV, and JM-B conducted the bioinformatic analysis. AV, MC, LG, RS, JM-B, and AL analyzed and discussed the data. AV wrote the manuscript. All authors contributed to the article and approved the submitted version.

Funding

This work was supported by grants from CONICET PIP 11220170100377CO to JM-B and AV, Agencia Nacional de Promoción Científica y Tecnológica (ANPCyT) PICT-2017-3536 to JM-B, PICT-2019-00074 to AL, and Ministerio de Ciencia, Tecnología e Innovación Productiva, Provincia de Santa Fe, Argentina, to AV and AL. MC is a former fellow of CONICET, LG is a fellow of ANPCyT, RC is a fellow of CONICET, JM-B, and AV are Career Researchers of CONICET, and AL is a Researcher of the National University of Rosario, Argentina.

Acknowledgments

We thank the collaboration of G. Repizo in the bioinformatic analysis.

Conflict of interest

The authors declare that the research was conducted in the absence of any commercial or financial relationships that could be construed as a potential conflict of interest.

Publisher's note

All claims expressed in this article are solely those of the authors and do not necessarily represent those of their affiliated organizations, or those of the publisher, the editors and the reviewers. Any product that may be evaluated in this article, or claim that may be made by its manufacturer, is not guaranteed or endorsed by the publisher.

Supplementary material

The Supplementary material for this article can be found online at: https://www.frontiersin.org/articles/10.3389/fmicb.2023.1057608/full#supplementary-material

References

Alattraqchi, A. G., Mohd Rani, F., A. Rahman, N. I., Ismail, S., Cleary, D. W., Clarke, S. C., et al. (2021). Complete genome sequencing of *Acinetobacter baumannii* AC1633 and *Acinetobacter nosocomialis* AC1530 unveils a large multidrug-resistant plasmid encoding the NDM-1 and OXA-58 carbapenemases. *mSphere* 6, e01076–e01020. doi: 10.1128/mSphere.01076-20

Allen, P. J., Naghski, J., and Hoover, S. R. (1944). Decomposition of guayule resins by microorganisms. *J. Bacteriol.* 47, 559–572. doi: 10.1128/jb.47.6.559-572.1944

Andam, C. P. (2019). Clonal yet different: understanding the causes of genomic heterogeneity in microbial species and impacts on public health. *mSystems* 4, e00097–e00019. doi: 10.1128/mSystems.00097-19

Antunes, L. C., Visca, P., and Towner, K. J. (2014). *Acinetobacter baumannii*: evolution of a global pathogen. *Path Dis.* 71, 292–301. doi: 10.1111/2049-632X.12125

Aziz, R. K., Bartels, D., Best, A. A., De Jongh, M., Disz, T., Edwards, R. A., et al. (2008). The RAST Server: rapid annotations using subsystems technology. *BMC Genomics* 9: 75. doi: 10.1186/1471-2164-9-75

Balalovski, P., and Grainge, I. (2020). Mobilization of pdif modules in *Acinetobacter*: A novel mechanism for antibiotic resistance gene shuffling? *Mol. Microbiol.* 114, 699–709. doi: 10.1111/mmi.14563

Baquero, F., Martínez, J. L., F. Lanza, V., Rodríguez-Beltrán, J., Galán, J. C., San Millán, A., et al. (2021). Evolutionary pathways and trajectories in antibiotic resistance. *Clin. Microbiol. Rev.* 34:e0005019. doi: 10.1128/CMR.00050-19

Blackwell, G. A., and Hall, R. M. (2017). The tet39 determinant and the msrE-mphE genes in Acinetobacter plasmids are each part of discrete modules flanked by inversely oriented pdif (XerC-XerD) sites. Antimicrob. *Agents Chemother.* 61, e00780–17. doi: 10.1128/AAC.00780-17

Bonnin, R. A., Girlich, D., Jousset, A. B., Gauthier, L., Cuzon, G., Bogaerts, P., et al. (2020). A single Proteus mirabilis lineage from human and animal sources: a hidden reservoir of OXA-23 or OXA-58 carbapenemases in Enterobacterales. *Sci. Rep.* 10:9160. doi: 10.1038/s41598-020-66161-z

Brito, B. P., Koong, J., Wozniak, A., Opazo-Capurro, A., To, JGarcia, P., et al. (2022). Genomic analysis of carbapenem-resistant *Acinetobacter baumannii* strains recovered from Chilean hospitals reveals lineages specific to South America and multiple routes for acquisition of antibiotic resistance genes. *Microbiol. Spectr.* 10:e0246322. doi: 10.1128/spectrum.02463-22

Brovedan, M., Repizo, G. D., Marchiaro, P., Viale, A. M., and Limansky, A. (2019). Characterization of the diverse plasmid pool harbored by the blaNDM-1-containing *Acinetobacter bereziniae* HPC229 clinical strain. *PLoS One* 14:e0220584. doi: 10.1371/journal.pone.0220584

Cameranesi, M. M., Morán-Barrio, J., Limansky, A. S., Repizo, G., and Viale, A. M. (2017). Three novel *Acinetobacter baumannii* plasmid replicase-homology groups inferred from the analysis of a multidrug-resistant clinical strain isolated in Argentina. *J. Infect. Dis. Epidemiol.* 3, 1–5. doi: 10.23937/2474-3658/1510046

Cameranesi, M. M., Morán-Barrio, J., Limansky, A. S., Repizo, G. D., and Viale, A. M. (2018). Site-specific recombination at XerC/D sites mediates the formation and resolution of plasmid co-integrates carrying a bla_{OXA-58}- and Tn*aphA6*-resistance module in *Acinetobacter baumannii*. *Front. Microbiol.* 9:66. doi: 10.3389/fmicb.2018.00066

Cameranesi, M. M., Paganini, J., Limansky, A. S., Moran-Barrio, J., Salcedo, S. P., Viale, A. M., et al. (2020). Acquisition of plasmids conferring carbapenem and aminoglycoside resistance and loss of surface-exposed macromolecule structures as strategies for the adaptation of *Acinetobacter baumannii* CC104O/CC15P strains to the clinical setting. *Microbial Genomi.* 6:mgen000360. doi: 10.1099/mgen.0.000360

Carattoli, A. (2013). Plasmids and the spread of resistance. *Int. J. Med. Microbiol.* 303, 298–304. doi: 10.1016/j.ijmm.2013.02.001

Carruthers, M. D., Harding, C. M., Baker, B. D., Bonomo, R. A., Hujer, K. M., Rather, P. N., et al. (2013). Draft genome sequence of the clinical isolate *Acinetobacter nosocomialis* strain M2. *Genome Announc.* 1, e00906–e00913. doi: 10.1128/genomeA.00906-13

Colloms, S. D., McCulloch, R., Grant, K., Neilson, L., and Sherratt, D. J. (1996). Xer-mediated site-specific recombination in vitro. *EMBO J.* 15, 1172–1181. doi: 10.1002/j.1460-2075.1996.tb00456.x

Cornet, F., Mortier, I., Patte, J., and Louarn, J. M. (1994). Plasmid pSC101 harbors a recombination site, psi, which is able to resolve plasmid multimers and to substitute for the analogous chromosomal *Escherichia coli* site dif. *J. Bacteriol.* 176, 3188–3195. doi: 10.1128/jb.176.11.3188-3195.1994

Crozat, E., Fournes, F., Cornet, F., Hallet, B., and Rousseau, P. (2014). Resolution of multimeric forms of circular plasmids and chromosomes. *Microbiol. Spectr.* 2. doi: 10.1128/microbiolspec.PLAS-0025-2014

Da Silva, G. J., and Domingues, S. (2016). Insights on the horizontal gene transfer of Carbapenemase determinants in the opportunistic pathogen *Acinetobacter baumannii*. *Microorganisms* 4:29. doi: 10.3390/microorganisms4030029

Didelot, X., Walker, A. S., Peto, T. E., Crook, D. W., and Wilson, D. J. (2016). Within-host evolution of bacterial pathogens. *Nat. Rev. Microbiol.* 14, 150–162. doi: 10.1038/nrmicro.2015.13

Dionisio, F., Zilhão, R., and Gama, J. A. (2019). Interactions between plasmids and other mobile genetic elements affect their transmission and persistence. *Plasmid* 102, 29–36. doi: 10.1016/j.plasmid.2019.01.003

Evans, B. A., and Amyes, S. G. (2014). OXA β-lactamases. *Clin. Microbiol. Rev.* 27, 241–263. doi: 10.1128/CMR.00117-13

Fu, Y., Jiang, J., Zhou, H., Jiang, Y., Fu, Y., Yu, Y., et al. (2014). Characterization of a novel plasmid type and various genetic contexts of Bla OXA-58 in *Acinetobacter* spp. from multiple cities in China. *PLoS One* 9:e84680. doi: 10.1371/journal.pone.0084680

García-Pastor, L., Puerta-Fernández, E., and Casadesús, J. (2019). Bistability and phase variation in Salmonella enterica. *Biochim. Biophys. Acta - Gene Regul. Mech.* 1862, 752–758. doi: 10.1016/j.bbagrm.2018.01.003

Hamidian, M., Ambrose, S. J., Blackwell, G. A., Nigro, S. J., and Hall, R. M. (2021). An outbreak of multiply antibiotic-resistant ST49:ST128:KL11:OCL8 *Acinetobacter baumannii* isolates at a Sydney hospital. *J. Antimicrob. Chemother.* 76, 893–900. doi: 10.1093/jac/dkaa553

Hamidian, M., and Nigro, S. J. (2019). Emergence, molecular mechanisms and global spread of carbapenem-resistant *Acinetobacter baumannii*. *Microb. Genom.* 5:e000306. doi: 10.1099/mgen.0.000306

Hamidian, M., and Hall, R. M. (2018). Genetic structure of four plasmids found in Acinetobacter baumannii isolate D36 belonging to lineage 2 of global clone 1. *PloS One.* 13:e0204357. doi: 10.1371/journal.pone.0204357

Harmer, C. J., Moran, R. A., and Hall, R. M. (2014). Movement of IS26-associated antibiotic resistance genes occurs via a translocatable unit that includes a single IS26 and preferentially inserts adjacent to another IS26. *MBio* 5, e01801–e01814. doi: 10.1128/mBio.01801-14

Jiang, X., Hall, A. B., Arthur, T. D., Plichta, D. R., Covington, C. T., Poyet, M., et al. (2019). Invertible promoters mediate bacterial phase variation, antibiotic resistance, and host adaptation in the gut. *Science* 363, 181–187. doi: 10.1126/science.aau5238

Jones, N. I., Harmer, C. J., Hamidian, M., and Hall, R. M. (2022). Evolution of *Acinetobacter baumannii* plasmids carrying the oxa58 carbapenemase resistance gene via plasmid fusion, IS26-mediated events and dif module shuffling. *Plasmid* 121:102628. doi: 10.1016/j.plasmid.2022.102628

Labrador-Herrera, G., Pérez-Pulido, A. J., Álvarez-Marín, R., Casimiro-Soriguer, C. S., Cebrero-Cangueiro, T., Morán-Barrio, J., et al. (2020). Virulence role of the outer membrane protein CarO in carbapenem-resistant *Acinetobacter baumannii*. *Virulence* 11, 1727–1737. doi: 10.1080/21505594.2020.1855912

Lean, S. S., and Yeo, C. C. (2017). Small, enigmatic plasmids of the nosocomial pathogen, *Acinetobacter baumannii*: good, bad, who knows? *Front. Microbiol.* 8:1547. doi: 10.3389/fmicb.2017.01547

Lin, D. L., Traglia, G. M., Baker, R., Sherratt, D. J., Ramirez, M. S., and Tolmasky, M. E. (2020). Functional analysis of the *Acinetobacter baumannii* XerC and XerD site-specific recombinases: potential role in dissemination of resistance genes. *Antibiotics* 9:405. doi: 10.3390/antibiotics9070405

Liu, H., Moran, R. A., Chen, Y., Doughty, E. L., Hua, X., Jiang, Y., et al. (2021). Transferable *Acinetobacter baumannii* plasmid pDETAB2 encodes OXA-58 and NDM-1 and represents a new class of antibiotic resistance plasmids. *J. Antimicrob. Chemother.* 76, 1130–1134. doi: 10.1093/jac/dkab005

Matos, A. P., Cayô, R., Almeida, L., Streling, A. P., Nodari, C. S., Martins, W., et al. (2019). Genetic characterization of plasmid-borne *bla*OXA-58 in distinct *Acinetobacter* species. *mSphere* 4, e00376–e00319. doi: 10.1128/mSphere.00376-19

Merrikh, C. N., and Merrikh, H. (2018). Gene inversion potentiates bacterial evolvability and virulence. *Nat. Commun.* 9:4662. doi: 10.1038/s41467-018-07110-3

Mindlin, S., Beletsky, A., Mardanov, A., and Petrova, M. (2019). Adaptive *dif* modules in permafrost strains of *Acinetobacter lwoffii* and their distribution and abundance among present day *Acinetobacter* strains. *Front. Microbiol.* 10:632. doi: 10.3389/fmicb.2019.00632

Mindlin, S., Beletsky, A., Rakitin, A., Mardanov, A., and Petrova, M. (2020). *Acinetobacter* plasmids: diversity and development of classification strategies. *Front. Microbiol.* 11:588410. doi: 10.3389/fmicb.2020.588410

Mussi, M. A., Limansky, A. S., and Viale, A. M. (2005). Acquisition of resistance to carbapenems in multidrug-resistant clinical strains of *Acinetobacter baumannii*: natural insertional inactivation of a gene encoding a member of a novel family of beta-barrel outer membrane proteins. *Antimicrob. Agents Chemother.* 49, 1432–1440. doi: 10.1128/AAC.49.4.1432-1440.2005

Piechaud, M., and Second, L. (1951). Etude de 26 souches de *Moraxella lwoffi* [studies of 26 strains of *Moraxella lwoffi*]. *Ann. Inst. Pasteur* 80, 97–99.

Rajeev, L., Malanowska, K., and Gardner, J. F. (2009). Challenging a paradigm: the role of DNA homology in tyrosine recombinase reactions. *Microbiol. Mol. Biol. Rev.* 73, 300–309. doi: 10.1128/MMBR.00038-08

Ramirez, M. S., Traglia, G. M., Lin, D. L., Tran, T., and Tolmasky, M. E. (2014). Plasmid-mediated antibiotic resistance and virulence in Gram-negatives: the *Klebsiella pneumoniae* paradigm. *Microbiol. Spectr.* 2, 1–15. doi: 10.1128/microbiolspec.PLAS-0016-2013

Ravasi, P., Limansky, A. S., Rodriguez, R. E., Viale, A. M., and Mussi, M. A. (2011). ISAba825, a functional insertion sequence modulating genomic plasticity and bla(OXA-58) expression in *Acinetobacter baumannii*. *Antimicrob. Agents Chemother.* 55, 917–920. doi: 10.1128/AAC.00491-10

Repizo, G. D., Espariz, M., Seravalle, J. L., Díaz Miloslavich, J. I., Steimbrüch, B. A., Shuman, H. A., et al. (2020). *Acinetobacter baumannii* NCIMB8209: a rare environmental strain displaying extensive insertion sequence-mediated genome remodeling resulting in the loss of exposed cell structures and defensive mechanisms. *mSphere* 5, e00404–e00420. doi: 10.1128/mSphere.00404-20

Repizo, G. D., Viale, A. M., Borges, V., Cameranesi, M. M., Taib, N., Espariz, M., et al. (2017). The environmental *Acinetobacter baumannii* isolate DSM30011 reveals clues into the Preantibiotic era genome diversity, virulence potential, and niche range of a predominant nosocomial pathogen. *Genome Biol. Evol.* 9, 2292–2307. doi: 10.1093/gbe/evx162

Roca, I., Espinal, P., Vila-Farrés, X., and Vila, J. (2012). The *Acinetobacter baumannii* oxymoron: commensal hospital dweller turned Pan-drug-resistant menace. *Front. Microbiol.* 3:148. doi: 10.3389/fmicb.2012.00148

Salgado-Camargo, A. D., Castro-Jaimes, S., Gutierrez-Rios, R. M., Lozano, L. F., Altamirano-Pacheco, L., Silva-Sanchez, J., et al. (2020). Structure and evolution of *Acinetobacter baumannii* plasmids. *Front. Microbiol.* 11:1283. doi: 10.3389/fmicb.2020.01283

Salto, I. P., Torres Tejerizo, G., Wibberg, D., Pühler, A., Schlüter, A., and Pistorio, M. (2018). Comparative genomic analysis of *Acinetobacter* spp. plasmids originating from clinical settings and environmental habitats. *Sci. Rep.* 8:7783. doi: 10.1038/s41598-018-26180-3

Schroeder, J. W., Sankar, T. S., Wang, J. D., and Simmons, L. A. (2020). The roles of replication-transcription conflict in mutagenesis and evolution of genome organization. *PLoS genetics.* 16, e1008987. doi: 10.1371/journal.pgen.1008987

Siguier, P., Perochon, J., Lestrade, L., Mahillon, J., and Chandler, M. (2006). ISfinder: the reference centre for bacterial insertion sequences. *Nucleic Acids Res.* 34, D32–D36. doi: 10.1093/nar/gkj014

Shintani, M., Sanchez, Z. K., and Kimbara, K. (2015). Genomics of microbial plasmids: classification and identification based on replication and transfer systems and host taxonomy. *Front. Microbiol.* 6:242. doi: 10.3389/fmicb.2015.00242

Trzilova, D., and Tamayo, R. (2021). Site-specific recombination - how simple DNA inversions produce complex phenotypic heterogeneity in bacterial populations. *Trends Genet.* 37, 59–72. doi: 10.1016/j.tig.2020.09.004

Varani, A. M., Siguier, P., Gourbeyre, E., Charneau, V., and Schlüter, A., and Chandler, M. (2011). ISsaga is an ensemble of web-based methods for high throughput identification and semi-automatic annotation of insertion sequences in prokaryotic genomes. *Genome Biol.* 12:R30. doi: 10.1186/gb-2011-12-3-r30

Wang, J., Wang, Y., Wu, H., Wang, Z. Y., Shen, P. C., Tian, Y. Q., et al. (2020). Coexistence of *bla*OXA-58 and *tet*(X) on a novel plasmid in *Acinetobacter* sp. from pig in Shanghai, China. *Front. Microbiol.* 11:578020. doi: 10.3389/fmicb.2020.578020

Zarrilli, R., Vitale, D., Di Popolo, A., Bagattini, M., Daoud, Z., Khan, A. U., et al. (2008). A plasmid-borne blaOXA-58 gene confers imipenem resistance to Acinetobacter baumannii isolates from a Lebanese hospital. Antimicrob. *Agents Chemother.* 52, 4115–4120. doi: 10.1128/AAC.00366-08

Zander, E., Fernández-González, A., Schleicher, X., Dammhayn, C., Kamolvit, W., Seifert, H., et al. (2014). Worldwide dissemination of acquired carbapenem-hydrolysing class D β-lactamases in *Acinetobacter* spp. other than *Acinetobacter baumannii*. *Int. J. Antimicrob. Agents* 43, 375–377. doi: 10.1016/j.ijantimicag.2014.01.012

Frontiers in Microbiology

Explores the habitable world and the potential of microbial life

The largest and most cited microbiology journal which advances our understanding of the role microbes play in addressing global challenges such as healthcare, food security, and climate change.

Discover the latest Research Topics

See more →

Frontiers

Avenue du Tribunal-Fédéral 34
1005 Lausanne, Switzerland
frontiersin.org

Contact us

+41 (0)21 510 17 00
frontiersin.org/about/contact